Atlas of Clinical Cases on Brain Tumor Imaging

Yelda Özsunar
Utku Şenol
Editors

Springer

Atlas of Clinical Cases on Brain Tumor Imaging

Yelda Özsunar • Utku Şenol
Editors

Atlas of Clinical Cases on Brain Tumor Imaging

Springer

Editors
Yelda Özsunar
Radiology Department
Adnan Menderes University
Aydın
Turkey

Utku Şenol
School of Medicine
Akdeniz University
Antalya
Turkey

ISBN 978-3-030-23272-6 ISBN 978-3-030-23273-3 (eBook)
https://doi.org/10.1007/978-3-030-23273-3

This Springer imprint is published by the registered company Springer Nature Switzerland AG
The registered company address is: Gewerbestrasse 11, 6330 Cham, Switzerland

Preface

With our well-known and accomplished authors who are competent in their fields, we believe that we have prepared a book which will be found interesting and beneficial about brain tumors.

Brain tumors are one of the most challenging diseases of neuroradiology not only in terms of diagnosis but also in management aspect. For example, glioblastomas (GBM), which encounter about half of the glial tumors, are still one of the most deadly tumors, despite the significant development of molecular and imaging technologies and advanced therapy methods.

In the last three decades, survival rates for GBM have shown no notable improvement. Therefore, we believe that the integration of most recent developments, such as genomic knowledge with clinical and imaging experience, might potentially improve the management of this devastating disease. In most cases, decision-making in diagnosis and therapy is complex and needs close interdiciplinary teamwork. Therefore, we tried to accomplish a multidiciplinary approach for preparing this book. We presented our book in two parts: The first part is the general, multidiciplinary explanation of most recent developments and basic knowledge about the brain tumors. The second part represents several imaging samples of brain tumors with brief but important explanations.

Translation of pathological and clinical findings to a simple and illustrative teaching tool is very important. Most radiologists and clinicians prefer not too complex and straightforward information with many cases presented with images. Simple pathological findings, such as increased neovascularity, should be easily translated into the dictionary of radiologist as increased perfusion and should be presented with numerous illustrations to enhance experience and knowledge of the interpreter. Therefore, this book will be a very useful and quick reference for primarily radiologists, neuroradiologists,

oncologists, radiation oncologists, neurosurgeons, and pathologists. The book also includes the most recent development of the imaging technology, management strategies, and pathological classifications.

In short, as editors and authors, we expected to present this book as a quick reference with brief and important illustrative explanations of brain tumors. The most recent multidiciplinary technical, clinical, molecular, and genetic developments have been also explained with simple explanations and images. We hope that this book will serve as a pleasant, informative, quick, and useful book in clinics of different disciplines which study brain tumors.

Aydın, Turkey — Yelda Özsunar
Antalya, Turkey — Utku Şenol

Contents

Part I

General Considerations in Brain Tumors

1 Pathology, Epidemiology, and WHO Classification of Brain Tumors

Özlem Yapıcıer

1.1 Epidemiology and Pathology of the Central Nervous System Tumors

The incidence of all brain tumors is reported to be ranged from 4.3 to 18.6 per 100,000 person-years [1]. Primary brain tumors constitute 50–75% of all central nervous system (CNS) tumors whereas secondary brain tumors, majority of which are carcinoma metastases, occur in the remaining 25–50%.

Although relatively rare in adults, primary CNS tumors are the most common type of solid tumors in infants and children. Pediatric CNS tumors differ from their adult counterpart with regard to the histological type and site of occurrence. For instance, the majority of the tumors occur in the supratentorial compartment in adults, whereas the infratentorial compartment is the most common site in the pediatric population. Regarding the tumor histology, the most common type encountered in adults is meningioma, followed by glioma, half of which being glioblastoma, and pituitary adenoma. On the other hand, the most common type seen in the pediatric population is glioma, majority of which is pilocytic astrocytoma, and embryonal tumors among which medulloblastoma is the leading type.

Ö. Yapıcıer (✉)
Department of Pathology, School of Medicine, Bahcesehir University, Istanbul, Turkey
e-mail: ozlem.yapicier@med.bau.edu.tr

Primary spinal cord tumors constitute 5–12% of all primary CNS tumors. Of these, 85% are extramedullary, with schwannoma and meningioma being the most common types. Intramedullary tumors, majority of which are ependymomas and astrocytomas, are much rarer. Regarding the metastatic spinal tumors, the most common primary malignancy in adults is lung cancer (adenocarcinoma in particular), followed by breast cancer, melanoma, renal cell carcinoma, and colorectal cancer. In the pediatric population, leukemia and lymphoma are the most common types of the metastatic tumors, followed by germ cell tumors, osteosarcoma, neuroblastoma, Ewing sarcoma, and rhabdomyosarcoma. Metastasis to the spinal cord, which constitutes 8–9% of spinal metastases, arises from the vertebral body or via direct infiltration from the paravertebral tissues. The most common culprit for intramedullary metastasis is small cell lung cancer, whereas for the spinal epidural disease, it is the prostate, breast, and lung.

CNS tumors arise from a number of different tissues that consist of various cell types, such as the brain parenchyma, the ventricles, pineal and sellar region, cranial and spinal nerves, and meninges. This is why CNS tumors are a very large and heterogenous group of tumors. A number of potential risk factors have been investigated in epidemiological studies with regard to the development of CNS tumors. Among these, ionizing radiation and genetic tendency have been shown to have a stronger correlation.

Y. Özsunar, U. Şenol (eds.), *Atlas of Clinical Cases on Brain Tumor Imaging*,
https://doi.org/10.1007/978-3-030-23273-3_1

However, although some brain tumor types occur in people with familial tumor syndromes such as neurofibromatosis or Li-Fraumeni syndrome, it is known that 95% of brain tumors are sporadic. Likewise, brain tumors may occur in individuals exposed to ionizing radiation; however, the majority of brain tumor patients have no history of prior ionizing radiation. Large epidemiological studies based on clinicopathological research are likely to shed more light on the immunological, genetic, and other potential risk factors that are likely to play a role on the development of CNS tumors.

1.2 An Overview of the WHO Classifications of Tumors of the Central Nervous System

The first edition of the "World Health Organization (WHO) Classification of Tumors of the Central Nervous System" published in 1979 was based mainly on the histogenesis of the tumors depending on their light microscopic features in routine hematoxylin and eosin-stained sections [2]. Since then, four classification updates have been published in 1993, 2000, 2007, and 2016, the last being the revised version of the 2007 edition (4th edition) rather than a new formal edition [3–6].

In the 1993 classification, immunohistochemical expressions of relevant proteins were added to the diagnostic algorithm in addition to histopathologic features. Although subsequent classifications of 2000 and 2007 put an emphasis on genetic factors in tumorigenesis as a result of greatly increased knowledge of the genetic basis of brain tumors, these not fully understood genetic changes fell short in specifying the tumors in the mentioned classifications. Through new genetic discoveries, the recent 2016 classification has been structured with a better understanding of the role of these genetic alterations play in prognosis and treatment response. In this context, the most important development in the field since the previous edition of the WHO classification 2007 has been the discovery of somatic mutations in the gene encoding isocitrate dehydrogenase (IDH) in adult diffuse gliomas. Sanson et al. [7] showed that diffuse gliomas in adults which do not contain IDH mutation show a more aggressive clinical behavior independent of the WHO grade. In 2014, the International Society of Neuropathology formulated guidelines [8] on how to incorporate molecular findings into CNS tumor classification. The proposed integrated diagnosis scheme was composed of four layers; Layer 2 containing the histological classification, Layer 3 tumor grade, and Layer 4 molecular information, while Layer 1 generating the integrated diagnosis by combining all the data from the other three layers. This "integrated" approach provided the fundamentals for the current classification. As such, the 2016 classification has emerged as one that builds biologically more homogeneous diagnostic categories by integrating well-established genotypic parameters along with phenotypic features.

1.3 Major Differences of WHO 2016 Classification

- The most significant changes took place in the category of glial neoplasms (Table 1.1) when compared to WHO 2007 classification [5]. All diffusely infiltrating gliomas whether astrocytic or oligodendroglial were grouped together based on their shared IDH gene mutation status along with the shared growth pattern and behaviors. Astrocytomas that lack IDH gene family mutations but with frequent BRAF alterations or tuberous sclerosis complex (TSC1/TSC2) mutations and circumscribed growth pattern were grouped separately from diffuse gliomas as "other astrocytic tumors." Molecular assay findings were incorporated into the diagnosis of diffuse gliomas as an extension of histopathological diagnosis (e.g., diffuse astrocytoma, IDH mutant)
- Medulloblastomas were reclassified as mutually complementary two broad groups containing genetically and histopathologically

Table 1.1 The comparison of 2007 and 2016 WHO CNS tumor classifications for glial neoplasms

2007—Glial neoplasms			2016—Glial neoplasms		
Astrocytomas	Oligodendrogliomas and oligoastrocytic tumors	Ependymomas	Diffuse astrocytic and oligodendroglial tumors	Other astrocytic tumors	Ependymal tumors
Diffuse astrocytomas Fibrillary[a] Gemistocytic Protoplasmic[a]	Oligodendroglioma	Subependymoma	Diffuse astrocytoma, ***IDH-mutant*** Gemistocytic astrocytoma, ***IDH-mutant*** ***Diffuse astrocytoma, IDH-wild type*** Diffuse astrocytoma, ***NOS***	Pilocytic astrocytoma Pilomyxoid astrocytoma	Subependymoma
Anaplastic astrocytoma	Anaplastic oligodendroglioma	Myxopapillary ependymoma	Anaplastic astrocytoma, ***IDH-mutant*** ***Anaplastic astrocytoma, IDH-wild type*** Anaplastic astrocytoma, ***NOS***	SEGA	Myxopapillary ependymoma
Glioblastoma Giant cell Gliosarcoma	Oligoastrocytoma	Ependymoma Cellular ependymoma[a] Papillary ependymoma Clear cell ependymoma Tanycytic ependymoma	Glioblastoma, ***IDH-wild type*** Giant cell glioblastoma Gliosarcoma ***Epithelioid glioblastoma*** Glioblastoma, ***IDH-mutant*** Glioblastoma, ***NOS***	PXA	Ependymoma Papillary ependymoma Clear cell ependymoma Tanycytic ependymoma
Gliomatosis cerebri[a]	Anaplastic oligoastrocytoma	Anaplastic ependymoma	***Diffuse midline glioma, H3 K27M mutant***	***Anaplastic PXA***	***Ependymoma, RELA fusion-positive***
Pilocytic astrocytoma Pilomyxoid astrocytoma			Oligodendroglioma, ***IDH-mutant/1p19q codeleted*** Oligodendroglioma, ***NOS***		Anaplastic ependymoma
SEGA			Anaplastic oligodendroglioma, ***IDH-mutant and 1p19q codeleted*** Anaplastic oligodendroglioma, ***NOS***		
PXA			Oligoastrocytoma, ***NOS*** Anaplastic oligoastrocytoma, ***NOS***		

IDH isocitrate dehydrogenase, *NOS* not otherwise specified, *SEGA* subependymal giant cell astrocytoma, *PXA* pleomorphic xanthoastrocytoma
Italicized terms: New designations
[a]Not included into the new (2016) classification

Table 1.2 2016 WHO classification of medulloblastomas

Medulloblastomas, histologically defined
Medulloblastoma, classic
Desmoplastic/nodular medulloblastoma
Medulloblastoma with extensive nodularity
Large cell/anaplastic medulloblastoma
Medulloblastomas, genetically defined
Medulloblastoma, WNT-activated
Medulloblastoma, SHH-activated and TP53-mutant
Medulloblastoma, SHH-activated and TP53-wild type
Medulloblastoma, non-WNT/non-SHH
Medulloblastoma, group 3
Medulloblastoma, group 4

Table 1.3 New entities, variants and patterns included in the 2016 WHO classification

Entities
Genetically defined diffuse gliomas
Glioblastoma, IDH-wild type, and IDH-mutant
Diffuse midline glioma, H3 K27M-mutant
Ependymoma, *RELA* fusion-positive
Genetically defined medulloblastomas
Embryonal tumor with multilayered rosettes (ETMR), C19MC-altered
Anaplastic pleomorphic xanthoastrocytoma
Diffuse leptomeningeal glioneuronal tumor
Variants
Epithelioid glioblastoma
Patterns
Glioblastoma with primitive neuronal component
Multinodular and vacuolating neuronal tumor of the cerebrum

defined tumors (Table 1.2). Anaplastic and large cell variants of medulloblastoma were combined as a single entity with two different morphological features of the same spectrum in the 2016 WHO classification

- The group of embryonal tumors of the CNS was reconstructed with the incorporation of genetically defined entities. Medulloepithelioma, CNS neuroblastoma, CNS ganglioneuroblastoma, and CNS embryonal tumor, NOS were grouped together as "other CNS embryonal tumors" since no specific genetic alteration has been shown pertaining to them yet. Ependymoblastoma, a separate entity under the embryonal tumors group in the 2007 classification, was regarded as one of the three histological patterns of embryonal tumor with multilayered rosettes (ETMRs), C19MC-altered in the current classification, on the basis of their molecular commonality. The primitive neuroectodermal tumor was removed from the classification
- Newly recognized entities, variants, and patterns were included in the current classification (Table 1.3)
- Some entities and variants were excluded from the classification. Fibrillary astrocytoma, protoplasmic astrocytoma, gliomatosis cerebri, cellular ependymoma, and primitive neuroectodermal tumor are no longer present in 2016 WHO classification. Gliomatosis cerebri, on the other hand, was considered merely as a growth pattern rather than being a distinct entity. Although this extensive involvement pattern of the neuroaxis can be seen in all subtypes of diffuse glioma, it is most commonly seen in anaplastic astrocytoma
- Chordoid glioma of the third ventricle, angiocentric glioma, and astroblastoma were grouped under "other gliomas" in 2016, not under the heading of "other neuroepithelial tumors" as in 2007 WHO classification
- Brain invasion was included as a criterion for the diagnosis of atypical meningioma
- Solitary fibrous tumor and hemangiopericytoma (SFT/HPC) were reconstituted as one entity and a new grading system as Grade I–II–III has been adapted for this entity
- The group of nerve sheath tumors was expanded by the addition of atypical neurofibroma, hybrid nerve sheath tumors, and malignant peripheral nerve sheath tumor with perineurial differentiation. Melanotic schwannoma was separated from other schwannomas
- The group of hematopoietic/lymphoid tumors was expanded in accordance with the changes in the classification of systemic lymphomas and histiocytic neoplasms over the past decade
- Pediatric diffuse gliomas showing similar histopathological features with their adult counterparts are addressed as separate entities due to a number of important differences

  - *Pediatric diffuse astrocytic tumors*: These tumors were shown to possess different clinicopathological (incidence, site, anaplastic progression) and genetic features as compared to the adult type. These include MYB and BRAF alterations, whereas the adult types harbor IDH1, IDH2, TP53, and ATRX mutations
  - *Pediatric high-grade diffuse astrocytic tumors*: Pediatric anaplastic astrocytoma (WHO Grade III) and glioblastoma (WHO Grade IV) were combined as a single category owing to the therapeutic implications. Like the low-grade counterparts, these tumors also show clinicopathological and genetic differences as compared to the adult types. One entity, which shows only H3F3A or K27M mutation on HIST1H3B/C and is mainly seen in the pediatric population and at sites like the spinal cord and midline structures such as the thalamus and the brainstem is included in the classification as a separate entity named "Diffuse midline glioma, H3 K27M-mutant"
  - *Pediatric-type oligodendroglioma* (oligodendroglioma lacking IDH mutation and 1p19q codeletion): These tumors were shown to constitute the majority of oligodendrogliomas in children and adolescents. It is emphasized that with the aid of molecular studies, these tumors could be distinguished from histopathologically similar tumors which show round cell morphology, such as the dysembryoplastic neuroepithelial tumor, angiocentric glioma, pilocytic astrocytoma, and extraventricular neurocytoma
- The term "oligoastrocytoma" is discouraged in the current classification since the use of both genotypical and phenotypical studies in these tumors results in more homogeneously defined categories as either astrocytoma or oligodendroglioma. With a simplified genotypic approach, IDH-mutant, *ATRX*-mutant, and 1p/19q-intact tumors are distinctively astrocytic while IDH-mutant, *ATRX*-wild-type, and 1p/19q-codeleted tumors are oligodendroglial
- No direct relevance between grade and biological behavior has been established in ependymomas to date [9, 10]. Consequently, the issue of the subjective nature of the histopathological criteria used in the classification of classical ependymoma (WHO Grade II) and anaplastic ependymoma (WHO Grade III) still remained in the most recent classification. A recent study by Pajtler et al. [11] suggests that ependymomas occurring in three principal anatomical locations have different genetic alterations and prognoses and utilizing transcriptome and methylome profiling might serve as the basis of molecular classification for ependymomas. However, for the time being, the only genetically defined subtype is *RELA* fusion-positive ependymoma constituting the majority of supratentorial tumors of childhood
- *Grade*:
  - Three grades were defined for the solitary fibrous tumor/hemangiopericytoma. The idea of a single entity encompassing different grades is not new for the tumors outside of the central nervous system. However, this is the first time this notion is introduced for central nervous system tumors
  - The majority of the diffuse leptomeningeal glioneural tumors, which has been recently included in the classification, are low-grade lesions. However, as a result of limited patient size and insufficient clinical follow-up, a grading has not been proposed for these tumors yet
  - Pilomyxoid astrocytomas show a wide spectrum of biological behavior. However, they do have a higher tendency for recurrence or cerebrospinal dissemination as compared to pilocytic astrocytomas. Since it is still not clear whether this aggressive behavior is a result of some inherent biological features or simply the unfavorable hypothalamic/chiasmatic location, a grading has not been applied to them
- *"NOS"* (not otherwise specified) designation is added to the diagnostic categories as an extension of the histopathological diagnosis when genetic testing is not done or done but is inconclusive

1.4 Diagnostic Algorithm Based on the 2016 CNS Tumor Classification

In this recent classification, some tumor groups are diagnosed by the combination of histomorphological and molecular/genetic features while many tumor groups are still diagnosed mainly by microscopic morphologic features. The former is predominantly used in diffuse astrocytic/oligodendroglial tumors and medulloblastoma categories.

1.4.1 Diffuse Astrocytic and Oligodendroglial Tumors

Although it is not necessary to follow a certain sequence, the first step recommended in the diagnosis algorithm of this tumor group in adults is to define the histomorphological subtype of diffuse glioma, followed by genetic testing for IDH status and 1p19q codeletion as depicted below and in Table 1.4.

1. Histomorphology: Astrocytoma, oligodendroglioma, oligoastrocytoma, or glioblastoma
2. IDH status: IDH mutant or IDH wild type
3. 1p19q codeletion: Presence or absence of 1p19q codeletion

Presence of 1p19q codeletion is essential in IDH mutated diffuse gliomas for the diagnosis of oligodendroglioma. Other genetic parameters including *ATRX* loss and TP53 mutation are characteristic but not required for the diagnosis of diffuse astrocytomas. Lack of nuclear ATRX immunoexpression is characteristic for astrocytomas while oligodendrogliomas have nuclear ATRX immunoexpression (Figs. 1.1 and 1.2).

However, if genetic tests are readily accessible, molecular/genetic data may precede histomorphological assessment throughout the course of integrated diagnosis.

IDH: Since the isocitrate dehydrogenase mutation has become a definitive marker for the adult diffuse glial tumors in the recent classification, it constitutes an important part of the diagnostic algorithm. Only IDH1 and IDH2 mutations, which are two of the three isoforms of IDH, have been detected in human gliomas. Mutations in the IDH1 isoform are much more common than those in the IDH2 isoform. IDH1 mutations are the earliest detectable genetic alteration in low-grade diffuse astrocytomas and in all oligodendrogliomas and also seen in secondary glioblastomas, which progress from a precursor diffuse astrocytoma or anaplastic astrocytoma [12]. The most frequent IDH1 mutation found in almost 90% of astrocytic and oligoden-

Table 1.4 Diagnostic algorithm for adult diffuse astrocytic and oligodendroglial tumors

Histomorphology	IDH status	1p19q codeletion	Diagnosis
Astrocytoma	Mutant	Absent	Diffuse astrocytoma, IDH mutant
	Wild type	Absent	Diffuse astrocytoma, IDH wild type
	Not done/ inconclusive	Absent	Diffuse astrocytoma, NOS
Oligodendroglioma	Mutant	Present	Oligodendroglioma, IDH mutant, 1p19q codeleted
	Wild type	No need to apply	Oligodendroglioma, NOS (after exclusion of histological mimics[a])
	Not done/ inconclusive	Not done/ inconclusive	Oligodendroglioma, NOS
Oligoastrocytoma	Very rare. Restricted to mixed gliomas with dual-genotype		
Glioblastoma	Mutant	No need to apply	Glioblastoma, IDH mutant (secondary glioblastoma)
	Wild type	No need to apply	Glioblastoma, IDH wild type (primary glioblastoma)
	Not done/ inconclusive	No need to apply	Glioblastoma, NOS

[a]Neurocytoma, dysembryoplastic neuroepithelial tumor, clear cell ependymoma, pilocytic astrocytoma

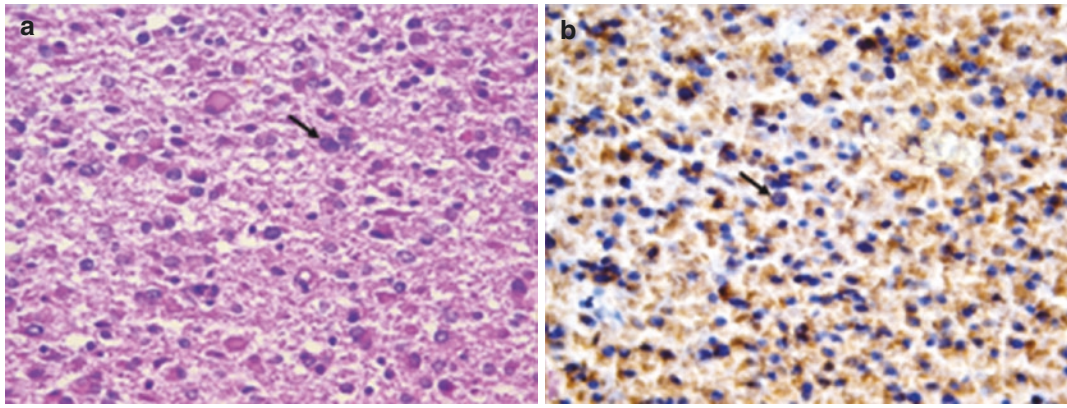

Fig. 1.1 Astrocytoma, ATRX-mutant. (**a**) H+E, ×100, tumor cells with oval nuclei (arrow) scattered in gliofibrillary matrix. (b) ATRX, ×400, loss of nuclear immunoexpression of ATRX in tumor cells (arrow)

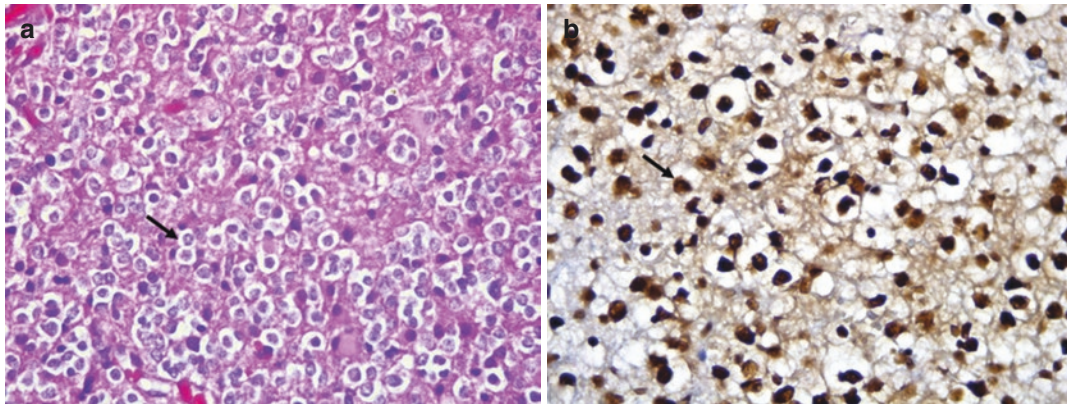

Fig. 1.2 Oligodendroglioma, ATRX-intact. (**a**) H+E, ×100, tumor cells showing typical (fried egg appearance) clear perinuclear halo of oligodendroglioma (arrow). (**b**) ATRX, ×400, immunoexpression of ATRX in tumor cells identified by nuclear brown color (arrow)

droglial gliomas, and IDH-mutant glioblastomas (secondary glioblastomas) are the R132H mutation [13]. The presence of this mutation can be detected by using an antibody for the specific gene product, immunohistochemically. The majority of diffuse astrocytomas and oligodendrogliomas demonstrate immunopositivity with the aforementioned antibody specific for R132H mutation, whereas the majority of glioblastomas (primary glioblastomas) are immunonegative [7]. Figures 1.3d and 1.4d show immunohistochemical staining with the specific R132H-mutant IDH1 antibody for an oligodendroglioma and a primary glioblastoma, respectively, along with their typical hematoxylin and eosin (H+E) stained sections and radiologic images. However, immunonegativity for R132H-mutant IDH1 antibody seen in diffuse gliomas does not rule out diffuse astrocytoma or oligodendroglioma since less common IDH1 and IDH2 mutations cannot be detected with the R132H-mutant IDH1 antibody. Assessment of IDH mutation status requires sequencing analysis for IDH1 codon 132 and IDH2 codon 172 mutations in cases that are immunohistochemically negative for the IDH1 R132H mutation. IDH-wild-type designation involves full assessment of IDH sequence analysis in addition to negative R132H-mutant IDH1 immunohistochemistry for diffuse astrocytomas and oligodendrogliomas after exclusion of other

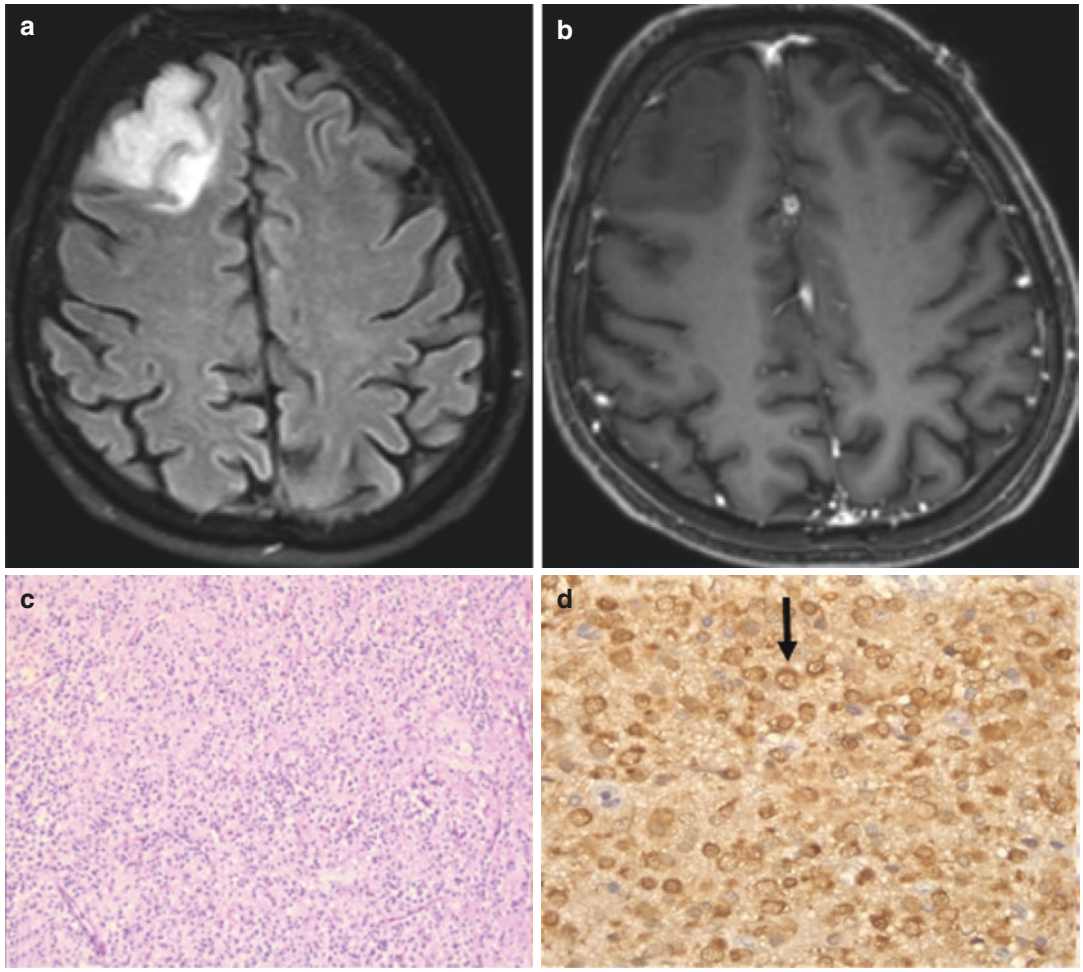

Fig. 1.3 Oligodendroglioma, IDH-mutant and 1p/19q codeleted. (**a**) Axial FLAIR MR image shows a peripherally located left temporal lobe heterogeneous hyperintense tumor with hemorrhagic signals and perifocal edema. (**b**) Axial T1-weighted contrast-enhanced MR image shows a well-defined hypointense nonenhancing mass in the right frontal lobe. (**c**) H+E, ×100, round uniform tumor cells with clear cytoplasm. (**d**) IDH1, ×400, immunoexpression of R132-mutant IDH1 protein in oligodendroglioma cells, identified by cytoplasmic brown color (arrow)

possible diagnoses. Nevertheless, IDH-wild-type designation can be applied to glioblastomas particularly in patients older than 54 years of age who do not have a lower-grade precursor lesion, without the need for IDH sequencing in the setting of negative IDH1 immunohistochemistry as proposed by Chen et al. [14].

Mutations in the IDH 1/2 genes cause overproduction of the oncometabolite 2-hydroxygluterate (2HG) within the tumor cells. 2HG can be detected by using magnetic resonance spectroscopy (MRS), albeit its routine use for this purpose is currently available only at a few institutions [15]. This modality has advantages over its alternatives in that genetic sequencing requires tissue containing at least 20% mutant alleles to be able to detect mutations on IDH1/2 [16], is time-consuming, expensive, and surrogate R132H-mutant IDH1 immunohistochemistry has false-negative results in gliomas harboring non-R132H IDH1 mutations. Besides, the availability of the information on the IDH mutation status before surgery

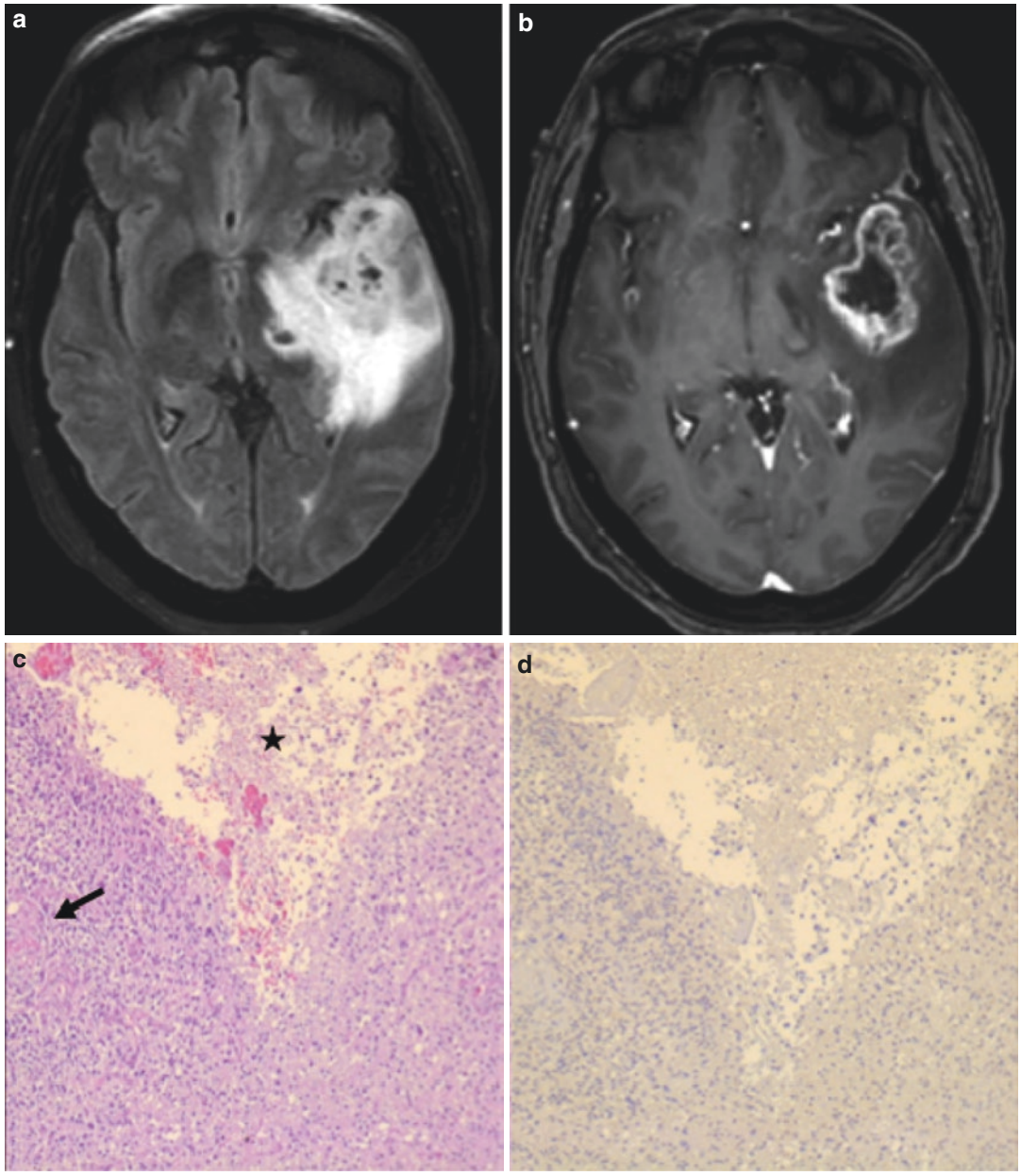

Fig. 1.4 Glioblastoma, IDH-wild type. (**a**) Axial FLAIR MR image shows a peripherally located left temporal lobe heterogeneous hyperintense tumor with hemorrhagic signals and perifocal edema. (**b**) Axial T1-weighted contrast-enhanced MR image shows irregular peripheral enhancement with central necrosis. (**c**) H+E, ×100, focus of ischemic necrosis (star) surrounded by densely accumulated tumor cells and microvascular proliferation (arrow). (**d**) IDH1, ×100, absence of R132-mutant IDH1 protein immunoexpression in tumor cell cytoplasms

is important not only for predicting prognosis but also for surgical decision-making and planning for neurosurgeons as well. In this regard, the ability to identify the IDH mutations in diffuse astrocytic and oligodendroglial tumors in the preoperative period would put the radiologists in a more critical position in the management of these patients.

1.4.2 Medulloblastomas

These tumors are classified according to their molecular characteristics based on transcriptome or methylome profiling as well as histological features. Histologically defined medullobastoma types including classic, desmoplastic/nodular, extensive nodular, and large cell/anaplastic (LCA) variants are maintained in the classification owing to its clinical usefulness when molecular tests are not available. Besides, these morphological variants have significant clinical associations. Genetically, medulloblastomas are divided into four principal subtypes: WNT (wingless)-activated, SHH (sonic hedgehog)-activated, group 3, and group 4. Histologically and genetically defined medulloblastomas show particular relationships. As a result, by combining their histological and molecular features through an integrative approach, the predictive and prognostic value of the pathological assessment increases. For instance, WNT-activated medulloblastomas with classic histological morphology have an excellent prognosis.

Although specific data is not available for each group of genetically defined medulloblastomas, some reports indicate that they have a tendency to arise in certain localizations [17, 18]. WNT-activated tumors tend to arise in the cerebellar midline/cerebellopontine angle, whereas SHH-activated tumors predominantly occur in the lateral cerebellar hemisphere and may involve the vermis. On the other hand, non-WNT/non-SHH medulloblastomas tend to present as midline tumors. By taking these into account, radiologists may predict the subtype of genetically defined medulloblastomas preoperatively.

Molecular analysis is still the gold standard in defining the genetic subgroups; however, several immunohistochemical antibodies have been found to be beneficial as surrogate markers in distinguishing WNT, SHH, and non-WNT/non-SHH medulloblastomas [19]. Nuclear β-catenin immunoreactivity is seen only in WNT-activated medulloblastomas while cytoplasmic GAB1 immunoreactivity is detected only in SHH-activated tumors. Non-WNT/non-SHH medulloblastomas can be distinguished from the other two groups by the presence of cytoplasmic β-catenin immunopositivity and GAB1 immunonegativity.

Likewise, given that immunohistochemistry is a reliable and widely available technology, certain immunohistochemical antibodies can be used instead of genetic tests also for the newly included entities and variants which have specific molecular alterations. The aforementioned antibodies are H3K27M, L1CAM, LIN28A, and VE1 and they are used as substitutes for genetic tests for diffuse midline glioma, RELA fusion-positive ependymoma, C19MC-altered ETMR, and epithelioid glioblastoma, respectively [6].

1.5 Advantages and Challenges of the 2016 CNS Tumor Classification

The new classification has several advantages and challenges. Assessment of genetic alterations with histological findings leads to the formation of more homogeneous and specific entities, thereby increasing diagnostic objectivity. This contributes to more accurate prediction of prognosis, improving patient management and response to targeted therapies. When taken into consideration that genetic tests are not available in many institutions, this classification is also useful in that it enables for the diagnosis to be made in the absence of molecular data. Classifying pediatric diffuse glial tumors that have similar morphology but different genetic features from their adult counterparts separately is a novel approach of this classification, which is likely to bring convenience for diagnosis and treatment.

Although a number of immunohistochemical surrogates are proposed by this new classification, specific assignment of certain assays as alternatives for the emphasized genetic tests is lacking in the classification. Therefore, higher interobserver variability in testing and reporting arises as a challenge of this classification. Nevertheless, with the increasing availability, reproducibility, and reliability of surrogate immunohistochemical antibodies, this challenge

is likely to be overcome in the near future. Since the integrative approach combining genotype and phenotype allows high diagnostic precision by forming more homogenous and narrower diagnostic groups, the tumors that do not fit into these categories are placed in "NOS" groups, which are essentially heterogenous "wastebasket" groups. On the other hand, these heterogeneous groups would likely serve as a source of future genetic studies aiming to improve the accuracy of the classification systems.

References

1. de Robles P, Fiest KM, Frolkis AD, Pringsheim T, Atta C, St Germaine-Smith C, et al. The worldwide incidence and prevalence of primary brain tumors: a systematic review and meta-analysis. Neuro-Oncology. 2015;17(6):776–83. https://doi.org/10.1093/neuonc/nou283.
2. Zülch KJ. Histological typing of tumours of the central nervous system. Geneva: World Health Organization; 1979.
3. Kleihues P, Burger PC, Scheithauer BW. Histological typing of tumours of the central nervous system. 2nd ed. Berlin: Springer; 1993.
4. Kleihues P, Cavenee WK. World Health Organization classification of tumours-pathology and genetics. Tumours of the nervous system. Lyon: IARC; 2000.
5. Louis DN, Ohgaki H, Wiestler OD, Cavenee WK, editors. WHO classification of tumours of the central nervous system. 4th ed. IARC: Lyon; 2007.
6. Louis DN, Ohgaki H, Wiestler OD, Cavenee WK, editors. WHO classification of tumours of the central nervous system. Revised 4th ed. Lyon: IARC; 2016.
7. Sanson M, Marie Y, Paris S, Idbaih A, Laffaire J, Ducray F, et al. Isocitrate dehydrogenase 1 codon 132 mutation is an important prognostic biomarker in gliomas. J Clin Oncol. 2009;27(25):4150–4. https://doi.org/10.1200/JCO.2009.21.9832.
8. Louis DN, Perry A, Burger P, Ellison DW, Reifenberger G, von Deimling A, et al. International Society of Neuropathology: Haarlem consensus guidelines for nervous system tumor classification and grading. Brain Pathol. 2014;24(5):429–35. https://doi.org/10.1111/bpa.12171.
9. Ellison DW, Kocak M, Figarella-Branger D, Felice G, Catherine G, Pietsch T, et al. Histopathological grading of pediatric ependymoma: reproducibility and clinical relevance in European trial cohorts. J Negat Results Biomed. 2011;10:7. https://doi.org/10.1186/1477-5751-10-7.
10. Figarella-Branger D, Civatte M, Bouvier-Labit C, Gouvernet J, Gamberelli D, Gentet JC, et al. Prognostic factors in intracranial ependymomas in children. J Neurosurg. 2000;93(4):605–13. https://doi.org/10.3171/jns.2000.93.4.0605.
11. Pajtler KW, Witt H, Sill M, Jones DT, Hovestadt W, Kratochwil F, et al. Molecular classification of ependymal tumors across all CNS compartments, histopathological grades, and age groups. Cancer Cell. 2015;27(5):728–43. https://doi.org/10.1016/j.ccell.2015.04.002.
12. Ohgaki H, Kleihues P. The definition of primary and secondary glioblastoma. Clin Cancer Res. 2013;19:764–72. https://doi.org/10.1158/1078-0432.CCR-12-3002.
13. Yan H, Parsons DW, Jin G, McLendon R, Rasheed BA, Yuan W, et al. IDH1 and IDH2 mutations in gliomas. N Engl J Med. 2009;360(8):765–73. https://doi.org/10.1056/NEJMoa0808710.
14. Chen L, Voronovich Z, Clark K, Hands I, Mannas J, Walsh M, et al. Predicting the likelihood of an isocitrate dehydrogenase 1 or 2 mutation in diagnosis of infiltrative glioma. Neuro-Oncology. 2014;16(11):1478–83. https://doi.org/10.1093/neuonc/nou097.
15. Pope WB, Prins RM, Albert Thomas M, et al. Non-invasive detection of 2-hydroxyglutarate and other metabolites in IDH1 mutant glioma patients using magnetic resonance spectroscopy. J Neurooncol. 2012;107(1):197–205. https://doi.org/10.1007/s11060-011-0737-8.
16. Arita H, Narita Y, Matsushita Y, Fukushima S, Yoshida A, Takami H, et al. Development of a robust and sensitive pyrosequencing assay for the detection of IDH1/2 mutations in gliomas. Brain Tumor Pathol. 2015;32:22–30. https://doi.org/10.1007/s10014-014-0186-0.
17. Gibson P, Tong Y, Robinson G, Thompson MC, Currle DS, Eden C, et al. Subtypes of medulloblastoma have distinct developmental origins. Nature. 2010;468(7327):1095–9. https://doi.org/10.1038/nature09587.
18. Teo WY, Shen J, Su JM, Yu A, Wang J, Chow WY, et al. Implications of tumor location on subtypes of medulloblastoma. Pediatr Blood Cancer. 2013;60(9):1408–10. https://doi.org/10.1002/pbc.24511.
19. Ellison DW, Dalton J, Kocak M, Nicholson SL, Fraga C, Neale G, et al. Medulloblastoma: clinicopathological correlates of SHH, WNT, and non-SHH/WNT molecular subgroups. Acta Neuropathol. 2011;121(3):381–96. https://doi.org/10.1007/s00401-011-0800-8.

2 When and How to Use Imaging in Brain Tumors, Protocols

Murat Alp Öztek

2.1 Introduction

Modern imaging techniques are the primary means of diagnosis of brain tumors [1]. They are also used to decide on best treatment options based on possible tumor grade, plan biopsy and surgery, evaluate extent of tumor resection, assess response to treatment, and detect recurrence.

This chapter will provide an overview of when to use imaging for brain tumors, a general overview of follow-up imaging, criteria used to assess treatment response, and recommended protocols. While the use of advanced imaging methods will be mentioned and some aspects of conventional MRI sequences will be discussed, these will be in the context of their utility in general terms. Details regarding specific uses, pearls and pitfalls of conventional sequences, and advanced imaging techniques will be discussed in other chapters of the book.

2.2 When to Use Imaging

2.2.1 Diagnosis

MRI remains the cornerstone of brain tumor imaging, and is considered the standard imaging method for diagnosis [2]. In cases where a brain tumor might be suspected, such as those with chronic headache with new features or increasing frequency, new onset headache with optic disc edema, nontraumatic seizure in patients older than 40 or with focal neurologic deficit, the most appropriate imaging is MRI with and without contrast [3, 4]. CT can be used in the emergency setting, or to look for calcification in selected patients.

While a specific histopathological diagnosis may not be possible based on the images, it is usually not needed. In many cases the distinction of low- and high-grade lesions is more important, and many patients will have biopsies or surgery for histopathologic diagnosis and molecular studies (and in case of surgery, for treatment) in any case.

2.2.2 Preoperative Planning

Surgery remains the cornerstone of treatment of brain tumors and maximum safe resection is recommended in all patients with newly diagnosed gliomas whenever feasible [2]. While some tumors in eloquent cortex or brainstem have been traditionally considered inoperable, recent advances in neurosurgery and mapping techniques make it possible to operate on at least some of those lesions [5].

In certain cases, biopsy may be preferred before (or instead of) surgery. It is well known

M. A. Öztek (✉)
Department of Radiology, University of Washington Medical Center, Seattle, WA, USA

Y. Özsunar, U. Şenol (eds.), *Atlas of Clinical Cases on Brain Tumor Imaging*,
https://doi.org/10.1007/978-3-030-23273-3_2

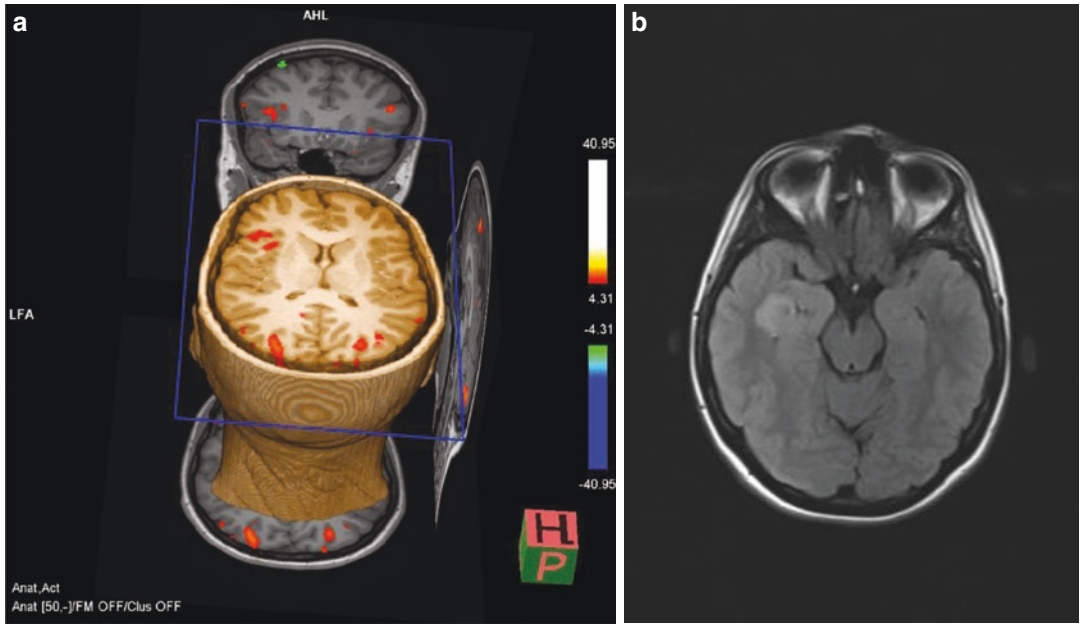

Fig. 2.1 fMRI study (**a**) to determine the location of the Broca area and plan surgery accordingly in a patient with a right temporal mass (**b**). The Broca region is demonstrated to be on the left side, which would have been impossible to determine with conventional MRI

that the heterogeneity of gliomas can cause undergrading and misdiagnosis due to sampling errors in biopsy [6]. In such patients, advanced imaging techniques can be used to target specific regions of interest to potentially improve diagnostic accuracy [6, 7].

MRI is also used in preoperative planning for navigational purposes. This is usually done with contrast-enhanced 3D-SPGR sequences that allow for high resolution and easy distinction of the tumor due to contrast enhancement. Coupled with some fiducials placed on the patient's head before the imaging study, these images can be used for intraoperative navigation. Imaging with head frames can also be performed for the same purpose in stereotactic radiosurgery or frame-based stereotactic biopsy.

Another factor with potential impact on surgery is the relation of the lesion to eloquent brain and critical white matter tracts [8]. Conventional anatomic MR imaging is insufficient to provide this information; for instance, while one can easily tell if a lesion is in the motor cortex provided one knows where the motor cortex is in that patient; brain mapping is not generalizable and must be done in a patient specific manner [9]. Functional MRI can be used to evaluate the location of the lesion with respect to eloquent brain (Fig. 2.1). The relationship of white matter tracts with the tumor can be delineated using diffusion tensor imaging (DTI) [8, 10]; thus DTI can also help improve tumor resection [11] and reduce the risk of new postoperative neurological deficits [12].

2.2.3 Intraoperative Imaging

Intraoperative MRI (iMRI) scans are beginning to get more widespread. The extent of resection is one of the factors improving overall survival in patients with gliomas [13] and use of intraoperative imaging makes it easier to ensure that as much of the lesion as is surgically feasible has been taken out [2]. This allows immediate further resection in the same session [14] and improved overall survival and progression-free survival have been reported by some groups [15, 16]. Despite these apparent benefits, there is a high cost of installation and an increase in the

healthcare cost and length of surgery [13]. There are also few studies providing high-quality evidence and evaluating whether the use of iMRI translates to improved progression-free survival or overall survival [14].

2.2.4 Postoperative Imaging

In the immediate postoperative period, unless there are operative complications or clinical concern, imaging is usually performed to determine the extent of tumor resection. In this situation, MRI is the modality of choice, provided the patient is clinically stable and there are no contraindications to an MRI scan.

Post-op imaging is also required to act as a baseline for further follow-up. The most appropriate time for baseline imaging to evaluate residual tumor is considered to be within 24–48 h of surgery and no later than 72 h [2, 17, 18]. Diffusion-weighted imaging (DWI) can also be included in the baseline imaging to determine if any future enhancement would be due to recurrence or ischemia related to surgery [18]. However, it should be noted that RANO criteria for diffuse low-grade gliomas recommend the baseline postoperative images to be preferably acquired 2–3 months after the surgery to minimize the effects of postsurgical changes such as edema, ischemia and enhancement and to better evaluate the extent of resection of non-enhancing tumors [19].

2.2.5 Follow-Up Imaging

There are two different scenarios where follow-up imaging is performed: To follow up the lesion after treatment for recurrence or progression of any non-resected parts of the mass; and to follow up lesions that did not receive any treatment. While the imaging protocol is similar in both cases, the distinction is important since it changes the differential diagnosis: new enhancement in a lesion that has been treated with chemoradiotherapy might be due to tumor progression as well as pseudoprogression or radiation necrosis in the appropriate timeframe, whereas the same change in a tumor that has not been treated would be very alarming for tumor progression.

Follow-up imaging should be performed using the same imaging modality as the baseline, which would be MRI in almost all cases [20]. Ideally, the same MRI scanner should be used, but if that is not possible or feasible, at least scanners with same magnet strength should be used (Fig. 2.2) [20].

Some clinical data can help with the interpretation of follow-up images: Type of treatment the patient received and when the treatment was completed would help determine if increasing or new enhancement could be due to pseudoprogression, radiation necrosis, or tumor progression; antiangiogenic therapy might cause decreased enhancement without true regression; changes in steroid dose can affect the size of T2/FLAIR hyperintense component and enhancement; knowledge of the radiation field could help differentiate progression or new disease outside the field from radiation-induced changes [17].

Edema, treatment-related changes, and postoperative gliosis surrounding the surgical cavity might make it difficult to determine the recurrence of the lesion using T2W or FLAIR images. Outside of the timeframe for treatment-related changes, increases in T2/FLAIR hyperintensity should be suspicious for progression of non-enhancing tumor or increasing edema. Similarly new or increasing contrast enhancement, especially outside the high-dose radiation zone, is also a red flag [17].

2.2.5.1 Pseudoprogression

Pseudoprogression is a temporary, new, or increased area of contrast enhancement without true tumor progression, caused by treatment-induced changes [21–23]. It has been described in 10–30% of GBM patients who receive radiotherapy and temozolomide, in GBM patients receiving immunotherapy, and in LGG patients receiving radiotherapy [21, 22, 24]. It occurs most commonly within 3–6 months following therapy [17, 25]. Pseudoprogression may be more frequent in patients with MGMT promoter

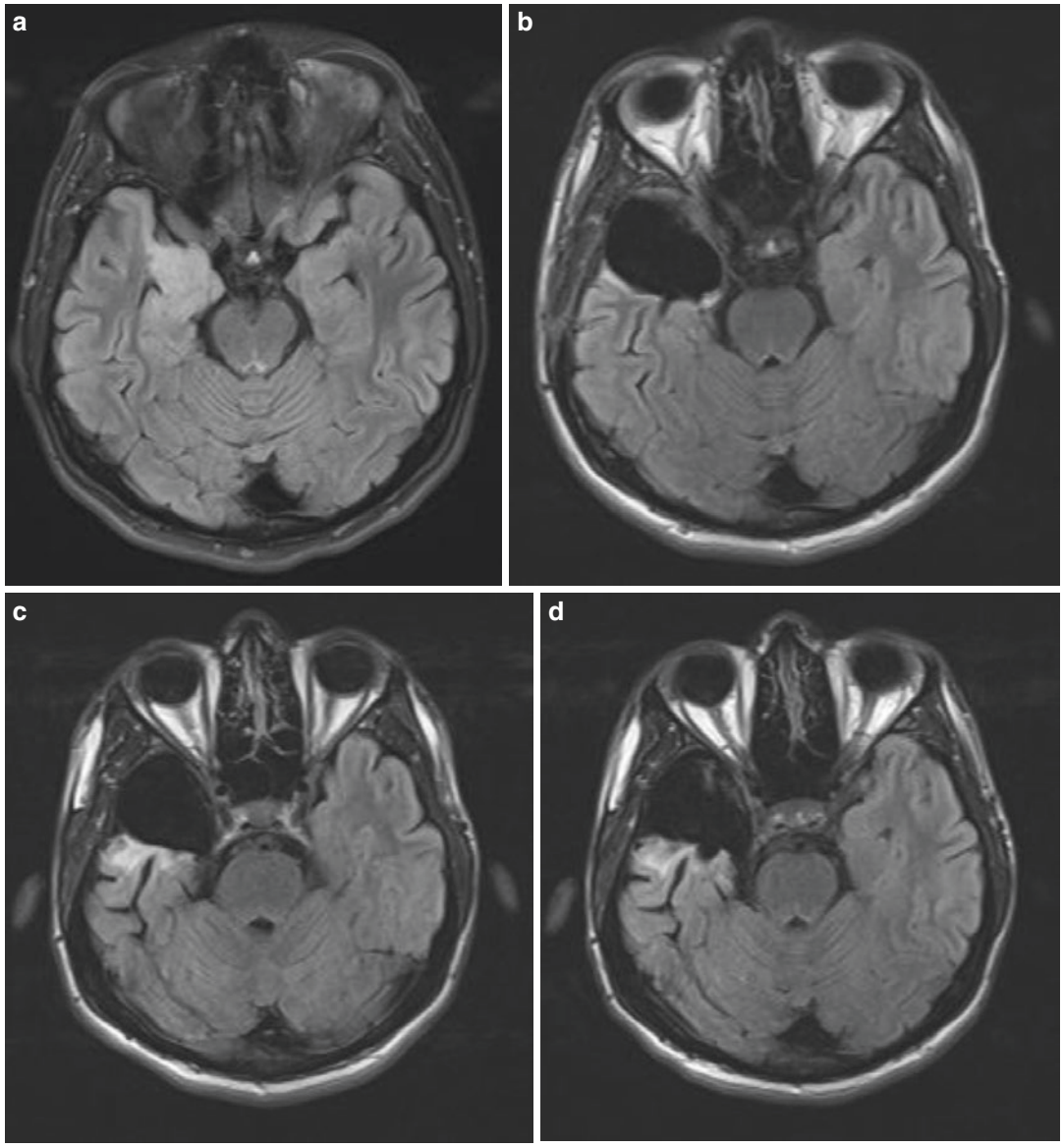

Fig. 2.2 Preoperative and follow-up FLAIR images of a 21-year-old (at time of four year follow-up) male patient with grade II glioma. (**a**) Preoperative, (**b**) 3 months post-op, (**c**) one year post-op, (**d**) four years post-op. Note the changes in FLAIR intensities surrounding the operation cavity, corresponding to gliosis

hypermethylation [17, 22]. Although most patients are asymptomatic, there may be deterioration in neurologic status or an increased need for steroids [22]. It typically resolves spontaneously [21].

Differentiating pseudoprogression from true tumor progression is challenging [24, 26]. Multifocality, the signal abnormality extending across the corpus callosum and subependymal involvement are suggestive of true progression, but there are no definitive conventional MRI findings to rule out true progression reliably [24]. Higher ADC values and lower perfusion parameters have been observed in pseudoprogression compared to true tumor progression [23, 24]; however, the thresholds reported in the literature

should be applied with care [23]. Clinical data can also help with the differential diagnosis: pseudoprogression occurs up to 6 months after treatment, and changes are expected to stabilize or improve in follow-up without any treatment [17, 24].

2.2.5.2 Radiation Necrosis

Another difficulty is radiation necrosis in patients who underwent radiotherapy. Radiation necrosis most commonly occurs 9–12 months after treatment but can be seen years after radiotherapy [17, 22]. Differentiating radiation necrosis from tumor progression is difficult using conventional MRI [17, 27]. Perfusion MRI might be helpful, but there is significant disparity in published results [17].

2.2.5.3 Pseudoresponse

Pseudoresponse or pseudoregression is a decrease in enhancement without a true antitumor effect [17, 22]. It is seen in 20–60% of patients receiving antiangiogenic therapy such as bevacizumab or cediranib and thought to be due to a normalization of abnormally permeable blood vessels which can cause marked decrease in contrast enhancement and peritumoral edema as early as day 1 after treatment [21, 24]. To distinguish this from true antitumor effect, patients under antiangiogenic therapy who demonstrate marked reduction in enhancement need to have another scan at least 4 weeks later to confirm the persistence of changes [18, 28]. Antiangiogenic therapies may select for hypoxic and invasive tumor that first grows as a non-enhancing mass before progressing to enhancing disease [24]. Therefore, careful consideration of T2/FLAIR intense non-enhancing parts of the mass is essential in this subset of patients.

2.3 Evaluating Treatment Response

In patients who underwent treatment, there is an obvious need to report whether the disease is stable, progressing, or regressing in follow-up studies. One way of doing this is simply reporting measurements and/or a subjective assessment by the radiologist. An alternative is creating an objective set of criteria to determine the response to treatment as well as provide a common terminology to be used in radiology reports. This would be beneficial especially for research purposes; however, easy-to-use, consistent, and objective terminology would certainly be useful in daily clinical practice as well. While RECIST criteria are widely used to this end for solid tumors in the body, different sets of rules are used for brain tumors [29].

The first set of such criteria was published by Levin et al. in 1977, followed by WHO oncology response criteria published in 1981 [30, 31]. The more widely used and well-known criteria (commonly referred to as Macdonald criteria) based on CT images, but later extrapolated to MRI, was proposed by Macdonald et al. in 1990. In the paper, the state of the tumor was described as complete response (CR), partial response (PR), stable disease (SD), or progression (progressive disease, PD) (Table 2.1) [32].

However, some limitations of the Macdonald criteria became apparent over time, such as not accounting for pseudoprogression, not evaluating non-enhancing component of the tumor, failing to address pseudoresponse in patients using antiangiogenic treatment, difficulty of measuring irregularly shaped tumors as well as in measuring enhancing lesions located on the walls of cysts or surgical cavities [18, 33]. To address these issues, Response Assessment in Neuro-Oncology (RANO) criteria for high-grade gliomas (RANO-HGG) was proposed in 2010 [18]. These criteria, commonly referred to as the RANO criteria, consider radiologic appearance, corticosteroid use and dose, and clinical status to define CR, PR, SD, or PD (Table 2.1). However, in the following section, only the radiographic criteria will be discussed. Interested readers are referred to the original paper for more information regarding clinical details [18].

Table 2.1 Comparison of various response assessment criteria

	RANO-HGG	RANO-LGG	RANO-BM	iRANO[g]	Macdonald
CR[a,b,d]	– No enhancement[g] – T2/FLAIR Stable to decreased[h] – No new lesions	– No lesion on T2/FLAIR, with complete resolution of enhancement if present before – No new T2/FLAIR abnormalities besides radiation effect – No new/increased enhancement – No new lesion	– No target lesions[j] – No non-target lesions[k] – No new lesions	Same as RANO-HGG, RANO-LGG or RANO-BM based on the type of tumor except for early progression[m]	– No enhancing disease – No new lesion
PR[a,c,d]	– ≥50% decrease in enhancing lesion[g,i] T2/FLAIR Stable to decreased[h] – No new lesions	– ≥50% decrease on T2/FLAIR[i] – No new T2/FLAIR abnormalities besides radiation effect – No new/increased enhancement – No new lesion	– ≥30% decrease in target lesions[j,l] – Stable or improved non-target lesions[k] – No new lesions	Same as RANO-HGG, RANO-LGG or RANO-BM based on the type of tumor except for early progression[m]	– ≥50% decrease in enhancing lesion[i] – No new lesions
SD[a,c,d]	– Enhancing lesion <50% decrease or <25% increase[i] – T2/FLAIR Stable to decreased[h] – No new lesions	– Stable on T2/FLAIR (not qualifying for other categories)[i] – No new T2/FLAIR abnormalities besides radiation effect – No new/increased enhancement – No new lesion	– Between <30% decrease and <20% increase in target lesions[j,l] – Stable or improved non-target lesions[k] – No new lesions	Same as RANO-HGG, RANO-LGG or RANO-BM based on the type of tumor except for early progression[m]	– Enhancing lesion <50% decrease or <25% increase[i] – No new lesions
PD[e,f]	– Enhancing lesion ≥25% increase[i] – Increased T2/FLAIR[h] – New lesion	– ≥25% increase on T2/FLAIR[i] – Increase in enhancement – New lesion	– ≥20% increase in target lesions[j,l] – Unequivocal progression of non-target lesions[k] – New lesion	Same as RANO-HGG, RANO-LGG or RANO-BM based on the type of tumor except for early progression[m]	– Enhancing lesion ≥25% increase[i] – New lesion
Minor Response	N/A	– 25–50% decrease on T2/FLAIR[i] – No new T2/FLAIR abnormalities besides radiation effect – No new/increased enhancement – No new lesion	N/A	If the tumor is LGG, same as RANO-LGG except for early progression[m]	N/A

BM brain metastases, *CR* complete response, *HGG* high-grade glioma, *iRANO* immunotherapy response assessment in neuro-oncology, *LGG* low-grade glioma, *PD* progressive disease, *PR* partial response, *RANO* response assessment in neuro-oncology, *SD* stable disease. Adapted from the relevant references for RANO-HGG, RANO-LGG, iRANO, RANO-BM, and Macdonald criteria [18, 19, 32, 34, 35]

[a]Patient should have all findings to qualify for the category

[b]CR requires the patient to be off corticosteroids or on physiologic replacement dose only

[c]PR and SD require the patient to be at the same or decreased corticosteroid dose compared to baseline scan

[d]CR, PR, and SD require the patient to be stable or improved clinically

Table 2.1 (continued)

[e]Any one of the findings is sufficient to qualify for progression. Neurologic deterioration not attributable to another cause also qualifies for PD by itself. Increase in corticosteroid dose by itself does not constitute PD

[f]To differentiate pseudoprogression from true tumor progression, unless progression is clearly outside the radiation field or there is pathologic confirmation, patients cannot be categorized as having PD within the first 12 weeks after chemoradiotherapy

[g]Findings should persist on a follow-up scan at least 4 weeks later

[h]Significant increase as determined qualitatively

[i]Lesion size measured as longest perpendicular two dimensions on an axial slice and multiplied. If there is more than one lesion, up to five lesions are chosen as described in the RANO-HGG section of the text and products of all lesions are summed to get a single value for comparison

[j]A measurable lesion is a contrast-enhancing lesion that can be accurately measured in at least one dimension, with a minimum size of 10 mm (or twice the slice thickness). The diameter perpendicular to the longest dimension should at least be 5 mm. Up to five largest measurable lesions that can be measured reproducibly can be picked as target lesions. Lesions not treated with local therapies are preferred if present

[k]All measurable lesions besides target lesions and all non-measurable lesions are non-target lesions. They should be recorded at baseline and classified as present, absent or unequivocal progression in follow-up

[l]Only the largest diameter in an axial slice is measured. In cases of multiple target lesions, the diameters are summed to get a single value for comparison in follow-up

[m]If there is radiological progression of lesions within 6 months of starting immunotherapy (including presence of new lesions), follow-up imaging is required 3 months later. If 3-month follow-up scan meet the criteria for CR, PR, or SD then the patient is categorized thus. If the 3-month follow-up scan demonstrates PD, the patient is considered to have PD. If there are new or increasing neurological symptoms not attributable to comorbid events in this time period, the patient is deemed to have PD. If radiological progression occurs more than 6 months after starting immunotherapy, the patient is considered to have PD and 3-month follow-up scan is not required for categorization

2.3.1 Response Assessment in Neuro-Oncology: High-Grade Glioma (RANO-HGG)[1]

RANO-HGG criteria (commonly referred to as only the "RANO criteria") define measurable disease as bidimensionally contrast-enhancing lesion(s) with clearly defined margins on CT or MRI, with two largest perpendicular diameters on an axial slice being at least 10 mm (Fig. 2.3). The lesion should be visible on at least two consecutive axial slices, and the slice thickness must preferably be at most 5 mm with 0 mm gap. If the slice thickness is greater than 5 mm, the size of the lesion should be at least two times the slice thickness to be considered measurable. If the lesion is unidimensionally measurable, lacks clearly defined margins, or smaller than 10 mm (or twice the slice thickness) in at least one dimension, it should be considered nonmeasurable. Special note is made of tumors around a cyst or surgical cavity: such lesions are to be considered nonmeasurable unless they have a clear nodular component that satisfies criteria for being measurable (i.e., at least 10 mm in two perpendicular dimensions).

If there is more than one lesion, two to five of the largest lesions should be measured in two dimensions, the area should be calculated as the product of the two diameters and then the areas of the measured lesions should be added to get a single final value. Comparisons in follow-up should be made using this single value. While typically the largest lesions are selected for measurement, care should be taken to ensure that these lesions allow reproducible measurements. In cases where the largest lesions do not lend themselves to reproducible measurements, the next largest lesion that can be measured reproducibly can be selected instead. The lesions picked for measurement and calculation of the final value for comparison are defined to be the "target lesions."

Non-enhancing components of the tumor are evaluated using T2W or FLAIR images, where they have similar appearance to peritumoral edema and radiation-related changes, making exact delineation of its margins quite difficult.

[1]Adapted from [18].

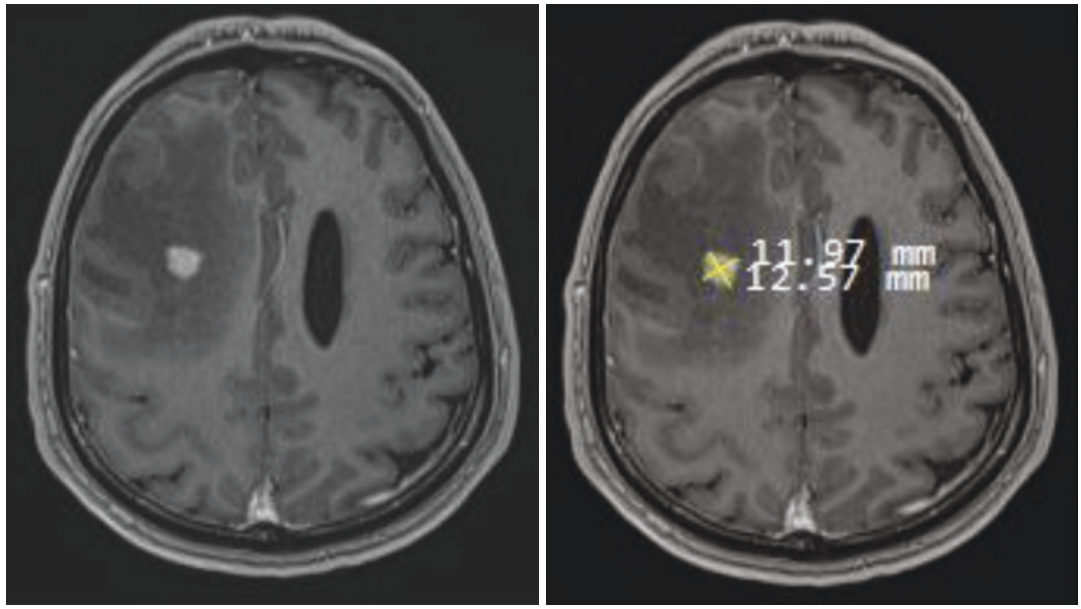

Fig. 2.3 Sample measurement of a high-grade glioma according to RANO criteria. With both dimensions of the enhancing part greater than 10 mm, this constitutes measureable disease

Signs of mass effect such as sulcal effacement or compression of the ventricles; infiltration of the cortical ribbon or simply the location being outside of the radiation field suggest infiltrating tumor. Sometimes, there might still be doubt as to whether the changes represent an increase in non-enhancing tumor. In such cases further follow-up usually confirms or refutes the idea. While objective measures of non-enhancing tumor would obviously be helpful, there are no widely accepted methods for this purpose and RANO criteria do not incorporate any such methods yet.

Response is determined in comparison to the baseline imaging to determine CR or PR, and the smallest tumor measurement (in pre-treatment baseline images or in follow-up images after the initiation of treatment) to determine PD. In cases where the changes are equivocal, close follow-up is indicated. Rules to classify response are provided in Table 2.1.

2.3.2 Other RANO Criteria

Patients receiving immunotherapy and patients with other types of brain tumors should not be evaluated using RANO-HGG criteria. There are different criteria described for brain metastases (RANO-BM), low-grade gliomas (RANO-LGG), and patients undergoing immunotherapy (iRANO) [19, 34, 35]. Major differences of these criteria and how they compare to RANO-HGG are provided in Table 2.1. Response assessment for leptomeningeal metastases (RANO-LM) is handled in a totally different manner and interested readers are referred to the original paper for details on how to score imaging data [36]. Criteria for spine tumors (SPINO), pediatric brain tumors (RAPNO), and meningiomas (RANO-meningioma) are also under development [37–39].

2.4 Imaging Protocol

To standardize neuro-oncologic imaging in clinical trials, Consensus Recommendations for a Standardized Brain Tumor Imaging Protocol (BTIP) have been reported [20]. While this protocol is concerned mostly with standardizing MRI acquisition to facilitate multicenter studies and comparison of different studies, it is also recommended to be used for routine, clinical brain tumor imaging [33]. According to BTIP, MRI

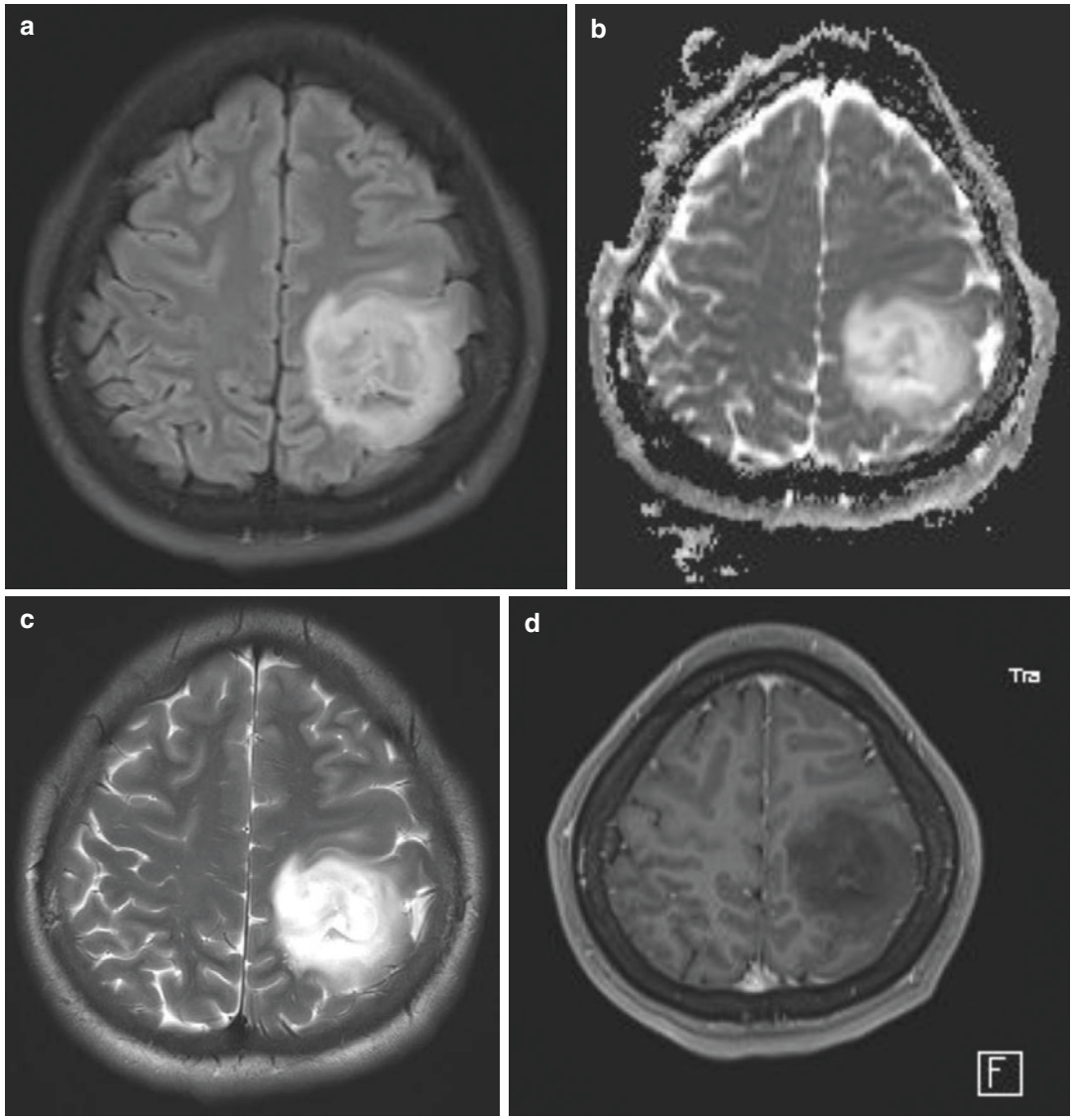

Fig. 2.4 Sample images for brain tumor imaging according to the recommended protocol: (**a**) 2D FLAIR, (**b**) ADC map acquired from DWI using 3 directions and b values 0, 500 and 1000 s/mm^2, (**c**) 2D T2W, (**d**) post-contrast 3D T1W. It should be noted that T1W images were acquired in the sagittal plane but are here demonstrated in the axial plane (using MPR) to be consistent with other images

imaging of brain tumors should include at least the following sequences (Fig. 2.4) [20]:

- Pre-contrast and post-contrast isotropic 3D inversion recovery-prepared T1W gradient-recalled echo (IR-GRE) images with matching parameters
- Axial 2D T2W TSE (dual echo preferred but not required) acquired after contrast injection but before post-contrast T1W images
- Pre-contrast axial 2D TSE T2W FLAIR
- Pre-contrast axial 2D three-directional DWI using echoplanar (EPI) or radial acquisition

The scanner used may be 1.5 T or 3 T [20]. There have been studies reported on 7 T scanners, but whether the use of 7 T scanners would translate into clinical benefit within the context of brain tumors is not clear [40]

Specific acquisition parameters as described by the consensus statements are provided in Table 2.2 [20]

Table 2.2 Consensus recommendations for a standardized brain tumor imaging protocol; recommended protocols for 3 T and 1.5 T scanners

	Pre-contrast T1W[a]		FLAIR[e]		DWI[h]		IV Contrast injection[j]	T2W[k]		Post-contrast T1W[a,l]	
Sequence	IR-GRE[b]		TSE[f]		EPI[i]			TSE[f]		IR-GRE[b]	
Plane of acquisition	Sagittal/axial[c]		Axial		Axial			Axial		Sagittal/axial[c]	
3D/2D	3D		2D		2D			2D		3D	
Field strength	3 T	1.5 T	3 T	1.5 T	3 T	1.5 T		3 T	1.5 T	3 T	1.5 T
TR (ms)	2100[d]	2100[d]	>6000	>6000	>5000	>5000		>2500	>3500	2100[d]	2100[d]
TE (ms)	Min	Min	100–140	100–140	Min	Min		80–120	100–120	Min	Min
TI (ms)	1100[d]	1100[d]	2500	2200	–	–		–	–	1100[d]	1100[d]
Flip angle	10–15°	10–15°	90°/≥160°	90°/≥160°	90°/180°	90°/180°		90°/≥160°	90° ≥ 160°	10–15°	10–15°
Frequency	256	≥172	≥256	≥256	128	128		≥256	≥256	256	≥172
Phase	256	≥172	≥256	≥256	128	128		≥256	≥256	256	≥172
NEX	≥1	≥1	≥1	≥1[g]	≥1	≥1[g]		≥1	≥1[g]	≥1	≥1
FOV (mm)	256	256	240	240	240	240		240	240	256	256
Slice thickness (mm)	1	≤1.5	3	≤4[g]	3	≤4[g]		3	≤4[g]	1	≤1.5
Gap/spacing	0	0	0	0	0	0		0	0	0	0
Parallel imaging	Up to 2×	No	Up to 2×	Up to 2×	Up to 2×	Up to 2×		Up to 2×	Up to 2×	Up to 2×	No

Adapted from [20]

DWI diffusion-weighted imaging, *EPI* echo planar imaging, *FLAIR* fluid attenuated inversion recovery, *FOV* field of view, *FSE* fast spin echo, *GRAPPA* generalized autocalibrating partial parallel acquisition, *IR-GRE* inversion recovery gradient-recalled echo, *NEX* number of excitations, *PD* proton density, *SNR* signal-to-noise ratio, *TE* echo time, *TI* inversion time, *TR* repetition time, *TSE* turbo spin echo

[a]Post-contrast T1W images should have identical parameters to pre-contrast T1W images

[b]3D acquisitions without inversion preparation should be avoided

[c]Sagittal preferred due to fewer required slices and thus shorter scan times

[d]The values provided are for Siemens and Hitachi scanners. GE, Philips and Toshiba scanners should use *TR* = 5–15 ms and *TI* = 400–450 ms

[e]3D FLAIR images are strongly endorsed, due to the possibility of multiplanar reconstruction, volumetry and less sensitivity to flow artifacts; but are considered optional due to not being universally available. The following parameters are recommended for 3D FLAIR: *TE* = 90–140 ms, *TR* = 6000–10,000 ms, *TI* = 2000–2500 ms (chosen based on vendor recommendations), GRAPPA ≤2, fat saturation, slice thickness ≤1.5 mm, FOV ≤250 mm × 250 mm, matrix ≥244 × 244, sagittal or axial acquisition

[f]TSE is equivalent to FSE in GE, Hitachi, and Toshiba scanners

[g]To get comparable SNR, older 1.5 T scanners can use images with 5 mm slice thickness with no interslice gap or increase NEX for slice thickness ≤4 mm

[h]DWI images should be acquired in at least 3 directions with $b = 0$, 500 and 1000 s/mm^2. If the scanner is an older scanner incapable of at least three b values, $b = 0$, 1000 s/mm^2 should be used

[i]If there is significant patient motion, radial acquisition schemes may be used. However, this should be a last option

[j]0.1 mmol/kg (up to 20 cc) gadolinium-chelated contrast injection at a rate of 3–5 cc/s, preferably using a power injector, as a single, full dose

[k]Dual echo PD/T2 TSE is optional. If used, the PD echo should have a TE <25 ms

[l]Advanced sequences can be substituted before the post-contrast T1W images as long as post-contrast 3D T1W sequences are acquired between 4–8 min following contrast administration

Other sequences such as high-resolution isovolumetric 3D T2W images and advanced imaging techniques can be included in the study based on clinical indications and whether they are needed for differential diagnosis or surgical planning, but are not included in the minimum required study. The protocol also allows for other additional post-contrast T1W imaging, such as 2D fat-saturated T1W TSE images. However, such images should be acquired after the recommended 3D T1W images to ensure consistency of the timing of the contrast injection and 3D T1W image acquisition.

Perfusion-weighted imaging has not yet made its way into standardized imaging protocols or treatment response criteria. Nonetheless, perfusion studies are very helpful during follow-up, to differentiate recurrence from treatment-related changes such as radiation necrosis or pseudo-progression. In the proper clinical setting, these images are invaluable as problem solvers and in our opinion should be included in every follow-up study where it is technically possible to do so. With dynamic susceptibility contrast (DSC) studies, tumor recurrence is expected to have a higher relative cerebral blood volume (rCBV) than radiation necrosis or pseudoprogression; however, there is considerable overlap and the findings can be dependent on the technique used [17]. Therefore, clinical findings and, more importantly, correlation with conventional MRI images are essential for an accurate diagnosis. A more detailed explanation of perfusion imaging is provided in another chapter of this book.

2.4.1 Contrast Use

0.1 mmol/kg gadolinium-chelated contrast agent should be injected at an injection rate of 3–5 cc/s with a power injector if possible [20]. The same contrast agent must be used for follow-up; in cases where this is not possible, at least contrast agents with the same chemical composition should be used [20]. Images should be acquired 4–8 min after contrast injection [20].

Regarding adverse reactions, complications and contraindications of gadolinium-based contrast agents, and their use in special patient groups such as children, those with renal failure, or pregnant women, relevant national or international guidelines such as ACR Manual on Contrast Media (https://www.acr.org/Clinical-Resources/Contrast-Manual) [41] or ESUR Guidelines on Contrast Agents (http://www.esur-cm.org/index.php/en/) [42] should be followed.

2.5 Conclusion

MRI is the preferred imaging method to diagnose and follow-up brain tumors. Consensus statements regarding imaging protocols recommend, at a minimum, 3D isotropic T1W parameter matched pre- and post-contrast images, 2D T2W and 2D FLAIR images, DWI using 3 b values (b = 0, 500, and 1000 s/mm^2) in at least three directions. Other advanced imaging methods are also useful and may be included in the routine protocol or on a case-by-case basis as needed.

MRI is essential for surgical planning, where advanced imaging modalities such as DTI and fMRI can be very useful. Intraoperative MRI can improve tumor resection, and thus prognosis. Postoperative imaging is necessary to ensure tumor resection and to provide baseline images for follow-up.

Follow-up is mainly concerned with the size of enhancing lesion as well as non-enhancing mass as demonstrated by T2W/FLAIR images. Based on the treatments used and the timeframe, pseudoresponse, pseudoprogression, and radiation necrosis should be taken into consideration where appropriate. DWI and perfusion images are very useful as problem solvers and to increase confidence in diagnosis of recurrence or treatment-related changes. Depending on whether the tumor is primary or metastatic, its histopathological type and grade, and the use of immunotherapy, different criteria to evaluate treatment response have been proposed and their use provide objective methods to assess response as well as a common terminology to use in reporting.

References

1. Langen KJ, Galldiks N, Hattingen E, Shah NJ. Advances in neuro-oncology imaging. Nat Rev Neurol. 2017;13(5):279–89. https://doi.org/10.1038/nrneurol.2017.44.
2. Weller M, van den Bent M, Tonn JC, Stupp R, Preusser M, Cohen-Jonathan-Moyal E, Henriksson R, Le Rhun E, Balana C, Chinot O, Bendszus M, Reijneveld JC, Dhermain F, French P, Marosi C, Watts C, Oberg I, Pilkington G, Baumert BG, Taphoorn MJB, Hegi M, Westphal M, Reifenberger G, Soffietti R, Wick W, European Association for Neuro-Oncology (EANO) Task Force on Gliomas. European Association for Neuro-Oncology (EANO) guideline on the diagnosis and treatment of adult astrocytic and oligodendroglial gliomas. Lancet Oncol. 2017;18(6):e315–29. https://doi.org/10.1016/S1470-2045(17)30194-8.
3. American College of Radiology. ACR appropriateness criteria: headache. 2019. Available at: https://acsearch.acr.org/docs/69482/Narrative/. Accessed 23 Apr 2019.
4. American College of Radiology. ACR appropriateness criteria: seizures and epilepsy. 2019. Available at: https://acsearch.acr.org/docs/69479/Narrative/. Accessed 23 Apr 2019.
5. Southwell DG, Birk HS, Han SJ, Li J, Sall JW, Berger MS. Resection of gliomas deemed inoperable by neurosurgeons based on preoperative imaging studies. J Neurosurg. 2018;129:567–75. https://doi.org/10.3171/2017.5.JNS17166.
6. McCullough BJ, Ader V, Aguedan B, Feng X, Susanto D, Benkers TL, Henson JW, Mayberg M, Cobbs CS, Gwinn RP, Monteith SJ, Newell DW, Delashaw J Jr, Fouke SJ, Rostad S, Keogh BP. Preoperative relative cerebral blood volume analysis in gliomas predicts survival and mitigates risk of biopsy sampling error. J Neurooncol. 2018;136(1):181–8. https://doi.org/10.1007/s11060-017-2642-2.
7. Ragel BT, Ryken TC, Kalkanis SN, Ziu M, Cahill D, Olson JJ. The role of biopsy in the management of patients with presumed diffuse low grade glioma: a systematic review and evidence-based clinical practice guideline. J Neurooncol. 2015;125(3):481–501. https://doi.org/10.1007/s11060-015-1866-2.
8. Mohammadzadeh A, Mohammadzadeh V, Kooraki S, Sotoudeh H, Kadivar S, Shakiba M, Rasuli B, Borhani A, Mohammadzadeh M. Pretreatment evaluation of glioma. Neuroimaging Clin N Am. 2016;26(4):567–80. https://doi.org/10.1016/j.nic.2016.06.006.
9. Silva MA, See AP, Essayed WI, Golby AJ, Tie Y. Challenges and techniques for presurgical brain mapping with functional MRI. Neuroimage Clin. 2017;17:794–803. https://doi.org/10.1016/j.nicl.2017.12.008.
10. Pope WB, Brandal G. Conventional and advanced magnetic resonance imaging in patients with high grade glioma. Q J Nucl Med Mol Imaging. 2018;62:239–53. https://doi.org/10.23736/S1824-4785.18.03086-8.
11. Yan JL, van der Hoorn A, Larkin TJ, Boonzaier NR, Matys T, Price SJ. Extent of resection of peritumoral diffusion tensor imaging-detected abnormality as a predictor of survival in adult glioblastoma patients. J Neurosurg. 2017;126(1):234–41. https://doi.org/10.3171/2016.1.JNS152153.
12. Mert A, Kiesel B, Wöhrer A, Martínez-Moreno M, Minchev G, Furtner J, Knosp E, Wolfsberger S, Widhalm G. Introduction of a standardized multimodality image protocol for navigation-guided surgery of suspected low-grade gliomas. Neurosurg Focus. 2015;38(1):E4. https://doi.org/10.3171/2014.10.FOCUS14597.
13. Rao G. Intraoperative MRI and maximizing extent of resection. Neurosurg Clin N Am. 2017;28(4):477–85. https://doi.org/10.1016/j.nec.2017.05.003.
14. Jenkinson MD, Barone DG, Bryant A, Vale L, Bulbeck H, Lawri TA, Hart MG, Watts C. Intraoperative imaging technology to maximise extent of resection for glioma. Cochrane Database Syst Rev. 2018;1:CD012788. https://doi.org/10.1002/14651858.CD012788.pub2.
15. Senft C, Bink A, Franz K, Vatter H, Gasser T, Seifert V. Intraoperative MRI guidance and extent of resection in glioma surgery: a randomised, controlled trial. Lancet Oncol. 2011;12(11):997–1003. https://doi.org/10.1016/S1470-2045(11)70196-6.
16. Wu JS, Gong X, Song YY, Zhuang DX, Yao CJ, Qiu TM, Lu JF, Zhang J, Zhu W, Mao Y, Zhou LF. 3.0-T intraoperative magnetic resonance imaging-guided resection in cerebral glioma surgery: interim analysis of a prospective, randomized, triple-blind, parallel-controlled trial. Neurosurgery. 2014;61(Suppl 1):145–54. https://doi.org/10.1227/NEU.0000000000000372.
17. Dalesandro MF, Andre JB. Posttreatment evaluation of brain gliomas. Neuroimaging Clin N Am. 2016;26(4):581–99. https://doi.org/10.1016/j.nic.2016.06.007.
18. Wen PY, Macdonald DR, Reardon DA, Cloughesy TF, Sorensen AG, Galanis E, Degroot J, Wick W, Gilbert MR, Lassman AB, Tsien C, Mikkelsen T, Wong ET, Chamberlain MC, Stupp R, Lamborn KR, Vogelbaum MA, van den Bent MJ, Chang SM. Updated response assessment criteria for high-grade gliomas: response assessment in neuro-oncology working group. J Clin Oncol. 2010;28(11):1963–72. https://doi.org/10.1200/JCO.2009.26.3541.
19. van den Bent MJ, Wefel JS, Schiff D, Taphoorn MJ, Jaeckle K, Junck L, Armstrong T, Choucair A, Waldman AD, Gorlia T, Chamberlain M, Baumert BG, Vogelbaum MA, Macdonald DR, Reardon DA, Wen PY, Chang SM, Jacobs AH. Response assessment in neuro-oncology (a report of the RANO group): assessment of outcome in trials of diffuse low-grade gliomas. Lancet Oncol. 2011;12(6):583–93. https://doi.org/10.1016/S1470-2045(11)70057-2.
20. Ellingson BM, Bendszus M, Boxerman J, Barboriak D, Erickson BJ, Smits M, Nelson SJ, Gerstner E, Alexander B, Goldmacher G, Wick W, Vogelbaum M, Weller M, Galanis E, Kalpathy-Cramer J, Shankar L, Jacobs P, Pope WB, Yang D, Chung C, Knopp

MV, Cha S, van den Bent MJ, Chang S, Yung WK, Cloughesy TF, Wen PY, Gilbert MR, Jumpstarting Brain Tumor Drug Development Coalition Imaging Standardization Steering Committee. Consensus recommendations for a standardized brain tumor imaging protocol in clinical trials. Neuro-Oncology. 2015;17(9):1188–98. https://doi.org/10.1093/neuonc/nov095.

21. Nowosielski M, Wen PY. Imaging criteria in neuro-oncology. Semin Neurol. 2018;38(1):24–31. https://doi.org/10.1055/s-0038-1627468.
22. Shiroishi MS, Booker MT, Agarwal M, Jain N, Naghi I, Lerner A, Law M. Posttreatment evaluation of central nervous system gliomas. Magn Reson Imaging Clin N Am. 2013;21(2):241–68. https://doi.org/10.1016/j.mric.2013.02.004.
23. Thust SC, van den Bent MJ, Smits M. Pseudoprogression of brain tumors. J Magn Reson Imaging. 2018;48:571–89. https://doi.org/10.1002/jmri.26171.
24. Villanueva-Meyer JE, Mabray MC, Cha S. Current clinical brain tumor imaging. Neurosurgery. 2017;81(3):397–415. https://doi.org/10.1093/neuros/nyx103.
25. Ellingson BM, Chung C, Pope WB, Boxerman JL, Kaufmann TJ. Pseudoprogression, radionecrosis, inflammation or true tumor progression? Challenges associated with glioblastoma response assessment in an evolving therapeutic landscape. J Neurooncol. 2017;134(3):495–504. https://doi.org/10.1007/s11060-017-2375-2.
26. Yun TJ, Park CK, Kim TM, Lee SH, Kim JH, Sohn CH, Park SH, Kim IH, Choi SH. Glioblastoma treated with concurrent radiation therapy and temozolomide chemotherapy: differentiation of true progression from pseudoprogression with quantitative dynamic contrast-enhanced MR imaging. Radiology. 2015;274(3):830–40. https://doi.org/10.1148/radiol.14132632.
27. Delgado-López PD, Riñones-Mena E, Corrales-García EM. Treatment-related changes in glioblastoma: a review on the controversies in response assessment criteria and the concepts of true progression, pseudoprogression, pseudoresponse and radionecrosis. Clin Transl Oncol. 2018;20:939–53. https://doi.org/10.1007/s12094-017-1816-x.
28. Wen PY, Chang SM, Van den Bent MJ, Vogelbaum MA, Macdonald DR, Lee EQ. Response assessment in neuro-oncology clinical trials. J Clin Oncol. 2017;35(21):2439–49. https://doi.org/10.1200/JCO.2017.72.7511.
29. Eisenhauer EA, Therasse P, Bogaerts J, Schwartz LH, Sargent D, Ford R, Dancey J, Arbuck S, Gwyther S, Mooney M, Rubinstein L, Shankar L, Dodd L, Kaplan R, Lacombe D, Verweij J. New response evaluation criteria in solid tumours: revised RECIST guideline (version 1.1). Eur J Cancer. 2009;45(2):228–47. https://doi.org/10.1016/j.ejca.2008.10.026.
30. Levin VA, Crafts DC, Norman DM, Hoffer PB, Spire JP, Wilson CB. Criteria for evaluating patients undergoing chemotherapy for malignant brain tumors. J Neurosurg. 1977;47(3):329–35.
31. Miller AB, Hoogstraten B, Staquet M, Winkler A. Reporting results of cancer treatment. Cancer. 1981;47(1):207–14.
32. Macdonald DR, Cascino TL, Schold SC Jr, Cairncross JG. Response criteria for phase II studies of supratentorial malignant glioma. J Clin Oncol. 1990;8(7):1277–80.
33. Huang RY, Wen PY. Response assessment in neuro-oncology criteria and clinical endpoints. Magn Reson Imaging Clin N Am. 2016;24(4):705–18. https://doi.org/10.1016/j.mric.2016.06.003.
34. Lin NU, Lee EQ, Aoyama H, Barani IJ, Barboriak DP, Baumert BG, Bendszus M, Brown PD, Camidge DR, Chang SM, Dancey J, de Vries EG, Gaspar LE, Harris GJ, Hodi FS, Kalkanis SN, Linskey ME, Macdonald DR, Margolin K, Mehta MP, Schiff D, Soffietti R, Suh JH, van den Bent MJ, Vogelbaum MA, Wen PY, Response Assessment in Neuro-Oncology (RANO) Group. Response assessment criteria for brain metastases: proposal from the RANO group. Lancet Oncol. 2015;16(6):e270–8. https://doi.org/10.1016/S1470-2045(15)70057-4.
35. Okada H, Weller M, Huang R, Finocchiaro G, Gilbert MR, Wick W, Ellingson BM, Hashimoto N, Pollack IF, Brandes AA, Franceschi E, Herold-Mende C, Nayak L, Panigrahy A, Pope WB, Prins R, Sampson JH, Wen PY, Reardon DA. Immunotherapy response assessment in neuro-oncology: a report of the RANO working group. Lancet Oncol. 2015;16(15):e534–42. https://doi.org/10.1016/S1470-2045(15)00088-1.
36. Chamberlain M, Junck L, Brandsma D, Soffietti R, Rudà R, Raizer J, Boogerd W, Taillibert S, Groves MD, Le Rhun E, Walker J, van den Bent M, Wen PY, Jaeckle KA. Leptomeningeal metastases: a RANO proposal for response criteria. Neuro-Oncology. 2017;19(4):484–92. https://doi.org/10.1093/neuonc/now183.
37. Rogers L, Barani I, Chamberlain M, Kaley TJ, McDermott M, Raizer J, Schiff D, Weber DC, Wen PY, Vogelbaum MA. Meningiomas: knowledge base, treatment outcomes, and uncertainties. A RANO review. J Neurosurg. 2015;122(1):4–23. https://doi.org/10.3171/2014.7.JNS131644.
38. Thibault I, Chang EL, Sheehan J, Ahluwalia MS, Guckenberger M, Sohn MJ, Ryu S, Foote M, Lo SS, Muacevic A, Soltys SG, Chao S, Gerszten P, Lis E, Yu E, Bilsky M, Fisher C, Schiff D, Fehlings MG, Ma L, Chang S, Chow E, Parelukar WR, Vogelbaum MA, Sahgal A. Response assessment after stereotactic body radiotherapy for spinal metastasis: a report from the SPIne response assessment in Neuro-Oncology (SPINO) group. Lancet Oncol. 2015;16(16):e595–603. https://doi.org/10.1016/S1470-2045(15)00166-7.
39. Warren KE, Poussaint TY, Vezina G, Hargrave D, Packer RJ, Goldman S, Wen PY, Pollack IF, Zurakowski D, Kun LE, Prados MD, Rutkowski

S, Kieran MW. Challenges with defining response to antitumor agents in pediatric neuro-oncology: a report from the response assessment in pediatric neuro-oncology (RAPNO) working group. Pediatr Blood Cancer. 2013;60(9):1397–401. https://doi.org/10.1002/pbc.24562.

40. Barrett TF, Sarkiss CA, Dyvorne HA, Lee J, Balchandani P, Shrivastava RK. Application of ultrahigh field magnetic resonance imaging in the treatment of brain tumors: a meta-analysis. World Neurosurg. 2016;86:450–65. https://doi.org/10.1016/j.wneu.2015.09.048.
41. ACR Committee on Drugs and Contrast Media. ACR manual on contrast media version 10.3. Published Jun 2017. https://www.acr.org/Clinical-Resources/Contrast-Manual. Accessed 25 Jun 2018.
42. The Contrast Media Safety Committee of the European Society of Urogenital Radiology (ESUR). ESUR Guidelines on Contrast Agents, version 10.0. Published Mar 2018. Available at: http://www.esur-cm.org/index.php/en/. Accessed 25 Jun 2018.

3 Pearls in Conventional Imaging Methods for Brain Tumors

Robert Y. Shih and James G. Smirniotopoulos

3.1 Pearl #1: As You Work to Practice and Improve Your Diagnostic and Interpretative Skills (the "What"), Seek Also to Learn About the Underlying Physics (the "How") and History of Our Specialty (the "Why")

If a colleague asked us what are the best sequences to perform in conventional MRI for brain tumors, we might answer that there is no one single perfect protocol and inquire what are they currently offering at their institution. We could direct them to published consensus recommendations [1] developed by a working group on imaging endpoints in clinical trials: (1) pre-contrast 3D T1 IR-GRE (e.g., MPRAGE), (2) pre-contrast axial 2D T2 FLAIR, (3) pre-contrast axial 2D DWI, (4) post-contrast axial 2D T2, and (5) post-contrast 3D T1 IR-GRE. While one valid option is to simply copy the recommended sequences and parameters (the "what") as a starting point, we would also suggest reading the entire document, because it provides the scientific and practical justifications (the "why") behind the recommendations, which are equally valuable. As radiologists and medical imaging experts, it is our duty to understand the decision process on 3D versus 2D, IR-GRE versus TSE, post-contrast sequence timing, etc.

One way to develop a healthy curiosity for the complex physics and technology underlying our specialty is through the lens of history [2]. Our modern day "conventional" imaging methods CT and MRI were born not so long ago (younger than many radiologists!) and were enabled by preceding advances in computer science and quantum physics. While it may not immediately elevate your ability to read a CT or MRI, it is both a worthy and a humbling exercise to learn about the historical steps and missteps that led us to where we are today, even if we no longer have to diagnose brain tumors by injecting air throughout the subarachnoid space or by detecting displacement of pineal calcifications or vessels on cerebral angiography. Before we move on to our next "pearl," here are two brief case studies (Figs. 3.1 and 3.2) in cancer patients that illustrate how a basic understanding of the underlying physics and technology can help us to solve problems in the reading room for our patients and our technologists.

R. Y. Shih (✉)
American Institute for Radiologic Pathology,
Silver Spring, MD, USA

J. G. Smirniotopoulos
George Washington University,
Washington, DC, USA

Y. Özsunar, U. Şenol (eds.), *Atlas of Clinical Cases on Brain Tumor Imaging*,
https://doi.org/10.1007/978-3-030-23273-3_3

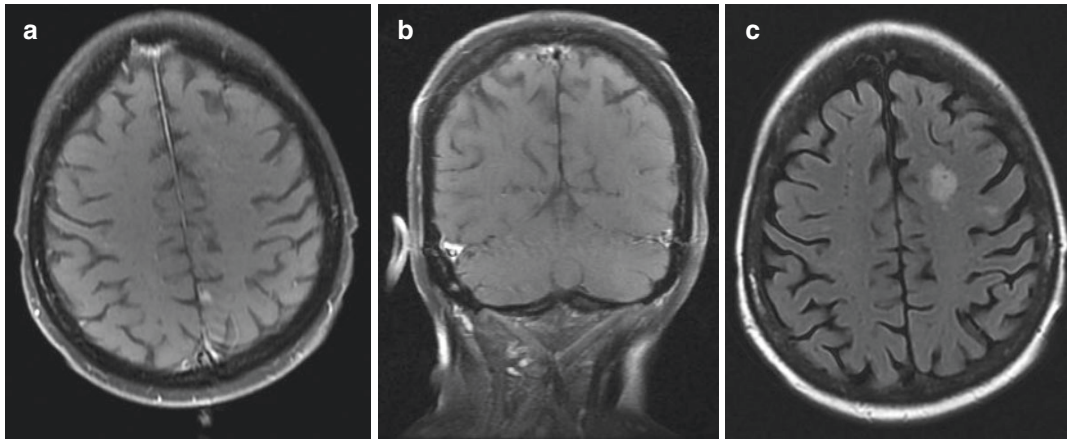

Fig. 3.1 70-year-old woman with extensive stage small cell lung cancer (SCLC) for metastatic workup. (**a**, **b**) Post-contrast T1 FS (fat saturated) images reveal a tiny enhancing focus in the medial left parietal cortex on the axial image that is not seen on the coronal image. The trainee was initially unsure whether to call a metastatic lesion, until the staff explained how the motion or pulsation of the superior sagittal sinus was producing artifactual hyperintensities, both intracranial and extracranial, in the phase encoding direction, which is also known as "ghosting." (**c**) The trainee had noted a lack of corroborating signal abnormality on the axial T2 FLAIR image; however, a true small cortical metastasis may not necessarily produce significant edema. There is incidental and non-enhancing small vessel disease in the left frontal white matter

3.2 Pearl #2: The Process of Image Interpretation to Generate Differential Diagnoses Is Largely an Exercise in Pattern Recognition, Which in the Case of Brain Tumors, Begins with Accurate Anatomic Localization

As diagnostic radiologists, we cannot make a diagnosis that we do not know exists. With regard to CNS tumors, a very useful reference is the most recent 2016 update to the World Health Organization classification [3], which lists all officially recognized entities from a neuropathological perspective within a two-page table. In addition to knowing what is possible, we need to know what is probable (the relative frequencies or likelihood of occurrence) in order to be successful radiologists; remember that post-test probabilities depend not only on test characteristics (sensitivity/specificity) and results, but also on pre-test probabilities. While a sense of what is likely and unlikely can certainly be developed through actual practice or exposure in the reading room, another useful reference are statistical reports [4] published by the Central Brain Tumor Registry of the United States (www.cbtrus.org), e.g., glioblastoma, meningioma, and pituitary adenoma together account for two-thirds of primary CNS tumors.

Once presented with images from a brain tumor patient, it comes time to select from the list of what is possible and probable in order to generate a reasonable and ordered differential diagnosis. This is largely an exercise in pattern recognition (Figs. 3.3 and 3.4), for which there is an innumerable supply of excellent educational texts [5] and articles to choose from. Also, there is usually an innumerable set of clinical and radiological data to mentally integrate, from the patient's age or gender or past medical history,

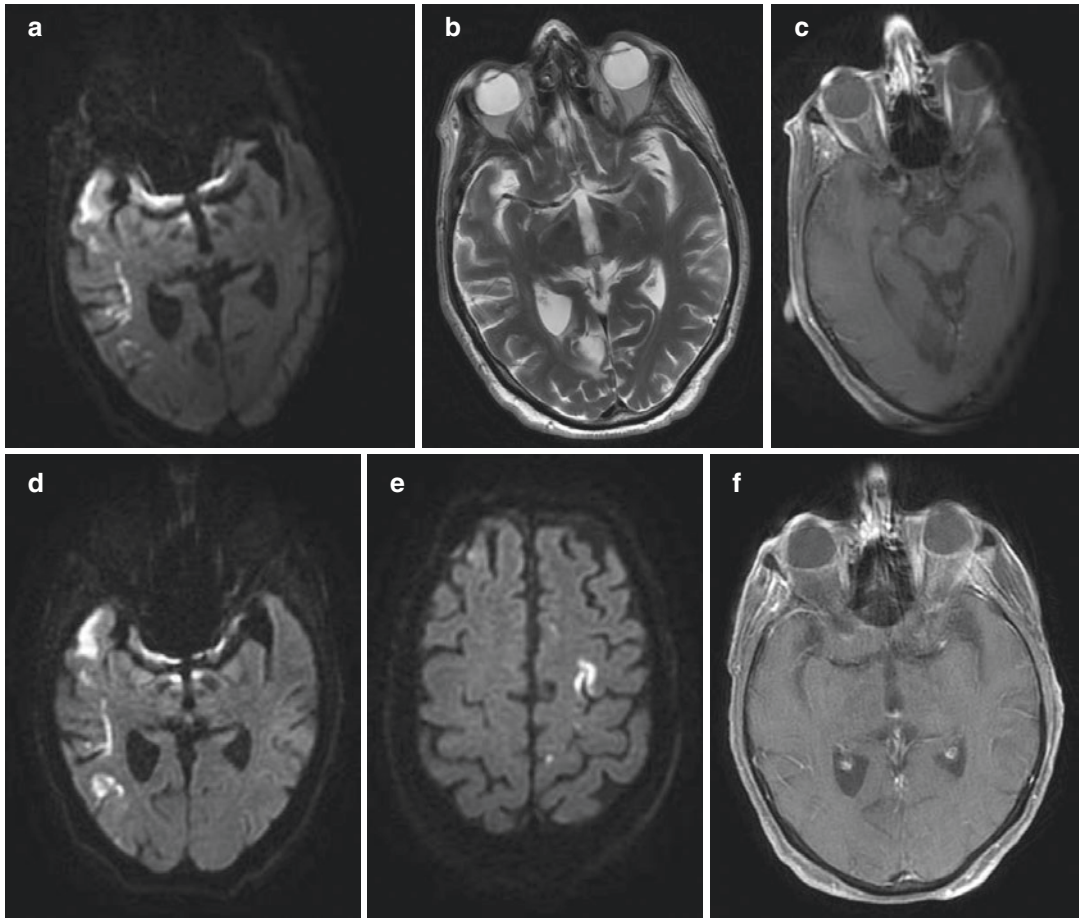

Fig. 3.2 74-year-old man with altered mental status and history of metastatic melanoma (not to CNS). (**a**–**c**) Axial DWI, axial T2 PROPELLER, and axial post-contrast T1 FS images show a bizarre banding with signal loss along the left cerebral convexity that affected multiple sequences. The technologist had attributed the artifact to patient motion (PROPELLER sequence was relatively spared) and unsuccessfully repeated multiple sequences, before calling the radiologist for help. The radiologist suggested repeating just one sequence with phase encoding direction flipped from left–right to anterior–posterior, which did not flip the artifact and therefore excluded patient motion. (**d**–**f**) Axial DWI and post-contrast T1 FS images after changing from the 32-channel head coil to a different head/neck/spine (HNS) coil resolved the artifact and successfully revealed small bilateral non-enhancing strokes—not metastases

to the tumor's CT features or MRI features and also the temporal evolution of the condition. Out of all of these factors, the most critical is accurate anatomic localization, i.e., where is the tumor centered and where is it likely arising from—the Real Estate mantra of "Location, Location, Location." For example, failure to identify or describe a meningioma as an extra-axial dural-based mass will make it difficult to recognize; conversely, successful localization of an extra-axial dural-based mass will lead to a differential diagnosis of meningothelial (most common/likely), mesenchymal, and dural metastatic tumors.

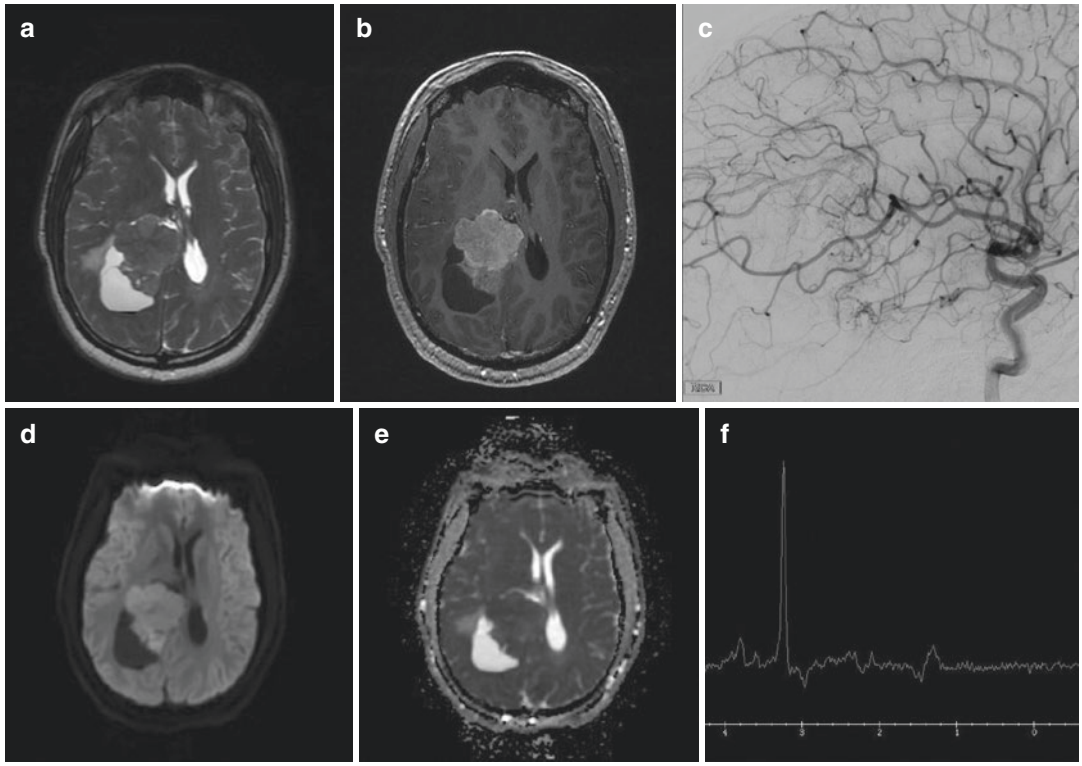

Fig. 3.3 Successful exercise in pattern recognition for a 34-year-old man with right lateral ventricular tumor. (**a**, **b**) Axial T2 and post-contrast 3D T1 GRE images reveal a large enhancing mass centered in the right ventricular atrium or trigone. A posterior cystic component may be related to ventricular trapping (obstruction of CSF flow from the temporal horn). Correct localization of this mass as centered on and arising from the choroid plexus—rather than from the ventricular wall or brain parenchyma—led to a differential diagnosis of choroid plexus tumor, meningioma, and metastasis. (**c**) Preoperative angiography identified slow filling from the choroidal arteries, but no good embolization targets. (**d**–**f**) Axial DWI/ADC and spectroscopy (*TE* = 144 ms) show low diffusivity and high choline suggestive of a highly cellular tumor, which matches the low T2 signal on conventional imaging. Excisional biopsy confirmed a diagnosis of anaplastic meningioma (WHO grade 3)

3.3 Pearl #3: Don't Mistake Edema for Tumor—Or Tumor for Edema—On CT or T2-Weighted Images and Be Wary of Interpreting Vasogenic Edema ("Leaky BBB") Without Pathologic Enhancement ("Intact BBB")

Many pathological processes are associated with increased water content and therefore present as hypoattenuating lesions on CT or T2 hyperintense lesions on MRI. Chronic gliosis or encephalomalacia will generally demonstrate volume loss, whereas both edema and tumor will demonstrate "mass effect" or volume gain. It is not always easy to determine whether an expansile T2 signal abnormality is edema versus tumor (Figs. 3.5 and 3.6), and there are certainly situations where they coexist, e.g., the non-enhancing "infiltrative edema" around an enhancing glioblastoma lesion. When making a diagnosis of edema, check whether the imaging features support the proposed pathophysiology (Table 3.1), e.g., vasogenic edema from a leaky blood-brain barrier should be accompanied by a contrast-enhancing lesion. When making a diagnosis of neoplasm, check whether the imaging features could be explained by ischemic or inflammatory edema, e.g., subacute cerebral or cerebellar stroke masquerading as an expansile mass.

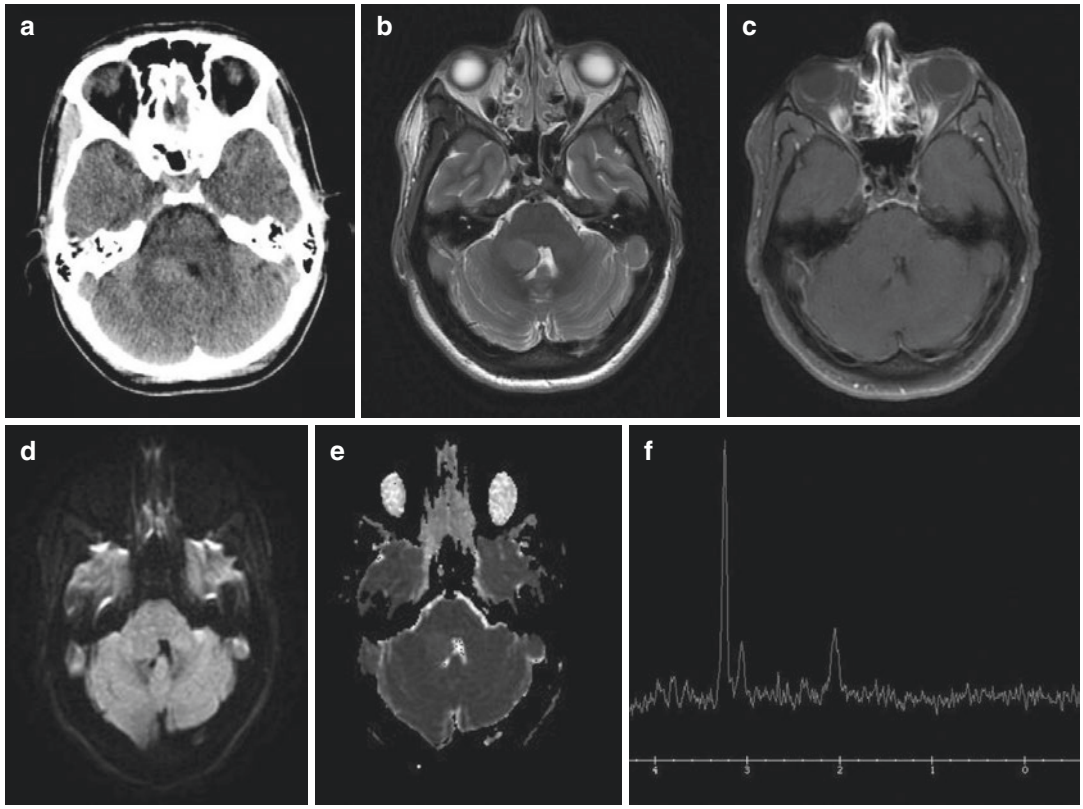

Fig. 3.4 Unsuccessful exercise in pattern recognition for a 35-year-old woman with incidental finding of right middle cerebellar peduncle tumor. (**a**) Head CT after fall on stairs showed a round high attenuation lesion mildly effacing the right side of the fourth ventricle. (**b**, **c**) Subsequent axial T2 and post-contrast T1 FS images revealed low T2 signal (like gray matter) and no enhancement. (**d**–**f**) Axial DWI/ADC and spectroscopy (*TE* = 144 ms) depict low diffusivity and high choline suggestive of a highly cellular tumor. This pattern—a possible hypercellular tumor in the posterior fossa of a young patient—led to an erroneous suspicion for medulloblastoma. Excisional biopsy confirmed a diagnosis of pilocytic astrocytoma (WHO grade 1). This case study illustrates how pattern recognition is not an infallible process and is especially prone to error with rare brain tumors or variant clinical presentations (e.g., adult pilocytic astrocytoma). Pilocytic tumors usually show a fluid component and are usually low attenuation with increased ADC. Adult pilocytic astrocytomas are often atypical on imaging and do not enjoy the same benign prognosis as childhood forms

3.4 Pearl #4: Remember Not to Overestimate the Significance of Post-contrast Images, Which Inform Us About Blood-Brain Barrier Integrity, But Are Often Less Dispositive Than Structural Findings on CT/T2

To oversimplify, we often administer intravenous contrast in the setting of "itis" (inflammation) or "oma" (neoplasms), both inside and outside the cranial vault. At the same time, we know that not all enhancing lesions are tumors and that not all brain tumors will enhance. The popular mnemonic for ring enhancing lesions ("MAGICDR") includes only two neoplastic letters (Metastasis and Glioblastoma); the other letters encompass inflammatory (Abscess and Demyelinating), reparative (Infarct and Contusion), or iatrogenic (Radiation) etiologies for a leaky blood-brain barrier (Fig. 3.7). While intravenous contrast definitely provides valuable information during initial and follow-up imaging, by helping with detection and characterization of brain tumors, it is foolish to discount or ignore

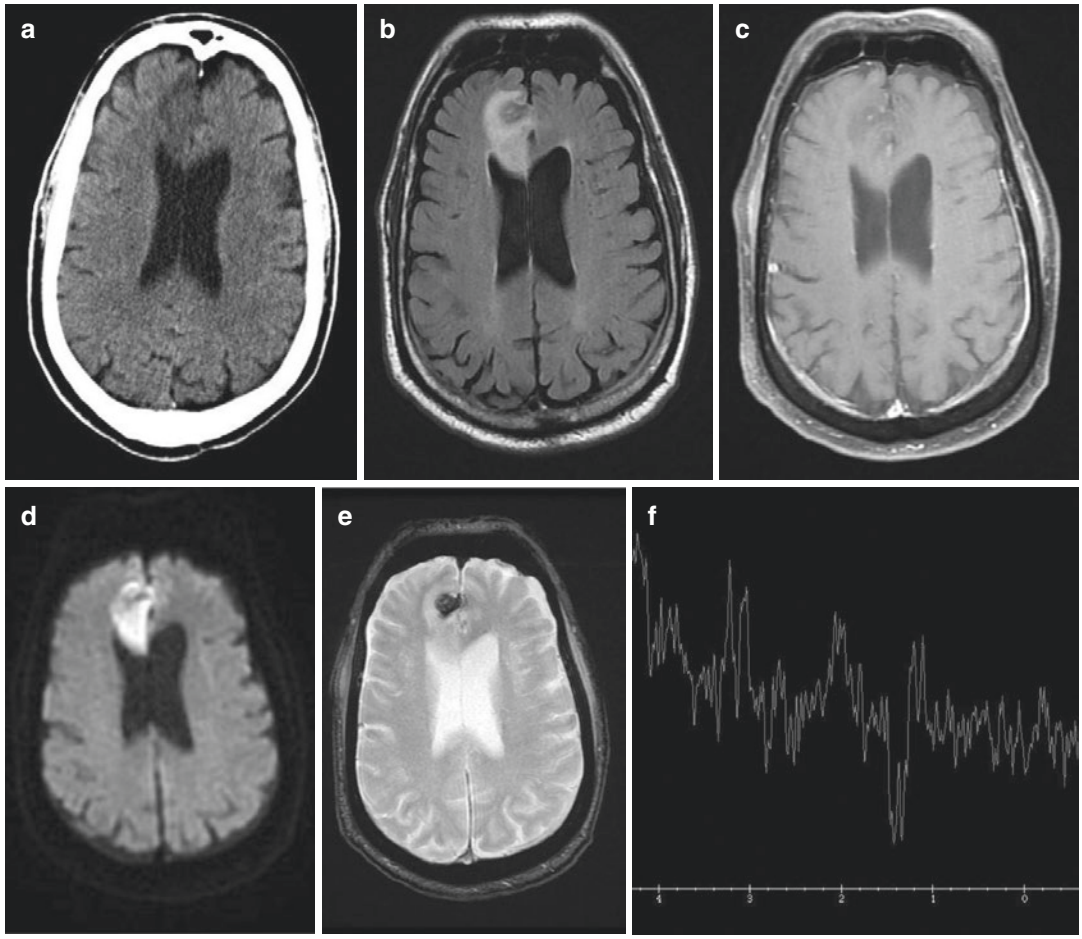

Fig. 3.5 Case study of edema mistaken for tumor in a 79-year-old man. (**a**) Outside head CT performed after an accidental fall shows an expansile hypodense lesion in the right medial frontal lobe. This patient was transferred to our hospital for "right frontal mass" evaluation. (**b**, **c**) Axial T2 FLAIR and post-contrast T1 FS images confirm an expansile T2 hyperintense lesion without enhancement. While a diffuse glioma is possible, the location may also prompt consideration of a right ACA territory stroke (cytotoxic edema). There was an incidental finding of thin subdural hematomas along the posterior cerebral convexities. (**d**, **e**) Axial DWI and GRE images make a diagnosis of right ACA infarct with petechial microhemorrhages. (**f**) Spectroscopy (*TE* = 144 ms) was ordered as part of the "tumor" workup. It is partially "contaminated" by blood products, but you can see an inverted lactate doublet at 1.3 ppm (from tissue hypoxia)

the value of noncontrast images. This is especially important in light of recent discoveries about gadolinium chelate dissociation and deposition disease (keep in mind that gadolinium, unlike iodine, is a known toxic element).

Due to the blood-brain barrier, most normal brain parenchyma should not enhance; however some normal enhancing structures include intracranial vessels, choroid plexus, and endocrine glands (pituitary/pineal). Reasons for parenchymal enhancement in the setting of a brain tumor may include non-neural (systemic-type) vasculature in the setting of metastatic disease or "leaky" microvascular proliferation in the setting of both low-grade circumscribed and high-grade diffuse gliomas. Reasons for parenchymal enhancement in the setting of posttreatment follow-up (Fig. 3.8) may include true residual/recurrent tumor or "leaky" vessels due to the effects of surgery and/or radiation. In the published RANO

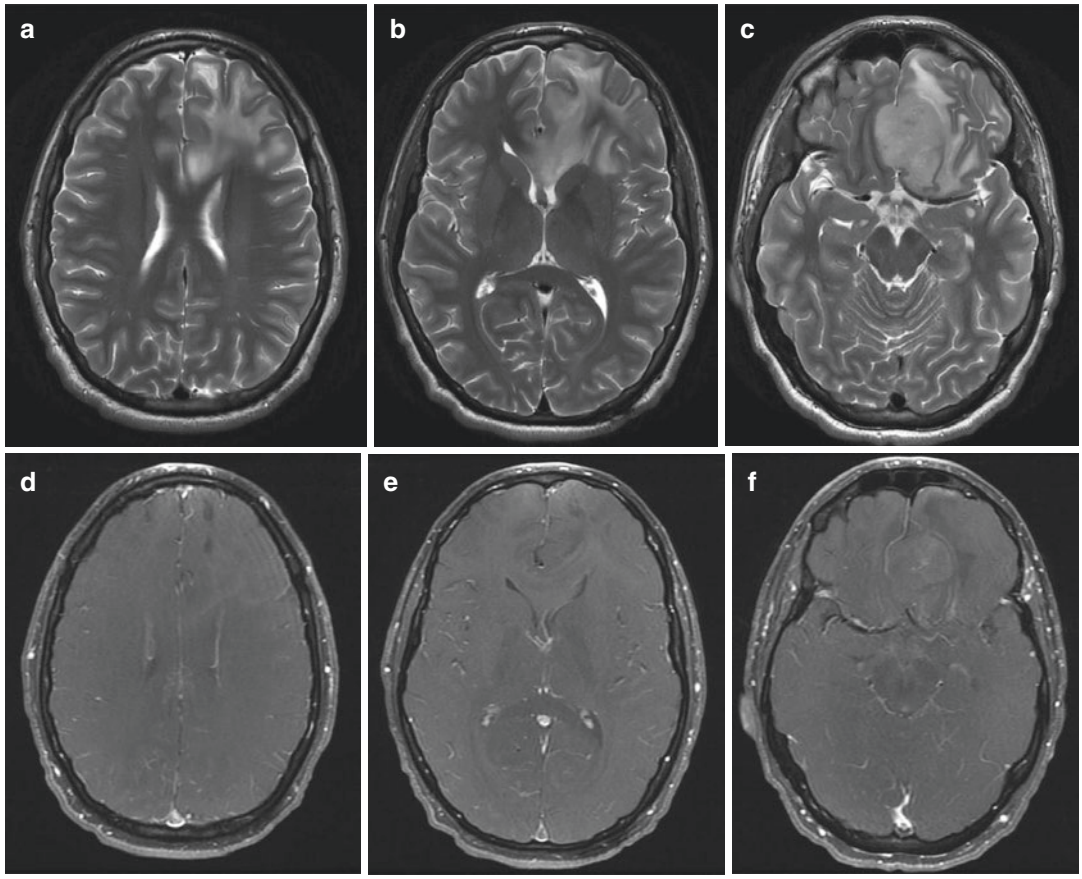

Fig. 3.6 Case study of tumor mistaken for edema in a 20-year-old man. (**a**–**c**) Axial T2 images reveal T2 signal abnormality in the left anterior frontal white matter with a rounded or nodular component more inferiorly that crosses the falx cerebri. Outside MRI films from thirteen years earlier were available for review and showed similar white matter findings (inferior nodular component was smaller at that time), which had been attributed to contusion or edema, since the initial MRI had been performed for a closed head injury. (**d**–**f**) Axial post-contrast T1 FS images demonstrate no significant pathologic enhancement, which indicates that the white matter T2 signal abnormality is not vasogenic edema, but infiltrative tumor. Excisional biopsy confirmed a diagnosis of anaplastic oligodendroglioma (with 1p/19q co-deletion)

Table 3.1 Three types of brain edema that may present as expansile T2 hyperintensity on neuroimaging

Types of edema (Greek: "swelling")	Cytotoxic ("cell poisoned")	Vasogenic ("vessel produced")	Hydrostatic/osmotic ("pressure or osmolarity produced")
Location of water	Intracellular (decreased diffusion)	Extracellular (increased diffusion)	Extracellular (increased diffusion)
Blood-brain barrier	Intact (please note that BBB may open later during the subacute phase)	Disrupted (extravasation of fluid and plasma proteins in setting of leaky BBB)	Intact (extravasation of fluid only from hydrostatic or osmotic gradient)
Common example	Cellular swelling from ischemic failure of ATP-dependent Na/K membrane pump	Formation of abnormal vessels by glioblastoma (neo-angiogenesis)	Periventricular edema from hydrocephalus with elevated pressure

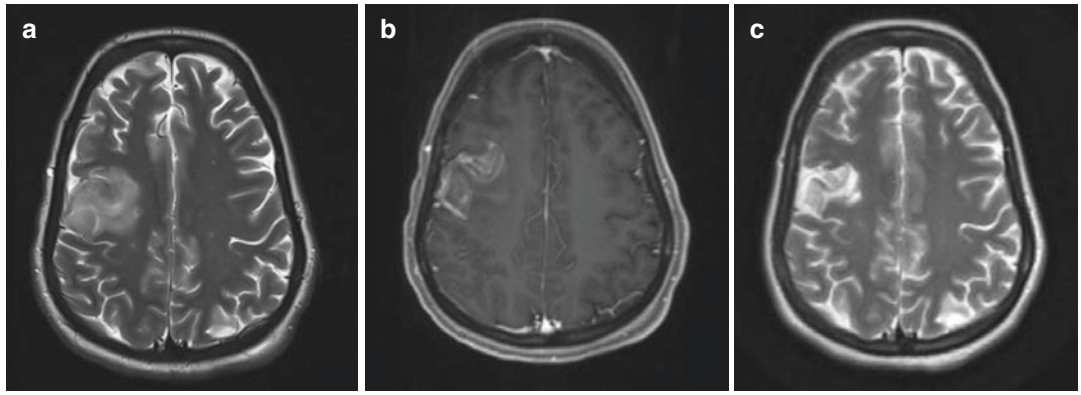

Fig. 3.7 Subacute enhancement due to tissue reactive repair in a 28-year-old woman. (**a**, **b**) Axial T2 and post-contrast T1 images reveal an expansile T2 hyperintense lesion with enhancement in the right frontal lobe. Based on the available information (complicated history including sepsis), both inflammatory (e.g., cerebritis) and neoplastic (e.g., glioma) causes are still possible. This was a subacute stroke with leaky vessels in the reparative phase. (**c**) Axial T2 image from 3 months later shows expected evolution into chronic gliosis with volume loss. Short interval follow-up can be helpful for questions of edema versus tumor

(Response Assessment in Neuro-Oncology) criteria for glioblastoma, contrast-enhancing lesion measurements are only one criterion in determining response versus progression. Serial evaluation of both enhancing and non-enhancing T2/FLAIR lesions to identify growth may help avoid diagnostic pitfalls of "pseudoprogression" or "pseudoresponse."

3.5 Pearl #5: The Truest Measure of the Value of Your Radiology Report Is Whether It Guides Patient Care in the Correct Direction, Not Whether It Includes the Final Pathological Diagnosis Somewhere in the Text

By definition, only the "gold standard" or definitive test will achieve 100% accuracy; with regard to brain tumors, this will generally be a pathologic diagnosis based on histologic and molecular features. Other diagnostic tests, for example, the radiologic interpretation of preoperative imaging, will achieve performance somewhere lower along the ROC (receiver operating characteristic) curve. For example: "is it glioblastoma or not?" has trade-offs in sensitivity versus specificity (e.g., do I call everything a possible glioblastoma?). While an accurate differential diagnosis is a noble goal—and the traditional focus of radiology education—it is not as important as our systems-based role in guiding clinicians' decisions to improve patients' outcomes. For example, a shotgun differential diagnosis that includes the correct diagnosis but leads to confusion or excess testing (due to distracting or extraneous considerations) is less valuable than a concise report that lists fewer—if any—diagnoses but clarifies the next step (e.g., biopsy, follow-up, or other confirmatory tests).

Remembering our ultimate purpose is especially useful when faced with a case whose pattern you do not recognize. This scenario is part of being a radiologist and should not be a source of guilt nor shame! When offering the differential diagnosis, you have the option of providing a few best guesses, which has the disadvantage of possibly missing the correct answer, versus throwing out a large and vague "fishing net" of possible

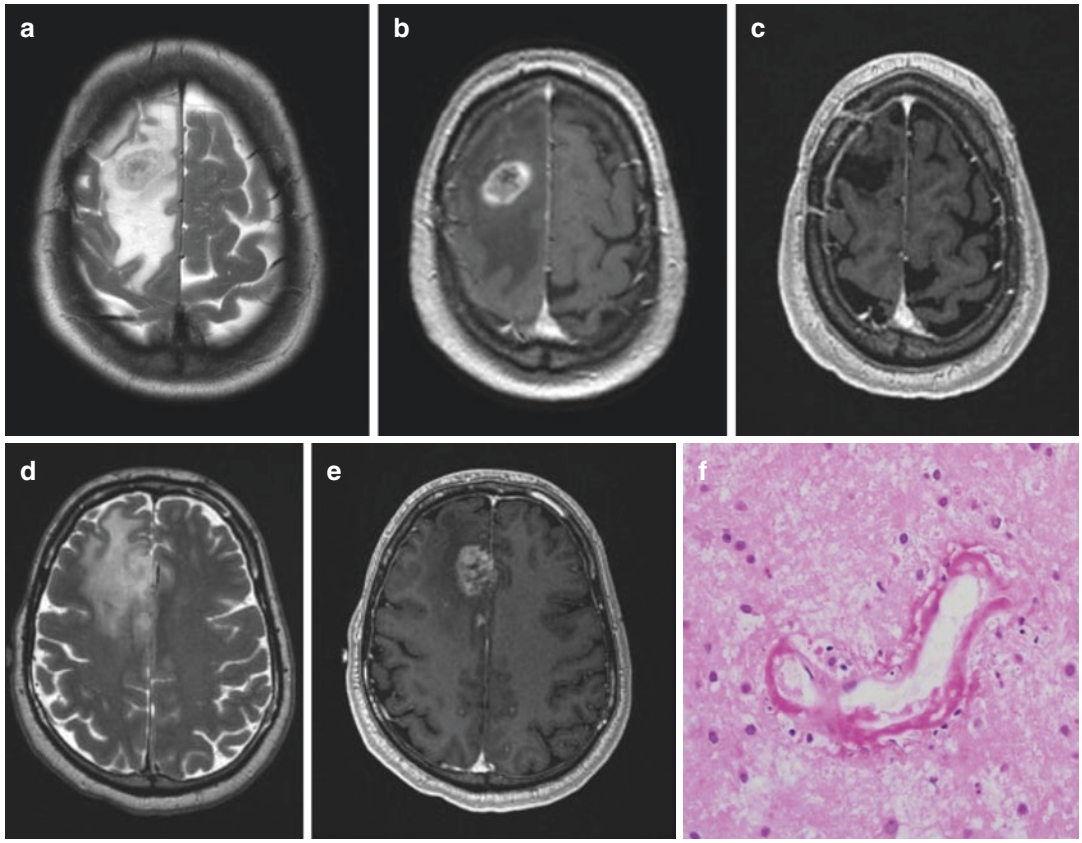

Fig. 3.8 Enhancement due to tumor vs. radiation in a 54-year-old man. (**a**, **b**) Axial T2 and post-contrast T1 images show a heterogeneously enhancing mass with surrounding vasogenic edema in the right frontal lobe. (**c**) Follow-up post-contrast T1 image confirms gross total resection of the enhancing lesion. The diagnosis was glioblastoma, and the enhancement was due to leaky tumor vessels (microvascular proliferation). (**d**, **e**) Axial T2 and post-contrast T1 images from a later scan after surgery, radiation, and 6 cycles/months of temozolomide chemotherapy reveal a new enhancing lesion with vasogenic edema inferior to the original resection cavity. Pseudoprogression usually occurs within 3 months of radiation; therefore the lesion was resected out of concern for true disease progression. (**f**) H&E photomicrograph shows an abnormal fibrosed/hyalinized blood vessel, consistent with radiation necrosis—not neoplasm

diagnoses, which has the disadvantage of not being helpful to anybody. By redirecting attention away from "nailing" the correct diagnosis to identifying the correct next steps, we serve as better members of the health care team (Figs. 3.9 and 3.10). Compared with possible diseases and diagnoses, there are also much fewer options to choose from too, e.g., neurology or neurosurgery consult, follow-up imaging, CSF analysis, biopsy, etc. Last but not least, multidisciplinary conferences (tumor boards) are a fantastic opportunity to discuss cases, to share knowledge, to stumble together, and to ultimately improve patient care/outcomes.

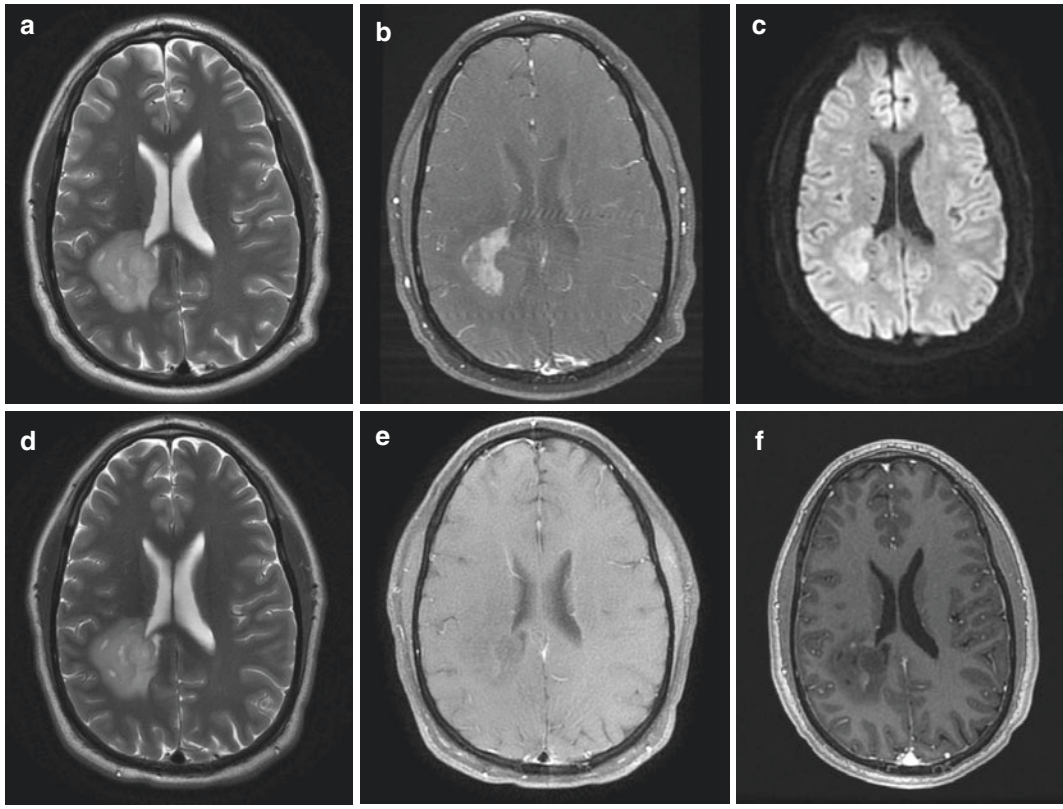

Fig. 3.9 Successful identification of the best next step in a 25-year-old man. (**a**–**c**) Axial T2, post-contrast T1 FS (fat-saturation), and diffusion images reveal a partially enhancing T2/DWI hyperintense lesion in the right parietal white matter. This was a puzzling case, and there was initial concern for a high-grade glioma. (**d**, **e**) Follow-up axial T2 and post-contrast T1 FS images from 4 days later show dramatic decrease in enhancement on intravenous steroids, raising the possibility of a demyelinating/inflammatory process or lymphoma. While the diagnosis was unclear, the recommendation was fairly straightforward: a stereotactic needle biopsy (not excisional biopsy). (**f**) Axial post-contrast T1 BRAVO image from the subsequent preoperative brain MRI depicts partial return of mildly enhancing foci, which were targeted for biopsy and confirmed a final pathologic diagnosis of an active tumefactive demyelinating lesion (TDL). This could be considered a variant of the "open ring" sign, because the enhancement is discontinuous, neither a ring nor a nodule

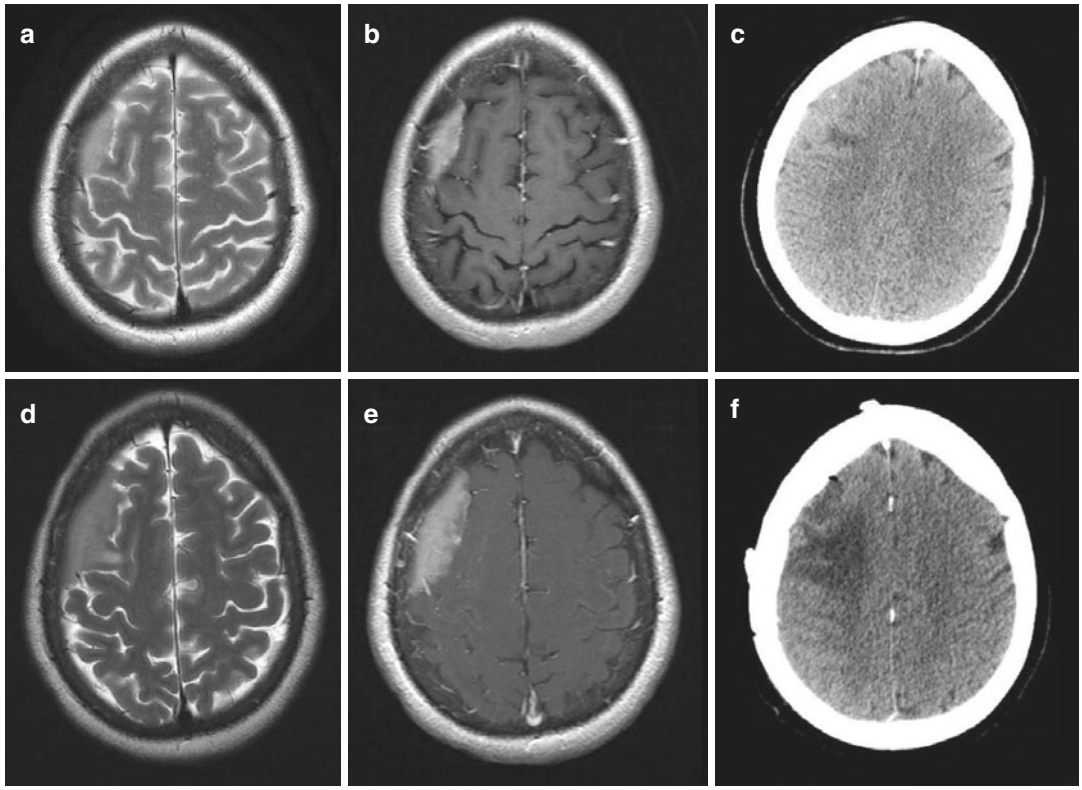

Fig. 3.10 Unsuccessful identification of the best next step in a 55-year-old woman. (**a**, **b**) Axial T2 and post-contrast T1 images reveal a small enhancing T2 isointense dural-based mass along the right frontal convexity. The indication for the study was upper extremity paresthesias; the impression for the report was probable meningioma. (**c**–**e**) Three years later, an outside head CT after a motor vehicle accident led to a subsequent outside brain MRI; the axial T2 and post-contrast T1 images show interval enlargement of the dural-based mass. The patient was unaware she had a meningioma; a retrospective investigation suggested that the primary care physician who ordered the initial brain MRI may not have told her and may not have known what to do with the results. (**f**) Postoperative head CT depicts gross total resection that was unfortunately complicated by a hypoattenuating venous infarct in the right frontal lobe. With the benefit of hindsight, a recommendation in the original radiology report for nonurgent neurosurgery consult or follow-up imaging may have helped, beyond predicting the correct diagnosis

References

1. Ellingson BM, Bendszus M, Boxerman J, Barboriak D, Erickson BJ, Smits M, Nelson SJ, Gerstner E, Alexander B, Goldmacher G, Wick W, Vogelbaum M, Weller M, Galanis E, Kalpathy-Cramer J, Shankar L, Jacobs P, Pope WB, Yang D, Chung C, Knopp MV, Cha S, van den Bent MJ, Chang S, Yung WK, Cloughesy TF, Wen PY, Gilbert MR, Jumpstarting Brain Tumor Drug Development Coalition Imaging Standardization Steering Committee. Consensus recommendations for a standardized brain tumor imaging protocol in clinical trials. Neuro-Oncology. 2015;17(9):1188–98.
2. Castillo M. History and evolution of brain tumor imaging: insights through radiology. Radiology. 2014;273(2 Suppl):S111–25.
3. Louis DN, Perry A, Reifenberger G, von Deimling A, Figarella-Branger D, Cavenee WK, Ohgaki H, Wiestler OD, Kleihues P, Ellison DW. The 2016 World Health Organization classification of tumors of the central nervous system: a summary. Acta Neuropathol. 2016;131(6):803–20.
4. Ostrom QT, Gittleman H, Liao P, Vecchione-Koval T, Wolinsky Y, Kruchko C, Barnholtz-Sloan JS. CBTRUS statistical report: primary brain and other central nervous system tumors diagnosed in the United States in 2010–2014. Neuro-Oncology. 2017;19(Suppl 5):v1–v88.
5. Shih RY, Koeller KK. Chapter 5: Central nervous system neoplasms and tumor-like masses. In: Gaensler EL, editor. Brant and Helms' fundamentals of diagnostic radiology. 5th ed. Philadelphia, PA: Lippincott Williams & Wilkins; 2018.

Diffusion, Perfusion, and PET Imaging of Brain Tumors

4

Angel Alberich-Bayarri, Fabio García Castro, Ismael González-Valverde, and Irene Mayorga Ruiz

4.1 Introduction

Magnetic resonance (MR) imaging is the reference modality for brain tumor diagnosis, staging, and prognosis evaluation [1]. High-grade malignant gliomas are frequently surgically resected as a first step. Identifying tumor persistence and recurrence after surgery is still one of the open issues for the multidisciplinary teams managing these patients, including neurosurgeons, radiologists, pathologists, and oncologists. Several studies have evaluated the effectiveness of conventional MR examinations for brain tumor grading and follow-up. Nevertheless, the conventional approach mainly relies on morphological evidences (lesion, edema, and necrosis volumes) and on the disruption of the blood-brain barrier as evaluated by the relative enhancement after the administration of Gadolinium (Gd)-based contrast agents. Published results of the effectiveness of these techniques showed that they are not suitable to support therapeutic decision-making because of their low efficacies, ranging between 55% and 83% [2, 3].The inclusion of MR imaging biomarkers able to characterize the presence and properties of malignant cells, angiogenesis, vasculogenesis, and tumor vascular heterogeneity may improve tumor grading and follow-up prognosis [4–6]. Furthermore, the combination of this quantitative information as radiomics data with nuclear medicine modalities such as single proton emission computed tomography (SPECT) and positron emission tomography (PET) to evaluate metabolic activity through ^{99m}Tc tetrofosmin and 18F-FDG radiotracer may provide complementary information (see Fig. 4.1). For multimodality and multiparametric analysis, an appropriate alignment and spatial registration of images is mandatory to guarantee spatial coherence, being a specific voxel the same across the different modalities and techniques (see Fig. 4.2). These imaging biomarkers give useful information for tissues' identification (tissue signaling) such as different tumor grades, normal parenchyma, vessels, edema, necrosis, and cerebrospinal fluid in the volume of interest. This information is crucial for the differentiation of tumoral, infiltrating peritumoral, and non-infiltrated regions to monitor tumor follow-up.

A. Alberich-Bayarri (✉)
Biomedical Imaging Research Group, La Fe Health Research Institute and Polytechnics and University Hospital, Valencia, Spain

Quantitative Imaging Biomarkers in Medicine (QUIBIM S.L.), Valencia, Spain
e-mail: angel@quibim.com

F. G. Castro · I. González-Valverde · I. M. Ruiz
Quantitative Imaging Biomarkers in Medicine (QUIBIM S.L.), Valencia, Spain

Y. Özsunar, U. Şenol (eds.), *Atlas of Clinical Cases on Brain Tumor Imaging*,
https://doi.org/10.1007/978-3-030-23273-3_4

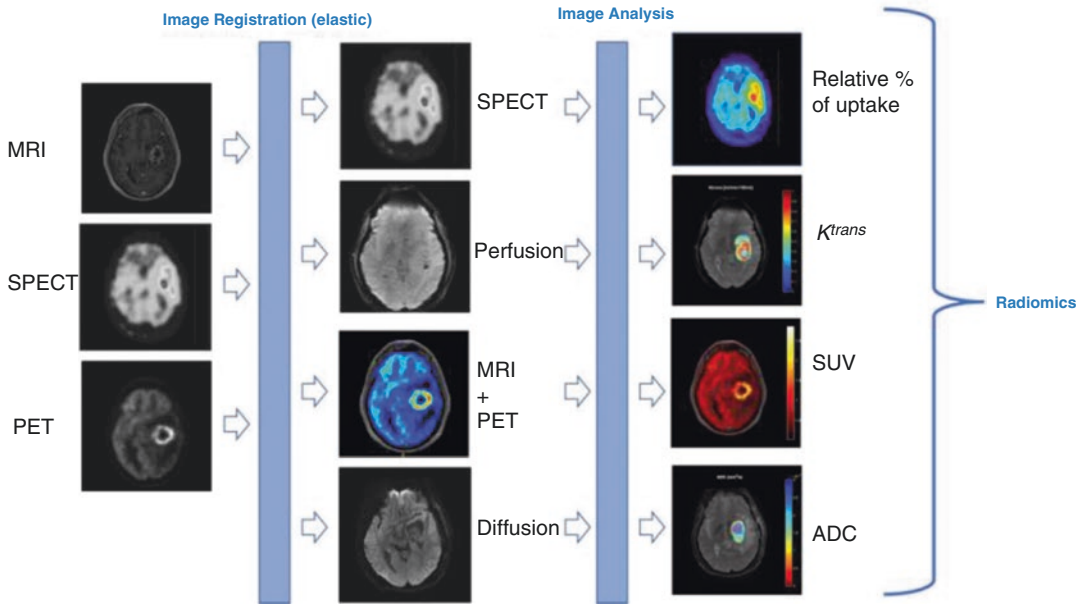

Fig. 4.1 Combination of different modalities, extraction of imaging biomarkers, and combination into a set of radiomics data

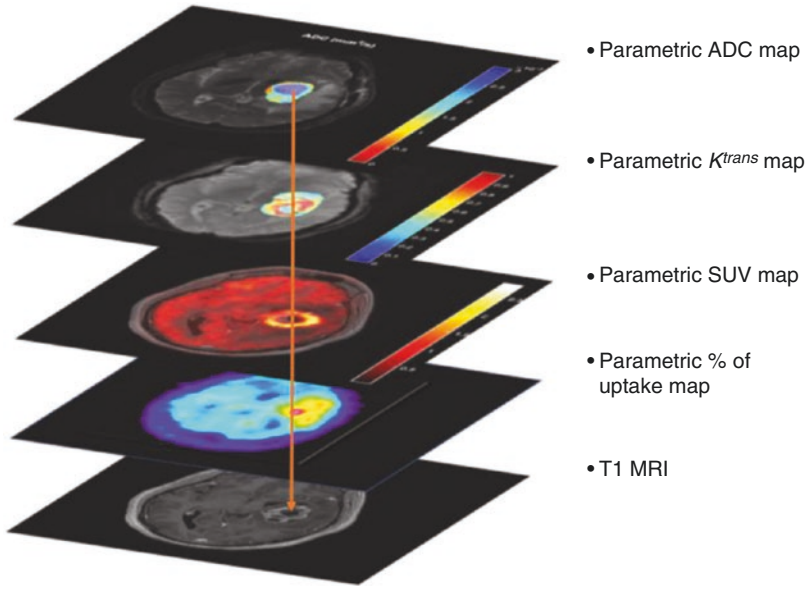

Fig. 4.2 Spatial coherence of different parametric maps of imaging biomarkers extracted after performing the quantitative analysis on previously registered examinations

4.2 Diffusion

Diffusion-weighted MR images allow characterization of tissue cellularity based on the free diffusion of water molecules in interstitial space [7, 8]. This sensitivity to diffusion can be used to classify organs and tissues in different tissue types and to extract quantitative descriptors of the water molecules diffusivity as the diffusion coefficient.

One of the most promising techniques for the quantification of the diffusion properties is

derived from the intra-voxel incoherent motions (IVIM) theory introduced by Le Bihan [9], which was not explored for survival prediction in gliomas until very recently by Puig et al. [10]. IVIM allows to differentiate between blood microcirculation in the capillary network and water diffusion in interstitial space. The signal amplitude in the diffusion MR acquisition is reduced bi-exponentially as the *b*-value parameter is increased. The *b*-value is used to control the degree of sensitivity to the water molecules with restricted diffusion and is related to the diffusion gradients intensity and separation. The bi-exponential signal decay is explained by an initial significant loss of energy by the fast-moving protons (rapid diffusion) mainly in the capillary network followed by a slight signal decay due to the slow-moving protons (restricted diffusion) within interstitial space in tissue regions with a high cell density. As it can be inferred, diffusion is also sensitive to perfusion since the water molecules within capillaries behave as a diffusion process [10]. IVIM analysis allows the calculation of three diffusion coefficients characterizing the restriction to molecular diffusion: the diffusion coefficient (*D*) (in some literature it is also named as "pure" diffusion coefficient), the pseudodiffusion coefficient (D^*) related to microcirculation, and finally the third parameter, called perfusion fraction (*f*), describes the portion of signal with a vascular contribution in each voxel.

Regarding MR acquisition properties, IVIM modeling requires the acquisition of diffusion-weighted images at different *b*-values. The advance in the hardware technology of MR scanners has allowed for reduced acquisition time with several *b*-values and improved signal-to-noise (SNR) ratio. This has made IVIM to be increasingly applied for the characterization of brain tumors and predicting and evaluating the response to treatment [10–12]. Reported evidence shows that *f* has a moderate correlation with the perfusion parameter of relative cerebral blood volume (rCBV) [11] and that in low- and high-grade gliomas the *f* values are significantly different, establishing *f* as a phenotyping parameter [12]. Finally, *f* has been demonstrated to correlate positively with vessel density and histology in rodent models of glioma [13].

4.3 Perfusion

Perfusion-weighted MR images may provide biological and physiological information. Dynamic susceptibility contrast (DSC) MR has been widely used to retrieve information on glioblastoma perfusion [14, 15]. There are two models to address the quantification of in vivo hemodynamic biomarkers obtained after the administration of contrast agents: the single-compartment model which analyzes the uptake curves characteristics and the two-compartment pharmacokinetic criteria [16, 17]. Bulakbasi et al. (2005) showed a statistically significant correlation between the rCBV obtained from the single-compartment model and tumor grade [18]. Awasthi et al. (2012) demonstrate that several perfusion index values, especially the extraction coefficient (k_{ep}), correlate with patient survival [19]. Moreover, several studies have established the relationship between survival prognosis and tumor vessel permeability (K^{trans}) obtained from two-compartment studies. Mills et al. (2006) and our group (Sanz-Requena 2013) demonstrated the relationship between K^{trans} and glioma grades [20, 21].

4.4 PET Imaging

Positron emission tomography (PET) images are increasing in relevance in the diagnosis, characterization, and treatment response evaluation of brain tumors. Nuclear medicine modalities, especially PET images, can provide additional information about tumor biology. This allows a noninvasive classification of the lesion through the semiquantitative parameter standard-uptake value (SUV).

18F-FDG PET imaging biomarkers provide information about the metabolic activity of the lesion which is directly correlated with aggressiveness. The most important biomarkers that can

be quantified from PET images are the metabolic tumor volume (MTV) and the total lesion glycolysis (TLG). Those biomarkers are defined as the volume of tumor with high metabolic activity and the amount of glucose uptake by the MTV, respectively.

The difference SUV (dSUV) biomarker can be applied for the longitudinal evaluation of brain tumors. This biomarker compares the SUV values of different time point studies giving as a result a parametric map. The results allow the evaluation of appearing/disappearing lesions. In addition, the SUV value difference allows the evaluation of metabolic activity response in the lesion after treatment.

4.4.1 Tissue Signatures Through Nosologic Imaging

Heterogeneity of high-grade brain tumors like glioblastoma is a key hallmark in the understanding of their resistance to effective therapies and a factor clearly related to the high aggressiveness of these lesions [22, 23]. Other hallmarks characterizing glioblastoma are high degrees of both deep infiltration and invasion. From the pathology perspective, low-grade gliomas can be well differentiated from high-grade gliomas by the vascular proliferation, angiogenesis, and microvasculature of the last ones, factors that influence patient prognosis. Specifically, neovascularization of the tumor detected on high-resolution blood-pool-contrast-enhanced magnetic resonance angiography (MRA) of glioblastoma is a candidate to be a useful biomarker since it is related to a worse survival [24]. Therefore, the early assessment of the highly heterogeneous vascular regions architecture of glioblastomas can provide powerful information to improve therapeutic decision-making.

The analysis of different tumor regions is mainly performed by manual delineation. A common practice is segmenting regions of interest (ROIs) within the tumor according to their intensity in T2, post-contrast T1 and DSC. Nevertheless, the manual approach hinders the applicability of this technique with well-defined criteria and defines a need for an automated clustering of different lesion regions that may be related to cancer hallmarks. In our group, a characterization of the vascular heterogeneity of glioblastomas through a multiparametric analysis of tumor habitats extracted from an unsupervised machine learning algorithm was implemented [25]. We found that the habitats obtained were good early predictors of overall survival in patients undergoing standard-of-care treatment. The method was termed as hemodynamic tissue signature (HTS) and was applied to automatically delineate a set of vascular habitats within the glioblastoma lesion. HTS includes consideration of four different habitats (see Fig. 4.3):

- The high-angiogenic tumor (the highest perfused area of the enhancing tumor in post-contrast T1)
- The low-angiogenic tumor (the area of the enhancing tumor in post-contrast T1 with a lower angiogenic profile)
- The potentially infiltrated peripheral edema (surrounding non-enhancing region adjacent to the tumor with elevated perfusion parameters)
- The vasogenic peripheral edema (remaining edema with a lower perfusion profile)

Survival analysis on the basis of perfusion measures obtained from the HTS in patients undergoing standard-of-care treatment provided satisfactory results [25]. An improvement of approximately 230 days in overall survival was observed for patients who had lower rCBV and rCBF in the high- and low-angiogenic habitats.

Multiparametric analysis can also be applied to evaluate regions that may be characterized by a hypoxic environment, since cells contained in

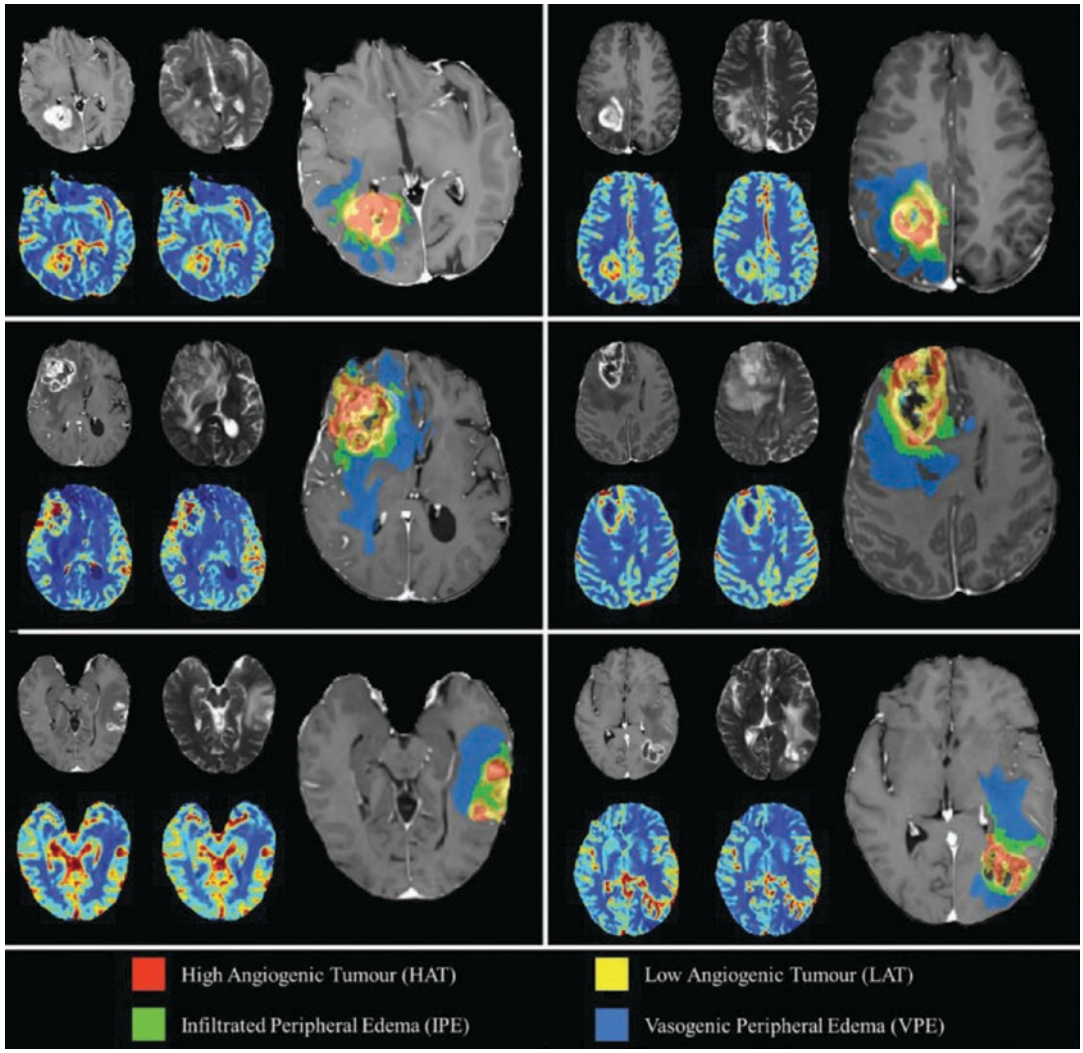

Fig. 4.3 Examples of the HTS habitat's map placed over the Gd-enhanced T1-weighted MR image for six patients. In addition, for each patient, Gd-enhanced T1-weighted MR image, T2-weighted MR image, CBV map, and cerebral blood flow (CBF) map are also shown in small images (left to right, top to bottom)

these regions are more radiation-resistant than others and this information is relevant for effective radiotherapy planning. In this regard, an indirect hypoxia parametric map was implemented in our group by the combination of the transfer constant information (K^{trans}) from the pharmacokinetics analysis of perfusion and the apparent diffusion coefficient (ADC) extracted from diffusion-weighted MR. Specifically, regions with a reduced permeability (low K^{trans}) are inferred to have a lower degree of oxygenation. Furthermore, if these regions present a high celularity (low ADC), we can affirm that a high number of cells with low permeability exists. These hand-crafted logics with MR perfusion and diffusion imaging biomarkers allow for the depiction of parametric maps with probable hypoxia (see Figs. 4.4 and 4.5).

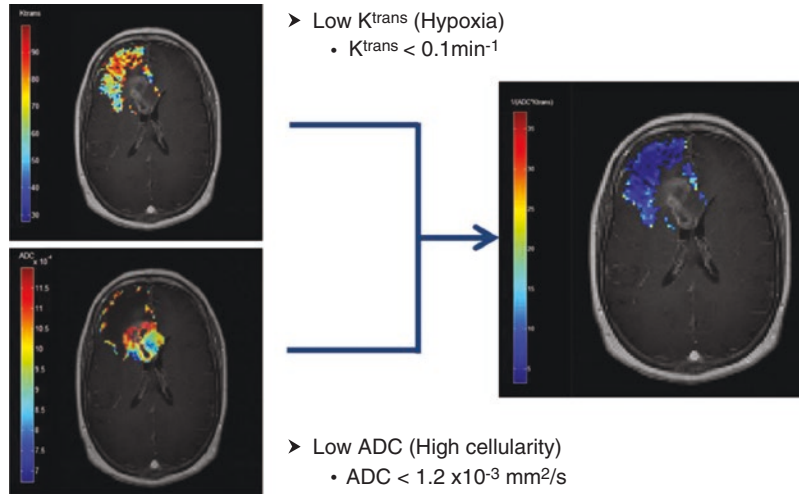

Fig. 4.4 Combination of K^{trans} and ADC into a new map depicting 1/(ADC × K^{trans}) showing those voxels where co-exist a high cellularity with a low vascular permeability in a case with glioblastoma

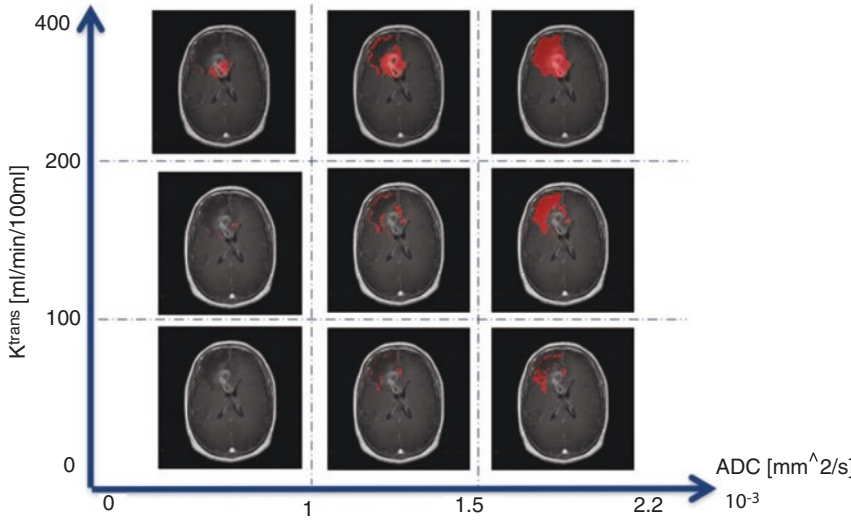

Fig. 4.5 Visualization of apparent hypoxia parametric maps by setting different threshold for ADC and K^{trans} in a case with glioblastoma

4.5 Conclusion

Although different imaging biomarkers have been proven useful for the characterization of brain tumors in different grades or phenotypes, a single imaging technique is not enough to provide relevant prognostic information in patients suffering from high-grade brain tumors such as glioblastoma. The combination of multiple imaging biomarkers and parametric maps in classifiers allows to predict relevant clinical endpoints for the clinician like overall survival.

References

1. Wen PY, Macdonald DR, Reardon DA, Cloughesy TF, Sorensen AG, Galanis E, et al. Updated response assessment criteria for high-grade gliomas: response assessment in neuro-oncology working group. J Clin Oncol. 2010;28:1963–72.
2. Asari S, et al. Assessment of the pathological grade of astrocytic gliomas using an MRI score. Eur Radiol. 1999;9:1047–54.
3. Upadhyay N, Waldman AD. Conventional MRI evaluation of gliomas. Br J Radiol. 2011;84:107–11.
4. Du R, et al. HIF1alpha induces the recruitment of bone marrow-derived vascular modulatory cells to

regulate tumor angiogenesis and invasion. Cancer Cell. 2008;13(3):206–20.
5. Petit I, et al. The SDF-1-CXCR4 signaling pathway: a molecular hub modulating neo-angiogenesis. Trends Immunol. 2007;28:299–307.
6. Mantovani A, et al. Cancer-related inflammation. Nature. 2008;454:436–44.
7. Zhou M, Scott J, et al. Radiomics in brain tumor: image assessment, quantitative feature descriptors, and machine-learning approaches. Am J Neuroradiol. 2018;39:208–16.
8. Padhani AR, Liu G, Koh DM, et al. Diffusion-weighted magnetic resonance imaging as a cancer biomarker: consensus and recommendations. Neoplasia. 2009;11:102–25.
9. Le Bihan D, Breton E, Lallemand D, Aubin ML, Vignaud J, Laval-Jeantet M. Separation of diffusion and perfusion in intravoxel incoherent motion MR imaging. Radiology. 1988;168:497–505.
10. Puig J, Sánchez-González J, Blasco G, Daunis-i-Estadella P, Federau C, Alberich-Bayarri A, Biarnes C, Nael K, Essig M, Jain R, Wintermark M, Pedraza S. Intravoxel incoherent motion metrics as potential biomarkers for survival in glioblastoma. Intravoxel incoherent motion metrics as potential biomarkers for survival in glioblastoma. PLoS One. 2016;11(7):e0158887. https://doi.org/10.1371/journal.pone.0158887.
11. Federau C, O'Brien K, Meuli R, Hagmann P, Maeder P. Measuring brain perfusion with intravoxel incoherent motion (IVIM): initial clinical experience. J Magn Reson Imaging. 2014;39:624–32. https://doi.org/10.1002/jmri.24195.
12. Bisdas S, Koh TS, Roder C, Braun C, Schittenhelm J, Ernemann U. Intravoxel incoherent motion diffusion-weighted MR imaging of gliomas: feasibility of the method and initial results. Neuroradiology. 2013;55:1189–96. https://doi.org/10.1007/s00234-013-1229-7.
13. Iima M, Reynaud O, Tsurugizawa T, Ciobanu L, Li JR, Geffroy F, et al. Characterization of glioma microcirculation and tissue features using intravoxel incoherent motion magnetic resonance imaging in a rat brain model. Investig Radiol. 2014;49:485–90. https://doi.org/10.1097/RLI.0000000000000040.
14. Knopp EA, Cha S, Johnson G, et al. Glial neoplasms: dynamic contrast-enhanced T2*-weighted MR imaging. Radiology. 1999;211(3):791–8.
15. Lupo JM, Cha S, Chang SM, Nelson SJ. Dynamic susceptibility-weighted perfusion imaging of high-grade gliomas: characterization of spatial heterogeneity. AJNR Am J Neuroradiol. 2005;26(6):1446–54.
16. Revert Ventura AJ, et al. Análisis nosológico con parámetros de perfusión tisular de RM obtenidos mediante los modelos monocompartimental y farmacocinético en los gliobastomas cerebrales. Radiologia. 2010;52:432–41.
17. Law M, et al. Comparison of cerebral blood volume and vascular permeability from dynamic susceptibility contrast-enhanced perfusion MR imaging with glioma grade. AJNR Am J Neuroradiol. 2004;25:746–55.
18. Bulakbasi N, Kocaoglu M, Farzaliyev A, Tayfun C, Ucoz T, Somuncu I. Assessment of diagnostic accuracy of perfusion MR imaging in primary and metastatic solitary malignant brain tumors. AJNR Am J Neuroradiol. 2005;26(9):2187–99.
19. Awasthi R, Pandey CM, Sahoo P, Behari S, Kumar V, Kumar S, et al. Dynamic contrast-enhanced magnetic resonance imaging-derived kep as a potential biomarker of matrix metalloproteinase 9 expressions in patients with glioblastoma multiforme: a pilot study. J Comput Assist Tomogr. 2012;36(1):125–30.
20. Mills SJ, et al. Do cerebral blood volume and contrast transfer coefficient predict prognosis in human-glioma? AJNR Am J Neuroradiol. 2006;27:853–8.
21. Sanz-Requena R, et al. Quantitative MR perfusion parameters related to survival time in high-grade gliomas. Eur Radiol. 2013;23:3456–65.
22. Lemée JM, Clavreul A, Menei P. Intratumoral heterogeneity in glioblastoma: don't forget the peritumoral brain zone. Neuro-Oncology. 2015;17(10):1322–32.
23. Soeda A, Hara A, Kunisada T, Yoshimura S, Iwama T, Park DM. The evidence of glioblastoma heterogeneity. Sci Rep. 2015;5(1):7979. [Published correction appears in Sci Rep. 2015;5:9630].
24. Puig J, Blasco G, Daunis-I-Estadella J, Alberich-Bayarri A, Essig M, Jain R, Remollo S, Hernández D, Puigdemont M, Sánchez-González J, Mateu G, Wintermark M, Pedraza S. High-resolution blood-pool-contrast-enhanced MR angiography in glioblastoma: tumor-associated neovascularization as a biomarker for patient survival. A preliminary study. Neuroradiology. 2016;58(1):17–26. Epub 2015 Oct 5. https://doi.org/10.1007/s00234-015-1599-0.
25. Juan-Albarracín J, Fuster-Garcia E, Pérez-Girbés A, Aparici-Robles F, Alberich-Bayarri Á, Revert-Ventura A, Martí-Bonmatí L, García-Gómez JM. Glioblastoma: vascular habitats detected at preoperative dynamic susceptibility-weighted contrast-enhanced perfusion MR imaging predict survival. Radiology. 2018;287:944–54.

5 Role of Magnetic Resonance Spectroscopy in Clinical Management of Brain Tumors

Adrien Heintz and Jean-Marc Constans

5.1 Introduction

5.1.1 Basic Principles

Magnetic resonance spectroscopy (MRS) analyzes the frequency of different atomic groups of molecules. Each atomic group corresponds to a free induction decay signal (FID) in the time domain.

In a molecule as well as in cerebral tissue, several different atomic groups correspond to different FIDs resonating at different frequencies after Fourier transform. Each atomic group, and thus FID, appears as a peak at a particular frequency allowing biochemical characterization. MRS has therefore become a useful analytical and diagnostic tool in biomedicine.

In the past two decades, human localized MRS (single voxel or multivoxel-spectroscopy or spectroscopic imaging) has emerged as an in vivo MR-based spectroscopic approach to translational and clinical research of parenchymal human tissues of interest.

One of the greatest advantages of cerebral MRS techniques is their ability to detect multiple tissue-specific physicochemical metabolites in a single experiment compared to Positron-emission tomography (PET) tracers (with membrane receptor affinity assumptions or hypotheses). The quantitative nature and translational component of in vivo MRS biomarkers come from the spectral and metabolic biomarkers discovered in in vitro/ex vivo and preclinical research studies. For these reasons, these in vivo MRS biomarkers can be easily translated and integrated into noninvasive spectroscopic and cerebral imaging protocols.

Disadvantages of in vivo MRS include low sensitivity, poor spectral resolution due to the inherently wider lines of "in vivo" metabolites, and B0 and B1 inhomogeneities. This will lead to overlapping resonances that are difficult to model and measure very accurately. It also suffers from poor time resolution, therefore offering fewer metabolic biomarkers to be measured and followed in vivo. Other disadvantages of the technique could be the difficulty in integrating all MRS measurements into a clinical protocol because it sometimes is perceived as taking too long.

In this chapter, we will reiterate several known MRS techniques and situations and provide considerations for establishing reliable indications and protocols, metabolite detection, measurement and quantification of in vivo brain tumor MR spectra. We will also explain how these techniques can contribute to diagnosis, follow-up, prediction, and monitoring of brain tumors. In this chapter, we will also present an overview of the role of cerebral MRS and when MRS could be used, and we will provide practical

A. Heintz · J.-M. Constans (✉)
Neuroradiology Department, Amiens Picardie University Hospital and EA7516 CHIMERE of University Picardie Jules Verne, Amiens, France
e-mail: Constans.Jean-Marc@chu-amiens.fr

Y. Özsunar, U. Şenol (eds.), *Atlas of Clinical Cases on Brain Tumor Imaging*,
https://doi.org/10.1007/978-3-030-23273-3_5

tables and examples of clinical cases of brain tumor spectroscopy.

5.1.2 Basic Protocol

For 3 T and 1.5 T, perform 1 min of calibration that encompasses the rough setup of the center frequency, then the optimization of the transmit and receiver gains, then the fine setup of center frequency, then the optimization of water suppression, and finally the single voxel MRS acquisition with 2 or 3 Echo Times (TEs):

- 35 ms (with 64 acquisitions for 2min12)
- 144 ms (with 96 acquisitions for 3min00)
- 288 ms (with 128 acquisitions for 3min48) = total 6–10 min

For new 3 T (with more head coil elements and better signal-to-noise ratios):

- 35 ms (with 16 or 32 acquisitions for 32 s or 1min34)
- 144 ms (with 64 acquisitions for 2min10)
- 288 ms (with 96 acquisitions for 3min00) = total 5–7 min

Monovoxel acquisition and processing are fast and relatively easy. However, there is not enough information about the extension and the heterogeneity of the tumor. On the other hand, we can easily quantitate, using monovoxel MRS, the most aggressive part of the tumor, which is most often used along with anatomo-pathology, to predict the prognosis the treatment response and make therapeutic decisions during the neuro-oncologic multidisciplinary staff meeting.

The basic protocol in multivoxel MRS could be Chemical Shift Imaging (CSI) of one slice with 12 × 12 or 16 × 16 phase encoding at TE 144 ms in 3 min with a 1min30 calibration.

Basic and frequent applications are brain tumors, metabolic brain diseases, inflammation and demyelination diseases, intensive care unit and epilepsy patients (cf. Chap. 3).

5.2 Important Metabolites Affecting Clinical Management

5.2.1 Metabolites

The main metabolites detected in proton MRS, in brain tumors, are, as you can see in Fig. 5.1, from 0 to 6 ppm: CH3-Lipids (CH_3-Lip → 0.9 ppm), CH2-Lipids + Lactate (CH_2-Lip + Lac → 1.3 ppm), *N*-Acetylaspartic Acid (NAA → 2.02 ppm), Glutamate + Glutamine (Glu + Gln → from 2.05

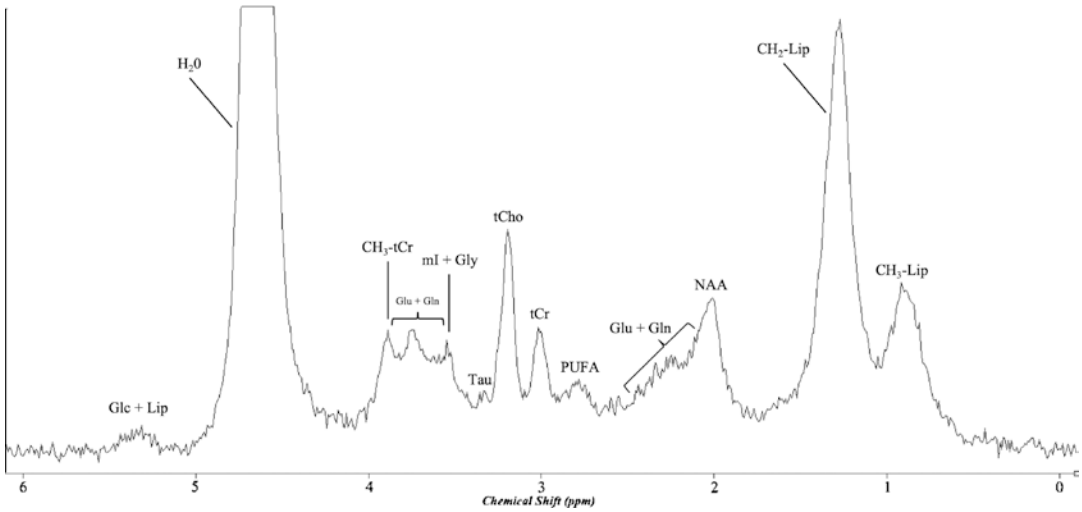

Fig. 5.1 Representative proton spectrum (TE/TR = 35/1500 ms) of the aggressive part of a Glioblastoma (GBM) with the main metabolite described above

to 2.55 ppm), PolyUnsaturated Fatty Acid (PUFA → 2.8 ppm), CH3-Total Creatine (CH3-tCr → 3.03 ppm), Total Choline (tCho → 3.22 ppm), Taurine (Tau → 3.4 ppm), Myoinositol + Glycine (mI + Gly → 3.56 ppm), Glutamate + Glutamine (Glu + Gln → from 3.6 to 3.9 ppm), CH2-Total Creatine (CH_2-tCr → 3.93 ppm), Water (H_2O → from 4.5 to 4.9 ppm), Glucose + Lipids (Glc + Lip → 5.24 ppm).

All metabolites are often measured as ratios over Creatine because this is the most stable metabolite in the brain in the most common brain diseases.

5.2.1.1 Cho/Cr and Cho/NAA

The first ratio to measure is the Choline/Creatine ratio (Cho/Cr), which is estimated at TE = 144 ms [1] (cf. Fig. 5.2). This ratio corresponds to tumor proliferation: the higher the ratio (above 2.5), the more proliferation and the mitotic index (Ki-67) reflecting proliferative activity is elevated [2]. We determine the grade of glioma based primarily on this ratio [3]. The ratio of Cho/NAA also allows us to confirm the tumor grade [1].

5.2.1.2 Lactate and Lac/Cr

The presence of lactate in a tumor lesion gives us information about the aggressiveness of the tumor. Its presence in large quantities can sometimes differentiate a lymphoma from a GBM and a transition to a higher grade of a glioma [4].

The detection of lactate is particular because its resonance frequency is located at the same frequency position as a part of necrotic CH2 phospholipids (1.3 ppm). For this, several TEs are needed as shown in Fig. 5.3: a TE at 35 ms to detect the presence of lactate and lipids, both at 1.3 ppm, at TE = 144 ms: if the 1.3 ppm signal goes negative, then there is more lactate than necrotic CH2 phospholipids. The concentration can be estimated at TE = 288 ms [5]. We should be cautious on 3 T MRS because the lactate detection is decreased at TE = 144 ms [5, 6]. Its concentration is therefore underestimated because of the chemical shift error and the PRESS sequence. We should thus use a third TE at 288 ms.

It is important, especially in low-grade gliomas, to associate Cho/Cr and Lac/Cr. When the glycolytic metabolism (Lac/Cr) is increased (>12 Mmol as in Fig. 5.3), it is a sign that a glioma transformation has resulted in a high-grade glioma, even though there is limited proliferation and almost no contrast enhancement.

5.2.1.3 Glucose

The amount of glucose [7] in a tumor is usually related to lactate [8].

5.2.1.4 Glutamine

The glutaminergic complex also confirms the aggressiveness of a tumor [9]. Its detection and measurement without processing software is more complex for distinguishing difference between glutamate and glutamine in particular [10] because of the overlapping resonances. They are added most of the time, but it is possible to differentiate them. The most useful energetic proton tumor

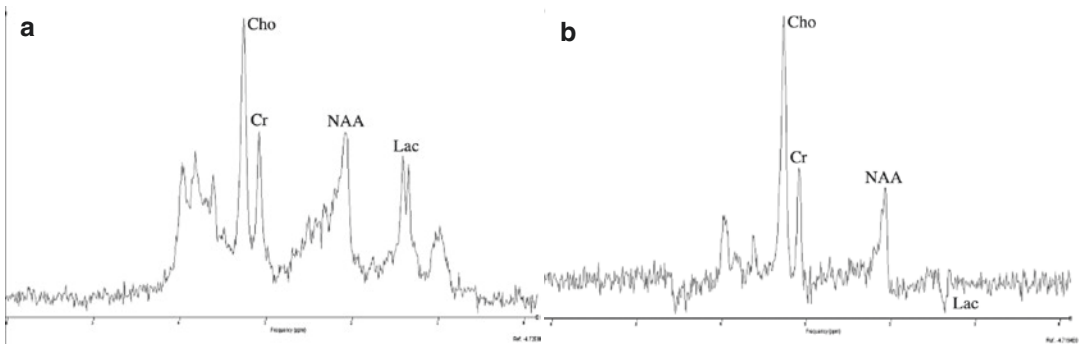

Fig. 5.2 Spectrum of a glioblastoma at TE/TR = 35/1500 ms (**a**) and TE/TR = 144/1500 ms (**b**) The ratio of Cho/Cr is measured by the neuroradiologist on the TE/TR = 144/1500 ms and correspond to the ratios of areas under the resonances of Choline (3.22 ppm) and Creatine (3.03 ppm). Here, the Cho/Cr ratio is a little above 2

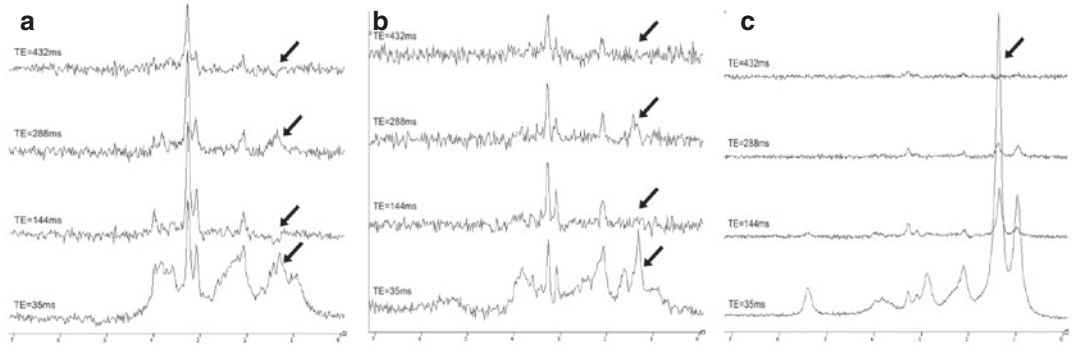

Fig. 5.3 A multi-TE study (TE = 35, 144, 288 and 432 ms) can, in some cases, help with the quantification of lactate and the differentiation between Lipids and lactate. If at TE = 144 ms the lactate doublet appears (**a**), it means that the lactate is predominant in the Volume of Interest (VOI). If it does not appear, it is that the resonances are of the same intensity (**b**). If, on the contrary, the resonance remains positive, it is that the lipids are still predominant (**c**)

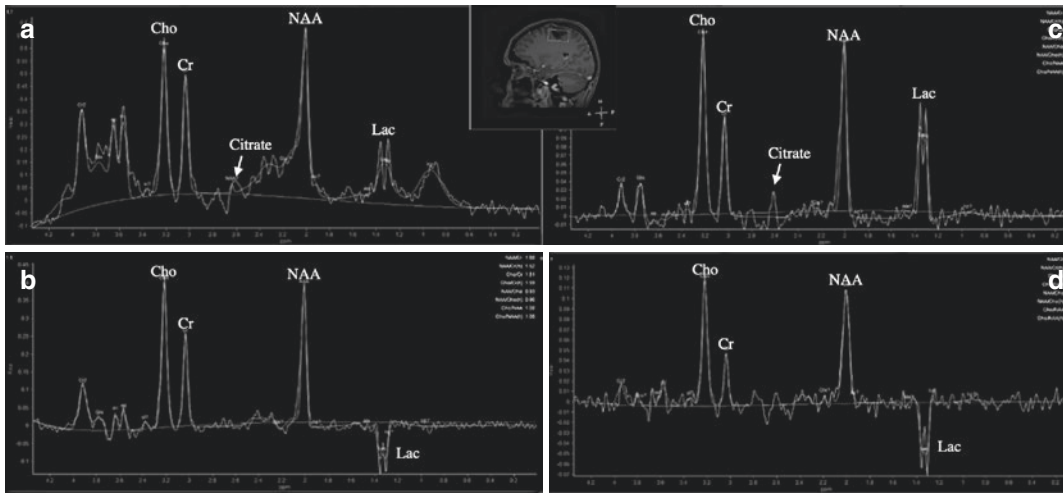

Fig. 5.4 MRS Glioblastoma spectra with citrate at TE/TR = 35/1500 ms (**a**); at TE/TR = 144/1500 ms (**b**); at TE/TR = 288/1500 ms (**c**); and at TE/TR = 432/1500 ms (**d**). Where we can detect citrate at 2.6 ppm, more visible at TEs 35ms and 288 ms

biomarker for detection is glutamine, which is closer to CH2 creatine (while glutamate is closer to the higher mI resonance at 3.56 ppm). Glutamine shows the metabolic activity of the tumors and is predictive of future proliferation [11].

5.2.1.5 CH2-Lipids

CH2 phospholipids are not present in substantial quantity in the normal human brain. The presence of lipids and the amount of CH2-Phospholipids (1.3 ppm) tells us about several elements. Before treatment initiation, they allow us to estimate the grade of the tumor. The higher they are, the higher the grade is. After treatment has been started, if the ratios detected are significantly different, they can indicate the effectiveness of the treatment [12] in producing necrosis [13].

5.2.1.6 Taurine

The Glucose/Taurine peaks (3.40 ppm), positioned to the left of Choline (3.22 ppm), can also indicate tumor grade [14].

5.2.1.7 Citrate

Citrate can be found in aggressive pediatric glial tumors [15] and active glioblastomas as in Fig. 5.4 below, and can be correlated to citrate synthase activity.

5.2.1.8 Alanine

When alanine is detected at 1.47 ppm in cerebral tumors, we should suspect meningioma [16].

5.2.1.9 Miscellaneous

Polyamines (between creatine and choline at 35 ms) could help to follow embolization and therapies of some GBM.

Myoinositol (at 35 ms) and glycine (at 35 and 144 ms) at around 3.56 ppm are elevated in glial tumors.

Polyunsaturated fatty acids (PUFA) at 2.8 ppm could be detected [17].

5.2.2 Etiologies

Table 5.1 below is giving a brief overview of main metabolites and ratios in main etiologies of brain tumors. It is sometimes important to consider spectral frequency resonances of metastases that could be detected in tumors, necrosis, and edema. This may suggest etiologic types of metastasis, or when the scale of the intensity changes, could give us information on the distribution. In the future, pharmacokinetics of some concentrated therapies such as Solumedrol, Diprivan, or antiepileptics could be followed.

5.2.3 Importance of Analysis of the Whole Spectral Profile

All of these ratios can be analyzed together (by multidimensional analysis with main compound analysis (MCA), correspondence factorial analysis (CFA) with discriminant analysis, or hierarchical classification), increasing the discriminative

Table 5.1 Brief overview of main metabolites and ratios in brain tumors

Metabolites	Etiologies
Cho/Cr	– Tumor proliferation (Cho/Cr >3) – Malignant (glial tumor, metastasis) or benign (meningioma) tumor setting: Clinical MRI
NAA/Cr	– Infiltration
Cho/NAA	– Tumor grade, proliferation, and infiltration
Lac/Cr	– Tumoral glycolytic metabolism – Intensive sport practice → Lactate <4 Mmol/L (288 ms) – Ischemia (stroke, vasospasm of subarachnoid hemorrhage, embolization) → Lactate >15 Mmol/L (288 ms) – Mitochondrial disease → Lactate often >20 Mmol/L (288 ms) – Inflammation, macrophages → Lactate between 5 and 10 Mmol/L (288 ms)
Glucose	– Glucose infusion, food, diabetes (ketone bodies) (35 ms)
Glutamine, glutamate	– Glial tumors and metabolic disease → Gln between 5 and 15 Mmol/L (35 ms) – Seizures → Glx >10 Mmol/L (35 ms) – Hepatic encephalopathy → Glx >15 Mmol/L (35 ms) – Excitotoxicity → Glu >15 Mmol/L (35 ms)
CH2 lipids (before treatment)	– Tumoral necrosis (Glial) → 15 >CH2Lip/Cr >2 (35 ms) – Tumoral necrosis (metastasis) → CH2Lip/Cr >15 (35 ms) – Infectious necrosis → CH2Lip/Cr >15 (35 ms) (e.g., bacterial, toxoplasmosis) – Demyelination (stroke) → CH2Lip/Cr <10 (35 ms) – Demyelination (MS) → 2 >CH2Lip/Cr >0.5 (35 ms) – Mental retardation → 10 >CH2Lip/Cr >5 (35 ms) – Apoptosis → CH2Lip/Cr <1 (35 ms) – Drug (alcohol) → CH2Lip/Cr <1 (35 ms)
Taurine	– Low-grade tumor and inflammation → Tau/Cr between 0.1 and 0.4 (35 ms) – Energetic drinks (e.g., Red Bull) → Tau/Cr between 0.2 and 0.6 (35 ms)
Citrate	– Pediatric tumor cases → Cit/Cr between 0.1 and 0.3 (35 ms) – Aggressive tumors (GBM) → Cit/Cr 0.2 (±0.1) (35 ms)
Alanine	– Meningioma → Ala/Cr = 0.4 (±0.3) (35 ms) – Intensive care unit patients Ala/Cr = 0.2 (±0.1) (35 ms)
Miscellaneous	– Polyamine between Cr and Cho (35 ms) – Myoinositol and glycine (at 3.56 ppm) increased – Polyunsaturated fatty acids (PUFA) (at 2.8 ppm)

If the TE is not indicated, it is at TE = 144 ms ratio

power of MRS. Performing multiple TEs at different sites of the tumor and brain allows for better differentiation of coupled spins from noise. It also allows the collection of as much relevant information as possible from tumoral processes, differential diagnoses, and treatment responses (included in contralateral normal appearing brain). Artificial intelligence and neuronal networks as well as deep learning could, of course, be helpful after evaluation and validation of a sufficient number of relevant and well-labeled data.

5.3 Role of MRS in Clinical Management of Brain Tumors

MRS provides additional quantitative information about the aggressive part of the tumor and the different pathological processes, acquired within a regular MR examination in 3–5 min.

MRS facilitates additional metabolic analysis far more inexpensively and quickly than PET, with physicochemical measurements, independent of the affinity of the receptor, and in real time (and with membrane changes). MRS is sometimes diagnostic, particularly for necrotic masses and for distinguishing tumoral from infectious processes, notably bacterial infection. For other tumoral conditions, and after registration, association with morphologic MRI 3D sequences, perfusion, and different PET tracers are always informative.

Once the tumoral process is confirmed (Cho/Cr >3), MRS used along with MRI increases the likelihood of detecting malignant tumors in some cases. It could help to measure the spectral and metabolic treatment response in vivo and monitor some highly concentrated treatments. In the future, monitoring biomarkers for responses to treatment could be possible. These biomarkers and their combinations could allow us to predict early survival (if the patient is still alive at 6, 8, or 10 months after relapse) and to predict the response to costly therapies such as antiangiogenics. It is particularly useful when contrast enhancement and hyperperfusion disappear while proliferation continues [18] or with antihypoxia or antimetabolite therapies. It could be possible to follow therapies in real time and monitor metabolic pharmacology [19].

MRS, which detects tumoral processes (Cho/Cr >3), allows early detection of brain tumors, the extension of their progression, and their boundaries, in CSI or multivoxel for glial tumors and their relapses under treatment, MRS can detect early response to specific treatments and their combinations (e.g., costly antiangiogenics, signaling pathway inhibitors, and new sources of radiation). Therefore, this technique is able to change the monitoring and treatment combinations used in brain tumor patients. MRS techniques and sequences should be adapted to the clinical question: Is there a malignant or benign tumor process? What is the extension assessment and stage? How is the tumor lesion progressing under therapy (degree of proliferation, necrosis, glycolytic, and glutamatergic metabolism)?

In metastasis, MRS will help to first differentiate multiple lesions, MS lesions, or vascular lesions from metastasis, then with more difficulty from some infectious diseases. In cases of unique necrotic masses, as we will see below, MRS helps to differentiate metastasis from abscess and GBM. In addition, in some cases it could help to evaluate or monitor treatment effectiveness, e.g., Solumedrol effectiveness.

Moreover, MRS is useful for better understanding and following the physiopathology of brain tumors and the different pathological processes that occur over time, particularly in treatment responses. Indeed, the volumetric response criteria (RECIST, RANO) are often not sufficient although they are used in clinical research protocols because they are more reproducible and quantifiable than clinical criteria. More sensitive, discriminant, and informative (regarding the pathological processes) measurements, such as multidimensional analysis of the different spectroscopic ratios and spectral profiles and their combinations over time, are needed. Artificial intelligence, neuronal networks, and deep learning could naturally be helpful after evaluation and validation of enough relevant and well-labeled data.

5.4 Clinical Features in Which MRS Will Be Used for Clinical Management

5.4.1 MRS Before Brainstem Biopsies of Brainstem Lesions with Mass Effect

Spectroscopy with perfusion and diffusion first helps to rule out differential diagnoses of brain tumor processes such as infectious, inflammatory, granulomatous, or autoimmune diseases [20].

Among brainstem tumors, we can justify differentiating between lymphomas, metastases, and necrotic or non-necrotic lesions, with increased CH2 phospholipids. Spectroscopy could subsequently predict the grade and the progression as well as short-term survival of the patients, followed by the differentiation between low-grade and high-grade gliomas.

5.4.2 Differentiation of Necrotic Masses

Diffusion and spectroscopy (with acetate, valine, leucine, isoleucine, and succinate) will confirm the diagnosis of abscesses with an accuracy rate of more than 99% [21, 22].

In non-treated necrotic masses, spectroscopy results with a CH2 phospholipids to creatine ratio >15 and a Cho/Cr ratio <3, in metastasis can help to differentiate them from glioblastomas.

Spectroscopy showing the amount of lactate, CH2 phospholipids and the value of Cho/Cr and mI/Cr, could help to differentiate GBM from lymphomas, especially when there is involvement of the corpus callosum in both cases.

5.4.3 Prediction of Survival, Tumor Activity, Early Progression, and Treatment Response

Usually, in cancer, four kinds of responses are used to evaluate treatment efficacy: complete and partial response, stability, and progression. To be classified into one of these responses, size comparisons using previous exams are done.

Two imaging exams are often used: the initial exam (baseline, before treatment) and the NADIR (the imaging exam in which the patient achieved the best treatment response). If the size increases by more than 20% compared to the NADIR, we classify it into "tumor progression," which often leads to a treatment change. In the same way, spectroscopy criteria could be set up and optimized to define best tumoral progression. For example, comparisons between two exams, or between the last exam and the initial or first one after treatment or the NADIR. Thus, these criteria are easier for proliferation and glycolytic metabolites, but more difficult for glutamine and other metabolites. To find MRS differences between necrosis and apoptosis in a clinical setting is still very challenging.

The complete response in spectroscopy is not seen often because the different tumoral pathological processes do not disappear quickly and easily. In contrast, we can see various combinations of changes, therefore the tumoral stability is difficult to define and the partial response needs further MRS/MRI studies and evaluations.

Within heterogeneous glial tumors, we can try to define target(s) such as the most aggressive parts of the tumor that could be good target(s) for localizing therapies such as stereotaxic radiation, boost radiation, or intra-tumoral therapy delivery. MRS in GBM and in metastasis could be predictive of volumetric changes.

Segmentation in the VOI to obtain a percentage of gray/white matter and the different tumoral compartments is useful in multivoxel and in monovoxel as well, allowing the correction of certain effects of the partial volume effect.

Any sign of spectral, or metabolic, progression needs to be thoroughly evaluated when there is no proliferation and when there is a combination of spectral changes. As mentioned before, it could be useful to study the relationship between the volume of necrosis in post-gadolinium T1-weighted imaging and the CH2 necrotic phospholipids to creatine ratio.

5.4.3.1 Chemotherapy (Temozolomide)

It is possible to detect Temozolomide (TMZ) in vitro and, in some cases, in vivo during glioma and GBM chemotherapy [23].

5.4.3.2 New Sources of Radiation

MRS could help to monitor stereotaxic, proton and Hadron therapy and to detect proliferation and relapse from radio-necrosis or pseudo-progression, or tissular antioxidant level [24].

5.4.3.3 Antiangiogenic Therapy

Some tumors, such as GBM, after genomic analysis with functional assays for identifying patients specific targetable alterations [25], can respond well to antiangiogenic therapy, with disappearance of hyper-perfusion and contrast enhancement. However, the glycolytic metabolism and proliferation persist [18]. Some other GBM have nevertheless shown decreased neo-angiogenesis (with disappearance of contrast enhancement and hyper-perfusion). They have, however, increased in size, mostly due to necrosis (in T1-weighted imaging post-gadolinium), and are confirmed by a markedly increased quantity of CH2 necrotic phospholipids without proliferation or glycolytic metabolism.

5.4.3.4 Immunotherapy: Detection of Inflammation and Immune Response

MRS, in some cases, can detect inflammation and immuno-response secondary to immunotherapy.

5.4.4 Interventional Therapeutic Monitoring of Tumors

Biopsies could be studied with HR-MAS. Tumoral ablation could be studied by thermo or cryoablation, focus ultrasound, or lasers, and could be monitor by spectroscopy.

Embolization in tumors such as meningiomas [16] could be monitored by MRS to follow experimental ischemia, embolization agents, metabolism changes, and glial tumor follow-up with glucose and polyamine. MRS could help to follow venous perfusion of medication, intra-arterial or intra-tumoral chemotherapy, or therapy delivery such as microbubbles and nanoparticles under ultrasound, laser, or radiation.

5.4.5 Symptomatic Treatment

MRS could detect and measure in vitro and in vivo symptomatic treatments such as antiepileptics, antibiotics, mannitol, steroids (Solumedrol), and Diprivan.

5.4.6 Summary of Clinical Features of Brain Tumors Pathologies for Which MRS Is Useful

Table 5.2 below is giving a summary of the main clinical features of brain tumors pathologies with metabolic changes for which MRS is useful.

Table 5.2 Summary of the main clinical features of brain tumor pathologies for which MRS is useful

Clinical management used	Pathologies	Metabolites
Brainstem biopsy	Brainstem tumors and their differential diagnosis	Cho/Cr, acetate, leucine, isoleucine, valine, CH2 phospholipids, CH3/Cr, Glx/Cr, mI/Cr
Necrotic masses	Abscesses, metastases, GBM, lymphoma	Acetate, leucine, isoleucine, valine, succinate, CH2 Creatine >15, Cho/Cr >3
Survival and tumor progression prediction	GBM, low-grade gliomas	Cho/Cr, Lac/Cr, Gln/Cr, Glc/Cr, ratio combinations
Monitoring treatment response	GBM, low-grade gliomas	Cho/Cr, Lac/Cr, Gln/Cr, CH2/Cr, NAA/Cr
Chemotherapy	GBM, low-grade gliomas	Cho/Cr, Lac/Cr, Gln/Cr, NAA/Cr, TMZ/Cr
Radiotherapy (stereotaxic, proton)	GBM	Cho/Cr, CH2/Cr, NAA/Cr
Antiangiogenics	GBM	Cho/Cr, Lac/Cr, Gln/Cr
Immunotherapy, inflammation	GBM	Cho/Cr, Lac/Cr
Interventional therapies	Meningioma embolization	Glucose, Cho/Cr, Lac/Cr, Glx/Cr, Gln/Cr, polyamines
Treatments	GBM, low-grade gliomas	TMZ, antiepileptics, antibiotics, Mannitol, Solumedrol, Diprivan

5.5 Brief Overview of Practical Clinical Cases: Examples of Brain Tumor MRS

For each pathology, a brief summary of the usefulness of MRS with examples are reviewed. Then, necrotic tumors and differential diagnosis of brain tumors will be discussed.

5.5.1 Glioblastoma

The usefulness of conventional, advanced MR imaging and MRS become clear when the biopsies are negative as in these two cases (Figs. 5.5 and 5.6).

The study of the agreement with anatomopathology features is also essential (Fig. 5.7).

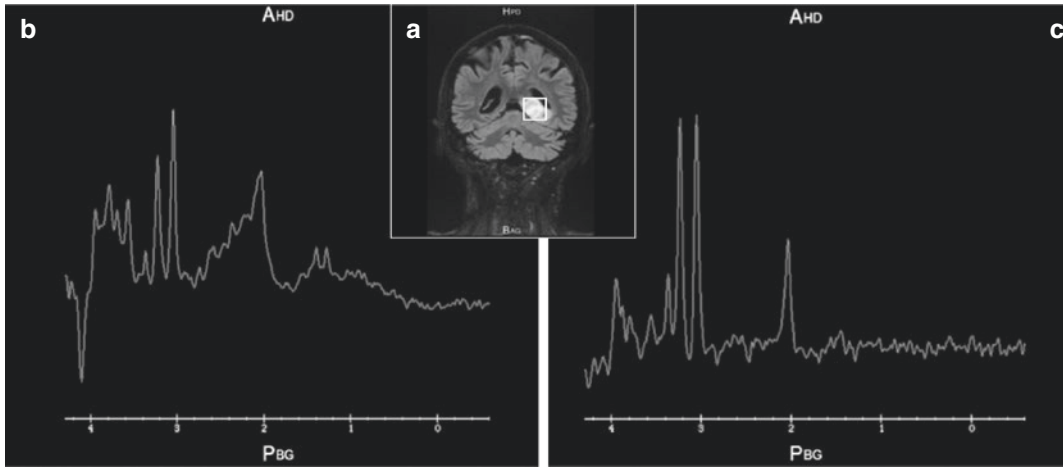

Fig. 5.5 MRI and MRS of a glioblastoma secondary to a glial tumor, with a negative biopsy and no proliferation T2 FLAIR (**a**) with infiltration, no proliferation (TE/TR = 144/2500 ms (**c**)), Glutamine and glycolytic metabolism (MRS TE/TR = 35/1500 ms (**b**)) Glucose - Taurine resonances can be seen around 3.4 ppm. If the glucose peak appears at 5.24 ppm, glucose is predominant

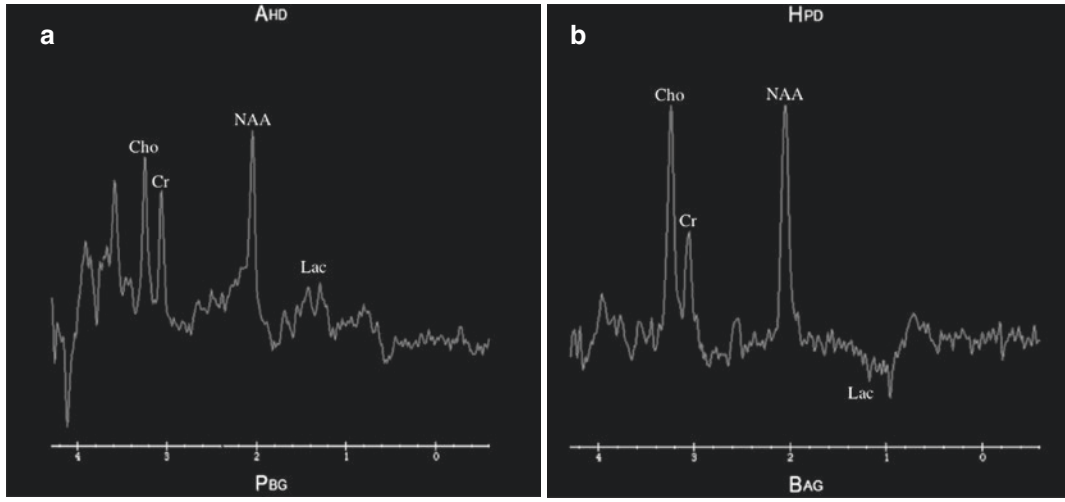

Fig. 5.6 MRI and MRS of a glioblastoma with a negative first biopsy. Although there is no significative infiltration, the proliferation (Cho/Cr at TE/TR = 144/1500 ms (**b**)) and the lactate (TE/TR = 35/1500 ms (**a**) and (**b**)) confirm the metabolic activity in high grade glioma (GBM confirmed by a 2nd biopsy)

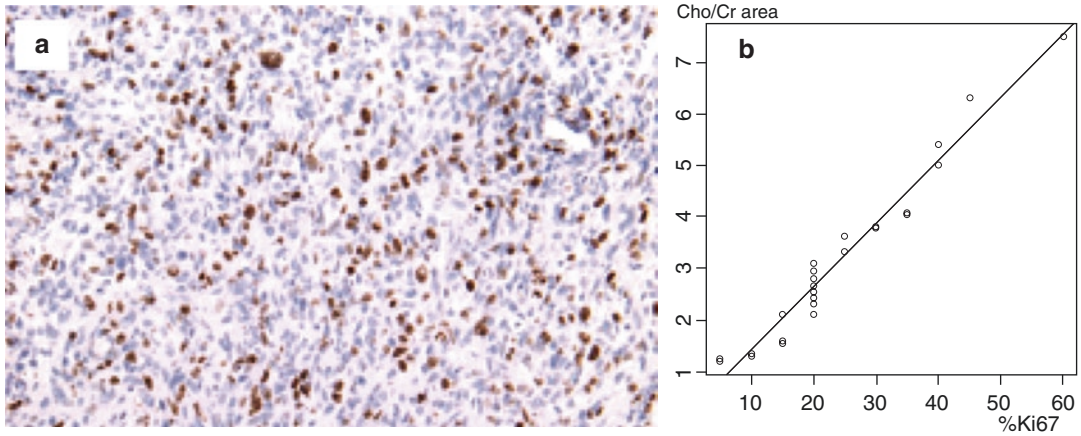

Fig. 5.7 There is good agreement between Ki-67 reflecting the number and percentage of mitosis found in anatomopathology (**a**) and the Cho/Cr ratio (**b**)

It would be useful to do a longitudinal spectral variation follow-up to predict survival, progression, and proliferation (Fig. 5.8), glycolytic (Fig. 5.9) metabolism, and treatment monitoring.

Usefulness of separation of short responders from long responders (Fig. 5.10).

5.5.2 Low- and High-Grade Gliomas

Usefulness of perfusion and spectral profiles in predicting progression or improvement, particularly in low-grade and diffuse infiltrative gliomas (Fig. 5.11).

5.5.3 Metastasis

MRI and MRS are useful for differential diagnosis of multiple lesions (number and size), edema assessment (Fig. 5.12), for treatment, prognosis prediction, and sometimes type of the metastasis.

5.5.4 Lymphoma

Lymphoma (Fig. 5.13) is a differential diagnosis from gliomas [26]. Lymphoma can also be differentiated from toxoplasmosis (Fig. 5.14).

5.5.5 Meningioma

MRS is helpful in the diagnosis of meningioma by showing the presence of alanine and sometimes very low Cr (Fig. 5.15). There are at least five meningioma spectra profile types showing different metabolic activity [16]. MRS could also be useful in following treatment (embolization, surgery, and/or radiation).

5.5.6 Necrotic Tumors

In front of necrotic tumors MRS could be very useful to distinguish abscesses from metastasis and GBM.

5.5.6.1 Abscess

Together with diffusion imaging, MRS with branched amino acid, acetate, and succinate (Fig. 5.16) helps to recognize bacterial abscess.

5.5.6.2 Metastasis

MRS shows usually a very high quantity of necrotic CH2-Phospholipids (Fig. 5.17).

5.5.6.3 Glioblastoma

MRS from GBM shows usually high proliferation and relatively low CH2-Phospholipids before treatment (Fig. 5.18).

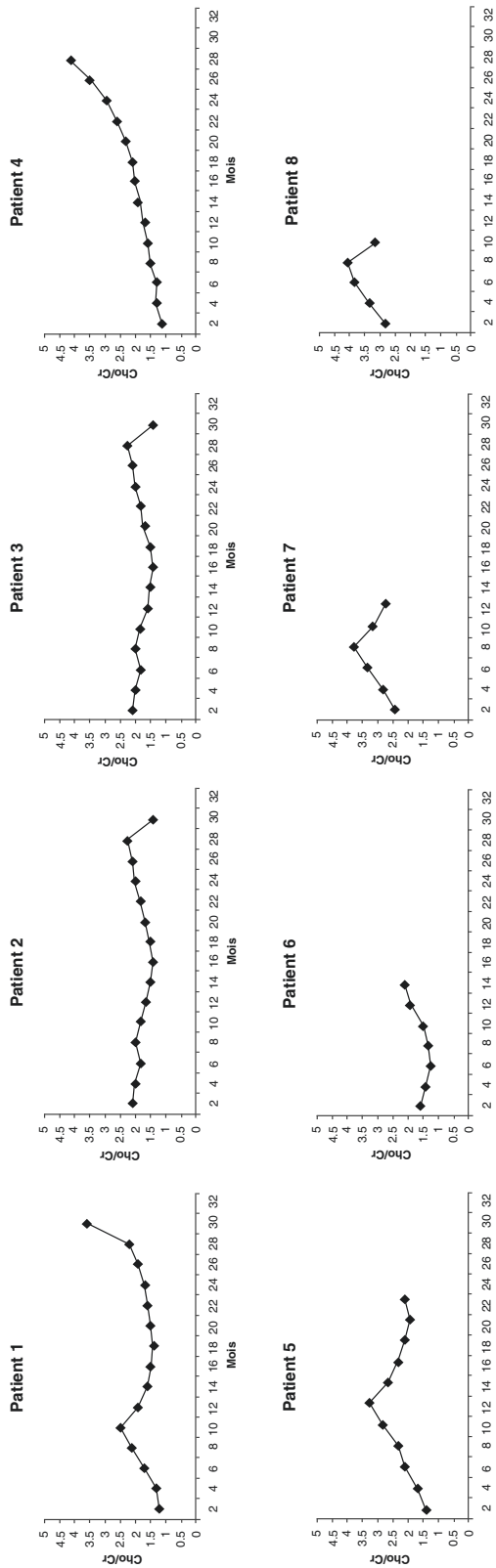

Fig. 5.8 Follow-up of Cho/Cr ratio in 8 patients showing periods of proliferation with increased Cho/Cr ratio in a long period for long responders (patients 1 to 5) and a short period for short responders (patients 6, 7 and 8)

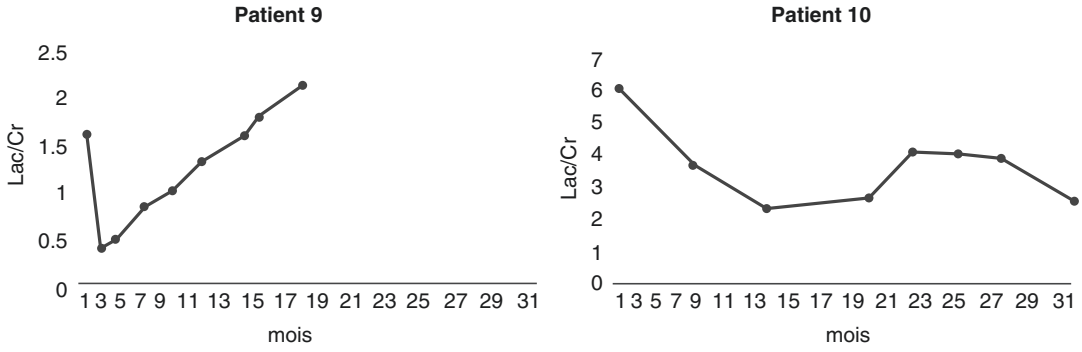

Fig. 5.9 Follow-up of Lac/Cr ratio in 2 patients showing increased and variable glycolytic metabolism

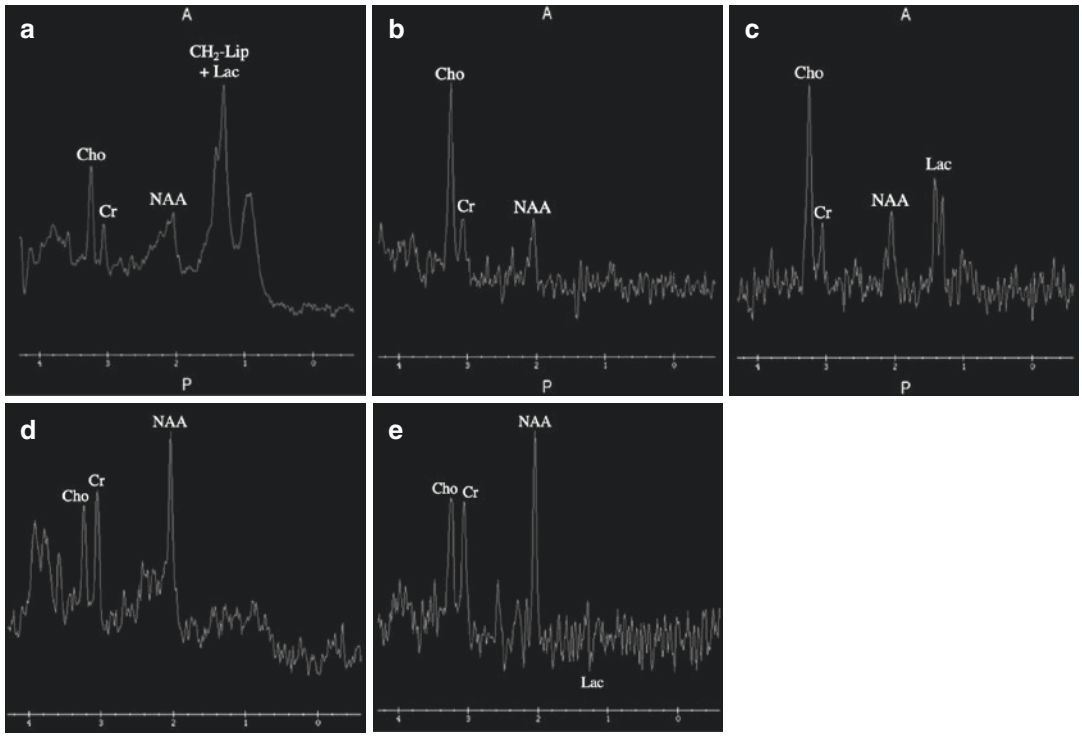

Fig. 5.10 MRS of short responder patient with glioblastoma with high metabolic activity (higher proliferation, higher lactate and glutamine) at TE/TR = 35/1500 ms (**a**); TE/TR = 144/1500 ms (**b**); TE/TR = 288/1500 ms (**c**) Compared to GBM long responder patient TE/TR = 35/1500 ms (**d**) and TE/TR = 144/1500 ms (**e**) without proliferation or high lactate

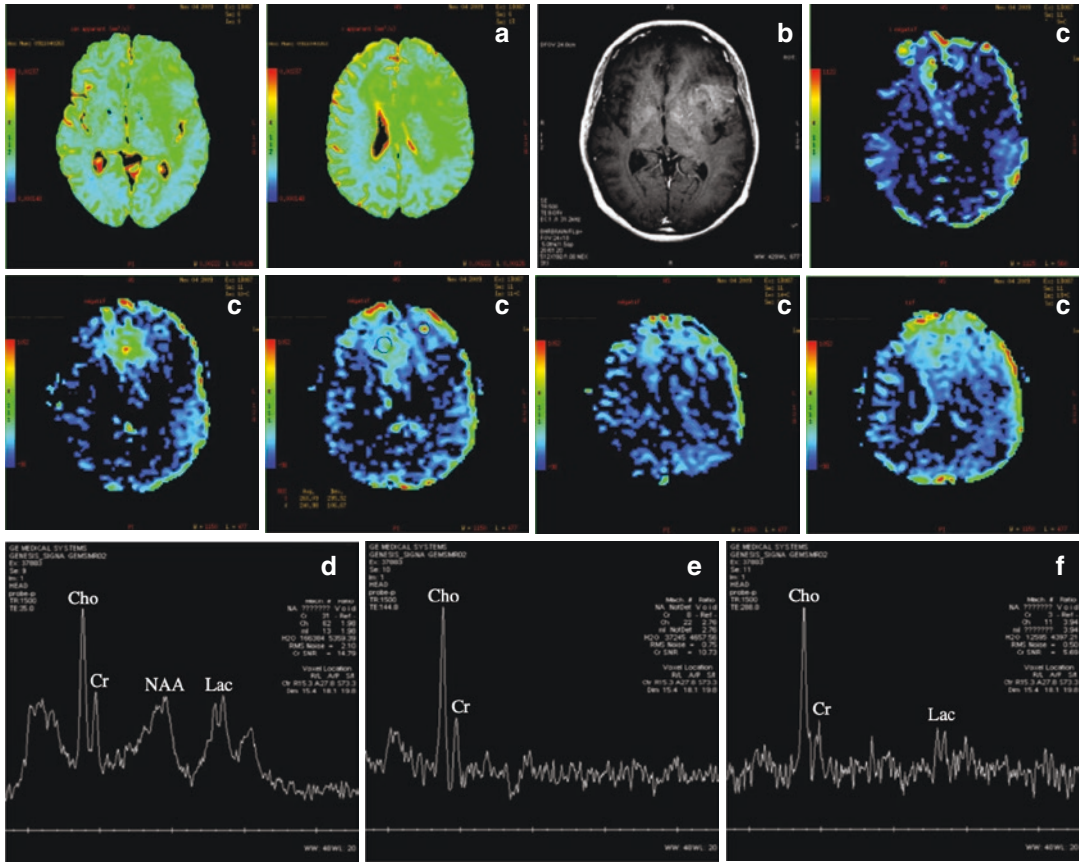

Fig. 5.11 Stability of ADC map (**a**), Disappearance of significative contrast enhancement (**b**) and not any more hyper perfusion (**c**) under antiangiogenics, but with persistence of glycolytic metabolism followed by increased proliferation. (TE/TR = 35/1500 ms (**d**); TE/TR = 144/1500 ms (**e**); TE/TR = 288/1500 ms (**f**))

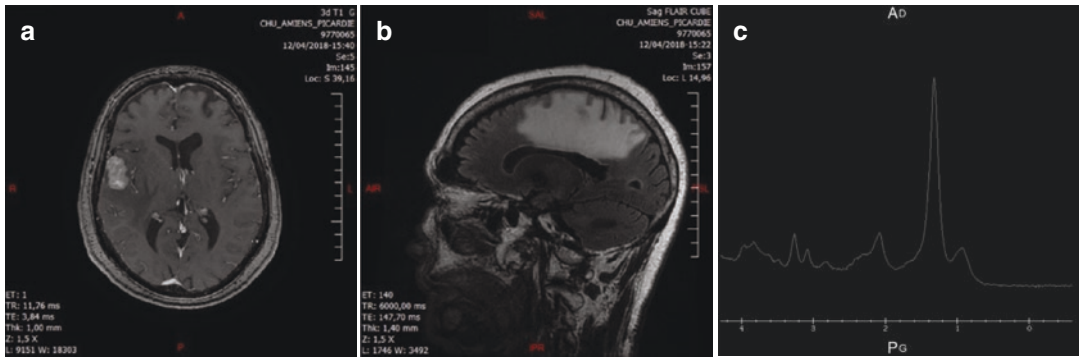

Fig. 5.12 MRI of metastasis (**d**), (**e**) and (**f**) images were done 3 months after (**a**), (**b**) and (**c**) Hyper Signal FLAIR (Edema) is reduced due to Cyber Knife treatment (like the proliferation, the CH2-Phospolipids and the Glx in the metastasis spectra)

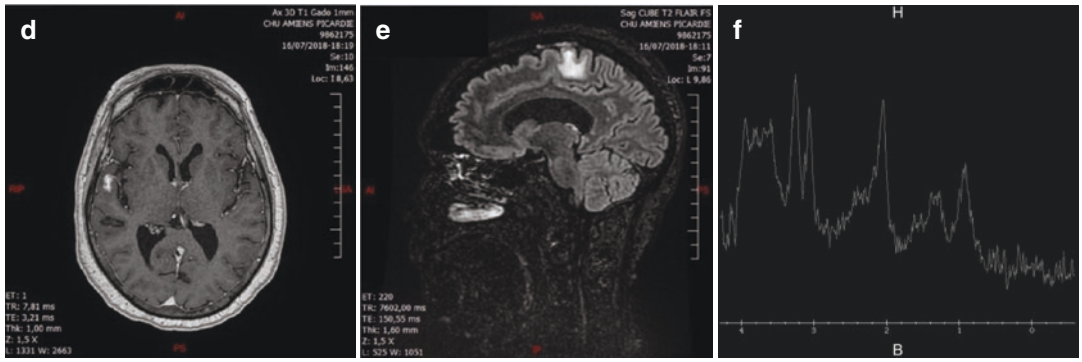

Fig. 5.12 (continued)

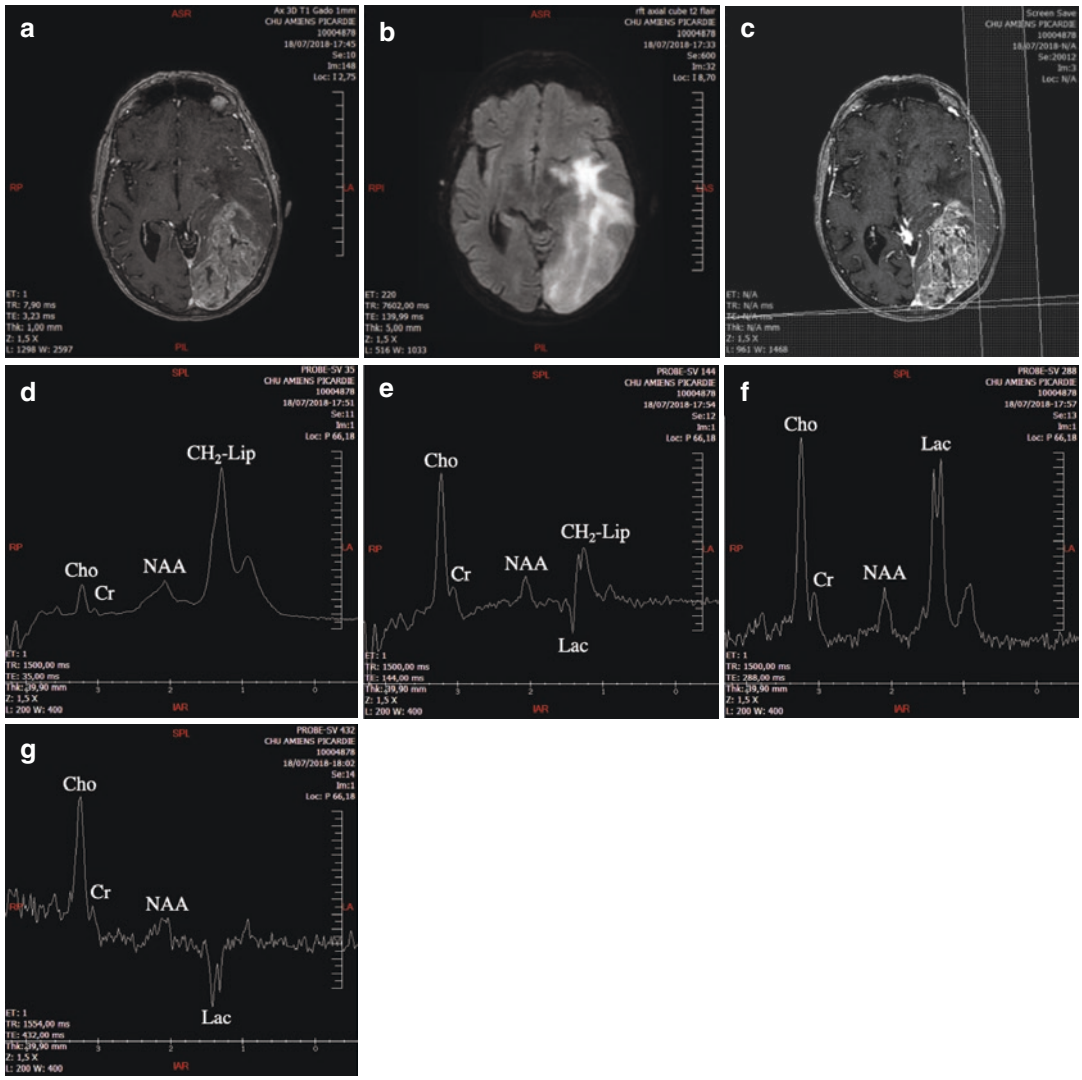

Fig. 5.13 MRS of patient with lymphoma at Tl gado (**a**); Axial FLAIR (**b**); Voxel placement with saturation bands (**c**); 1H-NMR Spectroscopy at TE/TR = 35/1500 ms (**d**); 144/1500 ms (**e**); 288/1500 ms with high lactate (**f**); 432/1554 ms (**g**)

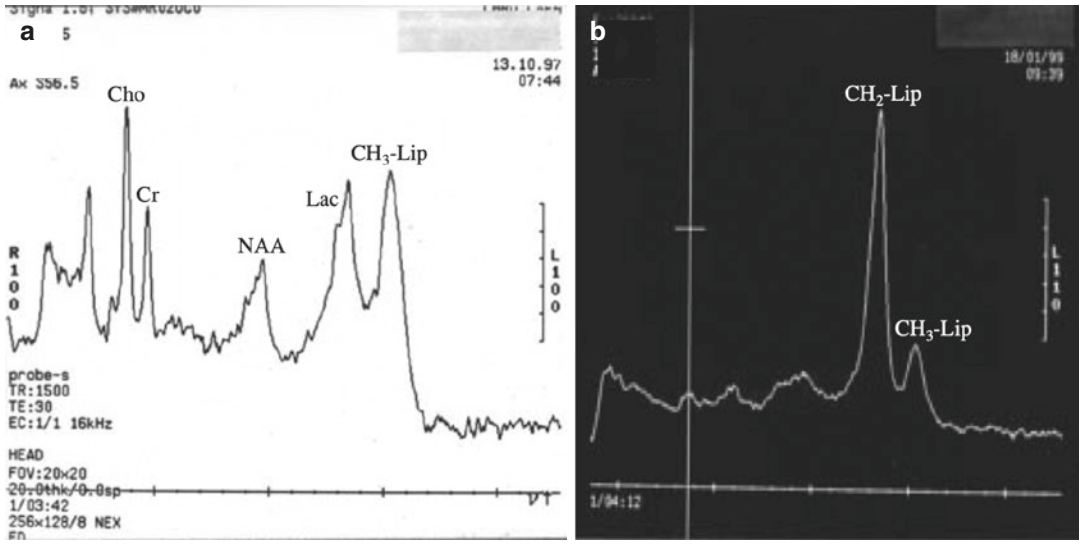

Fig. 5.14 When necrosis is present: More lactate at 1.27–1.33 ppm and CH3 lipids (0.9 ppm) in Lymphoma at TE/TR = 35/1500 ms (**a**); More CH_2-Lipids in necrotic toxoplasmosis (**b**). The lactate doublet (**a**) can be seen on the left of the CH2 lipids resonances

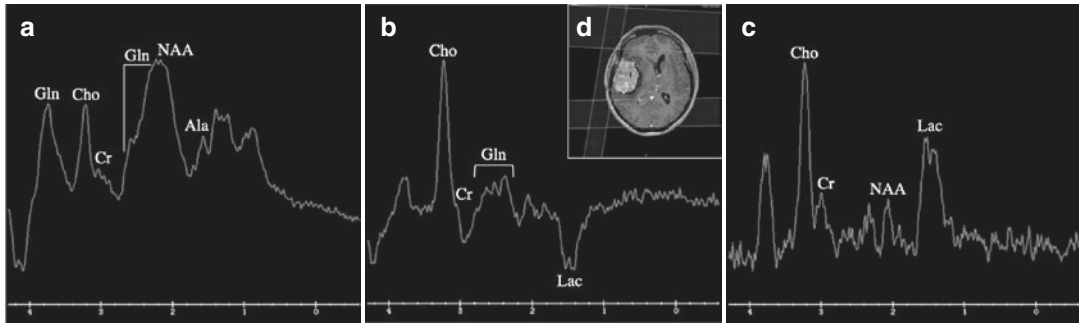

Fig. 5.15 Spectra from a meningioma at TE/TR = 35/1500 ms (**a**); TE/TR = 144/1500 ms (**b**); TE/TR = 288/1500 ms (**c**); Axial T1 Gado (**d**) Alanine is detected at 1.47 ppm (to the left of Lactate) at TE = 35 ms In this type of menigioma, glutamine is very high and creatine is very low

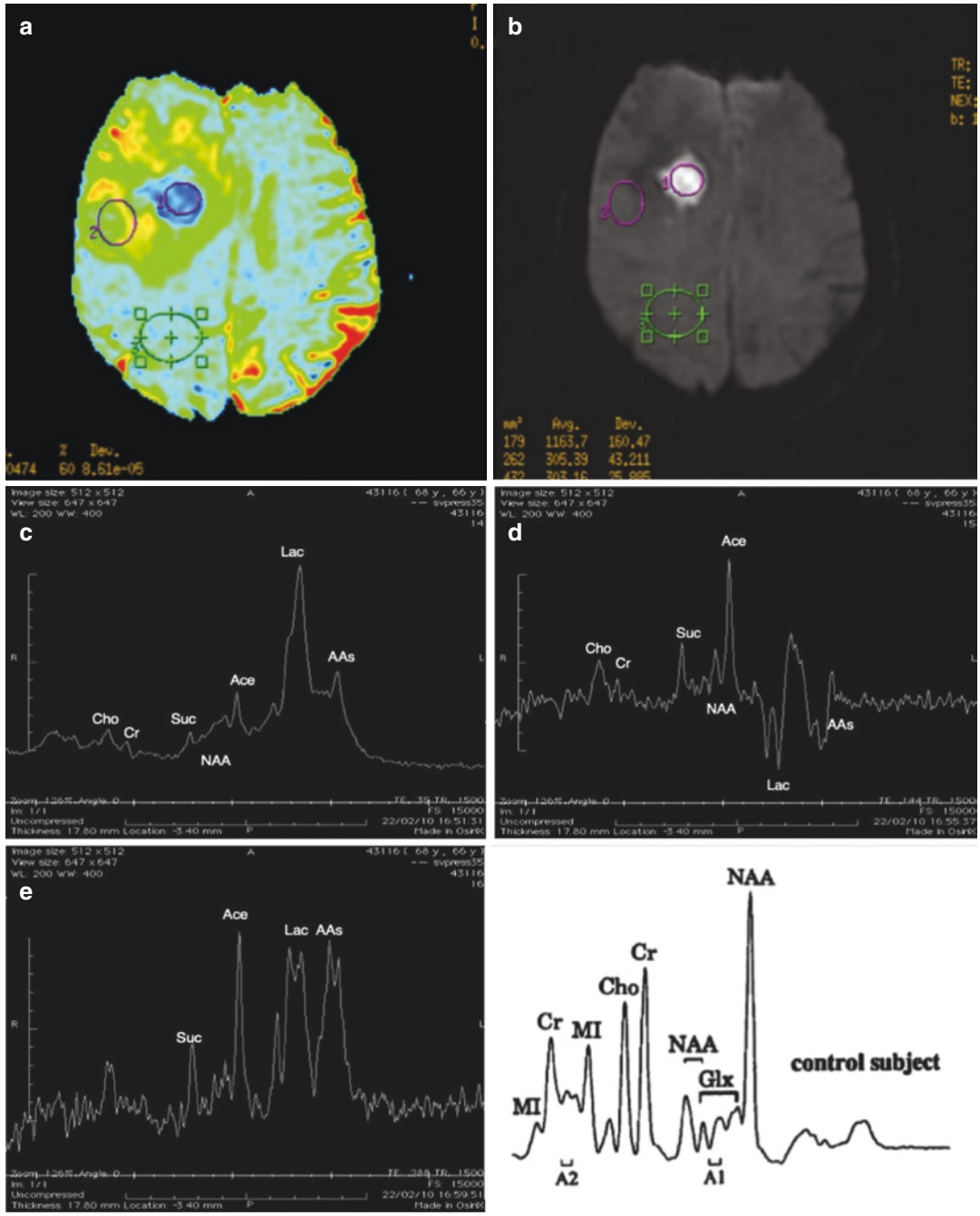

Fig. 5.16 ADC (**a**) and diffusion imaging (**b**), MRS from a necrotic bacterial abscess (TE/TR = 35/1500 ms (**c**); TE/TR = 144/1500 ms (**d**); TE/TR = 288/1500 ms (**e**)) and normal spectra from a healthy control subject (**f**). The abscess spectra are not normal. Very high resonances of acetate, lactate, and branched amino acids (leucine, isoleucine, and valine) that are coupled (positive at TE = 35 ms (**c**), negative at TE = 144 ms (**d**) and again positive at TE = 288 ms (**e**) are seen. Acetate and branched amino acids specific for bacterial abscesses are seen. In addition, the elevated succinate resonance seen here are indicative of anaerobic bacteria

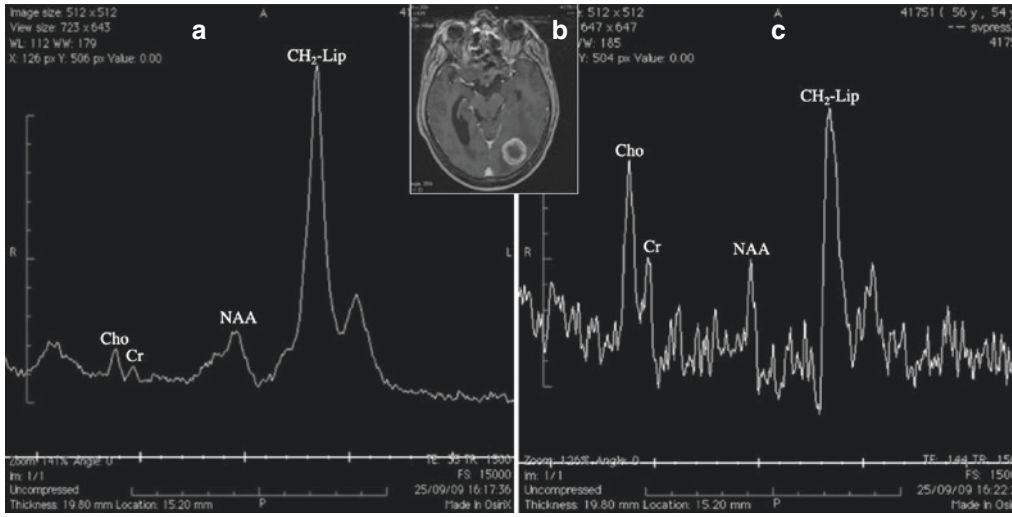

Fig. 5.17 TE/TR = 35/1500 ms (**a**) and TE/TR = 144/1500 ms (**c**) from a metastasis with a typical MRI appearance (**b**). There is a very high quantity of necrotic CH2-PhosphoLipids (CH_2-Lip/Cr ratio greater than 24 (**a**)) and a Cho/Cr ratio less than 3 (**c**)

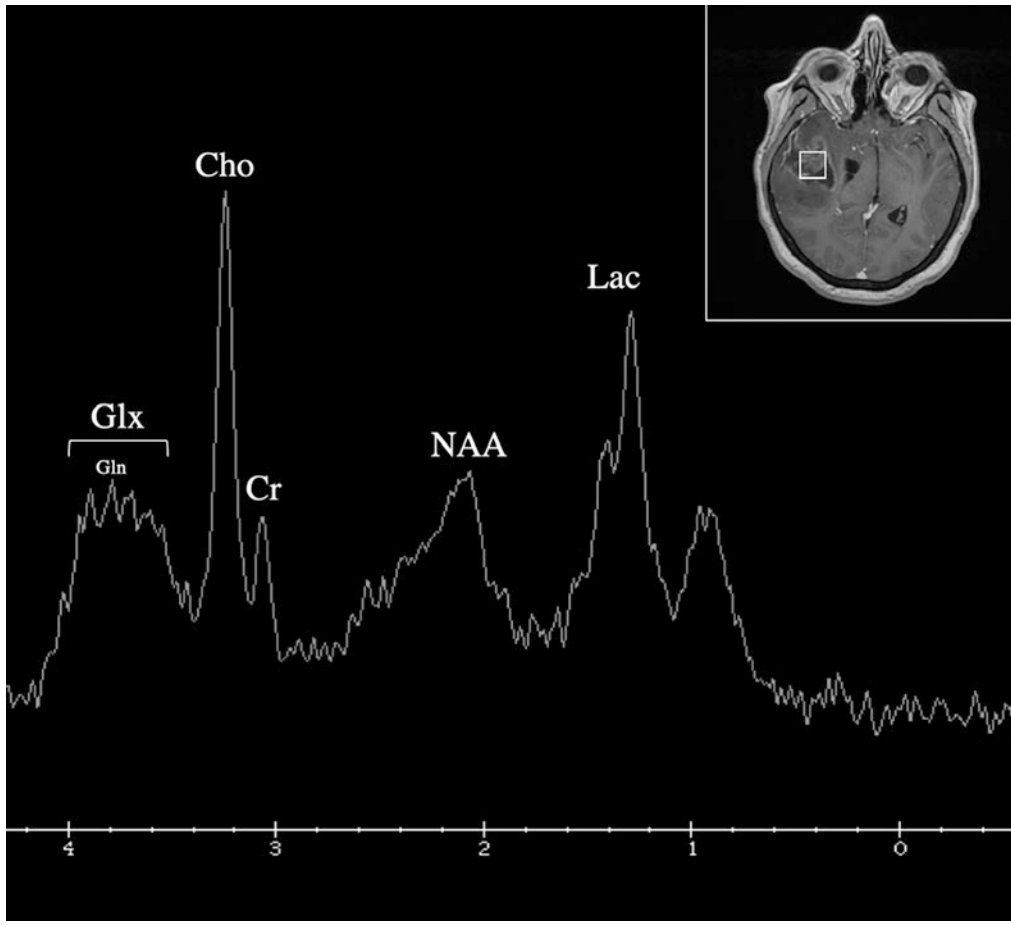

Fig. 5.18 TE/TR = 35/1500 ms spectrum from a GBM. High Cho/Cr ratio (over 4), high Glx and glutamine, high lactate (Lac/Cr over 2), and low CH_2-Lip/Cr (under 2) are seen

Table 5.3 Main and frequent ratio variations for the most frequently encountered brain tumors

Pathologies	MRS main metabolites ratios variations found
GBM	– Proliferation: • Cho/Cr >3 → High • Cho/Cr <1.8 → Stable or in regression – Glycolytic metabolism: • High Lac/Cr (288 ms) • High Glc/Cr (35 ms) – Glutaminergic metabolism: • High Gln/Cr (35 ms) • High Glx/Cr (35 ms) – High CH2PLip/Cr (>2) before treatment (35 ms) – Short responder (versus long responder): • Higher Cho/Cr, Glc/Cr (35 ms), and Lac/Cr (288 ms) • Higher Lip/Cr before treatment (35)
High- and low-grade gliomas	– Low grade: • Cho/Cr >1.5 • NAA/Cr >1.2 • Lac/Cr <0.5 (288 or 35 ms) • mI/Cr <0.9 (35 ms) – High grade: • Cho/Cr >3 • NAA/Cr <0.8 • Lac/Cr >2 (35 ms) • mI/Cr >1 (35 ms)
Lymphoma	– CH2Lip/Cr and CH3Lip/Cr high (35 ms) – Lac/Cr high (288 ms) – mI/Cr <0.9 (35 ms)
Meningiomas	– Ala/Cr >0.4 (35 ms) – Glx/Cr >2 (35 ms) – Lac/Cr >1 (288 ms) – Low creatine (Cr/Cho <0.3)
Necrotic tumors (metastasis and glial)	– Tumoral necrosis (metastasis) • CH2Lip/Cr >15 (35 ms) – Tumoral necrosis (glial) → • 10 >CH2Lip/Cr >5 (35 ms) • Cho/Cr >3

If TE is not indicated, it is a TE = 144 ms ratio

5.5.7 Summary of Main Metabolite Ratios Variations

Table 5.3 shows the summary of the main metabolite ratios variations found for the most frequently encountered brain tumors.

References

1. Weybright P, et al. Differentiation between brain tumor recurrence and radiation injury using MR spectroscopy. AJR Am J Roentgenol. 2005;185(6):1471–6.
2. Herminghaus S, et al. Increased choline levels coincide with enhanced proliferative activity of human neuroepithelial brain tumors. NMR Biomed. 2002;15(6):385–92.
3. Ott D, et al. Human brain tumors: assessment with in vivo proton MR spectroscopy. Radiology. 1993;186(3):745–52.
4. Bruhn H, et al. Noninvasive differentiation of tumors with use of localized H-1MR spectroscopy in vivo: initial experience in patients with cerebral tumors. Radiology. 1989;172(2):541–8.
5. Yablonskiy DA, et al. Homonuclear J coupling effects in volume localized NMR spectroscopy: pitfalls and solutions. Magn Reson Med. 1998;39(2):169–78.
6. Lange T, et al. Pitfalls in lactate measurements at 3T. AJNR Am J Neuroradiol. 2006;27(4):895–901.
7. Griffin JL, et al. Metabolic profiles of cancer cells. Nat Rev Cancer. 2004;4(7):551–61.
8. Pfeuffer J, et al. Extracellular-intracellular distribution of glucose and lactate in the rat brain assessed non-invasively by diffusion-weighted 1H nuclearmagnetic resonance spectroscopy in vivo. J Cereb Blood Flow Metab. 2000;20(4):736–46.
9. Fan G, et al. In vivo single-voxel proton MR spectroscopy in the differentiation of high-grade gliomas and solitary metastases. Clin Radiol. 2004;59(1):77–85.
10. Michaelis T, et al. On the identification of cerebral metabolites in localized 1H NMR spectra of human brain in vivo. NMR Biomed. 1991;4(2):90–8.
11. Constans JM, et al. Importance of early spectral variations during 61 months of longitudinal follow MRI and MRS in 100 patients treated glioblastomes. In: ISMRM. 2018.
12. Hakumäki JM, et al. 1H-MRS detects poly unsaturated fatty acid accumulation during gene therapy of glioma: implications for the in vivo detection of apoptosis. Nat Med. 1999;5(11):1323–7.
13. Lehtimäki KK, et al. Metabolite changes in BT4C rat gliomas undergoing ganciclovir-thymidine kinase gene therapy-induced programmed cell death as studied by 1H NMR spectroscopy in vivo, ex vivo, and in vitro. J Biol Chem. 2003;278(46):45915–23. Epub 2003 Sept 3.
14. Kovanlikaya A, et al. Untreated pediatric primitive neuroectodermal tumor in vivo: quantitation of taurine with MR spectroscopy. Radiology. 2005;236(3):1020–5.
15. Blüml S, et al. Elevated citrate in pediatric astrocytomas with malignant progression. Neuro-Oncology. 2011;13(10):1107–17. Epub 2011 Jul 19. https://doi.org/10.1093/neuonc/nor087.

16. Constans JM, et al. 1H MRS of meningiomas before and after embolization. J Neuroradiol. 2002;29(HS 1):157–8.
17. Arias-Ramos N, et al. Metabolomics of therapy response in preclinical glioblastoma: a multi-slice MRSI-based volumetric analysis for non-invasive assessment of temozolomide treatment. Metabolites. 2017;7(2):E20. https://doi.org/10.3390/metabo7020020.
18. Constans JM, et al. Five-year longitudinal MRI follow-up and 1H single voxel MRS in 14 patients with gliomatosis treated with temodal, radiotherapy and antiangiogenic therapy. Neuroradiol J. 2011;24(3):401–14.
19. Tafreshi NK, et al. Carbonic anhydrase IX as an imaging and therapeutic target for tumors and metastases. Subcell Biochem. 2014;75:221–54.
20. Duran A, et al. P07.02 Diagnostic pitfalls in brainstem lesions mimicking gliomas in adults. Neuro-Oncology. 2016;18(Suppl 4):iv33–4.
21. Mishra AM, et al. Role of diffusion-weighted imaging and in vivo proton magnetic resonance spectroscopy in the differential diagnosis of ring-enhancing intracranial cystic mass lesions. J Comput Assist Tomogr. 2004;28(4):540–7.
22. Hanafi R, et al. Variations spectrales et IRM aident à différencier métastases et abcès dans les processus expansifs cérébraux nécrotiques. In: SFNR 2017 congres.
23. Delgado-Goñi T, et al. Molecular imaging coupled to pattern recognition distinguishes response to temozolomide in preclinical glioblastoma. NMR Biomed. 2014;27(11):1333–45. Epub 2014 Sept 10. https://doi.org/10.1002/nbm.3194.
24. Constans JM, et al. Effects of reactive oxygen species on metabolism monitored by longitudinal 1H single voxel MRS follow-up in patients with mitochondrial disease or cerebral tumors. J Phys Conf Ser. 2011;261:012011.
25. Loriguet L, et al. Combining genomic analyses with tumour-derived slice cultures for the characterization of an EGFR-activating kinase mutation in a case of glioblastoma. BMC Cancer. 2018;18(1):964. https://doi.org/10.1186/s12885-018-4873-9.
26. Hakumäki JM, et al. 1H MRS detects polyunsaturated fatty acid accumulation during gene therapy of glioma: implications for the in vivo detection of apoptosis. Nat Med. 1999;5(11):1323–7.

6 Diffusion Tensor Imaging and Functional Magnetic Resonance in Brain Tumor Imaging

Ömer Kitiş and Sevcan Türk

6.1 Introduction

The main goal of brain tumor surgery is to remove the mass as completely as possible while ensuring minimal neurological deficits. For this reason, prior to surgery, neurosurgeons must be able to recognize associations between the tumor and specific eloquent cortical areas (such as the motor-sensory cortex, speech center, visual cortex, and dominant hemisphere) as well as important white matter (WM) tracts (such as the corticospinal tract and arcuate fasciculus) (Table 6.1). Functional magnetic resonance imaging (fMRI) and diffusion tensor imaging (DTI) can provide sufficient data in this respect, and these modalities are preferable to other modalities of assessment. fMRI enables the noninvasive localization and lateralization of specific areas of brain function via the measurement of local hemodynamic changes coupled with neuronal activation. On the other hand, DTI also presents valuable imaging data via the estimation of major WM bundles. The advantages of both fMRI and DTI are their noninvasiveness, lack of ionizing radiation, data reproducibility, and practicality due to the broad availability of MRI scanners [1–8].

Table 6.1 The main goals of neuroimaging for presurgical planning

• Demonstrating the anatomic relationship between the area of surgery and the eloquent cortex as well as major WM fibers
• Determining the relationship between the brain tumor and the eloquent cortex as well as major WM fibers
• Identifying the dominant hemisphere
• Investigating the neuronal plasticity of specific brain functions

6.2 DTI

Because the surgical injury of WM tracts can result in significant permanent neurologic deficits, neurosurgeons generally employ tractography in routine preoperative planning. The most common identification method for WM tracts is DTI, which measures the direction of the diffusion of water molecules in order to locate the axis of these tracts. DTI presumes that axonal membranes and myelin directionally restrict the diffusion of water. In brain tissue, most water molecules move parallel to fiber tracts, which results in anisotropic diffusion in regions of tightly packed WM bundles. Conversely, these molecules disperse equally in all directions (isotropic) in cerebrospinal fluid (CSF) and gray matter. In DTI, magnetic gradients are applied in at least six directions. The diffusion tensor is calculated via a mathematical model that estimates the direction of maximum diffusivity of water molecules for each voxel, which corresponds to the main axis of

Ö. Kitiş (✉) · S. Türk
School of Medicine, Ege University, Bornova, Izmir, Turkey

Y. Özsunar, U. Şenol (eds.), *Atlas of Clinical Cases on Brain Tumor Imaging*,
https://doi.org/10.1007/978-3-030-23273-3_6

WM tracts in the respective location. DTI-based tractography—a three-dimensional mapping algorithm of WM tracts obtained by diffusion-weighted imaging (DWI)—is the most common neuroimaging technique used to reveal WM structure (Fig. 6.1). From DWI signals, it is possible to generate an anisotropic map showing WM tracts, their orientations, and their relation to possible brain lesions. DTI can successfully determine major WM tracts, including the corticospinal, corticobulbar, and corticopontine tracts; arcuate fasciculus (AF), uncinate fasciculus, superior and inferior occipitofrontal fasciculi, and occipitotemporal fasciculus; optic radiation; corpus callosum; cingulum; and anterior commissure. The corticospinal tract (CST) and AF are the most important WM pathways most commonly investigated by DTI-based tractography because of their importance to motor functions and language, respectively [1, 3, 4, 7].

DTI is a relatively stable method since it is neither user-dependent nor task-based. However, one of its disadvantages is its relatively long acquisition time, meaning that movement artifacts can affect image quality. Although DTI acquisition time depends on many parameters such as the number of gradient directions, imaging matrix, slice thickness, and number of acquisition, it can nevertheless be obtained at acceptable image quality within 3–4 min on a 3 T MRI scanner.

6.2.1 Alteration of DTI Patterns in WM Tracts by Tumors

The major effects of brain tumors on WM tracts include deviation, infiltration, and disruption (Figs. 6.2 and 6.3). Jellison et al. have described four major patterns in affected WM tracts categorized on the basis of anisotropy and fiber direction

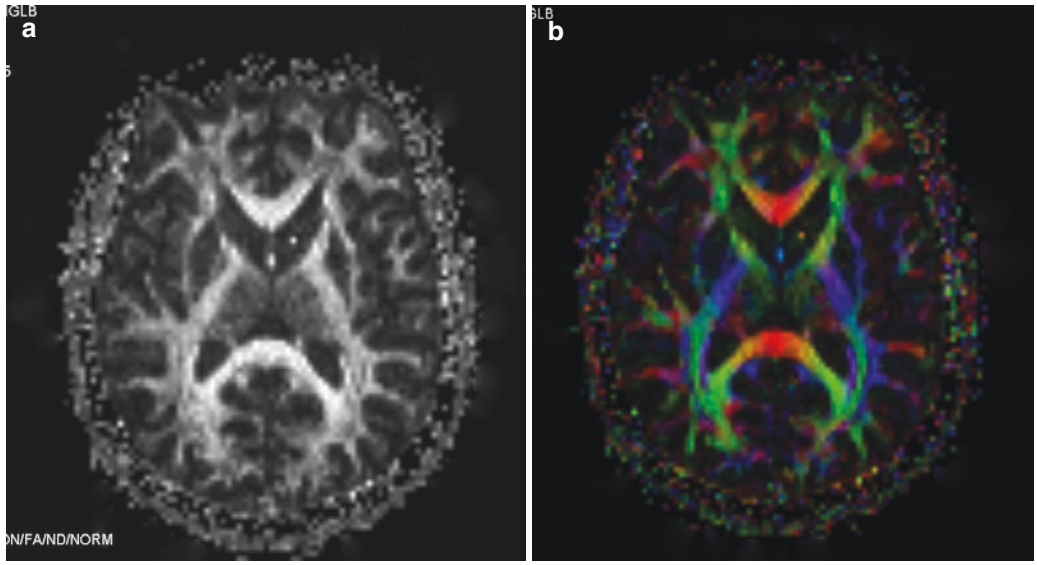

Fig. 6.1 DTI data set from a normal control case. (**a**) Gray-scale FA map showing the degree of anisotropy. Brighter areas (higher FA values) contain more anisotropy than darker areas (lower FA). (**b**) Color-coded FA map providing information regarding diffusion direction by using the largest eigenvalue within the voxel. The color red is used to indicate diffusion along the left/right axis, green for diffusion along the anterior/posterior axis, and blue for diffusion along the inferior/superior axis. (**c**) 3D fusion images including a color-coded FA map superimposed on 3D anatomical T1-weighted (MP-RAGE sequence) images. (**d**) DTI-based fiber tracking. The left CST (yellow arrows) has been reconstructed from DTI data by choosing a seed point at the level of cerebral peduncle. (**e**) 3D fiber tractography of the right AF (yellow arrows)

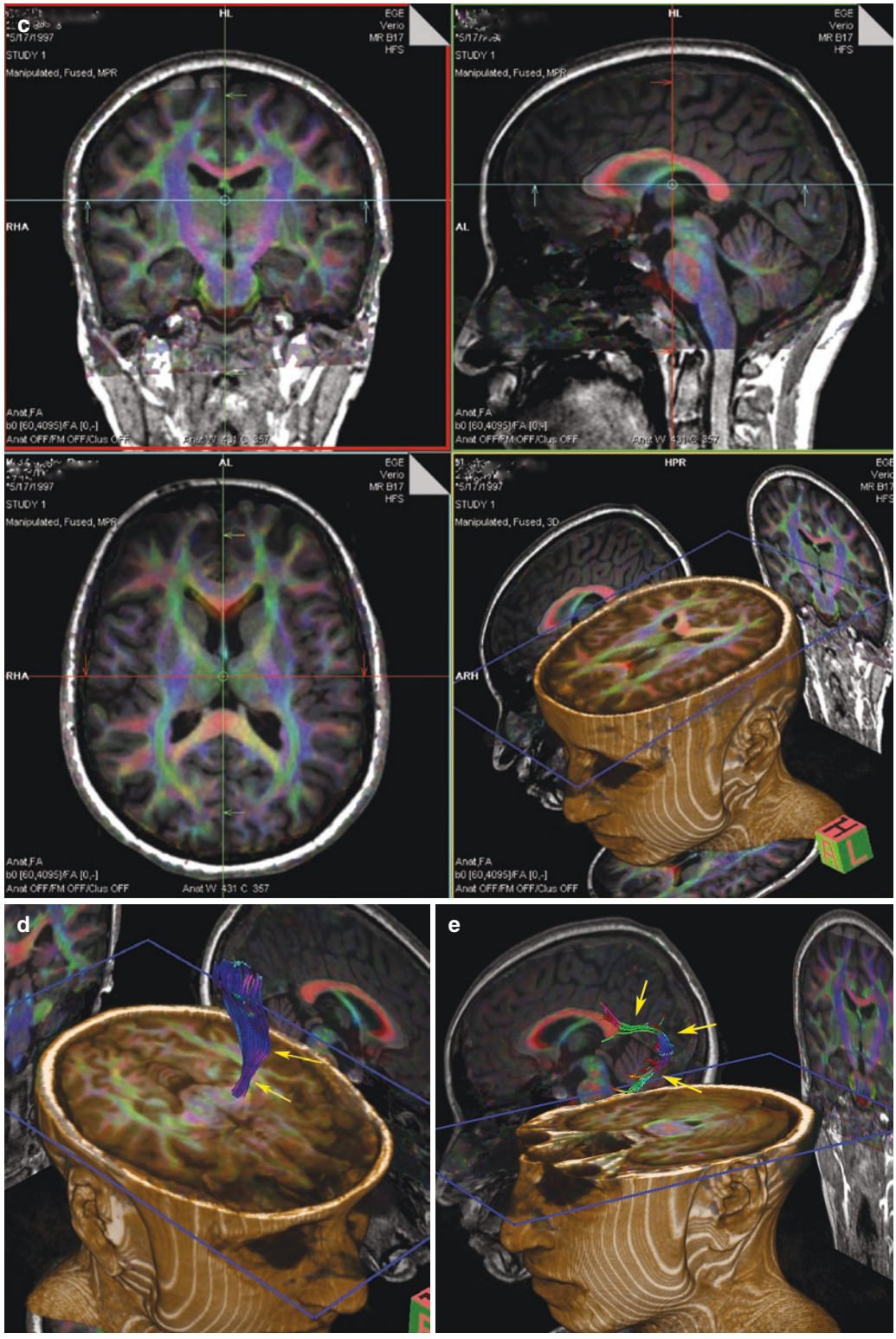

Fig. 6.1 (continued)

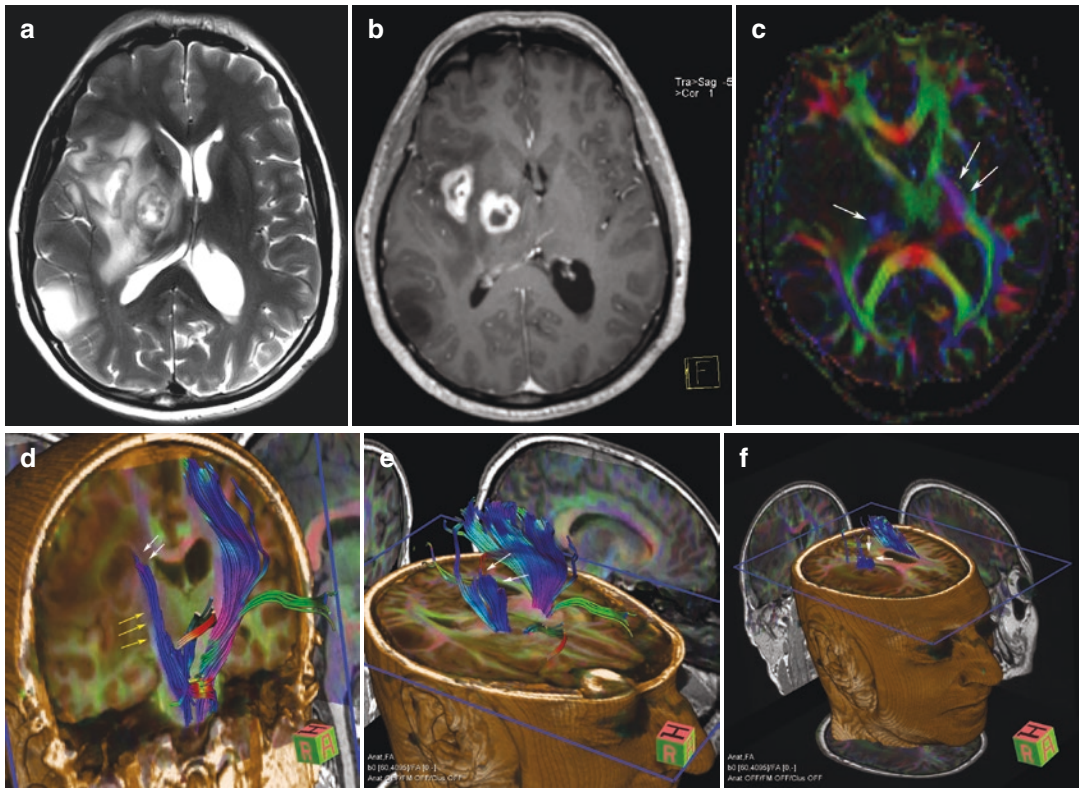

Fig. 6.2 A patient with multicentric glioblastoma in the right hemisphere. This patient complained of left hemiparesis, which had been caused by the infiltration of the tumor in the right posterior capsula interna. (**a**, **b**) Indicate right multicentric contrast-enhancing masses infiltrating the right basal ganglia and occipitotemporal cortex. (**c**) Involves a color-coded FA map which reveals the marked tumoral disruption of anisotropy in the infiltrated parenchyma. On the left side, normal CST (white arrows) is represented by magenta. However, the right CST (white arrow) appears in blue, secondary to the disruption of anisotropy. (**d**–**f**) Contain DTI tractography images, which show the displacement (yellow arrows) and interruption (white arrows) of the CST bundles

or orientation [4]. Pattern 1 involves normal or only slightly decreased fractional anisotropy (FA) with abnormal location and/or direction resulting from the mass effect of the tumor. This means that WM tracts are intact and can be preserved during surgery. Pattern 2 is typified by decreased FA with normal location and direction. This pattern is frequently observed in the vasogenic edema surrounding tumors such as metastases or meningiomas. Pattern 3 entails substantially decreased FA with abnormal hues on directional color maps. This pattern can be found in a small number of infiltrating gliomas. Finally, Pattern 4 involves isotropic (or near-isotropic) diffusion such that the tract cannot be identified on directional color maps. This pattern is observed when a part of a tract is completely disrupted by a tumor.

In addition to fiber tractography, DTI also enables the measurement of various parameters—such as the shape, magnitude, and degree of diffusion anisotropy—which may be used to differentiate brain tumors. DTI metrics such as mean diffusivity (MD), linear anisotropy coefficient (CL), planar anisotropy coefficient (CP), spherical anisotropy coefficient (CS), and FA can be used individually or in combination for brain tumor classification. However, these metrics play a limited role in the differentiation of brain tumors. Relatively newer and more advanced diffusion techniques such as diffusion kurtosis imaging (DKI) and diffusion spectrum imaging (DSI) may provide additional information [3] in this regard.

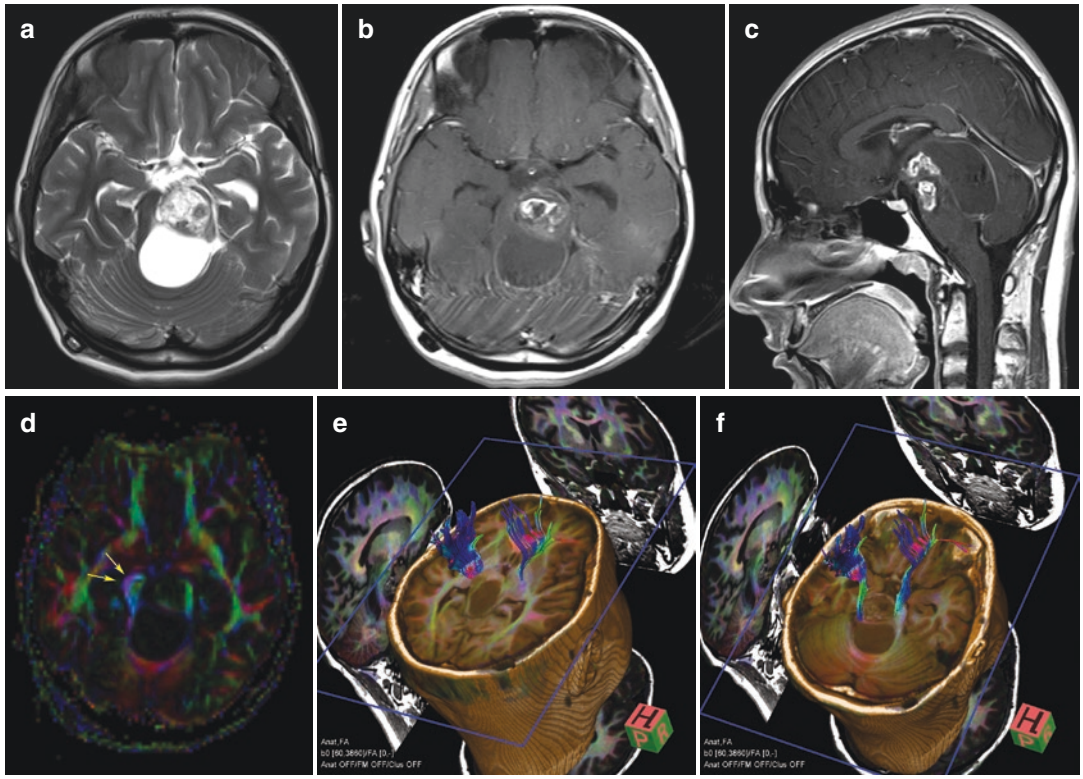

Fig. 6.3 Sixteen-year-old girl with brain stem glioma (pilocytic astrocytoma). A large mass containing a posterior cystic component and contrast-enhancing solid portions was observed in the brainstem (**a**–**c**) of this patient, the cyst had obliterated the fourth ventricle. A neurosurgeon advised an examination of the CST in order to assess the anatomic relation of the tumor to the CST inside the brainstem. A color-coded FA map (**d**) displays the right CST (yellow arrows) in magenta, but this was not visible on the left due to compression and a decrease in anisotropy. DTI tractography (**e**, **f**) revealed the exact bilateral location of CST fibers and anatomic relation to the tumor. In this case, tractography was enabled to plan an appropriate preoperative approach and safe surgical trajectory to neurosurgeon

6.3 fMRI

Blood-oxygen-level-dependent fMRI (BOLD fMRI) is a noninvasive brain mapping method that enables the indirect measurement of neuronal activity as a consequence of neurovascular coupling. During neuronal activation, local cerebral blood flow (CBF) increases with a consequent increase in oxyhemoglobin and decrease in deoxyhemoglobin concentration in venules. These molecular changes cause the transient distortion of local magnetic field homogeneity, and this effect can be detected by T2* gradient echo sequences. While oxyhemoglobin is diamagnetic, deoxyhemoglobin is a paramagnetic molecule. Since the increase in oxyhemoglobin is greater than the decrease in deoxyhemoglobin, the diamagnetic effect dominates local signal changes. This phenomenon results in the increase of transient T2* signals (BOLD signals) within the activated cerebral cortex. Since the magnitude of the BOLD signal is only around 2–4% at 1.5 T and 4–8% at 3 T, it is necessary to create multiple resting and activation conditions in order to detect activation-related signals and exclude noise [2].

fMRI examinations are performed using event-related and block-design paradigms, which consist of sensorimotor, cognitive, and visual tasks. In routine clinical practice, block-design fMRI is widely used due to its high

signal detection capability, easier design and implementation, and better patient participation. Neurosurgeons commonly advise patients with brain tumors to seek preoperative evaluation of the motor cortex and language lateralization in order to determine the exact anatomic location of the tumor and its association with eloquent brain regions.

6.3.1 Paradigms for the Primary Motor Cortex

Common paradigms used for the primary motor area are relatively easy tasks such as finger-tapping and tongue- and foot movement (Figs. 6.4 and 6.5). In most cases, patients can perform these tasks successfully, and these

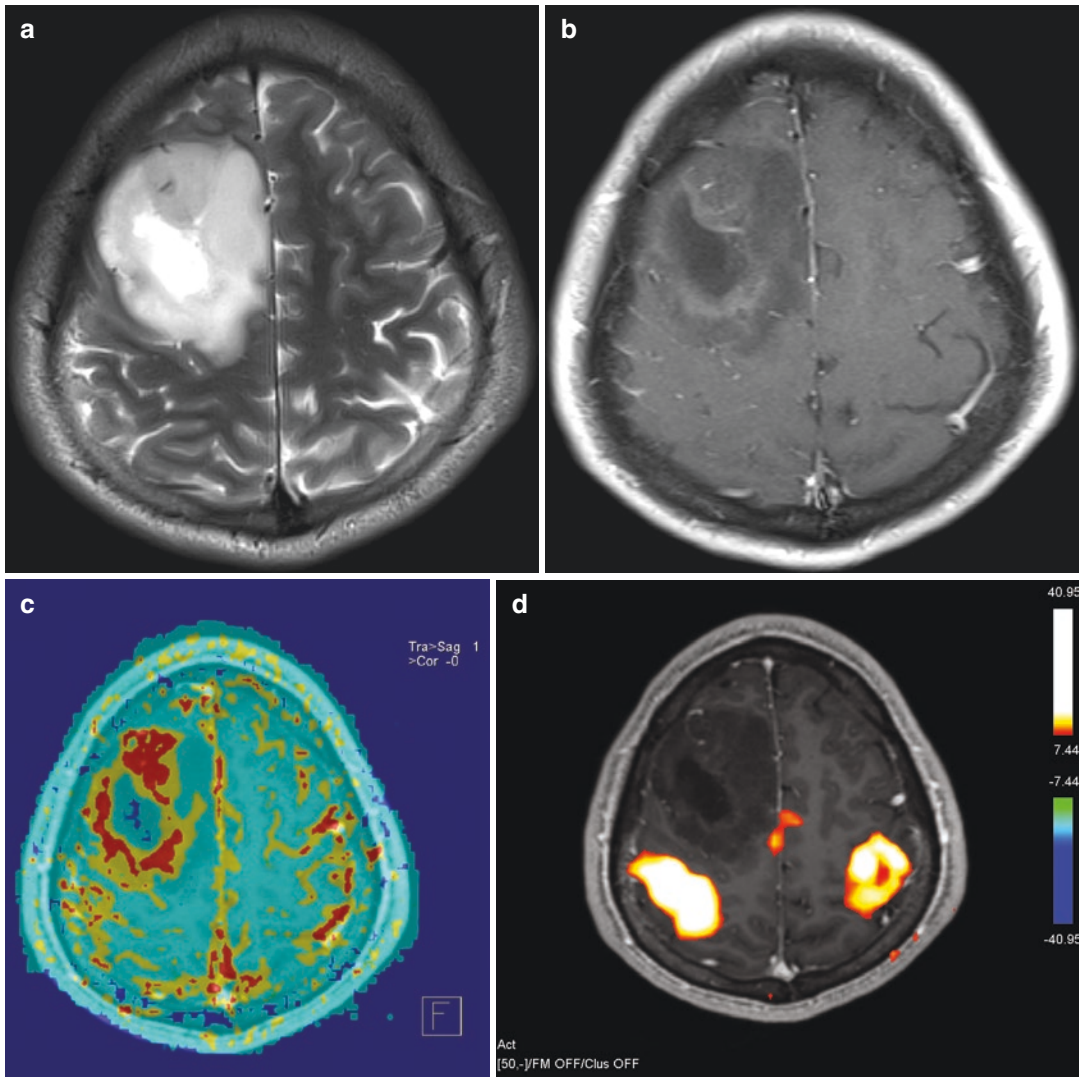

Fig. 6.4 These images indicate a right frontal mass possessing heterogeneity and moderate enhancement (**a**, **b**). The tumor displayed high perfusion (increased cerebral blood volume) on a relative cerebral blood volume (r-CBV) map (**c**, perfusion MRI), which is consistent with high grade. Since the tumor was located in the anterior Rolandic area, motor fMRI (finger-tapping) was conducted to identify the relation of the tumor to the eloquent motor cortex. fMRI activation maps overlaid with T2 and 3D T1-weighted images (**d**–**h**) reveal that there was no invasion in the motor-sensory cortex. Normal parenchyma can be seen between the tumor and adjacent precentral gyrus. On sagittal images (**f**, **h**), the superior part of the tumor can be seen in close proximity to the activation (white arrows), but this is possibly due to an exaggeration of the activation caused by a large cortical vein (venous effect) (yellow arrows). After surgery, the mass was diagnosed as an anaplastic astrocytoma, pathologically

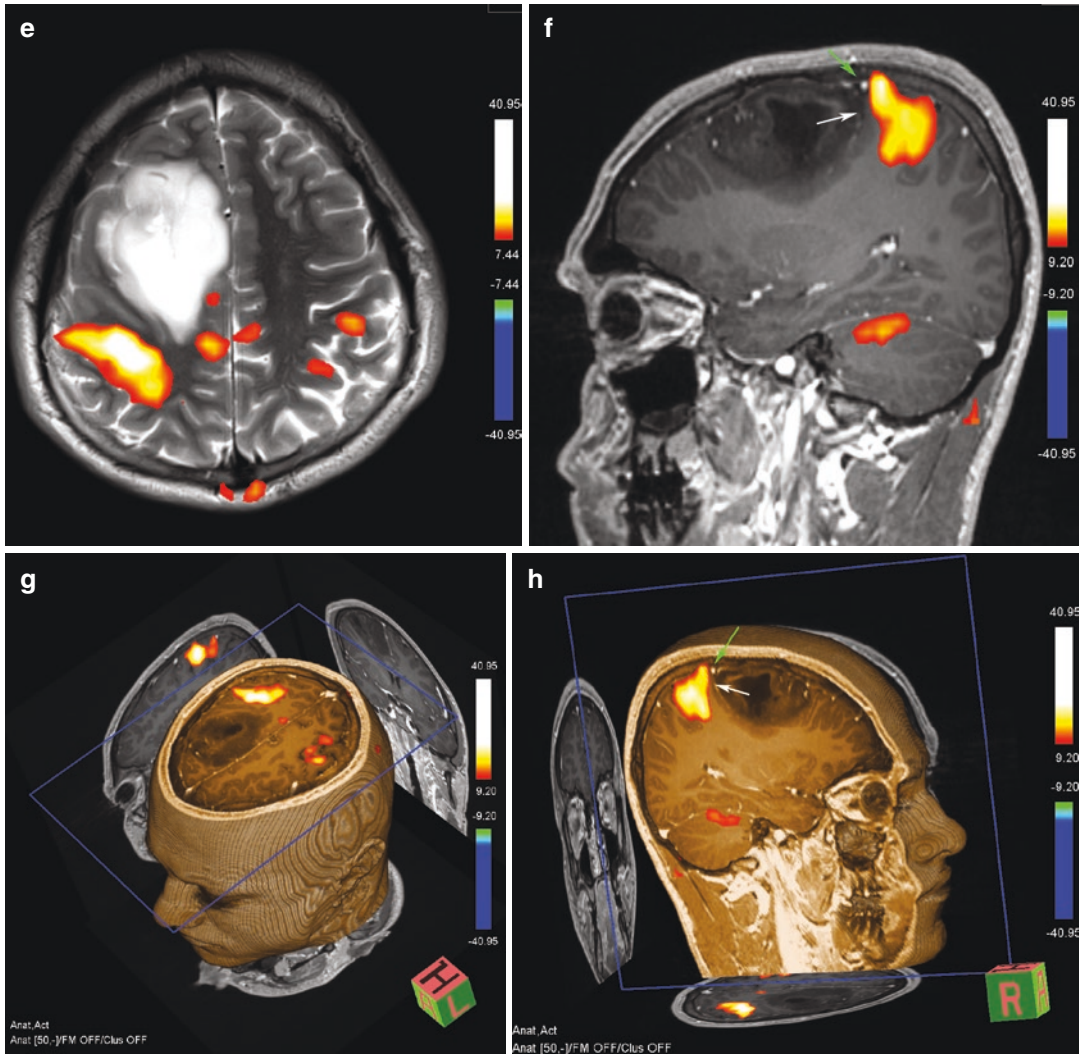

Fig. 6.4 (continued)

paradigms provide sufficient signal, especially at high-field strength.

6.3.2 Paradigms for Language Lateralization

The three main types of paradigms utilized for language lateralization are expressive, receptive, and semantic. Expressive paradigms are designed to demonstrate activation mainly in speech-production areas. The most commonly used expressive paradigms employed in fMRI for presurgical mapping are silent word generation, silent verb generation, and simple object naming (Figs. 6.5 and 6.6).

6.3.3 Statistical Analyses and the Creation of fMRI Maps

Following image acquisition and preprocessing, it is necessary to determine which voxels are of task-related activation. The most commonly used statistical method is the general linear model (GLM), which employs regression

analysis. The GLM includes modeling of both paradigm timing and expected hemodynamic response function (HRF), and the obtained model is fit to the acquired data at each voxel. Thus, the voxels with statistical significance can be displayed on a map superimposed on the anatomical image. In clinical settings, radiologists can change the thresholds of statistical significance (*t*-test, *z*-score, and *p*-value) in order to demonstrate appropriate activation and exclude noise or weak voxels.

fMRI can be processed on scanners during the performance of a paradigm (real-time processing), which is valuable in determining whether or not the task being performed is sufficient. Most clinical MRI centers contain hardware and software

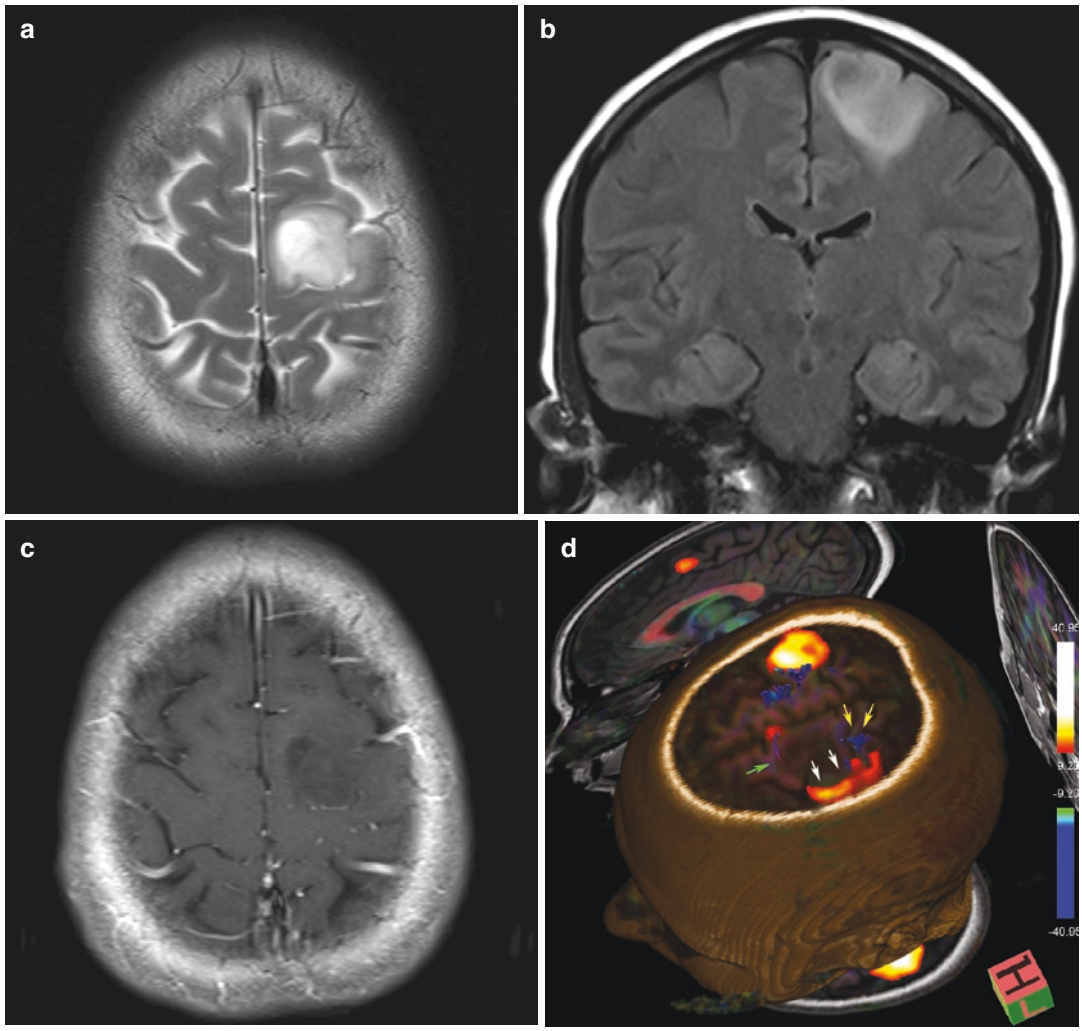

Fig. 6.5 Low-grade glioma (LGG) located in the left Rolandic region. The lesion was hyperintense on T2-weighted (**a**) and FLAIR (**b**) images and did not enhance with contrast (**c**). Both fMRI (motor-sensory activation by finger-tapping) and DTI examinations were performed and evaluated together at the preoperative stage. 3D fusion images (**d**–**f**) were formed by superimposing fMRI, DTI, and anatomical data at the workstation. Both activated motor cortex (red areas) and terminal CST fibers (blue bundles) could be seen on the 3D fusion images. The LGG had displaced the motor cortex (white arrows) laterally. The ventral CST fibers, however, seem to have been slightly separated (green arrows), and most of the CST fibers (yellow arrows) had been displaced posteriorly by the tumor

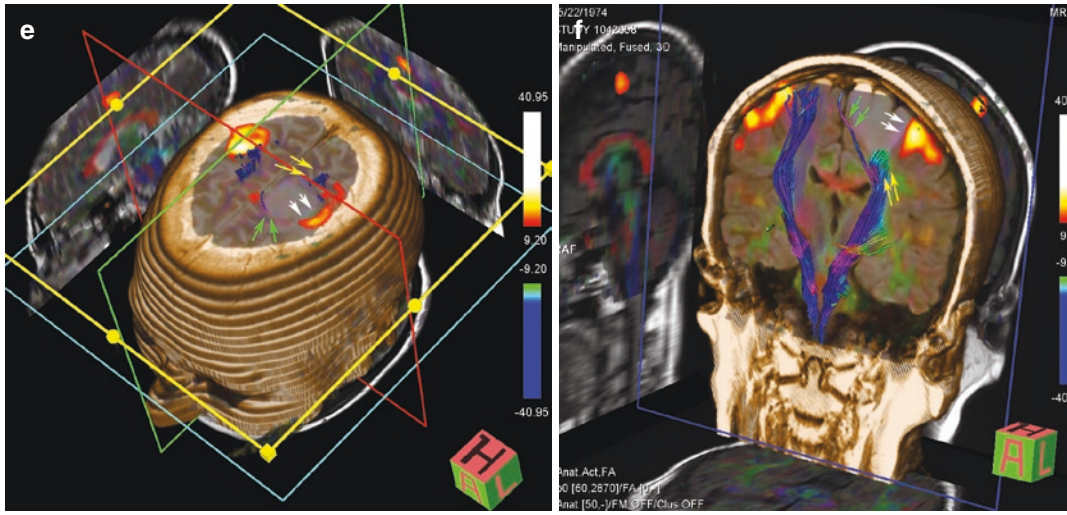

Fig. 6.5 (continued)

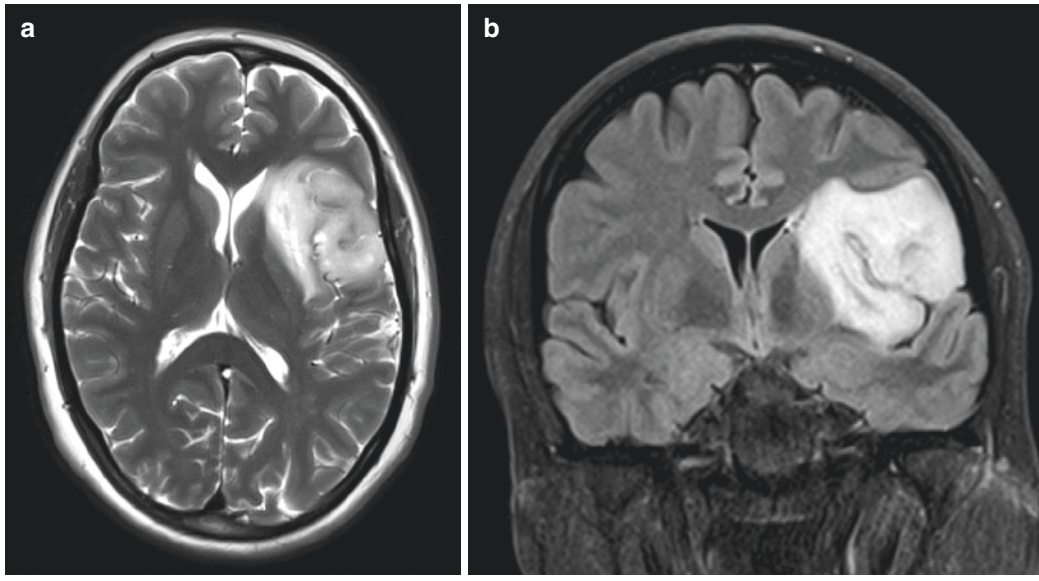

Fig. 6.6 Right-handed 48-year-old female patient with oligodendroglioma. T2-weighted and FLAIR images (**a**, **b**) show a mass in the left frontal operculum. Since the patient was right-handed, the left hemispheric dominancy possibility was 98%. Thus, it was suspected that this tumor may have infiltrated eloquent speech areas because of its location. Motor-sensory BOLD maps overlaid to T2-weighted images (**c**) reveal no close relationship between the motor-sensory cortex and the tumor, as was expected. In the second session of the fMRI exam, verb generation and word generation tasks were utilized to activate the dominant hemisphere and speech centers. The activation maps (**d**) obtained from the performance of a silent verb generation paradigm fused with T2 FLAIR structural images indicate that areas of neuronal activation were present at the superior and superoposterior margins of the lesion. DTI tractography images indicate that rostral AF was located at the posterior margin of the tumor (**e**). The DTI-fMRI fusion image (**f**) displays the anatomical relationship between the tumor with AF and language-related neuronal activation areas

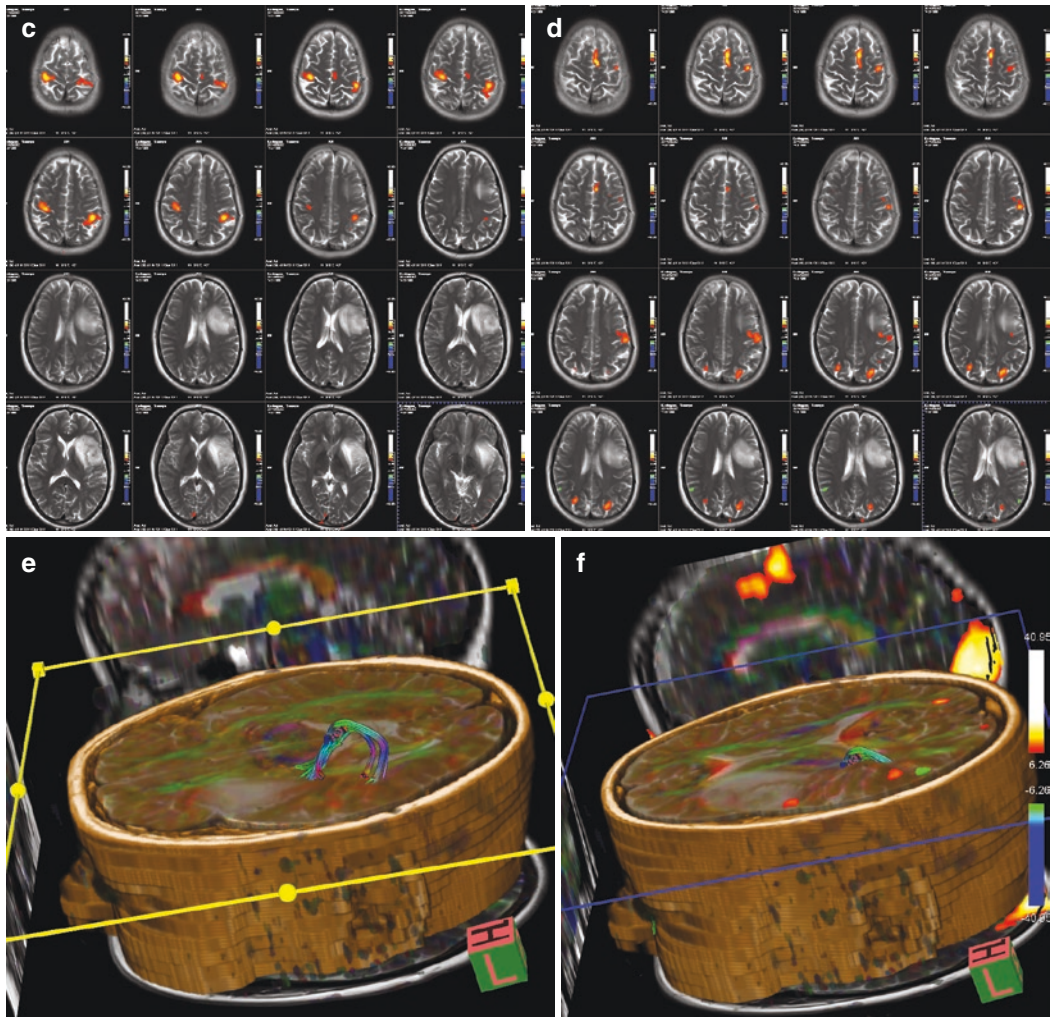

Fig. 6.6 (continued)

that allow the use of techniques such as motion correction, time correction, filtering, and anatomic co-registration in order to optimize the quality of the examination.

The paradigms used in motor-sensory fMRI are relatively simple, and the signal obtained from the task is strong, as well. Therefore, outlining the eloquent cortex by the use of a sensorimotor fMRI is a reliable method. In studies comparing electrocortical stimulation mapping (ESM) to sensorimotor fMRI, the accuracy of fMRI has been proven to be over 90% and the rate reaches 100% with the use of a 3 T scanner [8].

When compared with the Wada test and other invasive mapping techniques such as ESM, fMRI of language processing has proven 90% validity and higher. Thus, fMRI is widely utilized as the initial test of choice for determining language lateralization in preoperative patients. However, the use of language fMRI for identifying eloquent language areas has been proven as less accurate than that of sensorimotor fMRI. Therefore, the preoperative application of multiple language paradigms is essential for evaluating multiple language regions and recommended for enhancing sensitivity [8].

References

1. Mormina E, Longo M, Arrigo A, Alafaci C, Tomasello F, Calamuneri A, Marino S, Gaeta M, Vinci SL, Granata F. MRI tractography of corticospinal tract and arcuate fasciculus in high-grade gliomas performed by constrained spherical deconvolution: qualitative and quantitative analysis. AJNR Am J Neuroradiol. 2015;36:1853–8.
2. Stippich C. Clinical functional MRI presurgical functional neuroimaging. 2nd ed. Berlin: Springer; 2015.
3. Van Hecke W, Emsell L, Sunaert S. Diffusion tensor imaging: a practical handbook. New York: Springer; 2016.
4. Jellison BJ, Field AS, Medow J, Lazar M, Shariar Salamat M, Alexander AL. Diffusion tensor imaging of cerebral white matter: a pictorial review of physics, fiber tract anatomy, and tumor imaging patterns. Am J Neuroradiol. 2004;25(3):356–69.
5. Pillai JJ. Functional brain tumor imaging. New York: Springer; 2014.
6. Silva MA, See AP, Essayed WI, Golby AJ, Tie Y. Challenges and techniques for presurgical brain mapping with functional MRI. Neuroimage Clin. 2018;17:794–803.
7. Soni N, Mehrotra A, Behari S, Kumar S, Gupta N. Diffusion-tensor Imaging and tractography application in pre-operative planning of intra-axial brain lesions. Cureus. 2017;9(10):e1739.
8. Wang LL, Leach JL, Breneman JC, McPherson CM, Gaskill-Shipley MF. Critical role of imaging in the neurosurgical and radiotherapeutic management of brain tumors. Radiographics. 2014;34(3):702–21.

7 Brain Tumour Imaging: Developing Techniques and Future Perspectives

Paula L. Croal

7.1 Arterial Spin Labelling MRI

Arterial spin labelling (ASL) MRI is a noninvasive perfusion imaging technique, whereby water is magnetically labelled and acts as an endogenous diffusible tracer [1, 2]. Pairs of images are acquired (labelled and unlabelled), with the signal difference proportional to blood flow, or perfusion-weighted. Application of single or multiple compartment kinetic models enable the user to move from perfusion-weighted to absolute cerebral blood flow (CBF) while accounting for physiological and physical factors such as T1 (see Alsop et al. [3] for acquisition and modelling overview).

ASL offers an attractive approach in tumour imaging as an alternative to exogenous contrast-based techniques such as DSC MRI, where disruptions in the blood-brain barrier and resulting contrast leakages may complicate quantification [4]. There are additional challenges posed by gadolinium-based techniques, such as the inability to safely image patients with renal disease [5, 6], and recent evidence of long-term contrast deposition in brain structures [7]. Thus, the entirely noninvasive nature of ASL makes it easily repeatable and open to all patients. Studies have shown good agreement between ASL measures of both absolute and relative CBF with DSC MRI in tumours, with decreased susceptibility effects in ASL (Fig. 7.1), which may allow for improved delineation of tumour borders [8–10].

A key challenge in tumour imaging is that different pathologies, requiring different therapeutic strategies, often present with similar imaging characteristics on conventional/anatomic MRI. While biopsies remain the gold standard for tumour classification, they are not without increased patient risk, potentially prohibitive costs, and sample bias due to tumour heterogeneity. A noninvasive alternative is therefore desirable, and given the differences in microvasculature structure and blood-brain barrier integrity, physiological MRI is a potential candidate. Sunwoo et al. [11] report that ASL MRI was more effective than visual grading for differentiation between single brain metastasis and GBM, observing differences in both peritumoural and intratumoural CBF. Perfusion differences were attributed to differences in infiltrating tumour cells and vascular density, respectively, in line with previous findings [12–14]. The link between ASL measures of CBF and microvascular density has also been demonstrated in paediatric brain tumours, where routine MRI has lower diagnostic accuracy than in adults [15]. Both perfusion and vascular density increased with grade, leading to a recommendation of quantitative CBF thresholds, however, given the dependency of absolute CBF values

P. L. Croal (✉)
164 Nottingham Road, Stapleford, Nottingham, NG9 8AR, Institute of Biomedical Engineering, University of Oxford, Oxford, UK
e-mail: paula.croal@eng.ox.ac.uk

Y. Özsunar, U. Şenol (eds.), *Atlas of Clinical Cases on Brain Tumor Imaging*,
https://doi.org/10.1007/978-3-030-23273-3_7

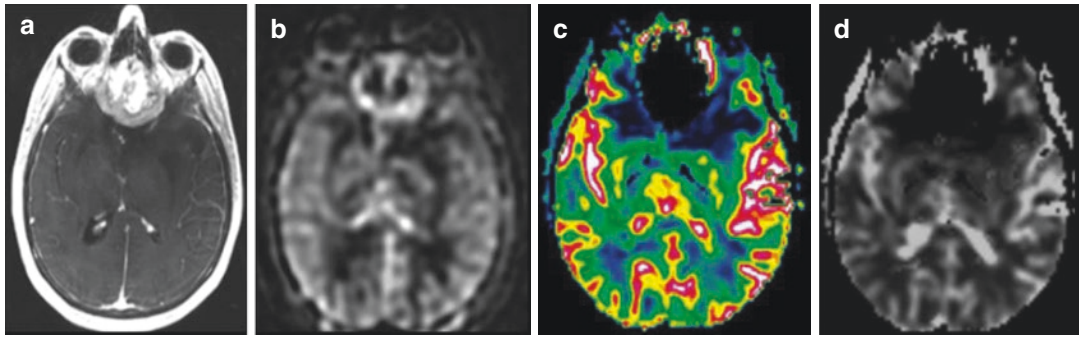

Fig. 7.1 An olfactory groove meningioma as shown on T1-weighted MRI post-gadolinium contrast (**a**). Susceptibility artefacts are not seen on ASL MRI (**b**), but are visible on DSC-based measures of relative CBF (**c**) and relative CBV (**d**). Reproduced with permission from [9]

on both acquisition and quantification techniques in ASL, as well as individual CBF differences, values normalised to 'normal appearing' tissue may be a more suitable metric [16].

Similarly, Yoo et al. [17] demonstrated that both absolute and relative CBF as quantified with ASL MRI was shown to be higher in adult High Grade Gliomas in comparison to lymphomas, in agreement with previous DSC MRI studies [18–20]. Interestingly, both absolute and relative CBF metrics significantly correlated to epidermal growth factor (EGFR) expression status, a predictor of poor prognosis. The potential for ASL MRI to provide information into genetic biomarkers puts it forward as a key player in a new era of imaging biomarkers and personalised medicine.

An additional challenge in tumour imaging is the differentiation of tumour recurrence from treatment effects (pseudo progression and/or radiation necrosis) using conventional MRI, with both presenting as T2 peritumoural hyperintensity [21, 22]. Xu et al. report both absolute and relative CBF measured with ASL discriminate recurrence from treatment effects with comparable performance to relative CBF with DSC MRI [23]. Again, ASL image quality was rated significantly better, attributed to less susceptibility artefacts than DSC MRI [23]. Similarly, Oszunar et al. [24] report semi-quantitative ASL superior to DSC MRI for distinguishing high-grade glioma from radiation necrosis, while Choi et al. [25] report that combining ASL and DSC enhances diagnostic accuracy for qualitative review.

Now available as a clinical sequence on all major scanner vendor, ASL MRI is establishing itself as a valuable technique in tumour imaging. However, there is a range of acquisition and quantification approaches for ASL MRI, both of which likely impact clinical performance, and this variability may hinder clinical uptake. Expert consensus, as summarised by Alsop et al. [3] for clinical ASL MRI studies reflect a significant move forward in clinical implementation, however prospective multi-centre trials in ASL MRI of brain tumours are needed to fully assess diagnostic/prognostic performance of both sequences and quantification methods.

7.2 Chemical Exchange Saturation Transfer MRI

Chemical exchange saturation transfer (CEST) MRI is a noninvasive molecular imaging technique whereby a series of frequency-selective saturation pulses are applied, to selectively image proton pools of interest. Typically, magnetisation of small proton pools would be difficult to image due to low signal, however CEST MRI indirectly images proton via their exchange with the much larger pool of water protons [26]. Amide Proton Transfer (APT) is an increasingly popular variant of CEST MRI which images endogenous amide

protons in intracellular protein and peptides, without the need for exogenous contrast [27].

Following initial reports of APT contrast increasing with glioma grade [28], Togao et al. [29] later reproduced these findings, reporting that APT MRI can predict the histological grading of adult diffuse glioma with increased sensitivity and specificity than routine MRI. Furthermore, using histogram analysis it was shown that APT imaging may provide a means for identification of contrast-enhancing low-grade brain tumour that mimics high-grade tumour, with improved accuracy over routine MRI [30]. While it is generally assumed that APT contrast in tumours arises from an increase in endogenous amide protons, APT MRI is also sensitive to proton exchange rate (pH-modulated). APT MRI has been shown to provide a measure of tissue pH in ischaemic stroke [31], but its role in tumours, where pH is also likely to be dysregulated, has not been established.

APT contrast could also provide an early and sensitive marker for differentiation malignancy from necrosis, as demonstrated both preclinically and in patients [32, 33] attributed to differences in cellularity. However, macromolecular CEST effects have more recently been reported to be sensitive to necrosis than APT [34]. It is possible that this discrepancy arises due to differences in quantification of APT effects, with some approaches more susceptible to effects such as pathological alterations in T1, magnetic field inhomogeneities and/or confounds from other proton pools [35]. Model-based quantification approaches [36] may help to elucidate true APT effects, while accounting for confounding effects from other proton pools, however their application in tumour patients remain to be assessed.

It is likely that molecular changes precede morphological changes, as such; APT may play a useful role in predicting or monitoring of treatment response (Fig. 7.2). Preclinical research suggests that in chemotherapy-resistant GBM, both APT contrast and ki67 (marker of cellular proliferation) continue to increase during short-term therapy, while tumour volume and cellular density remained constant in comparison to a reduction in APT contrast in the non-resistant group [33]. A recent study in patients with GBM was able to predict nonresponders to chemoradiation prior to treatment using APT CEST MRI, as well monitor therapeutic response as early as 2 weeks into treatment [34]. Again, CEST contrast arising from macromolecular effects rather than APT found to be of greater prognostic value, attributed to difficulty in isolating APT effects, as well as confounding factors such as T1.

APT contrast has the potential to provide unique molecular information in comparison to other MRI techniques; as such, clinical packages are currently in development across all major vendors. However, as with many advanced approaches, APT CEST MRI suffers from a lack of consensus over both acquisition and quantitative metrics, both of which may affect clinical interpretation. More research is needed in the form of large multicentre patient studies to both establish APT effects and understand the underlying pathophysiology.

7.3 Susceptibility-Weighted Imaging

Susceptibility-weighted imaging (SWI) is an MRI technique that provides a unique image contrast by exploiting the differences in magnetic susceptibility between blood and various tissues [38]. Rather than the more traditional approach in MRI of using magnitude images only, SWI combines $T2^*$-weighted magnitude images with corresponding phase images (filtered to enhance sensitivity to local phase changes) [39]. Due to the clinical potential of SWI, all major MR vendors now offer susceptibility-based sequences, and generation of susceptibility-weighted images.

Of particular interest for tumour imaging is the ability of SWI to image vascular architecture, providing insight into neoangiogenesis and microhaemorrhages, which is difficult to achieve with conventional MRI [40, 41]. SWI has proven to be of potential clinical value in the detection of

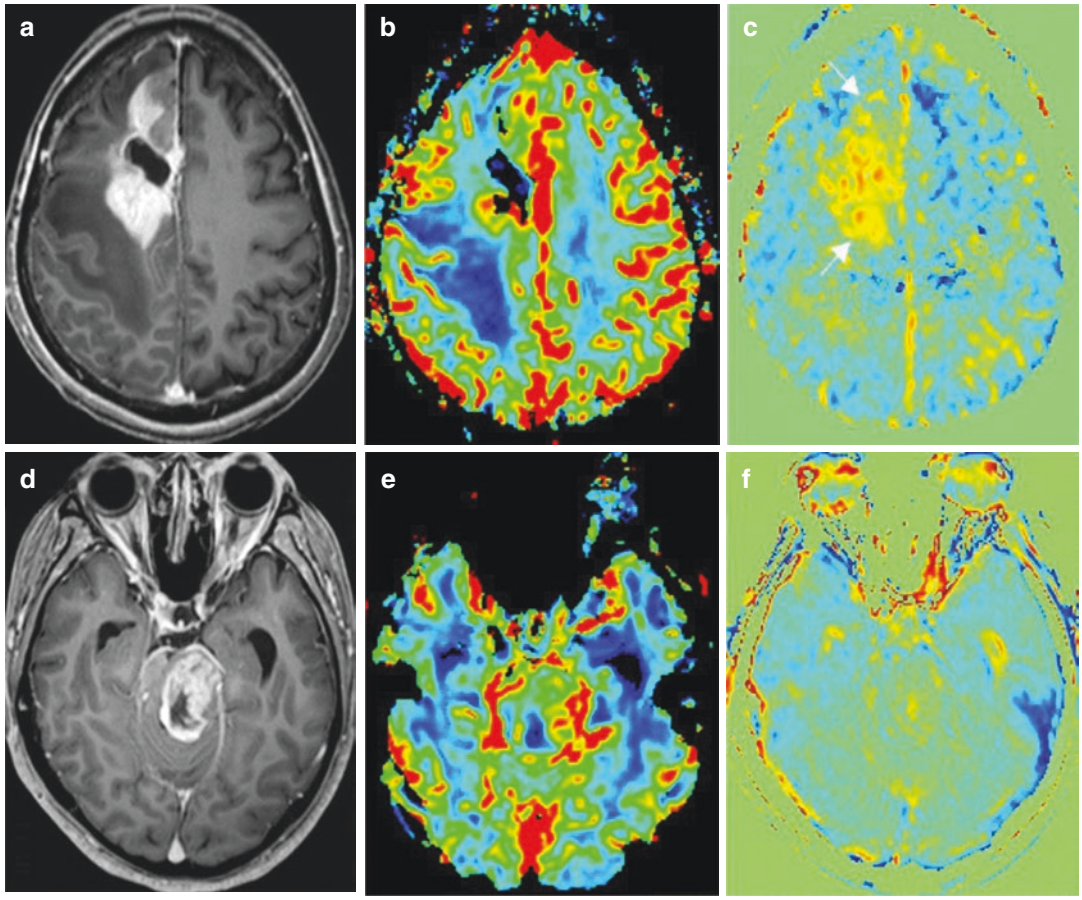

Fig. 7.2 Tumour progression presenting with (**a**) contrast enhancement on T1-weighted image, (**b**) increased cerebral blood volume on DSC MRI, and (**c**) APT hyperintensities (indicated by white arrow). Treatment effects were indistinguishable from tumour progression on (**d**) contrast-enhanced T1-weighted image and (**e**) DSC MRI, but did not show any APT contrast (**f**). Reproduced with permission from [37]

microhaemorrhages in response to anti-angiogenic therapy [42] and radiotherapy [43] as well as differentiating from radiation necrosis [44]. Furthermore, the ability to detect such microbleeds in conjunction with visualising vessel tortuosity and proliferation can lead to improved diagnosis and grading of astrocytoma [45] and early detection of basal ganglia germinomas [46]. Intratumoural susceptibility signal intensity (ITSS) refers to SWI signal hypointensities within the tumour (Fig. 7.3) and has been shown to correlate with glioma grade as confirmed with both PET and histopathology [47, 48]. It has been proposed that linear or dot-like ITSS correlate with neoangiogenesis, and dense conglomerates with microhaemorrhage and necrosis [49].

SWI may offer further advantage over conventional MRI in tumour imaging, in that it may be able to differentiate calcification from haemorrhage, an indicator of tumour malignancy, due to different magnetic properties of calcium phosphates and iron-based blood products. Previously requiring CT for differentiation, thus requiring ionising radiation [51, 52], it has recently been demonstrated that SWI can not only outperform conventional MRI but also CT for detection of intratumoural calcification [53, 54].

Despite the clinical potential of SWI, operating at lower field strength (e.g., 1.5 T) often seen in the clinic pose a challenge due to smaller phase shifts, and lower SNR. However, with higher field strengths becoming increasingly common,

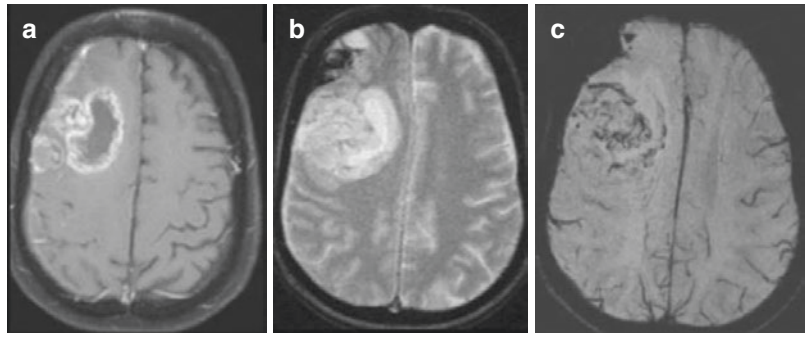

Fig. 7.3 Glioblastoma multiforme as imaged with (**a**) contrast-enhanced T1-weighted MRI, (**b**) T2-weighted imaging and (**c**) susceptibility-weighted imaging (SWI). Here, SWI is better able to define neovascularity and haemorrhage products than conventional MRI. Reproduced with permission from [50]

this hurdle should be overcome with time. A broader challenge regardless of field strength is the non-quantitative nature of SWI, with a lack of standardised approach for assessment of hypointensities. To minimise user-bias, semi-quantitative approaches could include post-processing techniques such as local image variance maps [55], fractal analysis [42] or quantitative susceptibility mapping [56, 57].

7.4 Quantitative Blood Oxygenation Level Dependent MRI

Oxygen tension and metabolic demand is an important marker of tissue viability [58] and helps predict treatment response [59]. Therefore a noninvasive, repeatable, and regional measure of oxygenation would be a valuable tool in tumour imaging for both grading and monitoring therapeutic efficacy [60]. Blood oxygenation level dependent (BOLD) MRI offers one such window into changes in oxygenation in the brain. Due to the differing magnetic properties of deoxyhaemoglobin and oxyhaemoglobin, the BOLD signal reflects changes in oxygenation, and so transverse relaxation ($T2^*$), between tissue and blood [61]. However, given the dynamic interplay of physiological and physical factors from which the BOLD response arises, it is not a quantitative measure. Furthermore, given the impact of microvascular and macrovascular field perturbations on $T2^*$ [62], $T2^*$-based oxygenation measurements may also be biased [63].

Christen et al. [64] proposed a multiparametric quantitative BOLD (qBOLD) approach which incorporates physiological (CBF, CBV) and physical parameters ($T2^*$, T2, T2′) with BOLD for regional oxygenation measures. An adaptation of the original qBOLD approach [65], the multiparametric approach requires multiple independent MR sequences to be acquired; however accuracy is less dependent on high SNR, with increased spatial coverage and resolution. Stadlbauer et al. [66] demonstrated the intraoperative utility of multiparametric qBOLD for mapping of oxygen extraction fraction (OEF) and metabolism ($CMRO_2$), observing increased oxygen metabolism and in peritumoural areas following resection, thus providing additional resection guidance.

There is a clear role for oxygenation and metabolism mapping in brain tumours, and qBOLD approaches offer a promising approach. However, both qBOLD and multiparametric qBOLD suffer from artefacts around air-tissue interfaces, and partial volume effects around cerebrospinal fluid. To address this, streamlined-qBOLD has been proposed [67], with increased robustness to such artefacts in a clinically feasible time. Streamlined-qBOLD offers a further step towards clinically feasible oxygenation mapping, however utility in brain tumours remains to be established.

7.5 Advanced Diffusion Techniques

7.5.1 Diffusion Kurtosis Imaging

Diffusion kurtosis imaging (DKI) [68] aims to more accurately model diffusion than previous diffusion-weighted and diffusion-tensor methods, in part by relaxing the assumption that the diffusion of water molecules follow a Gaussian distribution. This deviation from a normal distribution is thought to arise due to the complexity of intracellular and extracellular environments, and can be described by 'kurtosis'. DKI quantifies the degree of diffusion or tissue complexity, and as such is a potentially valuable imaging tool for identification of pathological tissue [69].

Diffusion kurtosis parameters have been proposed as potential biomarkers for glioma grading [70, 71], where tissue complexity may be increased in high-grade glioma due to increased cellularity, endothelial proliferation, haemorrhage and/or necrosis. A recent meta-analysis proposes the inclusion of DKI in routine clinical imaging of suspected gliomas, but notes diagnostic accuracy may be lower when limited to low grade gliomas [72]. DKI may also play a role in molecular profiling in glioma, as it has recently been demonstrated that mean kurtosis can differentiate between IDH1 mutation status [73] and predict ki-67 expression [74].

DKI has the advantage that it can be implemented on most clinical scanners, however it must be recognised that kurtosis is a dimensionless metric, which does not directly relate to a biophysical property. Thus while kurtosis is assumed to reflect overall tissue complexity, absolute physiological interpretation is currently lacking. To further interrogate the relationship between kurtosis and tissue microstructure, mean kurtosis can be separated into source components [75]; however, it is important to recognise the additional influence of scan parameters such as diffusion gradient strength and timing [76], as well as partial volume effects from CSF [77, 78].

7.5.2 Intravoxel Incoherent Motion

Intravoxel incoherent motion (IVIM) is an advanced diffusion imaging method, in theory allowing simultaneous measurement of perfusion and diffusion parameters [79]. It has been proposed that traditional diffusion-weighted signal reflect molecular motion arising from both diffusion and capillary flow, but at different temporal scales. By increasing the number of diffusion gradients (*b*-values), and applying a bi-exponential fitting approach, MR signal decay can be separated into molecular diffusion (D), pseudo (or macro) diffusion (D^*), and perfusion fraction (f).

While IVIM is not a new technique, to date, there are a limited number of applications in brain tumours. However, there is a need for advanced diffusion metrics in tumour environments, with the increased vascularity leading to a potential overestimation of ADC [80]. Such confounds may explain why ADC may not reliably differentiate between HGG and LGG [81, 82]. While Togao et al. [80] recently observed that ADC was significantly lower in HGG in comparison to LGG, they noted that the molecular diffusion component as measured with IVIM was significantly lower than ADC in both tumour grades. The largest discrepancy was observed in HGG, where an increased perfusion fraction [83, 84] reduces the 'true' diffusion component.

Le Bihan define the product of f and D^* (fD^*) proportional to CBF, and f proportional to CBV, however the reliability of these relationships is not fully established, particularly in the brain where tissue is much lower perfused in comparison to the body, challenging the accuracy of the bi-exponential relationship [85]. In healthy grey matter, LGG and HGG, a correlation between f and DSC measures of relative CBV has been observed [83, 86, 87]; however comparisons in healthy tissue between fD^* and both DSC and ASL measures of CBF did not establish a significant relationship [86, 88], challenging the robustness of D^* measurements. Further validation work is clearly needed, particularly against ASL measures of absolute CBF. However, regardless of physiological origin, perfusion fraction as

measured with IVIM has potential diagnostic value in tumour imaging, reported to be superior to both DSC MRI and DWI for discrimination between radiation necrosis and recurrent tumour [89, 90].

A lack of consensus on optimal acquisition and analysis poses a challenge to clinical implementation of IVIM. Factors such as number of *b*-values, corrections for relaxation time, number of averages, cardiac cycle, and number of parameters to be fitted have been shown to affect reliability and reproducibility of fitted parameters [79, 85, 87, 91, 92]. Furthermore, a particular challenge for IVIM in brain imaging is the potential confound of CSF [92], with it recently being proposed that the perfusion fraction actually reflects CSF signal rather than perfusion [88]. Such CSF confounds may be particularly problematic in brain tumours, due to increases in oedema or cystic/necrotic tumour regions. It remains to be seen how this may influence the reliability of IVIM in brain tumours, and whether potential CSF contributions can be accurately modelled or even exploited in the context of tumour imaging.

7.6 Radiogenomics

Genomic analysis has the potential to provide information regarding the biological underpinning behind diagnostics, prognostics and therapeutic response, with the 2016 World Health Organisation (WHO) guidelines for glioma classification now incorporating genetic parameters [93]. However, genetic profiling requires a tissue biopsy, and thus is not only associated with increased patient risk, a single sample may also not reflect the full tumour heterogeneity. Radiogenomics aims to identify imaging biomarkers for noninvasive genotyping, combining routine clinical imaging with non-routine genetic analysis with the goal of more personalised medicine [94].

A recent meta-analysis by Seow et al. [95] assessed the suitability of radiogenomics for glioma characterisation, highlighting the potential role of imaging biomarkers for precision therapy. Seow et al. report that EGFR overexpression (predictor of poor outcome [96]) is associated with contrast enhancement, increased perfusion, and restricted diffusion, with the heterogeneity observed in HGG a predictor of EGFR overexpression. GBM with IDH1 mutations (associated with more favourable clinical outcome [97, 98]) could be characterised by larger tumour size at the time of diagnosis, potentially non-enhancing, with reduced likelihood of vascular abnormalities, necrosis and oedema, but increased likelihood of cystic and diffuse components. Oligodendrogliomas with loss of chromosome arms 1p and 19q (associated with longer progression-free survival and increased chemotherapy sensitivity [99, 100]) was associated with indistinct tumour borders on T1-weighted images, mixed signal intensities on both T1- and T2-weighted images, and elevated CBV. Finally, elevated Ki-67 protein (histopathological marker of cellular proliferation [101]) was associated with increased Choline/Creatine ratio and restricted water diffusion.

While still an emerging field, radiogenomics represents a much needed step forward in diagnostics and therapeutic management of brain tumours. The field will most likely continue to develop as tumour imaging involves, incorporating additional MR-based metrics and advanced image processing techniques. However, radiogenomics remains subject to problems that challenge imaging biomarkers in general, namely the influence of acquisition protocols and quantification approaches between different institutions. Indeed, O'Connor et al. [102] highlight the need for both multicentre and multivendor reproducibility in order for imaging biomarkers to cross the translational gap between research and routine clinical use.

References

1. Detre JA, Leigh JS, Williams DS, Koretsky AP. Perfusion imaging. Magn Res Med. 1992;23:37–45.
2. Williams DS, Detre JA, Leigh JS, Koretsky AP. Magnetic resonance imaging of perfusion using spin inversion of arterial water. Proc Natl

Acad Sci. 1992;89:212–6. https://doi.org/10.1073/pnas.89.1.212.
3. Alsop DC, Detre JA, Golay X, et al. Recommended implementation of arterial spin-labeled perfusion MRI for clinical applications: a consensus of the ISMRM perfusion study group and the European consortium for ASL in dementia. Magn Reson Med. 2014;116:102–16. https://doi.org/10.1002/mrm.25197.
4. O'Connor JPB, Tofts PS, Miles KA, et al. Dynamic contrast-enhanced imaging techniques: CT and MRI. Br J Radiol. 2011;84:S112–20. https://doi.org/10.1259/bjr/55166688.
5. Grobner T. Gadolinium—a specific trigger for the development of nephrogenic brosing dermopathy and nephrogenic systemic brosis? Nephrol Dial Transpl. 2006;21:1104–8. https://doi.org/10.1093/ndt/gfk062.
6. Marckmann P. Nephrogenic systemic fibrosis: suspected causative role of gadodiamide used for contrast-enhanced magnetic resonance imaging. J Am Soc Nephrol. 2006;17:2359–62. https://doi.org/10.1681/ASN.2006060601.
7. Gulani V, Calamante F, Shellock FG, et al. Gadolinium deposition in the brain: summary of evidence and recommendations. Lancet Neurol. 2017;16:564–70. https://doi.org/10.1016/S1474-4422(17)30158-8.
8. Lehmann P, Monet P, de Marco G, et al. A comparative study of perfusion measurement in brain tumours at 3 Tesla MR: arterial spin labeling versus dynamic susceptibility contrast-enhanced MRI. Eur Neurol. 2010;64:21–6. https://doi.org/10.1159/000311520.
9. Järnum H, Steffensen EG, Knutsson L, et al. Perfusion MRI of brain tumours: a comparative study of pseudo-continuous arterial spin labelling and dynamic susceptibility contrast imaging. Neuroradiology. 2010;52:307–17. https://doi.org/10.1007/s00234-009-0616-6.
10. Reginster P, Martin B, Denolin V. Comparative study of pseudo-continuous arterial spin labeling and dynamic susceptibility contrast imaging at 3.0 Tesla in brain tumors. Neurooncol Open Access. 2017;2:1–13. https://doi.org/10.21767/2572-0376.100018.
11. Sunwoo L, Yun TJ, You S-H, et al. Differentiation of glioblastoma from brain metastasis: qualitative and quantitative analysis using arterial spin labeling MR imaging. PLoS One. 2016;11:e0166662. https://doi.org/10.1371/journal.pone.0166662.
12. Kelly PJ, Daumas-Duport C, Scheithauer BW, et al. Stereotactic histologic correlations of computed tomography- and magnetic resonance imaging-defined abnormalities in patients with glial neoplasms. Mayo Clin Proc. 1987;62:450–9.
13. Noguchi T, Yoshiura T, Hiwatashi A, et al. Perfusion imaging of brain tumors using arterial spin-labeling: correlation with histopathologic vascular density. Am J Neuroradiol. 2008;29:688–93. https://doi.org/10.3174/ajnr.A0903.
14. Yoo R-E, Yun TJ, Cho YD, et al. Utility of arterial spin labeling perfusion magnetic resonance imaging in prediction of angiographic vascularity of meningiomas. J Neurosurg. 2016;125:536–43. https://doi.org/10.3171/2015.8.JNS151211.536.
15. Dangouloff-Ros V, Deroulers C, Foissac F, et al. Arterial spin labeling to predict brain tumor grading in children: correlations between histopathologic vascular density and perfusion MR imaging. Radiology. 2016;281:553–66. https://doi.org/10.1148/radiol.2016152228.
16. Law-ye B, Schertz M, Galanaud D, et al. Arterial spin labeling to predict brain tumor grading: limits of cutoff cerebral blood flow values. Radiology. 2017;282:1–3.
17. Yoo RE, Choi SH, Cho HR, et al. Tumor blood flow from arterial spin labeling perfusion MRI: a key parameter in distinguishing high-grade gliomas from primary cerebral lymphomas, and in predicting genetic biomarkers in high-grade gliomas. J Magn Reson Imaging. 2013;38:852–60. https://doi.org/10.1002/jmri.24026.
18. Hartmann M, Heiland S, Harting I, et al. Distinguishing of primary cerebral lymphoma from high-grade glioma with perfusion-weighted magnetic resonance imaging. Neurosci Lett. 2003;338:119–22. https://doi.org/10.1016/S0304-3940(02)01367-8.
19. Ma JH, Kim HS, Rim NJ, et al. Differentiation among glioblastoma multiforme, solitary metastatic tumor, and lymphoma using whole-tumor histogram analysis of the normalized cerebral blood volume in enhancing and perienhancing lesions. Am J Neuroradiol. 2010;31:1699–706. https://doi.org/10.3174/ajnr.A2161.
20. Calli C, Kitis O, Yunten N, et al. Perfusion and diffusion MR imaging in enhancing malignant cerebral tumors. Eur J Radiol. 2006;58:394–403. https://doi.org/10.1016/j.ejrad.2005.12.032.
21. Mullins ME, Barest GD, Schaefer PW, et al. Radiation necrosis versus glioma recurrence: conventional MR imaging clues to diagnosis. Am J Neuroradiol. 2005;26:1967–72.
22. Linhares P, Carvalho B, Figueiredo R, et al. Early pseudoprogression following chemoradiotherapy in glioblastoma patients: the value of RANO evaluation. J Oncol. 2013;2013:690585. https://doi.org/10.1155/2013/690585.
23. Xu Q, Liu Q, Ge H, et al. Tumor recurrence versus treatment effects in glioma. Medicine (Baltimore). 2017;96:e9332. https://doi.org/10.1097/MD.0000000000009332.
24. Oszunar Y, Mullins ME, Kwong K, et al. Glioma recurrence versus radiation necrosis? A pilot comparison of arterial spin-labeled, dynamic susceptibility contrast enhanced MRI, and FDG-PET imaging. Acad Radiol. 2010;17:282–90. https://doi.org/10.1016/j.acra.2009.10.024.
25. Choi JC, Kim HS, Jahng G-H, et al. Pseudoprogression in patients with glioblastoma:

added value of arterial spin labeling to dynamic susceptibility contrast perfusion MR imaging. Acta radiol. 2013;54:448–54.
26. Liu G, Song X, Chan KWY, McMahon MT. Nuts and bolts of CEST MR imaging. NMR Biomed. 2013;26:810–28. https://doi.org/10.1002/nbm.2899.Nuts.
27. Zhou J, Payen J, Wilson DA, et al. Using the amide proton signals of intracellular proteins and peptides to detect pH effects in MRI. Nat Med. 2003;9:1085–90.
28. Zhou J, Blakeley JO, Hua J, et al. Practical data acquisition method for human brain tumor amide proton transfer (APT) imaging. Magn Reson Med. 2008;60:842–9. https://doi.org/10.1002/mrm.21712.
29. Togao O, Yoshiura T, Keupp J, et al. Amide proton transfer imaging of adult diffuse gliomas: correlation with histopathological grades. Neuro-Oncology. 2014;16:441–8. https://doi.org/10.1093/neuonc/not158.
30. Park JE, Kim HS, Park KJ, et al. Histogram analysis of amide proton transfer imaging to identify contrast-enhancing low-grade brain tumor that mimics high-grade tumor: increased accuracy of MR perfusion. Radiology. 2015;277:151–61. https://doi.org/10.1148/radiol.2015142347.
31. Harston GWJ, Tee YK, Blockley N, et al. Identifying the ischaemic penumbra using pH-weighted magnetic resonance imaging. Brain. 2015;138:36–42. https://doi.org/10.1093/brain/awu374.
32. Zhou J, Tryggestad E, Wen Z, et al. Differentiation between glioma and radiation necrosis. Nat Med. 2011;17:130–4. https://doi.org/10.1038/nm.2268.Differentiation.
33. Sagiyama K, Mashimo T, Togao O, et al. In vivo chemical exchange saturation transfer imaging allows early detection of a therapeutic response in glioblastoma. Proc Natl Acad Sci U S A. 2014;111:4542–7. https://doi.org/10.1073/pnas.1323855111.
34. Mehrabian H, Myrehaug S, Soliman H, et al. Evaluation of glioblastoma response to therapy with chemical exchange saturation transfer. Int J Radiat Oncol Biol Phys. 2018;101:713–23. https://doi.org/10.1016/j.ijrobp.2018.03.057.
35. Tee YK, Harston GWJ, Blockley N, et al. Comparing different analysis methods for quantifying the MRI amide proton transfer (APT) effect in hyperacute stroke patients. NMR Biomed. 2014;27:1019–29. https://doi.org/10.1002/nbm.3147.
36. Chappell MA, Donahue MJ, Tee YK, et al. Quantitative Bayesian model-based analysis of amide proton transfer MRI. Magn Reson Med. 2013;70:556–67. https://doi.org/10.1002/mrm.24474.
37. Park KJ, Kim HS, Park JE, Shim WH. Added value of amide proton transfer imaging to conventional and perfusion MR imaging for evaluating the treatment response of newly diagnosed glioblastoma. Eur Radiol. 2016;26:4390–403. https://doi.org/10.1007/s00330-016-4261-2.
38. Reichenbach JR, Venkatesan R, Schillinger DJ, et al. Small vessels in the human brain: MR venography with deoxyhemoglobin as an intrinsic contrast agent. Radiology. 1997;204:272–7. https://doi.org/10.1148/radiology.204.1.9205259.
39. Haacke EM, Xu Y, Cheng Y-CN, Reichenbach JR. Susceptibility weighted imaging (SWI). Magn Reson Med. 2004;52:612–8. https://doi.org/10.1002/mrm.20198.
40. Sehgal V, Delproposto Z, Haacke EM, et al. Clinical applications of neuroimaging with susceptibility-weighted imaging. J Magn Reson Imaging. 2005;22:439–50. https://doi.org/10.1002/jmri.20404.
41. Rauscher A, Sedlacik J, Barth M, et al. Magnetic susceptibility-weighted MR phase imaging of the human brain. Am J Neuroradiol. 2005;26:736–42. pii: 26/4/736.
42. Di Ieva A, Matula C, Grizzi F, et al. Fractal analysis of the susceptibility weighted imaging patterns in malignant brain tumors during antiangiogenic treatment: technical report on four cases serially imaged by 7T magnetic resonance during a period of four weeks. World Neurosurg. 2012;77:28–31. https://doi.org/10.1016/j.wneu.2011.09.006.
43. Lupo JM, Chuang CF, Chang SM, et al. 7-Tesla susceptibility-weighted imaging to assess the effects of radiotherapy on normal-appearing brain in patients with glioma. Int J Radiat Oncol Biol Phys. 2012;82:e493–500. https://doi.org/10.1016/j.ijrobp.2011.05.046.
44. Löbel U, Sedlacik J, Sabin ND, et al. Three-dimensional susceptibility-weighted imaging and two-dimensional T2*-weighted gradient-echo imaging of intratumoral hemorrhages in pediatric diffuse intrinsic pontine glioma. Neuroradiology. 2010;52:1167–77. https://doi.org/10.1007/s00234-010-0771-9.
45. Li C, Ai B, Li Y, et al. Susceptibility-weighted imaging in grading brain astrocytomas. Eur J Radiol. 2010;75:81–5. https://doi.org/10.1016/j.ejrad.2009.08.003.
46. Lou X, Ma L, Wang FL, et al. Susceptibility-weighted imaging in the diagnosis of early basal ganglia germinoma. Am J Neuroradiol. 2009;30:1694–9. https://doi.org/10.3174/ajnr.A1696.
47. Park MJ, Kim HS, Jahng GH, et al. Semiquantitative assessment of intratumoral susceptibility signals using non-contrast-enhanced high-field high-resolution susceptibility-weighted imaging in patients with gliomas: comparison with MR perfusion imaging. Am J Neuroradiol. 2009;30:1402–8. https://doi.org/10.3174/ajnr.A1593.
48. Pinker K, Noebauer-Huhmann IM, Stavrou I, et al. High-resolution contrast-enhanced, susceptibility-weighted MR imaging at 3T in patients with brain tumors: correlation with positron-emission tomography and histopathologic findings.

Am J Neuroradiol. 2007;28:1280–6. https://doi.org/10.3174/ajnr.A0540.
49. Hsu CC-T, Kwan GNC, Hapugoda S, et al. Susceptibility weighted imaging in acute cerebral ischemia: review of emerging technical concepts and clinical applications. Neuroradiol J. 2017;30:109–19. https://doi.org/10.1177/1971400917690166.
50. Thomas B, Somasundaram S, Thamburaj K, et al. Clinical applications of susceptibility weighted MR imaging of the brain—a pictorial review. Neuroradiology. 2008;50:105–16. https://doi.org/10.1007/s00234-007-0316-z.
51. Oot RF, New PFJ, Pile-Spellman J, et al. The detection of intracranial calcifications by MR. Am J Neuroradiol. 1986;7:801–9. https://doi.org/10.3174/ajnr.a1461.
52. Avrahami E, Cohn DF, Feibel M, Tadmor R. MRI demonstration and CT correlation of the brain in patients with idiopathic intracerebral calcification. J Neurol. 1994;241:381–4.
53. Berberat J, Grobholz R, Boxheimer L, et al. Differentiation between calcification and hemorrhage in brain tumors using susceptibility-weighted imaging: a pilot study. Am J Roentgenol. 2014;202:847–50. https://doi.org/10.2214/AJR.13.10745.
54. Zulfiqar M, Dumrongpisutikul N, Intrapiromkul J, Yousem DM. Detection of intratumoral calcification in oligodendrogliomas by susceptibility-weighted MR imaging. Am J Neuroradiol. 2012;33:858–64. https://doi.org/10.3174/ajnr.A2862.
55. Grabner G, Kiesel B, Wöhrer A, et al. Local image variance of 7 Tesla SWI is a new technique for preoperative characterization of diffusely infiltrating gliomas: correlation with tumour grade and IDH1 mutational status. Eur Radiol. 2017;27:1556–67. https://doi.org/10.1007/s00330-016-4451-y.
56. Schweser F, Deistung A, Lehr BW, Reichenbach JR. Quantitative imaging of intrinsic magnetic tissue properties using MRI signal phase: an approach to in vivo brain iron metabolism? Neuroimage. 2011;54:2789–807. https://doi.org/10.1016/j.neuroimage.2010.10.070.
57. Deistung A, Schweser F, Wiestler B, et al. Quantitative susceptibility mapping differentiates between blood depositions and calcifications in patients with glioblastoma. PLoS One. 2013;8:1–8. https://doi.org/10.1371/journal.pone.0057924.
58. Mendichovszky I, Jackson A. Imaging hypoxia in gliomas. Br J Radiol. 2011;84:145–58. https://doi.org/10.1259/bjr/82292521.
59. Brown JM, Wilson WR. Exploiting tumour hypoxia in cancer treatment. Nat Rev Cancer. 2004;4:437–47. https://doi.org/10.1038/nrc1367.
60. Preibisch C, Shi K, Kluge A, et al. Characterizing hypoxia in human glioma: a simultaneous multimodal MRI and PET study. NMR Biomed. 2017;30:1–13. https://doi.org/10.1002/nbm.3775.
61. Ogawa S, Lee TM, Kay AR. Brain magnetic resonance imaging with contrast dependent on blood oxygenation. Proc Natl Acad Sci USA. 1990;87:9868–72.
62. Yablonskiy DA, Haacke EM. Theory of NMR signal behavior in magnetically inhomogeneous tissues: the static dephasing regime. Magn Reson Med. 1994;32:749–63.
63. Christen T, Lemasson B, Pannetier N, et al. Is $T2^*$ enough to assess oxygenation? Quantitative blood oxygen level-dependent analysis in brain tumor. Radiology. 2012;262:495–502. https://doi.org/10.1148/radiol.11110518.
64. Christen T, Schmiedeskamp H, Straka M, et al. Measuring brain oxygenation in humans using a multiparametric quantitative blood oxygenation level dependent MRI approach. Magn Reson Med. 2012;68:905–11. https://doi.org/10.1002/mrm.23283.
65. He X, Yablonskiy DA. Quantitative BOLD: mapping of human cerebral deoxygenated blood volume and oxygen extraction fraction: default state. Magn Reson Med. 2007;57:115–26. https://doi.org/10.1002/mrm.21108.
66. Stadlbauer A, Merkel A, Zimmermann M, et al. Intraoperative magnetic resonance imaging of cerebral oxygen metabolism during resection of brain lesions. World Neurosurg. 2017;100:388–94. https://doi.org/10.1016/j.wneu.2017.01.060.
67. Stone AJ, Blockley NP. A streamlined acquisition for mapping baseline brain oxygenation using quantitative BOLD. Neuroimage. 2017;147:79–88. https://doi.org/10.1016/J.NEUROIMAGE.2016.11.057.
68. Jensen JH, Helpern JA, Ramani A, et al. Diffusional kurtosis imaging: the quantification of non-Gaussian water diffusion by means of magnetic resonance imaging. Magn Reson Med. 2005;53:1432–40. https://doi.org/10.1002/mrm.20508.
69. Wu EX, Cheung MM. MR diffusion kurtosis imaging for neural tissue characterization. NMR Biomed. 2010;23:836–48. https://doi.org/10.1002/nbm.1506.
70. Raab P, Hattingen E, Franz K, Zanella FE, Lanfermann H. Cerebral gliomas: diffusional kurtosis imaging analysis of microstructural differences. Radiology. 2010;254:876–81. https://doi.org/10.1148/radiol.09090819.
71. Van Cauter S, Veraart J, Sijbers J, et al. Gliomas: diffusion kurtosis MR imaging in grading. Radiology. 2012;263:492–501.
72. Falk Delgado A, Nilsson M, van Westen D, Falk Delgado A. Glioma grade discrimination with MR diffusion kurtosis imaging: a meta-analysis of diagnostic accuracy. Radiology. 2018;287:119–27. https://doi.org/10.1148/radiol.2017171315.
73. Hempel JM, Schittenhelm J, Brendle C, et al. Histogram analysis of diffusion kurtosis imaging estimates for in vivo assessment of 2016 WHO glioma grades: a cross-sectional observational study. Eur J Radiol. 2017;95:202–11. https://doi.org/10.1016/j.ejrad.2017.08.008.

74. Jiang R, Jiang J, Zhao L, et al. Diffusion kurtosis imaging can efficiently assess the glioma grade and cellular proliferation. Oncotarget. 2015;6:42380–93. https://doi.org/10.18632/oncotarget.5675.
75. Nilsson M, Englund E, Szczepankiewicz F, et al. Imaging brain tumour microstructure. Neuroimage. 2018; 182:232–50. https://doi.org/10.1016/j.neuroimage.2018.04.075.
76. Poot DHJ, den Dekker AJ, Achten E, et al. Optimal experimental design for diffusion kurtosis imaging. IEEE Trans Med Imaging. 2010;29:819–29. https://doi.org/10.1109/TMI.2009.2037915.
77. Metzler-Baddeley C, O'Sullivan MJ, Bells S, et al. How and how not to correct for CSF-contamination in diffusion MRI. Neuroimage. 2012;59:1394–403. https://doi.org/10.1016/j.neuroimage.2011.08.043.
78. Collier Q, Veraart J, Jeurissen B, et al. Diffusion kurtosis imaging with free water elimination: a Bayesian estimation approach. Magn Reson Med. 2018;80:802–13. https://doi.org/10.1002/mrm.27075.
79. Le Bihan D, Breton E, Lallemand D, et al. Separation of diffusion and perfusion in intravoxel incoherent motion MR imaging. Radiology. 1988;168:566–7.
80. Togao O, Hiwatashi A, Yamashita K, et al. Differentiation of high-grade and low-grade diffuse gliomas by intravoxel incoherent motion MR imaging. Neuro-Oncology. 2016;18:132–41. https://doi.org/10.1093/neuonc/nov147.
81. Server A, Kulle B, Gadmar ØB, et al. Measurements of diagnostic examination performance using quantitative apparent diffusion coefficient and proton MR spectroscopic imaging in the preoperative evaluation of tumor grade in cerebral gliomas. Eur J Radiol. 2011;80:462–70. https://doi.org/10.1016/j.ejrad.2010.07.017.
82. Lam WWM, Poon WS, Metreweli C. Diffusion MR imaging in glioma: does it have any role in the preoperation determination of grading of glioma? Clin Radiol. 2002;57:219–25. https://doi.org/10.1053/crad.2001.0741.
83. Federau C, O'Brien K, Meuli R, et al. Measuring brain perfusion with intravoxel incoherent motion (IVIM): initial clinical experience. J Magn Reson Imaging. 2014;39:624–32. https://doi.org/10.1002/jmri.24195.
84. Bisdas S, Koh TS, Roder C, et al. Intravoxel incoherent motion diffusion-weighted MR imaging of gliomas: feasibility of the method and initial results. Neuroradiology. 2013;55:1189–96. https://doi.org/10.1007/s00234-013-1229-7.
85. Meeus EM, Novak J, Withey SB, et al. Evaluation of intravoxel incoherent motion fitting methods in low-perfused tissue. J Magn Reson Imaging. 2017;45:1325–34. https://doi.org/10.1002/jmri.25411.
86. Wu WC, Chen YF, Tseng HM, et al. Caveat of measuring perfusion indexes using intravoxel incoherent motion magnetic resonance imaging in the human brain. Eur Radiol. 2015;25:2485–92. https://doi.org/10.1007/s00330-015-3655-x.
87. Catanese A, Malacario F, Cirillo L, et al. Application of intravoxel incoherent motion (IVIM) magnetic resonance imaging in the evaluation of primitive brain tumours. Neuroradiol J. 2018;31:4–9. https://doi.org/10.1177/1971400917693025.
88. Hare H V., Frost R, Meakin JA, Bulte DP. On the origins of the cerebral IVIM signal. bioRxiv. 2017. https://doi.org/10.1101/158014.
89. Kim DY, Kim HS, Goh MJ, et al. Utility of intravoxel incoherent motion MR imaging for distinguishing recurrent metastatic tumor from treatment effect following gamma knife radiosurgery: initial experience. AJNR Am J Neuroradiol. 2014;35:2082–90. https://doi.org/10.3174/ajnr.A3995.
90. Detsky JS, Keith J, Conklin J, et al. Differentiating radiation necrosis from tumor progression in brain metastases treated with stereotactic radiotherapy: utility of intravoxel incoherent motion perfusion MRI and correlation with histopathology. J Neurooncol. 2017;134:433–41. https://doi.org/10.1007/s11060-017-2545-2.
91. Federau C, Hagmann P, Maeder P, et al. Dependence of brain intravoxel incoherent motion perfusion parameters on the cardiac cycle. PLoS One. 2013;8:1–7. https://doi.org/10.1371/journal.pone.0072856.
92. Le Bihan D. What can we see with IVIM MRI? Neuroimage. 2019;187:56–67. https://doi.org/10.1016/j.neuroimage.2017.12.062.
93. Louis DN, Perry A, Reifenberger G, et al. The 2016 World Health Organization classification of tumors of the central nervous system: a summary. Acta Neuropathol. 2016;131:803–20. https://doi.org/10.1007/s00401-016-1545-1.
94. Rutman AM, Kuo MD. Radiogenomics: creating a link between molecular diagnostics and diagnostic imaging. Eur J Radiol. 2009;70:232–41. https://doi.org/10.1016/j.ejrad.2009.01.050.
95. Seow P, Wong J, Ahmad-Annuar A, et al. Quantitative magnetic resonance imaging and radiogenomic biomarkers for glioma characterisation: a systematic review. Br J Radiol. 2018;91:1–14.
96. Hait WN. Forty years of translational cancer research. Cancer Discov. 2011;1:383–90. https://doi.org/10.1158/2159-8290.CD-11-0196.
97. Parsons DW, Jones S, Zhang X, et al. An integrated genomic analysis of human glioblastoma multiforme. Science. 2008;321(5897):1807–12. https://doi.org/10.1126/science.1164382.
98. Nobusawa S, Watanabe T, Kleihues P, Ohgaki H. IDH1 mutations as molecular signature and predictive factor of secondary glioblastomas. Clin Cancer Res. 2009;15:6002–7. https://doi.org/10.1158/1078-0432.CCR-09-0715.

99. Law M, Brodsky JE, Babb J, et al. High cerebral blood volume in human gliomas predicts deletion of chromosome 1p: preliminary results of molecular studies in gliomas with elevated perfusion. J Magn Reson Imaging. 2007;25:1113–9. https://doi.org/10.1002/jmri.20920.
100. Khayal I, VandenBerg S, Smith K, et al. MRI apparent diffusion coefficient reflects histopathologic subtype, axonal disruption, and tumor fraction in diffuse-type grade II gliomas. Neuro-Oncology. 2011;13:1192–201. https://doi.org/10.1093/neuonc/nou223.
101. Mahajan A, Goh V, Basu S, et al. Bench to bedside molecular functional imaging in translational cancer medicine: to image or to imagine? Clin Radiol. 2015;70:1060–82. https://doi.org/10.1016/j.crad.2015.06.082.
102. O'Connor JPB, Aboagye EO, Adams JE, et al. Imaging biomarker roadmap for cancer studies. Nat Rev Clin Oncol. 2017;14:169–86. https://doi.org/10.1038/nrclinonc.2016.162.

8 The Basic Molecular Genetics and the Common Mutations of Brain Tumors

Handan Kayhan

8.1 Introduction

It is now a well-known fact that the accumulation of mutations in DNA may result in cancer, and furthermore, it can be a determinant for the type of tumor, its prognosis, and its outcome. Most of them are derived from a single abnormal cell that initially experienced some genetic changes. Most cancers are caused by 2–8 sequential mutations that develop over years [1]. Mutations are genetic alterations in DNA that affect genetic information. Gene mutations are results from changes in a single gene, while chromosomal mutations are in the whole chromosome. The general types of the mutations were summarized in Figs. 8.1 and 8.2.

8.2 Cancer-Causing Gene Mutations: Oncogenes, Tumor-Suppressor Genes, and microRNAs

Cancer-causing gene mutations can be categorized into two groups: oncogenes and tumor-suppressor genes (TSGs) [2]. Oncogenes are a mutant form of proto-oncogenes (activation). Proto-oncogenes are normal, protein-coding genes that regulate cell growth, survival, cell cycle, differentiation, and programmed cell death (apoptosis).

Oncogenes can be activated by five mechanisms (Fig. 8.3) and after activation, can be controlled by microRNAs (miRNAs). microRNAs are noncoding RNA molecules containing 21–25 nucleotides. These tiny RNAs can control gene expression by downregulation [3]. Mutations or epigenetic changes in such miRNAs can lead to activation of oncogenes. Such miRNAs are known as oncomirs. Recent developments show that miRNAs can play roles as TSGs and oncogenes [3, 4]. For instance, mir-21 (located at 17q23.2) was shown to be increased in glioblastoma (GB) at 5–100 fold than normal tissue and it controlled cell growth by inhibiting apoptosis, but not affect cell proliferation indicating its oncogenic role [5, 6].

TSGs are anti-oncogenes that protect cells from cancer. Inactivation of these genes as a result of some mutations can lead the cells to cancer. TSGs can be categorized into caretaker, gatekeeper, and landscaper genes. Caretakers correct mutations during replication and cell division so control genome integrity and stability, e.g., MLH1 and MSH2 [7]. Gatekeepers regulate proto-oncogenes. They block tumor growth by controlling cell cycle checkpoints (“gates”) and promoting apoptosis, e.g., p53 and retinoblastoma (RB) [8]. The landscapers are conductors that regulate caretakers and gatekeepers by

H. Kayhan (✉)
Faculty of Medicine, Department of Adult Haematology, Gazi University, Ankara, Turkey

Y. Özsunar, U. Şenol (eds.), *Atlas of Clinical Cases on Brain Tumor Imaging*,
https://doi.org/10.1007/978-3-030-23273-3_8

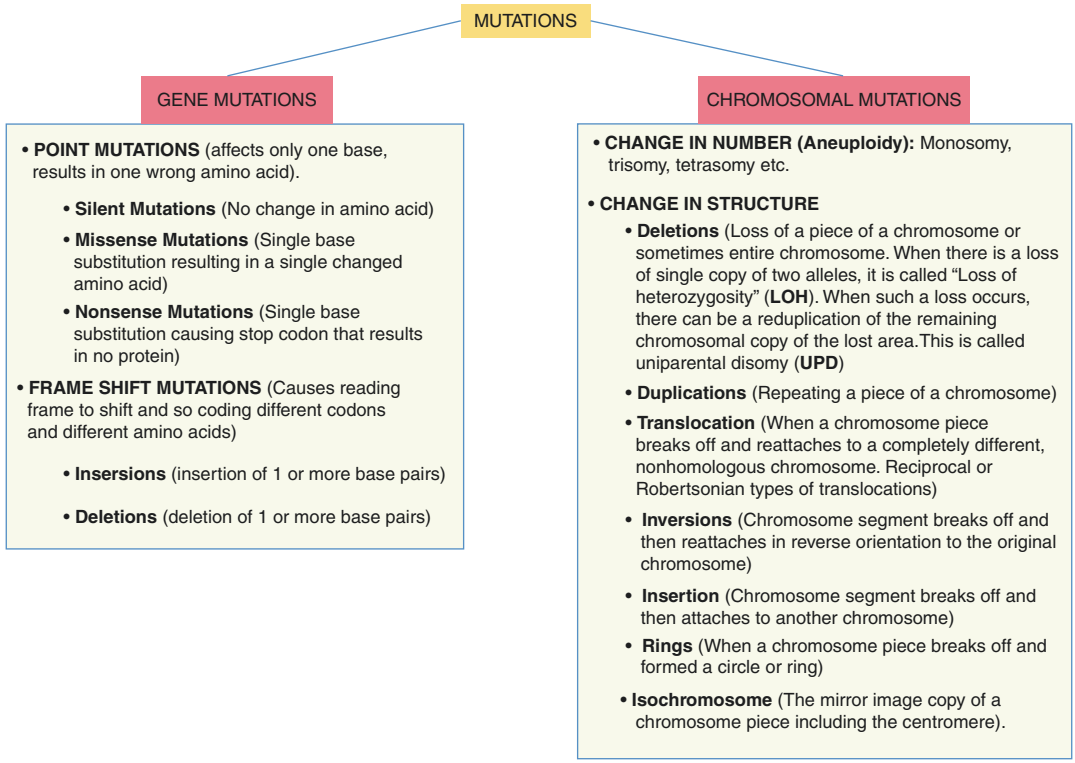

Fig. 8.1 A scheme that summarizes general mutation types. The gene mutations can occur in the coding region of a gene as well as in noncoding regions. Both of them can alter the expression of genes in different ways

involving major signalling pathways. They promote neoplastic growth by creating a microenvironment necessary for unregulated cellular proliferation, e.g., PTEN [9].

8.3 The Central Nervous System Tumors

The central nervous system (CNS) tumors are composed of the brain and spinal cord tumors including the meninges, pituitary gland, pineal gland, and nerves. Primary brain tumors are the most common cancer type after leukemia in children (0–19 years) while it is rare in adults [10]. Medulloblastomas (MBs), sellar region tumors, pilocytic astrocytomas, ependymomas, germ cell tumor, and embryonal tumors were the most prevalent brain tumors in children while meningiomas, diffuse astrocytic tumors, and oligodendrogliomas are the common CNS tumors in adults [11, 12]. Approximately 58% of CNS were nonmalignant while 42% of them were malignant [13]. Glioblastoma is the most prevalent and lethal tumor in adults (47.1%) while for all nonmalignant tumors was meningioma (53.0%) [13]. Glioblastoma and meningioma were diagnosed at older ages (median age of 64 and 66 years, respectively) [13].

CNS tumors were classified with the latest update, according to the criteria established by the "World Health Organization" (WHO) [14]. The WHO categorization of CNS tumors-2007 was largely dependent on histological and immunohistochemical properties of tumor cells while 2016 version of WHO classification revised according to molecular and genetic properties of tumor cells in addition to morphological characteristics [12, 14]. There are 152 types of primary central nervous system (CNS) tumors on the WHO's 2016 list with their official name and the ICD-O (International Classification of Diseases

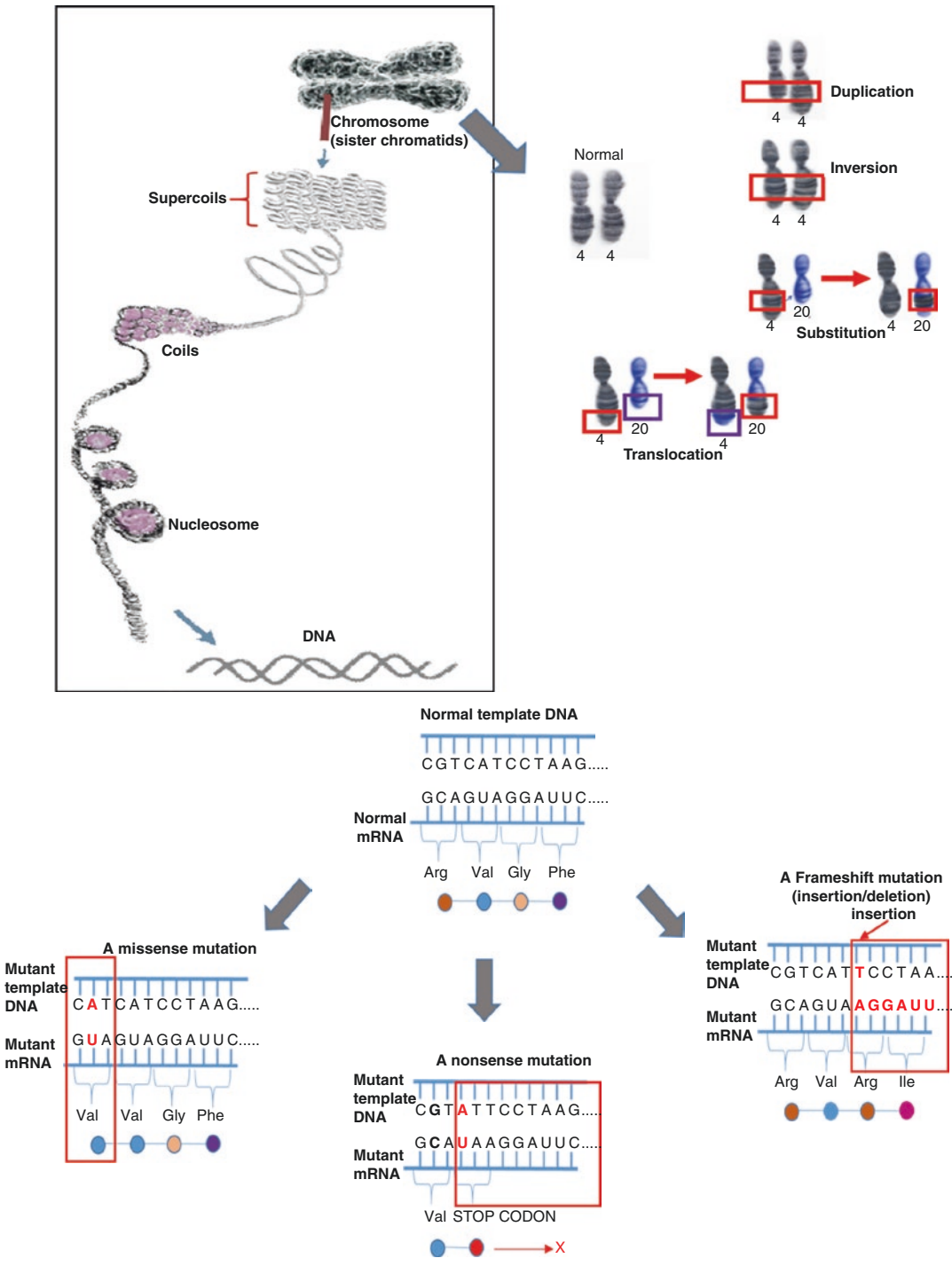

Fig. 8.2 Mutation types. Gene mutations and chromosomal mutations

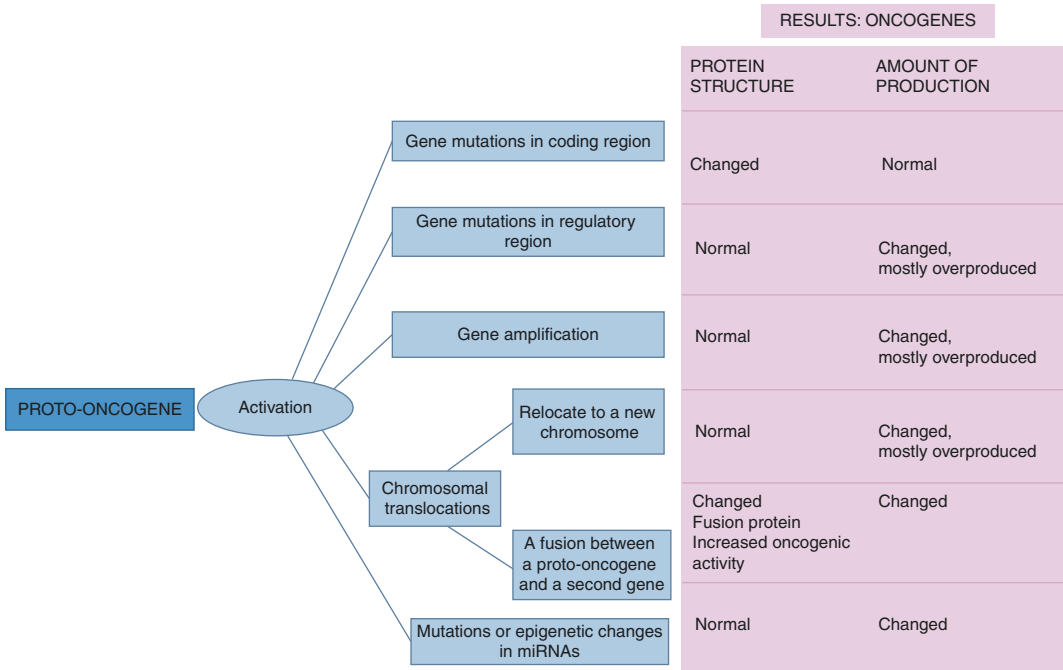

Fig. 8.3 A short summary of oncogenes activation options and the outcome of these activations. Some miRNAs may behave as oncogenes such as mir-21. In some cases, protein structure is changed but the final protein levels are the same as before the mutation. For the others, protein structure is the same as before the genetic alteration, but the final protein levels are changed. Epigenetic changes can affect final protein product levels. For all conditions, mutations and epigenetic changes are the basis for the formation of oncogenes, and oncogenes are the basis for the formation of tumor cells

for Oncology) codes [14]. These tumors have their own spectrum of clinical and genetic characteristics, treatments, and sequelae. For example, glial tumors are named according to their histological properties like astrocytomas (including glioblastoma), oligodendrogliomas, ependymomas, oligoastrocytoma (mixed glioma), not otherwise specified (NOS), and a few rare ones.

8.4 Molecular Markers

Along with other clinical data, some molecular markers that provide important biological and clinical understanding are commonly used in routine diagnostic. These molecular markers are mutations that can be determined by molecular genetic tests such as Sanger sequencing, next-generation sequencing, real-time PCR (RT-PCR), fluorescent in situ hybridization (FISH), comparative genomic hybridization (CGH), methylation-specific polymerase chain reaction (MSP-PCR), and immunohistochemistry IHC.

Each tumor has some typical mutations. For example, oligodendrogliomas are characterized by isocitrate dehydrogenase (IDH) mutations with a codeletion in 1p/19q and a mutation at the promoter region of telomerase reverse transcriptase (TERTp) [12]. Actually, the status of 1p/19q codeletion and IDH mutations are used as a classification marker as indicated by a diagnostic algorithm of WHO (Fig. 8.4).

The common genetic abnormalities that are pathologic markers in brain tumors are summarized in Table 8.1 and some important ones are below:

8.4.1 IDH1/2 Mutations

There is five isocitrate dehydrogenase (IDH) enzymes encoded in the human genome. The

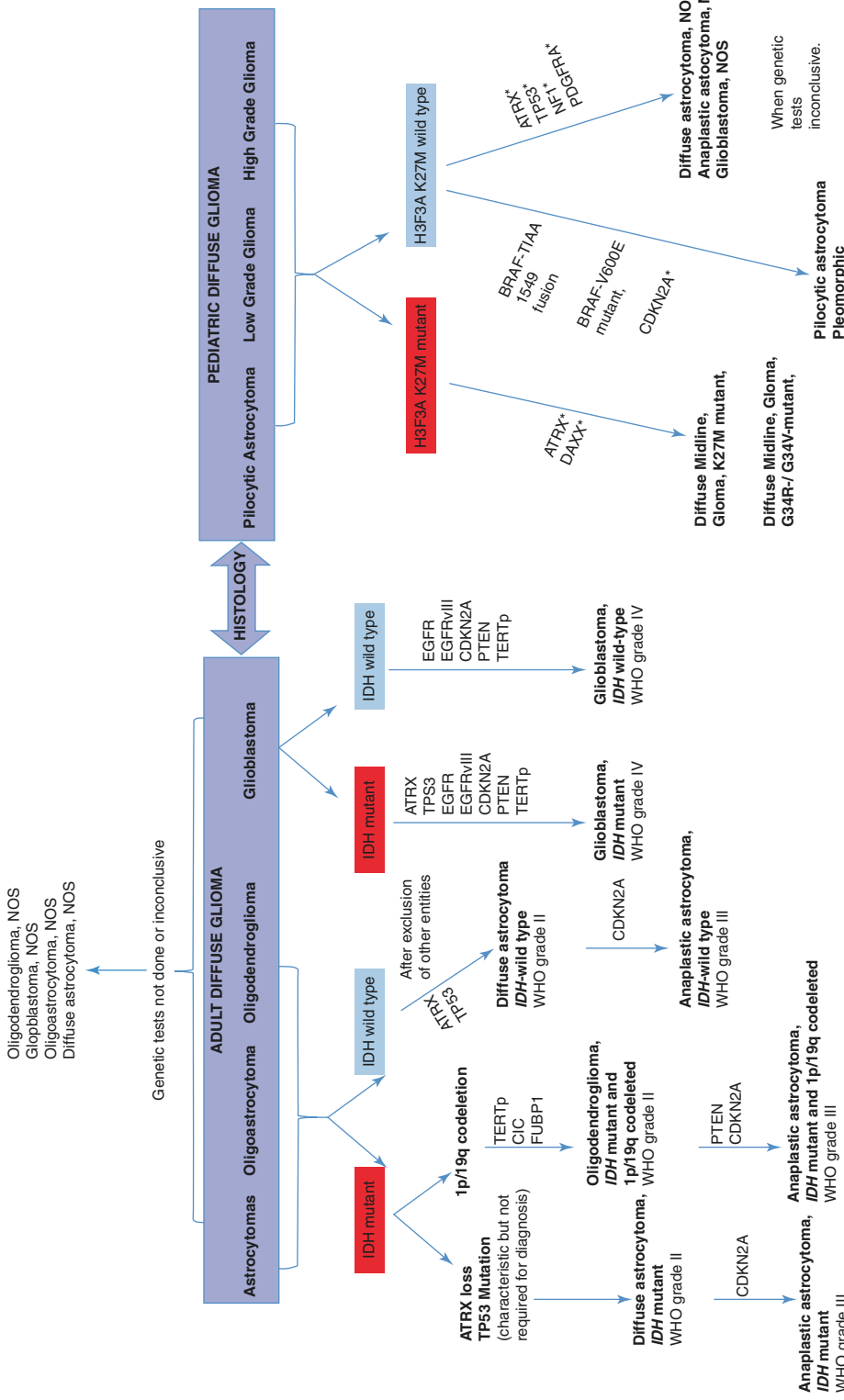

Fig. 8.4 A summary chart for classification of the diffuse gliomas based on genetic and histological features [12, 14]. *NOS* not otherwise specified. *Characteristic but not required for diagnosis

Table 8.1 The most common genetic changes in brain tumors [12, 15, 16]

Mutation name	Brain tumors	Location	Function	Mechanisms	FoGC (%)	Test method
1p/19q codeletion	Oligodendroglioma	1p36/19q	Undefined	Chromosomal deletion	100	FISH, IHC, Seq.
IDH1	Oligodendroglioma, Astrocytoma	2q33.3	Play roles in energy production. Magnesium ion binding and oxidoreductase activity, NAD or NADP as acceptor	R132 mutation	100	FISH, CGH, IHC, Seq.
IDH2		15q26.1		R172 mutation	65	FISH, CGH, IHC, Seq.
BRAF	Craniopharyngioma (papillary)	7q34	Serine/threonine protein kinase plays a role in regulating the MAP kinase/ERKs signalling pathway	V600E mutation	100	SNP-Array, FISH, RT-PCR, CGH, Seq.
BRAF	Pleomorphic xanthoastrocytoma			V600E mutation	66	
BRAF	Pilocytic astrocytoma			V600E mutation	9	
BRAF	Langerhans cell histiocytosis			M600E mutation	50–57	
BRAF	Ganglioglioma			W600E mutation	18	
BRAF-KIAA1549	Pilocytic astrocytoma			Oncogenic fusion	75	
TP53	Glioma, Medulloblastoma	17p13.1	TSG. Control of apoptosis, cell cycle progression, DNA repair	Missense mutations, LOH	96	Seq. DNA copy number analyses, RT-PCR, IHC
ATRX	Astrocytoma Glioma Glioblastoma	Xq21.1	Involved in transcriptional regulation and chromatin remodeling Abnormal telomere lengthening	Missense mutation (E991K), (X-linked) Loss of function	96 86 85	IHC, Seq.
TERT	Oligodendroglioma	5p15.33	Telomerase Reverse Transcriptase. It maintains telomere ends by addition of the telomere repeat TTAGGG	Promoter mutation	80–96	IHC, Seq.
TERT	Meningioma (fibrous)				10	IHC, Seq.
PTEN	Glioblastoma	10q23.3	Dual-specificity protein and lipid phosphatase, a negative regulator of phosphatidylinositol 3-kinase	Promoter methylation LOH, mutations	30	FISH, IHC, CGH, Seq.
EGFR amp.	Ependymoma, glioblastoma multiform	7p12	Epidermal growth factor receptor. A member of the protein kinase superfamily	Amplification	57	IHC, Seq., FISH, CGH, PCR
EGFRvIII mutation	Glioblastoma			Deletion	20	FISH, CGH, Seq.
PDGFRA	Glioblastoma, Oligodendrogliomas, High-grade astrocytoma	4q12	A tyrosine kinase receptor, that plays a role in organ development, wound healing, and tumor progression	Amplification	13	IHC, FISH, CGH, Seq.
					–	
					21–29	

CDKN2A	Glioblastoma,	9p21.3	Inhibitor of CDK4/6, CDK2A	Promoter methylation, homozygous deletion	60	IHC, Seq.
CDKN2B	Low-grade glioma		Cell growth regulator that controls cell cycle G1 progression		11	
CDKN2C	Glioblastoma	1p32.3			–	
CIC	Oligodendroglioma	19q13.2	Involved in brain development in concert with ATXN1 and ATXN1L	Mutation	56	Seq.
FUBP1	Oligodendroglioma	1p31.1	Binds RNA, and contains 3′–5′ helicase activity on both DNA–DNA and RNA–RNA duplexes. It may act both as activator and repressor of transcription	Mutation	29	FISH, CGH
TRAF7/ KLF4	Meningioma, fibrous type	16p13.3	Signal transducers for members of the TNF receptor superfamily	Mutation	100	
TSC1	Subependymal giant cell astrocytoma	9q34	Growth inhibitory protein product thought to play a role in the stabilization of tuberin	LOH	100	PCR-SSCP, Seq.
TSC2	Astrocytoma	16p13.3	Stimulation of specific GTPases	LOH	100	PCR-SSCP, Seq.
MYB-QKI fusion	Diffuse intrinsic pontine glioma, angiocentric glioma	6q22-q23	Transcription regulator	Oncogenic fusion	100	PCR
Histone H3F3A K27M	Diffuse intrinsic pontine glioma	1q42.12	Protein heterodimerization activity and RNA Polymerase II enhancer, sequence-specific binding to DNA	Mutation	80	FISH, CGH, IHC, Seq.
	Diffuse midline gliomas				70	
MGMT	Pleomorphic xanthoastrocytoma	10q26.3	DNA repair protein that is involved in cellular defense against mutagenesis and toxicity from alkylating agents	Promoter methylation	78.5	MSP-PCR, Pyrosequencing, IHC
	Oligodendroglioma				85	
	Glioblastoma				48–80	

FoGC frequency of genetic change, *TSG* tumor suppressor gene, *LOH* loss of heterozygosity, *CNS* central nervous system, *IHC* immunohistochemistry, *Seq* sequencing, *FISH* fluorescent in situ hybridization, *CGH* comparative genomic hybridization, *RT-PCR* real-time polymerase chain reaction,—not known, *MSP-PCR* methylation-specific polymerase chain reaction, *SNP-Array* single nucleotide polymorphism-based array analysis

mutations in cytoplasmic IDH1 and mitochondrial IDH2 have been identified as playing a decisive role in diagnosis and prognosis in brain tumors [17–19]. IDH1 (at chromosome 2q33.3) and IDH2 (at chromosome 15q26.1) encoded enzymes are NADP(+)-dependent and play roles in energy production. The most frequent mutations R132 (IDH1) and R172 (IDH2) occur in the active site of the enzymes. Both mutations were discovered by whole exome sequencing of glioblastomas (GB) [17–19].

IDH1 was an oncogene rather than a tumor suppressor gene [1]. The highest frequencies of IDH1 mutations were detected in secondary glioblastomas (88%), oligoastrocytomas (78%), oligodendrogliomas (69%), and diffuse astrocytomas (68%) [18]. IDH2 mutations have been associated with improved prognosis in gliomas.

The high frequencies of IDH mutations in astrocytic and oligodendroglial gliomas (WHO grade II, III) may be effective in early tumor development that can give rise to both astrocytes and oligodendrocytes [17, 18].

8.4.2 Codeletion of Chromosome 1p/19q

1p/19q abnormality was determined by fluorescence in situ hybridization (FISH) method with locus-specific colored probes. The loss of chromosome arms 1p and 19q has been characteristically detected in oligodendroglial tumors [20]. This codeletion is associated with a better prognosis and is an indicator of a good response to lomustine, procarbazine, and vincristine combination for chemotherapy [12]. However, other genetic changes have been reported as indicators of poor response to therapy and short survival, such as mutation of the PTEN gene at 10q23, homozygous deletion of the CDKN2A gene at 9p21, and amplification of the EGFR gene at 7p12 [20].

8.4.3 BRAF Mutations and BRAF-KIAA1549 Fusions

BRAF gene encodes B-Raf proto-oncogene protein that plays a role in regulating the MAP kinase/ERK signalling pathway affecting differentiation, cell division, and secretion. Missense BRAF mutations are found in many tumor-associated somatic alterations. Valine 600 to glutamic acid (V600E) is the most prevalent BRAF mutation. Missense V600E mutations and fusions of BRAF with KIAA1549 or FAM131B are characteristics of pilocytic astrocytomas.

Fusions between BRAF exon 9 and KIAA1549 exon 15 or FAM131B exon 2 in chromosome 7q34 can be detected by real-time polymerase chain reaction (RT-PCR), fluorescent in situ hybridization (FISH), and single nucleotide polymorphism (SNP)-based array analysis [21].

The BRAF V600E mutations were found in 66% in pleomorphic xanthoastrocytomas, 65% in xanthoastrocytomas with anaplasia, 18% in WHO grade I gangliogliomas, and 33% in pilocytic astrocytomas [22]. No mutations or low-frequency BRAF mutations occur in glioblastomas and other gliomas [22].

8.4.4 H3F3A Mutation

H3F3A (H3 histone family member 3A) encodes H3.3 histone that plays a central role in transcription regulation, DNA repair, DNA replication, and chromosomal stability. Histones are nuclear proteins that are responsible for the formation of chromosomal fibers in eukaryotes. There are four core histone molecules existing, H2A, H2B, H3, and H4. Two molecules of each of the four core histones form octamers and wrap DNA in repeating units.

H3F3A mutations have been detected in some cancers. For example, It has been reported that 80% of diffuse intrinsic pontine glioma (DIPG) cases, which is an aggressive pediatric brain tumor, and 70% of midline glioblastomas have a missense mutation at an allele of the H3F3A gene

at codon 27, replacing the lysine with methionine (K27M) [23, 24]. In addition, pyrosequencing analysis revealed that K27M mutations occurred in 27.1% of GBs and 17.9% of anaplastic astrocytomas [25].

8.4.5 P53 Mutation

TP53 is a very important TSG that encodes p53 protein locating in the nucleus. P53 is a gatekeeper protein that responds to diverse cellular stresses by regulating the expression of target key genes to control cell cycle arrest, apoptosis, senescence, and DNA repair. TP53 mutations are common in many other types of tumors. It is the first genetic alteration in astrocytic brain tumors [26]. The frequency of TP53 mutations in WHO class II and III astrocytic tumors are 94% [12, 27, 28]. Mostly, the mutations in TP53 are single nucleotide missense mutations. These point mutations are broadly distributed throughout the gene, but the majority of them localizing in the DNA-binding domain of p53. However, for some conditions, TP53 is completely deleted because of LOH or chromosomal aneuploidy. For example, monosomy 17 is the most common chromosomal mutation, with an approximately 50% frequency, in pediatric ependymomas [29]. TP53 has been altered or deleted in 25–40% of all glioblastoma multiforms (GBMs). The deletion is more severe in GBM and appears to be associated with tumors that occur in younger age groups of patients. Actually, TP53 mutations are classified into early progenitor-like (EPL) subtypes such as the pro-neural class of GB [15, 19].

8.4.6 ATRX Mutation

ATRX gene encodes a chromatin remodeler protein that plays roles in transcriptional regulation, helicase activity, chromatin binding, and remodelling. It may be involved in brain development and facial morphogenesis. ATRX protein commonly involved in ATRX–DAXX complex acts as histone chaperone molecule and facilitates deposition of histone H3.3 at telomeres. ATRX mutations correlate with abnormal telomeres in tumors of the central nervous system. The presence of ATRX mutations was shown correlated with alternative telomere lengthening in pediatric high-grade gliomas (HGGs) [30]. Mutations in this gene are related to X-linked syndromes and closely associated with TP53 mutations [31].

Loss-of-function ATRX mutations have been detected in astrocytoma with a frequency of 96% and neuroblastomas [12].

Most of lower-grade gliomas with IDH mutations and no 1p/19q codeletion had inactive ATRX (86%). In addition, ATRX mutations are observed in pediatric high-grade gliomas such as diffuse midline gliomas (DMGs) [16].

8.4.7 TERT Promoter Mutation

TERT gene encodes Telomerase Reverse Transcriptase that is a ribonucleoprotein polymerase maintaining telomere ends by addition of the telomere repeat TTAGGG. It is active in progenitor cells and almost all cancer cells while it is inactive, or have a low activity, in normal somatic cells. Overexpression of TERT mRNA was found to be associated with increased telomere length as in gliomas. The increased telomere length is associated with ATRX mutations. Telomerase activity is upregulated by point mutations in the promoter region of TERT, leading to high telomerase activity.

Atypical and anaplastic meningiomas usually have mutations in TERT promoter.

8.4.8 CDKN2A (p16) Homozygous Deletion

CDKN2A (cyclin-dependent kinase 2A) encodes p16 and p14arf. These alternatively spliced proteins are both tumor suppressors. P16 is a cyclin-dependent kinase inhibitor and inhibits cyclin-dependent kinase 4 and 6

(CDK4 and CDK6), and thereby activates retinoblastoma (Rb) family proteins for cell cycle control.

P14arf is the other protein encoded by CDKN2A, that transcribed by alternate open reading frame (ARF). P14arf activates p53 via MDM2.

CDKN2A is inactivated mostly by homozygous deletions or sometimes by promoter hypermethylation. A homozygous deletion or promoter hypermethylation of CDKN2A/2B is detected in 60% of GBMs and 11% of low-grade gliomas including oligodendroglioma, pleomorphic xanthoastrocytoma, and pilocytic astrocytoma [32].

8.4.9 EGFR Amplification and EGFRvIII Mutation

EGFR gene encodes "Epidermal Growth Factor Receptor" (EGFR) that is a cell membrane receptor playing a role in cell proliferation. When EGFR is activated by a gene amplification or by a deletion as in EGFR variant III (EGFRvIII) which is the most common rearranged form, it stimulates intracellular tyrosine kinase and triggers uncontrolled cell cycle division [33]. The EGFRvIII mutation is 801 bp deletion from exons 2 to 7 of the EGFR gene, causing a deletion protein's extracellular domain.

EGFR gene amplification and/or EGFRvIII may cause almost always active or overexpressed EGFR in high-grade astrocytomas, particularly glioblastomas [32] as well as prostate, non-small cell lung cancer and basal-like breast cancers. These alterations lead to constitutive activation of several signalling pathways including MAPK and PI3K/AKT that is critical for gliomagenesis and RAS-RAF-MEK-ERK and NF-kappa-B signalling cascades [34, 35].

EGFRvIII-positive tumor cells are the most proliferative and aggressive phenotype. Approximately 57% of glioblastoma cells exhibit EGFR overexpression [32].

8.4.10 PDGFRA Amplification

This gene encodes "Platelet-Derived Growth Factor Receptor" that is a cell surface tyrosine kinase receptor. Platelet-derived growth factor (PDGF) family of growth factors that are mitogens for mesenchymal origin cells bind these receptors. Binding of a ligand (PDGFA, PDGFB, PDGFC, and PDGFD) to the extracellular domain of the PDGFR results in oligomerization of two receptor molecules according to the functional polypeptides (alpha or beta), leading to the production of αα, ββ homodimers, or αβ heterodimers. After receptor-ligand binding, down-signalling begins, and some pathways including ERK, RAS/MAPK, and PI3K can be activated [15].

PDGFRA (PDGFR α) plays an important role in organ development while PDGFRβ is associated in early hematopoiesis. Amplified PDGFRA was seen in 13% of glioblastomas. Transcription of PDGFRA was also found to be upregulated in astrocytomas without gene amplification [32, 36]. Pediatric (29.3%) and adult (20.7%) high-grade astrocytomas also have PDGFRA amplification. In adults, PDGFR amplification was associated with significantly worse overall survival [37].

8.4.11 PTEN Mutation

PTEN ("Phosphatase and Tensin Homolog") is the most mutated tumor suppressor after p53 and mutated in a large number of cancers such as prostate cancer, glioblastoma, endometrial, lung, and breast cancer. It negatively regulates the PI3K-Akt signalling pathway. PTEN can act as both a phosphatase and a diphosphatase. When the phosphatase activity is lost due to LOH, promoter methylation, interference of miRNAs, and phosphorylation [38], PI3K-Akt signalling pathways are activated resulting in abnormal proliferation. PTEN mutations are found in 30% of GBMs. In IDH wild-type cases, PTEN inactivation often leads to GBM, and rarely to low-grade glioma. PTEN mutations are common in primary glioblastomas, while TP53 mutations are more common in secondary glioblastomas.

8.5 Concluding Remarks

Recent advances show that cancer is a genetic disease. Genetic alterations include not just mutations, they also include changes in epigenetic, transcriptional, and translational mechanisms (e.g., RNAi, miRNAs) of the cells that can be effective in the formation of diseases. Molecular biology is being used more and more intensively to diagnose cancer patients correctly, to determine subtypes of tumors and thus to decide the right treatment. Many methods such as PCR, RT-PCR, FISH, aCGH, Sanger sequencing, next-generation sequencing, pyrosequencing, mass spectrophotometry, and flow cytometry were discovered and have been used to for detection of genetic alterations.

All of these molecular mechanisms seem to be the key to understand cancer as well as hope for treatment. As a matter of fact, gene therapies and target-specific RNAi and CRISPR/Cas9 methods have been advancing at a dizzying pace and promises hope for cancer treatment.

References

1. Vogelstein B, Papadopoulos N, Velculescu VE, Zhou S, Diaz LA Jr, Kinzler KW. Cancer genome landscapes. Science. 2013;339(6127):1546–58.
2. Klein G. Oncogenes and tumor suppressor genes. Acta Oncol. 1988;27(4):427–37.
3. Negrini M, Ferracin M, Sabbioni S, Croce CM. MicroRNAs in human cancer: from research to therapy. J Cell Sci. 2007;120(Pt 11):1833–40.
4. Esquela-Kerscher A, Slack FJ. Oncomirs—microRNAs with a role in cancer. Nat Rev Cancer. 2006;6(4):259–69.
5. Ciafre SA, Galardi S, Mangiola A, Ferracin M, Liu CG, Sabatino G, et al. Extensive modulation of a set of microRNAs in primary glioblastoma. Biochem Biophys Res Commun. 2005;334(4):1351–8.
6. Chan JA, Krichevsky AM, Kosik KS. MicroRNA-21 is an antiapoptotic factor in human glioblastoma cells. Cancer Res. 2005;65(14):6029–33.
7. van Gent DC, Hoeijmakers JH, Kanaar R. Chromosomal stability and the DNA double-stranded break connection. Nat Rev Genet. 2001;2(3):196–206.
8. Michor F, Frank SA, May RM, Iwasa Y, Nowak MA. Somatic selection for and against cancer. J Theor Biol. 2003;225(3):377–82.
9. Stratakis CA. Genetics of adrenocortical tumors: gatekeepers, landscapers and conductors in symphony. Trends Endocrinol Metab. 2003;14(9):404–10.
10. Huttner A. Overview of primary brain tumors: pathologic classification, epidemiology, molecular biology, and prognostic markers. Hematol Oncol Clin North Am. 2012;26(4):715–32.
11. Dubuc AM, Northcott PA, Mack S, Witt H, Pfister S, Taylor MD. The genetics of pediatric brain tumors. Curr Neurol Neurosci Rep. 2010;10(3):215–23.
12. Park SH, Won J, Kim SI, Lee Y, Park CK, Kim SK, et al. Molecular testing of brain tumor. J Pathol Transl Med. 2017;51(3):205–23.
13. Ostrom QT, Gittleman H, Liao P, Vecchione-Koval T, Wolinsky Y, Kruchko C, et al. CBTRUS statistical report: primary brain and other central nervous system tumors diagnosed in the United States in 2010–2014. Neuro-Oncology. 2017;19(Suppl 5):v1–v88.
14. Louis DN, Perry A, Reifenberger G, von Deimling A, Figarella-Branger D, Cavenee WK, et al. The 2016 World Health Organization classification of tumors of the central nervous system: a summary. Acta Neuropathol. 2016;131(6):803–20.
15. Nasser MM, Mehdipour P. Exploration of involved key genes and signaling diversity in brain tumors. Cell Mol Neurobiol. 2018;38(2):393–419.
16. Cancer Genome Atlas Research Network, Brat DJ, Verhaak RG, Aldape KD, Yung WK, Salama SR, et al. Comprehensive, integrative genomic analysis of diffuse lower-grade gliomas. N Engl J Med. 2015;372(26):2481–98.
17. Parsons DW, Jones S, Zhang X, Lin JC, Leary RJ, Angenendt P, et al. An integrated genomic analysis of human glioblastoma multiforme. Science. 2008;321(5897):1807–12.
18. Balss J, Meyer J, Mueller W, Korshunov A, Hartmann C, von Deimling A. Analysis of the IDH1 codon 132 mutation in brain tumors. Acta Neuropathol. 2008;116(6):597–602.
19. Yan H, Parsons DW, Jin G, McLendon R, Rasheed BA, Yuan W, et al. IDH1 and IDH2 mutations in gliomas. N Engl J Med. 2009;360(8):765–73.
20. Reifenberger G, Louis DN. Oligodendroglioma: toward molecular definitions in diagnostic neuro-oncology. J Neuropathol Exp Neurol. 2003;62(2):111–26.
21. Roth JJ, Santi M, Pollock AN, Harding BN, Rorke-Adams LB, Tooke LS, et al. Chromosome band 7q34 deletions resulting in KIAA1549-BRAF and FAM131B-BRAF fusions in pediatric low-grade gliomas. Brain Pathol. 2015;25(2):182–92.
22. Schindler G, Capper D, Meyer J, Janzarik W, Omran H, Herold-Mende C, et al. Analysis of BRAF V600E mutation in 1,320 nervous system tumors reveals high mutation frequencies in pleomorphic xanthoastrocytoma, ganglioglioma and extracerebellar pilocytic astrocytoma. Acta Neuropathol. 2011;121(3):397–405.

23. Zhang R, Han J, Daniels D, Huang H, Zhang Z. Detecting the H3F3A mutant allele found in high-grade pediatric glioma by real-time PCR. J Neurooncol. 2016;126(1):27–36.
24. Liu KW, Pajtler KW, Worst BC, Pfister SM, Wechsler-Reya RJ. Molecular mechanisms and therapeutic targets in pediatric brain tumors. Sci Signal. 2017;10(470):eaaf7593.
25. Gielen GH, Gessi M, Hammes J, Kramm CM, Waha A, Pietsch T. H3F3A K27M mutation in pediatric CNS tumors: a marker for diffuse high-grade astrocytomas. Am J Clin Pathol. 2013;139(3):345–9.
26. Nigro JM, Baker SJ, Preisinger AC, Jessup JM, Hostetter R, Cleary K, et al. Mutations in the p53 gene occur in diverse human tumor types. Nature. 1989;342(6250):705–8.
27. Kyritsis AP, Saya H. Epidemiology, cytogenetics, and molecular biology of brain tumors. Curr Opin Oncol. 1993;5(3):474–80.
28. del Arco A, Garcia J, Arribas C, Barrio R, Blazquez MG, Izquierdo JM, et al. Timing of p53 mutations during astrocytoma tumorigenesis. Hum Mol Genet. 1993;2(10):1687–90.
29. von Haken MS, White EC, Daneshvar-Shyesther L, Sih S, Choi E, Kalra R, et al. Molecular genetic analysis of chromosome arm 17p and chromosome arm 22q DNA sequences in sporadic pediatric ependymomas. Genes Chromosomes Cancer. 1996;17(1):37–44.
30. Heaphy CM, de Wilde RF, Jiao Y, Klein AP, Edil BH, Shi C, et al. Altered telomeres in tumors with ATRX and DAXX mutations. Science. 2011;333(6041):425.
31. Klonou A, Piperi C, Gargalionis AN, Papavassiliou AG. Molecular basis of pediatric brain tumors. Neuromolecular Med. 2017;19(2–3):256–70.
32. Rodriguez FJ, Vizcaino MA, Lin MT. Recent advances on the molecular pathology of glial neoplasms in children and adults. J Mol Diagn. 2016;18(5):620–34.
33. Kuan CT, Wikstrand CJ, Bigner DD. EGFRvIII as a promising target for antibody-based brain tumor therapy. Brain Tumor Pathol. 2000;17(2):71–8.
34. Habib AA, Chatterjee S, Park SK, Ratan RR, Lefebvre S, Vartanian T. The epidermal growth factor receptor engages receptor interacting protein and nuclear factor-kappa B (NF-kappa B)-inducing kinase to activate NF-kappa B. Identification of a novel receptor-tyrosine kinase signalosome. J Biol Chem. 2001;276(12):8865–74.
35. Derrien A, Druey KM. RGS16 function is regulated by epidermal growth factor receptor-mediated tyrosine phosphorylation. J Biol Chem. 2001;276(51):48532–8.
36. Louis DN, Ohgaki H, Wiestler OD, Cavenee WK, Burger PC, Jouvet A, et al. The 2007 WHO classification of tumors of the central nervous system. Acta Neuropathol. 2007;114(2):97–109.
37. Phillips JJ, Aranda D, Ellison DW, Judkins AR, Croul SE, Brat DJ, et al. PDGFRA amplification is common in pediatric and adult high-grade astrocytomas and identifies a poor prognostic group in IDH1 mutant glioblastoma. Brain Pathol. 2013;23(5):565–73.
38. Georgescu MM. PTEN tumor suppressor network in PI3K-Akt pathway control. Genes Cancer. 2010;1(12):1170–7.

Treatment of Brain Tumor

9

İlknur Alsan Çetin

9.1 Treatment Options

Brain tumor treatment requires a multidisciplinary approach. Symptoms appear in the patient according to the area in which the tumor is located. A variety of therapies are used to treat brain tumors. The type of treatment recommended depends on the size, type, growth rate, and location of the tumor and performance status (PS) of the patient. Treatment options include surgery, radiation therapy, chemotherapy, targeted biological agents, or a combination of these.

9.1.1 Surgery

Brain tumors comprise a wide range of different neoplasms that grow within the central nervous system (CNS) [1]. The aim of neurosurgery in most brain tumors is maximal safe tumor resection. However, in selected cases such as certain deep-seated brain tumors or suspected brain lymphomas, either an open or stereotactic tumor biopsy is indicated. To optimize resection of brain tumors, specific intraoperative techniques were established in recent decades. The application of neuronavigation is nowadays considered as standard for preoperative approach planning, intraoperative localization, and guidance during surgery of brain tumors [2]. In recent years, the use of "advanced navigation" additionally enables the inclusion of multimodality image data such as magnetic resonance spectroscopy (MRS), perfusion magnetic resonance imaging (MRI), diffusion tensor imaging (DTI), and functional MRI in order to increase the precision of tissue sampling and patient safety [3, 4]. Furthermore, intraoperative ultrasound and MRI constitute the methods for visualization of brain tumors during surgery [5, 6].

9.1.2 Radiation Therapy (RT)

RT has been established as a mainstay of treatment for brain tumors, and for many brain tumor subtypes such as germinoma, may be curative [7]. Use of RT can also prolong survival or provide palliative relief and is a treatment modality used for both primary and metastatic tumors [8].

9.1.3 Chemotherapy

Chemotherapy, along with radiation (concurrent therapy), has become the standard of care for primary malignant brain tumors. It can be used before, during, or after surgery and/or radiotherapy to help.

İ. A. Çetin (✉)
Faculty of Medicine, Department of Radiation Oncology, Marmara University, Istanbul, Turkey

Y. Özsunar, U. Şenol (eds.), *Atlas of Clinical Cases on Brain Tumor Imaging*,
https://doi.org/10.1007/978-3-030-23273-3_9

9.1.4 Targeted Therapy

The focus on a specific element of a cell, such as molecules or pathways required for cell growth, in order to use them as a target.

9.2 Treatment Recommendations

9.2.1 Gliomas

Low-grade tumors (grade I and II), which are not aggressive, are treated with watchful monitoring or surgery alone. Surgery may be the only treatment needed especially if all of the tumor can be removed. Radiation therapy and chemotherapy is used for high risk patients. Radiotherapy has been the mainstay of treatment for glioma since the 1980s when it was established that postoperative treatment improves survival [9, 10]. No consensus exists regarding the proper timing of postoperative external beam radiation therapy (EBRT) in low-grade glioma. Although delaying RT in young, healthy patients without progressive neurologic decline can be controversial, there is a consensus to proceed with immediate postoperative RT in older patients after a less than total resection, because their survival is as poor as patients with anaplastic astrocytoma. High-risk patients with low-grade gliomas benefit with respect to both progression-free survival and overall survival with early up-front RT [11].

The standard RT dose for low-grade astrocytoma is 45–54 Gy, delivered in 1.8–2.0 Gy fractions [12]. Consider RT dose escalation to 59.4–60 Gy for isocitrate dehydrogenase (IDH)-wild-type low-grade gliomas, as these patients may have a more aggressive course of disease. Chemotherapy is not a traditional mainstay of upfront treatment for low-grade gliomas. There are some data that support temozolomide or PCV (procarbazine, lomustine, and vincristine) as adjuvant therapy especially in high-risk patients (age ≥40 following any resection or younger patients who were subtotally resected) [13, 14].

Higher grade tumors (grade III and IV), which are malignant and grow quickly, are more difficult to remove and require additional treatments beyond surgery, followed by RT and chemotherapy. Fractionated EBRT after surgery is standard adjuvant therapy for patients with high-grade astrocytoma [15]. The typical dose is 60 Gy in 1.8–2.0 Gy fractions. Use of hypofractionated courses of RT has been shown to be efficacious in poorly performing or older patients with glioblastoma. Typical schemes are 34 Gy in 10 fractions, 40 Gy in 15 fractions, or 50 Gy in 20 fractions. Alternatively, a shorter fractionation schedule of 25 Gy in 5 fractions may be considered for elderly and/or frail patients with smaller tumors for whom a longer course of treatment would not be tolerable [16–18]. Studies including a radiosurgery or brachytherapy boost to conventional RT did not show a survival benefit [19, 20].

Combined chemoradiation has emerged as a new standard of care for patients with 1p/19q co-deleted anaplastic oligodendroglioma or oligoastrocytoma as well as good PS non-elderly glioblastoma [21, 22]. Survival improves when chemotherapy is added to postoperative RT [23, 24]. Temozolomide, an alkylating agent, is now the standard of care in conjunction with postoperative RT for younger, good performance patients with glioblastoma [25, 26]. For frail patients, temozolomide or RT alone may be administered in old age [27].

Bevacizumab, an antiangiogenic agent, can be used for recurrent glioblastoma. Bevacizumab in combination with irinotecan, carmustine or lomustine, carboplatin or temozolomide has also been used in anaplastic gliomas. These combinations may be considered for patients who have failed bevacizumab monotherapy.

Alternating electric field therapy is a type of electromagnetic field therapy using low-intensity electrical fields to treat for recurrent glioblastoma [28].

9.2.2 Ependymoma

Surgery is the primary treatment for ependymoma. For more aggressive tumors or for

tumors that can't be removed completely with surgery, additional treatments, such as radiation therapy or chemotherapy, may be recommended. Whole brain and spine receive 36 Gy in 1.8 Gy fractions, followed by limited field to spine lesions to 45 Gy [29, 30]. For intracranial ependymomas, the primary brain site should receive a total of 54–59.4 Gy in 1.8–2.0 Gy fractions. To reduce toxicity from craniospinal irradiation (CSI) in adults, consider the use of intensity-modulated radiotherapy (IMRT) or protons if available. Stereotactic radiosurgery (SRS) has been used as a boost after EBRT or to treat recurrence with some success, although long-term results are still lacking [31]. Research on chemotherapeutic regimens has also centered on pediatric ependymomas, while the role of chemotherapy in the treatment of adult patients remains poorly defined.

9.2.3 Adult Medulloblastoma and Supratentorial PNET

There is consensus that surgical resection should be the routine initial treatment to establish diagnosis, relieve symptoms, and maximize local control. Complete resection is associated with improved survival. Adjuvant RT following surgery is the current standard of care. The conventional dose is 23.6–36 Gy of CSI and a boost to a total 54–58.8 Gy to the primary brain site with or without adjuvant chemotherapy. The use of post-irradiation chemotherapy to allow RT dose reduction is becoming increasingly common especially for children, but optimal use of adjuvant chemotherapy is still unclear for adult patients [32, 33].

9.2.4 Primary CNS Lymphomas

Methotrexate is the most effective agent in systemic therapy. It is commonly used in combination with other drugs such as vincristine, procarbazine, cytarabine, rituximab, and ifosfamide, but it may also be administered as monotherapy if toxicity tolerance is a concern [34, 35]. Chemotherapy is usually followed by consolidation RT to maximize response and improve outcome [36]. When used, low-dose whole brain radiation therapy (WBRT) should be limited to 23.4 Gy in 1.8 Gy fractions following a complete response (CR) to chemotherapy. For less than CR, consider WBRT to 30–36 Gy followed by a limited field to gross disease to 45 Gy.

9.2.5 Benign Brain Tumors

9.2.5.1 Meningiomas

Asymptomatic tumors 30 mm or larger should be surgically resected or observed. If neurologic impairment is imminent, surgery or RT (EBRT or SRS) is feasible. Complete surgical resection may be curative. Both the tumor grade and the extent of resection impact the rate of recurrence. Meningiomas may be treated by fractionated RT with doses of 45–60 Gy. The use of stereotactic RT in the management of meningiomas continues to evolve [37–39].

9.2.5.2 Vestibular Schwannomas

Tumors may be managed with microsurgical resection, SRS to 12–13 Gy, or fractionated stereotactic radiation therapy (FSRT) using either a standard approach (i.e., 45 Gy at 1.8 Gy per fraction) or a hypofractionated approach (i.e., 20 Gy at 4 Gy per fraction). Local control is more than 90% with all treatment modalities. There are no prospective randomized trials to guide treatment decisions, and multidisciplinary evaluation of each patient is an integral component of appropriate management [40, 41].

9.2.5.3 Pituitary Tumors and Craniopharyngiomas

Primary therapy is optimized by a multidisciplinary approach. Depending on the endocrine abnormality, tumor size, location, and clinical presentation, management strategies can range from observation to surgery, medical management,

radiation therapy, or a combination of these options. The standard surgical approach is transsphenoidal microsurgery. Adjuvant medical and radiation therapy options may be used to manage pituitary adenomas [42]. Gross total resection (GTR) or subtotal resection (STR) followed by EBRT may be used to manage craniopharyngiomas [43].

9.2.6 Brain Metastases

Advances in surgical technique have rendered upfront resection followed by WBRT, the standard of care for solitary brain metastases [44]. The advent of SRS offered a minimally invasive option as opposed to surgery. Accumulating evidence suggests that low disease volume is a better selection criterion for SRS than a low number of metastatic lesions [45, 46]. Additionally, patients with a favorable histology of the primary tumor (such as breast cancer) or controlled primary tumors can often benefit from SRS regardless of the number of brain metastases present [47].

Historically, WBRT was the mainstay of treatment for metastatic lesions in the brain. For WBRT, doses vary between 20 and 40 Gy delivered in 5–20 fractions. For SRS, maximum marginal doses from 24 to 15 Gy based on tumor volume is recommended.

For patients with limited (1–3) metastatic lesions, aggressive management (surgical resection plus postoperative WBRT and for SRS plus WBRT if only one lesion is involved) should be strongly considered. Other options include SRS alone or SRS following resection [48, 49]. All patients diagnosed with more than three metastatic lesions should be treated with WBRT or SRS as primary therapy. Systemic therapy is rarely used as primary therapy for brain metastases.

9.3 Radiotherapy Techniques

Radiation leads to DNA damage in irradiated cells, ultimately leading to cell death by apoptosis or necrosis. RT uses high-energy beams, such as X-rays or protons. A conventional form of radiation treatment delivery uses a specific arrangement of X-ray beams designed to conform to the shape of the tumor to maximize tumor dose and minimize normal surrounding tissue dose. Several techniques can help focus the radiation more precisely.

9.3.1 3-Dimensional Conformal Radiation Therapy (3D-CRT)

A conventional form of radiation treatment delivery that uses a specific arrangement of X-ray beams designed to conform to the shape of the tumor. This form of treatment is tailored to the patient's specific anatomy and tumor location. CT and/or MRI scan is often required for treatment planning. Intracranial tumor volumes are best defined using pre- and postoperative imaging, usually enhanced T1 and/or FLAIR (fluid-attenuated inversion recovery)/T2 (Fig. 9.1) [50, 51].

9.3.2 Intensity Modulated Radiation Therapy (IMRT)

IMRT is a type of 3D-CRT that can more directly target a tumor. In IMRT, the radiation beams are broken up into smaller beams and the intensity of each of these smaller beams can be changed. This means that the more intense beams, or the beams giving more radiation, can be directed only at the tumor (Fig. 9.2) [52, 53].

9.3.3 Volumetric Modulated Arc Therapy (VMAT)

In recent years, the combination of IMRT delivery and optimization methods with arc therapy, VMAT has become an important method for the delivery of conformal therapy. VMAT is a relatively new IMRT method that combines rotational delivery and MLC-based IMRT (Fig. 9.3) [54, 55].

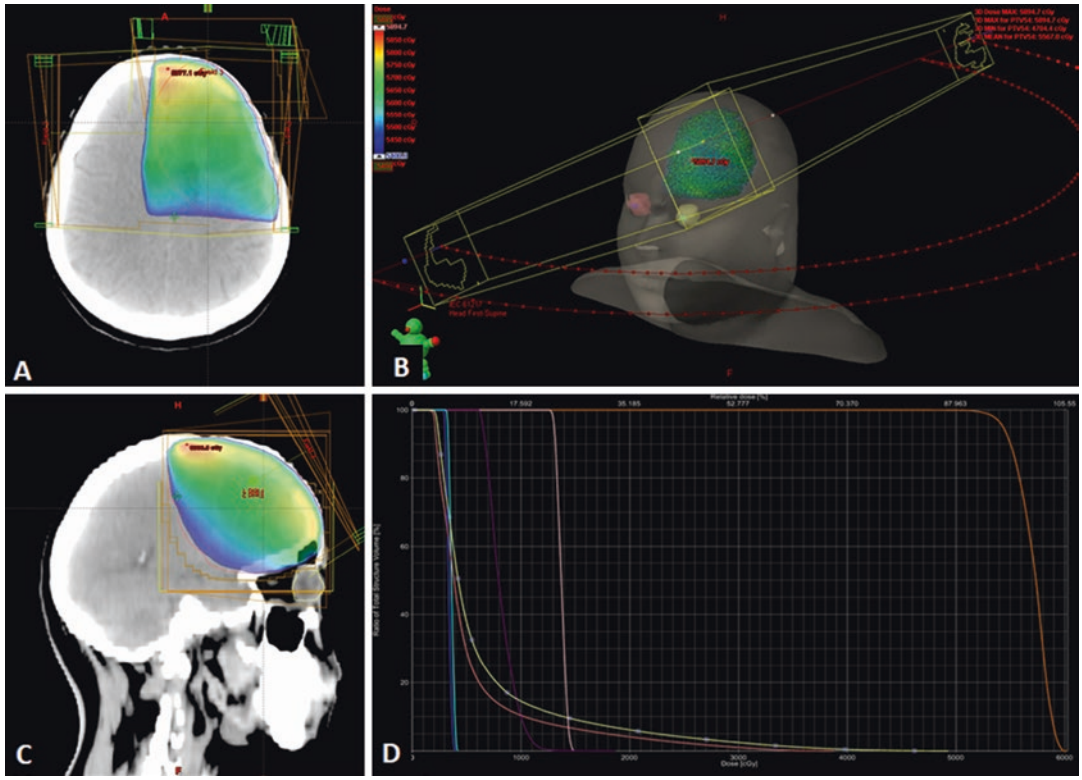

Fig. 9.1 Dose display for 3-D conformal plan. (**a**) Axial computed tomography (CT) with dose color wash. (**b**) Three-dimensional view dose color wash. (**c**) Sagittal CT with dose color wash. (**d**) The planning target volume (PTV) (orange), optic chiasm (pink), brainstem (purple), right eye (yellow), left eye (light orange), right and left lens (blue and dark blue) are shown in the cumulative dose-volume histogram (DVH)

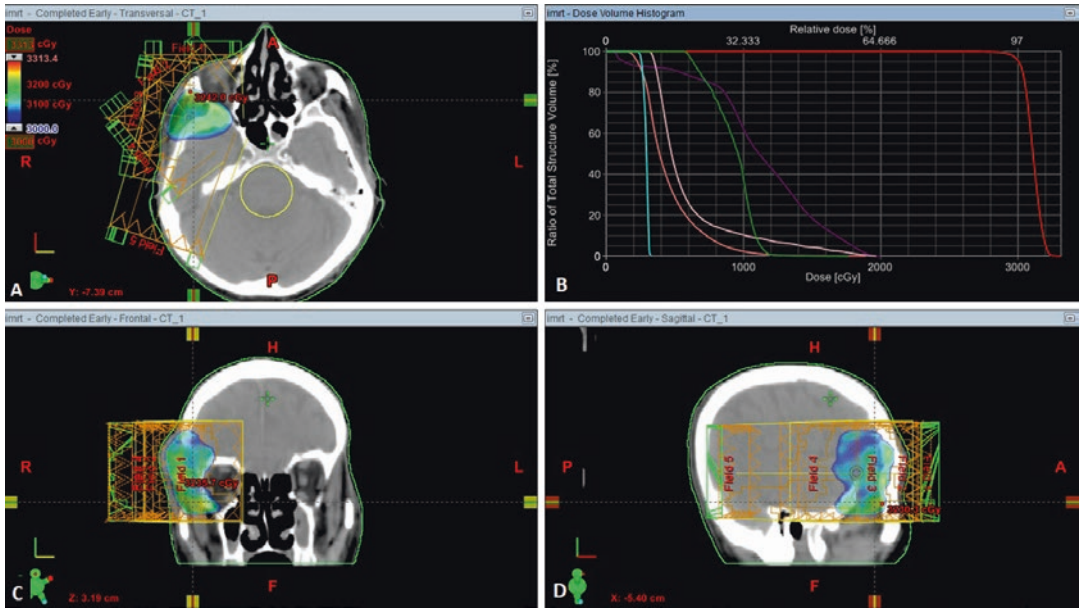

Fig. 9.2 Dose display for IMRT plan. (**a**) Axial CT with dose color wash. (**b**) PTV (red), brainstem (purple), right optic nerve (green), optic chiasm (pink), left eye (light orange), right lens (blue) are shown in the cumulative DVH. (**c**) Coronal and (**d**) sagittal CT with dose color wash

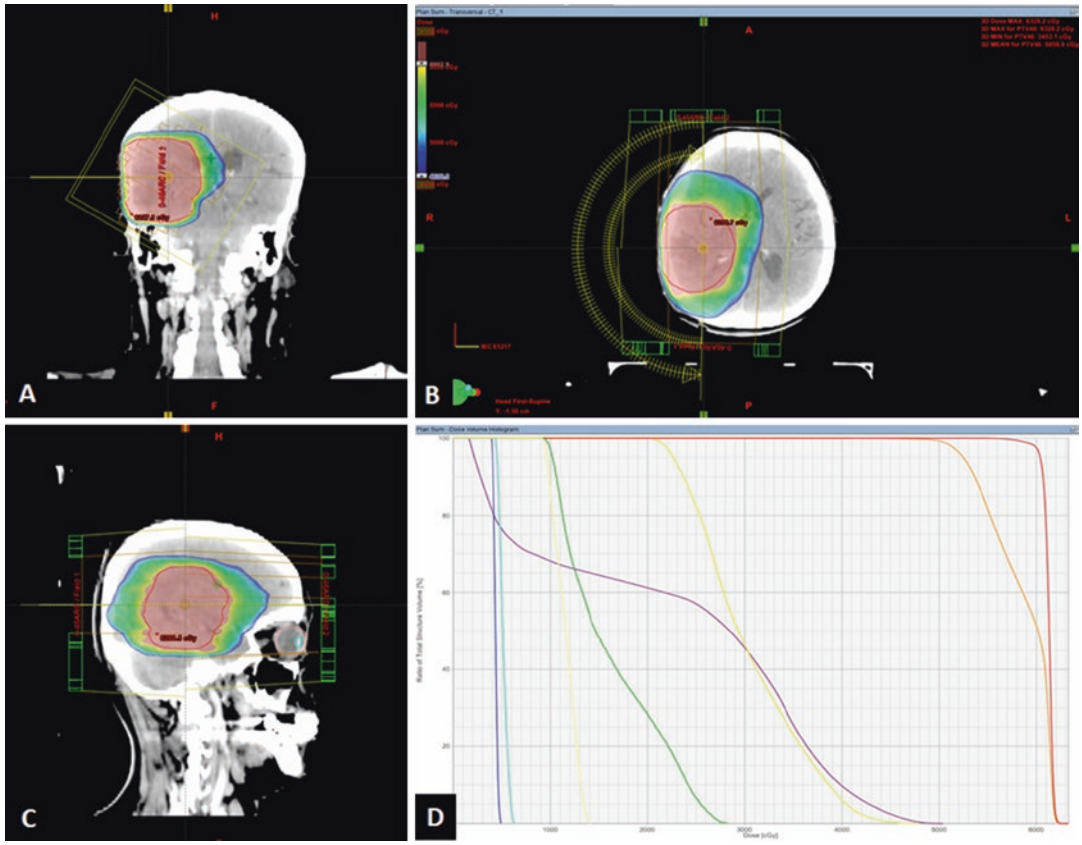

Fig. 9.3 A 63-year-old female patient underwent near-total excision and diagnosed glioblastoma multiforme (GBM). Total dose delivered is 60 Gy, in 2 Gy fractions administered 5 days per week for 5 weeks. In the VMAT plan coronal (**a**), axial (**b**), and sagittal (**c**) dose color wash are shown, along with the DVH (**d**) demonstrating PTV (red), brainstem (purple), right optic nerve (green), optic chiasm (yellow), left lens (dark blue), and right lens (blue)

9.3.4 Stereotactic Radiosurgery (SRS)

A highly precise form of radiation therapy that directs narrow beams of radiation to the tumor from different angles. There are different types of technology used in radiosurgery to deliver radiation to treat brain tumors, such as a Gamma Knife (Fig. 9.4) [56], a cyber knife, [57] or a linear accelerator [58]. In general, there can be many different combinations of technologies used to develop and implement sophisticated conformal therapy. SRS is an established method of ablating brain metastases and AVMs as well as treating certain benign intracranial neoplasms and trigeminal neuralgia.

All these conformal therapy delivery methods are greatly improved by the use of image-guided radiation therapy (IGRT) techniques to accurately position and set up the patient, using integrated megavoltage or kilovoltage diagnostic imaging, cone beam CT, radiofrequency beacons or radiographic fiducials, and other image-guidance methods.

9.4 Brachytherapy

The temporary placement of radioactive sources within the body, usually employed to give an extra dose or boost of radiation to the area of the excision site or to any residual tumor [59].

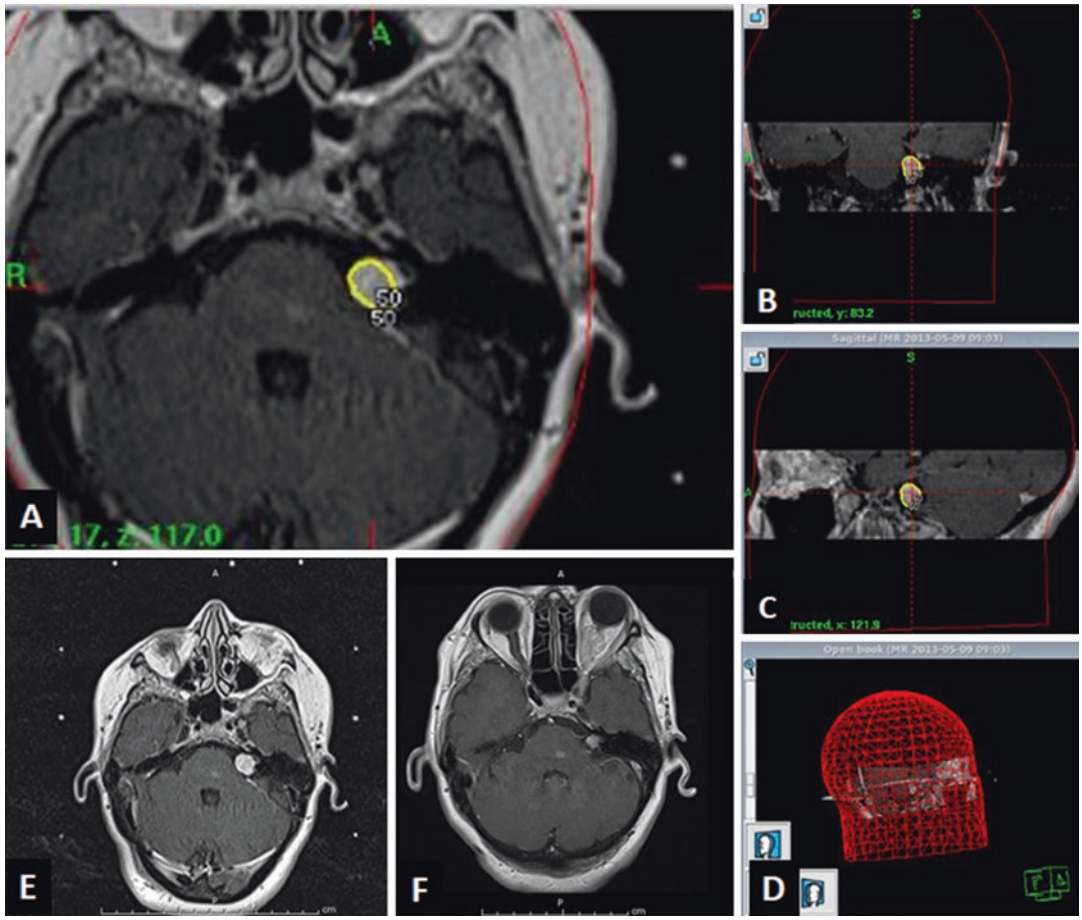

Fig. 9.4 Example of Gamma Knife radiosurgery treatment of a right-side vestibular schwannoma to a prescription dose of 12.5 Gy. The 50% isodose line (yellow) is shown on axial (**a**), coronal (**b**), sagittal (**c**) MRI, three-dimensional view (**d**) planes. MRI axial images of the patient before (**e**) and 55 months after (**f**) the treatment

9.5 Proton Beam

Proton irradiation may offer more localized delivery of radiation than conventional RT, which use photon irradiation. Therefore, it can permit higher radiation doses to the tumor with decreased risk of damage to surrounding tissue; this form of RT may be chosen for tumors with close proximity to important brain structures [60–62].

References

1. Louis D, Ohgaki H, Wiestler O, et al. World Health Organization histological classification of tumors of the central nervous system. Acta Neuropathol. 2016;131:803–20.
2. Roberts DW, Strohbehn JW, Hatch JF, et al. A frameless stereotaxic integration of computerized tomographic imaging and the operating microscope. J Neurosurg. 1986;65:545–9.
3. Mert A, Gan LS, Knosp E, et al. Advanced cranial navigation. Neurosurgery. 2013;72:A43–53.
4. Mert A, Kiesel B, Wöhrer A, et al. Introduction of a standardized multimodality image protocol for navigation-guided surgery of suspected low-grade gliomas. Neurosurg Focus. 2015;38:E4.
5. Black PM, Alexander E III, Martin C, et al. Craniotomy for tumor treatment in an intraoperative magnetic resonance imaging unit. Neurosurgery. 1999;45:423.
6. Moiyadi AV. Intraoperative ultrasound technology in neuro-oncology practice-current role and future applications. World Neurosurg. 2016;93:81–93.

7. Minniti G, Goldsmith C, Brada M. Radiotherapy. Handb Clin Neurol. 2012;104:215–28.
8. Nieder C, Berberish W, Schnabel K. Tumor-related prognostic factors for remission of brain metastases after radiotherapy. Int J Radiat Oncol Biol Phys. 1997;39:25–30.
9. Laperriere N, Zuraw L, Cairncross G. Radiotherapy for newly diagnosed malignant glioma in adults: a systematic review. Radiother Oncol. 2004;64:259–73.
10. Walker MD, Strike TA, Sheline GE. An analysis of dose–effect relationship in the radiotherapy of malignant gliomas. Int J Radiat Oncol Biol Phys. 2004;5:1725–31.
11. Karim AB, Afra D, Comu P, et al. Randomized trial on the efficacy of radiotherapy for cerebral low-grade glioma in the adult: European Organization for Research Council study BRO4: an interim analysis. Int J Radiat Oncol Biol Phys. 2002;52:316–24.
12. Shaw EG, Tater SB, Gj L, et al. Current controversies in the radiotherapeutic management of adult low-grade glioma. Semin Oncol. 2004;31:653–8.
13. Quinn JA, Reardon DA, Friedman AH, et al. Phase II trial of temozolomide in patients with progressive low-grade glioma. J Clin Oncol. 2003;21:646–51.
14. Shaw EG, Wang M, Coons SW, et al. Randomized trial of radiation therapy plus procarbazine, lomustine, and vincristine chemotherapy for supratentorial adult low-grade glioma: initial results of RTOG 9802. J Clin Oncol. 2012;30:3065–70.
15. Walker MD, Alexander E Jr, Hunt WE, et al. Evaluation of BCNU and/or radiotherapy in the treatment of anaplastic gliomas. A cooperative clinical trial. J Neurosurg. 1978;49:333–43.
16. Keime-Guibert F, Chinot O, Taillandier L, et al. Radiotherapy for glioblastoma in the elderly. N Engl J Med. 2007;356:1527–35.
17. Roa W, Brasher PM, Bauman G, et al. Abbreviated course of radiation therapy in older patients with glioblastoma multiforme: a prospective randomized clinical trial. J Clin Oncol. 2004;22:1583–8.
18. Malmstrom A, Gronberg BH, Morosi C, et al. Temozolomide versus standard 6-week radiotherapy versus hypofractionated radiotherapy in patients older than 60 years with glioblastoma: the Nordic randomized, phase 3 trail. Lancet Oncol. 2004;13:916–26.
19. Laperriere NJ, Leung PM, McKenzie S, et al. Randomized study of brachytherapy in the initial management of patients with malignant astrocytoma. Int J Radiat Oncol Biol Phys. 1998;41:1005–11.
20. Souhami L, Seiferheld W, Brachman D, et al. Randomized comparison of stereotactic radiosurgery followed by conventional radiotherapy with carmustine to conventional radiotherapy with carmustine for patients with glioblastoma multiforme: report of Radiation Therapy Oncology Group 93-05 protocol. Int J Radiat Oncol Biol Phys. 2004;60:853–60.
21. Cairncross G, Wang M, Shaw E, et al. Phase III trial of chemoradiotherapy for anaplastic oligodendroglioma: long-term results of RTOG 9402. J Clin Oncol. 2013;31:337–43.
22. Van den Bent MJ, Brandes AA, Taphoorn MJ, et al. Adjuvant procarbazine, lomustine, and vincristine chemotherapy in newly diagnosed anaplastic oligodendroglioma: long-term follow-up of EORTC brain tumor group study 26951. J Clin Oncol. 2013;31:344–50.
23. Stewart LA. Chemotherapy in adult high-grade glioma: a systematic review and meta-analysis of individual patient data from 12 randomized trial. Lancet. 2002;359:1011–8.
24. Fine HA, Dear KB, Loeffler JS, et al. Meta-analysis of radiation therapy with and without adjuvant chemotherapy for malignant gliomas in adults. Cancer. 1993;71:2585–97.
25. Stupp R, Mason WP, Van den Bent MJ, et al. Radiotherapy plus concomitant and adjuvant temozolomide for glioblastoma. N Engl J Med. 2005;352:987–96.
26. Stupp R, Hegi ME, Mason WP, et al. Effects of radiotherapy with concomitant and adjuvant temozolomide versus radiotherapy alone on survival in glioblastoma in a randomized phase III study: 5 year analysis of the EORTC-NCIC trial. Lancet Oncol. 2009;10:459–66.
27. Wick W, Platten M, Meisner C, et al. Temozolomide chemotherapy alone versus radiotherapy alone for malignant astrocytoma in the elderly: the NOA-08 randomized, phase 3 trail. Lancet Oncol. 2012;13:707–15.
28. Stupp R, Wong E, Kanner A, et al. Novo TTF-100A versus physician's choice chemotherapy in recurrent glioblastoma: a randomized phase III trial of a novel treatment modality. Eur J Cancer. 2012;48:2192–202.
29. Paulino AC, Wen BC, Buatti JM, et al. Intracranial ependymomas: an analysis of prognostic factors and patterns of failure. Am J Clin Oncol. 2002;25:117–22.
30. Reni M, Brandes AA, Vavassori V, et al. A multicenter study of the prognosis and treatment of adult brain ependymal tumors. Cancer. 2004;100:1221–9.
31. Kano H, Niranjan A, Kondziolka D, et al. Outcome predictors for intracranial ependymoma radiosurgery. Neurosurgery. 2009;64:279–87.
32. Chargari C, Feuvret L, Levy A, et al. Reappraisal of clinical outcome in adult medulloblastomas with emphasis on patterns of relaps. Br J Neurosurg. 2010;24:460–7.
33. Merchant TE, Kun LE, Krasin MJ, et al. Multi-institution prospective trial of reduced-dose craniospinal irradiation (23.4 Gy) followed by conformal posterior fossa (36 Gy) and primary site irradiation (55.8 Gy) and dose-intensive chemotherapy for average-risk medulloblastoma. Int J Radiat Oncol Biol Phys. 2008;70:782–7.
34. Batchelor T, Carson K, O'Neill A, et al. Treatment of primary CNS lymphoma with methotrexate and deferred radiotherapy: a report of NABTT 96-07. J Clin Oncol. 2003;21:1044–9.
35. Chamberlain MC, Johnston SK. High-dose methotrexate and rituximab with deferred radiotherapy for

newly diagnosed primary B-cell CNS lymphoma. Neuro-Oncology. 2010;12:736–44.
36. DeAngelis LM, Seiferheld W, Schold SC, et al. Combination chemotherapy and radiotherapy for primary central nervous system lymphoma: Radiation Therapy Oncology Group Study 93-10. J Clin Oncol. 2002;20:4643–8.
37. Soyuer S, Chang EL, Selek U, et al. Radiotherapy after surgery for benign cerebral meningioma. Radiother Oncol. 2004;71:85–90.
38. Aghi MK, Carter BS, Cosgrove GR, et al. Long-term recurrence rates of atypical meningiomas after gross total resection with or without postoperative adjuvant radiation. Neurosurgery. 2009;64:56–60.
39. Kondziolka D, Mathieu D, Lunsford LD, et al. Radiosurgery as definitive management of intracranial meningiomas. Neurosurgery. 2008;62:53–8; discussion 58–60.
40. Yang I, Aranda D, Han SJ, et al. Hearing preservation after stereotactic radiosurgery for vestibular schwannoma: a systematic review. J Clin Neurosci. 2009;16(6):742–7.
41. Anderson BM, Khuntia D, Bentzen SM, et al. Single institution experience treating 104 vestibular schwannomas with fractionated stereotactic radiation therapy or stereotactic radiosurgery. J Neurooncol. 2014;116(1):187–93.
42. Laws ER, Sheehan JP, Sheehan JM, et al. Stereotactic radiosurgery for pituitary adenomas: a review of the literature. J Neurooncol. 2004;69:257–72.
43. Masson-Cote L, Masucci GL, Atenafu EG, et al. Long-term outcomes for adult craniopharyngioma following radiation therapy. Acta Oncol. 2013;52:153–8.
44. Patchell RA, Tibbs PA, Regine WF, et al. Postoperative radiotherapy in the treatment of single metastases to the brain: a randomized trial. JAMA. 1998;280:1485–9.
45. Bhatnagar AK, Kondziolka D, Lunsford LD, Flickinger JC. Recursive partitioning analysis of prognostic factors for patients with four or more intracranial metastases treated with radiosurgery. Technol Cancer Res Treat. 2007;6:153–60.
46. Banfill KE, Bownes PJ, St Clair SE, et al. Stereotactic radiosurgery for the treatment of brain metastases: impact of cerebral disease burden on survival. Br J Neurosurg. 2012;26:674–8.
47. Karlsson B, Hanssens P, Wolff R, et al. Thirty years' experience with Gamma Knife surgery for metastases to the brain. J Neurosurg. 2009;111:449–57.
48. Mintz AH, Kestle J, Rathbone MP, et al. A randomized trial to assess the efficacy of surgery in addition to radiotherapy in patients with a single cerebral metastasis. Cancer. 1996;78:1470–6.
49. Andrews DW, Scott CB, Sperduto PW, et al. Whole brain radiation therapy with or without stereotactic radiosurgery boost for patients with one to three brain metastases: phase III results of the RTOG 9508 randomized trial. Lancet. 2004;363:1665–72.
50. Fraass BA, McShan DL. 3D treatment planning. I. Overview of a clinical planning system. In: IAD B, van der Giessen FH, van Kleffens HJ, et al., editors. The use of computers in radiation therapy. North Holland: Amsterdam; 1987. p. 273–6.
51. Webb S. Optimization by simulated annealing of three-dimensional treatment planning for radiation fields defined by a multileaf collimator. Phys Med Biol. 1991;36:1201–26.
52. Boyer AL, Butler EB, DiPetrillo TA, et al. Intensity Modulated Radiation Therapy Collaborative Working Group. Intensity modulated radiotherapy: current status and issues of interest. Int J Radiat Oncol Biol Phys. 2001;51:880–914.
53. Kessler ML, McShan DL, Epelman MA, et al. Costlets. A generalized approach to cost functions for automated optimization of IMRT treatment plans. Optim Eng. 2005;6:421–48.
54. Shepard DM, Cao D, Afghan MK, et al. An arc-sequencing algorithm for intensity modulated arc therapy. Med Phys. 2007;34:464–70.
55. Otto K. Volumetric modulated arc therapy. IMRT in a single gantry arc. Med Phys. 2008;35:310–7.
56. Larson E, Peterson H, Lamoreaux W. Clinical outcomes following salvage Gamma Knife radiosurgery for recurrent glioblastoma. World J Clin Oncol. 2014;5:142–8.
57. Veeravagu A, Jiang B, Patil CG, et al. CyberKnife stereotactic radiosurgery for recurrent, metastatic, and residual hemangiopericytomas. J Hematol Oncol. 2011;4(1):1–7.
58. Lutz W, Winston KR, Maleki N. A system for stereotactic radiosurgery with a linear accelerator. Int J Radiat Oncol Biol Phys. 1988;14:373–81.
59. Tatter S. Recurrent malignant glioma in adults. Curr Treat Options Oncol. 2002;3:509–24.
60. Fuss M, Hug EB, Schaefer RA, et al. Proton radiation therapy (PRT) for pediatric optic pathway gliomas: comparison with 3D planned conventional photons and a standard photon technique. Int J Radiat Oncol Biol Phys. 1999;45(5):1117–26.
61. Weber DC, Lomax AJ, Rutz HP, et al. Spot-scanning proton radiation therapy for recurrent, residual or untreated intracranial meningiomas. Radiother Oncol. 2004;71(3):251–8.
62. Habrand JL, Haie-Meder C, Rey A, et al. [Radiotherapy using a combination of photons and protons for locally aggressive intracranial tumors. Preliminary results of protocol CPO 94-C1]. Cancer Radiother 1999;3(6):480–488.

Part II

Case Based Learning in Brain Tumors

Nonneoplastic Mass Lesions of the Brain

10

Simon Nicolay, Luc Van Den Hauwe,
Paul M. Parizel, and Johan W. Van Goethem

10.1 Arachnoid Cyst

24-year-old woman with recurrent headache. Unremarkable medical history. CT scan and subsequent MRI scan of the head were performed.

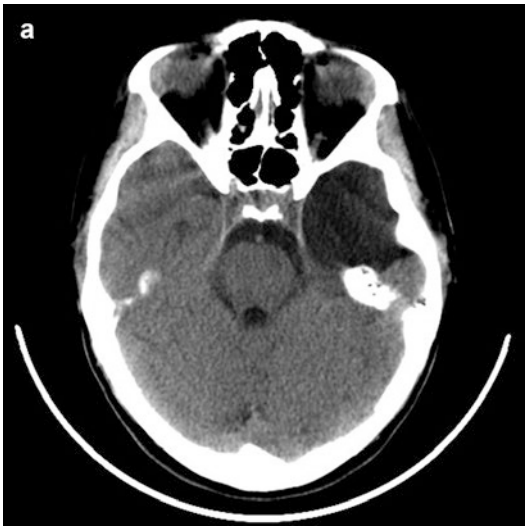

Fig. 10.1a Axial NECT of the head shows a large, well-demarcated mass in the left middle cranial fossa. The attenuation of the mass resembles CSF

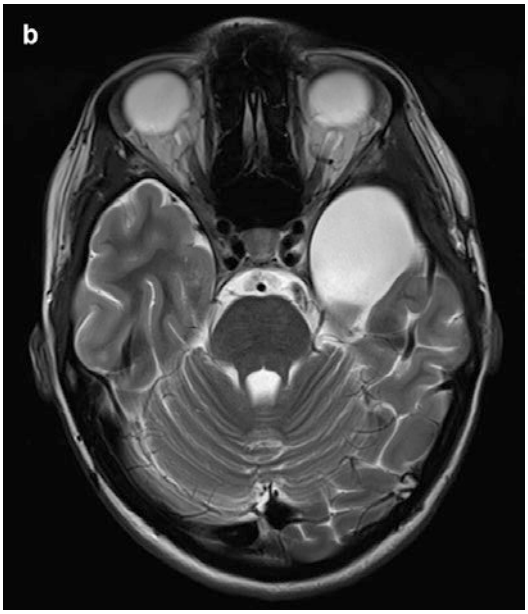

Fig. 10.1b Axial T2WI MRI confirms a homogeneous, well-demarcated, extra-axial cyst in the left middle cranial fossa, isointense with CSF

S. Nicolay (✉) · L. Van Den Hauwe · P. M. Parizel · J. W. Van Goethem
Department of Radiology, Antwerp University Hospital & University of Antwerp, Antwerp, Belgium

Y. Özsunar, U. Şenol (eds.), *Atlas of Clinical Cases on Brain Tumor Imaging*,
https://doi.org/10.1007/978-3-030-23273-3_10

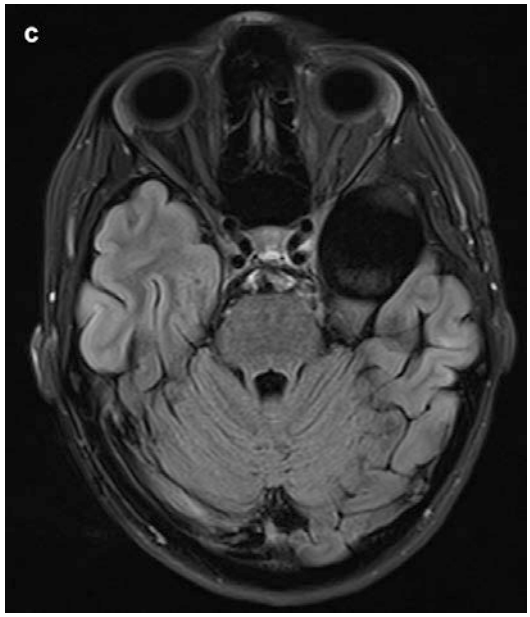

Fig. 10.1c Axial FLAIR image shows low signal of the cyst content, identical to CSF. No signal changes in the adjacent brain parenchyma

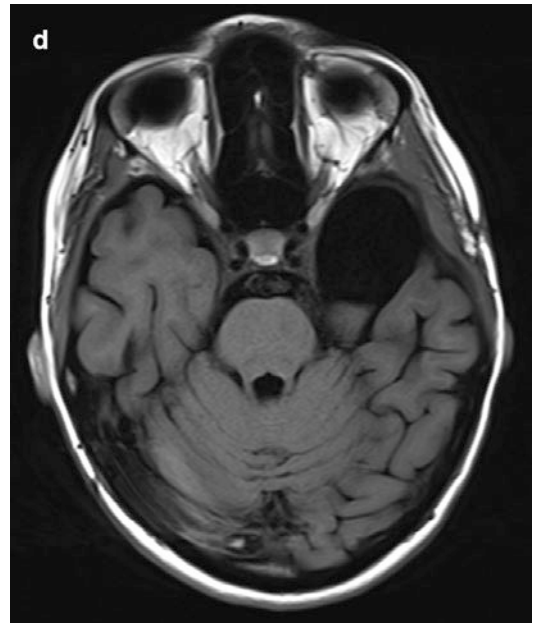

Fig. 10.1d On T1WI, the cyst is hypointense, similar to CSF

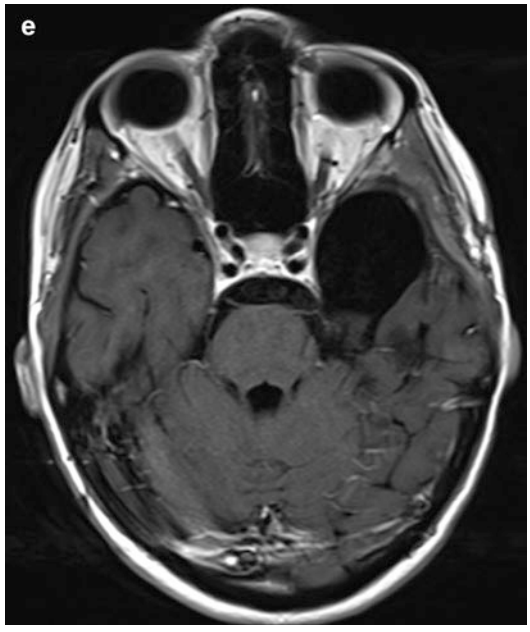

Fig. 10.1e Axial T1WI after contrast administration shows no enhancement

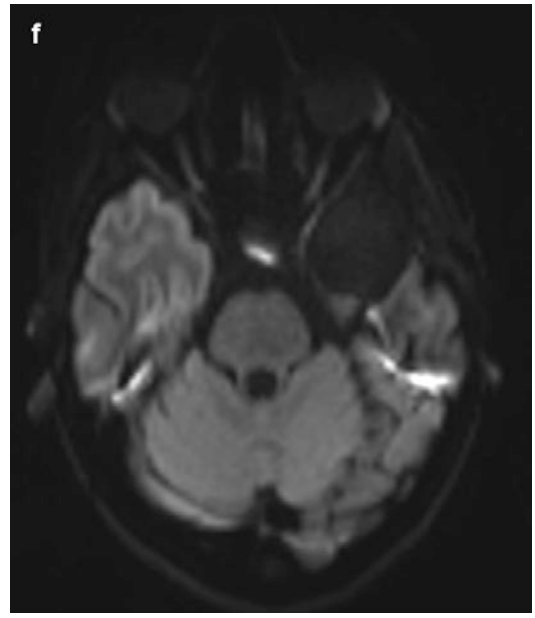

Fig. 10.1f No diffusion restriction on DWI

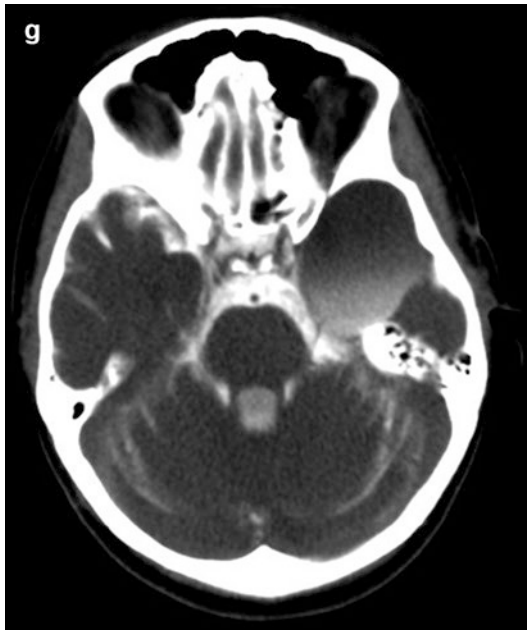

Fig. 10.1g Axial CT cisternography (after lumbar introduction of iodinated contrast in the intrathecal space) demonstrates a communication between the cyst and the subarachnoid space: contrast is pooling in the dependent part of the cyst

Epidemiology
- 1% of all intracranial masses
- Found at any age, the majority in children and young people
- No gender predilection

Pathology and Genetics
- Gross pathology: CSF containing, translucent cyst, not communicating with the ventricles
- Microscopy: the wall usually consists of arachnoid-like tissue and sometimes thicker, fibrous tissue or ciliated cells
- Etiology: probably failure to merge of the frontal and temporal embryonic meninges, leaving a space in between that fills with CSF
- Genetics: usually sporadic
- Associations:
  - Temporal lobe hypoplasia
  - Subdural hematoma (middle cranial fossa AC)
  - Hydrocephalus (giant periventricular AC)

Clinical Management
- Clinical presentation: usually incidental finding in asymptomatic patients
- Management:
  - Generally no treatment necessary
  - In selected cases, especially in cases with notable mass effect, endoscopic resection, or cyst marsupialization

Imaging Findings
- General:
  - Well-demarcated, rounded extra-axial cyst
  - Follows CSF density/signal on all sequences
  - More than half of cases are found in the middle cranial fossa. Other frequent locations include the cerebellopontine angle, the suprasellar region, the parafalcine space, and the quadrigeminal cistern
- MRI:
  - Isointense to CSF on all MR sequences
  - Complete nulling of the signal on FLAIR
  - No diffusion restriction
  - No enhancement

Take-Home Messages
- Arachnoid cysts are congenital intracranial extra-axial cysts that follow CSF attenuation/signal
- The majority are located in the middle cranial fossa
- The majority are incidentally found and asymptomatic
- No treatment necessary

Further Reading

- Osborn AG, Preece MT. Intracranial cysts: radiologic-pathologic correlation and imaging approach. Radiology. 2006;239(3): 650–664
- Adeeb N, Deep A, Griessenauer CJ et al. The intracranial arachnoid mater: a comprehensive review of its history, anatomy, imaging, and pathology. Childs Nerv Syst. 2013;29(1): 17–33
- Oprisan A, Popescu BO. Intracranial cysts: an imagery diagnostic challenge. Sci World J. 2013;2013: 172154

10.2 Epidermoid Cyst

36-year-old man with bilateral tinnitus, more on the left side. He is a professional drummer and music teacher. On imaging, a mass was detected in the left perimesencephalic cistern.

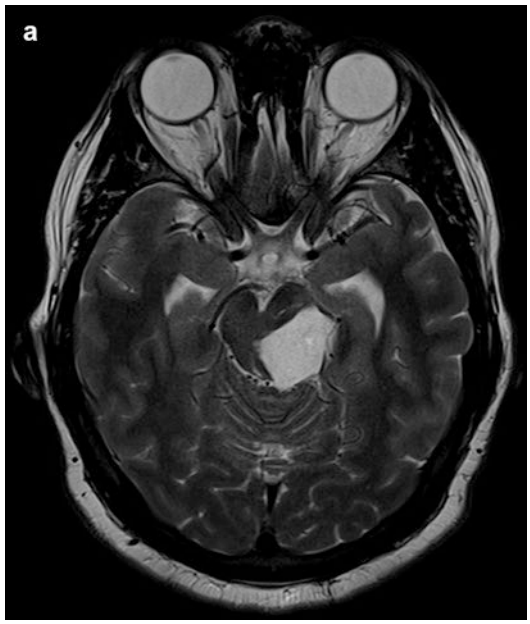

Fig. 10.2a Axial T2WI shows a well-demarcated, homogeneous, hyperintense/cystic mass in the left perimesencephalic cistern

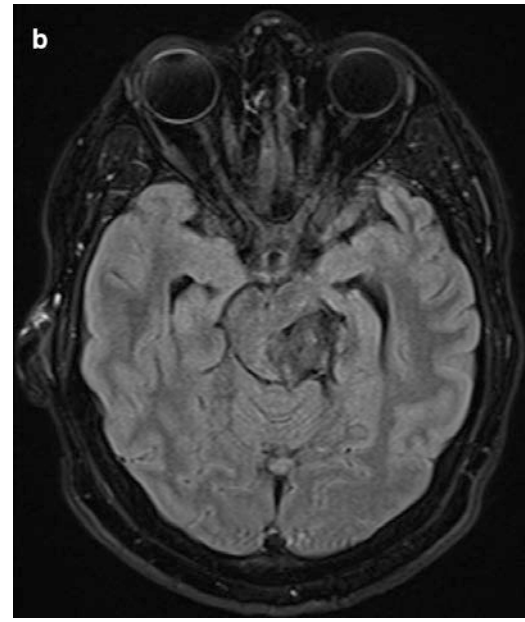

Fig. 10.2b On axial FLAIR, the signal is heterogeneous and lower than on T2WI but not completely suppressed

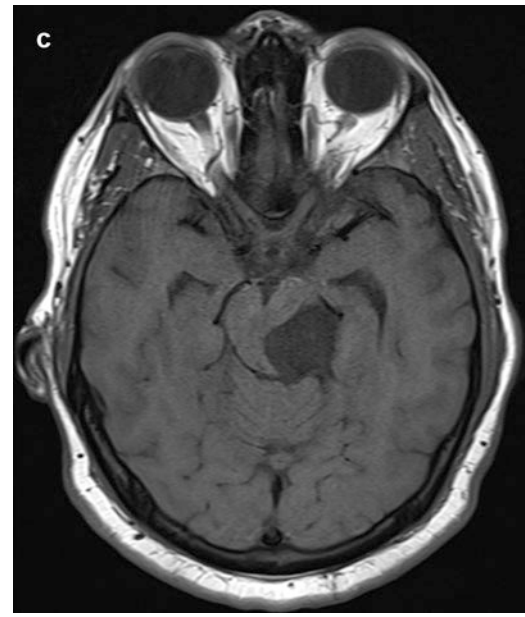

Fig. 10.2c Axial T1WI shows low signal intensity, slightly hyperintense to CSF

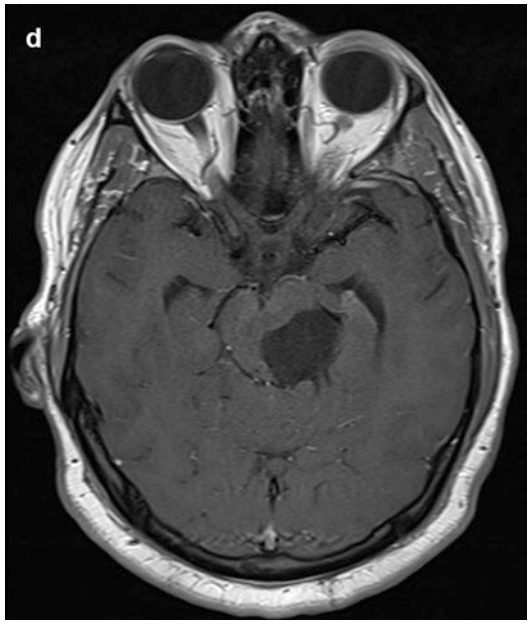

Fig. 10.2d Axial T1WI after gadolinium administration shows no enhancement

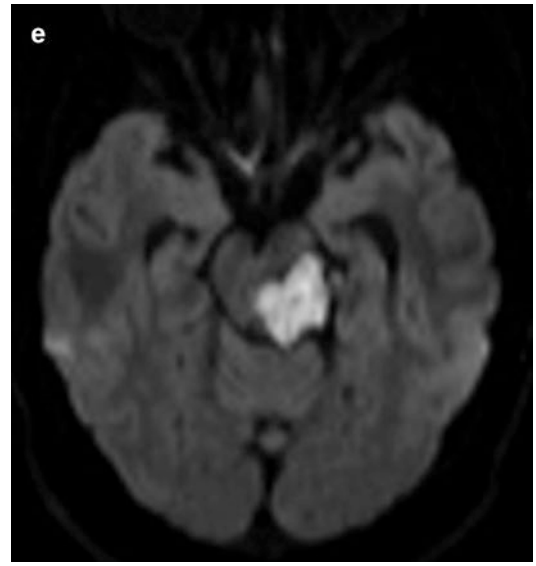

Fig. 10.2e Axial DWI shows marked restricted diffusion within the mass

Epidemiology
- 1% of all intracranial masses
- Third most common cerebellopontine angle mass after vestibular schwannoma and meningioma
- Most are found between 20 and 60 years, presentation in childhood is uncommon
- No significant gender predilection

Pathology and Genetics
- Gross pathology:
  - Soft and pliable cyst with shiny, mother-of-pearl surface
  - Contains soft, creamy keratinaceous material from desquamation of the cyst wall. No lipids
  - Extends through cisterns and conforms to the shape of adjacent nerves or vessels rather than displacing or invading them
- Microscopy: cyst wall is made up of squamous epithelium covered by a fibrous capsule. No dermal appendages
- Etiology:
  - Congenital: probably result of cutaneous ectoderm inclusion during closure of the neural tube in early embryogenesis
  - Acquired: post-surgical or post-traumatic implantation
- Genetics: usually sporadic
- Associations: may have occipital or nasofrontal fistulous connection to the skin: dermal sinus

Clinical Management
- Clinical presentation:
  - The majority are asymptomatic for a long time or present with aspecific symptoms like headache
  - Specific symptoms related to mass effect on neurovascular structures, most common CN V, VI, or VII neuropathy
  - Less frequently hypopituitarism, diabetes insipidus, and seizures
- Management:
  - Surgical resection if symptomatic
  - Nerve sparing complete resection is difficult. Recurrence is not uncommon

Imaging Findings

- General:
  - Lobulated, cauliflower-like mass intruding the subarachnoid space without displacing neurovascular structures
  - Majority intradural (90%): CPA (40–50%), fourth ventricle (17%), and parasellar/middle cranial fossa (15%). Extradural location mostly in the skull (10%)
- MRI:
  - Resembling CSF but no complete suppression on FLAIR
  - Diffusion restriction is typical and diagnostic
  - Slightly hyperintense to CSF on T1WI but generally no fat characteristics
  - No enhancement except minimal capsule enhancement
- CT: hypodense, resembling CSF; 10–25% show calcifications

Take-Home Messages

- Epidermoid cysts are the most common congenital intracranial cystic masses
- The majority are located in the CPA, the fourth ventricle, and the parasellar region
- Intrusion of the cisterns without invasion or displacement of the neurovascular structures
- Diffusion restriction is typical
- CSF-like behavior but no complete signal nulling on FLAIR

Further Reading

- Osborn AG, Preece MT. Intracranial cysts: radiologic-pathologic correlation and imaging approach. Radiology. 2006;239(3): 650–664
- Law EKC, Lee RKL, Ng AWH, Siu DYW, Ng H-K. Atypical intracranial epidermoid cysts: rare anomalies with unique radiological features. Case Rep Radiol. 2015;2015: 528632
- Hakyemez B, Aksoy U, Yildiz H, Ergin N. Intracranial epidermoid cysts: diffusion-weighted, FLAIR and conventional MR findings. Eur J Radiol. 2005;54(2): 214–220
- Oprisan A, Popescu BO. Intracranial cysts: an imagery diagnostic challenge. Sci World J. 2013;2013: 172154

10.3 Dermoid Cyst

59-year-old man with a history of seizures. Imaging shows a large mass in the anterior fossa.

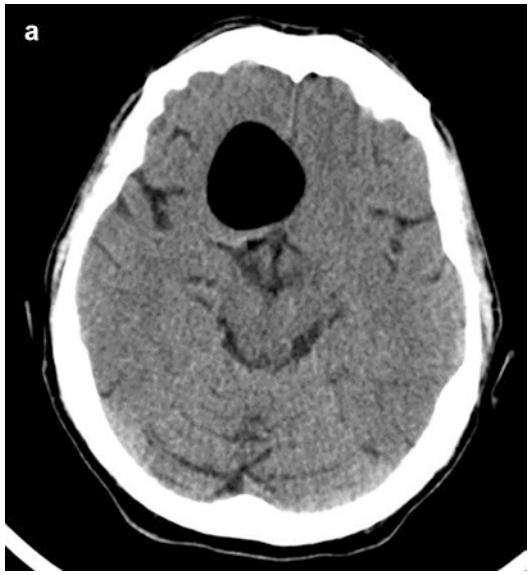

Fig. 10.3a Axial NECT of the head shows a large, well-circumscribed hypodense mass in the anterior fossa. The average density of the mass is −70 to −80 Hounsfield units

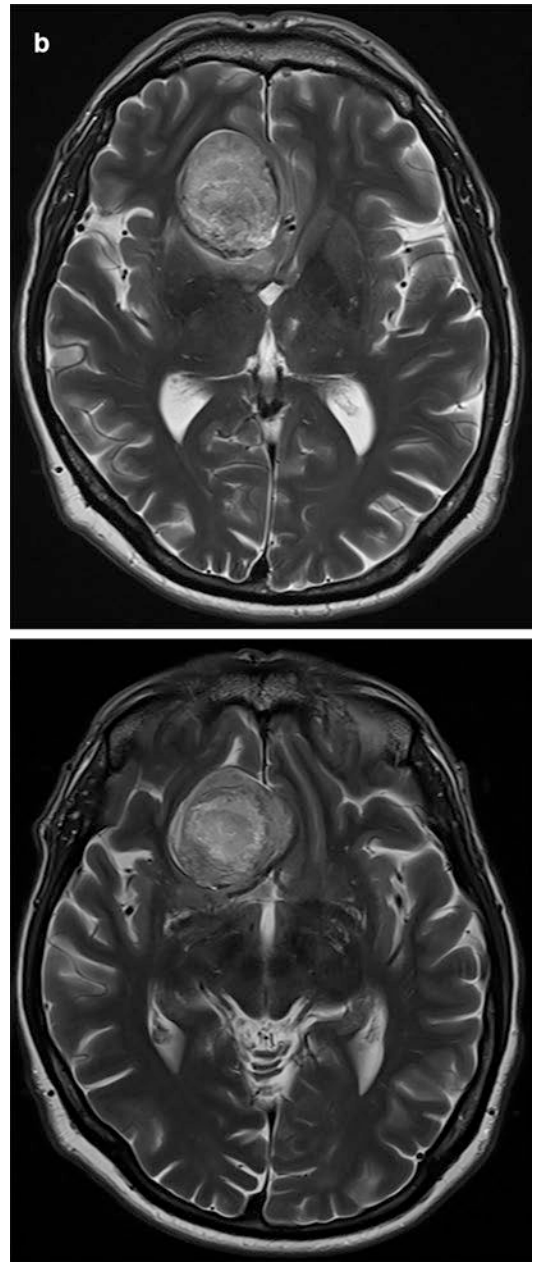

Fig. 10.3b Axial T2WI images show an extra-axial mass slightly off the midline to the right in the anterior fossa. The mass is well-demarcated, heterogeneous, and iso- to hyperintense

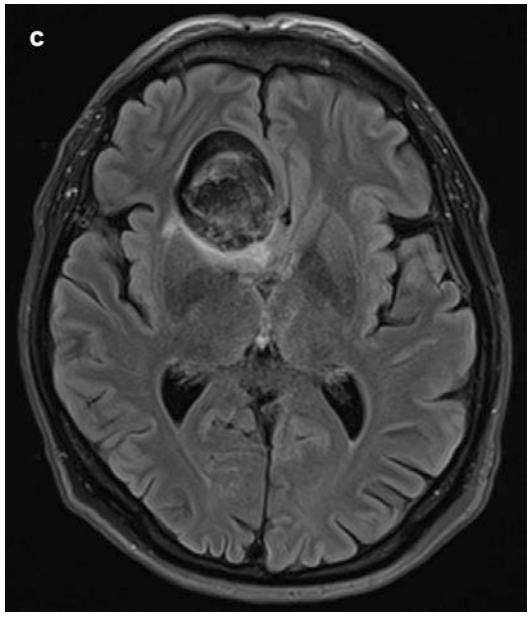

Fig. 10.3c On axial FLAIR images with fat suppression a signal drop is noted in a substantial part of the mass. Also note some perilesional edema

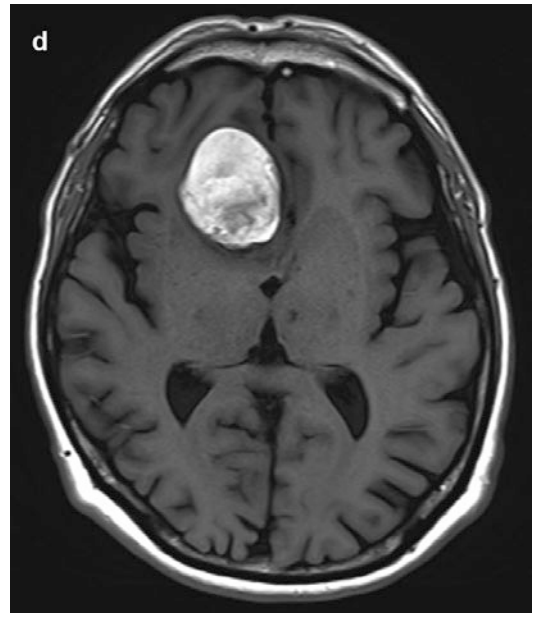

Fig. 10.3d On axial T1WI the mass is markedly hyperintense

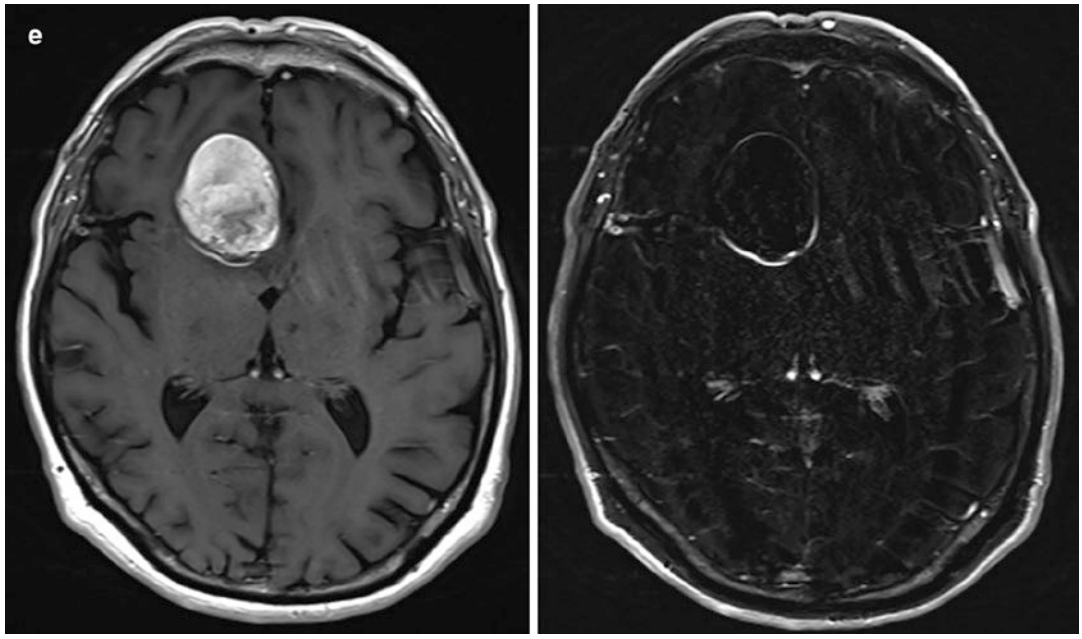

Fig. 10.3e Axial T1WI and subtraction images after gadolinium administration show mild peripheral enhancement

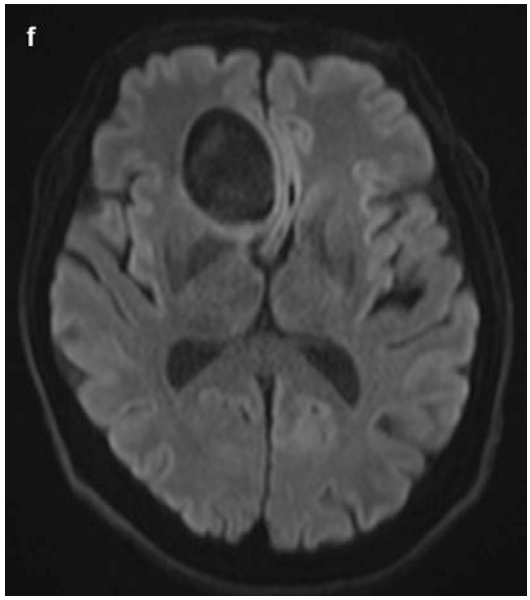

Fig. 10.3f No diffusion restriction on DWI

Epidemiology
- Less than 0.5% of all intracranial masses
- Most are found in the second or third decade
- No significant gender predilection

Pathology and Genetics
- Gross pathology: unilocular cyst with thick wall containing lipid and cholesterol from sebaceous secretions. No adipose tissue
- Microscopy: squamous epithelium on outer wall lining. Dermal elements such as hair follicles and sebaceous glands on inner wall lining
- Etiology: probably result of cutaneous ectoderm inclusion during closure of the neural tube in early embryogenesis
- Genetics: usually sporadic
- Associations:
  - Association with Goldenhar syndrome
  - Association with occipital and nasofrontal fistulous connection to the skin: dermal sinus

Clinical Management
- Clinical presentation:
  - Usually asymptomatic or aspecific symptoms like headache and seizures
  - Sometimes present with obstructive hydrocephalus, cranial nerve defects, or visual symptoms due to mass effect
  - Chemical meningitis in case of cyst rupture
  - Recurrent meningitis when associated with dermal sinus tract
- Management:
  - Complete surgical resection when symptomatic
  - Shunt for hydrocephalus

Imaging Findings
- General:
  - Midline, well-demarcated, intracranial mass that follows fat characteristics on imaging
  - Most frequently encountered in the suprasellar region or in the posterior fossa
  - Fat droplets in the cisterns, subarachnoid space, or ventricles when ruptured
- MRI:
  - High signal on T1WI, more heterogeneous than true lipomas
  - Signal suppression on fat-suppressed MR sequences
  - No diffusion restriction
  - No enhancement except for capsule
- CT: fat density, capsular calcifications in 20%

Take-Home Messages

- Dermoid cysts are congenital well-demarcated, midline intracranial cysts that contain fat
- Fat characteristics are confirmed on NECT, T1-WI, and fat-suppressed MRI sequences
- The majority are located in the suprasellar region and in the posterior fossa
- Frequently symptomatic due to local mass effect
- Risk of rupture with high morbidity and mortality

Further Reading

- Triplett TM, Griffith A, Hatanpaa KJ, Barnett SL. Dermoid cyst of the infratemporal fossa: case report and review of the literature. J Neurol Surg Rep. 2014;75(1): 33–37
- Muçaj S, Ugurel MS, Dedushi K, Ramadani N, Jerliu N. Role of MRI in diagnosis of ruptured intracranial dermoid cyst. Acta Inform Med. 2017;25 (2): 141–144
- Osborn AG, Preece MT. Intracranial cysts: radiologic-pathologic correlation and imaging approach. Radiology. 2006;239(3): 650–664
- Oprisan A, Popescu BO. Intracranial cysts: an imagery diagnostic challenge. Sci World J. 2013;2013: 172154

10.4 Lipoma

A 53-year-old patient who underwent a CT of the paranasal sinuses for nasal obstruction. Incidental finding of a mass around the corpus callosum.

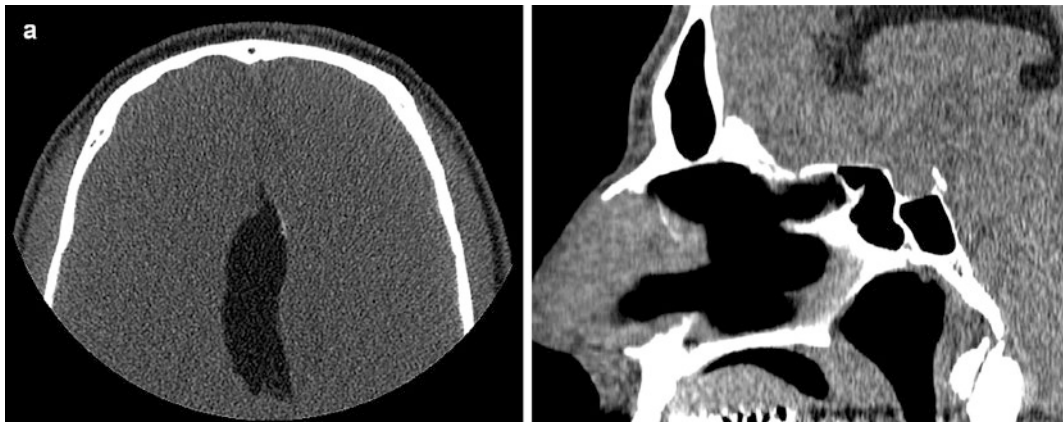

Fig. 10.4a Axial and sagittal reconstructions of a NECT of the paranasal sinuses show part of a hypodense mass around the corpus callosum. The average density of the mass is −100 Hounsfield units

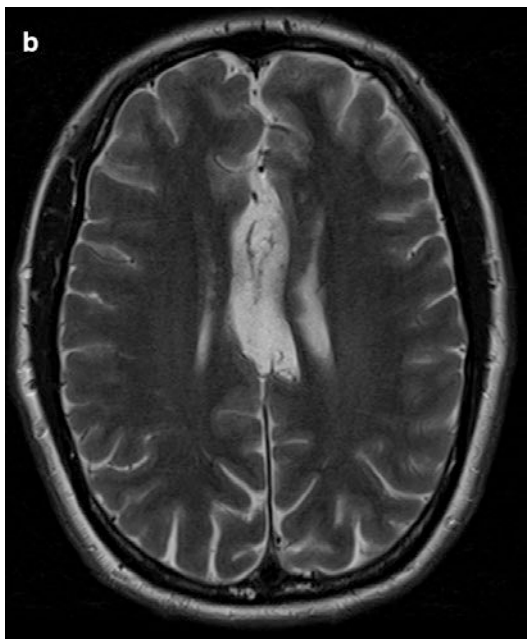

Fig. 10.4b Axial TSE T2WI shows a hyperintense mass around the corpus callosum. Linear hypointense structures, probably blood vessels or nerves, pass through the mass

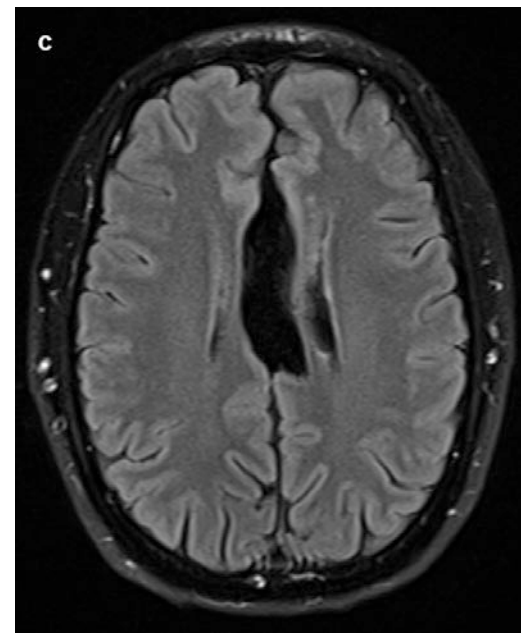

Fig. 10.4c On axial FLAIR with fat suppression the signal of the mass is completely suppressed

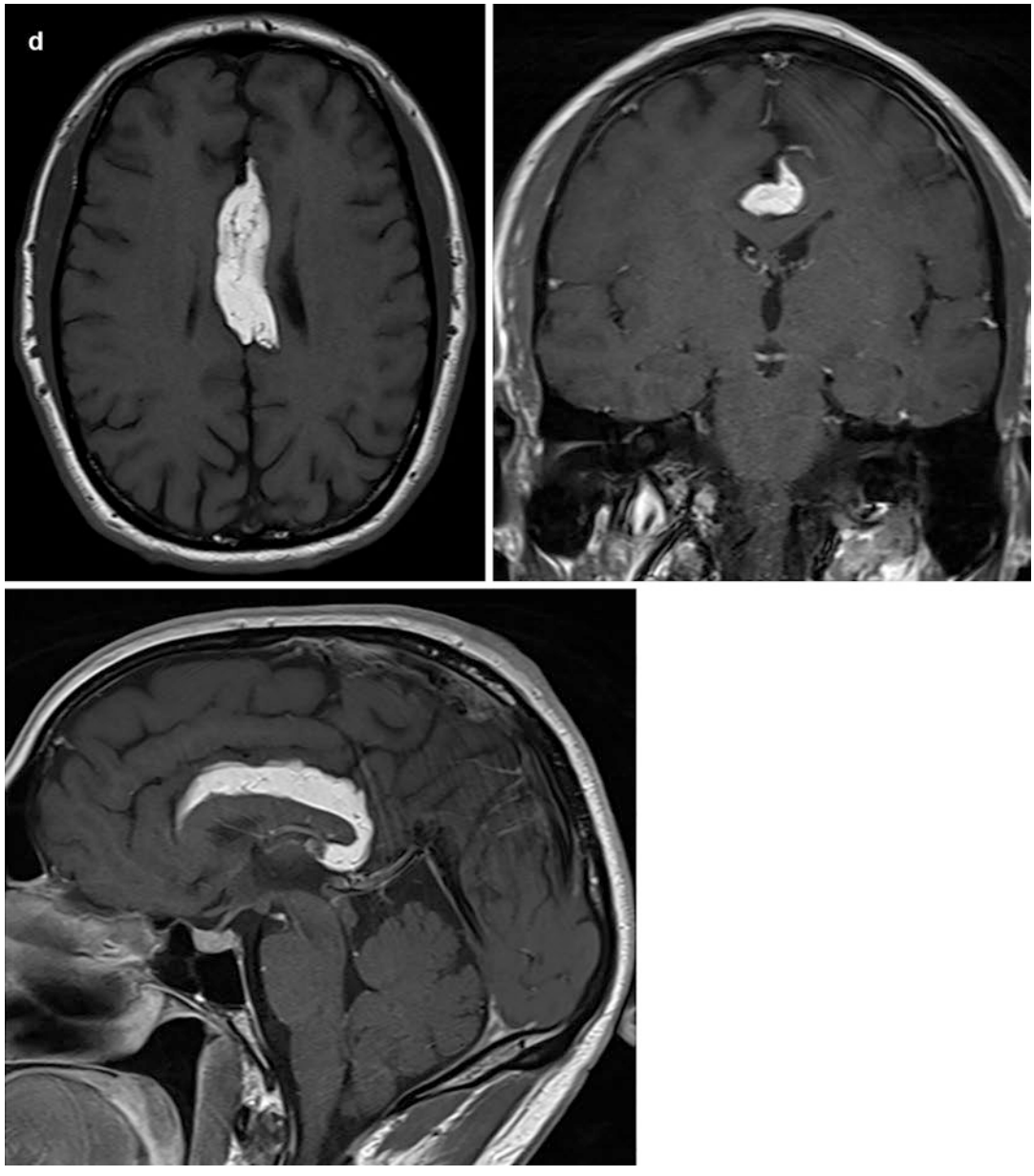

Fig. 10.4d Axial, coronal, and sagittal T1WI demonstrate homogeneous high signal intensity of the mass, which is wrapped around the corpus callosum. The splenium of the corpus callosum is not completely formed

Epidemiology
- Less than 0.5% of all intracranial masses (not a true tumor)
- Found at any age
- No significant gender predilection

Pathology and Genetics
- Gross pathology:
  - Yellow, lobulated fatty mass
  - Blood vessels and nerves run through the mass
- Microscopy: adipose tissue
  - Etiology: maldevelopment of embryonic primitive meninx into fat instead of leptomeninges
  - Genetics: usually sporadic
  - Associations:
    - Most common: corpus callosum anomalies
    - Other: cephaloceles, closed spinal dysraphism
    - Fishman syndrome, Pai syndrome (median cleft lip, corpus callosum lipoma, and fibroepithelial skin tag)

Clinical Management
- Clinical presentation:
  - Majority are asymptomatic and an incidental finding
  - Symptoms usually due to associated abnormalities, e.g. seizures
- Management:
  - No surgical indication
  - Avoid long-term corticosteriod use as this may expand the lipoma, leading to neural compression symptoms

Imaging Findings
- General:
  - Well-demarcated, lobulated extra-axial mass with fat characteristics
  - Midline location
  - Mostly supratentorial: interhemispheric over corpus callosum (45%), quadrigeminal cistern (25%), suprasellar (15%). Infratentorial: predominantly CPA (10%)
  - Encasement of blood vessels and nerves
- MRI:
  - Hyperintense on T1WI, more uniform than dermoid cyst
  - Hypointense on fat-suppressed sequences
  - Hypointense on SE T2WI, iso- to hyperintense on TSE T2WI
  - No diffusion restriction
  - No enhancement
- CT: uniform fat density (−50 to −100 HU); calcifications may be present

Take-Home Messages
- Intracranial lipomas are congenital masses of true adipose tissue
- The majority are located midline and supratentorial, typically around the corpus callosum
- Associated congenital malformations such as corpus callosum anomalies occur
- Uniform fat characteristics on imaging. Confirmation on fat-suppressed MR sequences
- Don't touch lesion

Further Reading

- Ginat DT, Meyers SP. Intracranial lesions with high signal intensity on T1-weighted MR images: differential diagnosis. Radiographics. 2012;32(2): 499–516
- Karakas E, Dogan MS, Cullu N, et al. Intracranial lipomas: clinical and imaging findings. Clin Ter. 2014;165(2): 134–138
- Yildiz H, Hakyemez B, Koroglu M, Koroglu M, Yesildag A, Baykal B. Intracranial lipomas: importance of localization. Neuroradiology. 2006;48(1): 1–7
- Jabot G, Stoquart-Elsankari S, Saliou G, Toussaint P, Deramond H, Lehmann P. Intracranial lipomas: clinical appearances on neuroimaging and clinical significance. J Neurol. 2009;256(6): 851–855

10.5 Neuroenteric Cyst

31-year-old woman with fainting spells since one year. She also has a throbbing headache when performing valsalva (e.g., during labor). Furthermore, she frequently wakes up at night with dormant arms. No significant medical history.

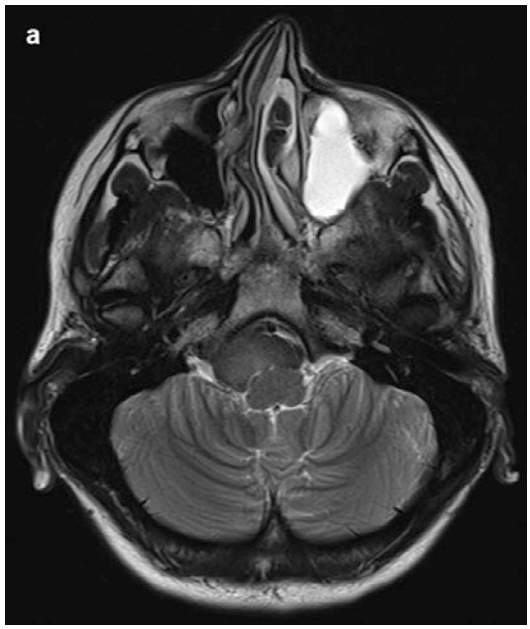

Fig. 10.5a Axial T2WI shows a mass in the cistern anterior to the medulla oblongata, hypointense to CSF

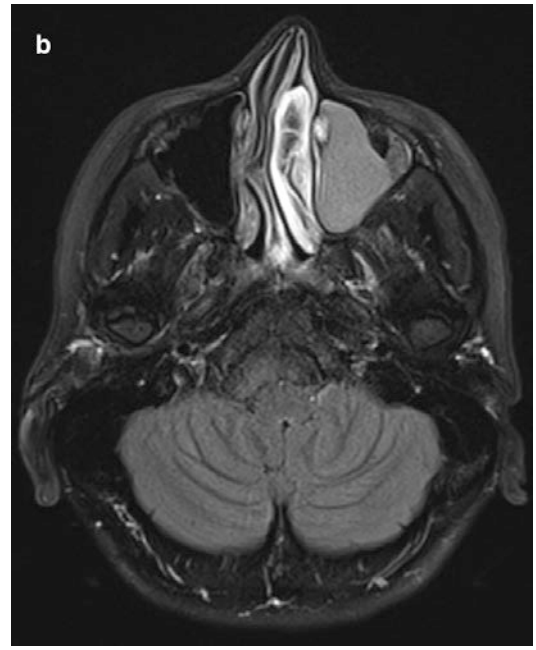

Fig. 10.5b Axial FLAIR with fat suppression shows iso- to slightly hyperintense signal to CSF

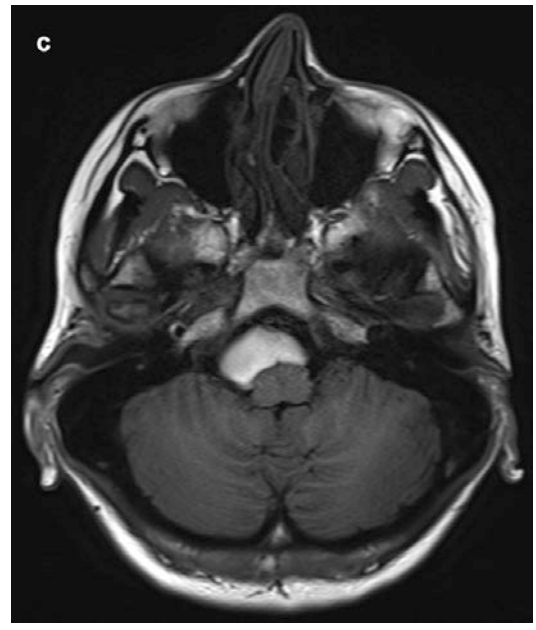

Fig. 10.5c Axial T1WI demonstrates high signal intensity within the mass

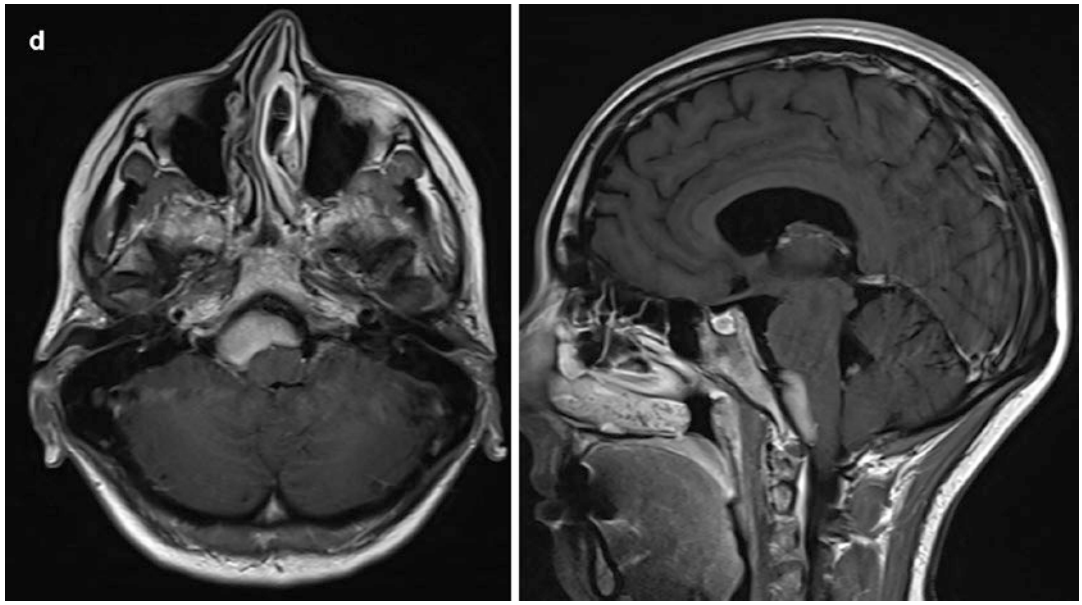

Fig. 10.5d Axial and sagittal T1WI after gadolinium administration show no clear enhancement

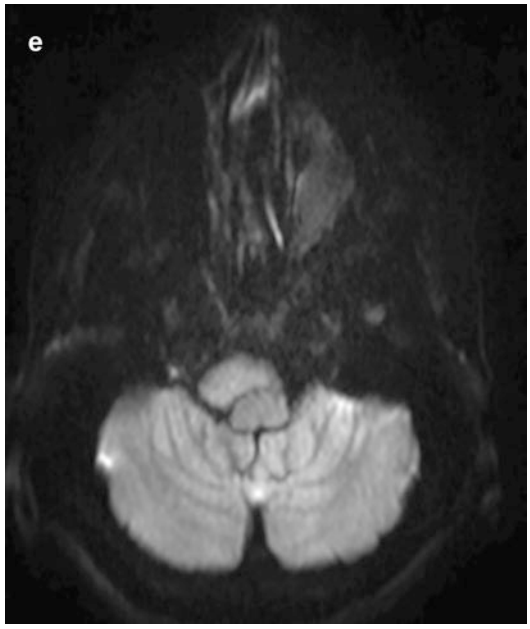

Fig. 10.5e No diffusion restriction on DWI

Epidemiology

- Rare entity
- More common in the spine than in the brain (3:1)
- Found at any age, peak in the fourth decade
- Female predilection (3:1)

Pathology and Genetics

- Gross pathology:
  - Translucent, thin-walled, round/lobulated cyst
  - Contains fluid varying from clear CSF-like to thick viscous/mucoid, depending on the type of epithelial lining
- Microscopy: two types of columnar epithelium in the cyst wall: rich in ciliated cells or rich in mucin-producing cells
  - Etiology: congenital endodermic cyst resulting from persistent connection between embryonic foregut and neural tube
  - Genetics: usually sporadic

Clinical Management

- Clinical presentation:
  - Intracranial: asymptomatic or aspecific symptoms like headache
  - Spine: symptoms due to spinal cord compression
- Management: surgery if symptomatic

Imaging Findings

- General:
  - Well-demarcated, lobulated extra-axial mass
  - 80% in the posterior fossa, typically anterior to the pontomedullary junction
  - 20% supratententorial: suprasellar, quadrigeminal cistern, cerebral hemispheres
- MRI:
  - Hyperintense to CSF on T1WI
  - Hyperintense to CSF on T2WI in 90%, hypointense in 10%
  - Usually hyperintense to CSF on FLAIR
  - Usually no diffusion restriction
  - No enhancement except for mild capsular enhancement
- CT: Iso- to slightly hyperattenuating to CSF, no calcifications

Take-Home Messages

- Intracranial neuroenteric cysts are congenital endodermal remnants
- Typically extra-axial in the posterior fossa, anterior to the pontomedullary junction
- Usually hyperintense to CSF on T1WI, T2WI, and FLAIR
- Surgical excision if symptomatic

Further Reading

- Intracranial Neurenteric Cysts: Imaging and Pathology Spectrum
- Preece MT, Osborn AG, Chin SS, Smirniotopoulos JG. Am J Neuroradiol. 2006;27(6): 1211–1216
- Arabi M, Ibrahim M, Camelo-Piragua S, Shah G. Supratentorial neurenteric cyst mimicking hydatid cyst: A case report and literature review. Avicenna J Med. 2013;3(3): 73–80
- Chakraborty S, Priamo F, Loven T, Li J, Insinga S, Schulder M. Supratentorial neurenteric cysts: case series and review of pathology, imaging, and clinical management. World Neurosurg. 2016;85: 143–152
- Gauden AJ, Khurana VG, Tsui AE, Kaye AH. Intracranial neuroenteric cysts: a concise review including an illustrative patient. J Clin Neurosci. 2012;19(3): 352–359

10.6 Colloid Cyst

56-year-old man with progressive gait disturbances and mild cognitive dysfunction since 2 months. CT scan reveals a supratentorial hydrocephalus due to an obstructing mass at the level of the foramina of Monro.

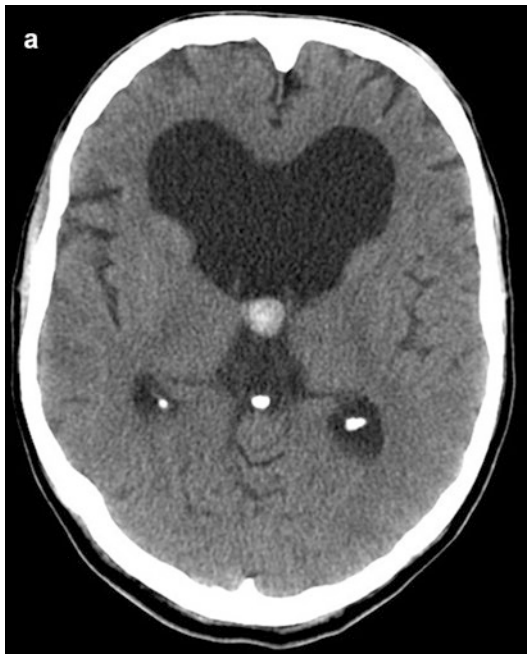

Fig. 10.6a Axial NECT of the head shows dilatation of the lateral ventricles due to an obstructing hyperattenuating mass anterior in the third ventricle, near the foramina of Monro

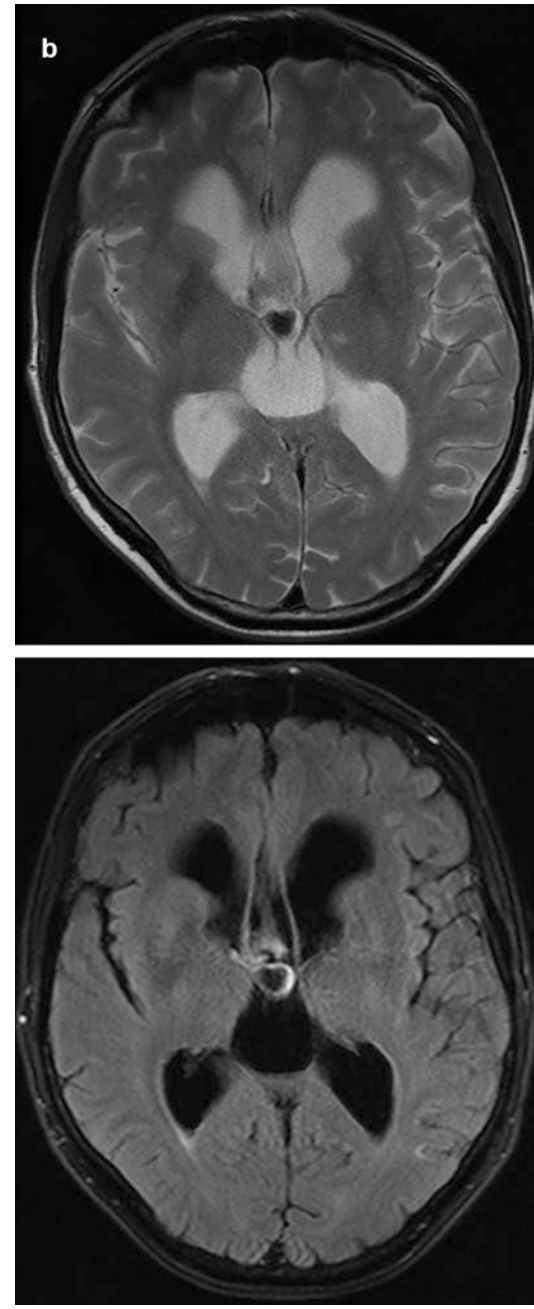

Fig. 10.6b The mass is hypointense with a hyperintense rim on T2WI and FLAIR

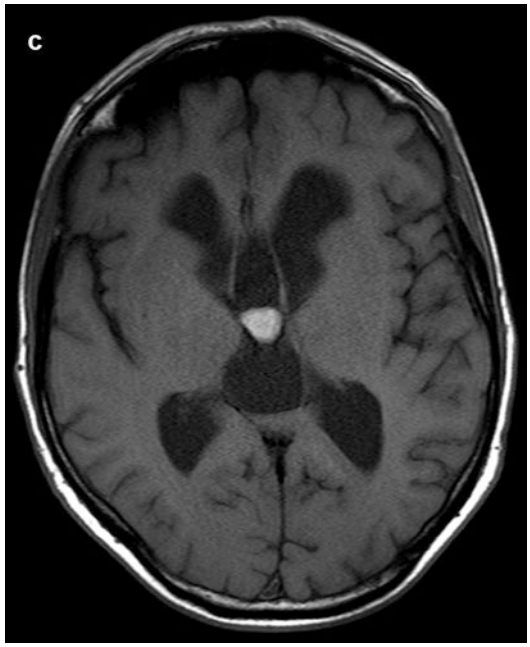

Fig. 10.6c On T1WI the mass is hyperintense

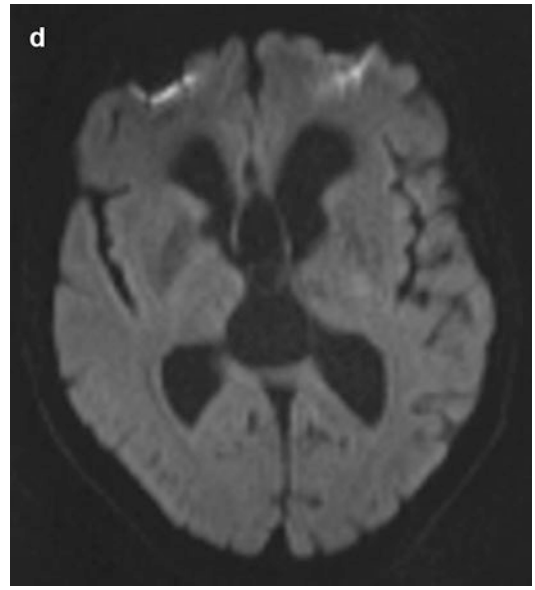

Fig. 10.6d No diffusion restriction on DWI

Epidemiology
- 15–20% of intraventricular masses
- Usually presents in the third and fourth decade, less in children
- No gender predilection

Pathology and Genetics
- Gross pathology:
  - Smooth, round, unilocular, well-demarcated cyst
  - Contains gelatinous "colloid" substance from mucinous secretions and epithelial desquamation, as well as cholesterol
- Microscopy: inner cyst wall lined with epithelium and goblet cells
  - Etiology: ectopic endodermal tissue migrated into the embryonic diencephalic roof
  - Genetics: usually sporadic
  - Associations: obstructive hydrocephalus

Clinical Management
- Clinical presentation:
  - Often asymptomatic and incidentally detected
  - Most common symptom is headache (50%)
  - Also nausea, vomiting, gait disturbances, visual changes, memory loss
  - Rapid clinical deterioration and possibly death in acute obstruction of foramen of Monro
- Management:
  - Endoscopic surgical resection
  - Good prognosis when diagnosed and resected early

Imaging Findings
- General:
  - Well-demarcated, round/ovoid mass
  - 99% anterosuperior midline in the third ventricle near or in the foramen of Monro
  - Signal/density variable, correlating with cyst content

- CT:
  - Hyperdense mass in the third ventricle at the level of the foramen of Monro is virtually pathognomonic
  - 66% hyperdense (low water content), 33% iso- or hypodense (high water content)
- MRI:
  - 66% hyperintense on T1WI (high cholesterol content), 33% hypointense (low cholesterol)
  - Generally isointense on T2WI. Sometimes hypointense: "black hole effect"
  - No suppression on FLAIR
  - No diffusion restriction
  - No enhancement except for mild capsular enhancement

Take-Home Messages

- Colloid cysts are congenital endodermal, mucin containing cysts
- 99% are located midline anterosuperior in the third ventricle near or in the foramen of Monro
- Hyperattenuating mass on NECT in this location is pathognomonic
- Risk of acute obstruction of foramen of Monro and rapid onset obstructive hydrocephalus
- Good prognosis when diagnosed and resected early

Further Reading

- Armao D, Castillo M, Chen H, Kwock L. Colloid cyst of the third ventricle: imaging-pathologic correlation. Am J Neuroradiol. 2000;21(8): 1470–1477
- Hamidi H, Faizi FR, Rasouly N, Hoshang MMS. CT and MRI features of pediatric-aged colloid cysts: Report of two cases. Case Rep Radiol. 2017;2017: 2467085
- Diyora B, Nayak N, Kukreja S, Sharma A. Hemorrhagic colloid cyst: Case report and review of the literature. Asian J Neurosurg. 2013;8(3): 162

10.7 Enlarged Perivascular Spaces

65-year-old man with aspecific symptoms like fatigue and difficulty in executing complex tasks. On imaging a multicystic mass in the midbrain is seen.

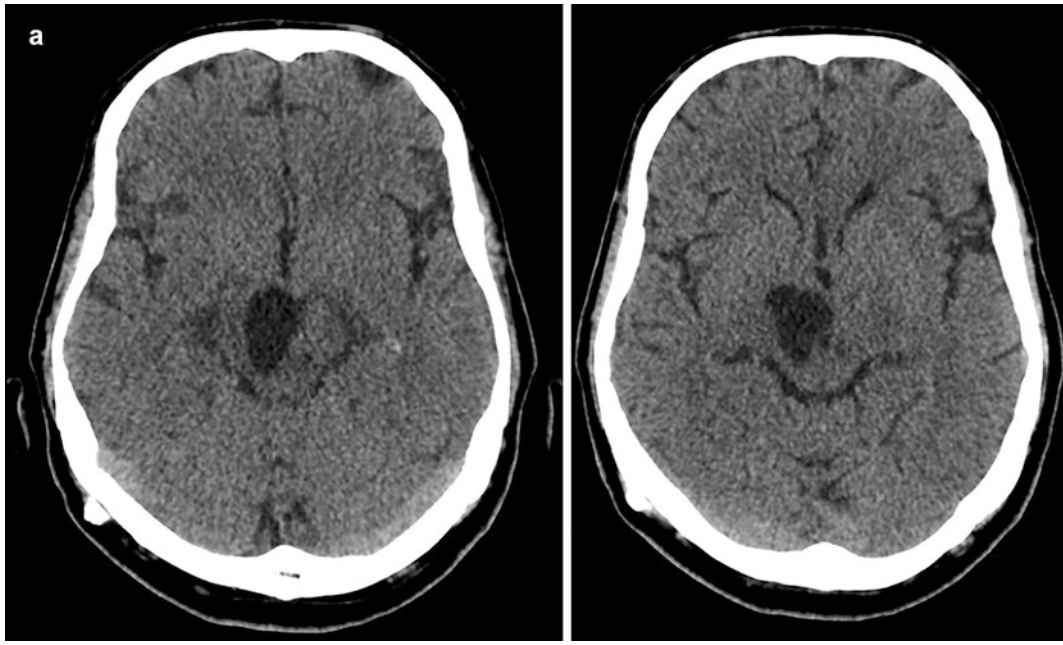

Fig. 10.7a Axial NECT images show a hypodense, probably cystic, mass in the mesencephalon and the right thalamus

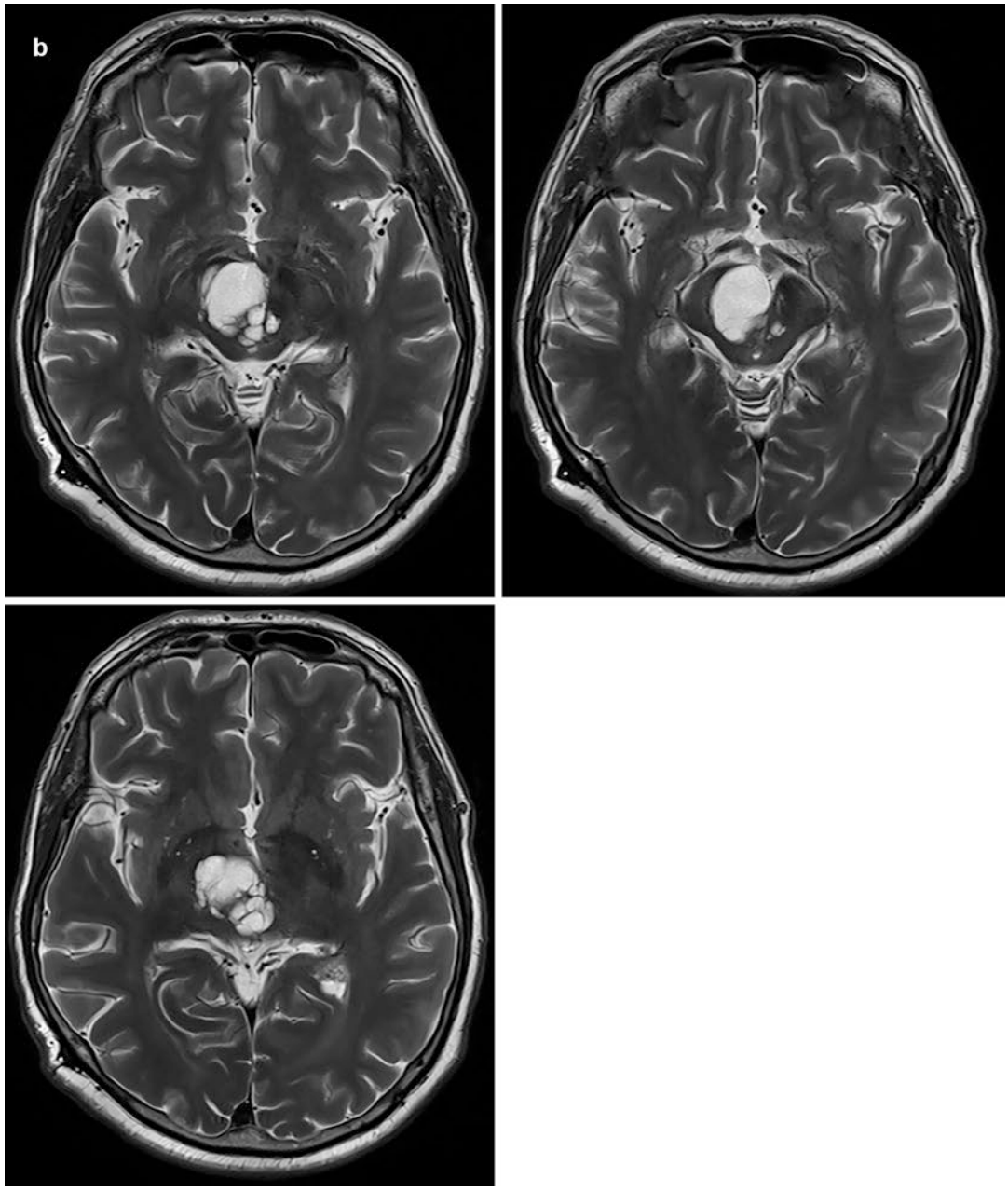

Fig. 10.7b Axial T2WI images show a multicystic mass in the mesencephalon. The cyst contents are hyperintense, resembling CSF

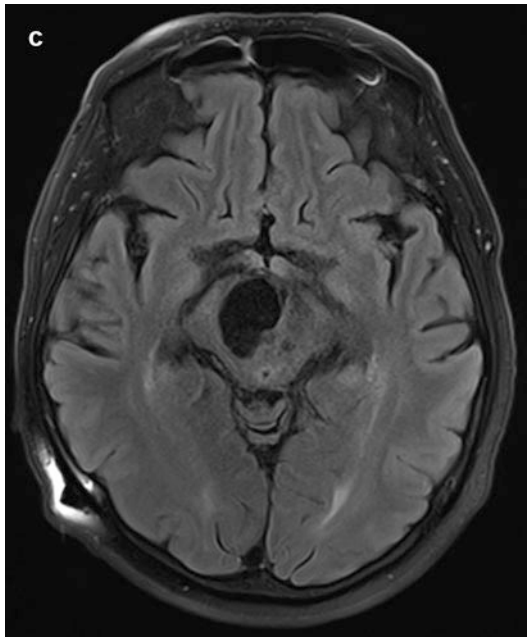

Fig. 10.7c Axial FLAIR image shows complete suppression of the signal in the cyst

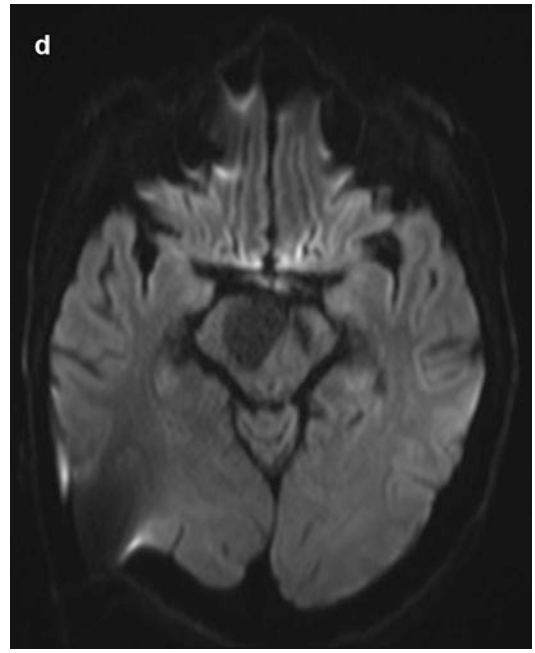

Fig. 10.7d No diffusion restriction on DWI

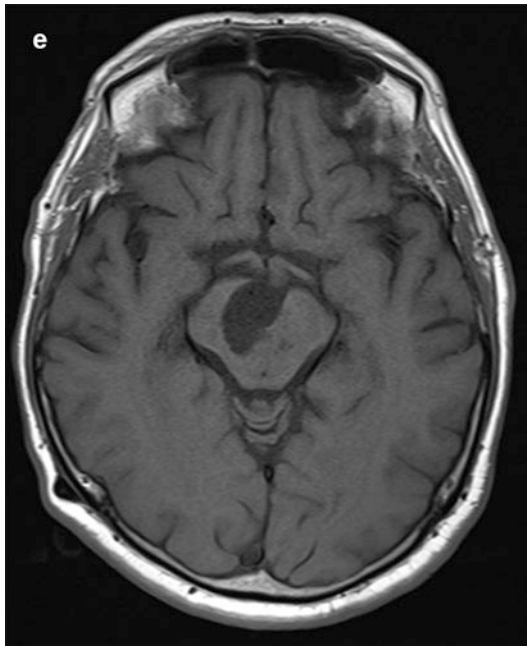

Fig. 10.7e On axial T1WI, the signal is hypointense, resembling CSF

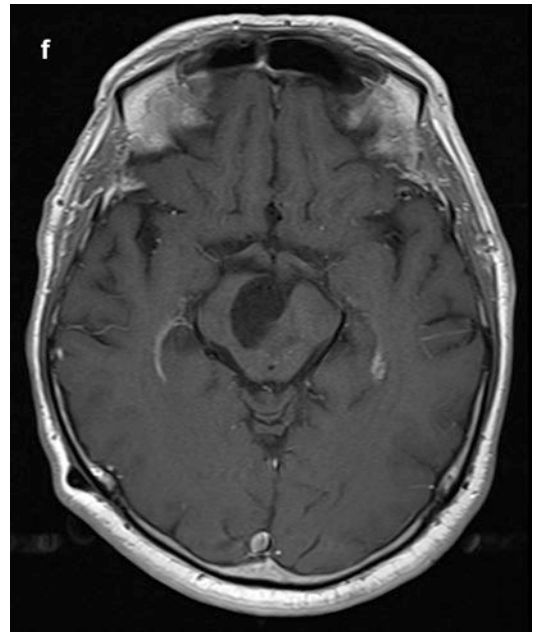

Fig. 10.7f Axial T1WI after gadolinium administration shows no enhancement

Epidemiology
- Perivascular spaces (PVS) seen at all ages, 30% in children. Normal variant
- Size and number increase with age
- Enlarged "giant" perivascular spaces more common in fifth decade, but not uncommon in children
- Giant PVS: male predilection (1.8:1)

Pathology and Genetics
- Gross pathology:
  - PVS: channels around penetrating arteries in brain parenchyma, lined by pia mater and filled with interstitial fluid. No communication with the subarachnoid space
  - Giant PVS: smooth, well-demarcated cysts
- Microscopy:
  - Wall of PVS/cysts = single or double layer of invaginated pia mater
  - Content = interstitial fluid, not CSF
- Etiology giant PVS: probably obstruction of interstitial fluid flow leading to accumulation
- Genetics: usually sporadic
- Associations:
  - Hydrocephalus due to aqueductal compression by midbrain PVS
  - PVS may facilitate spread of inflammation, infection, or tumor into the brain parenchyma
  - Probably increased risk of microvascular disease
  - Mucopolysaccharidoses

Clinical Management
- Clinical presentation:
  - Usually incidental finding in asymptomatic patients
  - Aspecific symptoms like headache
- Management:
  - Don't touch lesion
  - Ventricular shunt when midbrain giant PVS causes obstructive hydrocephalus

Imaging Findings
- General:
  - Enlarged PVS: intra-axial cluster(s) of variable-sized cystic spaces (usually less than 5 mm)
  - Enlarged PVS most frequently in the midbrain
  - Normal sized PVS found in all locations: most frequent in the basal ganglia (type 1) but also in the deep white matter (type 2) and the midbrain (type 3)
  - PVS/cyst content resembles CSF density/intensity
- CT: CSF-like density, no calcifications
- MRI:
  - Depiction best at 3 T
  - Appear isointense to CSF on all sequences
  - Usually complete suppression on FLAIR. 25% show surrounding gliosis, especially those located at the anterior superior temporal gyrus
  - No diffusion restriction
  - No enhancement

Take-Home Messages
- PVS are intra-axial fluid containing spaces, seen in all ages and locations as a normal variant
- Enlarged "giant" PVS may look like a multicystic mass
- Enlarged PVS commonly located in the midbrain
- Contains interstitial fluid, resembling CSF on imaging
- Almost always stable and asymptomatic: don't touch lesions

Further Reading

- Salzman KL, Osborn AG, House P, et al. Giant tumefactive perivascular spaces. Am J Neuroradiol. 2005;26(2): 298–305
- Kwee RM, Kwee TC. Virchow-Robin spaces at MR imaging. Radiographics. 2007;27(4): 1071–1086
- Osborn AG, Preece MT. Intracranial cysts: radiologic-pathologic correlation and imaging approach. Radiology. 2006;239(3): 650–664

Extra-Axial Tumors

11

Dora Zlatareva and Claude Nauer

11.1 Incidental Meningioma

A 77-year-old man undergoes brain MRI after a transient ischemic attack. An incidental asymptomatic meningioma is found. Follow-up 6 months later shows no change in size.

Companion case: asymptomatic 80-year-old woman, two asymptomatic meningiomas.

D. Zlatareva
Department of Diagnostic Imaging, Medical University Sofia, Sofia, Bulgaria

C. Nauer (✉)
Radiology, Kantonsspital Graubünden, Chur, Switzerland

Y. Özsunar, U. Şenol (eds.), *Atlas of Clinical Cases on Brain Tumor Imaging*,
https://doi.org/10.1007/978-3-030-23273-3_11

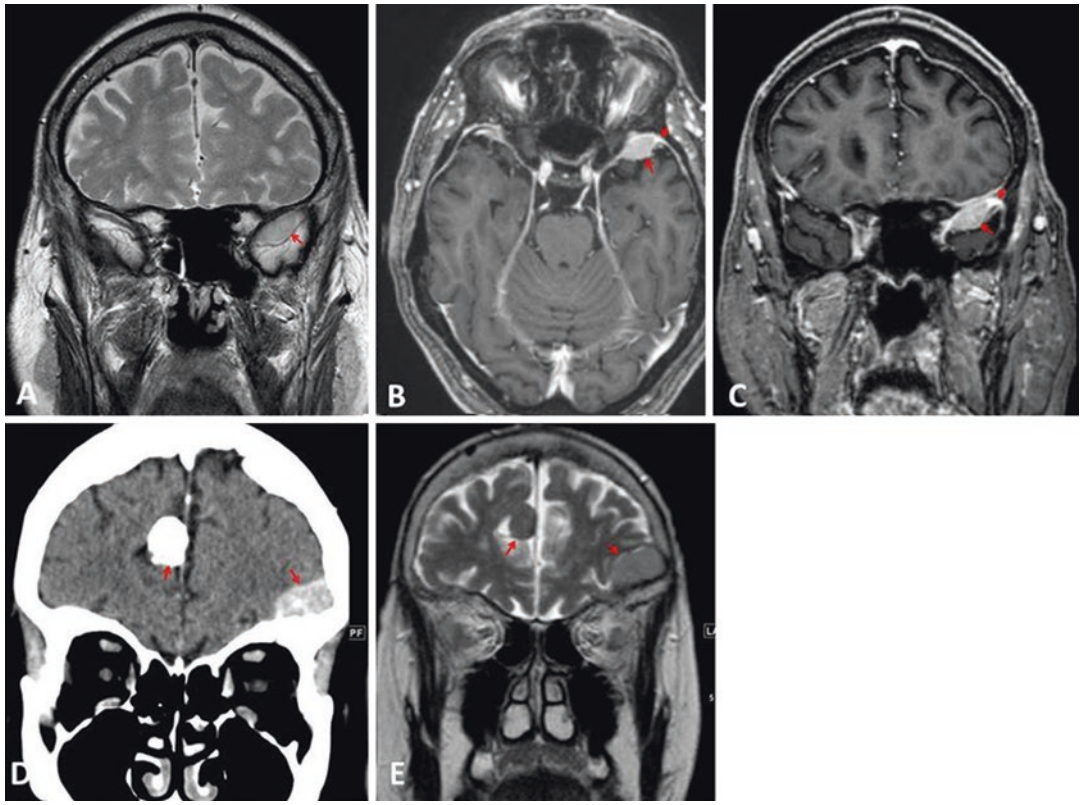

Fig 11.1 Coronal T2w MRI (**a**), transverse T1w with contrast (**b**), coronal section with contrast (**c**). Companion case: coronal CT (**d**) and T2w MR (**e**). MR shows an extra-axial well-circumscribed and ovoid-shaped lesion attached to the left greater sphenoid wing. Signal intensity on T2 weighted (**a**, red arrow) of the lesion is similar to gray matter, it shows typical homogenous enhancement on T1w after Gadolinium (**b**, **c**), somewhat lower than the abutting sphenoparietal sinus (short arrow on **b**, **c**). No evidence of bone or venous sinus infiltration. Companion case: coronal reformatted CT (**d**) show two densely calcified lesions on the falx and left frontal skull base (red arrows) with corresponding very low signal intensity on T2w MR (**e**)

11.1.1 Epidemiology/Most Commonly Seen Types

- Meningioma is a frequent, often asymptomatic tumor, prevalence in the elderly 2–3%
- Most meningiomas sporadic, 2–3 times more frequent in women
- Multiple meningioma typical in elderly women, in neurofibromatosis type 2 and after exposition to ionizing radiation
- Hemispheric location most frequent, other locations (skull base, spine) rarer, very rarely in the ventricles or in head and neck region

11.1.2 Pathology and Genetics

- Vast majority (>90%) WHO grade I, with many histological subtypes
- 5–7% WHO II, show higher mitose rate, more aggressive behavior and higher recurrence rate
- 1–3% WHO grade III, very high mitose rate, histologically overt aggressive features like brain invasion
- Brain invasion typical for WHO III tumors; however, calvarial or venous sinuses invasion and extensive trans-spatial growth are often seen in WHO grade I meningioma

11.1.3 Clinical Management

- Many meningiomas asymptomatic, frequent initial symptom epileptic seizure
- Focal neurologic symptoms when brain or cranial nerve compression
- Treatment not mandatory for asymptomatic tumor, "watchful waiting" often adequate: First clinical and imaging follow-up after 6 months, if stable in size, further controls yearly. After five years without significant change, control every second year
- Surgery generally first treatment option
- Radiosurgery alternative for unresectable meningioma

11.1.4 Imaging Findings and Differential Diagnosis

- Typically well defined, rather homogeneous, extra-axial tumor
- NECT isodense or hyperdense (40–50 HU) to gray matter
- MRI signal intensity similar to gray matter T2WI/T1WI
- Strong quiet homogenous enhancement typical; inhomogenous enhancement with cystic parts indicates regressive changes
- Dural tail (intense reactive dural enhancement around tumor) typical feature of meningioma, but not entirely specific, can be seen in other lesions as well
- Signal intensity very low on T2w when calcifications present (25%, see case e)
- Further typical imaging characteristics see subsequent cases

Typical meningioma can usually be diagnosed straightforward. However, wide variety in morphology/spreading pattern may make differential diagnosis challenging: Metastases, lymphoma, IgG4-associated inflammatory pseudotumor. Meningioma infiltrating adjacent structures indistinguishable from atypical (WHO II) or aggressive (WHO III) meningioma and hemangiopericytoma.

How to distinguish metastases from meningioma and differential diagnosis of en plaque meningioma (see case 11.2).

Take-Home Messages

- Meningioma is a frequent asymptomatic tumor found incidentally on imaging
- Typical meningioma usually has a very characteristic appearance and can be diagnosed reliably based on imaging only
- Many different spreading patterns and atypical morphology may make diagnosis difficult
- Treatment often not indicated, active surveillance with a first follow-up after 6 months and further yearly follow-up studies (after five years follow-up every second year) is a reasonable strategy

Further Reading

- Chourmouzi D, Potsi S, Moumtzouoglou A, et al. Dural lesions mimicking meningioma. A pictorial essay. World J Radiol. 2012;4(3):75–82
- Goldbrunner R, Minniti G, Preusser M, et al. EANO guidelines for the diagnosis and treatment of meningiomas. Lancet Oncol. 2016;17(9):e383–91
- Lee JH, editor. Meningiomas. Diagnosis, treatment and outcome. London: Springer; 2008
- Smith A, Horkanyne-Szakaly I, et al. Mass lesionsofthedura:Beyondmeningioma—radiologic-pathologic correlation. Radiographics. 2014;34:295–312
- Watts J, Box G, Galvin A, et al. Magnetic resonance imaging of meningiomas: a pictorial review. Insights Imaging. 2014;5:113–22

11.2 En-Plaque Meningioma

51-year-old woman with newly diagnosed neuroendocrine carcinoma, complaining of visual disturbances. MRI is performed to exclude brain or orbit metastasis. In retrospect, the symptoms were noted already for some time.

Companion case, 88-year-old woman. Asymptomatic meningioma.

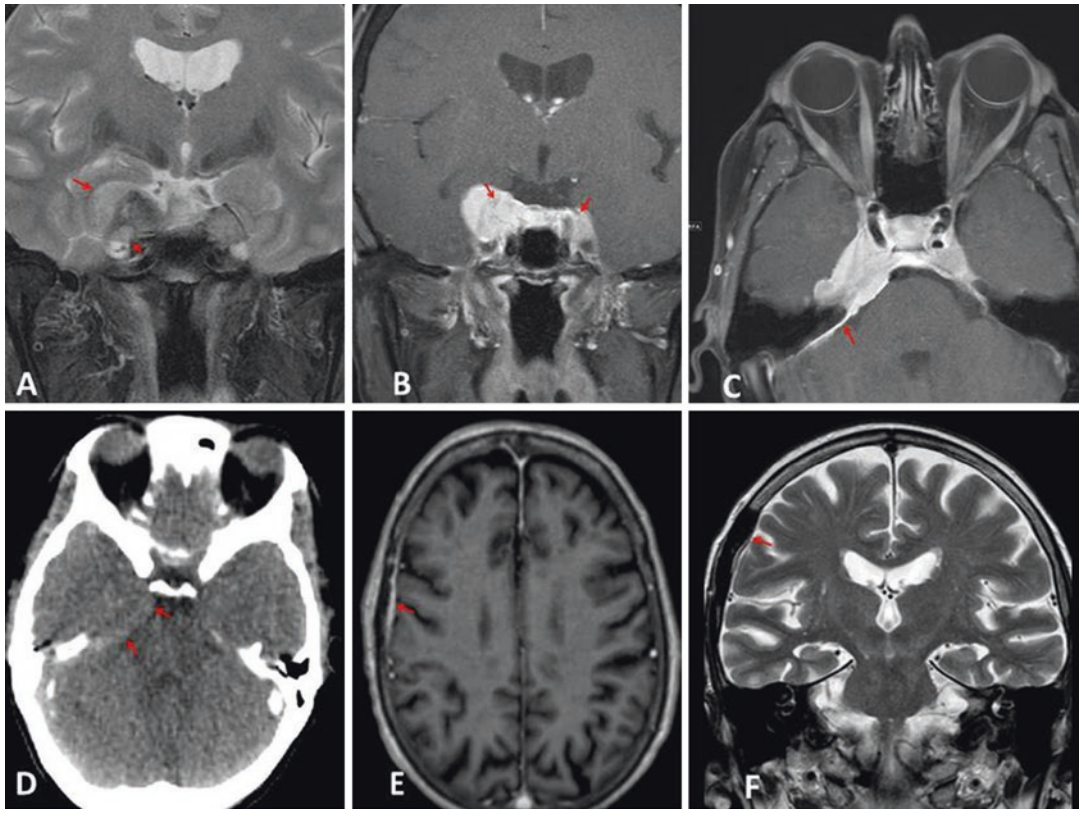

Fig. 11.2 Extra-axial enhancing mass extending bilaterally in the petrous apex/cavernous sinus region, with encasement of the right internal carotid artery, is evident on T1WI fat-saturated images after gadolinium (**b**, **c**). Note the oculomotor nerve encasement in the cavernous sinus, on coronal T1WI fat-saturated images after gadolinium (**b**, arrowheads) as well as infiltration of right Meckel's cave on T2WI fat-saturated image (**a**, short arrow). Note dural tail at petrous apex on **c** (red arrow). Signal intensities characteristic of meningioma (see case 1), as well as the spreading pattern typical of meningioma made the diagnosis probable. Recently acquired PET-CT showed no metabolic activity, but the mass can be discerned as faintly hyperdense to brain on NECT (**d**, red arrows). Companion case (**e**) (transverse T1WI with Gadolinium) shows the right frontotemporal en plaque meningiom, only a slightly thickened dura with enhancement is directly visible, however, significant thickening and sclerosis of the adjacent bone is evident T2WI (**f**)

11.2.1 Clinical Management

- Skull base meningioma can extend very far and cause cranial nerve symptoms because of invasion of neural foramina
- Due to slow growth, symptoms increase slowly and are often not noted by patients for a long time
- Symptomatology very important for distinction between skull base meningioma (symptoms growing over years) and two similarly looking entities: IgG4-related inflammatory pseudotumor (symptoms within days, pain, respond to steroids) and lymphoma (symptoms within weeks, respond to steroids)
- Meningioma and metastases frequent in the elderly, hence the two entities often found in the same study

11.2.2 Imaging Findings and Differential Diagnosis

- Differentiation of metastases and meningioma: Metastases from extracranial primary tumors usually intra-axial, meningioma extra-axial
- Dural metastases rare, distinction from meningioma may be challenging, check following:
  - Other (intra-axial) lesions present? Metastases likely
  - Reactive bone sclerosis? Meningioma likely

Differential diagnosis for en plaque meningioma: Smooth regional dural thickening may be scarring after subdural hematoma. Extensive Irregular dural thickening: IgG4-mediated inflammatory pseudotumor may involve cavernous sinus/skull base. Generalized dural thickening including the tentorium typical for chronic CSF loss.

Take-Home Messages

- Meningioma not always the typical round or ovoid-shaped well-defined tumor, and may extend "en plaque" over wide areas, covering or transgrowing neural foramina
- Meningioma typically show slow symptom increase often not perceived for a long time

11.3 Meningioma with Transosseous Spread

77-year-old man has been noticing a painless lump on his head for already three years, no growth during the past two years noted. No neurological symptoms. Imaging follow-up after 3 months and 6 months did not show growth.

Companion case: Rapidly growing lump on the head of a man with metastases of colon adenocarcinoma.

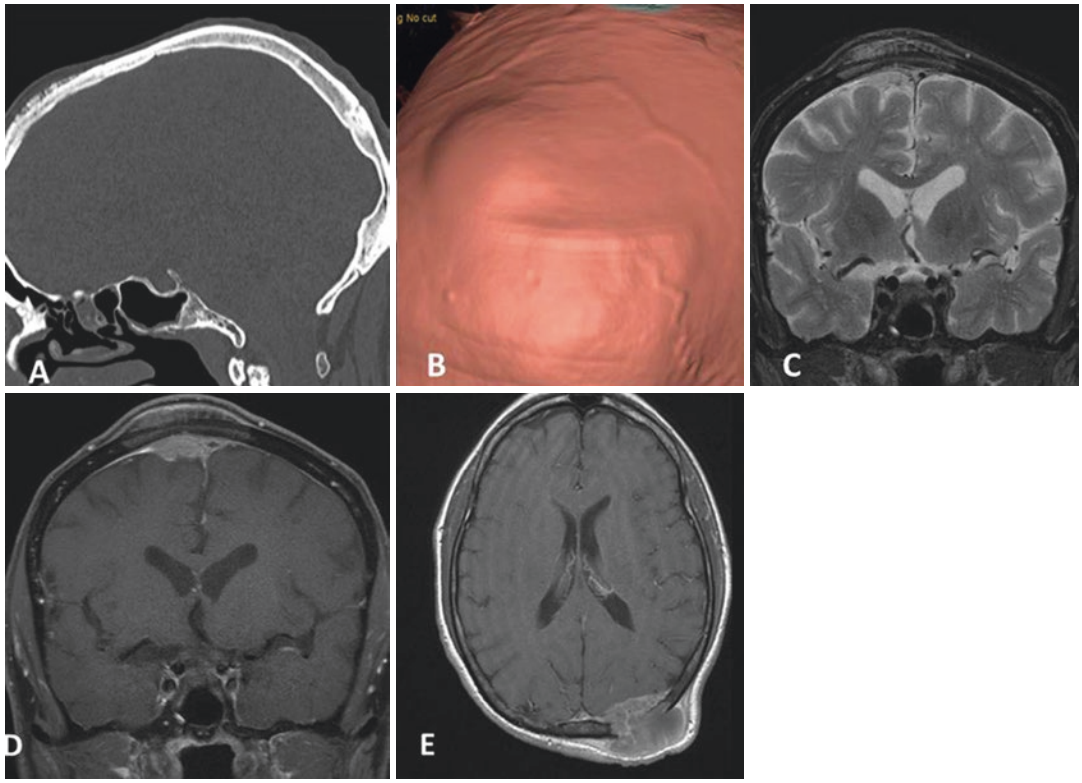

Fig. 11.3 An extra-axial frontal lesion growing through the frontal cranial vault, inducing reactive bone changes on the tabula externa, is evident on the sagittal reconstruction of bone kernel CT (**a**), the calvarium is not destructed (**b**). In the MRI T2WI fat saturated (**c**) and T1WI fat saturated after gadolinium (**d**) the invasive nature of the lesion is obvious; invasion of superior sagittal sinus as well as the cranial vault can be seen. The black dot (**c**, **d**) in the superior sagittal sinus is flow void, indicating that the sinus is not yet totally obstructed. (**e**) Companion case. Similar lesion but destructing the calvarial bone completely

11.3.1 Clinical Management

- Meningiomas often invade venous sinuses, due to slowly progressive lumen narrowing collaterals build up, hence sinus occlusion virtually never a clinical problem
- Neurosurgeons prefer to operate when sinus completely occluded, because then, infiltrated sinus can be safely removed
- Most important point for differentiation of meningioma from aggressive lesions is clinical history

11.3.2 Imaging Findings and Differential Diagnosis

- "Aggressive behavior" like bone or sinus invasion can be seen in meningioma WHO grade I
- From imaging perspective atypical (WHO II) or anaplastic (WHO III) meningioma, hemangiopericytoma or a metastases cannot be safely distinguished from WHO I meningioma in these cases
- Important to distinguish between bone infiltration with reactive sclerosis (meningioma) and frank bone destruction (metastases, hemangiopericytoma, other malignant tumors)

Take-Home Messages

- Meningiomas WHO I may infiltrate bone and venous sinuses
- Venous sinus invasion by meningioma is not as dangerous as it looks. The very slow progression of lumen narrowing lets enough time to build up collaterals
- Important to distinguish between transosseous growth with reactive sclerosis (meningioma) and frank bone destruction (malignant process)

11.4 Atypical Meningioma WHO II

A 68-year-old male presenting with headache, altered mental status, and urinary incontinence. MR shows a large frontal tumor. Histology reveals atypical meningioma (WHO grade II).

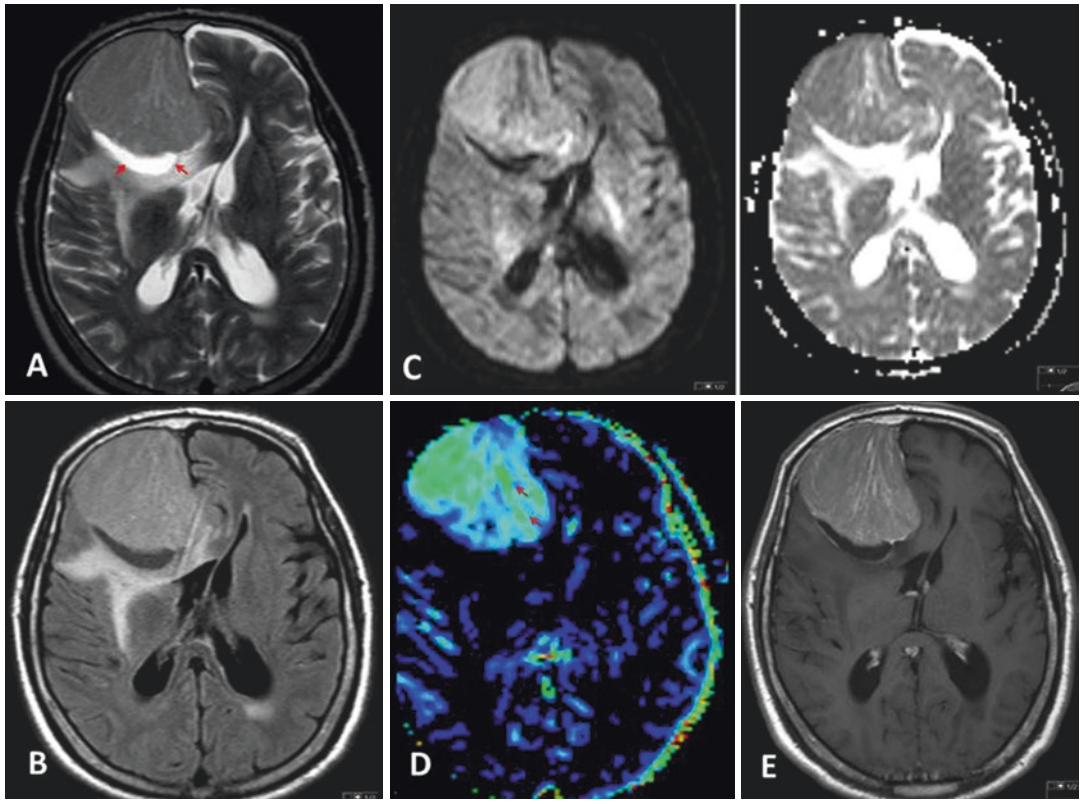

Fig. 11.4 The T2WI-weighted transverse section (**a**) shows an extra-axial tumor over the right frontal lobe with significant mass effect and edema in the adjacent brain. Transverse DSC perfusion map (**d**) shows areas of very high CBV values within the tumor. Striated vascular architecture is visible on perfusion map (**d**) as well as on T1WI after Gadolinium (**e**, red arrows). Note trapped CSF between brain surface and tumor (red arrow in **a**), typical sign of extra-axial tumor location. Inhomogenous signal on DWI and ADC map probably reflects areas with different degrees of cellularity

11.4.1 Epidemiology/Most Commonly Seen Types

- General remarks on meningioma WHO II/III see case 11.1
- Atypical and aggressive meningiomas mostly arise from the calvarial dura and are rare at the skull base
- Atypical and aggressive meningioma are rare (<10% of all meningioma)

11.4.2 Pathology and Genetics

- General remarks on meningioma WHO II/III see case 11.1
- Brain edema adjacent to meningiomas more frequent in higher grade tumors, but occurs also in meningiomas WHO grade I
- Brain edema indicates pial infiltration, making neurosurgeons task more difficult

11.4.3 Clinical Management

- Postoperative radiation therapy decreases the risk of recurrence
- Meningioma-induced brain edema correlates with seizures

11.4.4 Imaging Findings and Differential Diagnosis

- Reliable differentiation of meningioma WHO I and atypical/aggressive meningioma based on imaging alone generally not possible
- Imaging features helping to identify atypical and aggressive meningioma:
  - Lack of calcification
  - Indistinct tumor borders
  - Brain invasion and osseous destruction

Take-Home Messages

- Imaging-based differentiation meningioma WHO grade I vs. WHO II/III not reliably possible
- Atypical/aggressive meningioma tend to show indistinct tumor borders and brain invasion may be visible
- Brain edema adjacent to meningiomas not sign of atypical or aggressive (WHO II or III)

11.5 Hemangiopericytoma/ Malignant Solitary Fibrous Tumor (SFT)

A 36-year-old woman with history of a previous operation. Histology showed a hemangiopericytoma/malignant solitary fibrous tumor (SFT).

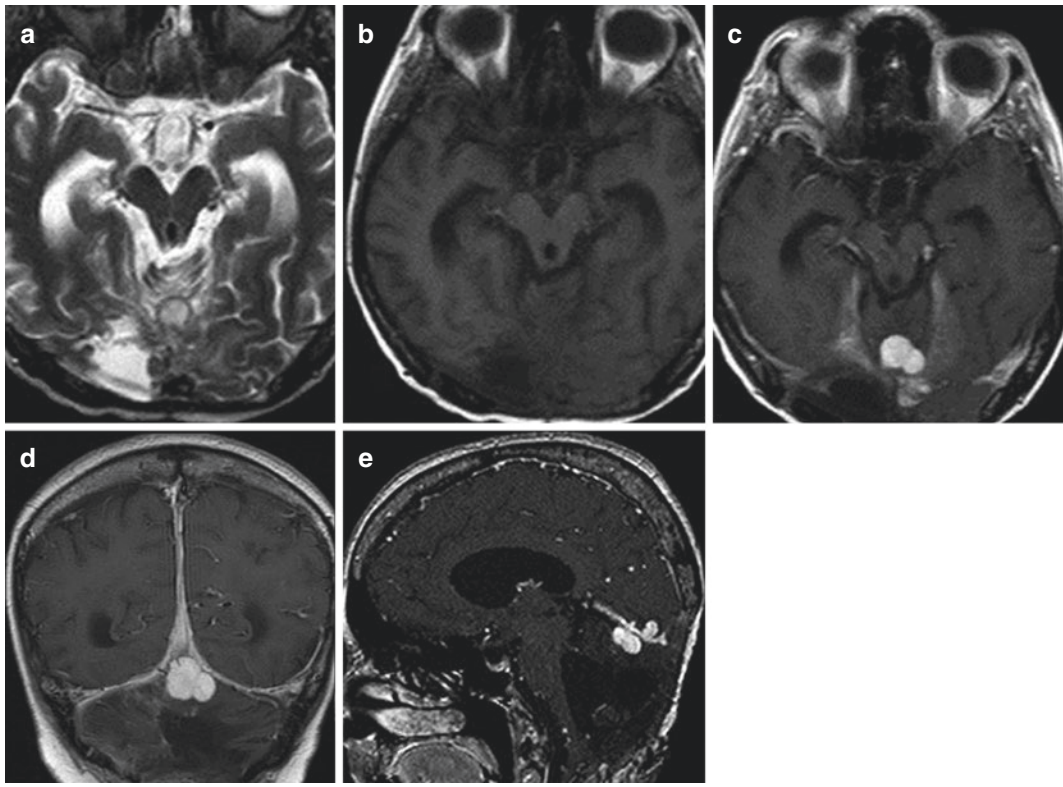

Fig. 11.5 A multinodular strongly enhancing extra-axial lesion is visible on T1WI-weighted images after gadolinium (**c**, **d**, **e**) extending on the lower and upper tentorial surface. Signal intensity on T2WI (**a**) is hyperintense and the lesion is unconspicuous on T1WI (**b**). Postoperative defects are present on the right cerebellar hemisphere as well as along the vermis

11.5.1 Epidemiology/Most Commonly Seen Types

- Rare tumor, accounting for less than 1% of all intracranial neoplasms
- Mostly middle aged persons
- Usually dural-based, most often along falx or tentorium

11.5.2 Pathology and Genetics

The tumor known as hemangiopericytoma was once thought to arise from vessel wall pericytes (hence its name).

- Derives from fibroblasts; hemangiopericytoma most aggressive variant of the solitary fibroblastic tumor (SFT) of the dura
- In 2016 WHO CNS tumor classification, these two entities are grouped together as SFT/hemangiopericytoma
- Most SFT arise in other body parts (namely the pleura), not CNS/meninges
- Malignant SFT/hemangiopericytoma highly vascular and cellular

11.5.3 Clinical Management

- Symptoms depend on tumor location and extent
- Surgery treatment of choice; preoperative embolization is an option, as well as postoperative radiotherapy, or radiotherapy alone in non-operable lesions
- 20% local recurrency, follow-up mandatory

11.5.4 Imaging Findings and Differential Diagnosis

- SFT usually lobulated, located along the falx or tentorium
- Gross infiltration of adjacent structures in malignant SFT
- Dural tail, as in meningioma, may be present
- Signal intensity generally isointense to brain, T2w hyperintense or inhomogenous parts may occur
- Calcification uncommon
- Avid enhancement
- As opposed to meningioma, malignant SFT causes osseous destruction, not hyperostosis
- May be undistinguishable from meningioma WHO grade II or III, and from dural metastases

Take-Home Messages

- Malignant solitary fibrous tumor/hemangiopericytoma is an aggressive fibroblastic tumor of the dura
- May be undistinguishable from meningioma on imaging
- Should be considered as a differential diagnosis when osseous destruction (not hyperostosis, as in meningioma) is evident
- High risk of recurrency, follow-up examinations are mandatory

Further Reading

- Drevelegas A, editor. Imaging of brain tumors with histological correlations. 2nd edn. Berlin: Springer; 2011
- Smith A, Horkanyne-Szakaly I, Schroeder J, Rushing E. Mass lesions of the dura: beyond meningioma—radiologic-pathologic correlation. Radiographics 2014;34:295–312

11.6 Pituitary Microadenoma

A 27-year-old female with history of secondary amenorrhea, headache, and galactorrhea. Prolactin serum level is elevated.

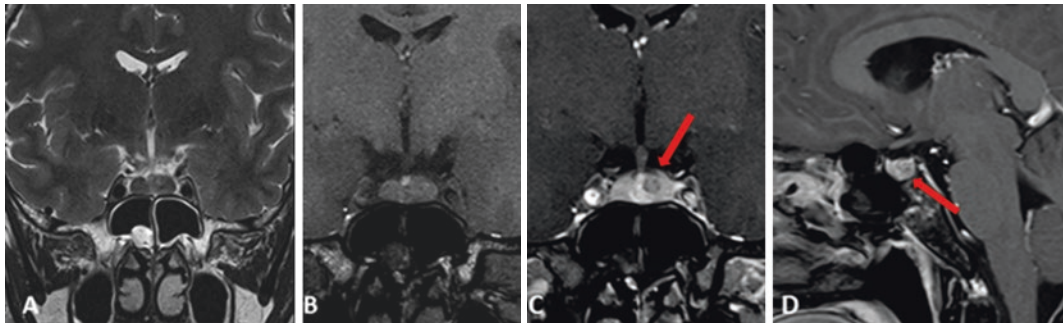

Fig. 11.6 Coronal T2WI (**a**) and T1WI (**b**) demonstrate increased convexity of the left cranial pituitary border. Coronal T1WI post-contrast (**c**) and sagittal T1WI post-contrast image (**d**) reveal well-delineated hypointense lesion with left paramedian location (arrow). No deviation of pituitary stalk

11.6.1 Epidemiology

- 90% of the intrasellar lesions, 10% of all primary intracranial neoplasms
- Smaller than 10 mm is microadenomas, and larger is macroadenomas
- Some are clinically silent and remain undetected resulting in much higher actual rate
- Female predilection, prolactin, and adrenocorticotrophic secreting tumors prevalence

11.6.2 Pathology and Genetics

- Most adenomas: WHO grade I, pituitary carcinoma is extremely rare
- Microadenomas: Circumscribed lesions within a normal sized pituitary
- Subclassified by immunohistochemical staining
- Prolactin (30–40% of symptomatic adenomas), growth hormone, ACTH, thyroid stimulating, luteinizing, or follicle-stimulating hormone
- Clinically nonfunctioning adenomas: 15–54%, majority asymptomatic
- Some are part of MEN syndrome type I, Carney complex, McCune Albright syndrome and familial isolated pituitary adenoma syndrome

11.6.3 Clinical Management

- Functional and nonfunctional, symptoms depend on hormones, age, and sex
- Women with hyperprolactinemia: amenorrhea, galactorrhea, and infertility
- Headache can occur with a lesion of any size
- Incidentalomas: most are small nonfunctional and asymptomatic
- Management
  - Incidentaloma: clinical investigation and follow-up imaging
  - Medical therapy with dopaminergic drug for prolactinomas
  - Transsphenoidal resection when medical therapy is ineffective

11.6.4 Imaging Findings and Differential Diagnosis

- Isodense on NECT, most are hypodense on post-contrast CT
- MRI: isointense on T2WI and T1W
- Hemorrhage is less common in microadenomas—increased T1 signal or blooming on gradient images
- May deviate the infundibulum or increase convexity of the cranial pituitary border but this could be a normal variant
- 70%: hypointense on post-contrast T1WI
- May show a delayed enhancement on dynamic contrast series

Differential diagnosis includes Pituitary "incidentaloma", Rathke's cleft cyst, pars, intermedia cyst, Pituitary hyperplasia, Intrasellar craniopharyngioma, and Hypophysitis

Take-Home Messages

- Dynamic contrast enhanced study to distinguish microadenoma on early images
- Clinical correlation is mandatory to differentiate between incidental lesions and clinically endocrine active lesions

Further Reading

- Molitch ME. Diagnosis and treatment of pituitary adenomas: A review. JAMA. 2017;317(5):516–24
- Osborne A. Pituitary microadenoma. In: Osborne A, editors. Diagnostic imaging BRAIN. Salt Lake City: Amirsys; 2007. p. II-2-20–23
- Smith A, Cha S. Sellar and juxtasellar tumors. In Naidich et al., editors. Imaging of the brain. Philadelphia: Elsevier, Saunders; 2013. p. 728–30

11.7 Pituitary Macroadenoma

A 35-year-old female with history of headache, bitemporal hemianopia, infertility, and galactorrhea. The prolactin serum level is elevated.

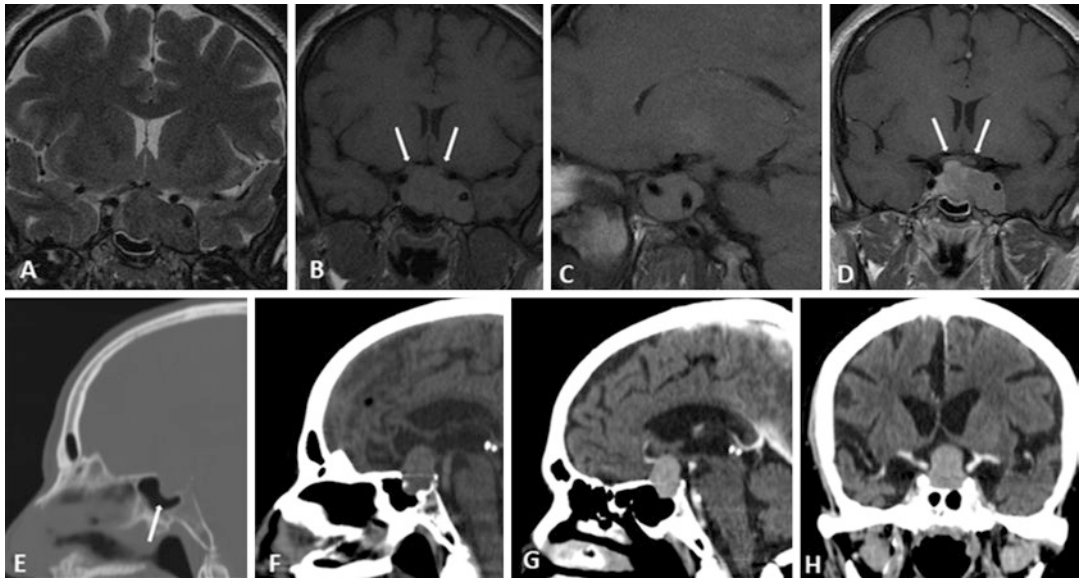

Fig 11.7 T2WI (**a**), T1WI coronal (**b**) and sagittal (**c**), contrast-enhanced T1WI coronal (**d**) MR images of pituitary. Large isointense sellar/parasellar mass is detected. The optic chiasm is displaced superiorly (arrows on **b** and **d**) and left internal carotid artery is encased but with normal flow void (**a**–**d**). Companion case, 56-year-old female with headache and visual field defects. Bone window CT (**e**) demonstrates enlarged sella with destruction of the floor (arrow). Non-enhanced (**f**) and post-contrast CT sagittal (**g**) and coronal (**h**) brain window image shows a homogeneously enhancing sellar and parasellar mass with a "snowman" shape

11.7.1 Epidemiology

- Around half of all suprasellar tumors are pituitary macroadenomas
- Female predilection for prolactin secreting tumors
- Nonfunctioning adenomas are more likely to diagnose at larger size
- Children and adolescents: frequency rate is less than 6% and macroadenoma has to be differentiated from more common secondary pituitary hyperplasia

11.7.2 Pathology and Genetics

- Well-delineated lobulated masses, extend into the suprasellar cistern, less commonly into the sphenoid sinus or into the cavernous sinus
- No capsule, but the intact pituitary gland is compressed
- Half of lesions show cystic or hemorrhagic components
- Subclassified by immunohistochemical staining
- Can occur in MEN syndrome type I
- MIB-1 and p53 immunoreactivity correlate with tumor invasion but not with malignant transformation. Elevated MIB indicates early recurrence and rapid regrowth

11.7.3 Clinical Management

- Symptoms vary with size, hormonal abnormalities, age and sex of the patient
- Two-thirds have hyperprolactinemia
- Nonfunctional tumors: headache and symptoms caused by optic chiasm compression
- Extension towards the cavernous sinus: palsies of CN III, IV, rarely V and VI
- May cause hypogonadism, secondary hypothyroidism, and adrenal insufficiency
- Medical therapy (prolactinoma), surgical resection or stereotactic radiosurgery and radiation therapy

11.7.4 Imaging Findings and Differential Diagnosis

- Sellar and parasellar location
- CT: sella is widened without calcifications. Larger lesions: erosion of the floor and inferior expansion towards sphenoid sinus or dorsal to clivus
- MRI: shape of “figure of eight” or “snowman” due to constriction by diaphragma sellae
- T1 isointense to the gray matter although small cysts or hemorrhages could be seen
- 20% absent posterior pituitary “bright spot” or displaced supradiaphragmatically in 80%
- T1WI bright spots in subacute hemorrhage. Fluid-fluid levels in apoplexy
- T2WI: isointense, less commonly heterogeneous mass with eccentric cyst or hemorrhage
- Compressed optic pathways may be seen with increased signal
- Blooming artifacts on gradient or SWI images in case of hemorrhage
- On post-contrast T1WI, diffuse slightly heterogeneous enhancement
- The intact pituitary is usually compressed against the sella
- Subtle dural thickening is detected in up to 10%
- Assessment of cavernous sinus invasion and displacement of internal carotid arteries

Differential diagnosis includes pituitary hyperplasia, meningioma of the sellar diaphragm, craniopharyngioma, aneurysm, metastasis, and hypophysitis.

Take-Home Messages

- Sellar or sellar/suprasellar mass with "snowman" configuration
- Isointense on T1WI and T2WI with contrast enhancement
- Increased T1 signal is suggestive of hemorrhage into, spontaneous or treatment-induced
- Assessment of optic chiasm, cavernous sinus and internal carotid arteries involvement is very important for clinical management

Further Reading

- Bonneville JF, et al. Magnetic resonance imaging of pituitary adenomas. Eur Radiol. 2005;15(3):543–8
- Osborne A, Pituitary adenoma. In Osborne A, editor. Osborne's brain Imaging, pathology, and anatomy. Salt Lake City: Amirsys; 2013. p. 699–706
- Smith A, Cha S. Sellar and juxtasellar tumors. In Naidich et al., editors. Imaging of the brain. Philadelphia: Elsevier, Saunders; 2013. p. 732–3

11.8 Pituitary Apoplexy

A 42-year-old male with history of acromegaly due to pituitary adenoma has been examined due to increased severity of headache and visual deficits.

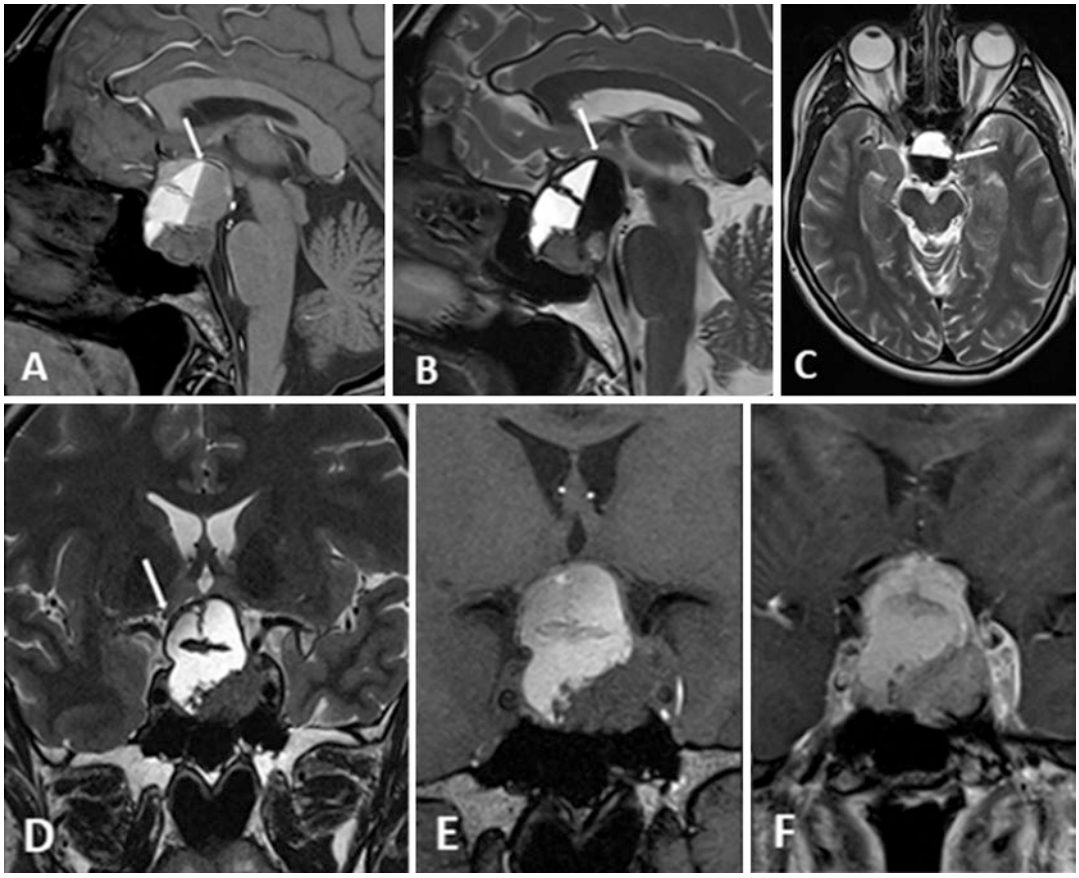

Fig. 11.8 Sagittal T1WI (**a**), T2WI (**b**), axial T2WI (**c**) demonstrate large sellar to parasellar mass with fluid debris level (arrow). The supernatant portion (free extracellular metHb) is hyperintense on T1W1 and T2WI and dependent portion is isointense on T1WI and hypointense on T2WI corresponding to a sediment of red blood remnants. Coronal T2WI (**d**), T1WI (**e**) and post-contrast T1WI (**f**) image shows displacement of the right optic tract (arrow on **d**) caused by suprasellar part of the tumor and encasement of internal carotid arteries. Nonhomogeneous enhancement is seen (**f**)

11.8.1 Epidemiology

- 1.9–26.5%, although many cases remain undiagnosed
- Male to female ratio of 2:1, mean age of onset of fifty seven years
- Subclinical hemorrhage (14–25%) is detected only on MRI

11.8.2 Pathology and Genetics

- Predisposing factors are hypertension, diabetes mellitus, administration of anticoagulants, bromocriptine, estrogens, and radiotherapy
- Can occur without any risk factor
- Histopathology: isolated infarction, hemorrhagic infarction, or hemorrhage alone

11.8.3 Clinical Management

- Severe and potentially fatal medical condition
- Frequently results in acute pituitary insufficiency
- Sudden onset headache, vomiting, visual impairment, coma, and panhypopituitarism
- First clinical manifestation in half of patients with undetected adenoma
- Sheehan syndrome: apoplexy within an intact pituitary during puerperium
- In some patients, recurrent hemorrhages
- Subclinical hemorrhage is a common finding in macroadenomas
- Conservatively or surgically with no significant difference in the frequency of recurrence

11.8.4 Imaging Findings and Differential Diagnosis

- Enlargement of the pituitary gland
- Radiological appearance depends on the duration of hemorrhage
- On CT acute hemorrhage is hyperdense, no or little contrast enhancement. Very rarely subarachnoid or ventricular hemorrhage
- With time, there is a gradual decrease of hyperdensity and ring enhancement
- Four days after the onset: hypodensity
- MRI evaluation of intra/suprasellar adenoma, possibility of estimating the onset
- After 12 h from onset, MRI is superior to CT in detection of bleeding
- Acute phase (0–7 days), T2 hypointense, T1 iso- or slightly hypointense
- Subacute phase (7–21 days), hyperintense on T1WI and T2WI
- Chronic phase (later than 21 days) a strong hypointensity on both T1WI and T2WI
- Fluid debris level within the mass (see images a, b, c) is suggestive of late subacute hemorrhage and is considered a specific sign of pituitary apoplexy. Another indicative finding is the reversible thickening of sphenoid sinus mucosa
- Gradient-echo (GE) T2∗-weighted images show bleeding products and hemosiderin deposits as strongly hypointense signal
- According to the recent UK guidelines for the management of pituitary apoplexy, an urgent MRI in case of clinical suspicion is recommended
- Follow-up MRI 3–6 months after onset and every year for five years to rule out adenoma growing and recurrent hemorrhage

Differential diagnosis includes posterior lobe of the pituitary gland, Rathke's cleft cyst, craniopharyngiomas, lipomas, dermoid cysts, aneurysms from the carotid siphon or Acom, metastatic melanomas, or any other hemorrhagic tumor.

Take-Home Messages

- Increased T1 signal is suggestive of pituitary apoplexy, but has to be differentiated from other conditions based on clinical and imaging findings
- Fluid debris level in the late subacute phase, hyperintense on T1WI and T2WI; in the subacute, chronic phase, strong hypointensity on T1WI and T2WI

Further Reading

- Boellis A, di Napoli A, Romano A, et al. Pituitary apoplexy: an update on clinical and imaging features. Review. Insights Imaging. 2014;5:753–62
- Bonneville JF, et al. Magnetic resonance imaging of pituitary adenomas. Eur Radiol. 2005;15(3):543–8
- Park M, Lee SK, Choi J, et al. Differentiation between cystic pituitary adenomas and Rathke cleft cysts: a diagnostic model using MRI. AJNR. 2015;36:1866–73

11.9 Craniopharyngioma

A 67-year-old male with long history of headache and recently noted visual deficits (bitemporal hemianopia).

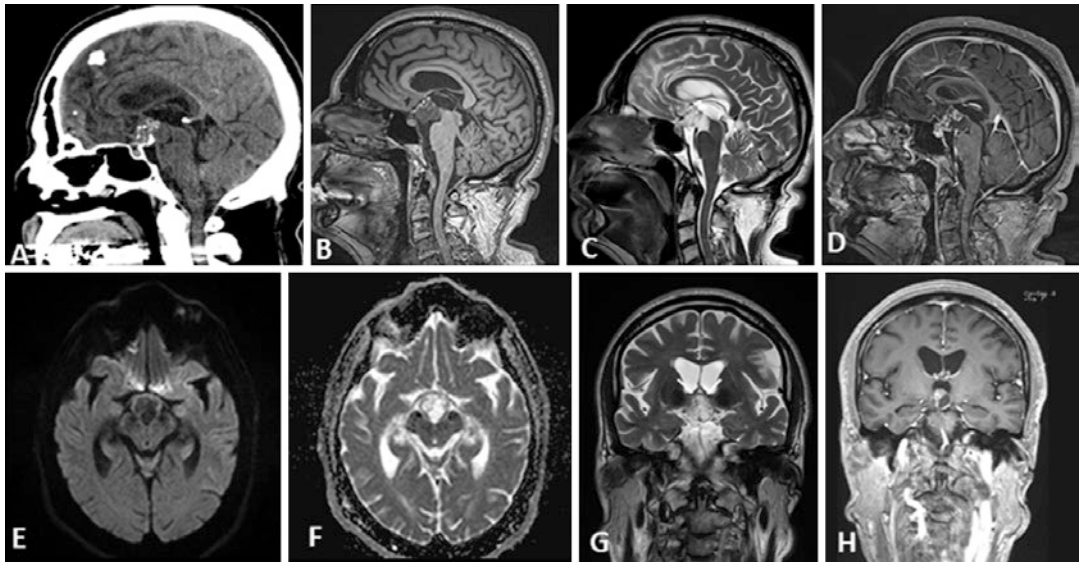

Fig. 11.9 Sagittal computed tomography (**a**) shows a suprasellar heterogeneous mass with calcifications. Sagittal T1WI (**b**) and T2WI (**c**) demonstrate suprasellar lesion with cystic and small solid components. Intact pituitary. Sagittal T1WI after Gadolinium (**d**) shows enhancement of the rim and solid components. DWI (**e**) and ADC (**f**) no evidence of restricted diffusion. Coronal T2W (**g**) elevated optic chiasm. Coronal T1WI post-contrast (**h**) dilation of the third ventricle up to 14 mm

11.9.1 Epidemiology

- 1–3% of intracranial tumors, the most common suprasellar tumor
- No gender predilection
- Bimodal age distribution, children (5–14 years), adults (65–74 years)
- More than 50% of craniopharyngiomas occur in children and young adults
- The most common nonglial intracranial tumors in the pediatric population

11.9.2 Pathology and Genetics

- 75% of craniopharyngiomas are suprasellar 20% are supra- and intrasellar
- WHO grade I, benign but locally aggressive, heterogeneous tumor
- Adamantinomatous: mixed solid and cystic areas (90%), calcifications in 90%, most common in children
- Squamous-papillary types: solid, rarely calcifies and is more common in adults

11.9.3 Clinical Management

- The location, size of the tumor, and age of the patient are important factors for the clinical symptoms
- Bitemporal hemianopia due to compression of the optic chiasm
- Endocrine dysfunctions, in particular growth hormone deficiency or hypothyroidism in children
- Hydrocephalus and morning headache in obstruction of foramina of Monro
- Management: gross total resection is curative, however, complications like hypothalamic injury or endocrine dysfunctions can occur
- When radical surgery is not possible, subtotal resection is followed by radiotherapy
- Another treatment is biopsy, cyst drainage and radiotherapy. ten-year survival: 64–96%. In tumors larger than 5 cm, the recurrence rate is 83%

11.9.4 Imaging Findings and Differential Diagnosis

- On CT, the adamantinomatus type is a suprasellar mass with calcifications in 90%, mixed solid and cystic areas in 90%, and contrast enhancement of the solid parts and capsule in 90%
- On T1WI, the cysts have different signal characteristics depending on their content. Hyperintensity reflects cholesterol, methemoglobin, or high protein content typical for adamantinomatous type
- Papillary type is T1 isointense solid tumor
- On T2WI, cysts are hyperintense while solid areas are iso/hyperintense. Hyperintensity in the surrounding brain parenchyma suggestive of gliosis, tumor infiltration or irritation as well as optic chiasm edema can be seen
- On FLAIR, cystic components are hyperintense; on DWI, the signal is varying
- Gradient echo images and susceptibility images (SWI) depict calcifications
- The solid parts and rim of the tumor enhance strongly after contrast administration
- On MR spectroscopy, a broad lipid spectrum can be demonstrated

Differential diagnosis includes Rathke's cleft cyst, pituitary adenoma, suprasellar arachnoid cyst, and chiasmatic astrocytoma

Take-Home Messages

- Craniopharyngioma is a WHO grade I tumor, predominantly suprasellar location with bimodal (children and adults) age distribution
- Heterogeneous appearance: solid, cystic components, calcifications. Strong enhancement of the solid components and the rim
- Unenhanced computed tomography can depict calcifications to assist diagnosis if MR images are doubtful

Further Reading

- Mollá E, et al. Craniopharyngiomas: identification of different semiological patterns with MR. Eur Radiol. 2002;12:1829–36
- Ruscalleda J. Parasellar lesions. Eur Radiol. 2005;15(3):549–59
- Shields R, et al. Magnetic resonance imaging of sellar and juxtasellar abnormalities in the paediatric population: an imaging review. Insights Imaging. 2015;6:241–60
- Smith A, Cha S, Sellar and juxtasellar tumors. In Naidich et al., editors. Imaging of the brain. Philadelphia: Elsevier, Saunders; 2013. p. 732–33

11.10 Vestibular Schwannoma

A 52-year-old female with a history of chronic left-sided sensorineural hearing loss and vertigo has been referred for MRI examination by the ENT specialist.

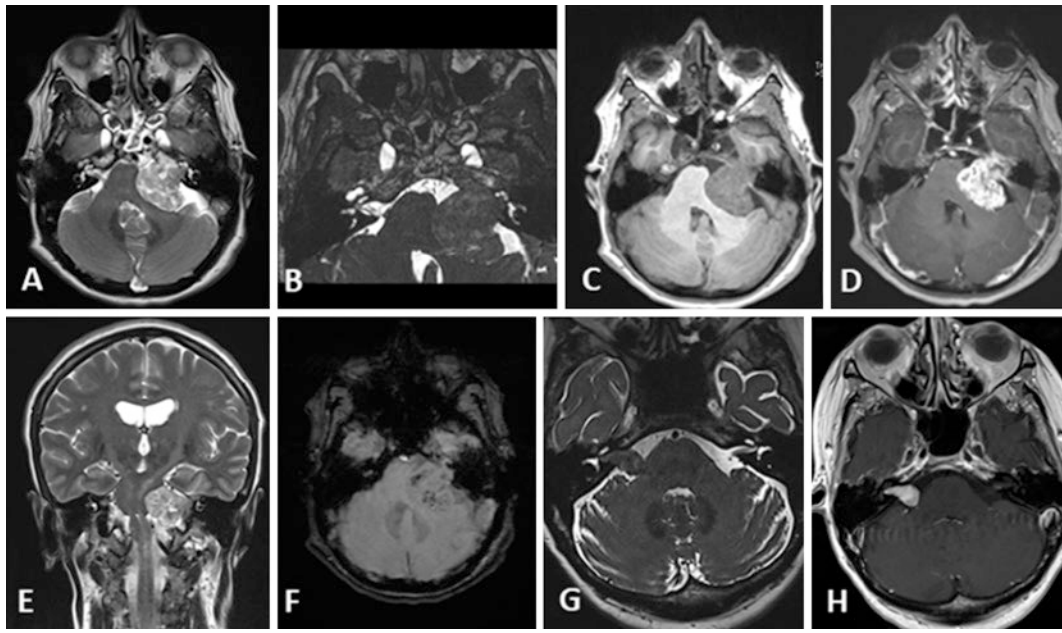

Fig. 11.10 Axial T2WI (**a**), 3D CISS (**b**), axial T1WI (**c**), contrast-enhanced T1WI (**d**) image demonstrates a large extra-axial mass in the left cerebellopontine angle. Widening of the internal acoustic canal (IAC), compression of the left middle cerebellar peduncle and pons, and fourth ventricle effacement. The tumor is heterogeneous on T2WI (**a**) with strong but heterogeneous enhancement (**d**). Coronal T2WI (**e**) shows brainstem compression and hyperintensity. SWI (**f**) reveals small hemorrhages within the lesion. Companion case: 68-year-old female, with right-sided hearing loss. 3D CISS (**g**) and contrast-enhanced T1WI (**h**) image show right intra-extrameatal tumor with homogeneous enhancement and widening of the IAC but intact brainstem

11.10.1 Epidemiology

- 10% of all intracranial neoplasms, the most common tumor of the cerebellopontine angle
- The second most common extra-axial tumors in adult patients, third to fifth decade
- All cranial nerves with exception of CN I and II have Schwann cell sheaths
- 90% from vestibular nerve, the majority of the rest from CN V or VII

11.10.2 Pathology and Genetics

- WHO grade I neoplasms
- Benign, slow-growing, well-delineated encapsulated lesion
- Typically arises within the internal auditory canal, centered at the porus acusticus
- Can be either purely intrameatal or intra-extrameatal, extends into the CP angle
- Associated hemorrhage and cysts are seen in 15–20%
- Vestibular schwannomas can be unilateral (sporadic 90%) or bilateral (NF2)

11.10.3 Clinical Management

- Chronic asymmetric sensorineural hearing loss in 90–95%, tinnitus or unsteadiness
- True vertigo, sudden hearing loss, facial pain, numbness, and weakness are uncommon
- Tumor may grow continuously or only to certain size and then stay stable or even shrink
- Enlargement can cause brainstem, cerebellar compression, and fourth ventricle effacement
- Microsurgical resection, stereotactic radiation, and conservative management

11.10.4 Imaging Findings and Differential Diagnosis

- Very difficult to be detected on NECT as extra-axial mass isodense or slightly hyperdense
- Enlargement of the internal acoustic canal, without calcifications. Strong homogeneous enhancement
- MRI: majority have both intra- and extracanalicular component, enlargement of the porus acusticus
- On T1WI, the lesion is iso- or mixed iso/hypointense, 15–20% cystic components
- Avid enhancement of the solid part or peripheral and heterogeneous enhancement
- T2WI for detection of surrounding edema. Tumor can be hyperintense or heterogeneous
- No restricted diffusion in the solid part. Increased signal on ADC
- Volumetric steady-state gradient-echo heavily T2WI (CISS or FIESTA) sequences have a high sensitivity

Differential diagnosis includes cerebellopontine angle meningiomas, leptomeningeal metastasis, lymphoma, meningeal melanocytoma, or malignant melanoma; facial nerve perineural spread, inflammatory processes as Bell palsy and neurosarcoidosis, aneurysms, and epidermoid cyst.

Take-Home Messages

- Unilateral enhancing mass, the most common tumor of the cerebellopontine angle
- Bilateral schwannomas are associated with NF2, always perform volumetric steady-state heavily T2WI and check bilaterally
- Cystic components and microhemorrhages can be seen

Further Reading

- Abele T, et al. Diagnostic accuracy of screening MR imaging using unenhanced axial CISS and coronal T2WI for detection of small internal auditory canal lesions. AJNR Am J Neuroradiol. 2014;35:2366–70
- Lin E, Crane B. The management and imaging of vestibular schwannomas. AJNR Am J Neuroradiol. 2017;38:2034–43
- Zou J, Hirvonen T. "Wait and scan" management of patients with vestibular schwannoma and the relevance of non-contrast MRI in the follow-up. J Otology. 2017;12(4):174–84

11.11 Chordoma

A 30-year-old male with a history of headache, diplopia, and bitemporal hemianopia. On previous CT, large intra-suprasellar mass and destruction of the clivus has been detected.

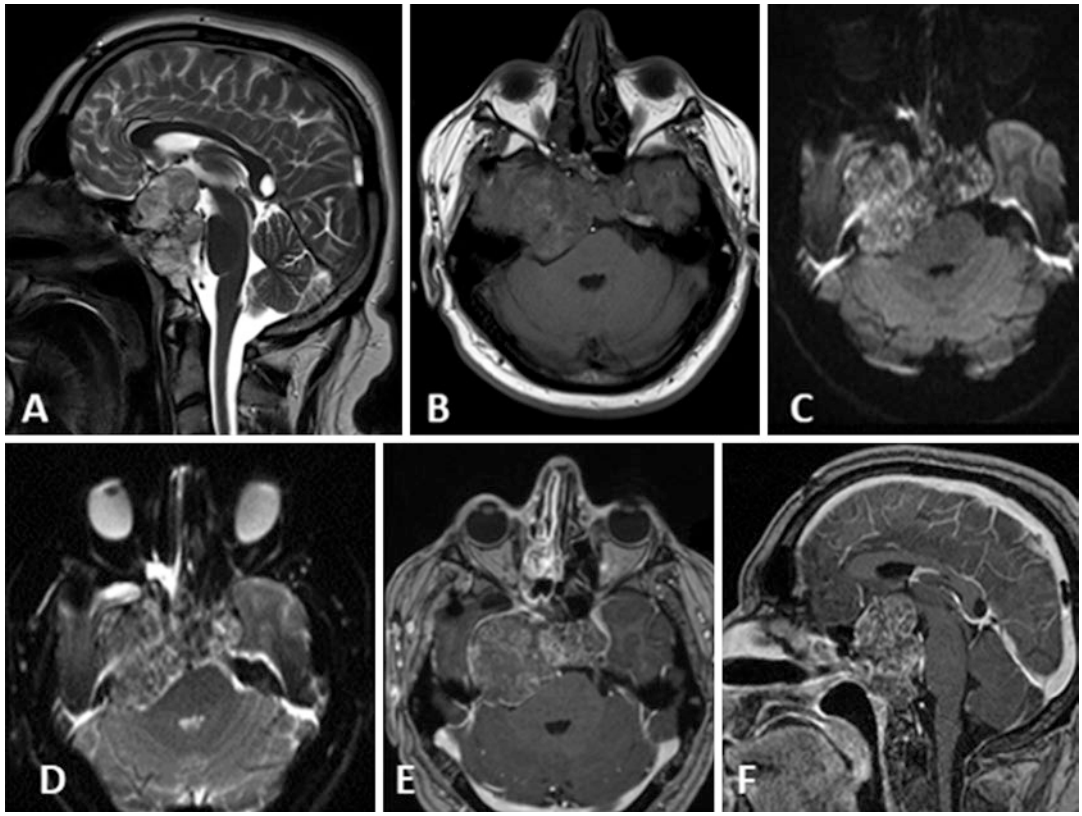

Fig. 11.11 Sagittal T2WI (**a**), axial T1WI (**b**), DWI (**c**), ADC (**d**), post-contrast T1WI axial (**e**) and sagittal (**f**) image demonstrates large mass destroying clivus that extends suprasellar, parasellar and towards right middle cranial fossa and right cerebellopontine angle. Right middle cerebellar peduncle and pons is compressed and fourth ventricle is effaced. On post-contrast images (**e**, **f**) honeycomb appearance is shown

11.11.1 Epidemiology

- Rare malignant tumor from embryonic notochord remnants in the craniospinal axis
- Second most common location is clivus (35%) after sacrococcygeal (50%)
- Most are found in fourth decade, rarely affects children and adolescents
- 2:1 male predominance

11.11.2 Pathology and Genetics

- Originate from the spheno-occipital synchondrosis along the clivus
- Midline, destructive, infiltrative slow-growing tumors, high risk of local recurrence
- At the time of diagnosis, they are large and have a poor prognosis
- Macroscopically: lobulated, heterogeneous tumor, necrotic areas, mucoid degeneration
- Hemorrhages, cartilage, calcifications, and sequestered bone fragments
- Incomplete pseudocapsule from surrounding tissue
- Three different histological variants: classical, chondroid, and dedifferentiated. The latter is an aggressive tumor more common in children

11.11.3 Clinical Management

- Symptoms occur mainly when cranial nerves are involved
- Depend on the location and extension from clivus to the sellar, parasellar, and retroclival
- Most common symptom is diplopia (CN VI palsy), occipital and retro-orbital headache
- Tinnitus, hearing loss, neck pain, facial pain, vertigo and gait disturbances
- Chordomas are invasive tumors, but they rarely metastasize
- Total removal is rarely possible as cavernous sinuses, basilar and carotid arteries are involved
- High local recurrence rates
- Radical or subtotal tumor removal, followed by radiation therapy or fractionated proton beam radiation therapy

11.11.4 Imaging Findings and Differential Diagnosis

- CT: Midline, well-delineated, heterogeneous mass, extensive osteolysis of clivus
- Hyperdense relative to the brainstem. Calcifications, sequestered fragments of clivus
- MRI for assessment of the tumor extent and relationship to the brainstem, cavernous sinuses, sellar region, optic chiasm, and other adjacent structures
- Characteristic is “thumb-printing” on the anterior brainstem, typically the pons
- On T1WI: low to intermediate signal, with hyperintense foci (mucus or hemorrhage)
- Normal clivus contains fat. Chordoma can be revealed on T1WI hyperintense background
- High T2 signal with areas of hypointensity, reflecting mucus, hemorrhage and calcifications. Gradient echo images and SWI detect hemorrhagic foci and calcification
- Moderate to marked contrast enhancement with honeycomb appearance
- Diffusion-weighted images show high signal intensity, due to the gelatinous structure
- Metastases within lungs, bone, skin and liver occur in 6–30% of all chordoma

Differential diagnosis icnludes chondrosarcoma and benign notochordal cell tumors

Take-Home Messages

- Soft-tissue masses with extensive osteolysis of the clivus. Involvement of the vital adjacent structures—basilar, carotid arteries, cavernous sinuses, sellar region, etc.
- CT for tumor detection, bone destruction, and dystrophic calcifications
- On T1WI, intermediate to low signal, very high T2 signal. Moderate to strong often heterogeneous enhancement

Further Reading

- Bourekas E, Slone W. Chordomas and other skull base tumors. In Newton H, Jolesz F, editors. Handbook of neuro-oncology neuroimaging. Academic Press, Elsevier; 2008 p. 460–8
- Erdem E, et al. Comprehensive review of intracranial chordoma. Radiographics. 2003;23(4):995–1009
- Santegoeds RGC, et al. State-of-the-art imaging in human chordoma of the skull base. Curr Radiol Rep. 2018;6:16. https://doi.org/10.1007/s40134-018-0275-7

11.12 Esthesioneuroblastoma (ENB)

A 46-year-old male with a history of anosmia, nasal obstruction, epistaxis, right proptosis, and headache.

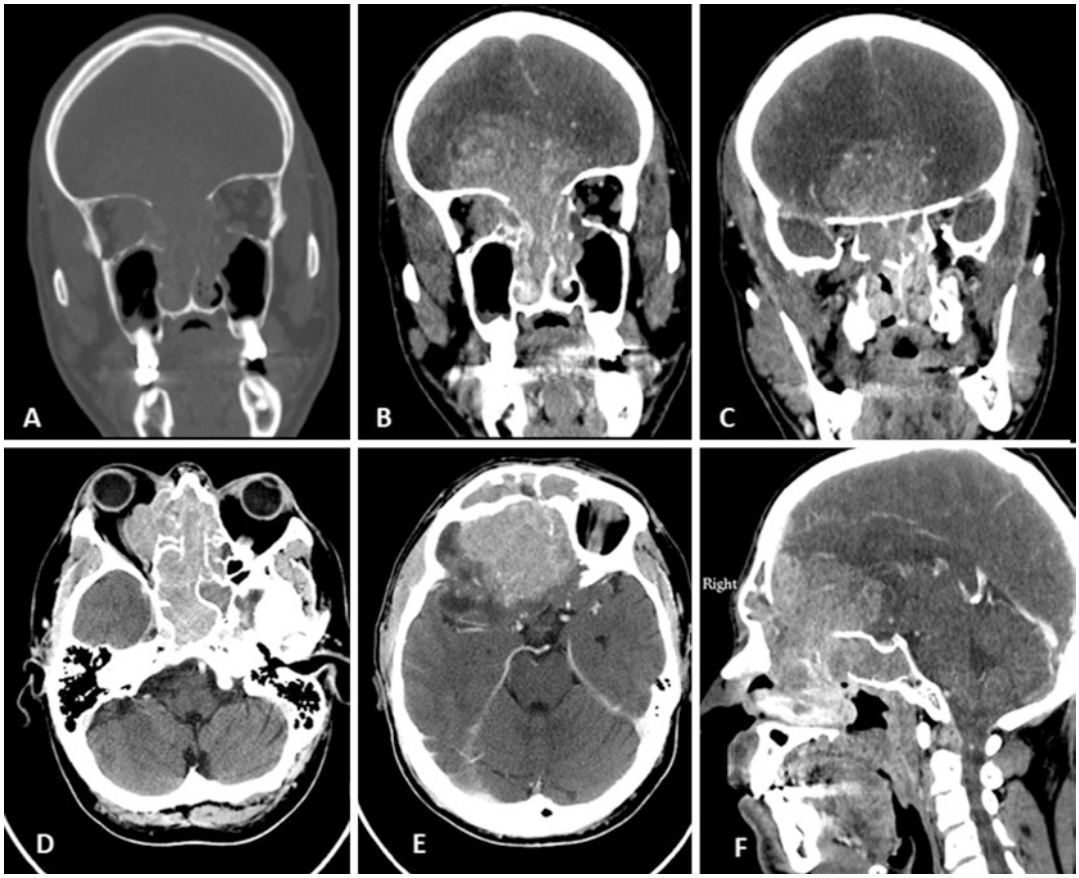

Fig. 11.12 Computed tomography, bone window (**a**), post-contrast coronal (**b**, **c**), axial (**d**, **e**) and sagittal (**f**) images. A large expansive soft tissue mass is shown with extensive bony destruction and involvement of nasal cavity bilateral, ethmoid cells, sphenoid sinus, frontal sinus, right orbit, and anterior cranial fossa. The mass shows strong enhancement

11.12.1 Epidemiology

- ENB or olfactory neuroblastoma is a rare malignant tumor
- 2–6% of all intranasal tumors, no gender predilection
- Bimodal age distribution, peak in second decade and at the fifth and sixth decade

11.12.2 Pathology and Genetics

- From the olfactory epithelium of the superior nasal cavity
- Classification for surgical staging is the Kadish system with A, B, and C groups
- Group **A**: tumor is confined to the nasal cavity; Group **B:** the tumor extends into the paranasal sinuses; Group **C:** cribriform plate, skull base, orbit, or intracranial cavity are involved
- On MRI, only few patients are classified as stage A at the time of diagnosis
- Histologic differentiation from other nasal cavity neoplasms is difficult

11.12.3 Clinical Management

- Varying biologic behavior: slow growth, diagnosed later, have a better prognosis
- With highly aggressive course metastasize earlier and have a very low survival rate
- Typically treated ENB are prone to multiple recurrences
- Metastasize within local lymph nodes, lungs, liver, and bones
- Most common symptoms are nasal obstruction and epistaxis. Anosmia can precede diagnosis by many years
- Symptoms related to tumor extension into the orbit (proptosis, visual field defects, pain), paranasal sinuses, anterior cranial fossa (headache), and inappropriate AD hormone secretion
- Combined treatment strategies, including surgery, radiation, and adjuvant chemotherapy

11.12.4 Imaging Findings and Differential Diagnosis

- CT: when a soft tissue dumbbell-shaped mass within the nasal vault is detected, the cribriform plate, fovea ethmoidalis, and lamina papyracea should be assessed
- Homogeneous mass or with scattered calcification, moderate homogeneous enhancement
- CT can be used for staging of local lymph nodes spreading
- MRI differentiates entrapped secretions from neoplasm and assessing the soft tissue extent especially within orbits, skull base, and intracranial
- Dural and parenchymal involvement can be also evaluated
- Hypointense on T1WI, intermediate to high T2 signal, some hemorrhages and necrosis
- Entrapped secretions are strongly T2 hyperintense
- On post-contrast images strong and homogeneous or slightly heterogeneous enhancement

Differential diagnosis includes sinonasal squamous cell carcinoma, non-Hodgkin's lymphoma, metastasis, malignant degeneration in inverted papilloma, sinonasal polyposis, Ewing sarcoma, and juvenile angiofibroma.

Take-Home Messages

- ENB: consider when CT or MRI detect soft tissue mass within the superior nasal cavity with bony destruction and local extension into orbits, paranasal sinuses or intracranial compartment
- CT and MRI are complementary imaging modalities for diagnosis, staging, and monitoring but definite diagnosis is based on histology
- Follow-up imaging is recommended due to the high recurrence rate

Further Reading

- Dublin A, Bobinski M. Imaging characteristics of olfactory neuroblastoma (Esthesioneuroblastoma). J Neurol Surg B. 2016;77:1–5
- Saad et al. MRI features of esthesioneuroblastoma. A descriptive analysis of 7 cases. ECR 2014. https://doi.org/10.1594/ecr2014/C-0369
- Taneja A, et al. Esthesioneuroblastoma. Arq Neuropsiquiatr 2009;67(3-A):704–6

Pediatric Brain Tumors

12

Korgun Koral

12.1 Medulloblastoma

9-month-old female.

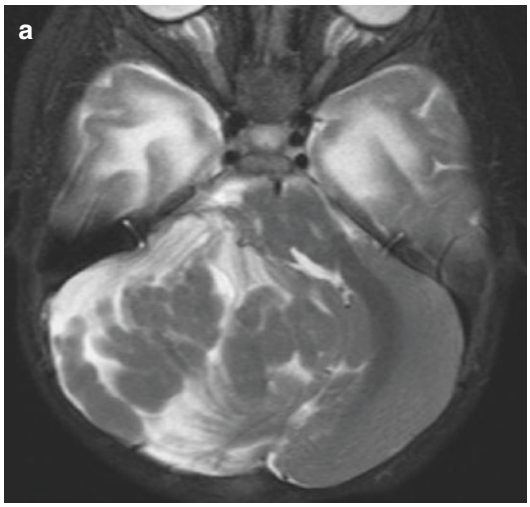

Fig. 12.1a Axial T2-weighted image demonstrates a mass involving the right cerebellar hemisphere and resulting compression of the fourth ventricle. The lesion has apparent nodularity and is relatively isointense to the normal left cerebellar hemisphere. There is marked vasogenic edema about the lesion

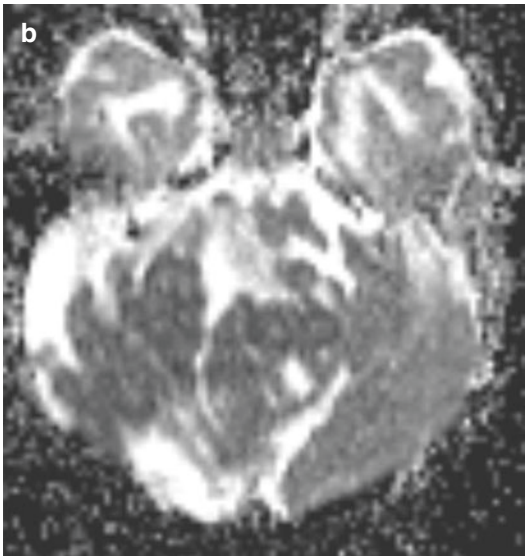

Fig. 12.1b Apparent diffusion coefficient (ADC) map shows that the tumor shows decreased signal compared with the normal left cerebellar hemisphere, indicating diffusion restriction. Vasogenic edema about the tumor appears hyperintense

K. Koral (✉)
Department of Radiology/Division of Pediatric Neuroradiology, Cohen Children's Medical Center of New York, Donald and Barbara Zucker School of Medicine at Hofstra University/Northwell Health, Queens, NY, USA
e-mail: kkoral@northwell.edu

Y. Özsunar, U. Şenol (eds.), *Atlas of Clinical Cases on Brain Tumor Imaging*,
https://doi.org/10.1007/978-3-030-23273-3_12

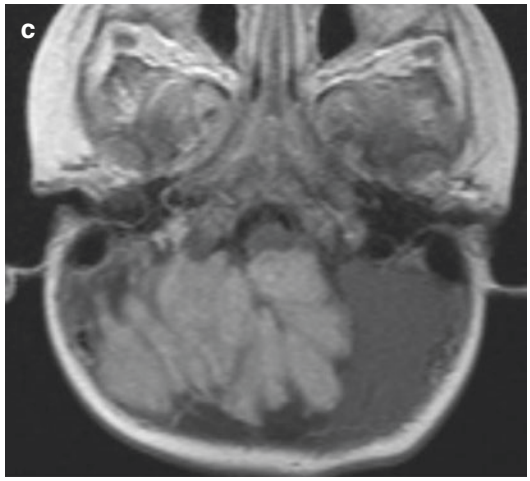

Fig. 12.1c Gadolinium enhanced axial and coronal T1-weighted images show intense enhancement and nodularity of the tumor

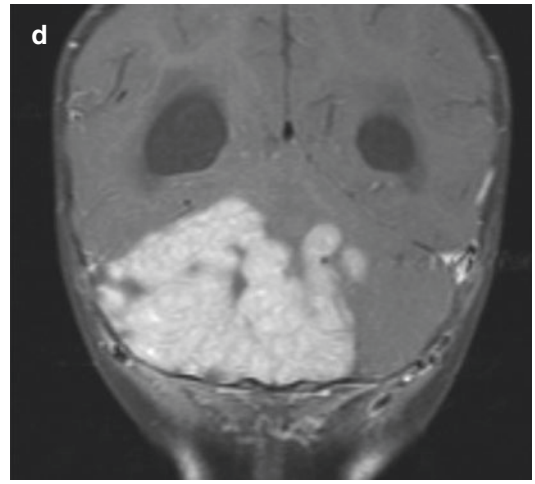

Fig. 12.1d Gadolinium enhanced axial and coronal T1-weighted images show intense enhancement and nodularity of the tumor

20-month-old patient.

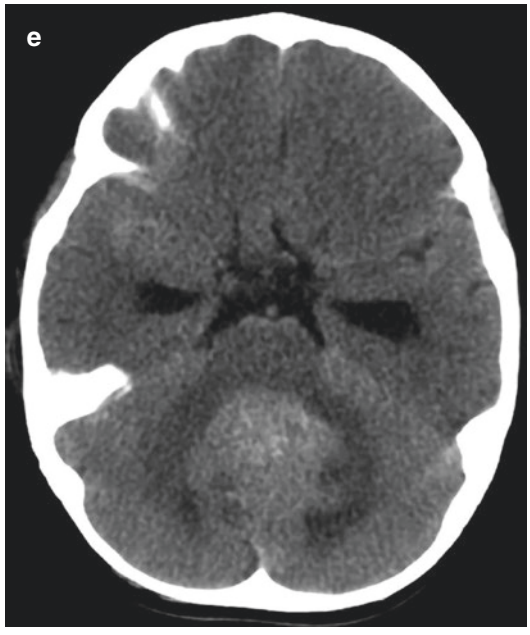

Fig. 12.1e Axial noncontrast CT shows a hyperdense mass at midline. There is obstructive hydrocephalus

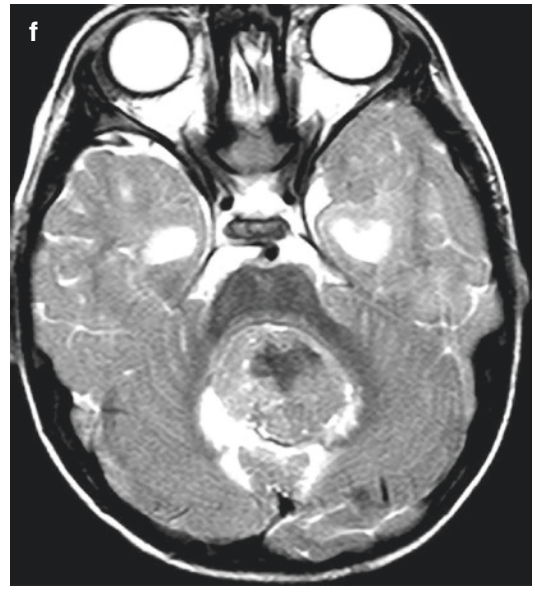

Fig. 12.1f Axial T2-weighted image shows that the solid components are isointense to normal brain

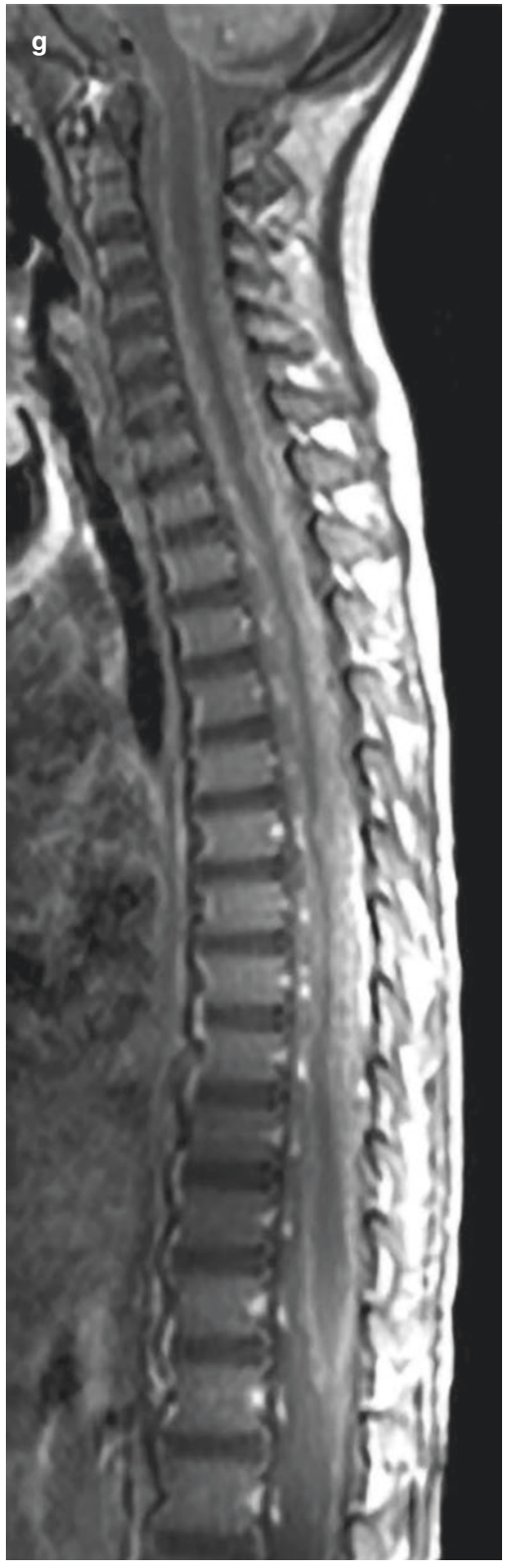

Fig. 12.1g Gadolinium enhanced sagittal T1-weighted image shows extensive drop metastasis coating the spinal cord

Epidemiology
- Most common embryonal CNS tumor
- Approximately 30% of all pediatric posterior fossa tumors
- 250–350 new cases in the United States annually
- Eighty percent of medulloblastomas diagnosed before fifteen years of age
- Median age at diagnosis 5–7 years

Pathology and Genetics
- Molecular subgroups were introduced in the latest WHO classification
- Histopathology-based classification is still performed
- Wnt and SHH groups are clearly defined, Group 3 and Group 4 less clearly defined
- Wnt group tumors tend to be off midline and better prognosis
- Medulloblastoma is a highly cellular neoplasm
- WHO grade IV

Clinical Management
- Usually present with hydrocephalus
- MRI of the spine should be performed prior to tumor resection
- Goal of surgery is to achieve gross total resection. Chemotherapy is always employed. Utilization of radiation therapy depends on molecular subgroup, histopathology, residual tumor, age of the patient, and metastases

Imaging Findings
- In general midline lesion
- Hyperdense on CT
- Isointense to gray matter on T2-weighted images
- Solid components show diffusion restriction
- Cysts and hemorrhage variable
- Enhancement generally present and intense
- Brainstem involvement in one-third of patients

Take-Home Messages
- Posterior fossa mass with diffusion restriction is likely to be medulloblastoma

- Atypical teratoid rhabdoid tumor is in differential diagnosis in younger children (<3 years)
- Preoperative spine MRI should be performed when a cerebellar mass is diagnosed

Further Reading

- Schwalbe EC, Lindsey JC, Nakjang S, Crosier S, Smith AJ, Hicks D, et al. Novel molecular subgroups for clinical classification and outcome prediction in childhood medulloblastoma: a cohort study. Lancet Oncol. 2017;18(7):958–71
- Eran A, Ozturk A, Aygun N, Izbudak I. Medulloblastoma: atypical CT and MRI findings in children. Pediatr Radiol. 2010;40(7):1254–62
- Koral K, Gargan L, Bowers DC, Gimi B, Timmons CF, Weprin B, et al. Imaging characteristics of atypical teratoid-rhabdoid tumor in children compared with medulloblastoma. AJR Am J Roentgenol. 2008;190(3):809–14

12.2 Pilocytic Astrocytoma (Cerebellar)

3-year-old. Headache.

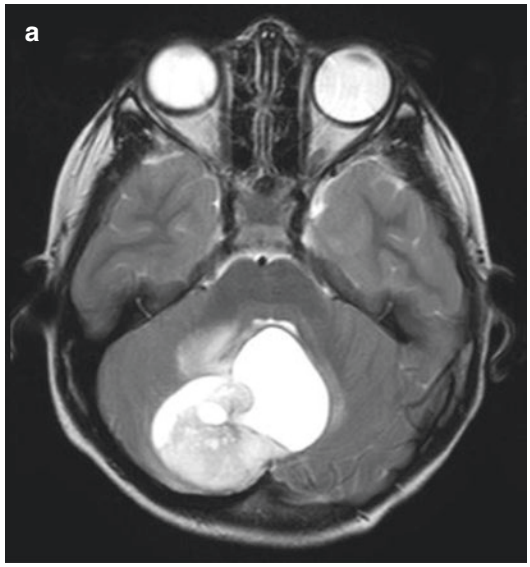

Fig. 12.2a Axial T2-weighted image show a partially cystic cerebellar lesion. The cystic component results in compression of the fourth ventricle. The solid component of the tumor is very hyperintense compared to normal cerebellum

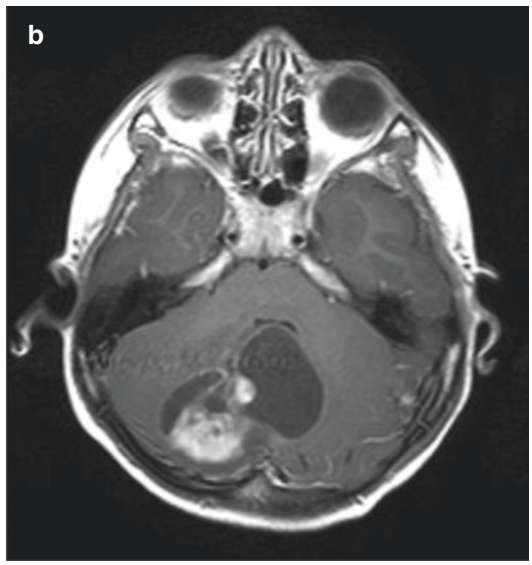

Fig. 12.2b Gadolinium enhanced axial T1-weighted image shows enhancement of the solid components of the tumor

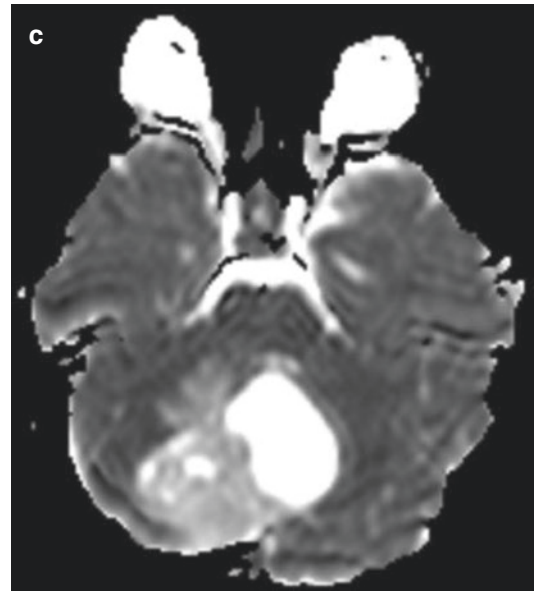

Fig. 12.2c ADC map shows that solid component of the tumor is hyperintense indicating increased diffusivity

Epidemiology

- Cerebellar pilocytic astrocytoma is the most common pediatric brain tumor comprising approximately 15% of all pediatric brain tumors
- Optic-hypothalamic region, cerebral hemispheres, brainstem, and spinal cord are other locations for pilocytic astrocytoma. Optic-hypothalamic astrocytomas are associated with neurofibromatosis type I
- The mean age at presentation for cerebellar pilocytic astrocytoma is seven years

Pathology

- WHO grade I
- Low cellularity compared with embryonal tumors
- Rosenthal fibers are characteristic on hematoxylin & eosin stain

Associations

- Unlike optic-hypothalamic pilocytic astrocytomas, there is no association between the cerebellar pilocytic astrocytomas and neurofibromatosis

Clinical Management

- Presentation is less acute than medulloblastoma
- Treatment is surgical resection. One-third of the lesions may have brainstem invasion
- Cystic components may be decompressed and not necessarily resected

Imaging Findings

- Approximately half of the tumors have large cystic components
- Solid components hypodense on CT and very hyperintense on T2-weighted images
- Solid components show intense enhancement
- Solid components always show increased diffusivity on ADC maps due to low cellularity
- Spinal drop metastases are very rare for cerebellar pilocytic astrocytomas

Take-Home Message

- Cerebellar tumor whose solid component demonstrating increased diffusivity on ADC map is very likely to be pilocytic astrocytoma

Further Reading

- Koeller KK, Rushing EJ. From the archives of the AFIP: pilocytic astrocytoma: radiologic-pathologic correlation. Radiographics. 2004;24(6):1693–708
- D'Arco F, Khan F, Mankad K, Ganau M, Caro-Dominguez P, Bisdas S. Differential diagnosis of posterior fossa tumours in children: new insights. Pediatr Radiol.2018;48(13):1955–63

12.3 Ependymoma

4-year-old with headache.

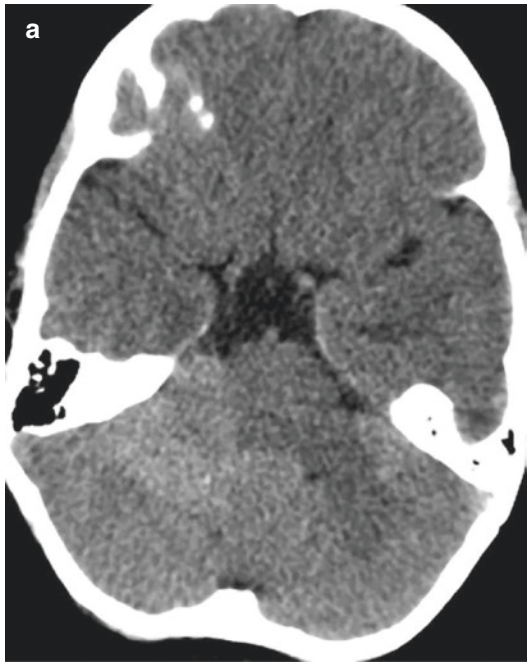

Fig. 12.3a Axial noncontrast CT shows a relatively hyperdense mass of the right cerebellar hemisphere and cerebellopontine angle cistern

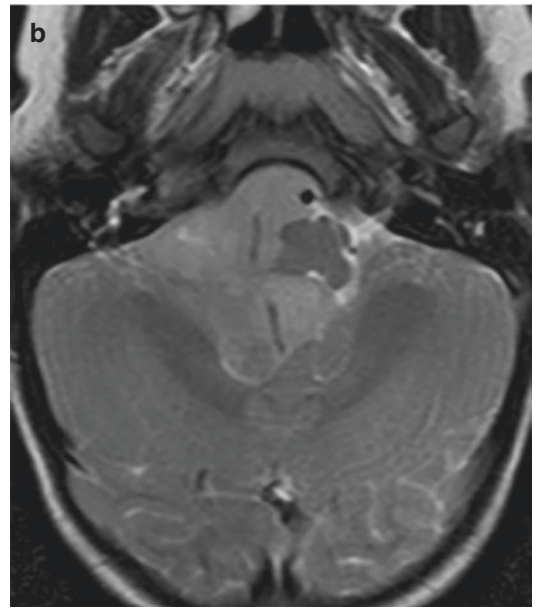

Fig. 12.3b Axial T2-weighted image shows a mass involving the cerebellopontine angle cistern and fourth ventricle, traversing the right foramen of Luschka. There is extension of the tumor to the premedullary cistern. The basilar artery is encased by the lesion

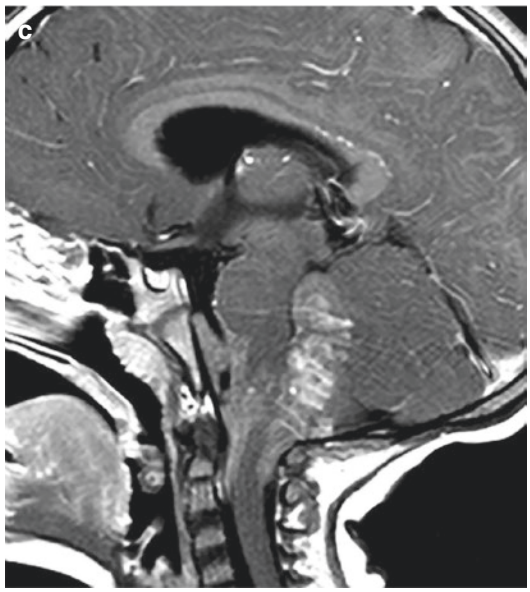

Fig. 12.3c Gadolinium enhanced T1-weighted images shows extension of the tumor into the cervical spinal canal through the foramen of magnum. There is enhancement of the lesion

Epidemiology

- Third most common pediatric cerebellar tumor following pilocytic astrocytoma and medulloblastoma
- Mean age at diagnosis is 4–6 years, one-third diagnosed before three years of age

Pathology

- Two-thirds of ependymomas are infratentorial
- Classic (WHO grade II) and anaplastic (WHO grade III) are still used, however, of questionable utility
- Ependymoma, *RELA fusion-positive* has been introduced in the WHO 2016 classification. The majority of the supratentorial ependymomas are *RELA fusion-positive*

Clinical Management

- Surgery is the mainstay of therapy with gross total resection being its goal. However, for tumors encasing the brainstem and vessels gross resection may not be possible
- Achievement of gross total resection significantly improves the outcome
- Radiation therapy is commonly used
- In younger children (younger than three years) chemotherapy may be employed

Imaging Findings

- Involvement of the surfaces of the cerebellum and brainstem is characteristic
- Extension through the foramen of Luschka into the cerebellopontine angle cistern and extension through the foramen of Magendie into the cervical spinal canal
- Calcifications, cyst, and hemorrhage can be seen, but not necessarily helpful in distinguishing ependymoma from other cerebellar tumors
- On diffusion weighted imaging, the solid components of cerebellar ependymomas show ADC values between those of medulloblastomas and pilocytic astrocytomas
- Spinal drop metastases can be seen

Further Reading

- D'Arco F, Khan F, Mankad K, Ganau M, Caro-Dominguez P, Bisdas S. Differential diagnosis of posterior fossa tumours in children: new insights. Pediatr Radiol. 2018;48(13):1955–63
- Louis DN, Perry A, Reifenberger G, von Deimling A, Figarella-Branger D, Cavenee WK, et al. The 2016 World Health Organization Classification of Tumors of the Central Nervous System: a summary. Acta Neuropathol. 2016;131(6):803–20
- Koral K, Mathis D, Gimi B, Gargan L, Weprin B, Bowers DC, et al. Common pediatric cerebellar tumors: correlation between cell densities and apparent diffusion coefficient metrics. Radiology. 2013;268(2):532–7

12.4 Atypical Teratoid Rhabdoid Tumor (ATRT)

21-month-old with imbalance.

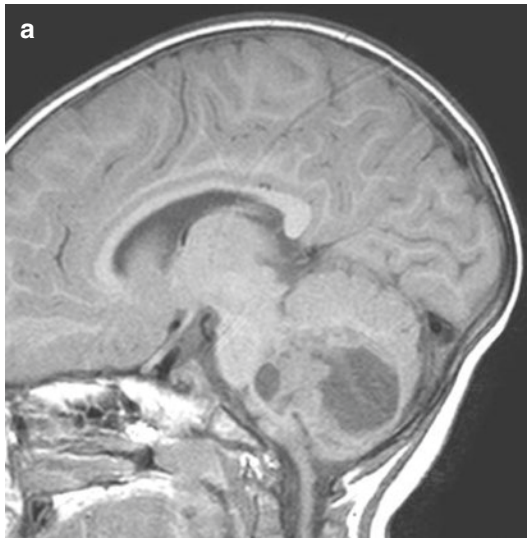

Fig. 12.4a Axial T1-weighted image shows a heterogenous, partially cystic mass of the cerebellum

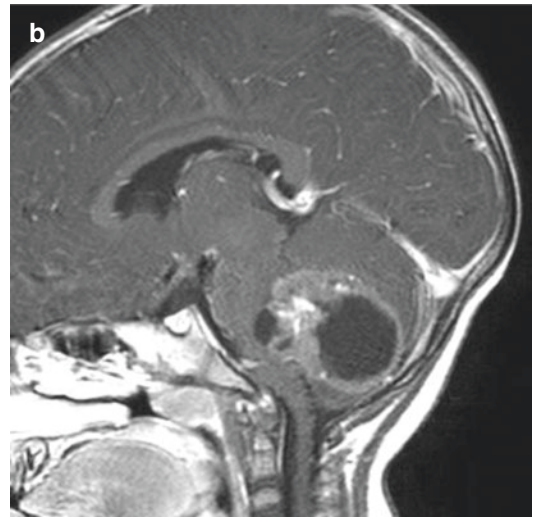

Fig. 12.4b The solid components show variable enhancement following administration of intravenous Gadolinium

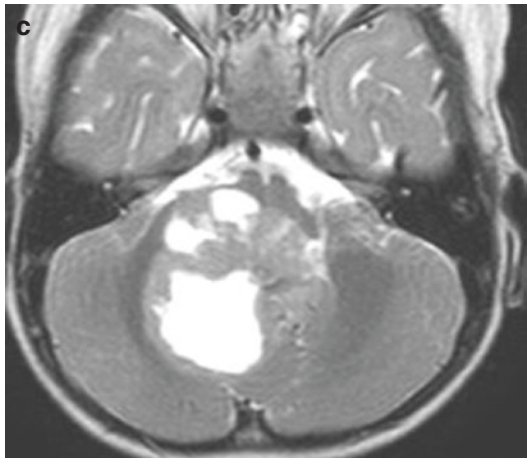

Fig. 12.4c The solid components of the tumor are relatively isointense to normal brain on T2-weighted images

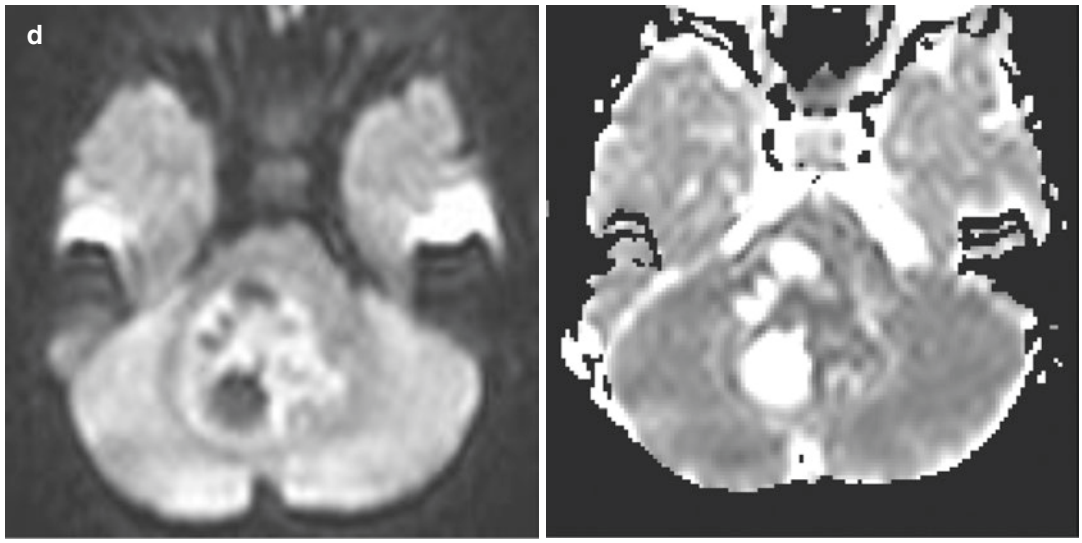

Fig. 12.4d Axial diffusion weighted image and axial apparent diffusion coefficient image show diffusion restriction within the solid tumor

Epidemiology
- Rare embryonal tumor encountered in children generally younger <3 years
- Incidence estimated to be 0.1–0.5/million children per year

Pathology & Genetics
- Highly malignant, hypercellular neoplasm
- Greater likelihood of disseminated disease at the time of diagnosis compared with medulloblastoma
- *INI-1* is pathognomonic for diagnosis of ATRT and not present in medulloblastoma

Associations
- Synchronous rhabdoid tumor of the kidney can be present, screening of the abdomen needs to be performed

Clinical Management
- Gross total resection is attempted depending on the site of the involvement
- Intense chemotherapy is used (more intense than medulloblastoma)
- Radiation therapy is problematic due to the patients age, however, is employed

Imaging Findings
- Similar to medulloblastoma
- Extracerebellar locations for primary ATRT include cerebral hemispheres, pineal region, cranial nerves (third and fifth), and orbit
- Solid components show relative T2 hypointensity and diffusion restriction
- Solid components enhance to variable degrees
- The likelihood of cerebellopontine angle cistern is greater than medulloblastoma
- Spine screening is performed for drop metastasis at the time of diagnosis and follow-up

Take-Home Message
- Differential diagnosis of an off-midline lesion in the posterior fossa with diffusion restriction in a young child (<3 years) should include ATRT

Further Reading

- Koral K, Mathis D, Gimi B, Gargan L, Weprin B, Bowers DC, et al. Common pediatric cerebellar tumors: correlation between cell densities and apparent diffusion coefficient metrics. Radiology. 2013;268(2):532–7
- Oh CC, Orr BA, Bernardi B, Garre ML, Rossi A, Figa-Talamanca L, et al. Atypical teratoid/rhabdoid tumor (ATRT) arising from the 3rd cranial nerve in infants: a clinical-radiological entity? J Neurooncol. 2015;124(2):175–83

12.5 Diffuse Midline Glioma

4-year-old with headache.

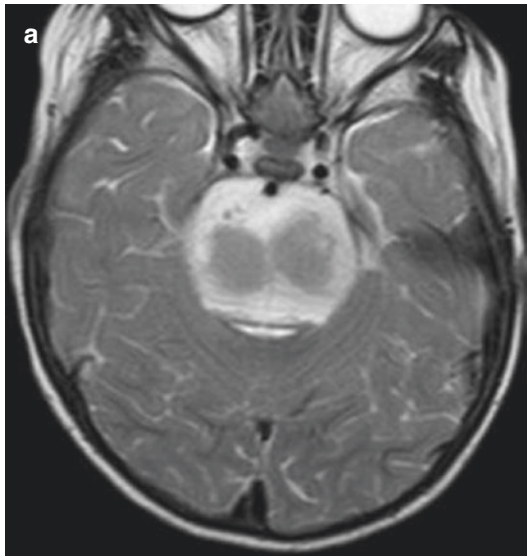

Fig. 12.5a Axial T2-weighed image shows an expansile, hyperintense mass expanding the pons

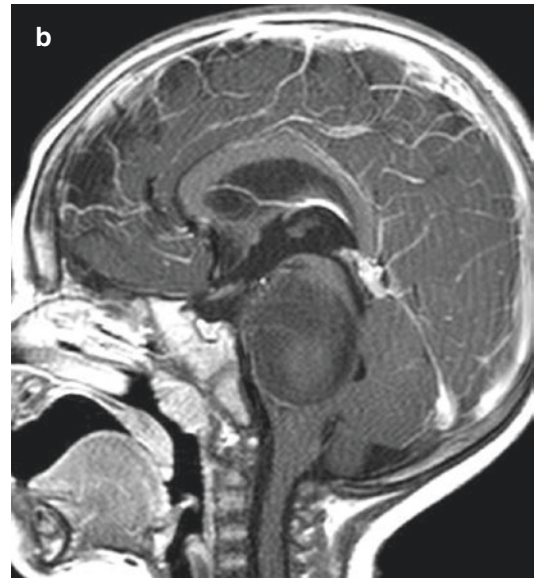

Fig. 12.5b Gadolinium enhanced T1-weighted sagittal image shows that there is no appreciable enhancement within the lesion. Biopsy showed characteristic *H3-K27M* mutation

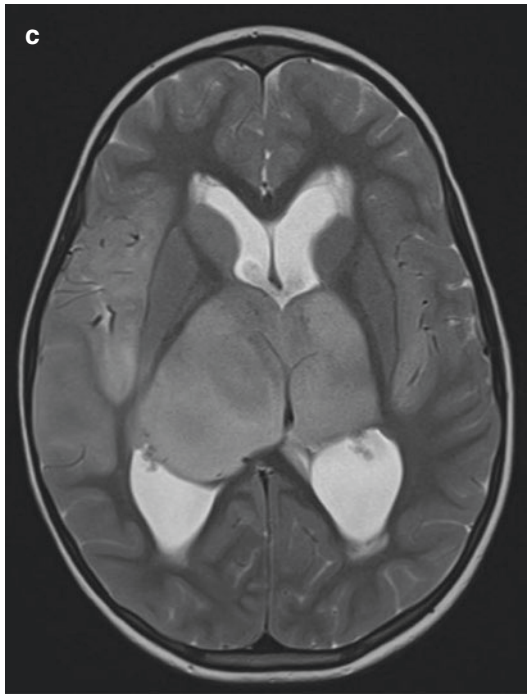

Fig. 12.5c Axial T2-weighted image shows expansile mass involving the bilateral thalami. There is abnormal increased T2 signal of the right parietal lobe and bilateral insulae

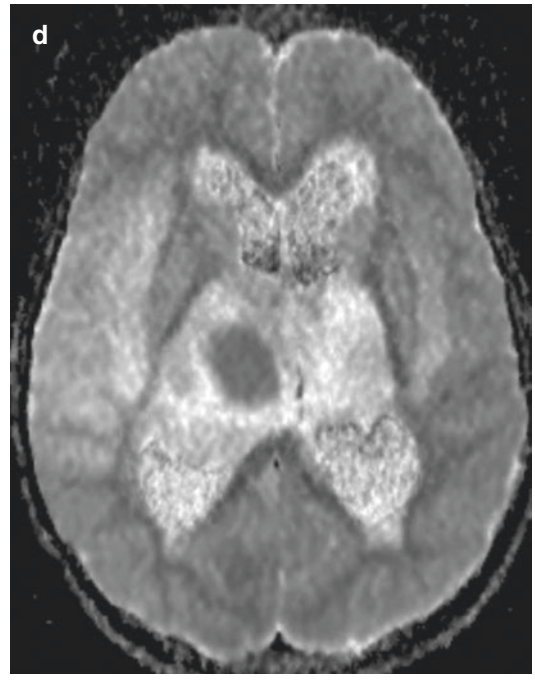

Fig. 12.5d ADC map shows diffusion restriction within the tumor involving the anterior aspect of the right thalamus

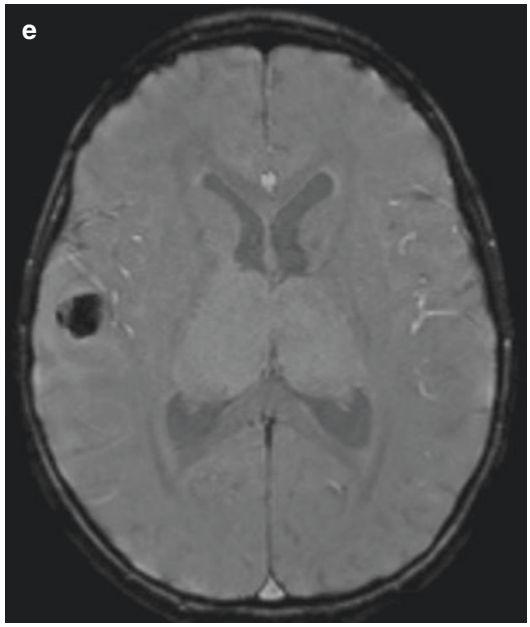

Fig. 12.5e Axial susceptibility weighted image shows a hemorrhagic focus involving the right superior temporal lobe. Biopsy was performed at this site which demonstrated the *H3-K27 M* mutation characteristic for diffuse midline glioma

Epidemiology
- Rare tumors of childhood

Pathology and Genetics
- Formerly known as diffuse intrinsic pontine glioma (DIPG)
- In the 2016 edition of WHO Classification diffuse midline glioma was chosen as a more accurate and inclusive term
- Histone H3K27M mutation is characteristic
- Grade IV neoplasm with unfavorable outcome

Clinical Management
- Biopsy is becoming more commonplace for pontine lesions
- If supratentorial involvement is present, biopsy may be performed at less dangerous sites
- Radiation therapy is universally used with limited utility of chemotherapy
- Dismal outcome despite therapy

Imaging Findings
- Expansile T1-weighted hypointense and T2-weighted hyperintense pontine lesion
- Compression of fourth ventricle and cerebral aqueduct, hydrocephalus common
- Enhancement and intralesional hemorrhage variable
- Occasional involvement of the supratentorial midline structures (i.e., thalami) and cerebral hemispheres
- Spinal drop metastases are unlikely

Take-Home Message
- Diffuse intrinsic pontine glioma is now an obsolete term

Further Reading

- D'Arco F, Khan F, Mankad K, Ganau M, Caro-Dominguez P, Bisdas S. Differential diagnosis of posterior fossa tumours in children: new insights. Pediatr Radiol. 2018;48(13):1955–63
- Louis DN, Perry A, Reifenberger G, von Deimling A, Figarella-Branger D, Cavenee WK, et al. The 2016 World Health Organization Classification of Tumors of the Central Nervous System: a summary. Acta Neuropathol. 2016;131(6):803–20

12.6 Suprasellar Germ Cell Tumor

2-year-old presenting with diabetes insipidus.

Companion case: 3-year-old with diabetes insipidus.

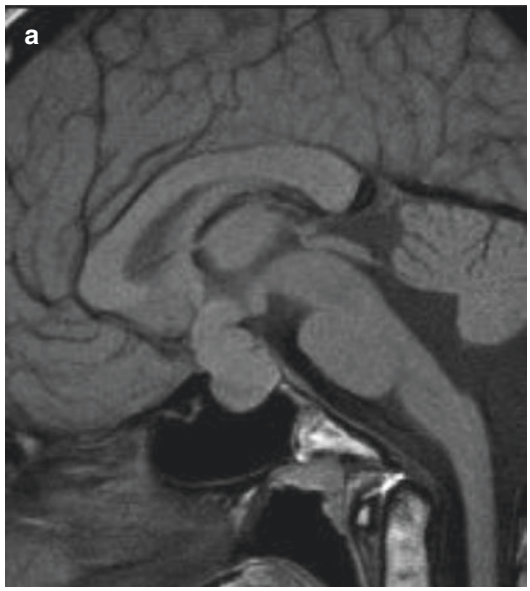

Fig. 12.6a Sagittal T1-weighted images demonstrate a sellar and suprasellar lesion. There is nonvisualization of the T1 shortening of the neurohypophysis in the posterior sella

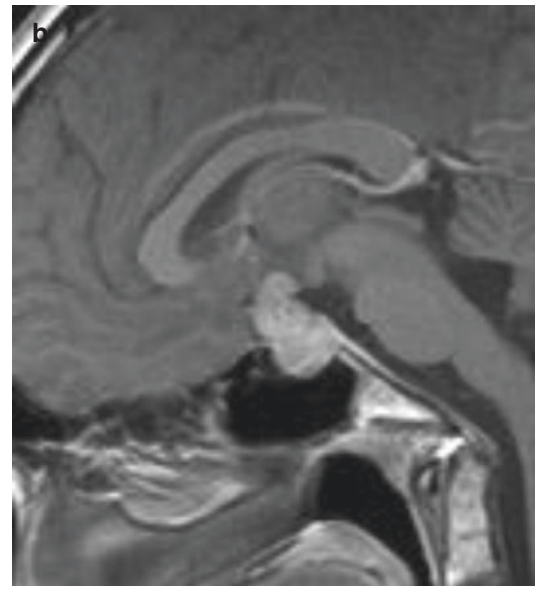

Fig. 12.6b Sagittal gadolinium enhanced T1-weighted image shows intense enhancement of the lesion

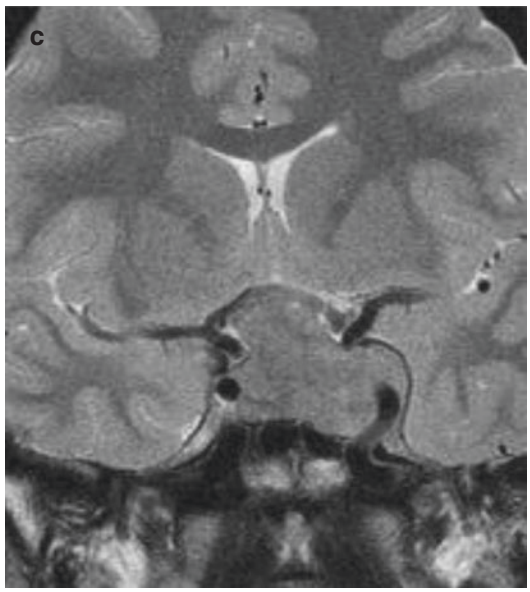

Fig. 12.6c Coronal T2-weighted image shows that the lesion is relatively isointense to normal brain, indicating hypercellularity. The mass involves the left cavernous sinus, circumscribing the normal signal void of the cavernous segment of the left internal carotid artery

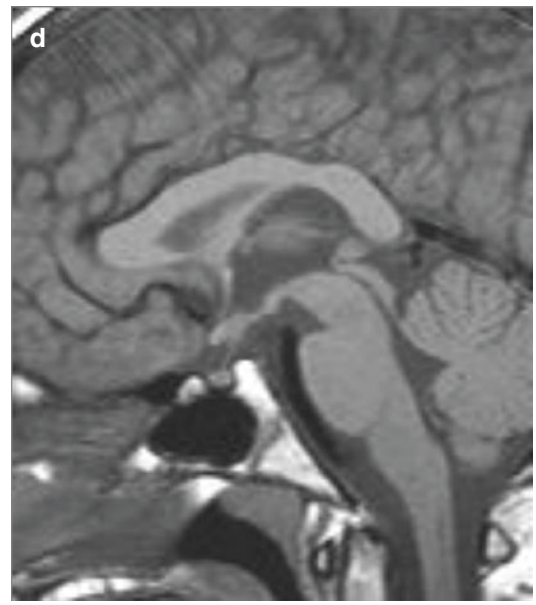

Fig. 12.6d Sagittal T1-weighted image demonstrates nonvisualization of the T1-shortening of the neurohypophysis

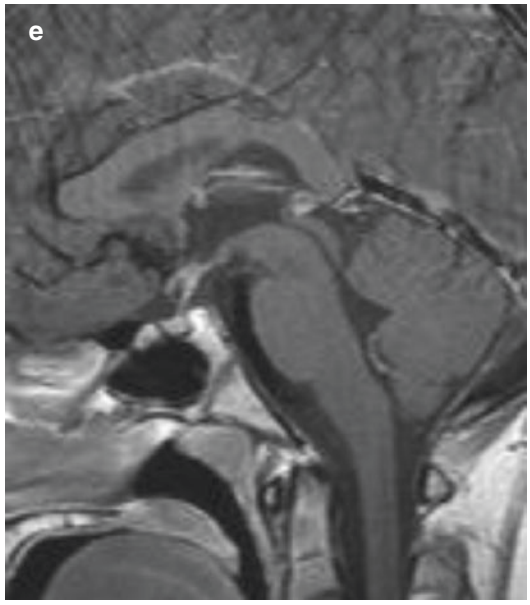

Fig. 12.6e Gadolinium-enhanced sagittal T1-weighted image shows mild thickening of the pituitary stalk without discreet mass

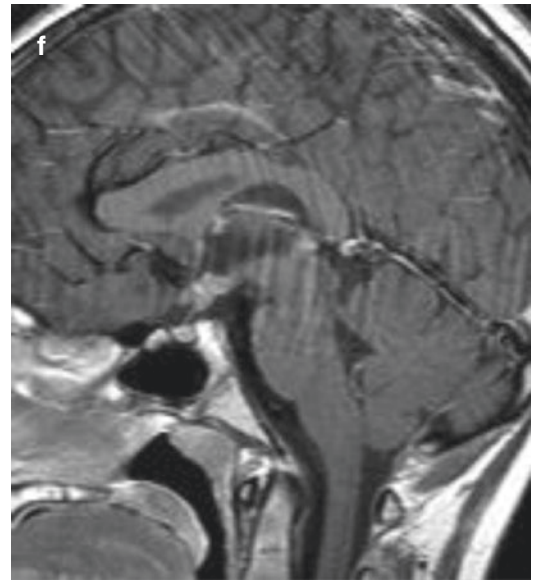

Fig. 12.6f Follow-up examination 5 months later demonstrates a nodular mass involving the floor of the third ventricle

Epidemiology
- 3–5% of pediatric intracranial tumors
- Peak incidence at 10–12 years of age

Pathology
- Germinomas arise from germ cells and typically occur at midline
- Hypercellular tumors
- Synchronous involvement of the pineal region in approximately 15%

Clinical Management
- If no mass is seen in child with diabetes insipidus and nonvisualization of the T1 shortening of the neurohypophysis repeat imaging should be performed in 3–6 months
- Alpha fetoprotein and beta-hCG may be elevated in certain germ cells tumors
- Highly sensitive to radiation therapy and chemotherapy

Imaging Findings
- Hyperdense on CT
- Nonvisualization of the T1 shortening of the neurohypophysis
- Occasional cavernous sinus involvement
- Primary differential consideration for suprasellar germinoma is Langerhans cell histiocytosis. Imaging can be identical in the absence of remote intracranial involvement or local tumor extension (e.g., pineal region or cavernous sinus involvement) which can be seen in germinoma. Involvement of the calvarium or mandible is seen in Langerhans cell histiocytosis

Take-Home Messages

- Nonvisualization of the T1 shortening of the neurohypophysis is always abnormal, its cause should be ascertained
- In a child with central diabetes insipidus and nonvisualization of the T1 shortening of the neurohypophysis, if no discreet mass is identified repeat imaging should be performed in 3–6 months

Further Reading

- Douglas-Akinwande AC, Mourad AA, Pradhan K, Hattab EM. Primary intracranial germinoma presenting as a central skull base lesion. AJNR Am J Neuroradiol. 2006;27(2):270–3
- Glastonbury CM, Osborn AG, Salzman KL. Masses and malformations of the third ventricle: normal anatomic relationships and differential diagnoses. Radiographics. 2011;31(7):1889–905

12.7 Langerhans Cell Histiocytosis (Sellar/ Suprasellar)

6-year-old with diabetes insipidus.

Companion case: 3-year-old with diabetes insipidus.

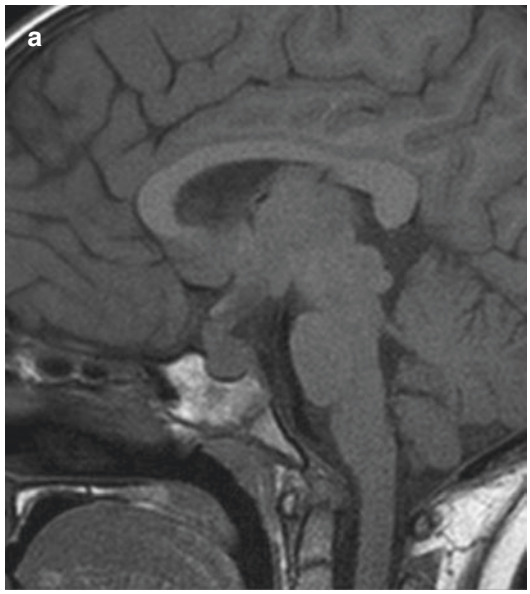

Fig. 12.7a Sagittal T1-weighted image shows nonvisualization of the T1 shortening of the neurohypophysis and thickening of the pituitary stalk

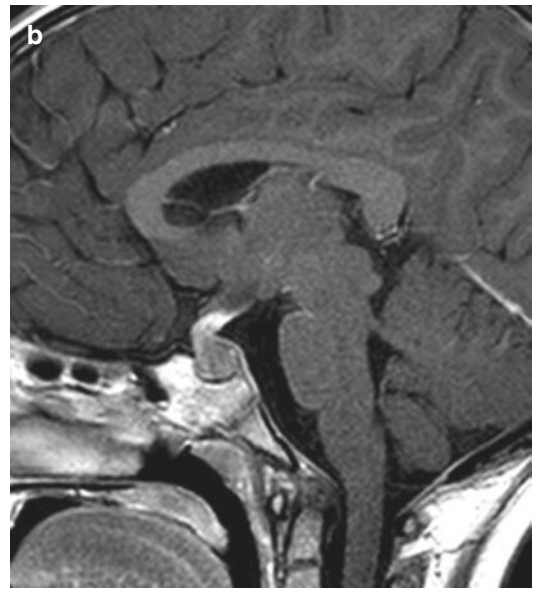

Fig. 12.7b Gadolinium enhanced sagittal T1-weighted image shows enhancement of the thickened stalk and enlargement of the pituitary gland

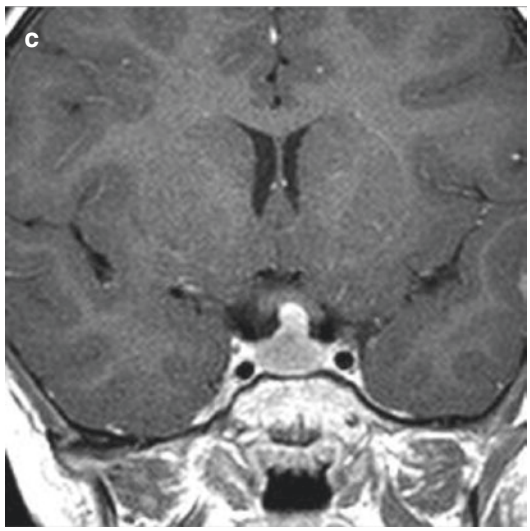

Fig. 12.7c Gadolinium enhanced coronal T1-weighted image shows thickening of the pituitary stalk. The cavernous sinuses are normal

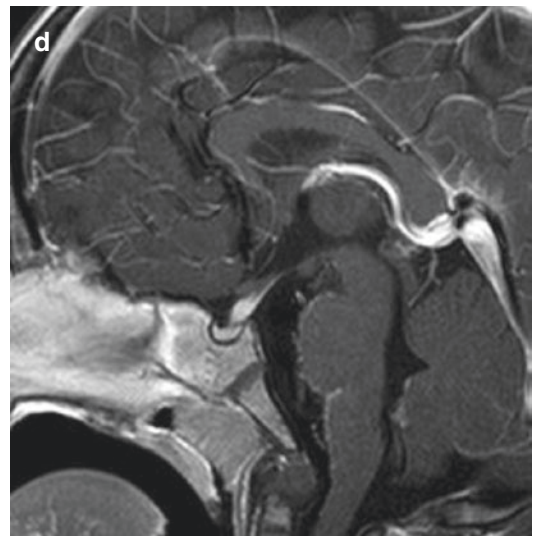

Fig. 12.7d Gadolinium enhanced T1-weighted sagittal image shows thickening of the pituitary stalk which shows enhancement. The pituitary gland is normal in size

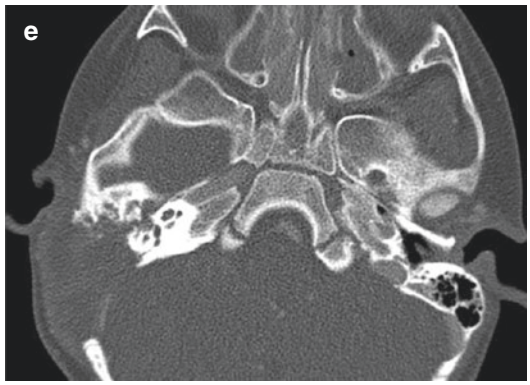

Fig. 12.7e Contrast enhanced axial CT shows a lytic lesion of the right temporal bone with an expansile soft tissue lesion

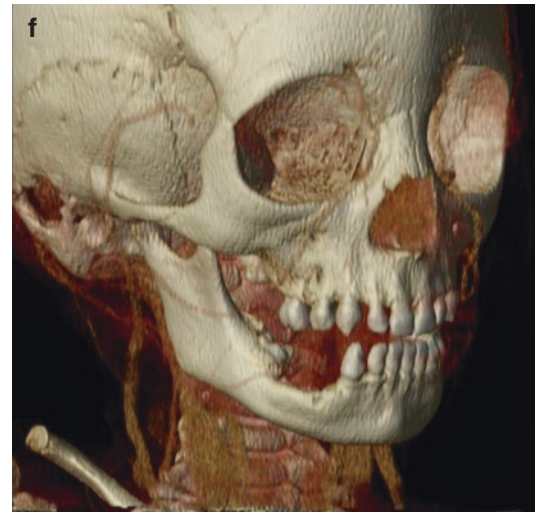

Fig. 12.7f Volume rendered 3D image shows the lytic lesions involving the right temporal bone and right hemimandible

Epidemiology
- Langerhans cell histiocytosis (LCH) is a rare disease with an incidence of 0.2–2.0 cases per 100,000 children under fifteen years of age
- Most common dendritic disorder

Pathology and Genetics
- Named because of its similarity to the Langerhans cells found in the skin and mucosa
- Abnormal cells in Langerhans cell histiocytosis are actually derived from myeloid dendritic cells that exhibit the same antigens (CD1a, S100, and CD207)

Associations
- Involvement of the pituitary stalk may be in isolation or in the presence of skeletal lesions

Clinical Management
- Screening with skeletal survey or whole body MRI may allow visualization of sites that are amenable to less invasive biopsy
- Treatment is with chemotherapy
- Neurodegenerative Langerhans cell histiocytosis is a late complication of the disease and/or treatment and is characterized by involvement of cerebellum, deep gray matter structures, and cerebral hemispheres

Imaging Findings
- Involvement of the pituitary stalk (and gland) with nonvisualization of the T1 shortening of the neurohypophysis is characteristic
- Germinoma is the primary differential consideration of Langerhans cell histiocytosis. Imaging findings are identical in the absence of cavernous sinus involvement and intracranial synchronous/ metastatic lesions which can be seen in germinoma
- Bone lesions are seen in Langerhans cell histiocytosis, but not in germinoma

Take-Home Message
- In the absence of secondary findings, when only the pituitary stalk and/or pituitary gland are involved germinoma and Langerhans cell histiocytosis cannot be discriminated from each other in a child presenting with diabetes insipidus

Further Reading

- Prayer D, Grois N, Prosch H, Gadner H, Barkovich AJ. MR imaging presentation of intracranial disease associated with Langerhans cell histiocytosis. AJNR Am J Neuroradiol. 2004;25(5):880–91
- Zaveri J, La Q, Yarmish G, Neuman J. More than just Langerhans cell histiocytosis: a radiologic review of histiocytic disorders. Radiographics. 2014;34(7):2008–24

12.8 Craniopharyngioma

12-year-old presenting with vision problems.
Companion case:
4-year-old with vision problems.

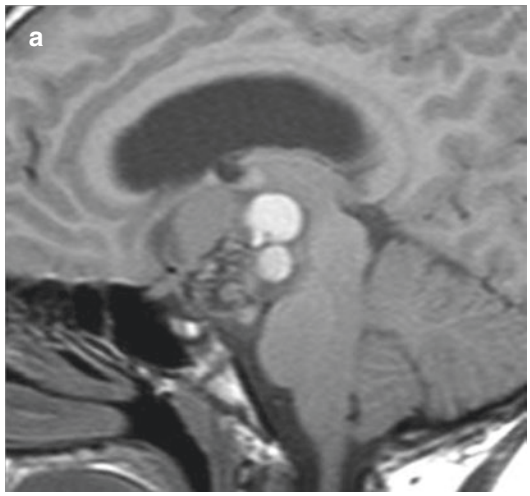

Fig. 12.8a Sagittal T1-weighted image shows a suprasellar mass with multiple small cysts. Some cysts show increased signal intensity due to proteinaceous content. The T1-shortening of the neurohypophysis is preserved

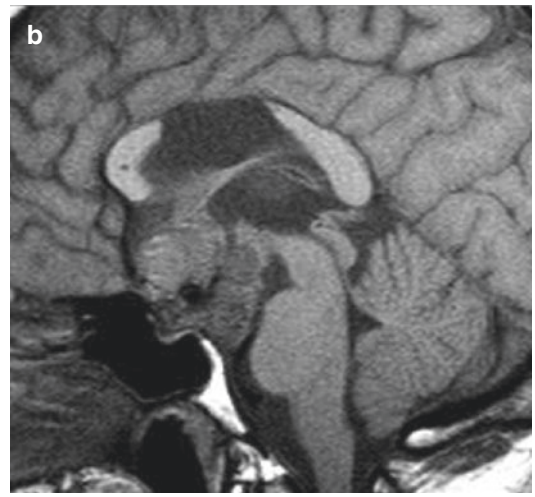

Fig. 12.8b Remote postoperative examination shows the surgical defect involving the corpus callosum. Residual tumor is present in the suprasellar cistern. The T1 shortening of the neurohypophysis is no longer visualized. The patient developed postoperative diabetes insipidus

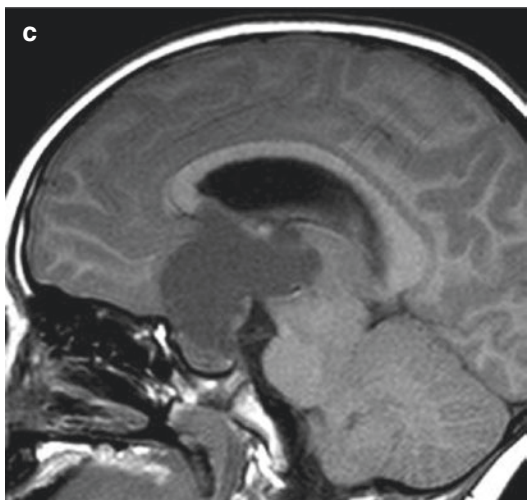

Fig. 12.8c Sagittal T1-weighted image shows a predominantly cystic sellar and suprasellar mass

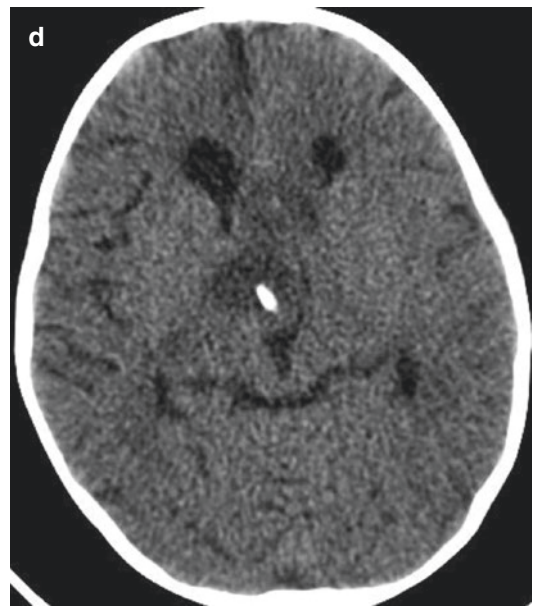

Fig. 12.8d Axial noncontrast CT shows the tip of a catheter connected to a Rickman reservoir. These are used for control of the cyst volume and occasionally instillation of P^{32} for local radiotherapy

Epidemiology
- May be seen at any age with the peak incidence encountered between 10 and 14 years

Pathology and Genetics
- Two types:
  - Adamantinomatous (pediatric), generally with cysts and calcifications
  - Papillary (adult), generally solid

Associations
- Generally, craniopharyngoma does not present with diabetes insipidus, 80% of the axons within the pituitary stalk need to be severed for development of diabetes insipidus

Clinical Management
- Involvement of optic chiasm and intracranial optic nerves makes resection and management difficult
- Regional vessels may be in close proximity of tumor
- Treatment has evolved, from attempted complete resection to management of mass effect and disease control by decompressing the cysts and radiation therapy

Imaging Findings
- Ninety percent of pediatric craniopharyngiomas show calcifications and 90% have cysts
- The cyst fluid may have high protein content and appear hyperintense on T1-weighted and FLAIR images

Take-Home Message
- Relationship of the tumor with optic apparatus and regional vasculature should be discussed in detail while describing the tumor

Further Reading

- Prieto R, Pascual JM, Barrios L. Topographic Diagnosis of Craniopharyngiomas: The Accuracy of MRI Findings Observed on Conventional T1 and T2 Images. AJNR Am J Neuroradiol. 2017;38(11):2073–80
- Saleem SN, Said AH, Lee DH. Lesions of the hypothalamus: MR imaging diagnostic features. Radiographics. 2007;27(4):1087–108

12.9 Optic Hypothalamic Glioma

4-month-old with macrocephaly
Companion case:
9-year-old with vision problems

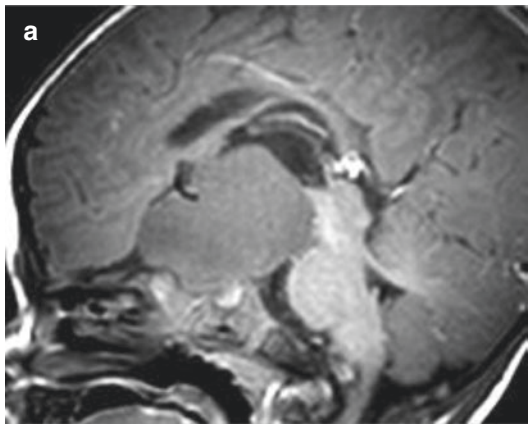

Fig. 12.9a Gadolinium enhanced sagittal T1-weighted image shows a large suprasellar mass which does not show enhancement

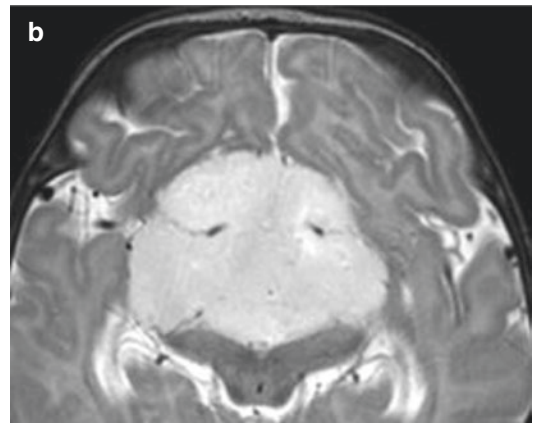

Fig. 12.9b The lesion is markedly hyperintense on the axial T2-weighted image

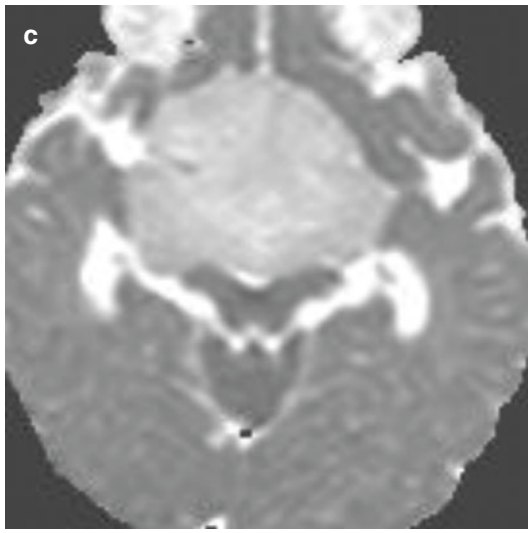

Fig. 12.9c Axial ADC map shows markedly increased diffusivity within the lesion

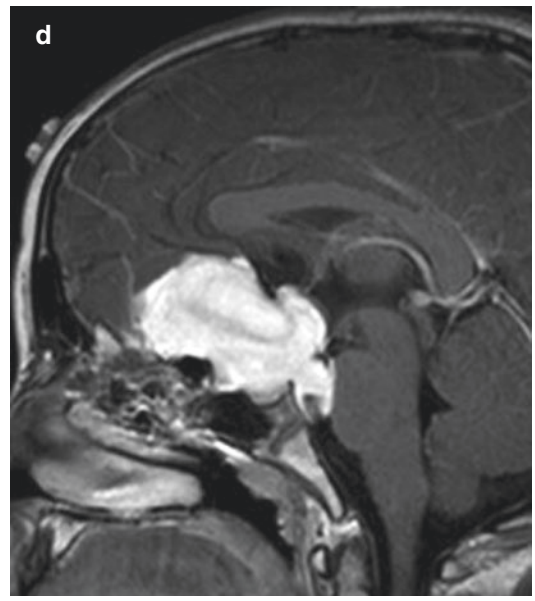

Fig. 12.9d Gadolinium enhanced sagittal T1-weighted image shows an intensely enhancing suprasellar tumor

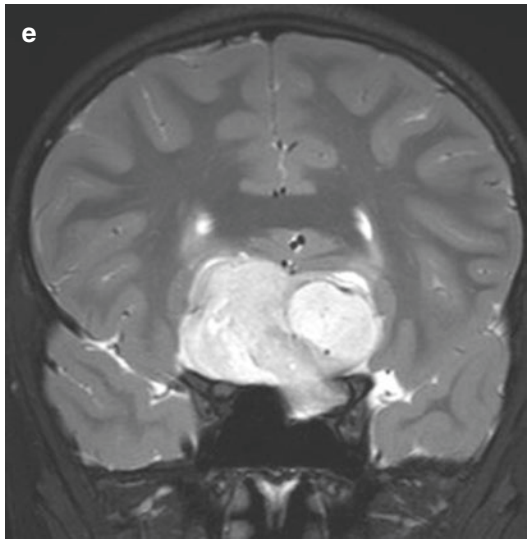

Fig. 12.9e Coronal STIR image shows extension of the tumor into the enlarged left optic canal

Epidemiology
- Optic hypothalamic gliomas constitute 5% of all brain tumors
- Ten percent of all may be seen at any age with the peak incidence encountered between 10 and 14 years

Pathology and Genetics
- Majority of the optic hypothalamic gliomas are pilocytic astrocytomas (WHO grade I)
- Pilomyxoidastrocytomas (WHO grade II) occasionally arise in this region

Associations
- Patients with neurofibromatosis type I should be screened for optic hypothalamic gliomas and vice versa

Clinical Management
- Although optic hypothalamic tumors are generally low grade, complete resection is rarely possible because of involvement of the optic apparatus and hypothalamus
- Chemotherapy is effective in disease control
- Regional vessels may be in close proximity of the tumor

Imaging Findings
- Markedly hyperintense on T2 weighted images, similar to cerebellar pilocytic astrocytomas
- Increased diffusivity is present in all optic hypothalamic gliomas
- Cysts are occasionally present
- Enhancement is variable
- T1 shortening of the neurohypophysis almost always preserved despite encasement of the pituitary stalk

Take-Home Messages
- Association with neurofibromatosis type I, 15% of patients with neurofibromatosis type I develop optic hypothalamic gliomas
- Preservation of the T1 shortening of the neurohypophysis and increased diffusivity are important in discriminating from other sellar/ suprasellar tumors

Further Reading

- Kornreich L, Blaser S, Schwarz M, Shuper A, Vishne TH, Cohen IJ, et al. Optic pathway glioma: correlation of imaging findings with the presence of neurofibromatosis. AJNR Am J Neuroradiol. 2001;22(10):1963–9
- Shofty B, Ben-Sira L, Kesler A, Jallo G, Groves ML, Iyer RR, et al. Isolated optic nerve gliomas: a multicenter historical cohort study. J Neurosurg Pediatr. 2017;20(6):549–55

12.10 Optic Hypothalamic Glioma

5-year-old with gelastic seizures.

Companion case:
10-year-old with learning difficulty.

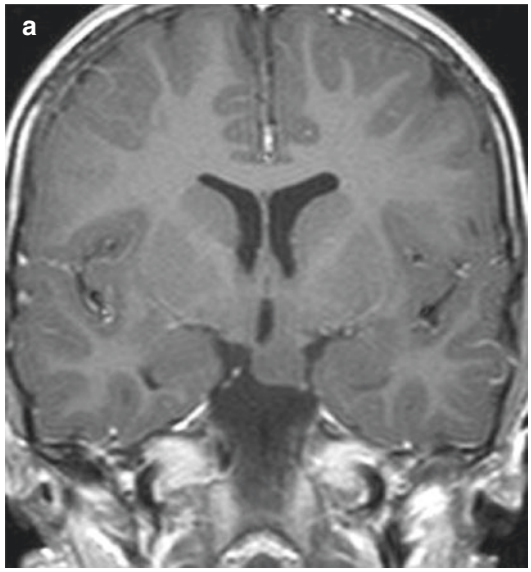

Fig. 12.10a Gadolinium enhanced T1-weighted coronal image shows a left-sided suprasellar mass which is isointense to normal brain

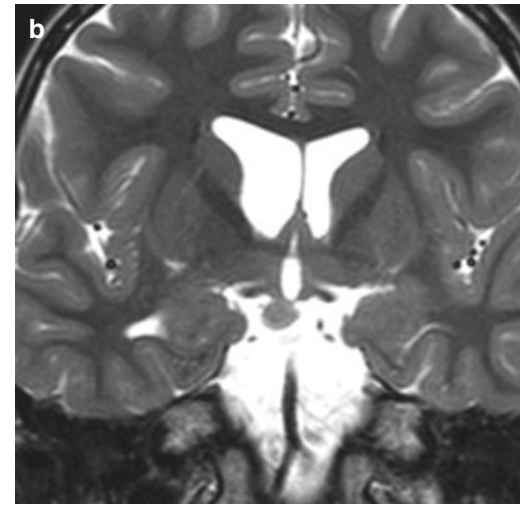

Fig. 12.10b Coronal T2-weighted image shows a pedunculated right-sided mass extending into the suprasellar cistern, separate from the optic apparatus

Epidemiology
- Rare developmental malformation

Pathology and Genetics
- Not a true neoplasm
- Developmental malformations arising from mature ganglionic tissue that involve the tuber cinereum

Associations
- Pallister-Hall syndrome: Hypothalamic hamartoma, polydactyly, syndactyly, dysplastic nails
- Precocious puberty

Clinical Management
- Gelastic "laughing" seizures
- Developmental delay, learning difficulty
- Treatment with surgery or image guided laser ablation

Imaging Findings
- Pedunculated or sessile
- Growing into the suprasellar cistern and occasionally deforming the third ventricle
- Generally isointense to normal brain
- No enhancement

Take-Home Message
- In patients with gelastic seizures, developmental delay, learning difficulty, and precocious puberty attention should be paid to hypothalamus

Further Reading

- Plaza MJ, Borja MJ, Altman N, Saigal G. Conventional and advanced MRI features of pediatric intracranial tumors: posterior fossa and suprasellar tumors. AJR Am J Roentgenol. 2013;200(5):1115–24
- Rolston JD, Chang EF. Stereotactic laser ablation for hypothalamic hamartoma. Neurosurg Clin N Am. 2016;27(1):59–67

Primary Intra-Axial Brain Tumours

13

Laura Oleaga, Javier Moreno, Mariano Werner, and Nuria Bargalló

13.1 Case 1

25-year-old female with a prior medical history of seizures non-responding to treatment.

Biopsy was performed; the pathological diagnosis was diffuse astrocytoma WHO grade II. Molecular and genetic features: isocitrate dehydrogenase (IDH1)-mutant, 1p/19q non-codeleted, and loss of ATRX expression, PFAG positive expression and P53 positive.

13.1.1 Images and Legends

L. Oleaga (✉) · J. Moreno · M. Werner · N. Bargalló
Radiology Department, Hospital Clínic Barcelona, Barcelona, Spain

Y. Özsunar, U. Şenol (eds.), *Atlas of Clinical Cases on Brain Tumor Imaging*,
https://doi.org/10.1007/978-3-030-23273-3_13

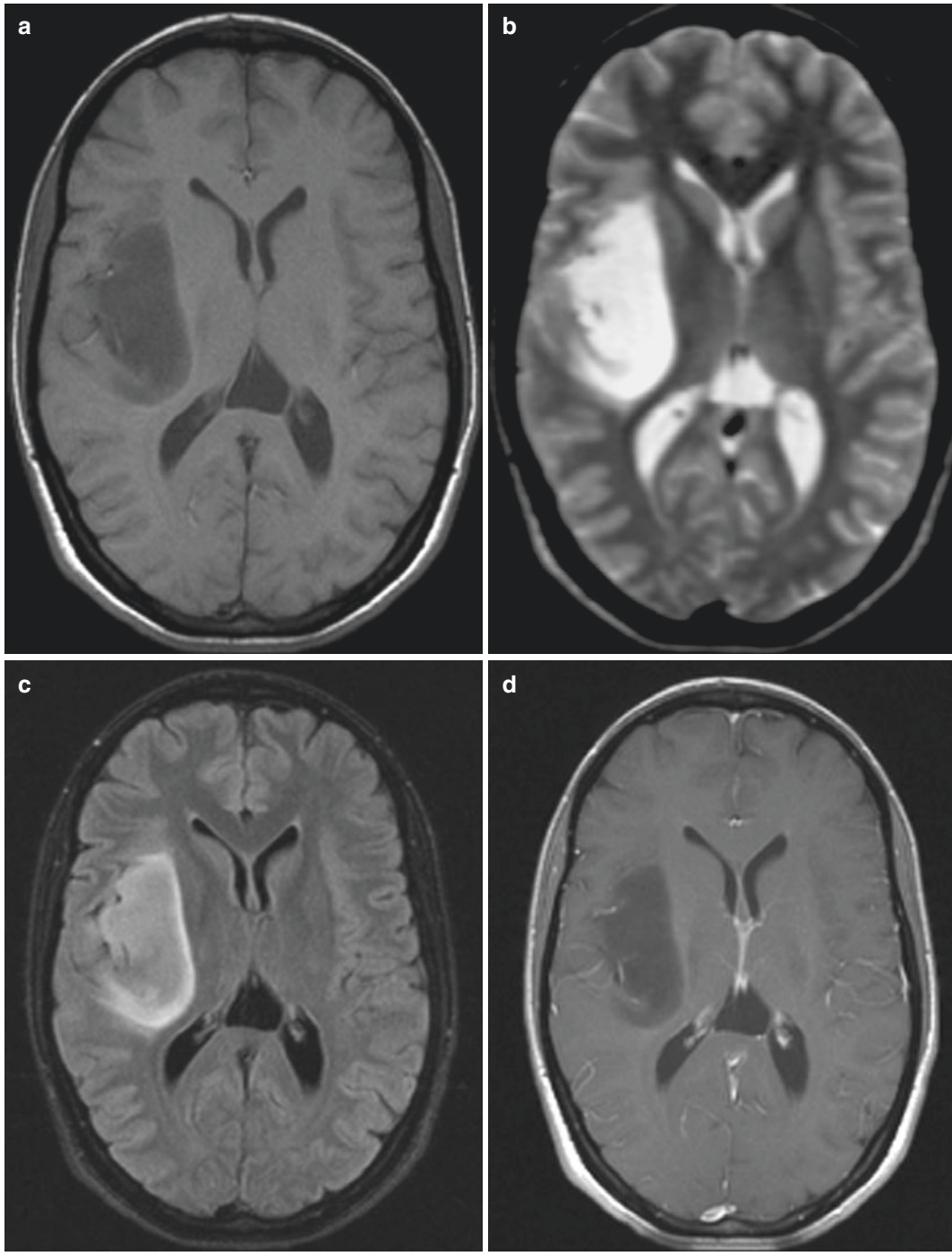

Fig. 13.1 (**a**) Axial T1-weighted MRI demonstrates low-signal intensity, well-defined mass on the right insular lobe. (**b**) 3D Sagittal T2-weighted MRI-axial reconstruction. Markedly T2-hyperintense right insular mass, similar to cerebrospinal fluid (CSF). (**c**) Axial FLAIR MRI, on this sequence the central part of the tumour, demonstrates substantially lower signal than the T2-weighted image (FLAIR/T2 mismatch). (**d**) Contrast-enhanced axial T1-weighted image demonstrates a well-defined non-enhancing insular mass. (**e**)Axial diffusion-weighted magnetic resonance imaging (DWI). Low signal is depicted on the tumour. (**f**) Apparent diffusion coefficient map (ADC). The tumour exhibits high ADC value. (**g**) Dynamic susceptibility contrast-enhanced MR image. Relative cerebral blood volume (rCBV) colour map shows a low rCBV, in keeping with a low-grade glioma. (**h**) ^{1}H-MR spectroscopy (TE 30 ms) shows a slightly elevated choline (Ch) peak with a diminished peak of N-acetyl aspartate (NAA) and increased myo-inositol (mIns)

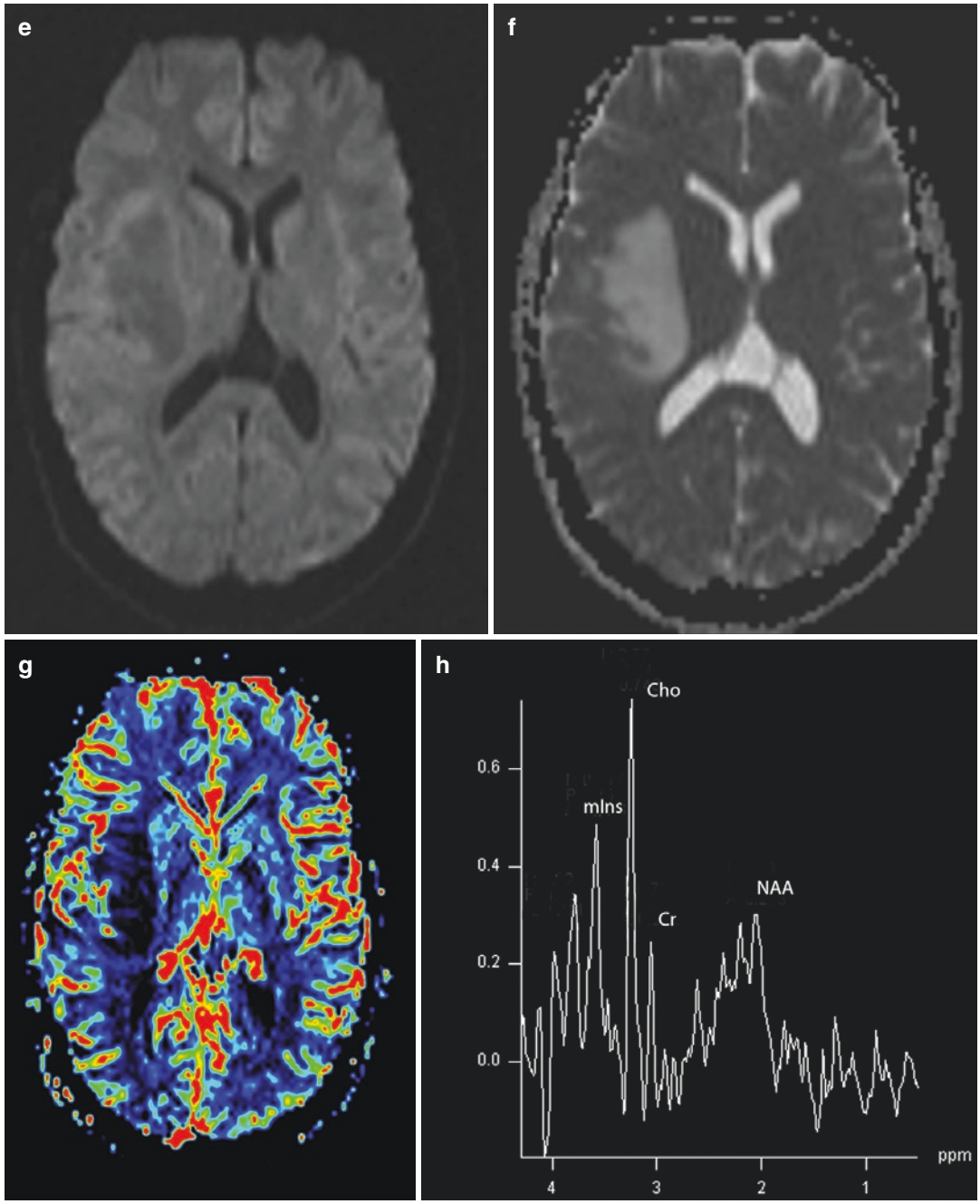

Fig. 13.1 (continued)

13.1.2 Epidemiology

Diffuse astrocytoma, IDH-mutant, are the most common WHO grade II astrocytomas.

13.1.3 Pathology and Genetics

The World Health Organization (WHO) has recently updated the diagnostic criteria for astrocytic and oligodendroglial tumours. Under the

new classification system, the diagnosis of diffuse glioma incorporates the mutation in the isocitrate dehydrogenase (IDH) genes, either type 1 (IDH1) or type 2 (IDH2) and simultaneous deletion of chromosomes 1p and 19q.

Maximum surgical resection, as feasible, is considered the best initial treatment option for WHO grade II astrocytomas (1p/19q non-codeleted). In cases of biopsy or incomplete resection, involved field radiotherapy and maintenance procarbazine, lomustine, and vincristine chemotherapy (RTOG 9802 trial) is recommended according to the European Association for Neuro-Oncology (EANO) guideline 2017.

13.1.4 Clinical Management

Molecular diagnostic tests are essential to select the appropriate treatment. Standard of care for WHO grade II astrocytomas IDH-mutant (1p/19q-non-codeleted) includes resection, as feasible, or biopsy followed by involved field radiotherapy and maintenance procarbazine, lomustine, and vincristine chemotherapy.

13.1.5 Imaging Findings and Differential Diagnosis

MR imaging feature labelled "T2-FLAIR mismatch" has been demonstrated in diffuse astrocytoma IDH-mutant 1p/19q non-codeleted. The lack of enhancement on the conventional MR image suggests a low-grade glioma.

rCBV measurements correlate with tumour grade and histologic findings of increased vascularity. Astrocytic low-grade tumours show low rCBV values.

ADC maps can also be used as grade tumour predictors. DWI quantifies the water diffusivity within the intra- and extracellular compartments, there is an inverse correlation between the minimum ADC values and histopathologic grade of the astrocytic supratentorial brain tumours. Low-grade tumours show low diffusivity and high ADC values.

Take-Home Messages

- The presence of >50% T2-FLAIR mismatch is highly predictive of a IDH-mutant 1p/19q non-codeleted tumour

Further Reading

1. Johnson DR, Guerin JB, Giannini C, Morris JM, Eckel LJ, Kaufmann TJ. 2016 Updates to the WHO Brain Tumor Classification System: What the Radiologist needs to know. RadioGraphics 2017; 37:2164–2180
2. Lasocki A, Gaillard F, Gorelik A, Gonzales M. MRI features can predict 1p/19q status in intracranial gliomas. Am J Neuroradiol. 2018; 39:687–692
3. Patel SH, Poisson LM, Brat DJ, Zhou Y, Cooper L, Snuderl M, Thomas C, Franceschi AM, Golfinos JG, Chi AS, Jain R. T2–FLAIR mismatch, an imaging biomarker for IDH and 1p/19q status in lower-grade gliomas: A TCGA/TCIA Project. Clin Cancer Res. 2017; 23:6078–6085
4. Broen MPG, Smits M, Wijnenga MMJ, Dubbink HJ, Anten MHME, Schijns OEMG, Beckervordersandforth J, Postma AA, van den Bent MJ. The T2–FLAIR mismatch sign as an imaging marker for non-Enhancing IDH-mutant, 1p/19q-intact lower grade glioma: a validation study. Neuro Oncol. 2018;3(20):1393–1399
5. Leu K, Ott GA, Lai A, Nghiemphu PL, Pope WB, Yong WH, Liau LM, Cloughesy TF, Ellingson BM. Perfusion and diffusion MRI signatures in histologic and genetic subtypes of WHO grade II–III diffuse gliomas. J Neurooncol 2017; 134:177–188

13.2 Case 2

35-year-old female, with a sudden loss of consciousness, prior history of hemiparesis and multiple cranial nerve palsies with a clinical suspicion of multiples sclerosis (MS). Steroid treatment was started with symptoms worsening.

Biopsy was performed; the pathological diagnosis was diffuse astrocytoma WHO II, negative isocitrate dehydrogenase (IDH) wild-type, 1p19q non-codeleted, loss of ATRX expression, PFAG positive expression and P53 positive. The tumour shows high proliferation index Ki67 17%.

The patient was treated with temozolamide and radiation therapy.

13.2.1 Images and Legends

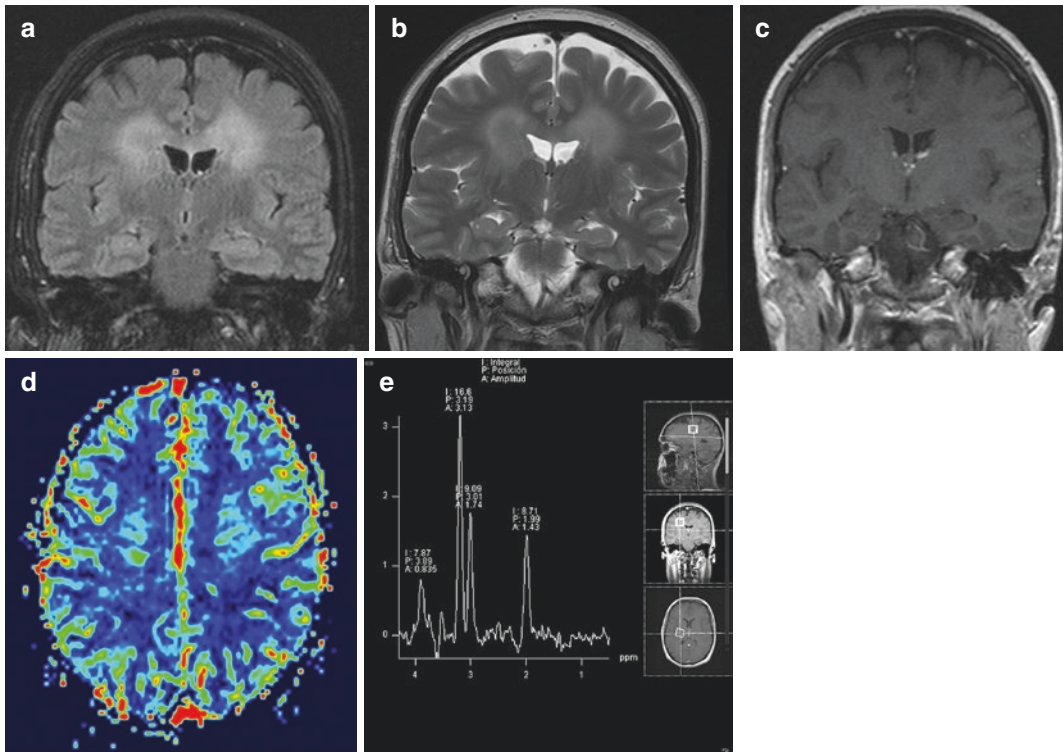

Fig. 13.2 (**a**) Coronal T2 FLAIR MRI demonstrates an ill-defined mass in both centrum semiovale with corpus callosum infiltration. (**b**) Coronal T2-weighted MRI. Slight mass effect of the lesion is shown. U-fibbers are spared. No mismatch on FLAIR images is demonstrated. (**c**) Coronal T1-weighted MRI post-Gd administration shows no enhancement whatsoever. (**d**) Dynamic susceptibility contrast-enhanced MR image. Relative cerebral blood volume (rCBV) colour map shows slight increase of perfusion possibly secondary to the high cellularity of the lesion. A possible pitfall may be the transcortical veins at this region. (**e**) MR spectroscopy shows a slightly elevated choline peak associated with a diminished peak of N-acetyl aspartate (NAA)

13.2.2 Epidemiology

Diffuse astrocytomas are tumours diagnosed in childhood or young adulthood (biphasic distribution 6–12 years and 26–46 years).

13.2.3 Pathology and Genetics

According to the new WHO 2016 classification of CNS tumours, there are three variants of diffuse astrocytoma: IDH-mutant, IDH no mutant (wild type) and NOS (no otherwise specified). Diffuse astrocytomas, IDH-wild type with no 1p19q codeletion, are the most aggressive grade II astrocytomas.

13.2.4 Clinical Management

Maximum surgical resection, as feasible, is considered the best initial treatment option for WHO grade II astrocytomas (1p/19q non-codeleted). In cases of biopsy or incomplete resection, involved field radiotherapy and temozolamide is recommended according to the European Association for Neuro-Oncology (EANO) guideline 2017.

13.2.5 Imaging Findings and Differential Diagnosis

Wild-type diffuse astrocytoma is usually a mass-like hyperintense on T2-weighted images, non-enhancing lesion, which follows white matter distribution. Cortical involvement is possible in late cases. In comparison with the IDH-mutant, the borders of the wild type are usually ill defined; also the FLAIR mismatch is absent. rCBV measurements correlate with tumour grade and histologic findings of increased vascularity. Astrocytic low-grade tumours show low rCBV values. High cellular tumours show high rCBV values.

Take-Home Messages

- Wild-type DA is usually a smaller lesion with ill-defined border in comparison with the more benign IDH-mutant DA

Further Reading

1. Louis DN, Perry A, Reifenberger G et al. The 2016 World Health Organization Classification of Tumors of the Central Nervous System: a summary. Acta Neuropathol. 2016; 131: 803–20
2. Patel SH, Poisson LM, Brat DJ, Zhou Y, Cooper L, Snuderl M, Thomas C, Franceschi AM. et al. T2–FLAIR mismatch, an imaging biomarker for IDH and 1p/19q status in lower-grade gliomas: A TCGA/TCIA project. Clin Cancer Res. 2017; 23:6078–6085
3. Brat DJ, Verhaak RG et al. Comprehensive, integrative genomic analysis of diffuse lower-grade gliomas. N. Engl. J. Med. 2015; 372: 2481–2498
4. Lasocki A, Gaillard F, Gorelik A, Gonzales M. MRI features can predict 1p/19q status in intracranial gliomas. Am J Neuroradiol. 2018; 39:687–692

13.3 Case 3

64-year-old male presents with first episode of seizures. The patient was previously asymptomatic.

The patient underwent complete surgical resection of the temporal mass. Biopsy was performed and pathology showed histologic features of glioblastoma (GB). The patient received TMZ + RDT according to Stupp Protocol. Four years later, the patient developed a right frontal superficial nodule. Surgical resection was performed. Pathology of the second lesion showed a conventional GB with meningeal infiltration and a region with cystic areas and small blue cells with positive synaptophysin. Final diagnosis was GB with primitive neuroectodermal tumour (PNET)-like component. There was no PNET component in the first pathology specimen.

13.3.1 Images and Legends

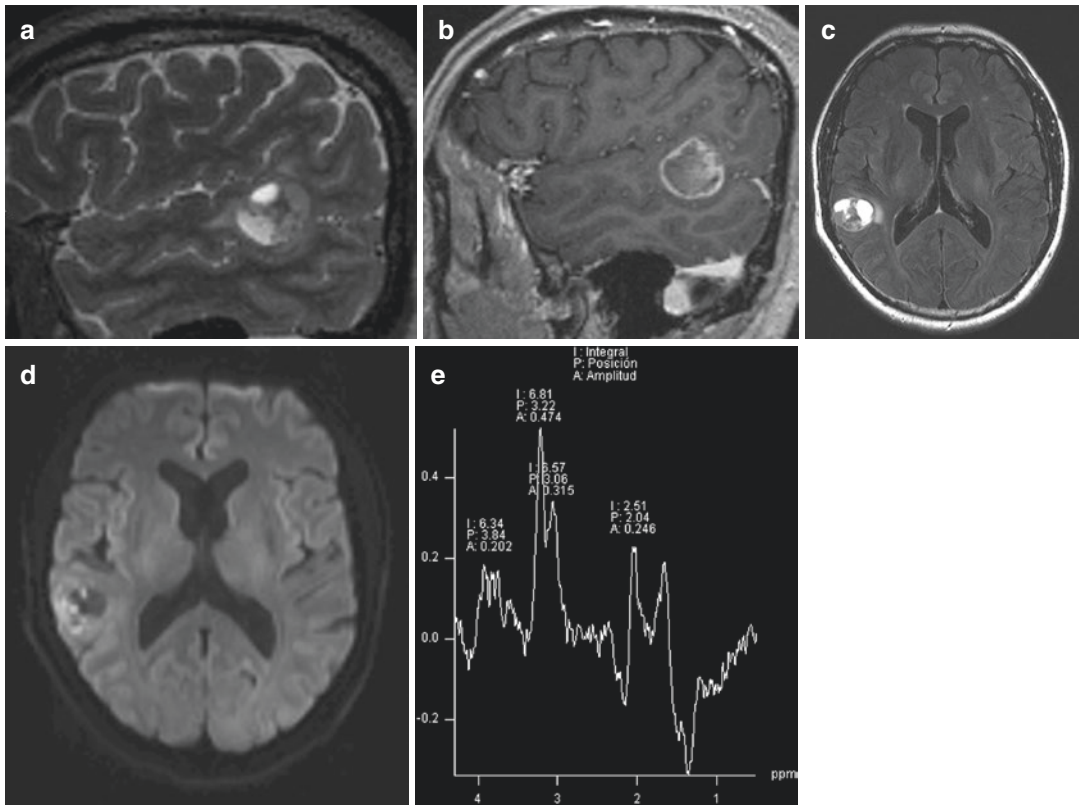

Fig. 13.3 (**a**) T2W 3D SPACE MRI. Right cortical tumour with anterior cystic and solid areas. (**b**) T1GRE 3D+Gd MRI. Enhancement of the solid part of the tumour and a peripheral enhancing rim. (**c**) T2 FLAIR MRI shows a rim of peripheral hyperintense oedema in adjacent white matter. (**d**) DWI MRI. The posterior nodular part of the lesion shows a hypercellular zone with high diffusion. (**e**) ^{1}H-MR spectroscopy (TE 30 ms) shows a Choline peak and reduction of the NAA

13.3.2 Epidemiology

GB with PNET-like components is a rare variant of GB. There is an increased propensity of these tumours for CSF dissemination and a benefit of "PNET-like" chemotherapy.

13.3.3 Pathology, Imaging and Genetics

GB with PNET component has two areas with different histological architectures:

The traditional astrocytic GB areas with high expression of GFA, 10q deletion, EGFR amplification and 1p/19q deletions. IDH mutations are variable. MR signal is very variable hence the name "multiforme". Enhancement and necrosis are common with an ill-defined lesion and severe mass effect. rCBV measurements are elevated in the viable tumour areas.

Hypercellular undifferentiated PNET areas, present lower expression of GFAP and variable neuronal immunophenotype (S-100, synaptophysin, NeuN, NSE and NFP). Also high Ki-67 index, N-myc or C-myc amplifications are reported. MR aspect of the region features cystic areas and high restriction (secondary to the high cellularity of the lesion).

GB-PNET tumours feature behaviour from both histologic regions, GB-PNET tumour tends to disseminate to CSF and has fewer local recurrence in comparison with conventional GB.

13.3.4 Clinical Management

There is no consensus with treatment; most series has been treated with TMZ and local RDT. There are some reports with possible benefit of carboplatin and whole spine RDT for reducing CSF dissemination.

Take-Home Messages

- GB-PNET lesions present both MR characteristics and behaviour from both histologic origins of the tumour. High restriction and CSF spread are some specific aspect of the tumour. Lower local recurrence rates are reported

Further Reading

1. Louis DN, Perry A, Reifenberger G et al. The 2016 World Health Organization Classification of Tumors of the Central Nervous System: a summary. Acta Neuropathol. 2016; 131: 803–820
2. Varlet P, Soni D, Miquel C, Roux FX, Meder JF, Chneiweiss H, Daumas-Duport C. New variants of malignant glioneuronal tumors: a clinicopathological study of 40 cases. Neurosurgery. 2004; 55:1377–1391
3. Lee APS, Brewer J, Back M, Wheeler H. Combination therapy for glioblastoma multiforme with primitive neuroectodermal tumor components: case series. J Clin Oncol. 2012; 30(Suppl 15):e12507
4. Perry A, Miller CR, Gujrati M, Scheithauer BW, Zambrano SC, Jost SC, Raghavan R, Qian J, Cochran EJ, Huse JT, Holland EC. Malignant gliomas with primitive neuroectodermal tumor-like components: a clinicopathologic and genetic study of 53 cases. Brain Pathology. 2009; 19:81–90

13.4 Case 4

57-year-old male. Sudden-onset of aphasia and vomiting. Biopsy was performed; the pathological diagnosis was GB, WHO grade IV, negative for ATRX, p53, IDH1 (wild-type) and IDH2. No MGMT hypermethylation is noted. High expression of EGFR is demonstrated.

The patient was treated with TMZ + RT. 8 months later the patient presented with severe progression of the disease with cranial hypertension, neurological deterioration and pneumonia. The patient died 9 months later.

13.4.1 Images and Legends

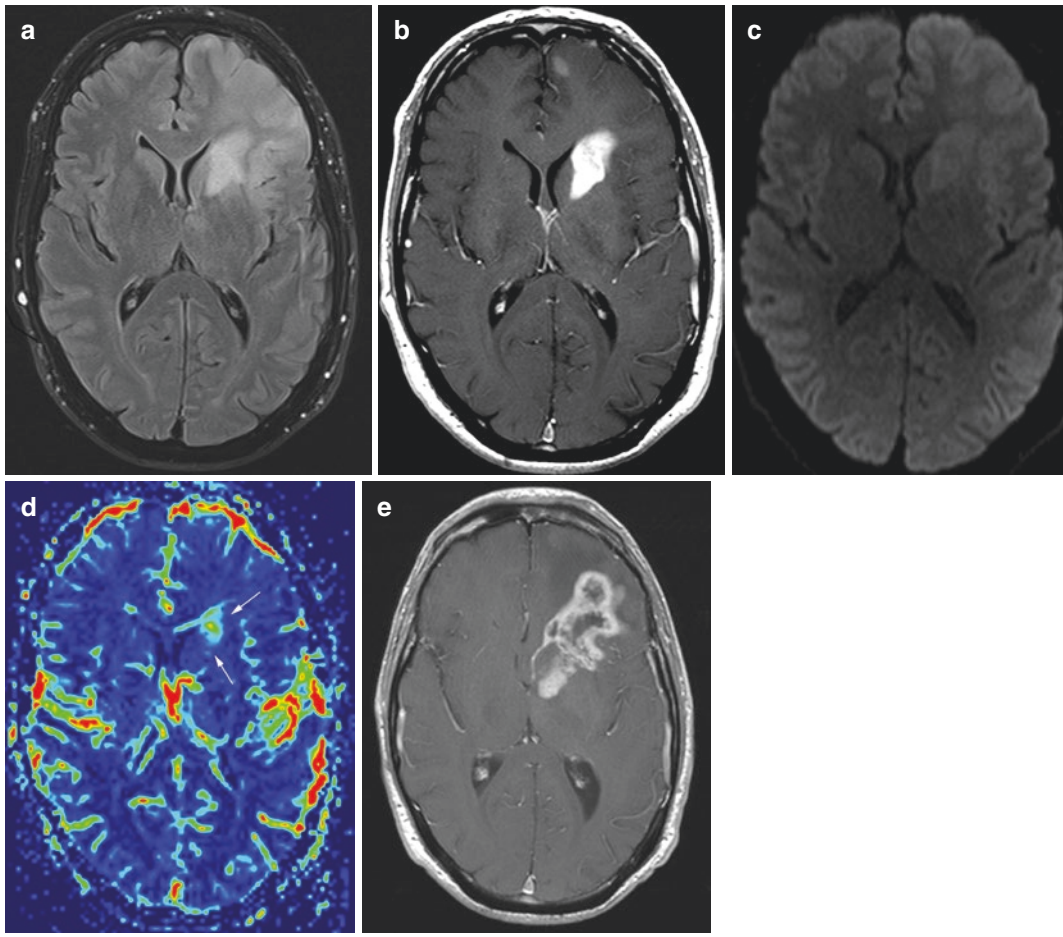

Fig. 13.4 (**a**) Axial FLAIR MRI. Left frontal mass involving the cortex and corona radiata. (**b**) Axial T1W + Gd MRI. Nodular deep enhancement is demonstrated with some foci in the sub-cortical areas. (**c**) Dynamic susceptibility contrast-enhanced MR image. Relative cerebral blood volume (rCBV) colour map shows increased rCBV (arrows) in the enhancing region. (**d**) DWI MRI. The mass shows slightly increased signal in keeping with hypercellular tumour. (**e**) 8 months follow-up MRI T1SE + Gd. Massive progression of the mass is noted with midline crossing at the callosum (butterfly lesion) and necrotic areas. Ependymal spread is noted in the frontal horn of the ventricle

13.4.2 Epidemiology

GB is a tumour with a global incidence of less than 10/100.000 people. GB accounts for 50% of all gliomas. It has a poor prognosis of 15 months survival rate.

13.4.3 Pathology and Genetics

Glioblastoma is the most aggressive, invasive and undifferentiated type astrocytic of tumour and has been designated Grade IV by WHO. According to the origin, 90% of the GBs are primary type, also known as "wild type" (without IDH mutation or MGMT methylation). Secondary GB is IDH mutated and arises from a previous low-grade glioma. Wild-type GB shows a typical EGFR amplification and aggressive behaviour.

13.4.4 Clinical Management

Surgical debulking or total excision + temozolomide and radiation therapy are the typical management of the lesion.

13.4.5 Imaging Findings and Differential Diagnosis

GB usually shows an extensive supratentorial lesion with variable enhancement (always present, although) with signs of hypercellularity and necrosis. Butterfly image is frequent. At the moment of diagnosis, some signs of extensive spread are more frequent on WT GBs, as ependymal or leptomeningeal spread. DWI and rCBV maps correlate with the histologic grade of the GBs.

Take-Home Messages

- Wild-type GBs are the most aggressive subtype of GB. They arise from a previous normal brain

Further Reading

1. Kumar V, Abbas AK, Fausto N et al. Robbins and Cotran pathologic basis of disease. W B Saunders Co. (2005) ISBN:0721601871
2. Rees JH, Smirniotopoulos JG, Jones RV et al. Glioblastoma multiforme: radiologic-pathologic correlation. Radiographics. 1996; 16: 1413–38
3. Omuro A, DeAngelis LM. Glioblastoma and other malignant gliomas: a clinical review. JAMA. 2013; 310:1842–1850
4. Osborn AG, Salzman KL, Jhaveri MD, Barkovich AJ. Diagnostic imaging: brain E-book. Elsevier Health Sciences; 2015 Dec 24
5. Lacroix M, Abi-Said D, Fourney DR, Gokaslan ZL, Shi W, DeMonte F, Lang FF, McCutcheon IE, Hassenbusch SJ, Holland E, Hess K. A multivariate analysis of 416 patients with glioblastoma multiforme: prognosis, extent of resection, and survival. Journal of neurosurgery. 2001; 95:190–198
6. Thakkar JP, Dolecek TA, Horbinski C, et al. Epidemiologic and molecular prognostic review of Glioblastoma. Cancer Epidemiol Biomarkers Prev. 2014; 23:1985–1985

13.5 Case 5

63-year-old man with headache, altered mental status and left-hand weakness from months ago.

Biopsy was performed; the pathological diagnosis was glioblastoma, WHO grade IV. Molecular and genetic features: isocitrate dehydrogenase (IDH1)-wild-type, methylguanine methyltransferase (MGMT) negative, P53 negative, EGFR negative, EGFRvIII negative. TERT mutation. c .–124C > T.

13.5.1 Images and Legends

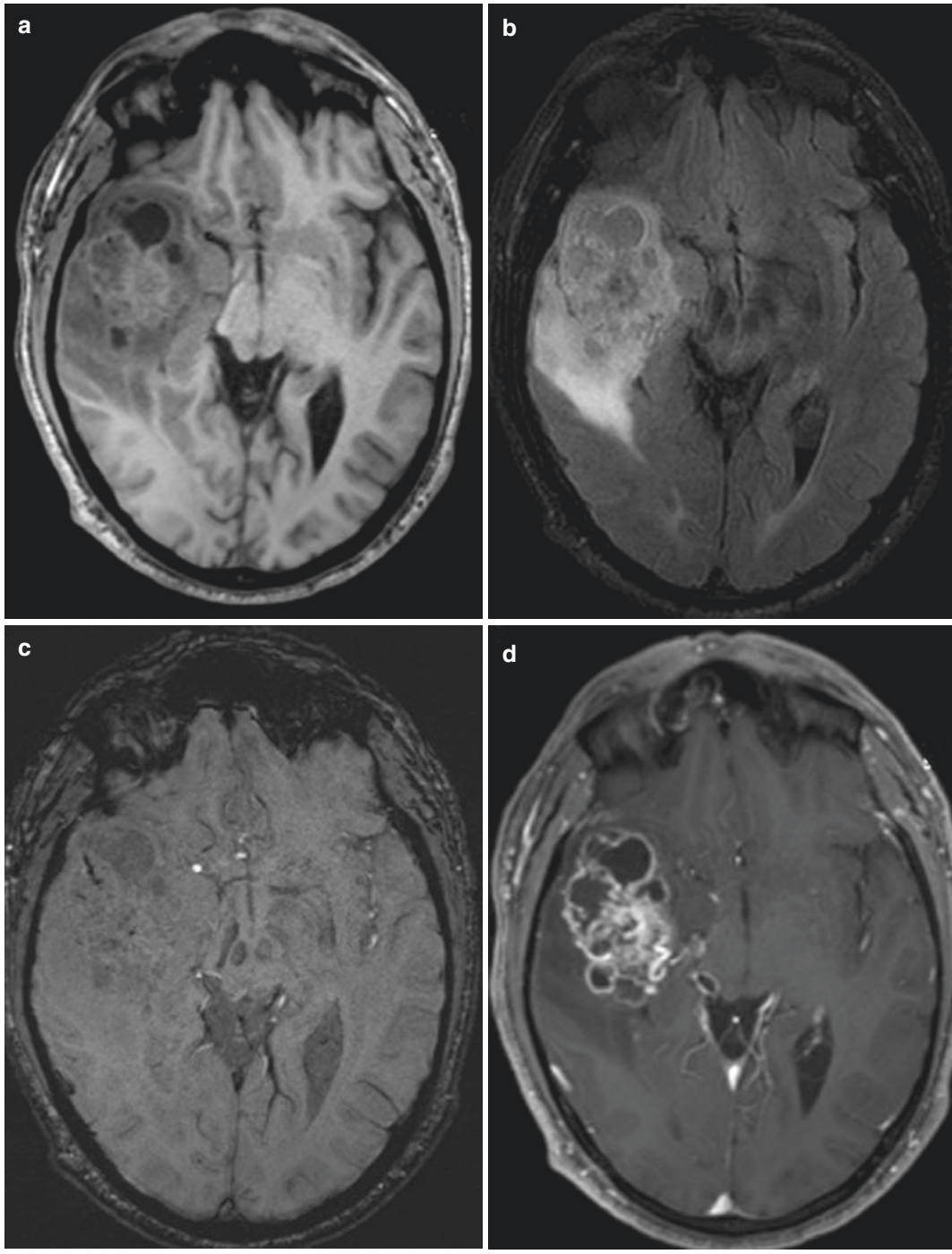

Fig. 13.5 (**a**) Axial T1-weighted MRI demonstrates a heterogeneous mass involving the temporo-insular region. (**b**) Axial FLAIR MRI shows hyperintense solid regions with central hypointense areas of necrosis surrounded by vasogenic oedema. (**c**) Axial SWI demonstrates susceptibility artefact inside the lesion due to presence of blood products. (**d**) Contrast-enhanced axial T1-weighted MRI demonstrates thick, irregular predominantly peripheral enhancement with central necrosis. (**e**) MR perfusion shows rCBV elevated in solid enhancing regions of the tumour. (**f**) DTI demonstrates high signal in solid parts related to hypercellularity. (**g**) Low ADC values correlated with high-grade gliomas

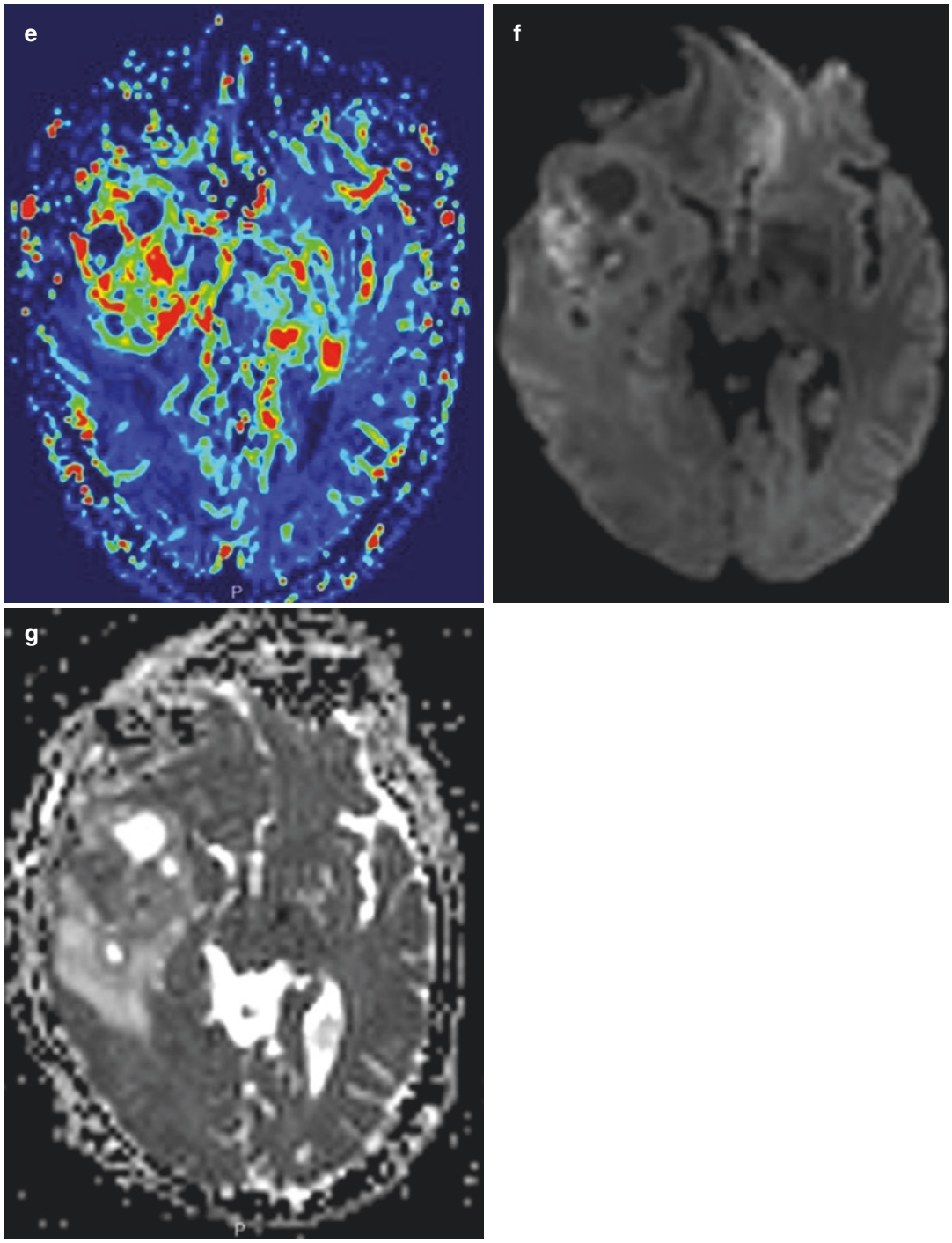

Fig. 13.5 (continued)

13.5.2 Epidemiology

There are two types of glioblastomas:

- Glioblastoma, IDH-wild type (90% of cases), which corresponds with the clinically defined primary glioblastoma and occurs in patients over 55 years of age
- Glioblastoma, IDH-mutant (10% of cases), which corresponds to secondary glioblastoma with a history of prior lower grade diffuse glioma and usually affect younger patients

13.5.3 Pathology and Genetics

- Glioblastoma, IDH-wild type. IDH negative, related to poor prognosis. MGMT methylation (60%). TERT promoter mutations (72%). TP53 mutations (27%). ATRX mutations (exceptional). EGFR amplification (35%). PTEN mutations (24%)
- Glioblastoma, IDH-mutant. IDH positive, related to better prognosis. MGMT methylation (80%). TERT promoter mutations (26%). TP53 mutations (81%). ATRX mutations (71%). EGFR amplification (exceptional). PTEN mutations (exceptional)

13.5.4 Clinical Management

After a complete surgical resection, the patient received standard treatment with temozolomide (TMZ) and radiation therapy.

The **Stupp protocol** (radiotherapy plus temozolomide) has become standard of care for the treatment of these patients since it has led to significant survival improvements.

13.5.5 Imaging Findings and Differential Diagnosis

Glioblastomas are usually seen as a heterogeneous enhancing mass. They tend to be hypointense in T1WI and hyperintense in T2/FLAIR surrounded by vasogenic oedema and may have susceptibility artefact on SWI from blood products. Lower ADC values in solid areas are related with high-grade tumours. They show heterogeneous enhancement on contrast images, irregular and predominantly peripheral. Perfusion images show increased rCBV in solid enhancing areas. MR spectroscopy demonstrates increased Choline, lactate and lipids and decreased NAA and myoinositol.

Differential diagnosis includes cerebral metastasis, primary CNS lymphoma, cerebral abscess and tumefactive demyelination.

Take-Home Messages

- Glioblastomas are heterogeneous enhancing intra-axial masses with poor prognosis despite treatment

Further Reading

1. Louis DN, Perry A, Reifenberger G, von Deimling A, Figarella-Branger D, Cavenee WK, et al. The 2016 World Health Organization Classification of Tumors of the Central Nervous System: a summary. Acta Neuropathol. Springer Berlin Heidelberg; 2016; 131:803–820
2. Stupp R, Mason WP, van den Beuf MJ. Radiotherapy plus concomitant and adjuvant temozolomide for newly diagnosed glioblastoma. N Engl J Med. 2005; 352: 987–96
3. Perry JR, Laperriere N, O'Callaghan CJ, Brandes AA, Menten J, Phillips C, et al. Short-Course Radiation plus Temozolomide in Elderly Patients with Glioblastoma. N Engl J Med 2017; 376:1027–1037
4. Yamashita K, Hiwatashi A, Togao O, Kikuchi K, Hatae R, Yoshimoto K, et al. MR Imaging – Based Analysis of Glioblastoma Multiforme: Estimation of IDH1 Mutation Status. AJNR 2016; 37:58–65
5. Krex D, Klink B, Hartmann C, Von Deimling A, Pietsch T, Simon M, et al. Long-term survival with glioblastoma multiforme. Brain. 2007;130:2596–2606
6. Hilario A, Ramos A, Perez-Nuñez A, Salvador E, Millan JM, Lagares A, et al. The added value of apparent diffusion coefficient to cerebral blood volume in the preoperative grading of diffuse gliomas. Am J Neuroradiol. 2012; 33:701–707

13.6 Case 6

66-year-old female with left facial pain and hypoesthesia, swelling in the left malar region and left retro-orbital pressure for a month.

Biopsy was performed; the pathological diagnosis was gliosarcoma, Ki67 40%, WHO grade IV. Molecular and genetic features: Isocitrate dehydrogenase (IDH1)-wild-type, Methylguanine methyltransferase (MGMT) promoter methylation, ATRX wild-type, P53 negative, EGFR negative.

13.6.1 Images and Legends

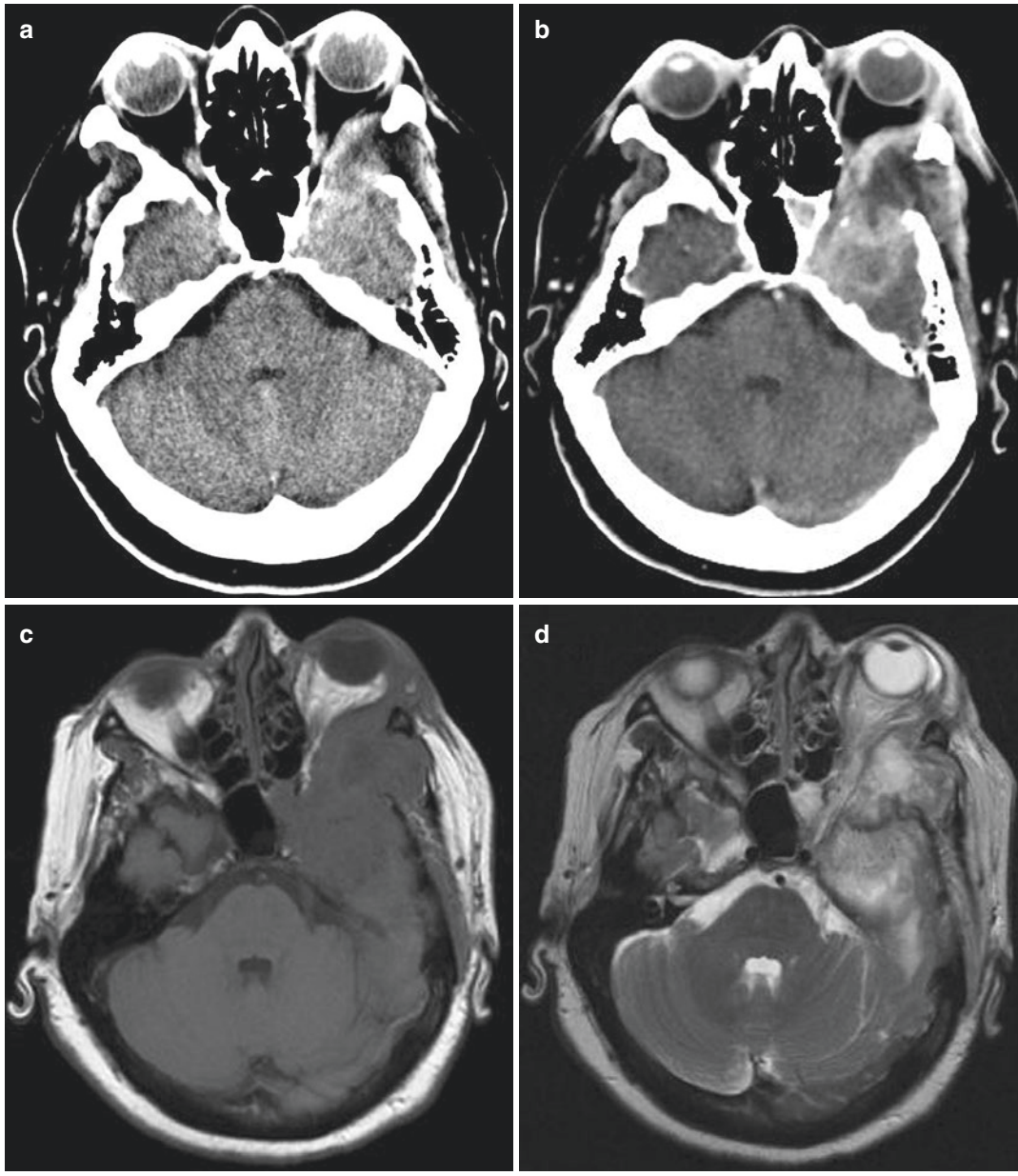

Fig. 13.6 (**a**) Axial non-contrast CT demonstrates a left temporal lobe mass destroying the greater wing of the sphenoid bone and invading into the orbit and the infratemporal fossa. (**b**) Axial contrast-enhanced CT better demonstrates the mass with heterogeneous enhancement. (**c**) Axial T1-weighted MRI demonstrated a heterogeneous hypointense mass involving the anterior left temporal lobe with left sphenoid bone destruction. (**d**) Axial T2-weighted MRI demonstrates the tumour to be heterogeneous isointense to brain cortex with central hyperintense areas of necrosis. (**e**) Contrast-enhanced axial T1-weighted MRI demonstrates heterogeneous enhancement with central necrosis intracranially. (**f**) Sagittal contrast-enhanced T1-weighted demonstrates heterogeneous enhancement in the anterior more solid part of the tumour and a posterior cystic component with an irregular rim of enhancement

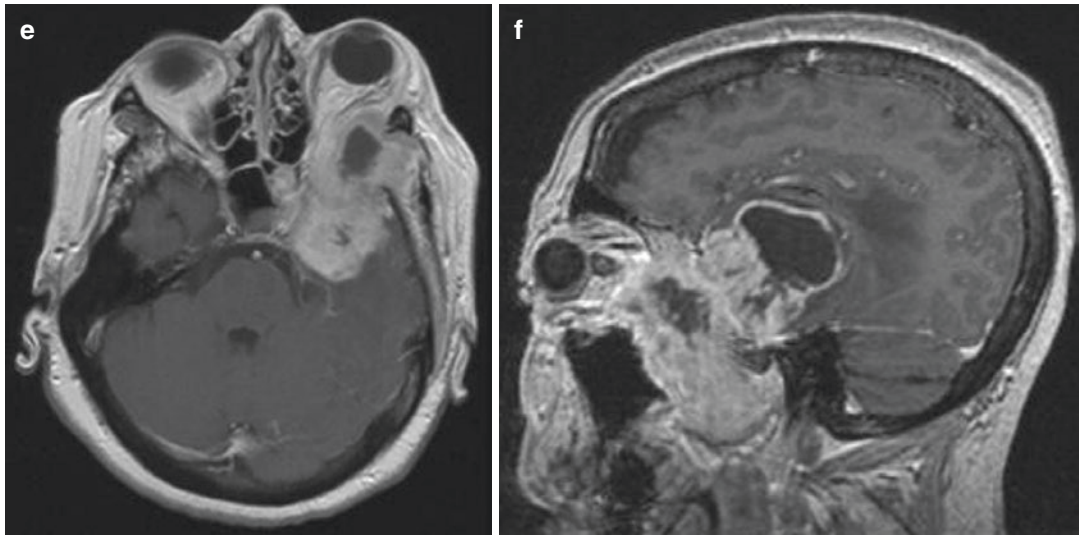

Fig. 13.6 (continued)

13.6.2 Epidemiology

Gliosarcomas represent 2% of the malignant primary glial tumours; they occur in the fifth to sixth decade of life, they are more frequently located in the temporal lobe.

Eleven percent of the cases present with haematogenous metastases, the most frequent sites are lung 72%, liver 41%, and lymph nodes 18%.

Skull base invasion is a rare feature, the mechanism o extradural and extracranial extension is not well understood, but it is thought to be by dural invasion.

13.6.3 Pathology and Genetics

Gliosarcoma is a rare central nervous system (CNS) tumour, characterised by a biphasic tissue pattern, with alternating areas of glial origin with mixed areas of malignant mesenchymal differentiation. The main prognostic factor is the predominance of the sarcomatous component with better prognosis in those cases.

13.6.4 Clinical Management

Gliosarcomas have similar clinical and radiological presentation as glioblastoma (GB) and an even poorer prognosis.

Chemotherapy and radiotherapy is the treatment of choice although there is a debate over the value of TMZ chemotherapy.

13.6.5 Imaging Findings and Differential Diagnosis

Gliosarcomas tend to show variable characteristics on Magnetic Resonance Images. They are generally hypointense on T1-weighted images and hyperintense on T2-weighted images in comparison to white matter, with marked peritumoural oedema. On contrast images they present heterogeneous enhancement, with intense peripheral or irregular ring and central necrosis or cystic changes. Perfusion images show increased rCBV in solid enhancing areas. On diffusion images the solid areas can depict decreased ADC values. MR

spectroscopy shows increased Cho and Lac values and decreased NAA and Cr values.

Differential diagnosis includes glioblastomas, meningiomas, embryonal tumours and brain abscesses.

Take-Home Messages

- Gliosarcomas are superficially located tumours with a dural base. The most common site is the temporal lobe

Further Reading

1. Sampaio L, Linhares P, Fonseca J. Detailed magnetic resonance imaging features of a case series of primary gliosarcoma. Neuroradiol J. 2017; 30:546–553
2. Yi X, Cao H, Tang H, Gong G, Hu Z, Liao W, Sun L, Chen BT, Li X. Gliosarcoma: a clinical and radiological analysis of 48 cases. Eur Radiol. 2019; 29:429–438
3. Kozak KR, Mahadevan A, Moody JS. Adult gliosarcoma: epidemiology, natural history, and factors associated with outcome. Neuro Oncol. 2009; 11:183–91
4. Zhang BY, Chen H, Geng DY, Yin B, Li YX, Zhong P, Wu JS, Wang XQ. Computed tomography and magnetic resonance features of gliosarcoma: a study of 54 cases. J Comput Assist Tomogr. 2011; 35:667–73
5. Han L, Zhang X, Qiu S, Li X, Xiong W, Zhang Y, Qu H, Chang R, Chen B, Wang W, Li S. Magnetic resonance imaging of primary cerebral gliosarcoma: a report of 15 cases. Acta Radiol. 2008; 49:1058–67

13.7 Case 7

40-year-old female with a 3-month history of gait disturbance, bilateral facial hypoesthesia and visual deficit.

The patient deteriorated rapidly, therefore surgical biopsy of the tumour was not feasible; no histopathological confirmation was possible.

Based on the imaging appearance, large infiltrating tumour, with areas of enhancement and necrosis, the diagnosis of diffuse midline glioma was made and the patient underwent treatment with radiotherapy and concomitant temozolomide.

13.7.1 Images and Legends

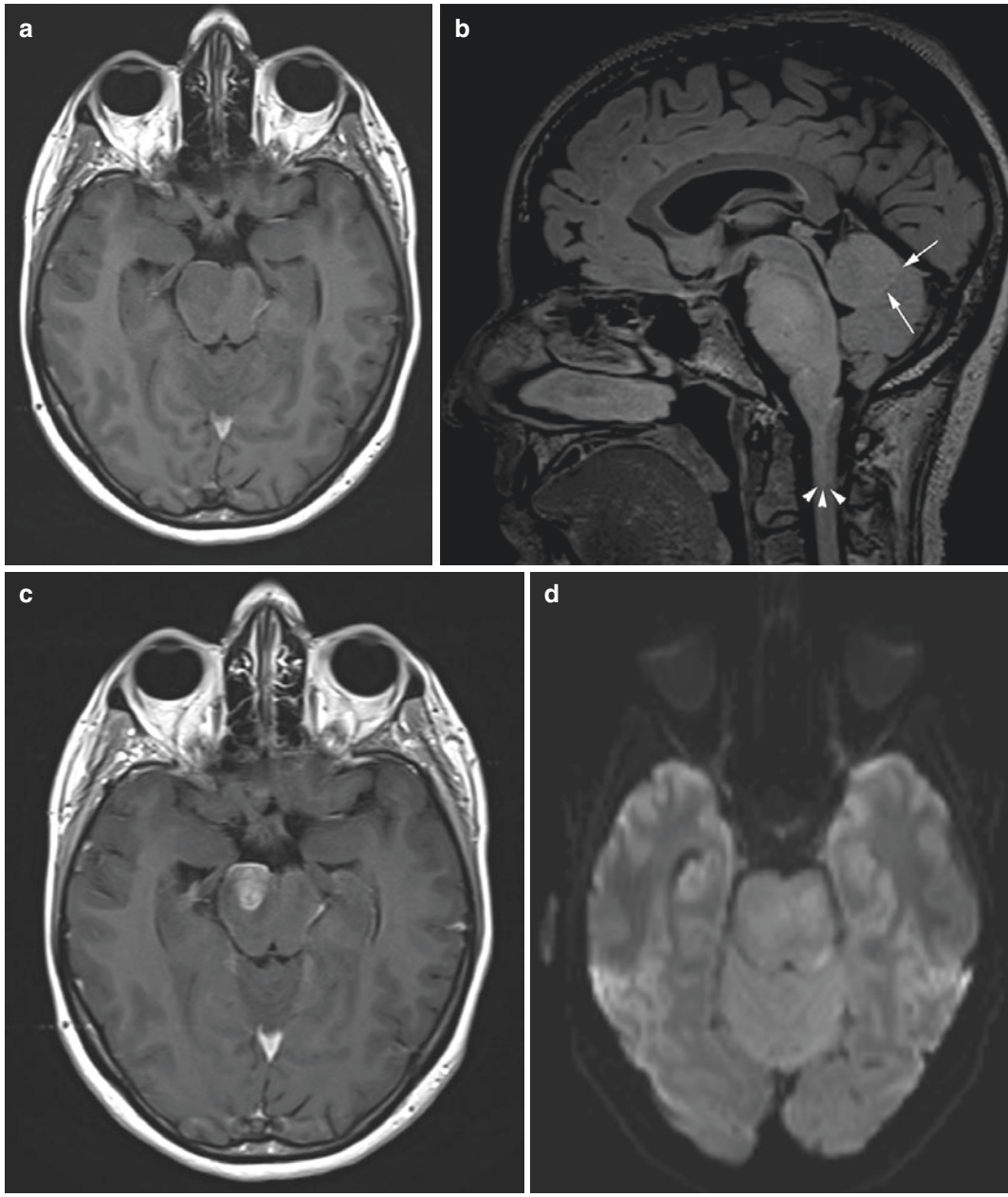

Fig. 13.7 (**a**) Axial T1-weighted MRI demonstrates a hypointense pontine mass with poorly defined margins. (**b**) Sagittal FLAIR MRI hyperintense shows the infiltrative expansile lesion involving the entire pons, vermis white arrows), caudal extension to the medulla (white arrowheads). (**c**) Contrast-enhanced axial T1-weighted image demonstrates a ringlike pattern of enhancement, suggesting central necrosis, on the right aspect of the pons, abutting the basilar artery. (**d**) Axial diffusion-weighted magnetic resonance imaging (DWI) the tumour demonstrates low signal on diffusion. (**e**) Apparent diffusion coefficient map (ADC). High ADC value is demonstrated within the tumour. (**f**) Dynamic susceptibility contrast-enhanced MR image. Relative cerebral blood volume (rCBV) colour map. Increased blood volume within the tumour. (**g**) ^{1}H-MR spectroscopy (TE 30 ms) shows an elevated choline (Ch) peak, reduced peak of N-acetyl aspartate (NAA) and elevated lipids and lactic acid peaks (lip-lac)

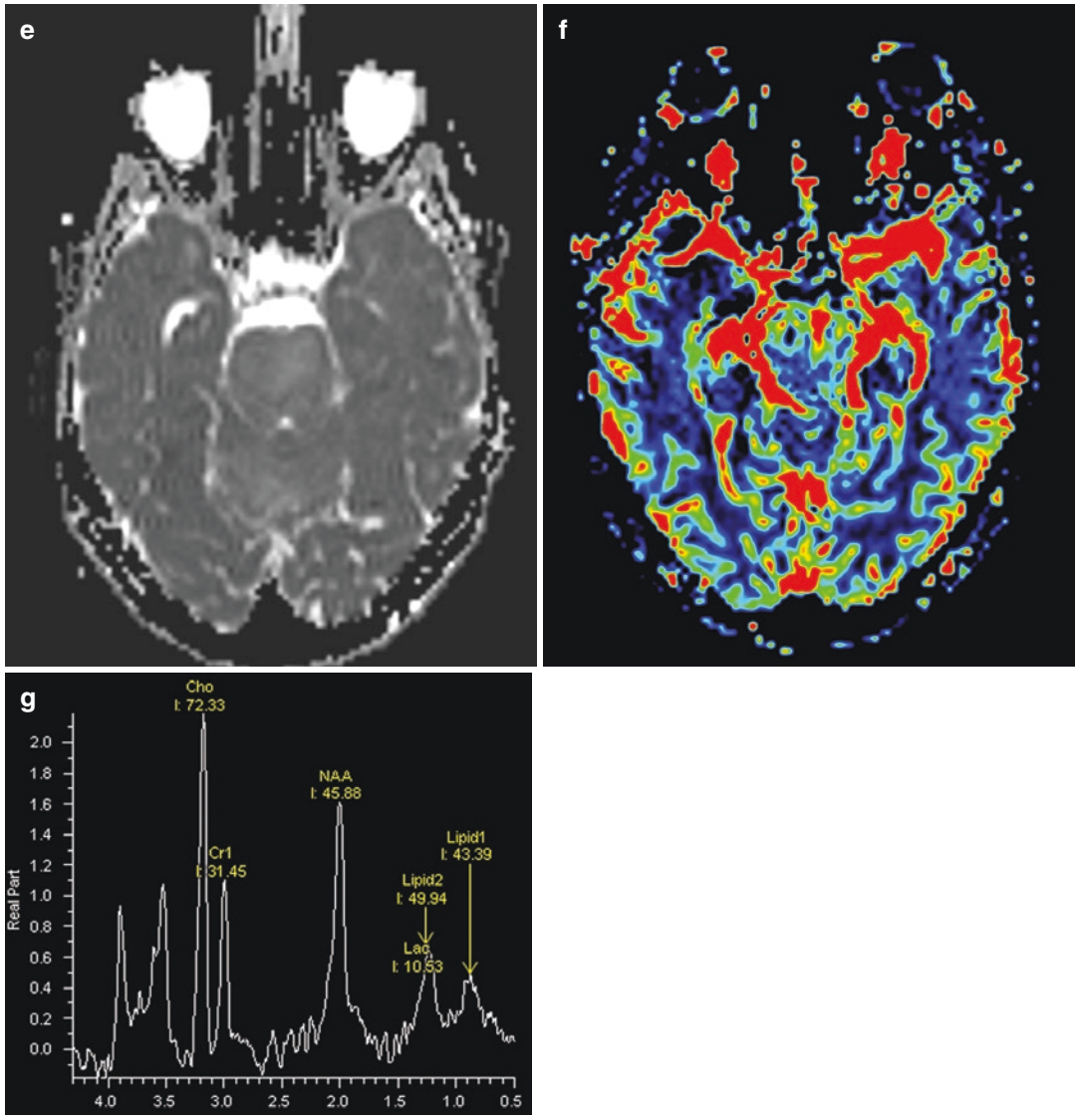

Fig. 13.7 (continued)

13.7.2 Epidemiology

Although brainstem tumours are more commonly encountered in children and represent 10% of all paediatric brain tumours, they represent only 1–2% of all brain tumours in adults.

Brainstem tumours are more frequently found in children, adult brainstem tumours represent 1–2% of all brain tumours in adults.

13.7.3 Pathology and Genetics

Based on the imaging features brain stem gliomas can be classified in four subgroups: diffuse intrinsic, low-grade brainstem gliomas involving>50% of the greatest dimension of the brainstem; focal, malignant brainstem gliomas; focal, tectal gliomas; and exophytically growing tumours.

In the revised 2016 World Health Organization classification, "Diffuse midline glioma, H3 K27M-mutant" is recognised as a distinct entity that corresponds to grade IV.

13.7.4 Clinical Management

These tumours occur in young adults in their third to fifth decade of life. The symptoms are insidious including gait disturbance, facial palsy, myasthenia, and cranial nerve deficits.

Radiotherapy is the standard treatment for adult brainstem gliomas, adjuvant chemotherapy is also used, although the role of chemotherapy remains unclear.

13.7.5 Imaging Findings and Differential Diagnosis

Diffusely infiltrating brainstem gliomas are characterised on MRI as ill-defined mass lesions T1-hypointense and T2-hyperintense with variable contrast enhancement. The presence of contrast enhancement within the tumour often is an indication of a higher pathologic grade and a worse prognosis.

Differential diagnosis includes demyelinating diseases, neuro-Behçet, lymphoma and sarcoidosis.

Take-Home Messages

- Diffuse midline gliomas present as infiltrating masses with expansion of the brainstem
- They depict increased signal on T2-weighted MRI sequences
- Frequently present contrast-enhancing areas with central necrosis

Further Reading

1. Aboian MS, Solomon DA, Felton E, Mabray MC, Villanueva-Meyer JE, Mueller S, Cha S. Imaging characteristics of pediatric diffuse midline gliomas with histone H3 K27 M mutation. AJNR 2017; 38:795–800
2. Louis DN, Perry A, Reifenberger G, von Deimling A, Figarella-Branger D, Cavenee WK, Ohgaki H, Wiestler OD, Kleihues P, Ellison DW. The 2016 World Health Organization Classification of Tumors of the Central Nervous System: a summary. Acta Neuropathol. 2016; 131:803–20
3. Eisele SC, Reardon DA. Adult Brainstem Gliomas. Cancer 2016; 122:2799–809
4. Donaldson SS, Laningham F, Graham Fisher PG. Advances Toward an Understanding of Brainstem Gliomas. J Clin Oncol 2006; 1266–1272
5. Purohit B, Kamli AA, Kollias SS. Imaging of adult brainstem gliomas. Eur J Radiol. 2015; 84:709–20

13.8 Case 8

45-year-old female presenting to the emergency room with generalised tonic-clonic seizure after a gustatory aura. The patient presented prior episodes of gustatory and olfactory sensations. She refers a yearlong period of fluctuating headache.

Patient underwent near complete total resection of the right frontal part of the tumour, no further treatment was implemented. She continues under close surveillance.

Histology revealed an oligodendroglioma WHO grade II. Molecular and genetic features: Isocitrate dehydrogenase (IDH1)-mutant, 1p/19q codeleted and P53 negative.

13.8.1 Images and Legends

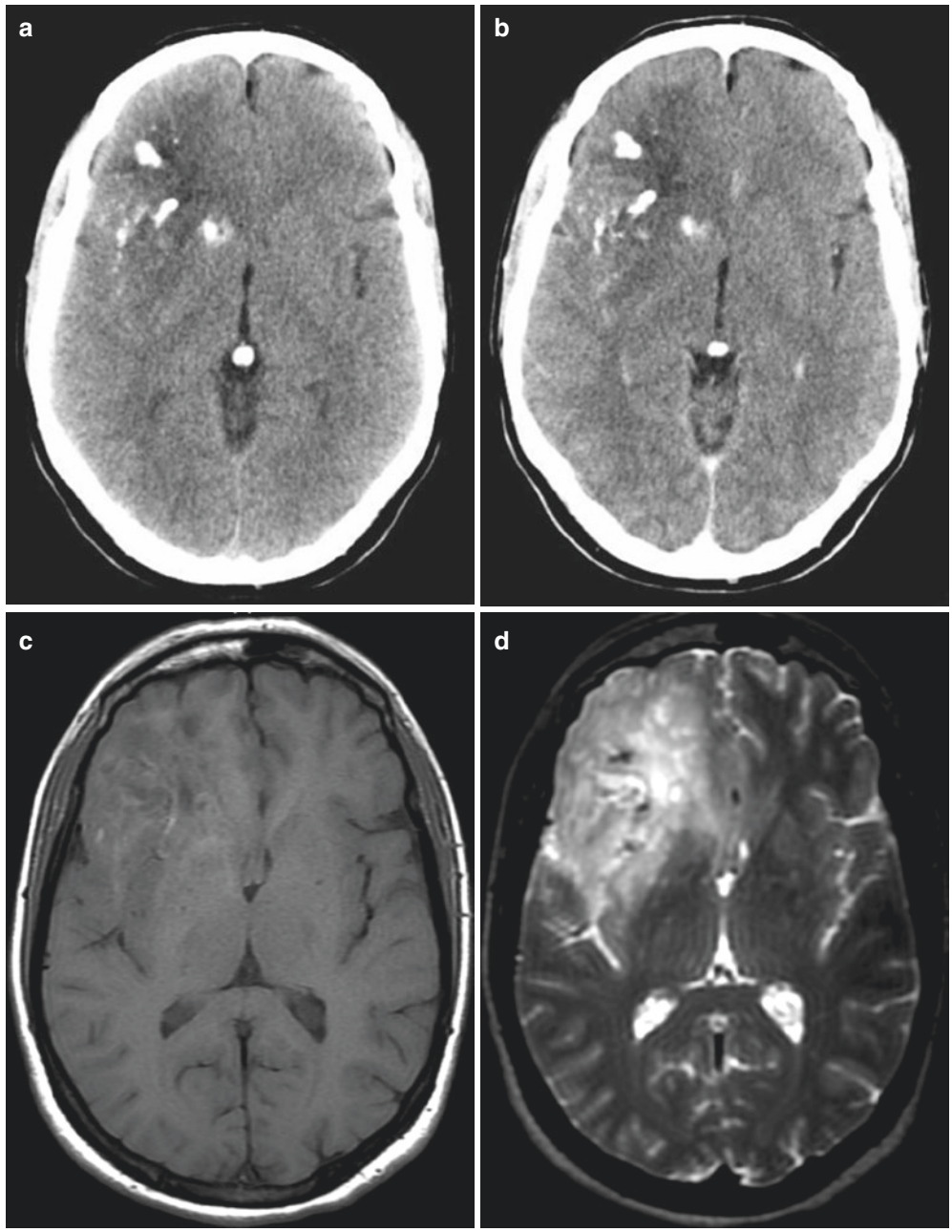

Fig. 13.8 (**a**) Axial non-enhanced brain CT demonstrates a large ill-defined, hypoattenuating frontal mass with coarse calcifications. (**b**) Axial contrast-enhanced CT demonstrating the same features with no areas of enhancement within the tumour. (**c**) Axial T1-weighted MRI shows a large right frontal mass with poorly defined borders and internal heterogeneity with some linear high signal intensity areas. (**d**) Axial T2-weighted MRI shows the mass predominantly hyperintense with internal heterogeneity and mass effect abutting the frontal horn of the right ventricle. (**e**) Axial FLAIR MRI better demonstrates the wide involvement in the cortex and subcortical white matter in the frontal and insular lobes extending through the genu of the corpus callosum into the left frontal lobe. (**f**) Contrast-enhanced axial T1-weighted image shows scattered areas of faint enhancement within the tumour. (**g**) Axial diffusion-weighted magnetic resonance imaging (DWI) shows low signal intensity of the mass. (**h**) Apparent diffusion coefficient map (ADC). The tumour shows high ADC value, indicating absence of restricted water diffusion. (**i**) Dynamic susceptibility contrast-enhanced MR image. Relative cerebral blood volume (rCBV) colour map. The tumour shows mildly increased rCBV. (**j**) ^{1}H-MR spectroscopy (TE 135 ms) shows a slightly elevated choline (Ch) peak and reduced peak of N-acetyl aspartate (NAA)

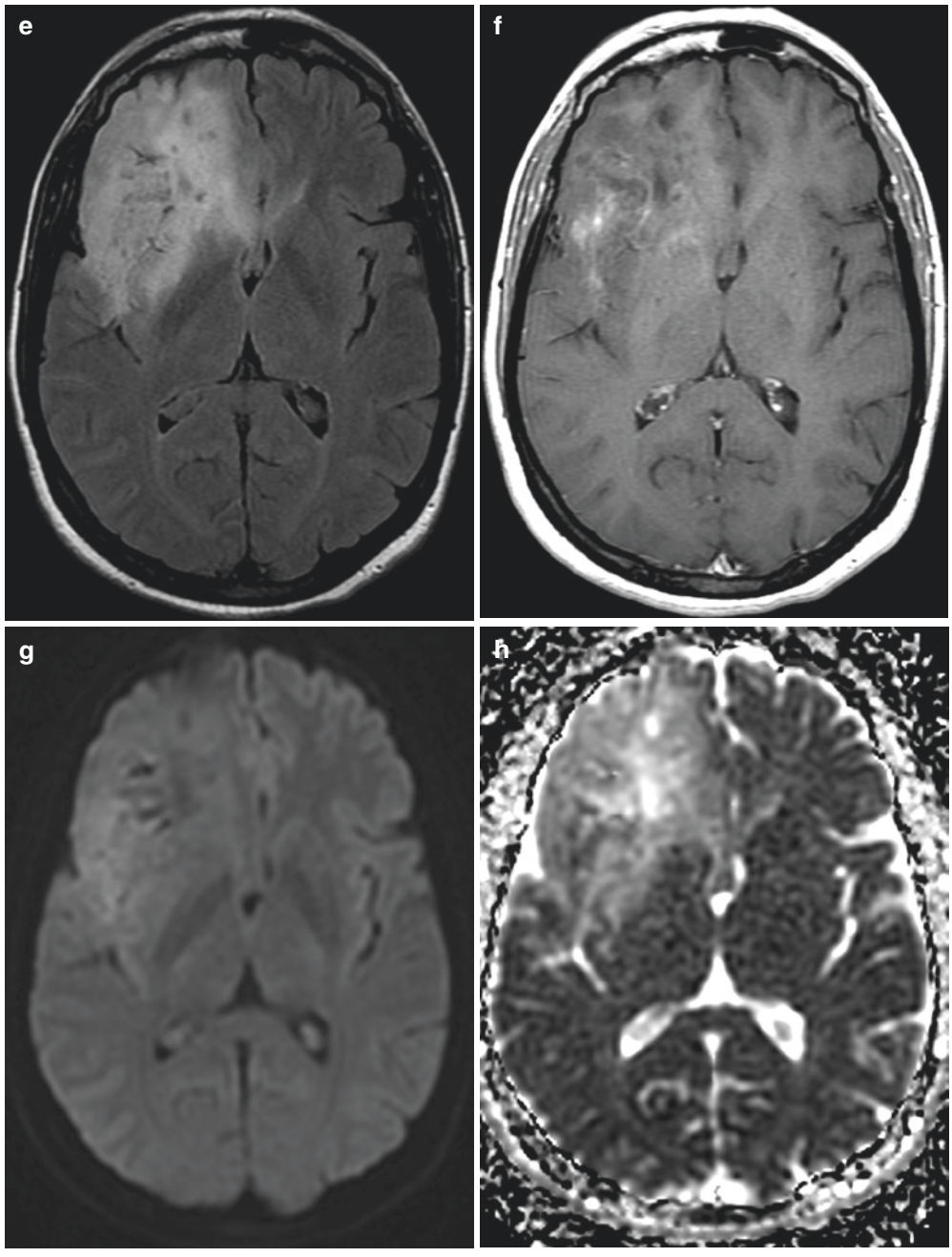

Fig. 13.8 (continued)

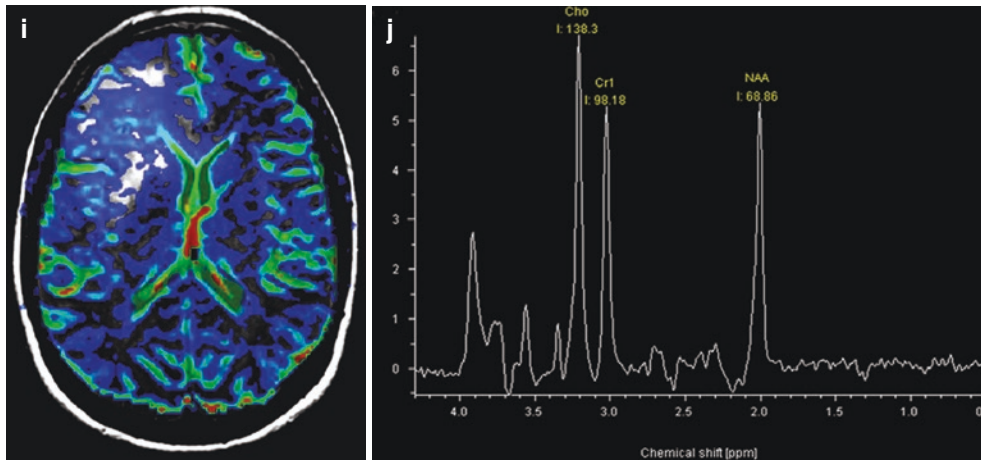

Fig. 13.8 (continued)

13.8.2 Epidemiology

Oligodendroglioma is the third most common glioma it accounts for 5–20% of all glial tumours. They occur predominantly in adults; with a peak between 40 and 60 years, males are more commonly affected. Seizure activity is the most common clinical presentation.

13.8.3 Pathology and Genetics

Oligodendrogliomas are defined as IDH-mutant and 1p/19q-codeleted grade II tumours by the 2016 WHO classification.

13.8.4 Clinical Management

Surgical resection and gross total resection is the principal form of therapy in oligodendrogliomas.

13.8.5 Imaging Findings and Differential Diagnosis

Frontal lobe location (50% of the cases), cortical involvement and calcification are common among low-grade oligodendrogliomas, mucoid or cystic degeneration are also frequently found. The temporal lobe is the second most common location.

On imaging oligodendrogliomas usually are hypointense compared to grey matter on T1-weighted images and hyperintense compared to grey matter on T2-weighted images, with heterogeneous signal intensity within the tumour. Vasogenic oedema surrounding the tumour is not commonly seen. Low-grade oligodendrogliomas usually do not enhance after contrast administration, some cases may depict minimal, multifocal enhancement with a dot-like or lacy pattern.

Oligodendrogliomas may have markedly elevated rCBV even when low-grade, elevated rCBV does therefore not necessarily indicate high-grade tumour in oligodendroglioma.

Low-grade oligodendroglioma shows moderately elevated Cho and decreased NAA without a lactate peak.

Take-Home Messages

- Cortical grey matter involvement, frontal lobe location and calcifications are highly distinctive features in oligodendrogliomas
- Oligodendroglioma might have markedly elevated rCBV even low grade ones; this finding is attributed to the presence of the short capillary segments in oligodendroglioma

Further Reading

1. Lin Y, Xing Z, She D, Yang X, Zheng Y, Zebin Xiao Z, Wang X, Dairong Cao D. IDH mutant and 1p/19q co-deleted oligodendrogliomas: tumor grade stratification using diffusion-, susceptibility-, and perfusion-weighted MRI. Neuroradiology 2017; 59:555–562
2. Fellah S, Caudal D, De Paula AM, Dory-Lautrec P, Figarella-Branger D, Chinot O, Metellus P, Cozzone PJ, Confort-Gouny S, Ghattas B, Callot V, Girard N. Multimodal MR Imaging (Diffusion, Perfusion, and Spectroscopy): Is it possible to distinguish oligodendroglial tumor grade and 1p/19q codeletion in the pretherapeutic diagnosis?. AJNR 2013; 34:1326–33
3. Johnson DR, Diehn FE, Giannini C, Jenkins RB, Jenkins SM, Parney IF, Kaufmann TJ. Genetically Defined Oligodendroglioma Is Characterized by Indistinct Tumor Borders at MRI. AJNR 2017; 38:678–684
4. Smits M. Imaging of oligodendroglioma. Br J Radiol 2016; 89: 20150857
5. Koeller KK, Rushing EJ. From the archives of the AFIP: Oligodendroglioma and its variants: radiologic-pathologic correlation. Radiographics. 2005; 25:1669–88

13.9 Case 9

45-year-old female with seizures.

Biopsy was performed; the pathological diagnosis was oligodendroglioma, Ki67 15%, WHO grade II. Molecular and genetic features: Isocitrate dehydrogenase (IDH1)-wild-type, ATRX positive (Wild-type), P53 negative. 1p19q codeletion positive. TERT mutation (c.-124 C > T).

13.9.1 Images and Legends

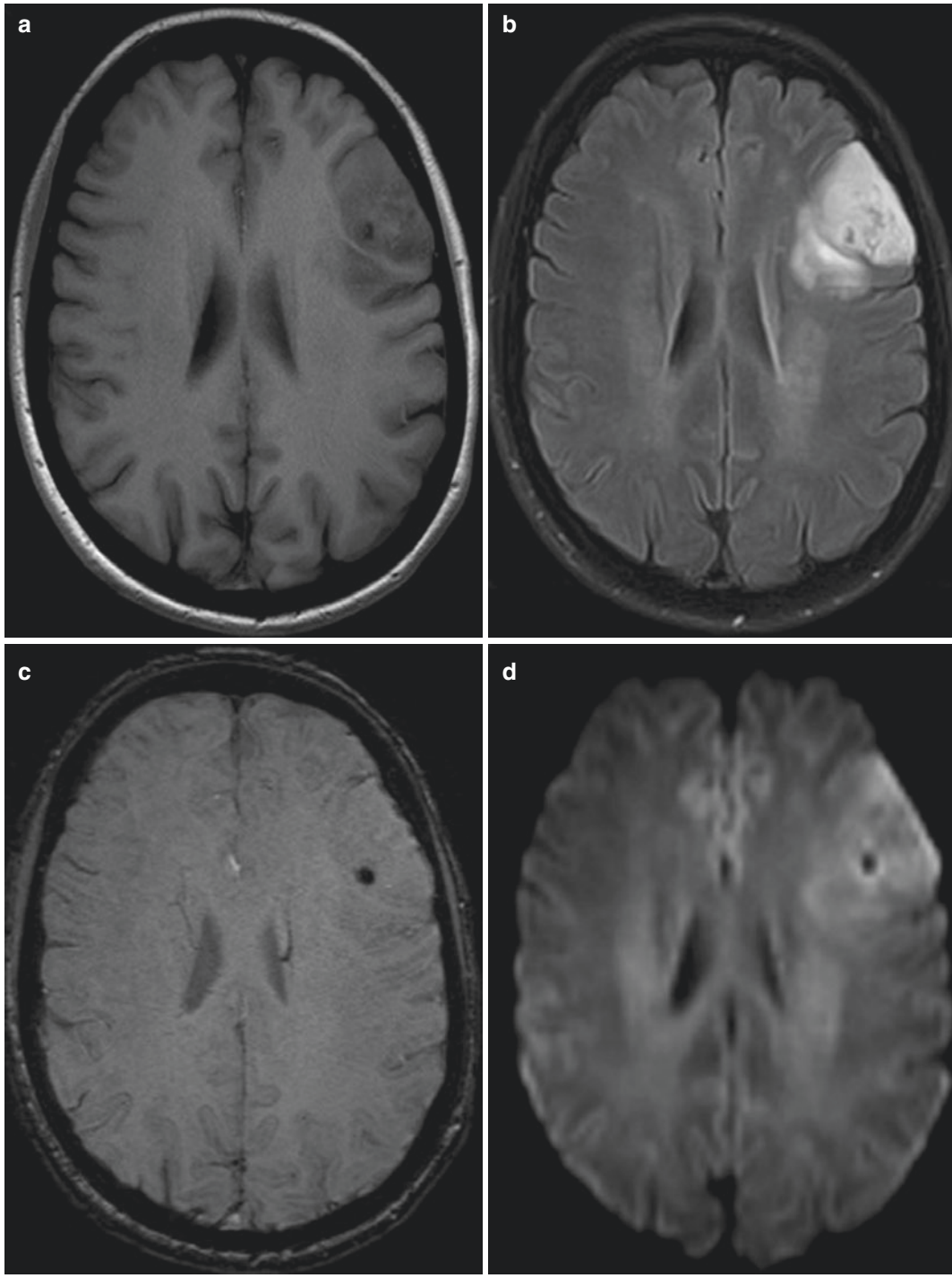

Fig. 13.9 (**a**) Axial T1-weighted MRI demonstrates an iso-hypointense solid mass involving the middle frontal gyrus. (**b**) Axial FLAIR MRI shows hyperintense heterogeneous solid mass with central hypointense areas surrounded by mild vasogenic oedema. (**c**) Axial SWI demonstrates susceptibility artefact inside the lesion from calcifications. (**d**) DTI demonstrates high signal in solid parts related to hypercellularity. (**e**) Low ADC values in solid enhancing areas. (**f**) MR perfusion shows rCBV elevated in solid enhancing regions of the tumour. (**g**) Contrast-enhanced axial T1-weighted MRI demonstrates heterogeneous mild enhancement. (**h**) MR spectroscopy shows increased Cho and decreased Cr and NAA

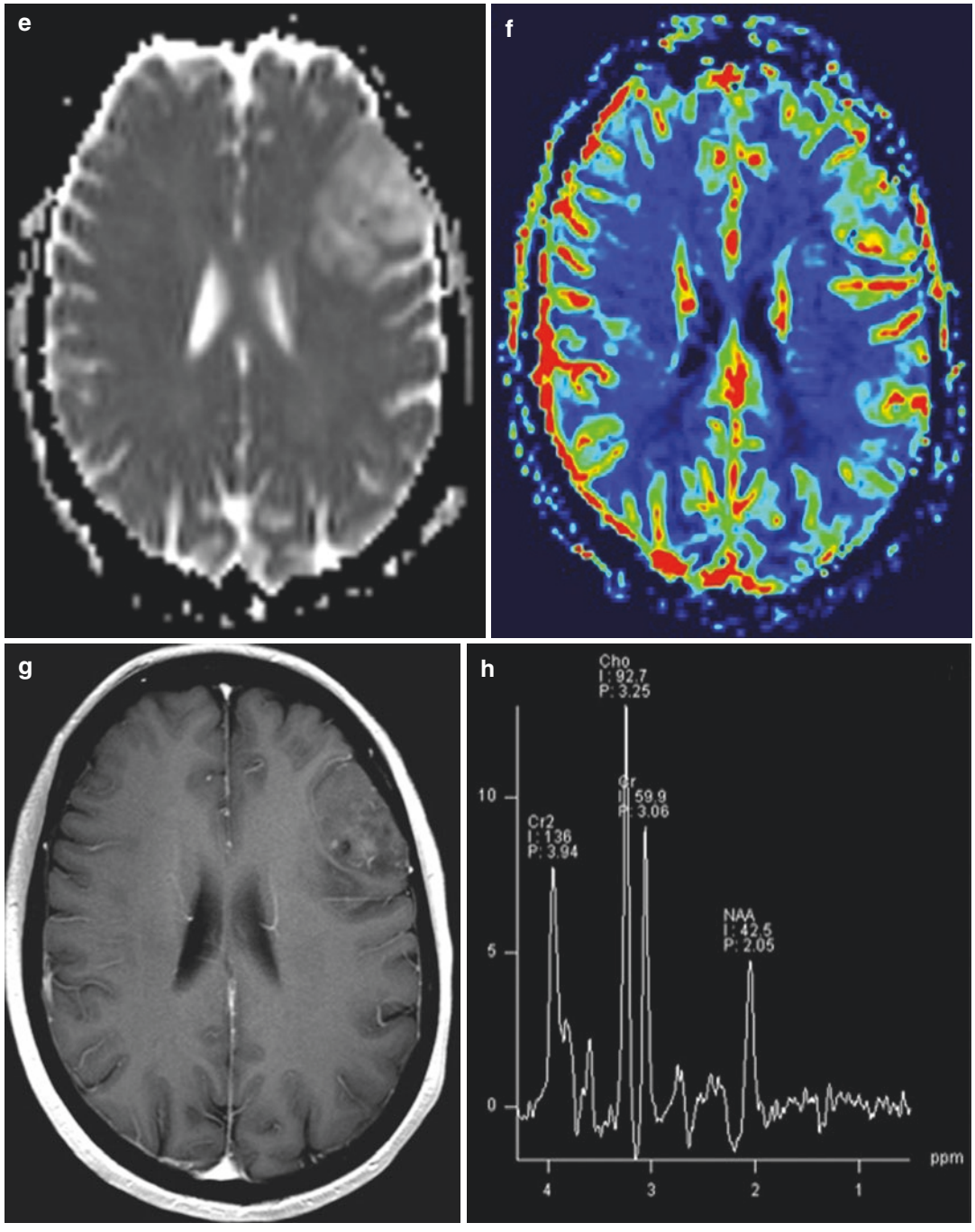

Fig. 13.9 (continued)

13.9.2 Epidemiology

Oligodendrogliomas are glial tumours more frequent in the fourth to fifth decade of life with slight male predilection. They account for 5–25% of all gliomas and 5–10% of all primary intracranial neoplasms.

13.9.3 Pathology and Genetics

The molecular hallmark of oligodendroglioma is codeletion 1p19q which is present in 60–90% of histopathologically diagnosed oligodendroglioma and have both diagnostic and prognostic value.

13.9.4 Clinical Management

The patient received surgical resection followed by radiotherapy plus chemotherapy (procarbazine + lomustine + vincristine).

The presence of 1p19q codeletion has prognostic and predictive relevance. Early chemotherapy + radiation therapy increases survival in patients with anaplastic oligodendroglioma compared with radiotherapy alone.

13.9.5 Imaging Findings and Differential Diagnosis

Oligodendrogliomas are usually well-circumscribed supratentorial cortical-based mass most commonly located in frontal lobes. They frequently appear hypointense in T1WI and hyperintense in T2/FLAIR with areas of signal loss/susceptibility artefact on SWI from calcifications and variable contrast enhancement.

Increased rCBV on perfusion-weighted imaging may be found in some low-grade oligodendrogliomas.

Signal heterogeneity, high rCBV and irregular borders of tumours are suggestive of the 1p/19q codeletion.

Differential diagnosis includes astrocytoma, ganglioglioma, dysembryoplastic neuroepithelial tumour (DNET) and pleomorphic xanthoastrocytoma.

Take-Home Messages

- Oligodendrogliomas are usually well-circumscribed supratentorial cortical-based mass most commonly located in the frontal lobes
- 1p/19q codeletion and IDH mutation are characterised by better prognosis and better response to chemotherapy

Further Reading

1. Fellah S, Caudal D, De Paula AM, Dory-Lautrec P, Figarella-Branger D, Chinot O, Metellus P, Cozzone PJ, Confort-Gouny S, Ghattas B, Callot V, Girard N. Multimodal MR imaging (diffusion, perfusion, and spectroscopy): is it possible to distinguish oligodendroglial tumor grade and 1p/19q codeletion in the pretherapeutic diagnosis? AJNR 2013; 34:1326–1333
2. Dumrongpisutikul N, Intrapiromkul J, Bonekamp D, Barker PB. Imaging Characteristics of Oligodendrogliomas. AJNR 2012; 33:1–6
3. Bourdillon P, Hlaihel C, Guyotat J, Guillotton L, Honnorat J, Ducray F, Cotton F. Prediction of anaplastic transformation in low-grade oligodendrogliomas based on magnetic resonance spectroscopy and 1p/19q codeletion status. J Neurooncol. 2015; 122:529–37
4. Spampinato MV, Smith JK, Kwock L, Ewend M, Grimme JD, Camacho DLA, et al. Cerebral blood volume measurements and proton MR spectroscopy in grading of oligodendroglial tumors. AJR 2007; 188:204–2012
5. Jenkinson MD, du Plessis DG, Smith TS, Joyce KA, Warnke PC, Walker C. Histological growth patterns and genotype in oligodendroglial tumours: correlation with MRI features. Brain. 2006; 129:1884–1891

13.10 Case 10

37-year-old man with headache, started several months ago.

Biopsy was performed; the pathological diagnosis was pilocytic astrocytoma, WHO grade I.

13.10.1 Images and Legends

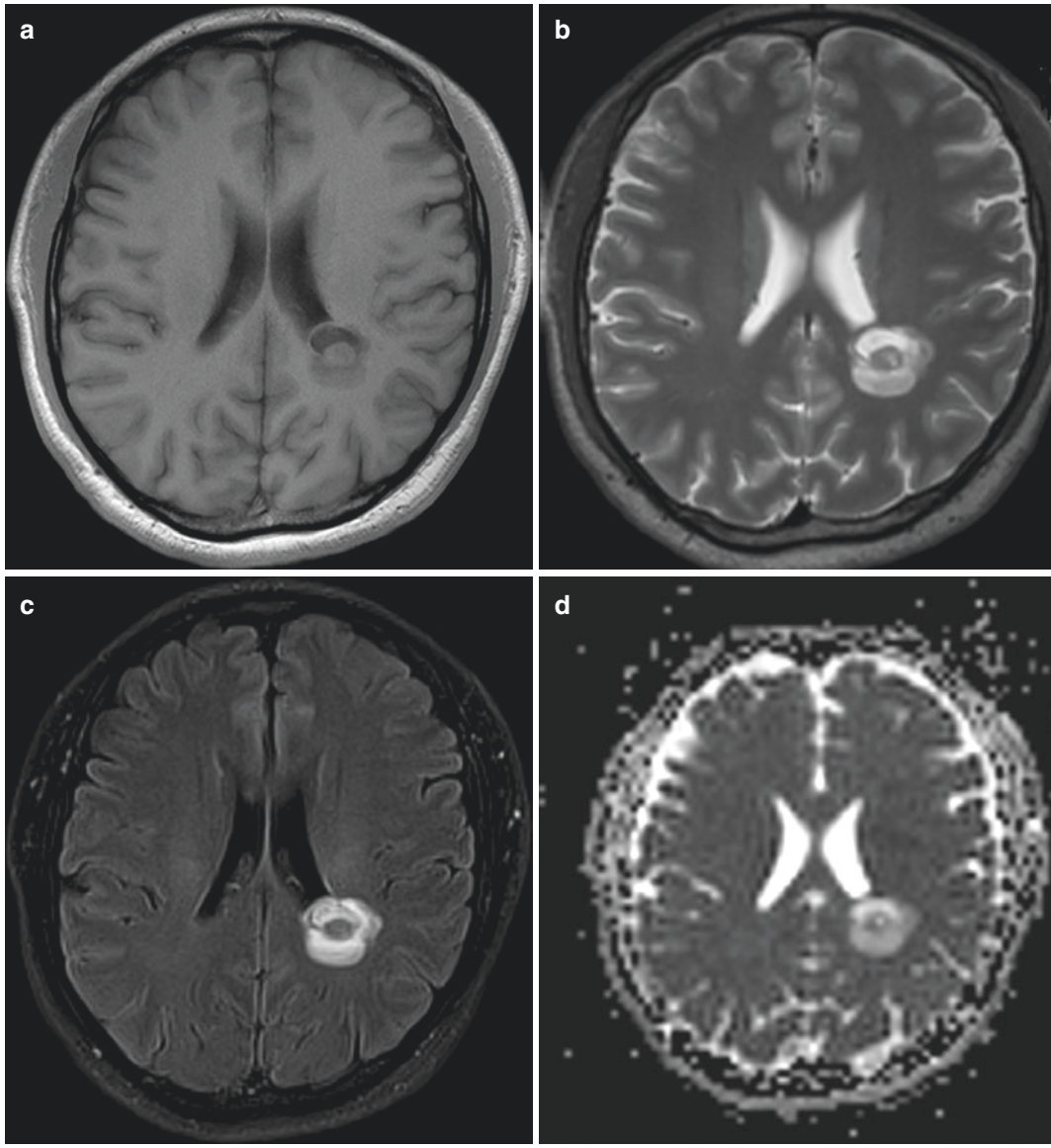

Fig. 13.10 (**a**) Axial T1-weighted MRI demonstrates a well-defined cystic mass with a hypointense peripheral nodule, adjacent to the occipital horn of the left lateral ventricle. (**b**) Axial T2WI demonstrates the solid and cystic components of the mass. No vasogenic oedema is seen. (**c**) FLAIR MRI shows the hyperintense solid nodule and the fluid signal cystic component. (**d**) Axial ADC map shows high signal with exception of the central nodule. (**e**) Axial SWI demonstrates small foci of signal loss that may be due to calcifications or haemorrhage. (**f**) Contrast-enhanced axial T1-weighted MRI demonstrates vivid enhancement in central nodule

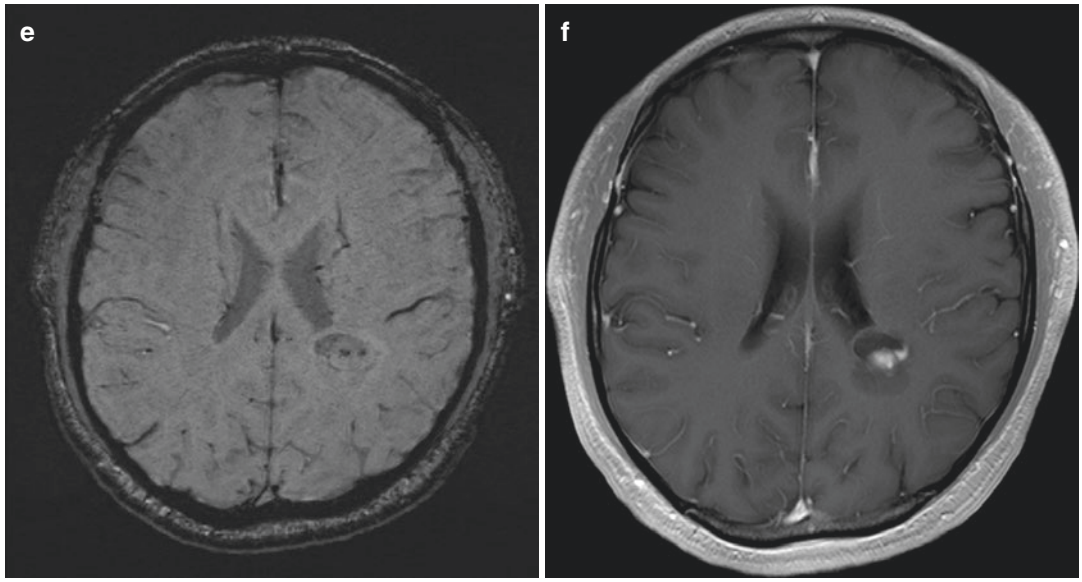

Fig. 13.10 (continued)

13.10.2 Epidemiology

Pilocytic astrocytomas tend to occur in young adults (first two decades of life), typically at 9–10 years.

They are the most common primary brain tumour of childhood and the most common paediatric cerebellar tumour (70–85% of all cerebellar astrocytomas).

13.10.3 Pathology and Genetics

The most common location is the cerebellum followed by the optic pathway, particularly in patients with NF1.

They frequently have BRAF alterations (about 70% of cases) and lack IDH and TP53 mutations.

13.10.4 Clinical Management

After a complete surgical resection, the patient remains disease-free until now.

13.10.5 Imaging Findings and Differential Diagnosis

Mixed masses with hypointense in T1WI and hyperintense in T2WI solid component, which shows strong enhancement, and fluid signal cystic component. ADC map shows typically high signal.

Differential diagnosis includes pleomorphic xanthoastrocytoma, medulloblastoma, ependymoma, haemangioblastoma, cerebellar abscess and ganglioglioma.

Take-Home Messages

- PA are the most common intracranial tumours in childhood and the most common paediatric cerebellar tumour
- There are mixed masses with solid component that shows vivid enhancement and cystic component

Further Reading

1. Chourmouzi D, Papadopoulou E, Konstantinidis M, Syrris V, Kouskouras K, Haritanti A, et al. Manifestations of pilocytic astrocytoma: A pictorial review. Insights Imaging. 2014; 5:387–402
2. Murakami R, Hirai T, Kitajima M, Fukuoka H, Toya R, Nakamura H, et al. Magnetic resonance imaging of pilocytic astrocytomas: Usefulness of the minimum Apparent Diffusion Coefficient (ADC) value for differentiation from high-grade gliomas. Acta radiol. 2008; 49:462–7
3. Koeller KK, Rushing EJ. From the Archives of the AFIP. RadioGraphics 2004; 24:1693–1708

13.11 Case 11

46-year-old female with a previous history of chronic headaches and depression. The patient present left face myoclonus and focal epilepsy with posterior generalisation. Surgery was performed. The specimen showed an oligodendroglial cell population with cystic component and small gliosis in the periphery of the tumour. Ki67 lower than 1%, no IDH or p53 mutation is demonstrated. The sample was positive in GFAP immunochemistry stain. No mitosis, necrosis or perivascular proliferation is noted. Dysembryoplastic neuroepithelial tumour (DNET) was diagnosed.

13.11.1 Images and Legends

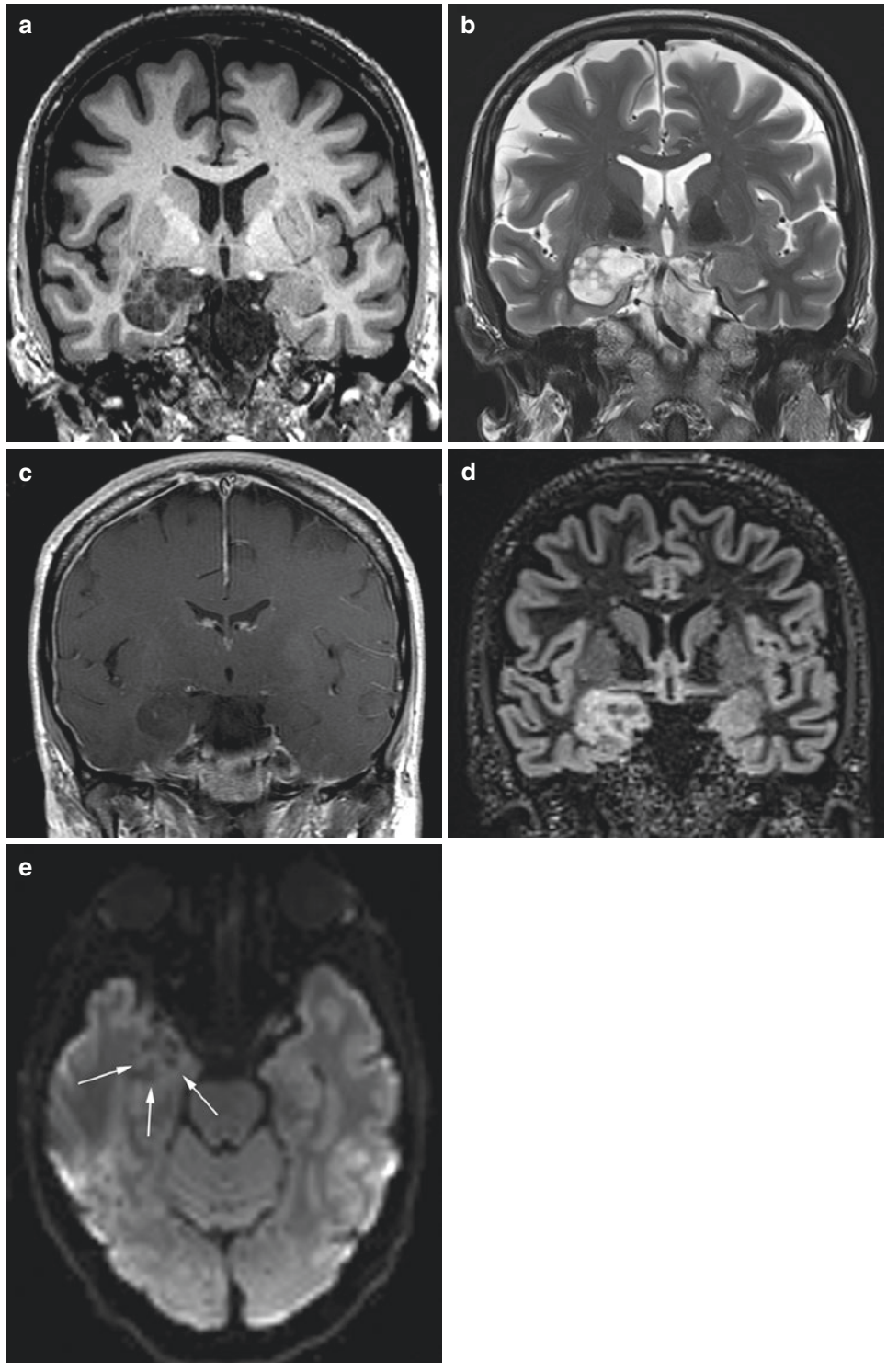

Fig. 13.11 (**a**) Coronal T1W MRI demonstrates a mass in the right hippocampus. (**b**) Coronal T2W MRI, the mass shows a multicystic "bubbly" appearance with cyst following the CSF signal and slight mass effect. (**c**) Coronal contrast-enhanced T1W MRI. No enhancement is noted in the lesion. (**d**) Coronal Double Inversion Recovery (DIR) MRI. High signal is noted in the lesion. There is a hyperintensity halo around the lesion. (**e**) Axial DWI MRI No restriction is demonstrated (arrows)

13.11.2 Epidemiology

DNET is juvenile or infantile tumour with a slight predilection in males.

13.11.3 Pathology and Genetics

DNET is a WHO I class tumour. It derivates from cortical grey matter and has a predilection for the temporal lobe. The characteristic pathologic feature is the Specific Glioneuronal Element (SGNE). There is association with focal cortical dysplasia. Intractable partial seizures are typical clinical debut.

DNETs are negative for IDH mutations, P53 mutations, and do not demonstrate 1p19q deletion. SGNE is positive for GFAP. Oligodendroglia inside the tumour shows S100 and OLIG2 positivity.

13.11.4 Clinical Management

DNET do not grow over time, however, seizures are usually intractable so surgery is warranted. Prognosis is excellent.

13.11.5 Imaging Findings and Differential Diagnosis

DNETs are cortical lesions with a "bubbly" appearance and cystic areas. Typically there is no enhancement. Susceptibility weighted images (SWI) or CT are very useful for demonstrating calcification of the lesion. No DWI restriction or rCBV hypervascularization is present. Temporal lobe is affected in over 50% of cases. Typical differentials are ganglioglioma, pleomorphic xanthoastrocytoma, oligodendroglioma and cystic lesions (neuroepithelial, choroid fissure).

Take-Home Messages

- Young patient with partial, persistent seizures and a temporal "bubbly" mass is typically a DNET

Further Reading

1. Takahashi A, Hong SC, Seo DW et al. Frequent association of cortical dysplasia in dysembryoplastic neuroepithelial tumor treated by epilepsy surgery. Surg Neurol. 2005; 64: 419–427
2. Makola M, Cecil KM. Dysembryoplastic neuroepithelial tumor (DNET) and focal cortical dysplasia: Case report of two pediatric patients with imaging features. International Journal of Diagnostic Imaging. 2017; 4:31
3. Isler C, Erturk Cetin O, Ugurlar D, Ozkara C, Comunoglu N, Kizilkilic O, Oz B, Kayadibi Y, Tanriverdi T, Uzan M. Dysembryoplastic neuroepithelial tumours: clinical, radiological, pathological features and outcome. British journal of neurosurgery. 2018; 23:1–6
4. Cosson RS, Varlet P, Beuvon F, Duport CD, Devaux B, Chassoux F, Fredy D, Meder JF. Dysembryoplastic neuroepithelial tumors: CT, MR findings and imaging follow-up: a study of 53 cases

13.12 Case 12

35-year-old male with a recent onset of seizures.

Biopsy was performed; the pathological diagnosis was Ganglioglioma, WHO grade I.

13.12.1 Images and Legends

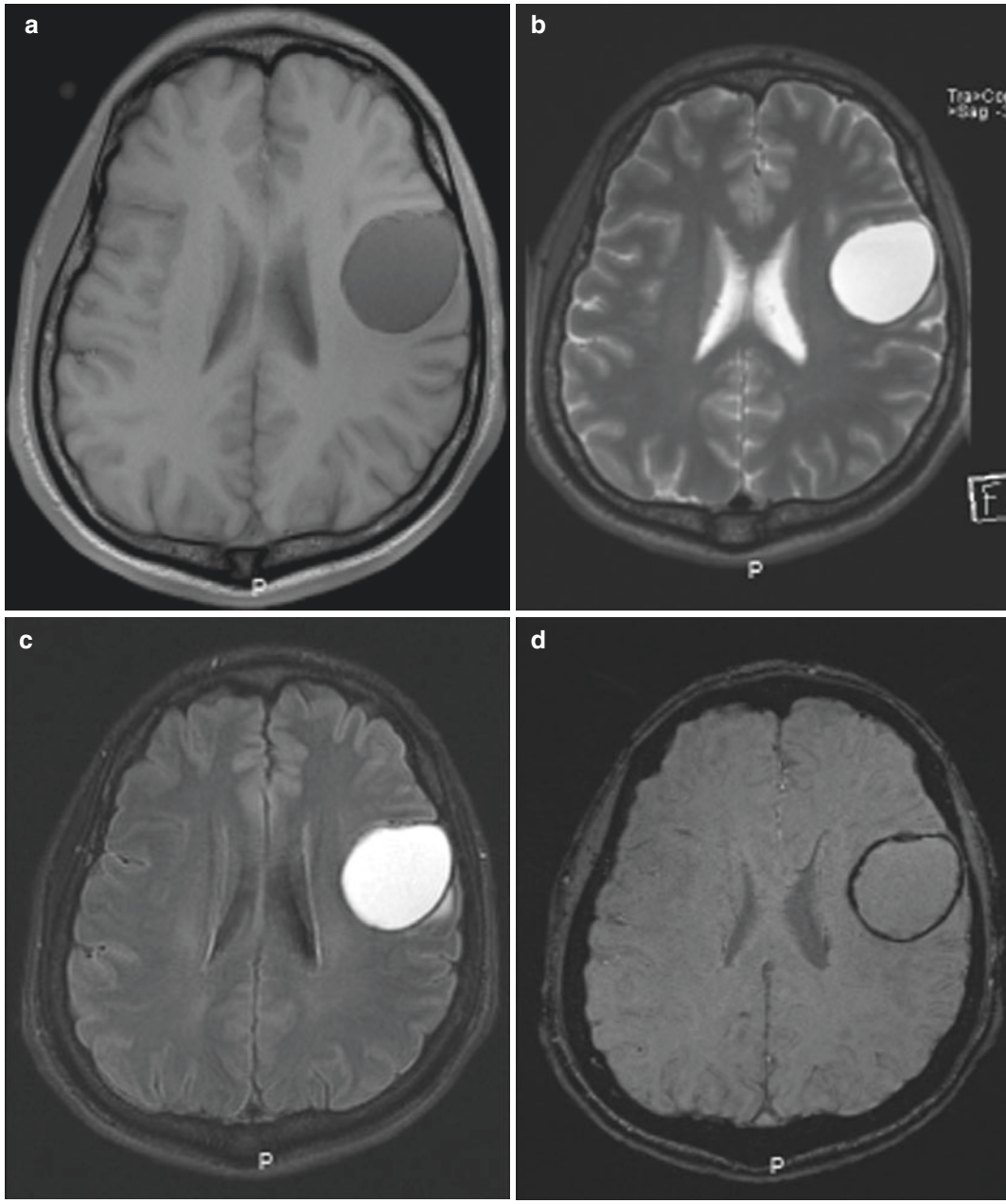

Fig. 13.12 (**a**) Axial T1-weighted MRI demonstrates a cortical-based hypointense mass in left frontal lobe surrounded by a hypointense thin rim. (**b**) Axial T2WI shows a fluid signal cystic mass in left frontal lobe. (**c**) Axial FLAIR MRI shows hyperintense content of the cystic lesion that could be related with high protein content. There is no vasogenic oedema. (**d**) Axial SWI demonstrates thin hypointense peripheral rim may be due to calcification. (**e**) Axial ADC map shows high signal within the mass. (**f**) Contrast-enhanced axial T1-weighted MRI demonstrates mild peripheral enhancement, which predominates in anterior part of the lesion. (**g**) Axial Non-Contrast CT scan confirms thin calcification of peripheral rim

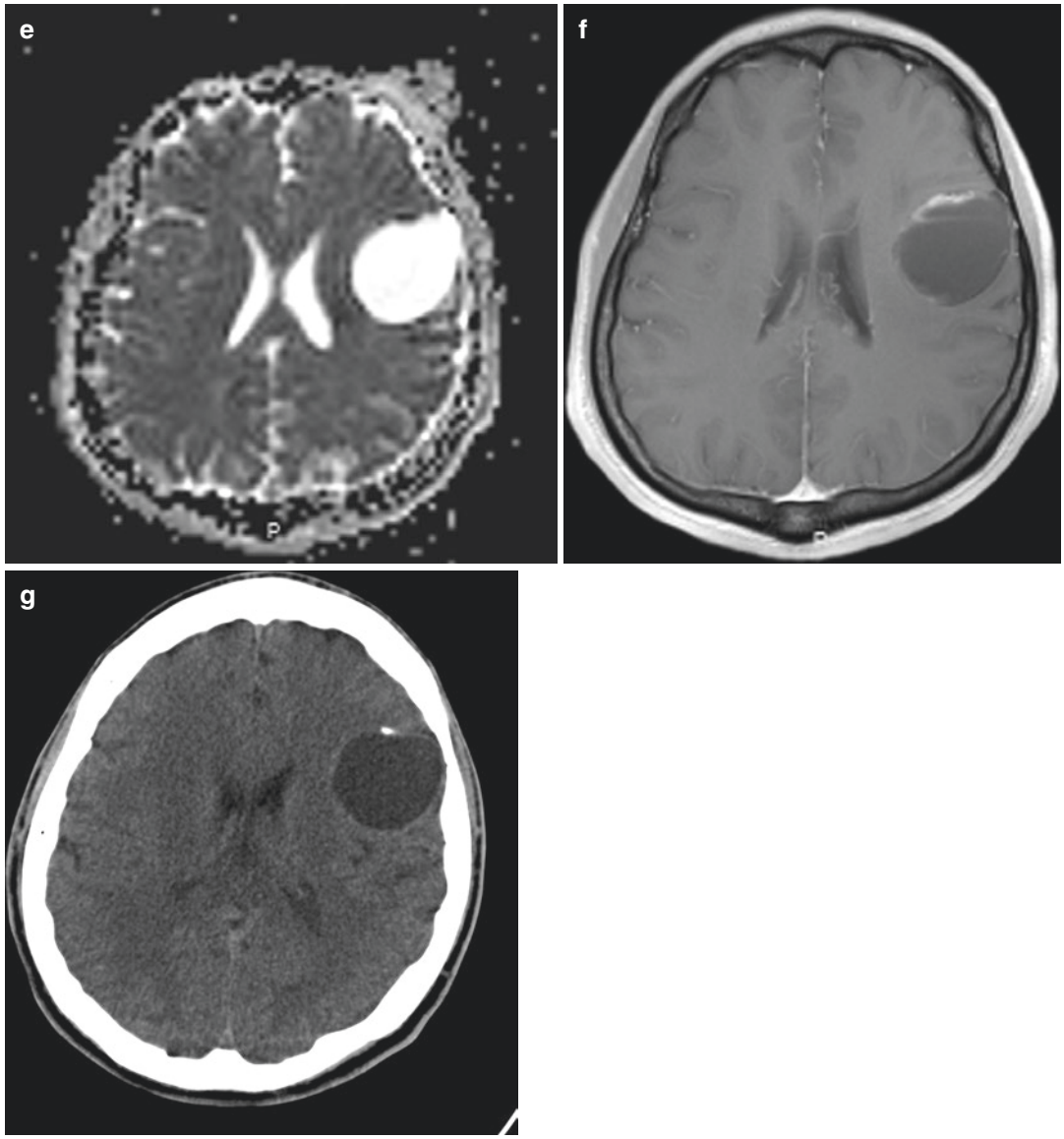

Fig. 13.12 (continued)

13.12.2 Epidemiology

These tumours represent 0.4–0.9% of all primary brain tumours in adults and about 10% of all primary brain tumours in children.

Most of gangliogliomas are found in infants or young individuals aged 8–31 years with no gender predominance.

13.12.3 Pathology and Genetics

The majority of them occur in temporal lobes and in the cerebellar hemispheres.

BRAF V600E mutations are found in 20–60% of cases. IDH negative.

13.12.4 Clinical Management

After a complete surgical resection, the patient remains disease-free until now.

13.12.5 Imaging Findings and Differential Diagnosis

Variable appearance on MRI. Predominantly cystic masses with variable signal in the cystic component in T2WI related to the amount of proteinaceous material or blood products. Iso to hypointense solid component in T1WI with variable contrast enhancement. Blooming signal loss in T2*/SWI due to calcified areas.

Differential diagnosis includes dysembryoplastic neuroepithelial tumours (DNET), pleomorphic xanthoastrocytoma, oligodendroglioma and desmoplastic infantile astrocytoma and ganglioglioma.

Take-Home Messages

- Tumours with peripheral location within cerebral hemispheres with predilection for temporal and frontal lobes and variable appearance on MRI

Further Reading

1. Castillo M. Gangliogliomas: Ubiquitous or not? Am J Neuroradiol. 1998; 19:807–809
2. Jong Won Kwon, Kim IO, Cheon JE, Woo Sun Kim, Je Geun Chi, Wang KC, et al. Cerebellopontine angle ganglioglioma: MR findings. Am J Neuroradiol. 2001; 22:1377–1379
3. Provenzale JM, Ali U, Barboriak DP, Kallmes DF, Delong DM, McLendon RE. Comparison of patient age with MR imaging features of gangliogliomas. AJR Am J Roentgenol. 2000; 174:859–862

13.13 Case 13

23-year-old male who consulted the emergency department for cervical pain, headache, confusion and general deterioration with walking difficulty.

Patient underwent surgery; the mass was attached to the tentorium and completely removed.

The pathological diagnosis was classic medulloblastoma with some areas of the desmoplastic variant, Ki67 30%, WHO grade IV. Molecular and genetic features: CD45, CD20, p53, CD99 and c-erbB2 negative.

The patient underwent radiotherapy after surgery.

13.13.1 Images and Legends

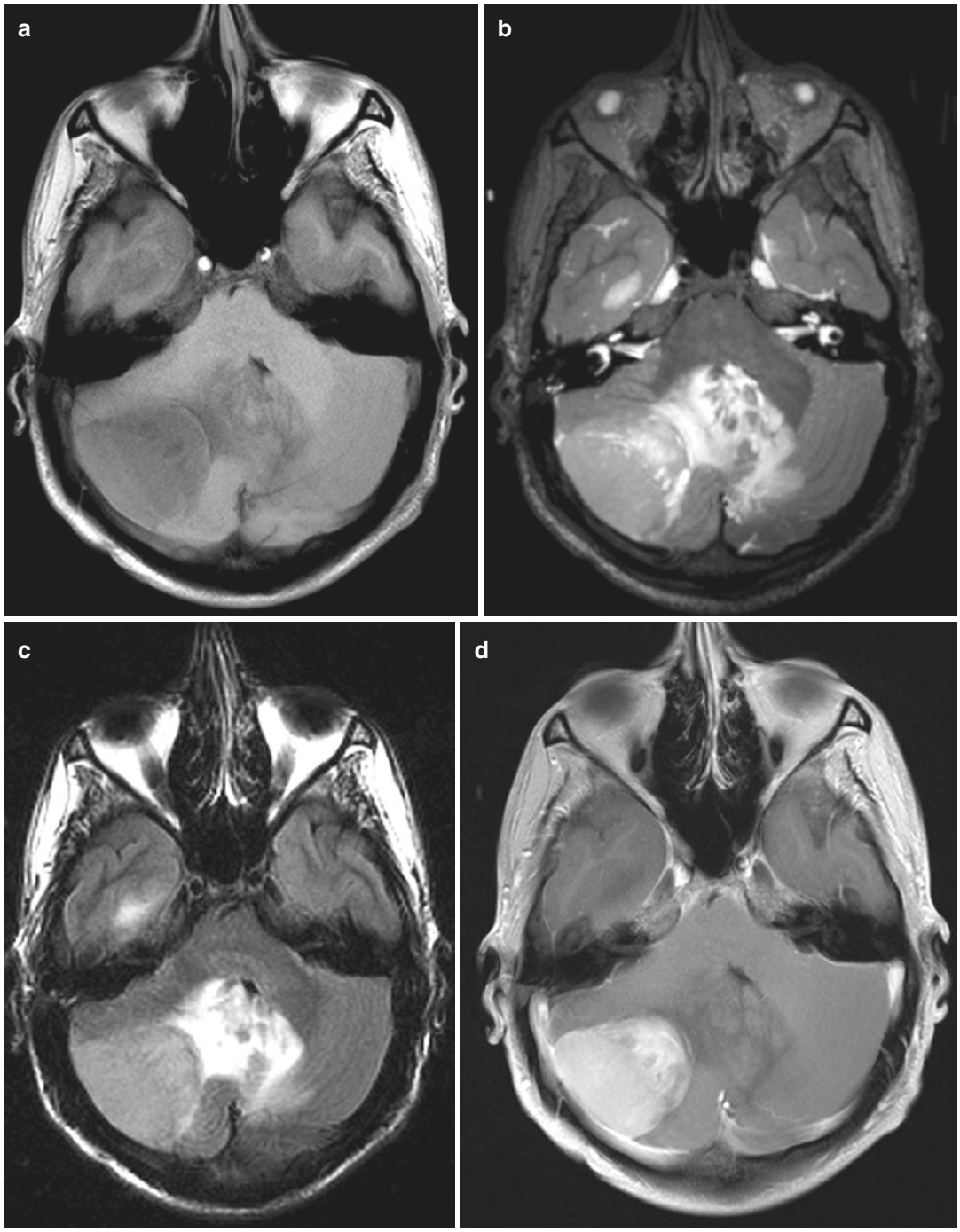

Fig. 13.13 (**a**) Axial T1-weighted MRI reveals a right cerebellar isointense, hemispheric mass. (**b**) Axial T2-weighted MRI. Heterogeneous mostly isointense mass with cysts and necrotic changes. (**c**) Axial FLAIR MRI demonstrating the mass, severe vasogenic oedema, midline shift and mass effect over the fourth ventricle. (**d**) Contrast-enhanced axial T1-weighted image shows a well-defined mass with heterogeneous enhancement. (**e**) Axial diffusion-weighted magnetic resonance imaging (DWI) shows increased diffusion signal due to water movement limitation. (**f**) Apparent diffusion coefficient map (ADC). The tumour demonstrates low ADC value, which reflects high cellular density. (**g**) Dynamic susceptibility contrast-enhanced MR image. Relative cerebral blood volume (rCBV) colour map. The tumour shows mainly a low rCBV, with some central areas with slightly increased rCBV. (**h**) ^{1}H-MR spectroscopy (TE 30 ms) shows an elevated choline (Ch) peak, reduced peak of N-acetyl aspartate (NAA) and elevated lipids and lactic acid peaks (lip-lac)

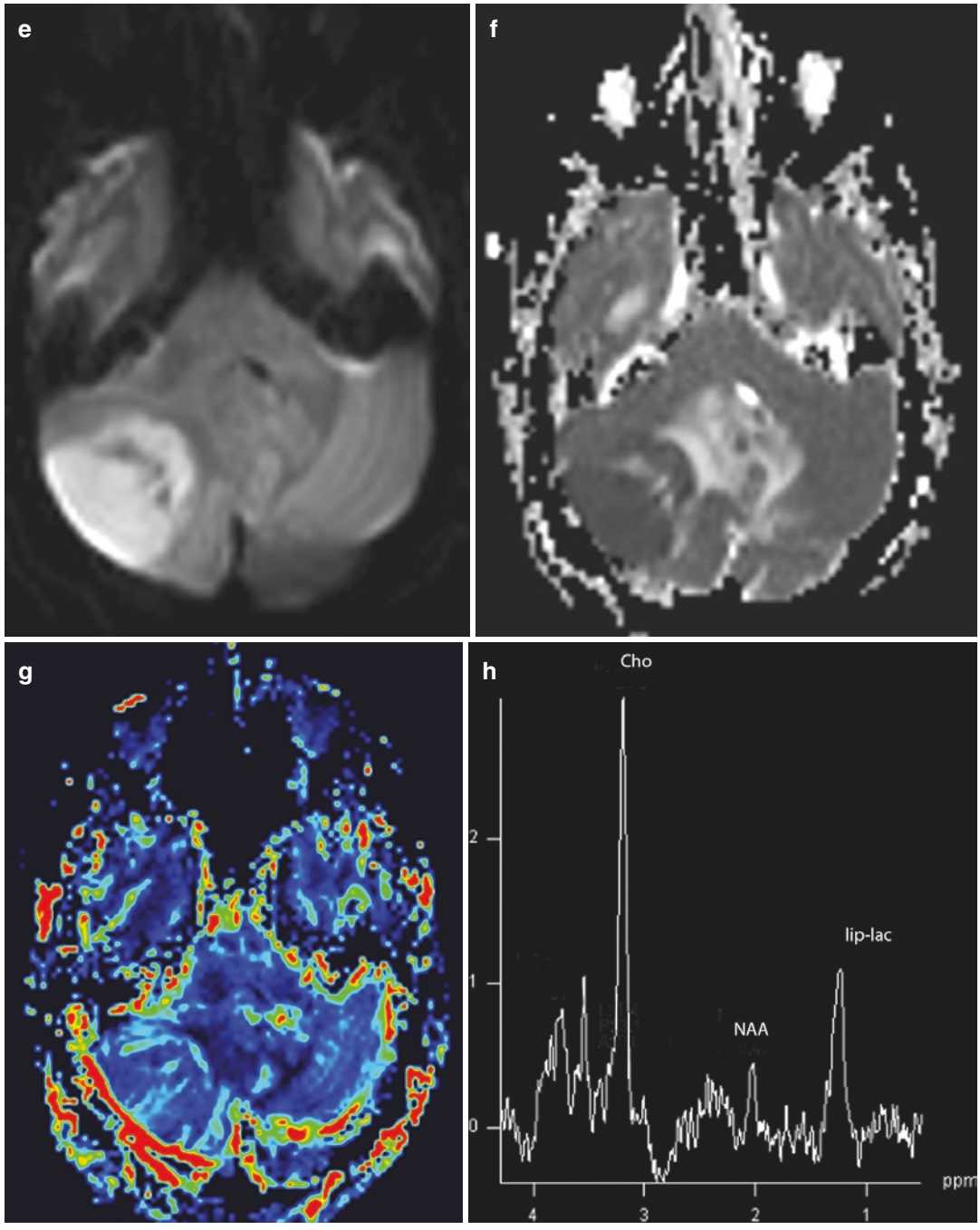

Fig. 13.13 (continued)

13.13.2 Epidemiology

Medulloblastoma is the most common cerebellar tumour in children <20 years. One-fourth occur in adulthood, mean age 31-years-old and more often are lateral hemispheric not midline vermian as in childhood.

13.13.3 Pathology and Genetics

The WHO regards all medulloblastomas as grade IV neoplasms. There are four major histologic subtypes: classic, desmoplastic/nodular, extensively nodular, and large cell/anaplastic. In the new 2016 CNS WHO classification there are four genetically defined subtypes of medulloblastoma based on the presence or absence of activation in the wingless integration (WNT) or sonic hedgehog (SHH) signalling pathways: WNT-activated, SHH-activated and TP53-mutant, SHH-activated and TP53 wild-type, Non-WNT/non-SHH (groups 3 and 4).

13.13.4 Clinical Management

The four distinct molecular subgroups of medulloblastoma are clinically important. The definition of genetic and histologic features of medulloblastoma is necessary to define the adequate personalised therapy.

13.13.5 Imaging Findings and Differential Diagnosis

On imaging studies, medulloblastoma commonly appears as a well-defined enhancing posterior fossa mass with surrounding oedema, cyst formation, haemorrhage and occasional areas of calcification can be seen. Leptomeningeal seeding is common as high as 33% of the cases.

Medulloblastomas exhibit variable perfusion and permeability characteristics, with some lesions showing elevated perfusion and permeability and others not. Desmoplastic cases do not show elevation of the blood volume, which could be due to their fibrous matrix.

On MR spectroscopy, medulloblastomas demonstrate increased Cho peak and decreased NAA. Significant elevated Taurine (Tau) concentration at 3.3 ppm is seen in the classic subtype of medulloblastoma.

Take-Home Messages

- Four genetically defined subtypes of medulloblastoma have been added in the new WHO 2016 classification
- Medulloblastoma in the adulthood is more commonly located in the cerebellar hemispheres
- Medulloblastoma exhibits a variable perfusion and permeability characteristics
- MR imaging of the spinal axis should be performed at the time of initial work up of the primary tumour to rule out leptomeningeal spread

Further Reading

1. Shih RY. Smirniotopoulos JG. Posterior fossa tumours in adult patients. Neuroimag Clin N Am 2016; 26:493–510
2. de Oliveira F, Landeiro JA, de Castro I. Adult hemispheric cerebellar medulloblastoma. Surg Neurol Int. 2018; 9:34–47
3. Keil VC, Warmuth-Metz M, Reh C, Enkirch SJ, Reinert C, Beier D, Jones DTW, Pietsch T, Schild HH, Hattingen E, Hau P. Imaging biomarkers for adult medulloblastomas: genetic entities may be identified by their MR imaging radiophenotype. Am J Neuroradiol. 2017; 38:1892–1898
4. Shih RY, Koeller KK. Embryonal Tumors of the Central Nervous System. RadioGraphics 2018; 38:525–541
5. Koeller KK, Rushing EJ. Medulloblastoma: a comprehensive review with radiologic-pathologic correlation. RadioGraphics 2003; 23:1613–1637

13.14 Case 14

41-year-old male with gait disturbance and ataxia. The patient has a history of pancreatic cystic tumours and suspicion of Von Hippel-Lindau disease. MRI was performed, and a cerebellar mass was found. Surgery was performed. Histology showed a highly vascular tumour with vacuolated cells and cystic areas. No mitosis was demonstrated. Cells show positivity for NSE and S-100. Final diagnosis was haemangioblastoma of the CNS (WHO I).

13.14.1 Images and Legends

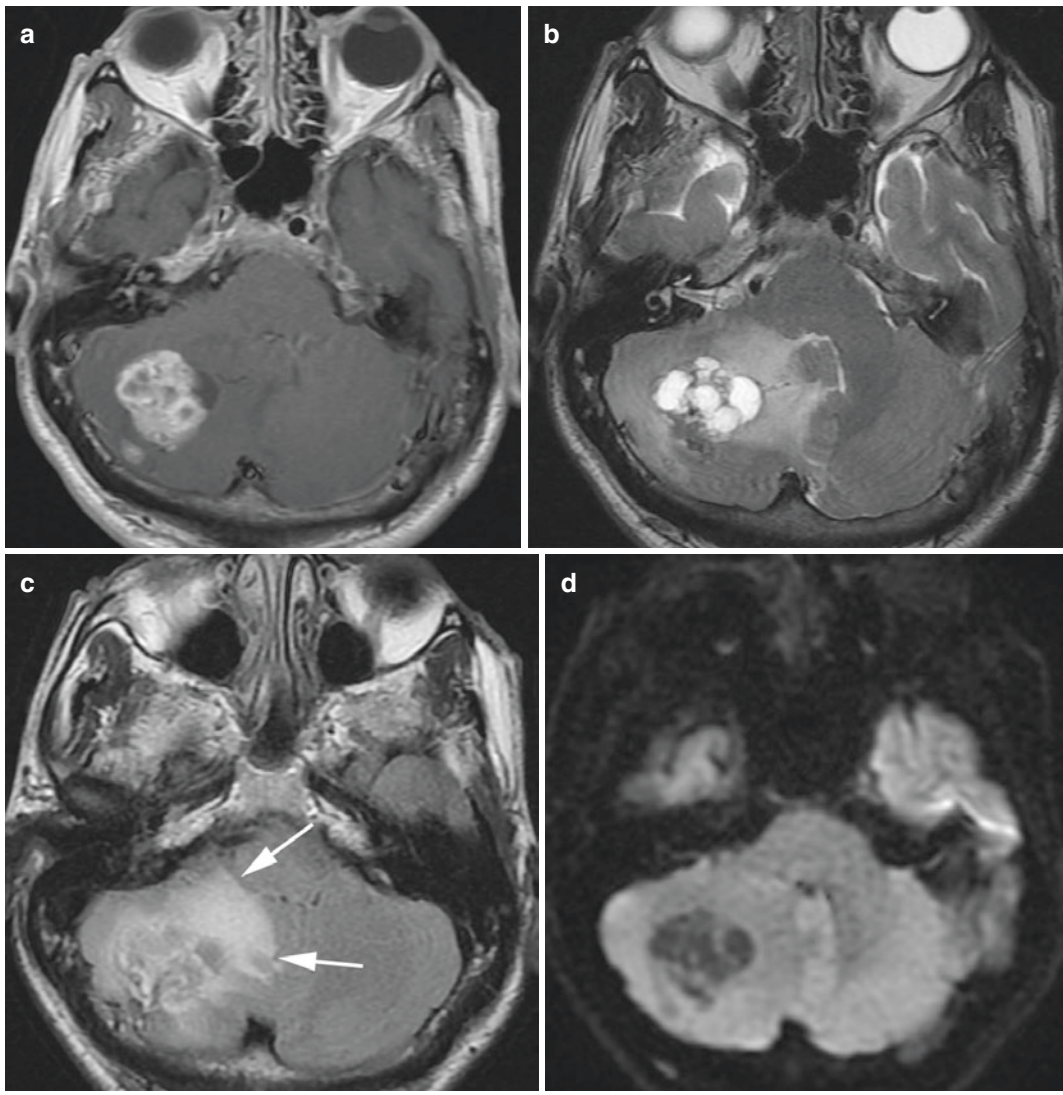

Fig. 13.14 (**a**) Axial T1-weighted contrast-enhanced MRI demonstrates an enhancing mass in the right cerebellar hemisphere. (**b**) Axial T2-weighted MRI. Multiple cystic areas are demonstrated within the mass. (**c**) Axial FLAIR MRI, white matter oedema in the periphery of the tumour (arrows) with mass effect on the fourth ventricle and secondary hydrocephalus. (**d**) Axial DWI MRI. No diffusion restriction is noted. (**e**) Susceptibility-weighted images (SWI) low signal intensity areas indicating the presence of blood products. (**f**) Axial contrast-enhanced abdominal CT, 1- basal and 2- portal phase. Multicystic pancreatic mass is shown

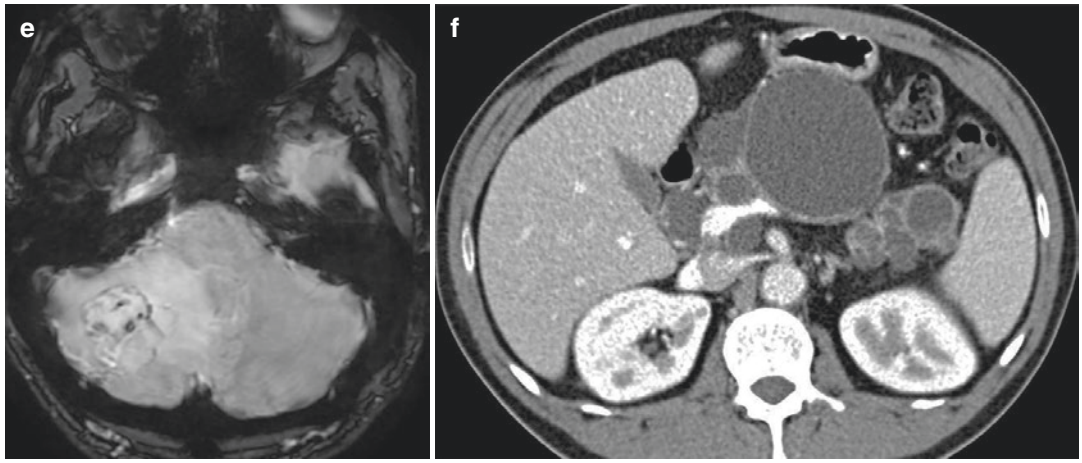

Fig. 13.14 (continued)

13.14.2 Epidemiology

Haemangioblastoma of the CNS are tumours diagnosed in young to middle aged adults. Most cases are sporadic, but younger patient tends to be related to VHL disease. Typical symptoms are related to mass effect in the posterior fossa.

13.14.3 Pathology and Genetics

Haemangioblastoma features the nodule within a cyst appearance. It is a highly vascular tumour with flow voids, sometimes, enlarged arterial feeders are demonstrated. Is suggested that the cystic component most likely arises by exudation from the solid nodule vascular component. 95% are in the posterior fossa. Usually it does not grow and has a very low Ki67 index (WHO I).

13.14.4 Clinical Management

Most patients are cured with surgical resection. In patients with very large tumours, pre-surgical embolisation makes easier the resection. Incomplete surgery is treated with RDT.

13.14.5 Imaging Findings and Differential Diagnosis

The lesion features a cystic mass with a mural nodule that vividly enhances and often has prominent flow voids. Arterial feeders may be demonstrated. Calcification is possible. Perfusion rCBV shows high ratios. The typical differential is the pilocytic astrocytoma and brain metastases.

Take-Home Messages

- Cystic mass with a peripheral enhancing nodule in the posterior fossa suspect haemangioblastoma. Differential diagnosis with unique cystic metastasis (lung, breast…)

Further Reading

1. Quadery FA, Okamoto K. Diffusion-weighted MRI of haemangioblastomas and other cerebellar tumours. Neuroradiology. 2003; 45:212–219
2. Gnanalingham KK, Apostolopoulos V, Chopra I, Mendoza N, Peterson D. Haemangioblastoma: a rare cause of a cerebellar mass in the elderly. British journal of neurosurgery. 2003; 17:461–4
3. Osborn AG, Hedlund GL, Salzman KL. Osborn's Brain E-Book. Elsevier Health Sciences; 2017 Nov 2
4. Slater A, Moore NR, Huson SM. The natural history of cerebellar hemangioblastomas in von Hippel-Lindau disease. AJNR 2003; 24:1570–1574

13.15 Case 15

13.15.1 Images and Legends

44-year-old male with altered mental status.

Biopsy was performed; the pathological diagnosis was diffuse large B-cell lymphoma. CD20+.

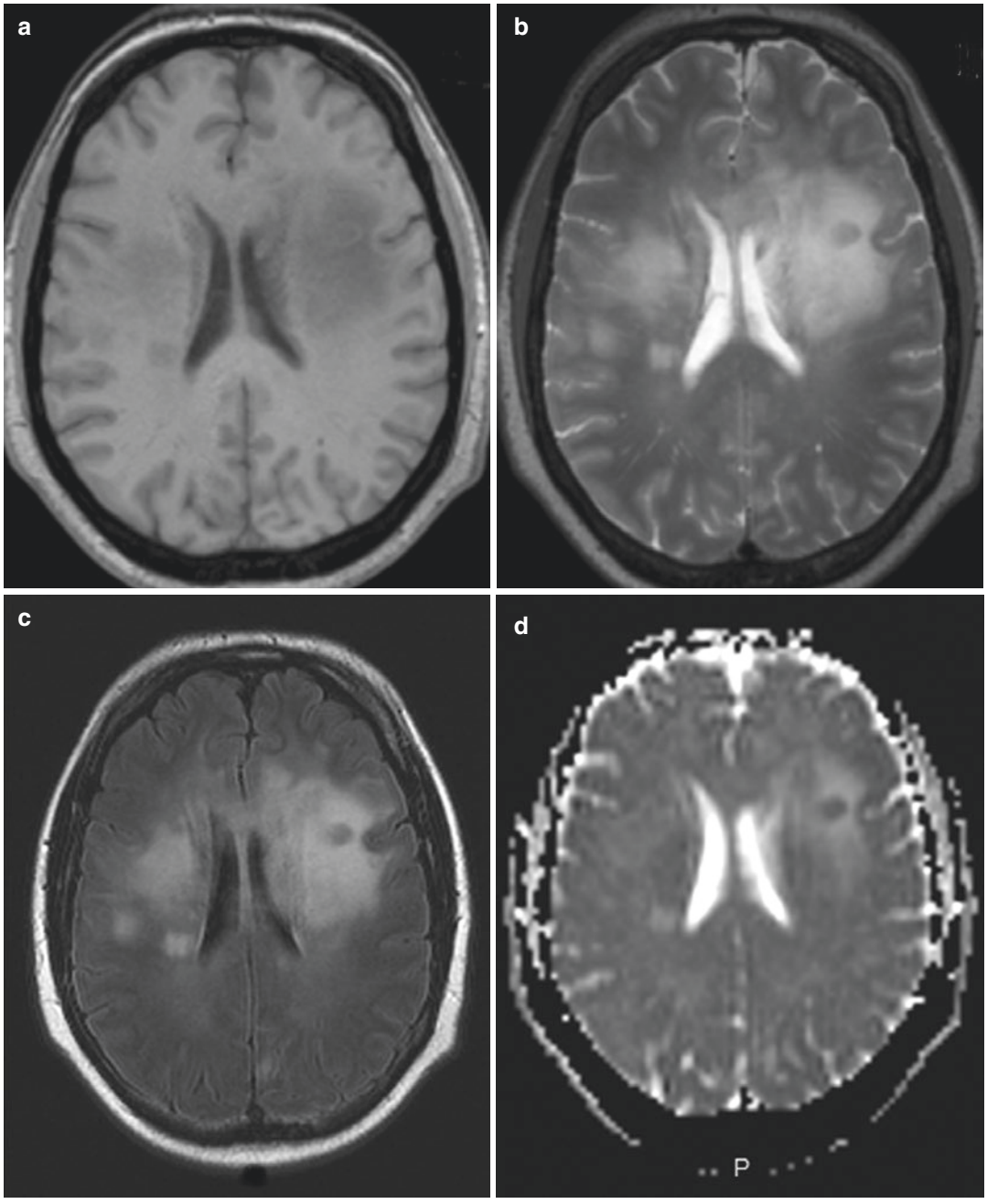

Fig. 13.15 (**a**) Axial T1WI demonstrates a hypointense subcortical left frontal lobe mass. (**b**) Axial T2WI shows subcortical WM high signal intensity with central hypointense component. (**c**) Axial FLAIR shows the same findings than T2WI. (**d**) ADC map demonstrates restricted diffusion with lower ADC values than normal brain in the central area. (**e**) PWI shows elevated rCBV in the central portion. (**f**) Contrast-enhanced axial T1-weighted MRI demonstrates several areas of enhancement. (**g**) MR spectroscopy shows increased Cho and decreased NAA and Cr values

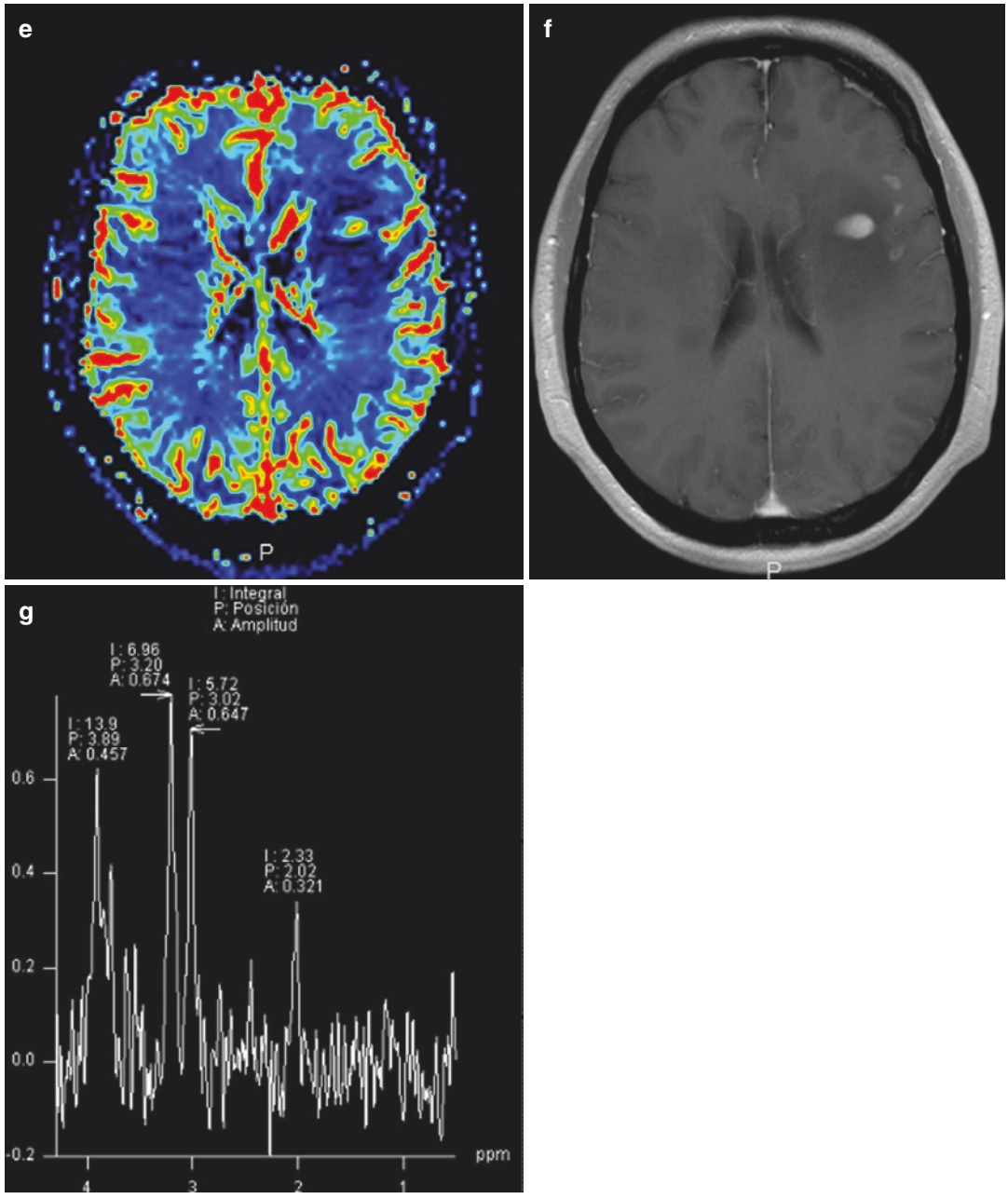

Fig. 13.15 (continued)

13.15.2 Epidemiology

Primary CNS lymphoma accounts for 1–5% of all brain tumours. The incidence rates of PCNSL are increasing among immunocompetent patients. Immunocompromised patients have an increased risk of PCNSL.

13.15.3 Pathology and Genetics

The majority (>90%) of PCNSL are B-cell tumours: diffuse large B-cell lymphoma and high-grade Burkitt-like B-cell lymphoma. Diffuse large B-cell lymphoma is the most common type

and is characterised by reactivity for CD19, CD20, CD22, CD79a and PAX-5.

13.15.4 Clinical Management

The patient was treated with steroids plus chemotherapy and radiotherapy.

These tumours are often high grade and have a poor prognosis despite treatment.

13.15.5 Imaging Findings and Differential Diagnosis

PCNSL are hypointense to grey matter in T1WI with intense homogeneous enhancement in high-grade tumours. They are usually iso-hypointense in T2WI with lower ADC values than normal brain.

Perfusion images show mild increase rCBV in enhancing areas. MR spectroscopy shows increased Cho and markedly decreased NAA and Cr values.

Differential diagnosis includes secondary CNS lymphoma, glioblastomas, cerebral toxoplasmosis, tumefactive MS and brain abscesses.

Take-Home Messages

- PCNSL are generally B-cell high-grade tumours that have a poor prognosis despite treatment
- MRI plays an important role in diagnosis and detection of treatment-related complications

Further Reading

1. Royer-Perron L, Hoang-Xuan K, Alentorn A. Primary central nervous system lymphoma. Curr Opin Neurol. 2017; 30:669–676
2. Mansour A, Qandeel M, Abdel-Razeq H, Abu Ali HA. MR imaging features of intracranial primary CNS lymphoma in immune competent patients. Cancer Imaging. 2014; 14:1–9
3. Haldorsen IS, Espeland A, Larsson EM. Central nervous system lymphoma: Characteristic findings on traditional and advanced imaging. Am J Neuroradiol. 2011; 32:984–92
4. Slone HW, Blake JJ, Shah R, Guttikonda S, Bourekas EC. CT and MRI findings of Intracranial Lymphoma. AJR 2005; 184: 1679–1685

Secondary Brain Tumors

14

Melda Apaydın

14.1 Malign Melanoma Metastasis

A 65-year-old man with medical history of malignant melanoma underwent brain MRI after the complaints of balance problems, speech impairment, and fatigue.

M. Apaydın (✉)
Department of Radiology, Izmir Atatürk Education and Training Hospital, Izmir, Turkey

Y. Özsunar, U. Şenol (eds.), *Atlas of Clinical Cases on Brain Tumor Imaging*,
https://doi.org/10.1007/978-3-030-23273-3_14

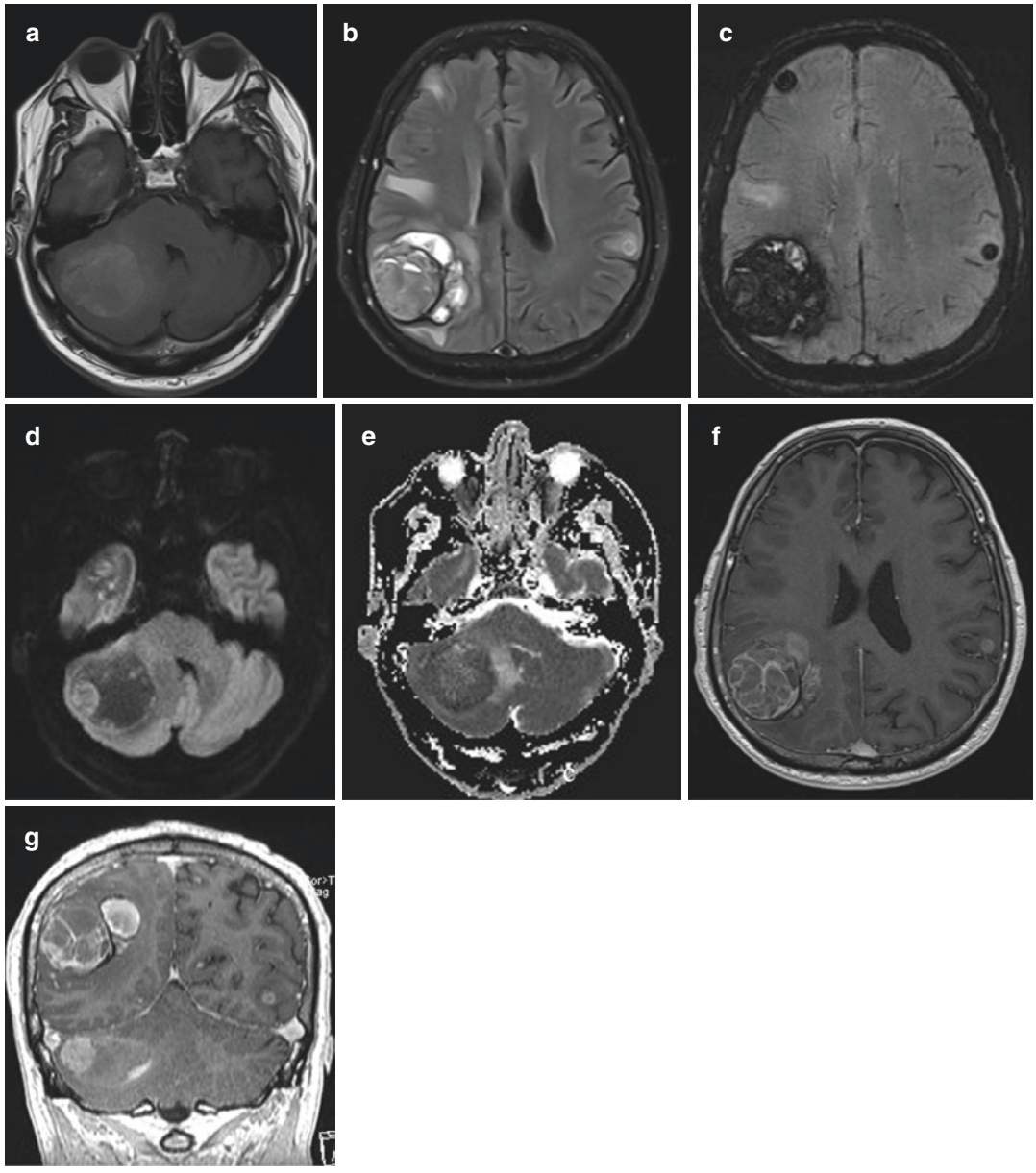

Fig. 14.1 (**a**) Axial T1WI shows heterogeneous hyperintense right cerebellar and temporal lobe lesions. (**b**) Axial T2 FLAIR image shows significant edema around the lesion. (**c**) The SWI is more sensitive than other sequences for the detection of hemorrhagic metastases. (**d**, **e**) DWI and ADC confirm restricted diffusion and hemorrhagic nature in some tumoral areas. (**f**, **g**) Gadolinium-enhanced axial and coronal T1WI show intense heterogeneous enhancement of the metastases

14.1.1 Epidemiology

- Brain metastases which can develop in 10–40% of cancer patients are the most common intracranial brain tumor
- Lung cancer (40%), breast cancer (20%), melanoma (10%), and enteric cancers (10%) are the common causes

- They are usually the result of hematogenous spread or less frequently from nearby tissue such as bone metastasis
- The majority of metastases (about 80%) are located in the supratentorial region. The cerebellum and brain stem are less affected (10–15% and 2–3%)
- In adults, the most common intra-axial neoplastic lesion in the posterior fossa is cerebellar metastasis

14.1.2 Pathology

- The pathological features are generally similar to the primary tumor
- Most metastatic tumors clearly demarcated from the adjacent brain on both macroscopic and microscopic examination
- They usually show microinvasion into the brain parenchyma via perivascular (Virchow–Robin) spaces. This is usually seen in metastases of small-cell carcinoma, melanomas, and lymphomas
- Significant reactive gliosis occurs surrounding metastatic nodules
- Various immunohistochemical algorithms are used to diagnose the origin of metastases, and molecular genetic analysis is very helpful for the detection of unknown metastatic origin

14.1.3 Clinical Management

- Most patients with a known cancer undergo imaging studies when neurologic signs and symptoms arises
- Headache, seizure, nausea, vomiting, cognitive and motor dysfunction are the most commonly seen symptoms
- The number, size, and content of the metastatic brain lesions are very important for choosing the right treatment
- Medical treatment and chemotherapy can be used for symptomatic or systemic treatment. Surgical treatment and radiation therapy can be used for radical treatment

14.1.4 Imaging Findings

- Metastases are usually seen in the border zones (watershed zones) of the cerebral arterial regions. The posterior watershed area (border of the middle and posterior cerebral arteries) is more commonly involved than the anterior watershed area (border of middle and anterior cerebral arteries)
- They usually involve the cortex near the white-gray matter junction, resembling a hematogenous or embolic lesion
- Chest X-ray, mammography, PET CT, and abdominal USG should be performed on multiple cerebral metastases, originating from an unknown source
- Metastatic brain cancer can be safely diagnosed in a patient with a known primary cancer with multiple enhancing solid lesions in the gray matter-white matter junction with marked edema
- In cancer patients, 11% of the brain mass lesions are not metastases. Abscess, granuloma, demyelinating disorders, radiation necrosis, primary brain tumors (GBM, astrocytoma, oligodendroglioma), stroke, and cerebral venous thrombosis are among the lesions in the differential diagnosis
- Leptomeningeal carcinomatosis and dural metastases are different forms of brain metastasis. Dural metastases form dural plaques which infiltrate the cortical surface. Meningioma, CNS lymphoma, granulomatous disease, and chronic subdural hemorrhage are the most common lesions in the differential diagnosis

14.1.5 MRI

- Contrast-enhanced MRI is the most sensitive and specific method in determining the location and number of metastases. It can detect metastases 2–3 times more than contrast-enhanced CT, especially the lesions smaller than 5 mm
- Usually hypointense on T1WI but sometimes hyperintense on T1WI, especially in hemor-

rhagic metastases and nonhemorrhagic melanoma (due to melanin pigment) metastases
- Usually hyperintense on T2WI and FLAIR imaging. Peritumoral edema is more prominent with FLAIR imaging
- On DWI, metastases typically show increased diffusion, but high cellular metastases such as mucinous and other tumors (breast, colon, testicular, and small and non-small cell lung carcinoma) can show restricted diffusion. SWI is very sensitive for the detection of small hemorrhagic metastases
- Calcification, cystic, and hemorrhagic changes commonly seen with metastasis. Calcification is always hyperdense (bright) on CT, can be hyperintense on T1WI and hypointense on T2WI. Hemorrhage has variable appearance depending on the stage of its evolution
- Although contrast material is usually used on T1WI, postcontrast FLAIR images may improve the detection of leptomeningeal metastases
- Dynamic susceptibility and contrast-enhanced (DSC, DCE) MRI, and arterial spin labeling (ASL) techniques can be used for the detection of tumor perfusion
- MRS, DTI, FDG, and non-FDG PET are the other advanced imaging techniques for brain metastases imaging

Take-Home Messages

- Brain metastasis, which is the predominant cause of significant morbidity and mortality in oncology patients, is the most common intracranial malignancy
- The number, size, and content of the metastatic brain lesions are very important for choosing the right treatment
- Contrast-enhanced MRI is the most important method for the detection of brain metastases

Further Reading

- Lopes MBS. Metastatic diseases of the central nervous system-neuropathologic aspects. Handb Clin Neurol. 2018;49:67–73
- Pope WB. Brain metastases: neuroimaging. Handb Clin Neurol. 2018;149:89–112

14.2 Leptomeningeal Metastases

A 20-year-old woman with a huge abdominal mass underwent brain MRI due to vomiting and headache. Leptomeningeal tumoral infiltration was detected in the subarachnoid space, which was more prominent in vertex and in the posterior fossa.

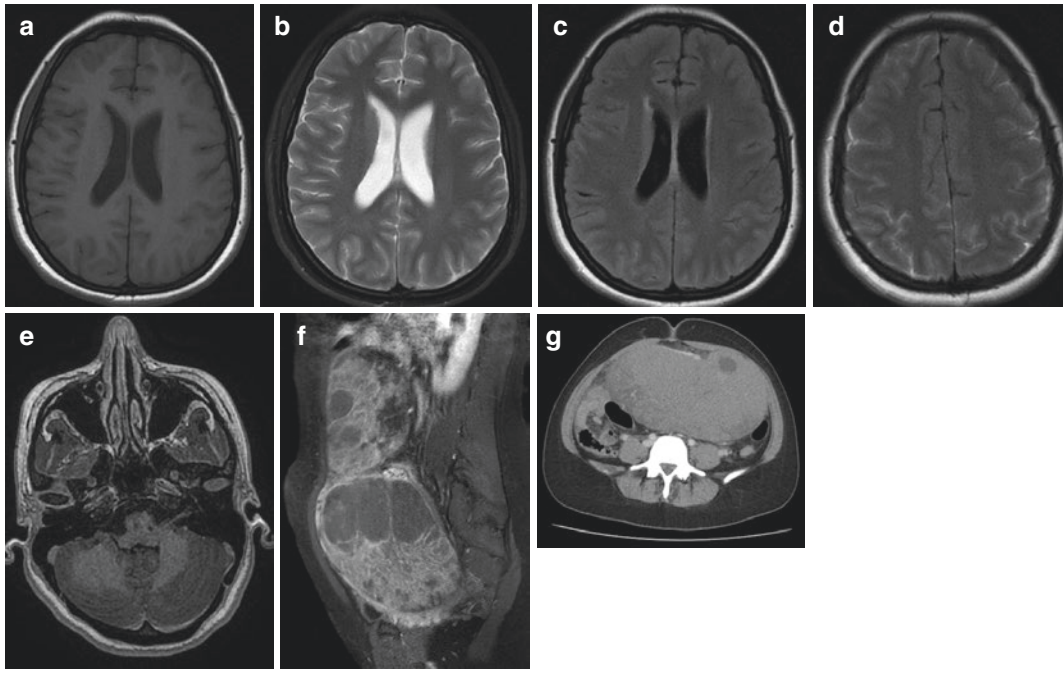

Fig. 14.2 (**a**–**c**) There is no pathology on axial T1WI and T2WI (**a**, **b**), but increased signal in the *subarachnoid space* on T2W FLAIR image, and periventricular high intensity is also seen due to increased CSF pressure (**c**). (**d**) FLAIR T2WI with contrast shows enhancement in the subarachnoid spaces. (**e**) Volumetric axial 3D-T1WI with contrast shows left 7./8. nerve root enhancement and ventricular dilatation. (**f**, **g**) There was a huge mass in the abdomen from diaphragmatic level to the pelvis on the sagittal contrast-enhanced abdominal MRI and axial CT images. The patient had diagnosed with lymphoma and CNS metastases

14.2.1 Epidemiology

- Leptomeningeal metastases which usually show diffuse infiltrations of the leptomeninges
- Involves the base of the brain, cranial and spinal nerve roots, and occurs in the 4–15% of the patients with solid tumor
- Leptomeningeal metastases are seen (70% and more) in advanced stages of cancer, rarely occur at the onset of the disease
- Headaches, gait/ memory/sensory problems, and cranial nerve disturbances are the most commonly seen clinical findings

14.2.2 Pathology

- Cancer cells disseminate to the leptomeninges (pia and arachnoid) and CSF compartment usually from lymphoma, leukemia, melanoma, breast and lung cancer
- This spread is usually caused by direct tumor involvement of the leptomeninges or cancer spread from the perineural or perivascular space
- Pelvic cancer spreads via arterial or venous (plexus of Batson) route
- Since the CSF circulation is slower in the subarachnoid space of the spinal cord (cauda equina) and in the base of the brain (basilar cisterns), cancer cells may multiply fast

14.2.3 Clinical Management

- Mean survival without treatment in these patients is approximately 6 weeks, and the results are not satisfactory even with treatment

14.2.4 Imaging Findings

- MRI sensitivity for leptomeningeal metastases ranges from 20% to 91%. Therefore, the display with normal MRI findings is possible
- Brain contrast-enhanced CT, which is 40% less sensitive compared to MRI, should be used for patients who cannot tolerate MRI

14.2.5 MRI

- T1WI and T2WI are usually normal. T2W FLAIR images are the best sequence for the evaluation of subarachnoid spaces. They show abnormally high signal within sulci
- T2W FLAIR images with contrast are also very helpful for delineating sulci and leptomeningeal infiltrates correctly. Postcontrast FLAIR images may improve the detection of leptomeningeal metastases
- Volumetric T1WI with contrast provides better sensitivity for leptomeningeal disease than 2D T1W or FLAIR images such as in our case
- Leptomeningeal contrast enhancement pattern shows either sheetlike pattern or nodular patterns on the leptomeningeal surfaces
- Contrast enhancement may be seen in cranial nerves and nerve roots
- Ependymal, sulcal, and parenchymal nodules can be seen with contrast administration
- Cerebellum and occipital lobes, CN VII/VIII, and the ependymal lining of the lateral ventricles are mostly involved in leptomeningeal metastasis
- Brain parenchymal involvement occurs in 40–75% of these patients with leptomeningeal metastases
- Hydrocephalus may be seen as a result of CSF flow obstruction. The spine involvement is reported in 15–25% of patients
- The differential diagnosis is usually with among infectious, granulomatous disease, and rarely subarachnoid hemorrhage
- Before MRI, lumbar puncture should be avoided. Propofol, high oxygen tension may also shows hyperintensity in T2W FLAIR images

Take-Home Messages

- Leptomeningeal metastasis is a diffuse infiltration of leptomeninges with tumor metastasis. MRI with T1W contrast, FLAIRW contrast, and T2W sequence is diagnostic in this case. There are some diagnostic pitfalls such as subarachnoid hemorrhage, propofol, high oxygen tension and previous Gd contrast administration
- Leptomeningeal metastases can also be diagnosed with typical MR findings and clinical findings, without CSF studies

Further Reading

- Debnam JM, Mayer RR, Chi TL, Ketonen L, Weinberg JS, Wei W, Groves MD, Guha-Thakurta N. Most common sites on MRI of intracranial neoplastic leptomeningeal disease. J Clin Neurosci. 2017;45:252–6
- Taillibert S, Chamberlain MC. Leptomeningeal metastasis. Handbook of clinical neurology, vol 149 (3rd series). p. 169–204

14.3 Seizures in Patient with Metastatic Brain Tumor

A 53-year-old woman with medical history of breast and ovarian malignancy underwent brain MRI after seizure.

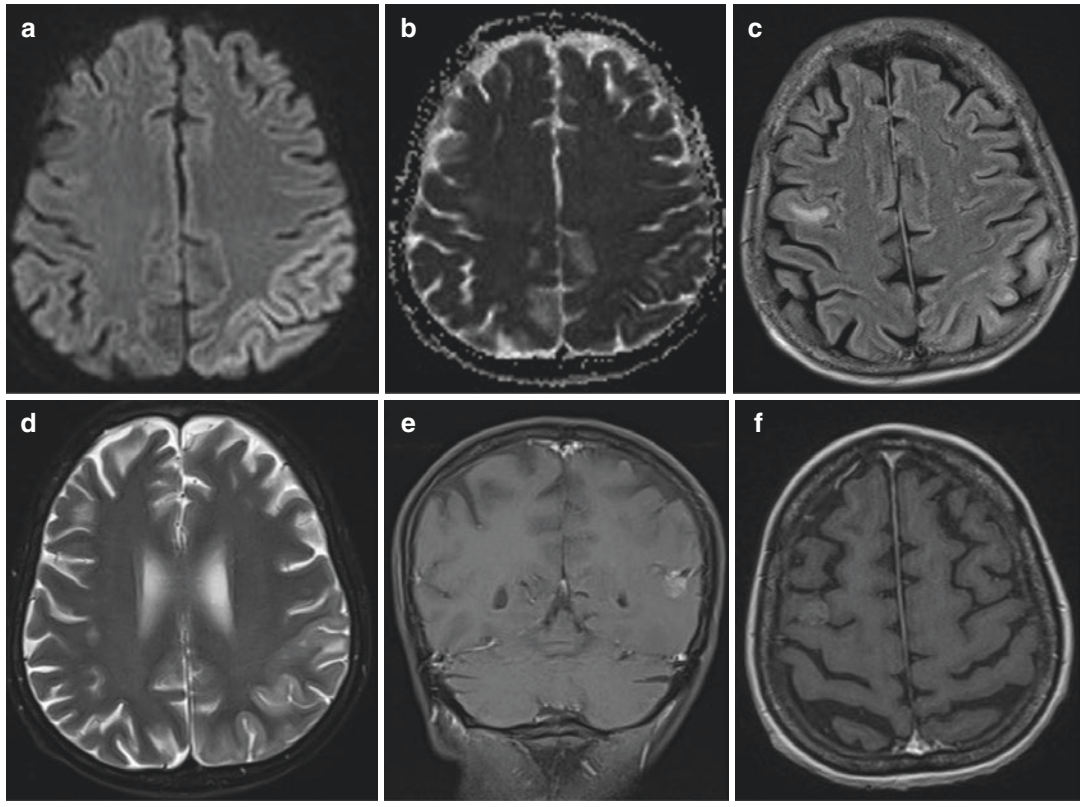

Fig. 14.3 (**a**, **b**) DWI (**a**) and ADC (**b**) map show gyral pattern of restricted diffusion on the left parieto-occipital region. (**c**, **d**) Axial T2 FLAIR image (**c**) and T2WI (**d**) show hyperintensity on the left parieto-occipital cortex. (**e**, **f**) Coronal and axial contrast-enhanced T1WI show metastatic lesions and cortical enhancement

14.3.1 Epidemiology

- Seizures can be seen in patients with primary or secondary brain tumors and may be the first sign of the tumor
- Tumor type, location, and cortical gray matter proximity are important factors of the seizure development
- Up to 50% of patients with brain metastases have seizure. Seizures can be seen in the end stage of the disease
- Epilepsy due to brain tumors accounts for about 4% of all epilepsy patients
- Although the pathogenesis is indeterminate, there may be multiple factors such as tumor histology and location, neurotransmission differences, peritumoral area, deterioration of the blood–brain barrier, and changes in molecular and cellular gap junctions
- Supratentorial tumors are more epileptogenic than infratentorial tumors, and tumors in the temporal, parietal, and occipital lobes cause epilepsy more often than the frontal lobe tumor
- Metastatic brain lesions often have fewer seizures than those with primary brain masses

14.3.2 Pathology

- The incidence of seizures varies between different metastatic lesions. However, 67% of seizures occur in metastatic melanomas
- Multiple lesions with hemorrhage and cortical gray matter involvement can cause seizure. Increased glutamate (brain-stimulating neurotransmitter) induces neuronal hyperexcitability and seizure activity in the peritumoral region
- Upregulation of adenosine kinase in peritumoral tissue may facilitate tumor-associated epilepsy Blood–brain barrier deterioration, gap junction (which allow communication of the adjacent cells) status, molecular genetics, and peritumoral environmental changes are the factors of seizure

14.3.3 Clinical Management

- Seizure or epilepsy, which develops secondary to brain metastases, is a very important clinical issue and requires very careful evaluation, and should be treated with caution
- Treatment choices for controlling the brain tumor such as radiotherapy and/or chemotherapy may reduce seizure control

14.3.4 Imaging Findings

- With both cortical and hippocampal patterns of seizure activity, increased DWI and decreased ADC signal may represent cytotoxic edema
- T2W and DWI without decreased ADC may represent vasogenic edema
- Also PRESS syndrome and acute ischemia are in the differential diagnosis of these findings
- Cerebral metastases with clinical findings are very helpful to reach the final diagnosis

Take-Home Messages

- Identification of seizure-related imaging abnormalities is important to initiate appropriate treatment, to avoid unnecessary treatment and/or investigation of the patients with brain metastases

Further Reading

- Chhetri SK, Mathur S, Soh C, Gosal D. Seizure-induced MRI changes mimicking metastatic brain disease. J Clin Neurosci. 2014;21:869–72
- Cianfoni A, Caulo M, Cerase A, Della Marca G, Falcone C, Di Lella GM, et al. Seizure-induced brain lesions: a wide spectrum of variably reversible MRI abnormalities. Eur J Radiol. 2013;82:1964–72
- Koekkoek JAF, Dirven L, Reijneveld JC, Postma TJ, Grant R, Pace A, et al. Epilepsy in the end of life phase of brain tumor patients: a systematic review. Neuro-Oncol Pract. 2014;1(3):134–40

14.4 Sellar Metastatic Tumor

A 56-year-old man without any medical history of malignancy underwent brain and pituitary MRI after the complaints of decreased vision, headache, and right eye ptosis. A mass in the sellar and suprasellar region was found.

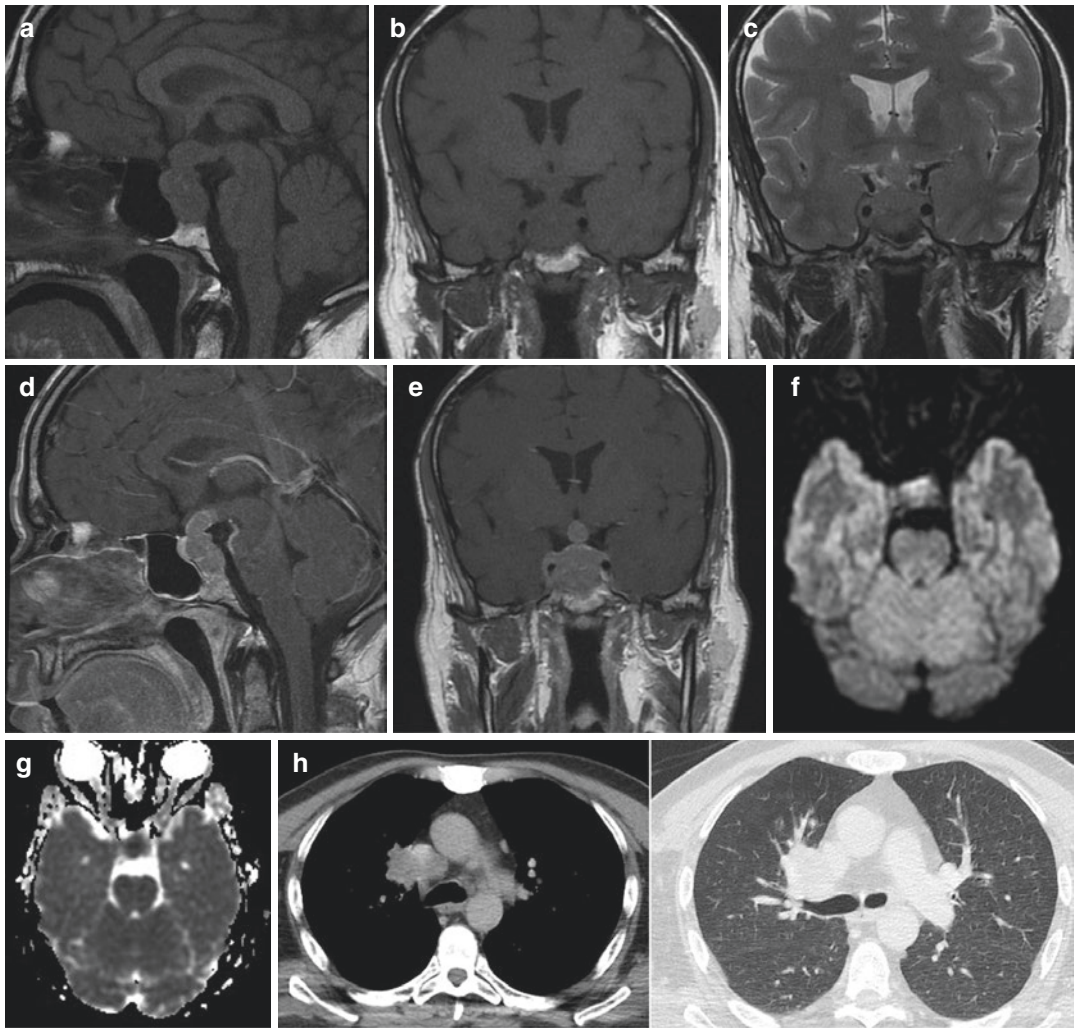

Fig. 14.4 (**a**–**c**) Sagittal T1WI (**a**), coronal T1WI (**b**), sagittal T2WI (**c**) pituitary MRI shows isointense sellar and suprasellar mass with infundibular involvement. There was loss of normal posterior pituitary bright signal on T1WI. (**d**, **e**) Contrast-enhanced sagittal T1WI (**a**) and coronal T1WI (**b**) show a moderately enhancing sellar and suprasellar mass with infundibulum, optic chiasm, and right cavernous sinus invasion. (**f**, **g**) There was no lesion in the brain and the mass showed restriction on DWI (**f**) and ADC (**g**) MRI. (**h**) Right mediastinal metastatic lymphadenopathy and central lung tumor are seen on thorax CT

14.4.1 Epidemiology

- Metastatic pituitary tumors are seen in about 1% of the tumors in the sellar region in patients who had transsphenoidal surgery
- The metastatic involvement in autopsy cases was reported as high as 28%
- Breast (40%) and lung (33%) cancers were the most common metastasizing tumors to this area
- Lymphoma and prostate cancer are the common and RCC, colon, thyroid, and liver are the rare cause of metastasis in the sellar region
- Sellar metastasis is mostly seen in patients in their sixties or seventies, and usually with bone metastasis. It is very rare to be as a first manifestation of a metastatic disease such as in our case

14.4.2 Pathology

- Prolactin-rich environment of the pituitary enables and promotes the proliferation of breast cancer metastases
- The blood-borne metastases spread to the pituitary via neurohypophysis or posterior pituitary, infundibulum, clivus, dorsum sella, cavernous sinus, and also leptomeningeal infiltration of the pituitary capsule
- Posterior pituitary lobe, which has direct arterial systemic supply, is prone to develop metastatic involvement and the close continuity with dural surfaces enhances the effect
- •Anterior pituitary metastatic involvement is usually secondary to contiguous spread by posterior lobe

14.4.3 Clinical Management

- Sellar metastasis diagnosis without malignancy is very difficult
- According to the anatomic involvement site of the sellar tumor, diabetes insipidus and visual/oculomotor/hormonal disturbances can be seen
- Rarely it can be as a first manifestation of a metastatic disease
- Biopsy has to be done for indeterminate cases
- The treatment depends on clinical symptoms and primary malignancy. Surgery, chemotherapy, and radiotherapy can be used. Definitive diagnosis is crucial for choosing appropriate treatment
- If an active treatment is indicated, surgery is generally the method of choice. Conventional radiation therapy alleviates symptoms. Radiosurgery can also help to control the tumor. Chemotherapy currently used alone or as an adjunct to radiotherapy for palliative care
- Prognosis is very poor and survival is usually less than two years

14.4.4 Imaging Findings

- Infundibular involvement, neurohypophysis signal loss/change, hypothalamic infiltration, optic chiasm and optic nerve invasion, and Turkish saddle wall bony destruction were also frequent accompanying imaging characteristics for sellar metastases
- Atypical pituitary adenomas, and infiltrating lymphocytic and granulocytic tumors of the pituitary must be in the differential diagnosis
- Incidental hypophysis adenoma may be present in the patients with malignancy

14.4.5 MRI

- Iso-hypointense mass on T1WI, hyperintense on T2WI, loss of normal posterior pituitary bright signal in T1WI, and intense enhancement with contrast
- Infundibular, optic chiasm, optic nerve, hypothalamic, cavernous sinus involvement, dorsum sella infiltration, and bony destruction are commonly seen
- The lymphocytic and granulocytic pituitary involvement is in the differential diagnosis

Take-Home Messages

- Sellar metastases are a very rare manifestation of CNS metastases
- It is usually seen in patients with known malignancy but very rarely can be an early manifestation of a malignant disease
- Sudden onset pituitary hormone imbalance, and visual and cranial nerve disorders in a cancer patient can be suspicious signs for pituitary metastasis

Further Reading

- Altay T, Krisht KM, Couldwell WT. Sellar and parasellar metastatic tumors. Int J Surg Oncol. 2012;2012:647256
- Habu M, Tokimura H, Hirano H, Yasuda S, Nagatomo Y, Iwai Y, et al. Pituitary metastases: current practice in Japan. J Neurosurg. 2015;123:998–1007
- Yi HJ, Kim CH, Bak KH, Kim JM, Ko Y, Oh SJ. Metastatic tumors in the sellar and parasellar regions: clinical review of four cases. J Korean Med Sci. 2000;15:363–7

Tumor-Like Conditions of the Brain

15

Agapi-Alexandra Katsarou, Sotirios Bisdas, and Vasileios K. Katsaros

15.1 62-Year-Old Woman, with Left Extremities Weakness and Seizures

Findings: Brain MRI shows pathological intensity (Fig. 15.1a), heterogeneous enhancement after i.v. gadolinium administration (Fig. 15.1b), restricted diffusion (Fig. 15.1c, d), and perfusion parameters (Fig. 15.1e) within the right frontal and parietal lobes, as well as over the motor cortex of the frontal lobes. T2 prolongation is noted in all the locations where restricted diffusion is seen.

Diagnosis: Multiple **infarcts** in the distribution of right middle cerebral artery in a background of diabetes mellitus and dyslipidemia.

Key Points

- Increased T2 signal lesions with restricted diffusion have a broad differential
- Clinical history, distribution (vascular territories involved, unilateral vs. bilateral), number (single vs. multiple), the presence or absence of mass effect, and the presence or absence of a peripheral ring or central necrosis are key diagnostic clues
- Abscesses may be single or multiple, may be unilateral or bilateral, often have a peripheral ring, and often display mass effect
- Tumors often have mass effect, often have a peripheral ring, may be single or multiple, may be unilateral or bilateral, and may show central necrosis
- Hemorrhage is often in the subdural or subarachnoid space, but may be intraparenchymal, especially if there is history of head trauma or associated fracture
- In acute infarct, there is no mass effect, no peripheral ring, and no central necrosis and the lesions are usually in a single vascular distribution and are usually—but not always—unilateral
- Examples of multiple acute infarcts, as seen in this patient, are watershed infarcts occurring in typical watershed zones and infarcts occurring secondary to cardiac emboli or vasculitis, both of

A.-A. Katsarou
Department of Diagnostic and Interventional Radiology, Euroclinic of Athens, Athens, Greece

Department of Neurosurgery, National and Kapodistrian University of Athens School of Medicine, Athens, Greece

S. Bisdas
Department of Brain Repair and Rehabilitation, Neuroradiology Academic Unit, University College of London (UCL), London, UK
e-mail: s.bisdas@ucl.ac.uk

V. K. Katsaros (✉)
Department of Diagnostic and Interventional Radiology, Euroclinic of Athens, Athens, Greece

Department of Brain Repair and Rehabilitation, Neuroradiology Academic Unit, University College of London (UCL), London, UK

Department of Advanced Imaging Methods, MRI Unit, General Anti-Cancer and Oncological Hospital of Athens "St. Savvas", Athens, Greece

Department of Neurosurgery, National and Kapodistrian University of Athens School of Medicine, Athens, Greece
e-mail: vaskkatsaros@med.uoa.gr

Y. Özsunar, U. Şenol (eds.), *Atlas of Clinical Cases on Brain Tumor Imaging*,
https://doi.org/10.1007/978-3-030-23273-3_15

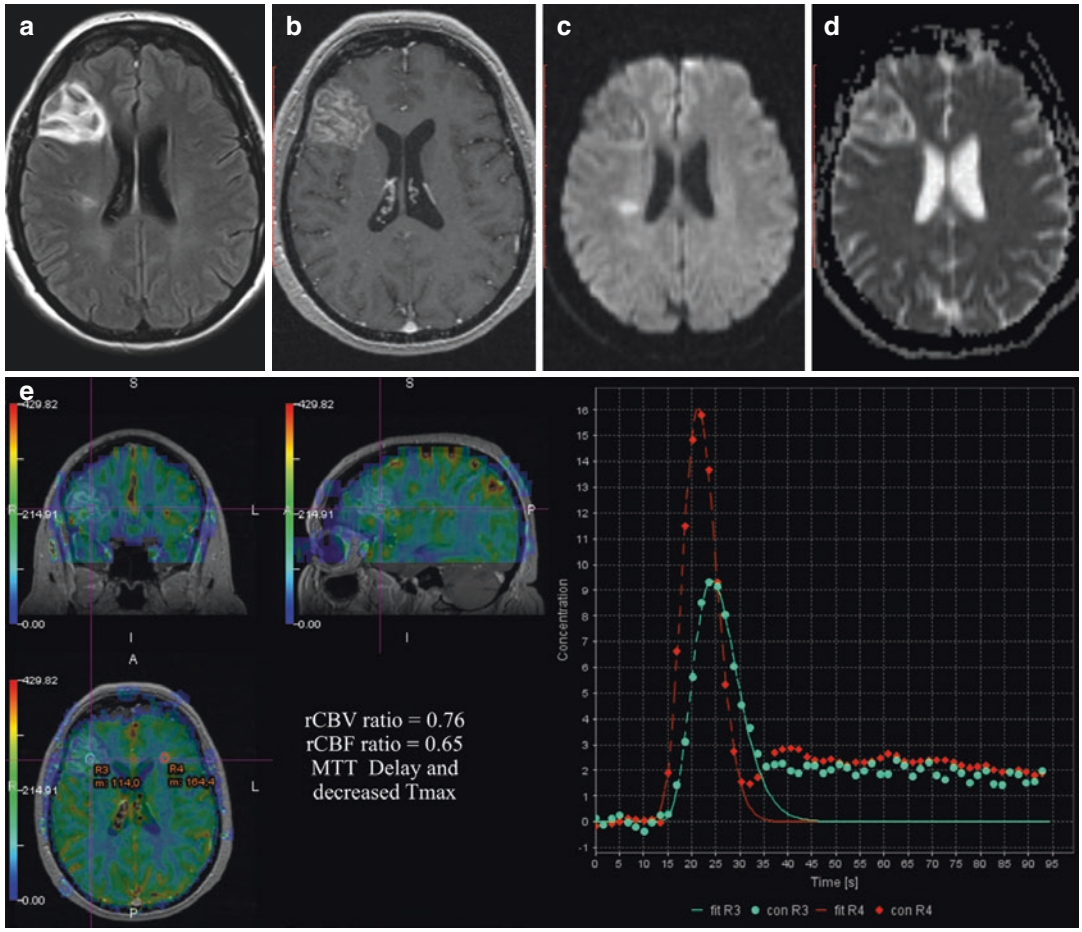

Fig. 15.1 (**a**) FLAIR, (**b**) T1 post-gadolinium, (**c**) diffusion b = 1000, (**d**) ADC map, (**e**) DSC-T2∗ perfusion

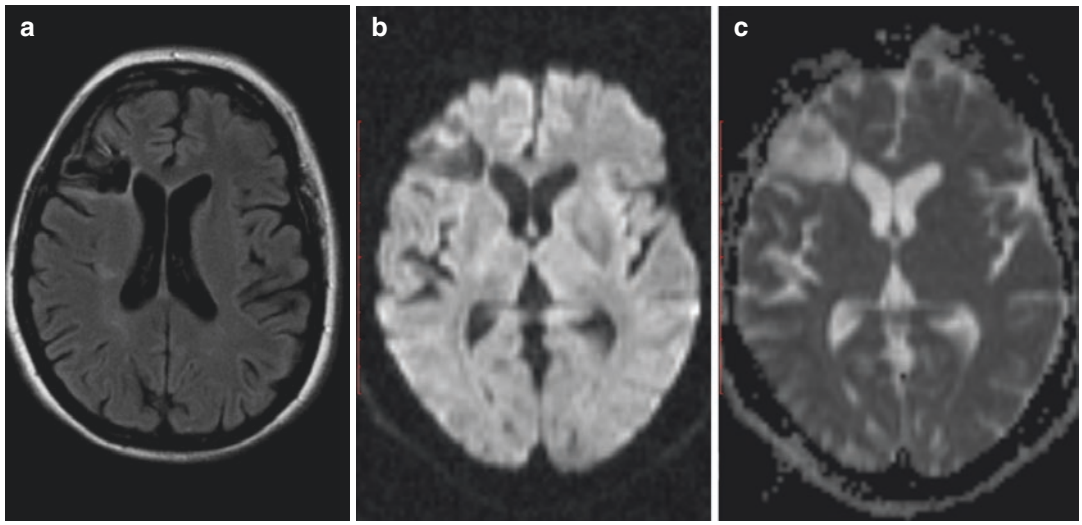

Fig. 15.2 Follow-up after one year confirming ischemic lesions in chronic phase, (**a**) FLAIR, (**b**) diffusion b = 1000, (**c**) ADC map

which are not distributed with respect to single vascular territories
- Besides IV drug abuse, cerebral vasculitis with secondary infarct can be seen in bacterial meningitis, tuberculous meningitis, viral, mycotic, syphilitic or postradiation arteritis, cell-mediated arteritis, collagen vascular disease, sarcoid, Wegener's granulomatosis, and Moyamoya disease

References

1. Stadnik, TW, et al. "Imaging Tutorial: Differential Diagnosis of Bright Lesions on Diffusion-weighted MR Images." Radiographics 2002; Nov. 1.
2. Imbesi, SG; Bradley, WG. Vasculitis, Intracranial. STATdx. 2 May 2008.

15.2 Man, with Headache and Seizures

Findings: A space-occupying lesion of the left frontal lobe is demonstrated. The wall is smooth and thinner on the periventricular surface. The contents show a fluid/fluid level. There is local mass effect and midline shift caused by vasogenic edema (Fig. 15.3a). On diffusion-weighted imaging there is restricted diffusion within portions of the lower fluid level (Fig. 15.3b). There is concurrent signal loss on ADC mapping (Fig. 15.3c). There is activation of the primary motor cortex left by task fMRI with right hand finger-tapping (Fig. 15.3c). Rim

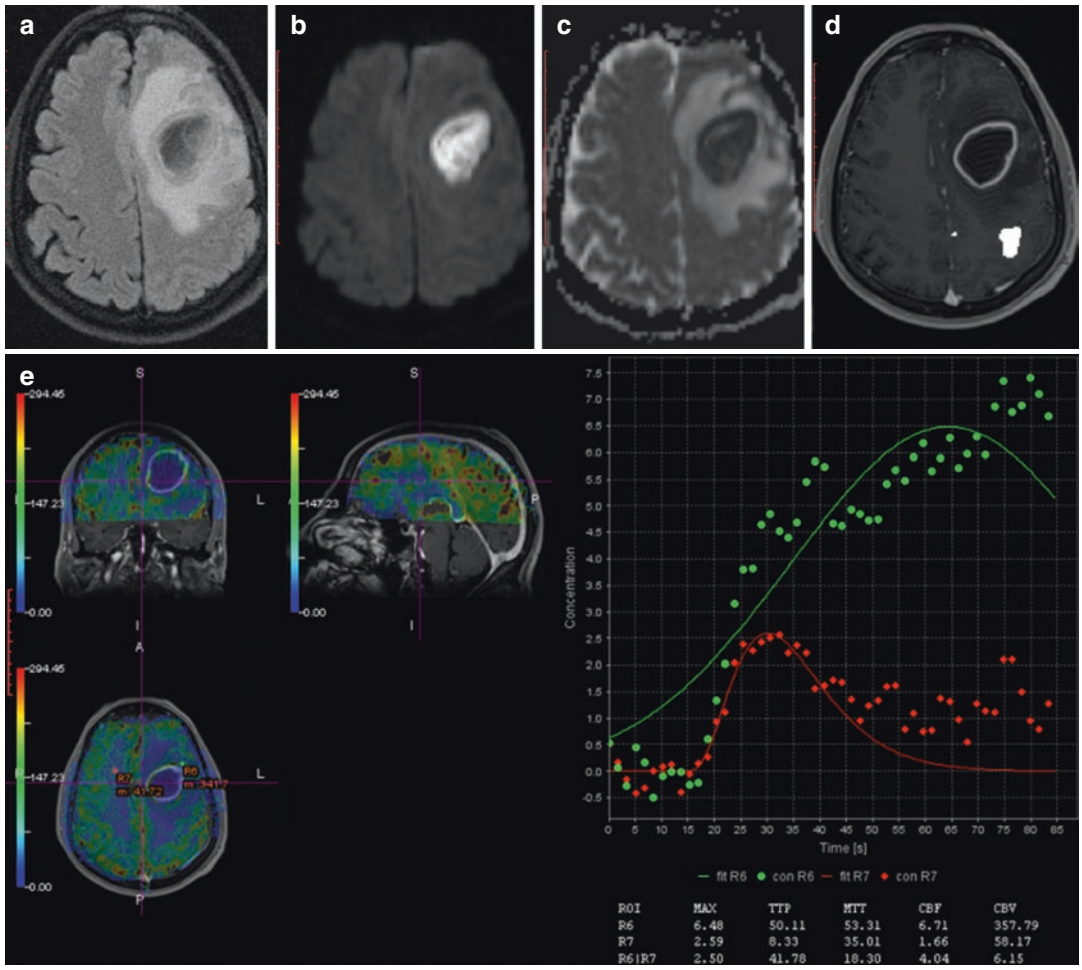

Fig. 15.3 (**a**) FLAIR, (**b**) diffusion b = 1000, (**c**) ADC map, (**d**) T1 post-gadolinium and fMRI sensorimotor activation left and e: DSC-T2∗ perfusion analysis

enhancement is demonstrated (Fig. 15.3d). Perfusion MRI showing extra-axial origin of the lesion (Fig. 15.3e) with "mother-in-law" sign in the time intensity curve (green curve, Fig. 15.3e).

15.2.1 Differential Diagnosis

- Pyogenic abscess
- Cysticercosis
- Neoplasm
- Tuberculoma
- Infarct
- Resolving hematoma

Diagnosis: Pyogenic **brain abscess** extending from frontal sinus infection.

15.2.2 Brain Abscess

15.2.2.1 Pathogenesis

Brain abscesses have been described clinically for thousands of years, yet the pathogenesis, diagnosis, and therapy of brain abscesses continue to be challenging. The pathogenesis of brain abscesses depends upon predisposing conditions. The three most common risk factors include:

1. Hematogenous spread, e.g., endocarditis
2. Penetrating wounds from trauma or iatrogenic injury
3. Venous retrograde septic thrombosis from paranasal sinus and mastoid air cell disease

Immuno-suppressed patients are at risk. This has become increasingly important, especially in patients with AIDS and posttransplant patients.

Brain abscesses typically undergo 4 stages in its development and neuroimaging features are a reflection of pathophysiological changes:

- Stage I (days 1–3) is characterized by perivascular cuffing with inflammatory cells in the region surrounding the developing necrotic center, with marked cerebral edema developing peripherally (early cerebritis, pre-encapsulation)
- Stage II (days 4–9) is characterized by early capsule formation via fibroblasts, as well as neovascularization
- Stage III (days 10–13) shows definite capsule formation with concomitant increase in fibroblast numbers, as well as shrinkage of the necrotic center and diminishing cerebritis
- Stage IV (days 14 on), a well-defined necrotic center and a dense collagenous capsule produced by fibroblasts with peripheral cerebral edema can be seen

15.2.3 Diagnostic Imaging

The older techniques used to diagnose brain abscess included pneumoencephalography, ventriculography, carotid arteriography, and nuclear brain scan. CT revolutionized the diagnosis and management of brain abscesses with refinements occurring with the advent of MRI. They can define the number, size, and locations of abscesses with a high degree of sensitivity and specificity. On CT scans, the typical appearance is of a hypodense center with circumferential ring enhancement and surrounding hypodense edema. Delayed scans with an increased enhancement in the center of the lesion may differentiate between cerebritis (medical management possible) and a true encapsulated abscess (surgical intervention is more likely needed), the latter showing a paucity of central contrast.

MRI can further delineate the lesion. Combined with gadolinium the differentiation of the central abscess, abscess rim, and surrounding edema with MRI is more accurate than contrasted CT scans. Diffusion and perfusion MR are becoming more useful in differentiating abscess from neoplasm, particularly in the patient with AIDS.

Differentiating an abscess from a metastasis may be difficult. While both of them may localize to the corticomedullary junction, a metastasis usually shows focal nodular thickening in the wall of the capsule.

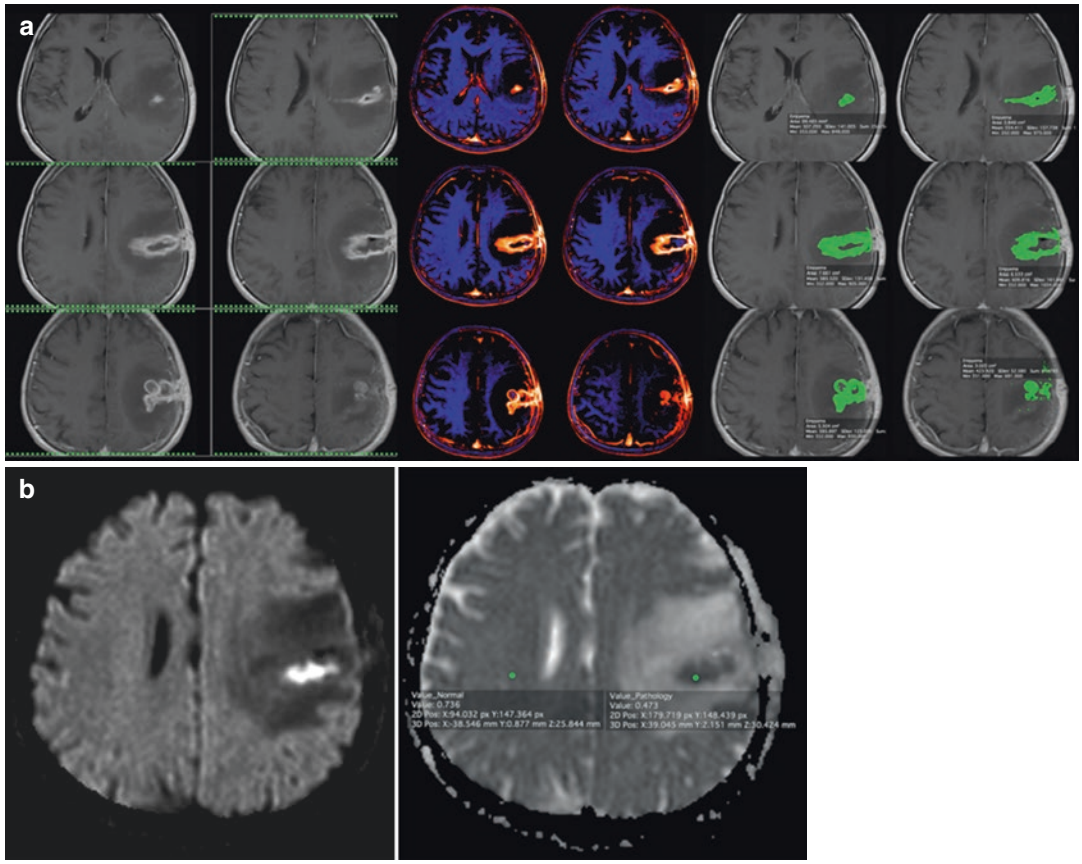

Fig. 15.4 Another example (above) of a postsurgical **empyema** showing ring-like enhancement (**a**) and marked diffusion restriction (**b**)

Selected Readings

- Patrick CC, Kaplan SL. Current concepts in the pathogenesis and management of brain abscesses in children. Pediatric Clinics of North America 1988;35(3):625–636
- Saez-Llorens XJ, Umana MA, Idio CM, et al. Brain abscess in infants and children. Pediatric Infectious Disease Journal 1989;8:449–458
- Brook I. Aerobic and anaerobic bacteriology of intracranial abscesses. Pediatric Neurology 1992;8(3):210–4
- Wispelwey B, Dacey RG, and Scheld WM: Brain Abscess, in Infections of the Central Nervous System, second edition, edited by Scheld WM, Whitley RJ, and Durack DT, Lippincott-Raven Publishers, Philadelphia, 1997;463–92
- Mathisen GE and Johnson JP: Brain Abscess. Clinical Infectious Diseases 1997;25:763–81
- Robert A. Zimmerman, Wendell A. Gobby: Neuroimaging, Clinical and Physical Principles, Springer-Verlag, NewYork, 2000;911

15.3 Fever and Headache for Several Days with Onset of Seizures

15.3.1 Diagnosis: Herpes Encephalitis

15.3.1.1 Herpes Encephalitis: Discussion

Herpes encephalitis can be caused by either the type 1 (HSV-1) or type 2 (HSV-2) viruses. HSV-2 occurs principally in neonates delivered vaginally and leads to gross brain destruction. HSV-1

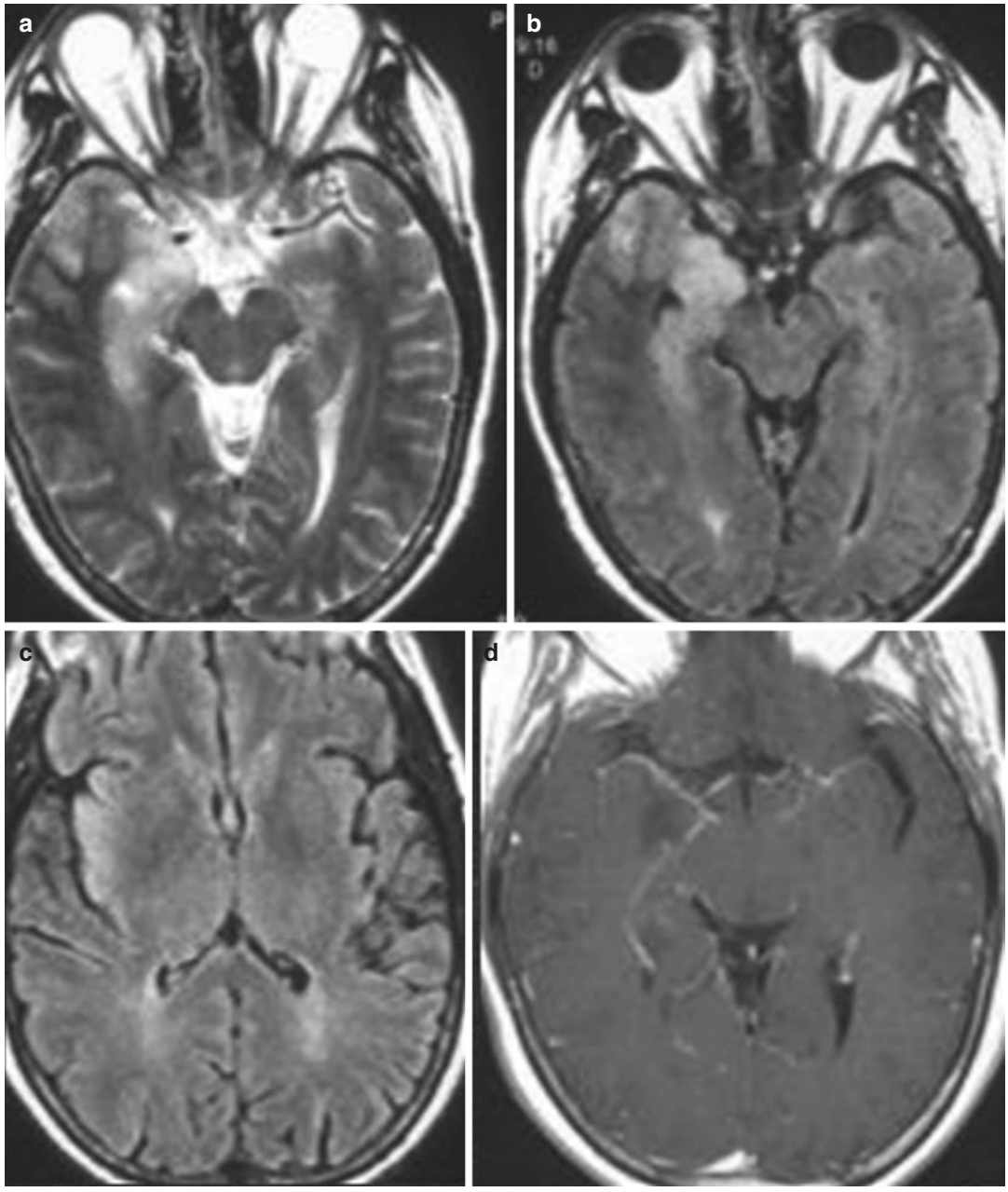

Fig. 15.5 T2WI (**a**) and FLAIR (**b**) show abnormal hyperintensity in the right deep temporal lobe involving the uncus and hippocampus and also in the insula. There is also involvement of the inferior lateral right frontal lobe. There is questionable subtle hyperintensity involving the left uncus and insula, but this could be artifactual (**c**). Postcontrast T1WI shows no abnormal enhancement, but abnormal hypo-intensity is seen (**d**)

infection in immunocompetent patients is often the result of reactivation of latent infection of the trigeminal nerve. Primary infection or reinfection can also occur, often extending from the nasal cavity to the olfactory nerves. When latent infection in cranial nerve V is reactivated, the virus spreads along branches of the nerve that supply the meninges of the anterior and middle cranial fossae, resulting in meningoencephalitis involving the inferior temporal and frontal lobes.

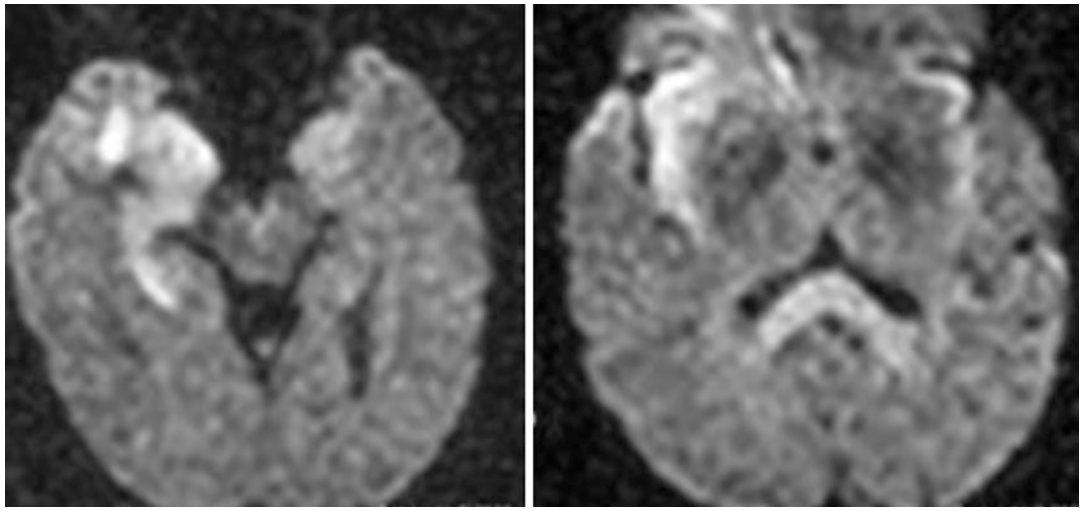

Fig. 15.6 Diffusion images (b = 1000) (above, Figure) show prolonged diffusion (high signal) in these areas. There is also slight increased signal noted in the left uncus and insula which could be artifact but also could represent early presence of infection. No definite abnormal signal is noted on the left on the FLAIR or T2WI, but there is questionable minimal hyperintensity on the FLAIR in these locations

Infection is often bilateral. Cases of localized involvement of the brainstem are believed to be related to latent infection in cranial nerves IX and X. Both HSV-1 and HSV-2 infections are seen in immunocompromised patients and often involve multiple locations.

There are approximately 2000 cases of HSV-1 encephalitis reported in the United States each year. It occurs most often in patients younger than 20 or older than 40. Temporal lobe involvement is found in 90% of cases. Clinical presentation includes headache and fever. Lethargy develops and seizures (40%) and hemiparesis (33%) are common.

Radiology: MRI is more sensitive in the detection of herpes encephalitis than CT or nuclear studies and will generally reveal the disease as early as the second day. Abnormal hyperintensity involving both gray and white matter on T2WI are noted and mass effect is eventually seen. On T1WI, involved areas may be isointense or hypointense. Postcontrast studies early in the course of the disease generally show lack of abnormal enhancement. After 3 or 4 days, abnormal enhancement similar to that seen with infarction may be noted. Decreased diffusion through involved areas leads to abnormal signal on diffusion studies. Unlike infarction, perfusion studies fail to show decreased diffusion in our experience. Focal areas of hemorrhage may be detected by gradient-recalled or T2-weighted spin echo sequences and are rarely detected by CT. Hemorrhage is always present on pathological evaluation of specimens. As mentioned, involvement of the inferior temporal and frontal lobes, including the insula and hippocampus, is seen in the vast majority of cases and should lead to the correct diagnosis. MRI often reveals bilateral, often asymmetrical, involvement when CT only shows involvement on the more severe side.

Diagnosis and Treatment: Diagnosis can be established least invasively by polymerase chain reaction (PCR) analysis when lumbar puncture is not precluded by mass effect associated with the disease process. This test has been shown to be more sensitive and specific than brain biopsy [1]. Open biopsy has been shown to be more sensitive than stereotactic biopsy. Increased white cells are also noted in the CSF. EEG is usually abnormal.

Treatment is with Acyclovir which is often administered empirically as soon as the disease is clinically considered. Treatment reduces mortality from >70% to 19%, and 38% return to normal function after therapy.

Reference

1. Domingues RB, Tsanaclis AM, Pannuti CS, Mayo MS, Lakeman FD: Clin Infect Dis 1997 Jul;25(1):86–91.

15.4 Woman with Headaches, Fatigue, and Shortness of Breath

Findings: Head CT shows numerous foci of nodular enhancement located throughout bilateral cerebral hemispheres, mostly at the gray-white junction with a few involving gray matter. A few small parenchymal calcifications are seen (Fig. 15.7)

Diagnosis: Cysticercosis of CNS

15.4.1 Cysticercosis

Cysticercosis is a parasitic infection caused by the larvae of the pork tapeworm, Taenia solium. This is the most common parasitic infection of the human central nervous system worldwide and is seen in both immunosuppressed and immunocompetent individuals. Cysticercosis is endemic in Mexico, Central and South America, India, and China. Increased prevalence in the United States results from immigration.

Humans may be infected with a tapeworm or infected with the cysticercus (larval form). When humans ingest insufficiently cooked pork that contains the viable larvae of *T. solium*, the larva develops in the small intestine into a tapeworm 1 to 8 meters in length. This tapeworm is usually asymptomatic, but it releases eggs that are passed in the stool. Pigs and humans become infected by the cysticercus after ingestion of food or water contaminated with the ova. The gastric juices within the stomach dissolve the outer thick shell of the ova and oncospheres are released. These oncospheres, the primary larvae, penetrate the intestinal tract and enter the blood stream. While they may deposit in any tissue, they show a predilection for the brain, retina, skeletal muscle, heart, and subcutaneous tissues.

The cysticerci that reach the CNS may infest the parenchyma, meninges, ependyma, choroid plexus, or spinal cord (rarely). Parenchymal neurocysticercosis is the most common. Initial cerebral infection by the larva results in a small edematous lesion which is usually asymptomatic. The secondary larvae then develop into cysts which are present approximately 2–3 months

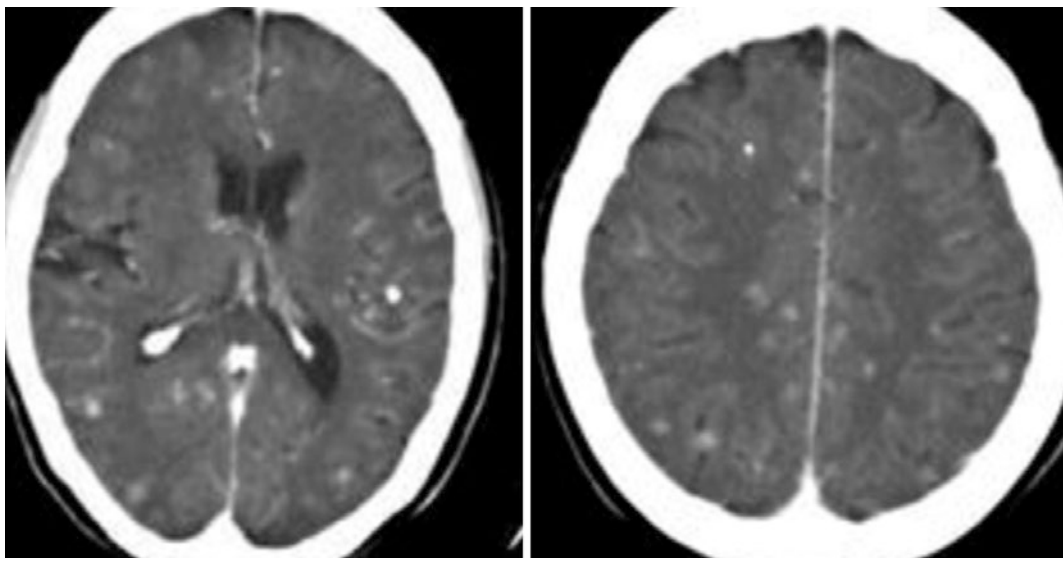

Fig. 15.7 A few small parenchymal calcifications are seen on CT images above

after the original host ingestion of ova. Each cyst contains a scolex and remains viable for 2–6 years after infestation. As the cyst dies, antigens and metabolic products are released into the surrounding brain which incite an intense inflammatory reaction with edema and mass effect. The patient may become symptomatic, and seizures occur in 30–90% of patients. The cyst then degenerates, decreases in size, and calcifies.

The infection may involve the ventricular system and/or the subarachnoid space. The subarachnoid cysts resemble a "cluster of grapes." This is known as the racemose form, and the scolex is absent. The racemose cyst can cause obstructive hydrocephalus and also a granular ependymitis from the release of toxic substances from the permeable cyst wall of the dead larvae. The racemose cyst usually does not calcify after degeneration. Chronic meningitis and/or ventriculitis can occur over years with this form.

Recurrent ingestion of ova leads to cysts in different stages of evolution. In the untreated host, the entire process of resolution of a single lesion will take 2 to 10 years. Treatment is with drugs such as praziquantel and albendazole. Intraventricular cysts may require surgical treatment if ventricular obstruction occurs.

References

1. Atlas, S.W. Magnetic Resonance Imaging of the Brain and Spine, 2nd ed. Philadelphia: Lippincott-Raven, 1996: 757–63.
2. Brant, W.E.; Helms, C.A. Fundamentals of Diagnostic Radiology, 2nd ed. Philadelphia: Lippincott Williams & Wilkins, 1999: 150–52.

15.5 A 78-Year-Old Man Presents with a Worsening Headache, Blurry Vision, and Nausea

Findings and Diagnosis: A 2-cm basilar artery thrombosed fusiform aneurysm. The finding is better demonstrated in FLAIR sequence (Fig. 15.8a) and the raw data of 3D-Time Of Flight (TOF) MRA (Magnetic Resonance Angiography) (Fig. 15.8b), than in 3D-MIP (Maximum Intensity Projection) reconstruction (Fig. 15.8c), which is giving the false impression of stenosis of the basilar artery. Thus, it is strongly recommended to evaluate MRA by combining raw data with MIP reconstructions.

15.5.1 Discussion

15.5.1.1 Epidemiology and Pathogenesis

Aneurysms are focal outpouchings of arteries containing all three vessel layers and that usually arise at arterial bifurcations. The prevalence of saccular or "berry" cerebral aneurysms has been reported in a wide range, 0.2% to 8.9% of asymptomatic individuals, while the incidence of rupture is around 6 to 8 per 100,000 per year. There is a strong genetic component, whereby patients who have more than two first-degree relatives with a history of aneurysms have around a 30% chance of having an aneurysm themselves. There is increased risk in females (1.5 times) and people of African, Japanese, and Finnish descent. There are also associations with hypertension and abnormal connective tissue disorders, such as Ehlers-Danlos syndrome, autosomal polycystic kidney disease, and fibromuscular dysplasia.

The most common cause of subarachnoid hemorrhage is secondary to trauma. Ruptured cerebral aneurysm is the most common cause of nontraumatic subarachnoid hemorrhage (85% of cases). Other, much less common causes include perimesencephalic hemorrhage from venous sources (10%), bacterial or granulomatous meningitis, or bleeding from ruptured arteriovenous fistulas or malformations. Non-contrast CT is extremely sensitive in ruling out aneurysmal subarachnoid hemorrhage. Although its sensitivity is dependent upon the amount blood and time since hemorrhage, recent research suggests that a normal head CT within six hours of headache and normal neurologic exam approaches 100% sensitivity, and a lumbar puncture may not be necessary (Dubosh et al., 2016).

Clinically, subarachnoid hemorrhage classically presents with a "thunderclap" headache, which is the worst of the patient's life and often associated with photophobia and meningism.

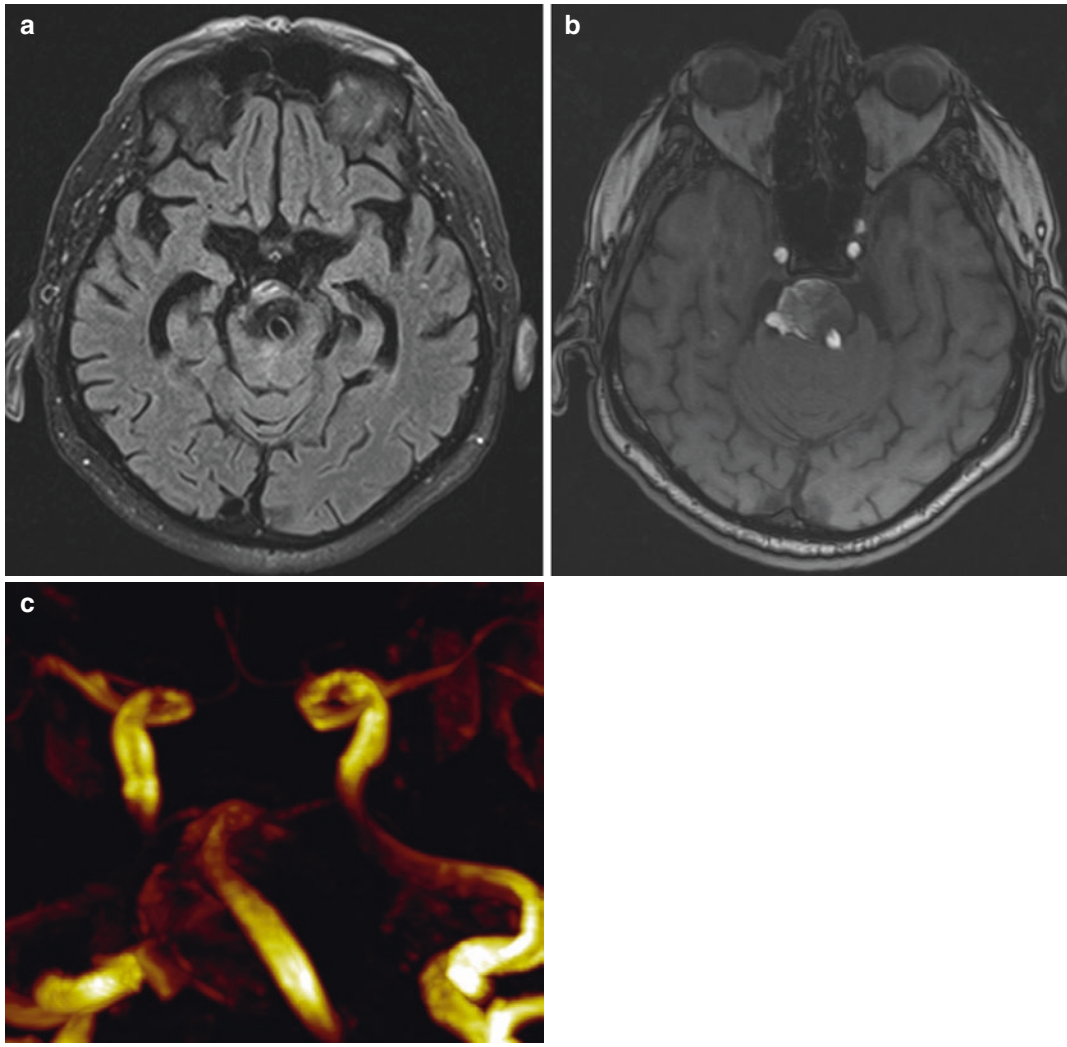

Fig. 15.8 The thrombosed aneurysm is better demonstrated in FLAIR sequence (**a**) and the raw data of 3D-Time Of Flight (TOF) MRA (Magnetic Resonance Angiography) (**b**), than in 3D-MIP (Maximum Intensity Projection) reconstruction (**c**), which could be false interpreted as stenosis of the basilar artery

Around 4% to 22% of patients presenting with thunderclap headaches are found to have subarachnoid hemorrhage. The degree of symptoms is highly correlated to both the degree of hemorrhage and the morbidity and mortality, with more severe cases presenting with complete loss of consciousness and high rates of mortality.

15.5.2 Imaging Findings

CT

- Blood will be seen as hyperattenuating material (40–60 HU) filling the subarachnoid space, including within the suprasellar cisterns and perimesencephalic cisterns, and can be seen extending into the fissures and cerebral convexities
- The most sensitive place is within the interpeduncular fossa

Locations of cerebral aneurysms: Around 85% are found in the anterior circulation, with 30% to 40% arising from the anterior cerebral or anterior communicating artery, 30% from the posterior communicating artery, 20% to 30% at the middle cerebral artery bifurcation, and 5% to 10% within the internal carotid artery. Around

15% arise from the posterior circulation, which includes within the basilar tip, superior cerebellar artery, and posterior inferior cerebellar arteries.

CT/CTA

- On CT, aneurysms are usually well-defined, round, slightly hyperattenuating lesions, sometimes with peripheral calcification
- On postcontrast CT images, there will be bright and uniform enhancement within the aneurysm sac, whereas in a thrombosed aneurysm there will be a filling defect and rim enhancement
- CTA allows for detailed anatomy of the vasculature and detection/characterization of aneurysms larger than 3 mm

MRI/MRA

- MRI is more sensitive with hyperintensity seen on fluid-attenuated inversion recovery (FLAIR) images and magnetic susceptibility seen on gradient-recalled echo (GRE) sequences
- Aneurysms can sometimes be seen as large flow voids on T2-weighted sequences
- Three-dimensional time-of-flight MR angiograms can generate detailed images of the vasculature without radiation or contrast, but the spatial resolution is lower, and it is prone to motion artifacts

Digital subtraction angiography (DSA)

- DSA is more accurate and sensitive for detecting small aneurysms. Has both higher spatial and temporal resolution, as CTA often overestimates size compared with angiography
- It is associated with higher procedural risks, including stroke
- Allows for a more careful analysis of the size and shape of the body and neck, which is important for treatment planning

15.5.3 Treatment and Prognosis

Despite improvements in diagnosis and treatment of ruptured aneurysms, the mortality is still high, around 50%. Management relies heavily on reimaging to assess for re-hemorrhage, hydrocephalus, vasospasm, and cerebral edema. The Hunt and Hess grading system can be used to predict mortality and depends on the neurologic deficit produced from the subarachnoid hemorrhage, which ranges from 5% in patients with severe headaches but no neurologic deficit to 77% in patients with a deep coma.

Treatment of ruptured aneurysms includes endovascular intervention, which includes coiling in most cases and additional supporting treatments such as prevention of vasospasm.

The prognosis/treatment of unruptured aneurysms is somewhat controversial. The larger the aneurysm and interval increase in size are highly predictive of future rupture. Traditionally, aneurysms less than 7 mm were thought to have a low risk of rupture. Additional important factors include increase in size and whether the patient is a smoker (Villablanca et al., 2013). On average, they found about 1.8% of aneurysms ruptured per year.

References

1. Dubosh NM, Bellolio MF, Rabinstein AA, Edlow JA. Sensitivity of early brain computed tomography to exclude aneurysmal subarachnoid hemorrhage. *Stroke*. 2016;47(3):750–755.
2. Hacein-Bey L, Provenzale JM. Current imaging assessment and treatment of intracranial aneurysms. *AJR Am J Radiol*. 2011;196(1):32–44.
3. Tomandl BF, Köstner NC, Schempershofe M, et al. CT angiography of intracranial aneurysms: A focus on postprocessing. *Radiographics*. 2004;24(3):637–655.
4. Villablanca JP, Duckwiler GR, Jahan R, et al. Natural history of asymptomatic unruptured cerebral aneurysms evaluated at CT angiography: Growth and rupture incidence and correlation with epidemiologic risk factors. *Radiology*. 2013;269(1):258–265.

15.6 Thirty-Year-Old Woman with Left Arm and Leg Paresis

15.6.1 Radiographic Findings

Multifocal areas of T1-dark, T2-bright lesions in periventricular, bilateral internal capsule. One large area in the periventricular region right show central necrosis (Fig. 15.9a). Ring and arc enhancement is seen (Fig. 15.9b).

15.6.2 Proposed Differential Diagnosis

- Multiple Sclerosis (considered most likely)
- Lyme disease or other vasculitis
- Tumor
- Abscesses
- ADEM

Diffusion (Fig. 15.9c, d) and perfusion (Fig. 15.10) studies exclude the possibility of glioma, lymphoma, and metastasis

Actual Pathology: Based on clinical presentation, negative serologic work up, lack of mass effect, propensity for white matter, and lack of a consistent enhancement pattern, the findings were presumed to represent "**tumefactive" multiple sclerosis**.

15.6.3 Multiple Sclerosis

Multiple sclerosis is the most common demyelinating disease; it is primarily a disease of the oligodendroglia and consists of multifocal well-demarcated areas of demyelination with little or no axonal degeneration. The diagnosis of MS is a clinical one, and the cornerstone of the diagnosis is the neurological exam. The diagnosis is based on symptoms as well as objective evidence of white matter lesions in the CNS, disseminated both temporally and spatially. The most common symptoms at initial presentation are disturbances in sensation (53%), gait (50%), and visual loss (22%). Support for the diagnosis as well as exclusion of other disease processes comes from additional examinations such as examination of the CSF for evidence of a CNS inflammatory process (increased gamma globulins as well as oligoclonal bands), and evoked potential studies. However, MRI is the most frequently performed study to evaluate the presence of white matter lesions as well as exclude other neurological disorders. Diagnostic criteria have been developed and in patients with "clinically definite" MS, MRI is able to support the diagnosis in up to 95% of cases, and in approximately 70% of "clinically suspected".

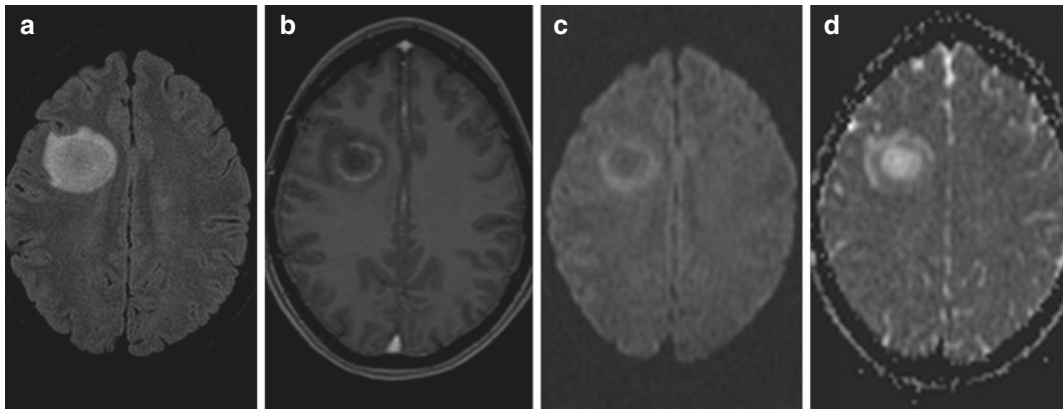

Fig. 15.9 (**a**) FLAIR, (**b**) T1 post-gadolinium, (**c**) diffusion b = 1000, (**d**) ADC map

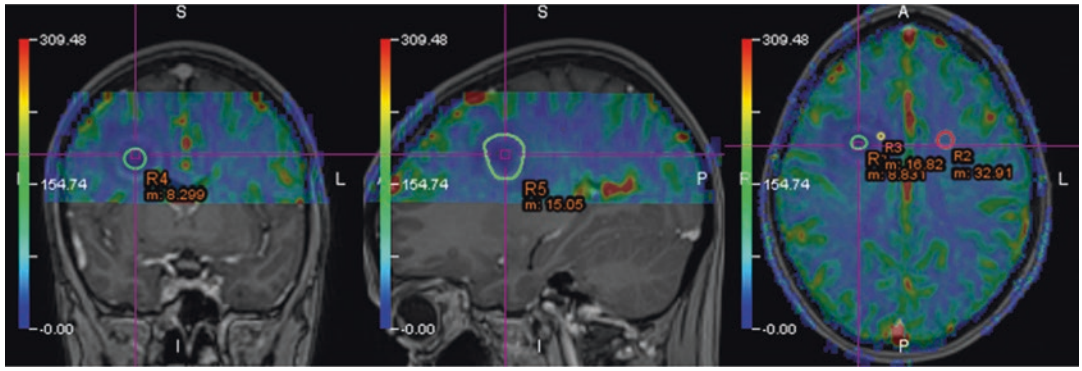

ROI	MAX	TTP	MTT	CBF	CBV
R4	0.99	5.69	23.01	0.36	8.34
R2	3.24	5.87	23.61	1.38	32.59
R4IR2	0.30	–0.18	–0.60	0.26	0.26

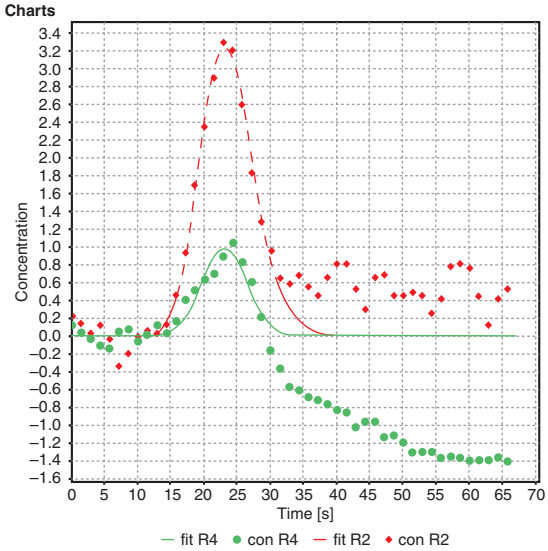

Fig. 15.10 DSC-T2*Perfusion study showing very low rCBV ratio = 0.26 (lesion compared to normal appearing white matter), as well as a curve with severe T1 contamination effect (in the late phase, the green curve is returning below the baseline), which is characteristic of significant blood-brain barrier disruption and pathognomonic for an inflammatory process

15.6.4 Epidemiology/Etiology

The prevalence of MS is 58/100,000 in the US or 0.058%. It is primarily a disease of young adults and the median age at presentation is 33, with 13% of patients presenting <20, 30% 20–29, 28% 30–39, 14% 40–49, and 15% at 50+ years. The disease is more common in woman (63%) and the average age of onset is 2–3 years younger for women. It is also more common in whites; different races appear to have different susceptibilities to the disease. A great deal of evidence is available to suggest that the disease is somehow acquired prior to the first clinical presentation. The disease incidence varies with latitude, with the high frequency zones being between 45 and 65 degrees. All studies of Asia and Africa show a low prevalence, and there is no well-documented case of the disease arising in an African black.

A large amount of evidence also suggests that the disease is caused by an infectious agent, possibly a slow virus. In support of this theory is the finding that with migration the person acquires the risk of the new residence if migration takes place at <15 years, or keeps the risk of the birthplace if it occurs at >15 years. Several studies

have pointed out a relationship to MS and canine distemper, as well as the similarities between the epidemiology of MS and the poliovirus before vaccination. One theory is that perhaps MS is an unusual manifestation of a common enteric virus in those people who have had less contact with this agent during their early life, and who have failed to develop immunity by late childhood. There also appears to be a genetic or familial disposition to the disease, with an increased risk of developing the disease in twins, sibs(20X), and in children (12X) of the afflicted individual. Approximately 10% of patients have a positive family history. Certain HLA types seem to have an increased risk, as with polio.

15.6.5 Pathology

The early stages of the disease are characterized histologically by an altered staining in the white matter with an irregular bubbly expansion within the myelin sheath. Neuroglial proliferation is seen, and the affected area of the CNS becomes soft. After several weeks an infiltration of phagocytic cells is present which have become laden with phagocytized fragments of myelin and its degeneration products, which are sudanophilic. As a rule, the axons are intact but there may be a loss in cases of rapidly progressive demyelination. The nerve cell bodies appear normal. With increasing time, well-defined plaques are formed which may no longer stain positively for myelin. Frequently perivascular lymphocytic cuffing of small vessels is seen. Minimal regenerating myelin may be seen, which is of limited extent. Regenerative astrocytes with prominent cytoplasm and cellular processes are seen within and surrounding the lesion. The oligodendrocytes are decreased but may be preserved at the periphery. In old or inactive lesions there is moderate to advanced fibrillary gliosis, and the lesions are devoid of oligodendrocytes. This dense gliosis accounts for the original histologic description of this process as multiple "sclerosis." Little or no perivascular inflammatory changes remain. Large plaques may show varying histology, with the center showing chronic changes with active or acute changes seen in the periphery of the lesions.

15.6.6 Distribution

Any white matter within the CNS may be affected by this process, but most frequently these lesions are present within the periventricular white matter (approximately 40% of lesion). Lesions within the brain are roughly symmetrical. MS is frequently found within the brainstem and the cerebellum; surrounding the third and fourth ventricles is an additional common location. However, the distribution of the lesions is highly variable and there may be extensive spinal cord involvement with minimal brain involvement. Approximately 10% of lesions are said to involve the gray matter but this is difficult to visualize pathologically and is not seen on either CT or MR images. Lesions may involve the optic nerves, chiasm, or tracts. Root involvement of the cranial and spinal nerves is possible but rare. The plaques may vary greatly in size, occasionally they may be very large and simulate a mass lesion.

15.6.7 Radiology

It is now well known that MRI is much more sensitive than CT for the detection of plaques with definite MS; MRI was abnormal in >90% of cases, as compared to approximately 25% of CTs, 74% of CSF examinations, and 80% of paraclinical studies. It is also more sensitive than the physical examination in the detection of active disease; this is not surprising as many lesions may occur in clinically "silent" areas. Typically, the lesions are of increased signal intensity on T2-weighted images; Tl-weighted images are frequently normal but may have decreased signal intensity. These findings are presumed secondary to demyelination with subsequent increase in tissue water content. It must be remembered, however, that the MR findings are relatively nonspecific, and that with increasing patient age foci of increased signal intensity are frequently seen. These lesions have been termed "UBOs" or unidentified bright objects. They are, however, rare in patients <40 and infrequent in the 40–49 age group. At ages >50 it becomes increasingly difficult to differentiate

age related changes from changes associated with MS: the "classic" aged brain of patients >50 may be identical in appearance to the "classic" MS patient <50. Other disease may also show similar abnormalities on T2, secondary to degeneration, infarction, gliosis, or demyelination. Atrophy is frequently associated with MS in 21–78% of cases, both centrally and peripherally. Rarely there may be evidence of mass effect, particularly with large active plaques. In this situation it may be extremely difficult to differentiate MS from tumor.

Increased signal on Tl images has been described. This has been proposed secondary to an increase in tissue protein, the presence of lipid-laden macrophages or free radicals within the macrophages, or possibly areas of hemorrhage. An additional, albeit rare, finding is evidence of increased iron deposition within the basal ganglia on susceptibility sequences in severe cases.

Contrast enhancement has been used to determine the presence of active lesions, as enhancement represents breakdown in the blood brain barrier that is felt to accompany active disease. A very good correlation has been shown between active disease pathologically and the presence of MR enhancement; it is felt that the BBB breakdown may be related to the early macrophage infiltration. MR is also, not surprisingly, much more sensitive than CT in the detection of active MS. Longitudinal MR studies have revealed the dynamism of MS plaques. They have shown that areas of enhancement may develop from areas of previously T2 bright white matter, or alternatively from areas of previously "normal" brain. In addition, areas of previous enhancement may revert to isointensity or hyperintensity on T2 images. The disappearance of signal suggests that perhaps a reparative process such as demyelination may take place, or alternatively inflammation with edema and little demyelination may resolve. MR has been used to gauge treatment efficacy in the past, as steroids can cause "healing" of the BBB and decrease in enhancement. However, these newer studies show that caution may be warranted in the use of MR in gauging the efficacy of therapy.

CT is used much less frequently in the evaluation of patients with MS, as it is much less sensitive than MR. However, findings present in "old" lesions are decreased attenuation in the region of plaques (also due to increased tissue water), and hypo or isodense lesions with contrast enhancement in active lesions. Delayed scanning with higher contrast volumes has been reported in the past to increase sensitivity. CT is poor in the evaluation of cord and brainstem lesions.

15.6.8 Prognosis

The prognosis in patients with MS is extremely variable and does not appear to relate to the relapse rate. At least 20% of patients have a benign course for 15 or more years. One study showed the percent of patients ambulatory twenty five years after diagnosis to be greater than 2/3. In general, better prognostic factors include the female sex, age less than 40 at presentation, initial symptoms referable to sensation rather than motor, and the absence of disability at five years after the initial diagnosis.

Tumefactive Multiple Sclerosis: ("tumefactive" = swollen or puffy condition, a visual characteristic lending to this description of one or more MS plaques). In tumefactive MS, the lesions show less mass effect and usually respect gray matter when compared to tumor or abscess.

References

1. Grossman RI et al. Multiple sclerosis: serial study of gadolinium enhanced MR imaging. Radiology 1988 169:117–122.
2. Latchaw RE.MR and CT Imaging of the Head Neck and Spine.2nd Ed.1991 Mosby Year Book.
3. Nesbit GM et al. Multiple Sclerosis: histopathologic and MR and/or CT correlation in 37 cases at biopsy and three cases at autopsy. Radiology Aug 1991 180(2):467–74.
4. PatyDw et al. MRI in the diagnosis of MS: a prospective study with comparison of evoked potentials, oligoclonal banding, and CT. Neurology 1988 38: 180–85.

5. Swanson JW. Multiple sclerosis: update in diagnosis and review of prognostic factors. Mayo Clin Proc 1989 64:577–86.
6. Tourtelotte WW. Current concepts about multiple sclerosis. Mayo Clin Proc 1989 64:592–5.

15.7 Seventy-Year-Old Man with Headache

Findings: Heterogeneous right temporal lobe mass (Figs. 15.11, 15.12, 15.13 and 15.14). There is associated susceptibility on gradient images (Figs. 15.11d, 15.12a, 15.12c, 15.13, 15.14), however, no diffusion restriction (Fig. 15.11c). There are also multiple punctate/small foci of susceptibility distributed throughout the cerebral hemispheres centered at the corticomedullary junction (Fig. 15.13). Also noted were foci of T2 prolongation scattered throughout the centrum semiovale, corona radiata, and subcortical white matter, consistent with microvascular disease (Fig. 15.11a) without enhancement (Fig. 15.11b).

Also, the longitudinal follow-up is shown, without any notifiable change (Fig. 15.14).

15.7.1 Differential Diagnosis

- Hypertensive micro hemorrhages
- Ischemic stroke with micro hemorrhage
- Multiple vascular malformations
- Traumatic diffuse axonal injury

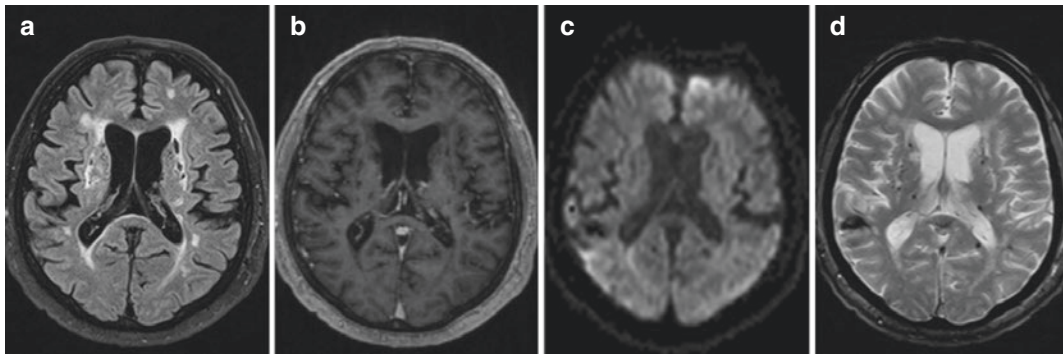

Fig. 15.11 (**a**) FLAIR, (**b**) T1 post-gadolinium, (**c**) diffusion b = 1000, (**d**) gradient-echo T2∗

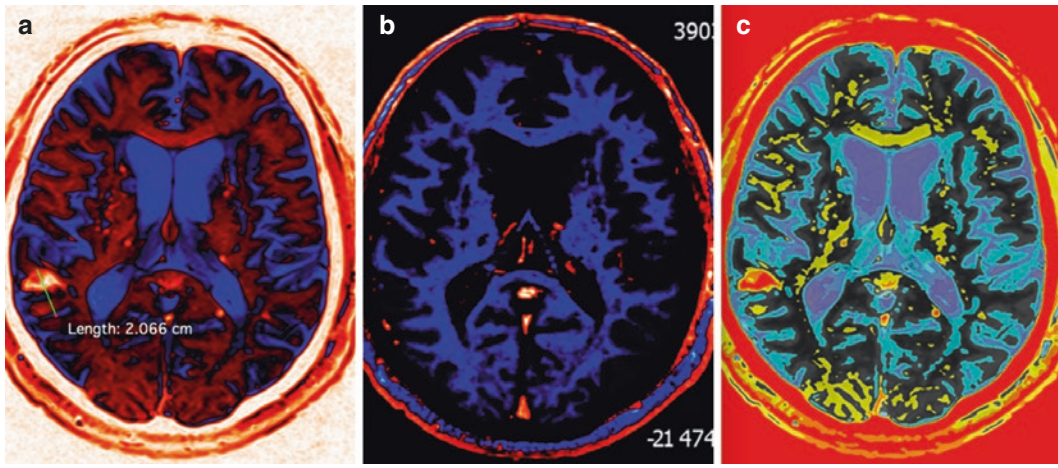

Fig. 15.12 (**a**) Color-encoded Gradient-echo T2∗, (**b**) Color-encoded T1-W Subtracted Image, (**c**) Fused **a** + **b** image

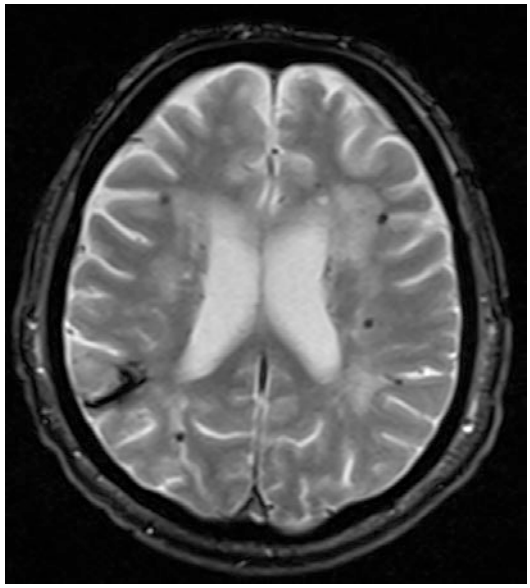

Fig. 15.13 Gradient-echo T2∗ (Haemo)

- Amyloid angiopathy
- Hemorrhagic metastasis
- CADASIL (cerebral autosomal dominant arteriopathy with subcortical infarcts and leukoencephalopathy)
- Metallic microemboli from artificial heart valves

Diagnosis: **Amyloid angiopathy** with right temporal lobe hemorrhage.

- Amyloidosis—rare systemic disease caused by extracellular deposition of ß-amyloid
- 10–20% localized form, inclusive of CNS
- Can be idiopathic/primary or secondary/reactive (dialysis related amyloidosis)
- Cerebral amyloid deposition: 3 varieties
  - Cerebral amyloid angiopathy (most common)

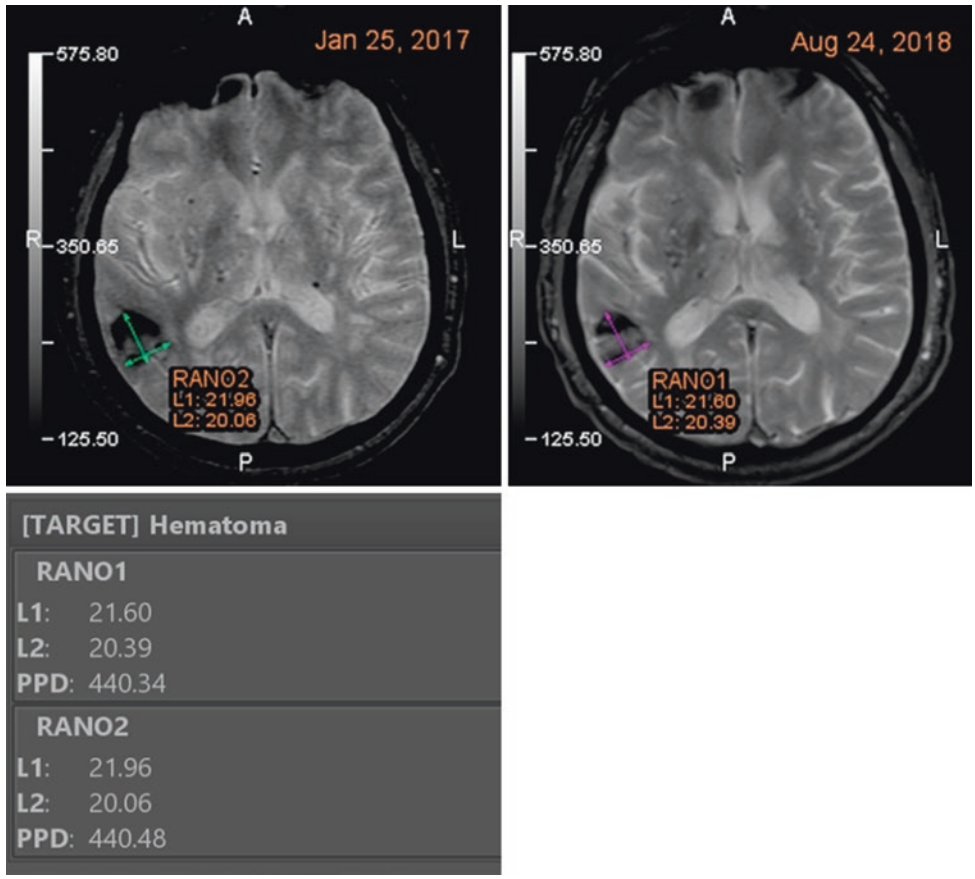

Fig. 15.14 Gradient-echo T2∗ (Haemo)

  - Amyloidoma (rare)
  - Diffuse white matter involvement (rare)
- Common cause of spontaneous lobar hemorrhage in elderly (1% of all strokes)
- Responsible for 15–20% of ICH in patients >60 years old
  - 27–32% of normal elderly (autopsy)
  - 82–88% in Alzheimer's disease
  - Common in Down's syndrome

15.7.2 Imaging Features

- Multifocal "black dots" representing chronic micro hemorrhages
- Lobar hemorrhages of different ages
- Involves subcortical WM (gray/white junction), parietal and occipital lobes (autopsy), also frontal and temporal lobes
- Less commonly involves brainstem, deep gray matter, cerebellum, hippocampus
- Acute lobar hemorrhages tend to be large and irregular with dependent blood sedimentation
- Punctate foci of dark susceptibility on T2∗GRE sequences (blooming) seen with chronic micro hemorrhages
- Focal or patchy/confluent WM disease associated in approximately 70%

Key Points

- Non-contrast CT best initial screening study (evaluate for acute hemorrhage)
- Consider T2∗GRE sequence in all patients >60

Reference

1. Osborne A, Blaser S, Salzman K, et al. Diagnostic Imaging Brain. Salt Lake City: Amirsys, 2004.

15.8 Follow-Up Imaging Status 4 Months Postradiation Treatment in a Grade IV Tumor

15.8.1 Radiographic Findings

MRI shows a residual enhancing mass in the left frontal region with low signal within suspicious for central necrosis. There is peripheral enhancement with gadolinium and surrounding edema and volumetric segmentation of the lesion (Fig. 15.15, green color and Fig. 15.16, blue color).

Diffusion, permeability, and DSC-T2∗ perfusion (Fractional Tumor Burden Histogram, Fig. 15.17) imaging show characteristical biomarkers (mean ADC = 1.678 > 1.1 × 10^3 mm^2/s, mean K^{trans} = 0.009 < 0.08 min^{-1} and mean rCBV ratio = 0.35 < 1.75) compatible with radiation necrosis (Fig. 15.18).

References

1. Katsaros VK, Nikiforaki K, Manikis G, Marias K, Liouta E, Boskos C, Kyriakopoulos G, Stranjalis G, Papanikolaou N. Whole tumor MR Perfusion histogram analysis in the preoperative assessment of patients with gliomas: Differentiation between high- and low-grade tumors. Hell J Radiol 2017; 2(1): 30–38.
2. Ulyte A, Katsaros VK, Liouta E, Stranjalis G, Boskos C, Papanikolaou N, Usinskiene J, Bisdas S. Prognostic value of preoperative dynamic contrast-enhanced MRI perfusion parameters for high-grade glioma patients. Neuroradiology. 2016;58(12):1197–1208.

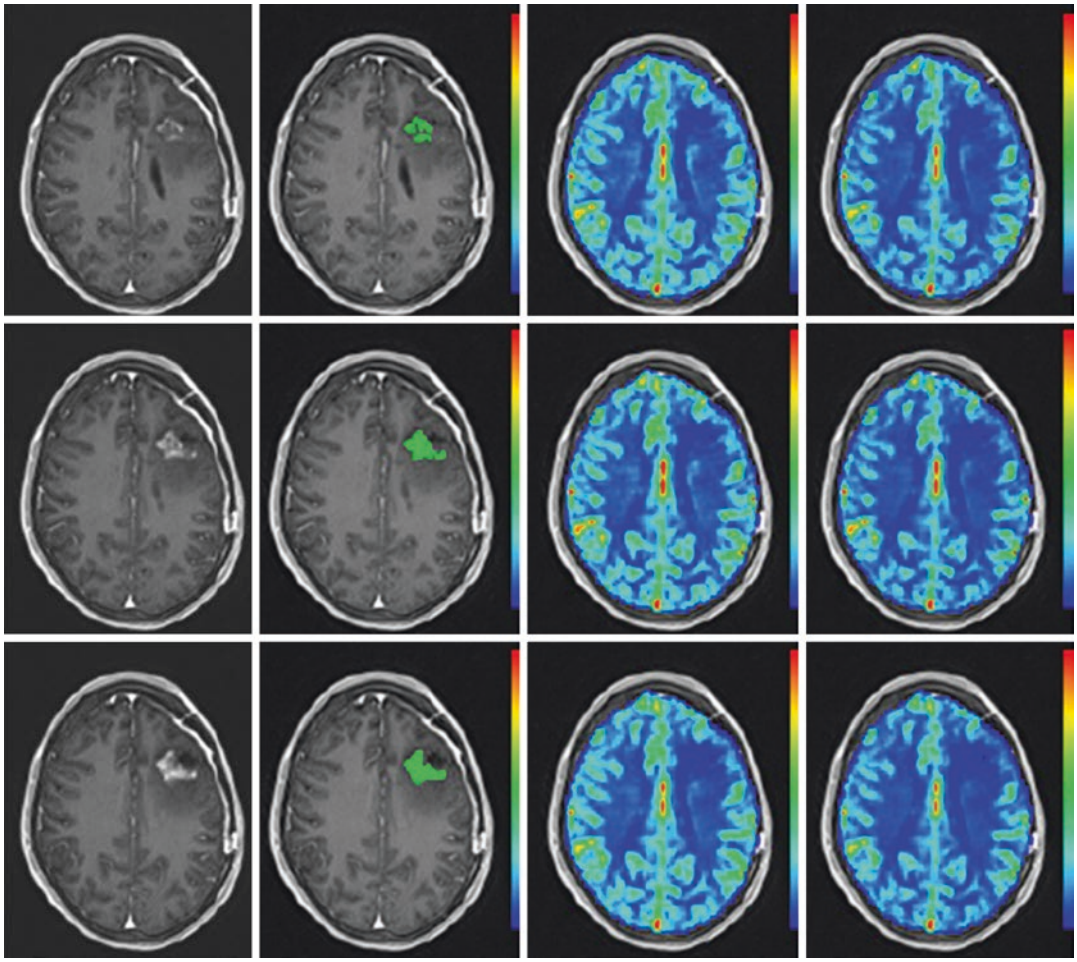

Fig. 15.15 Volumetric segmentation of the enhancement region (green)

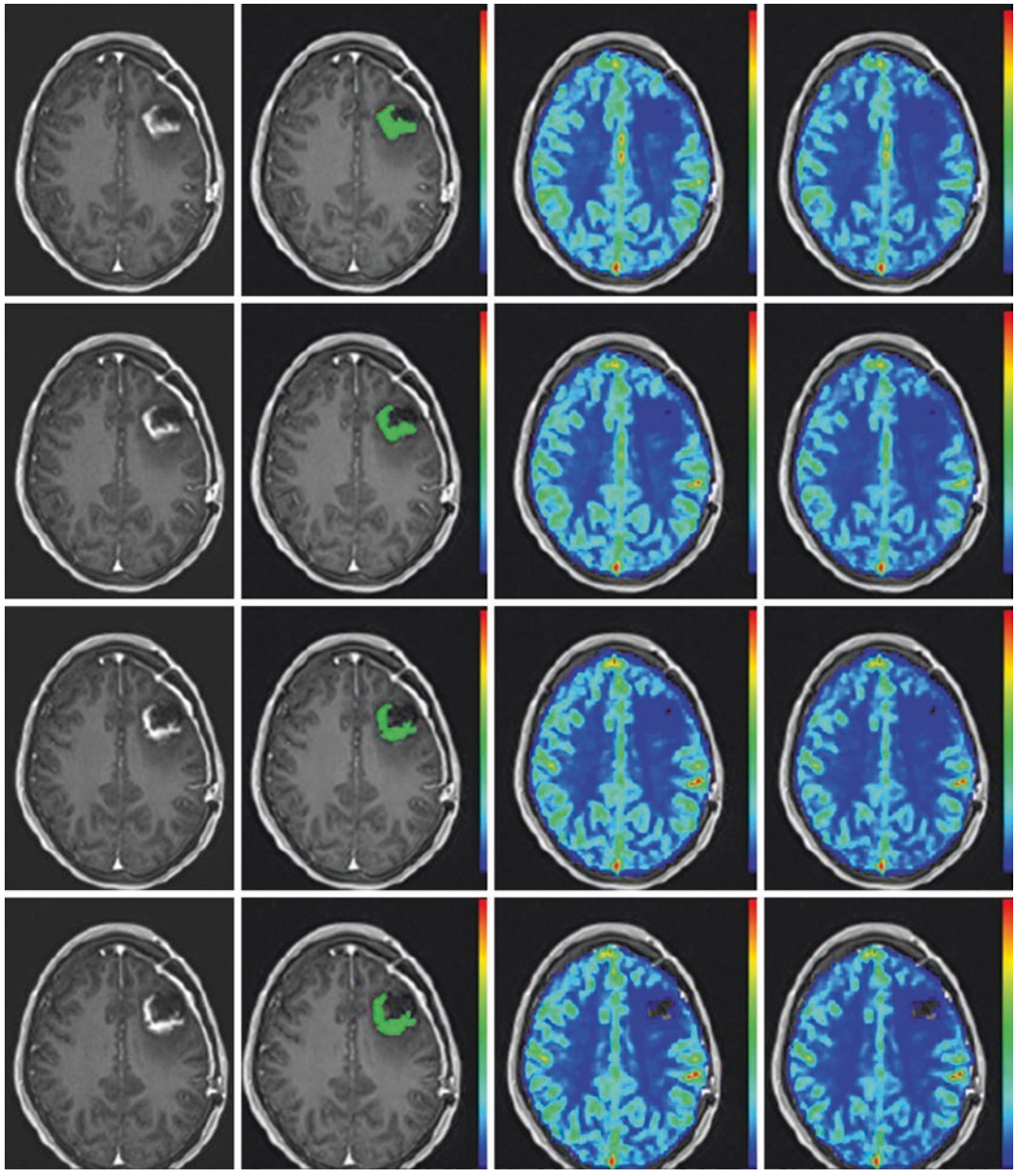

Fig. 15.15 (continued)

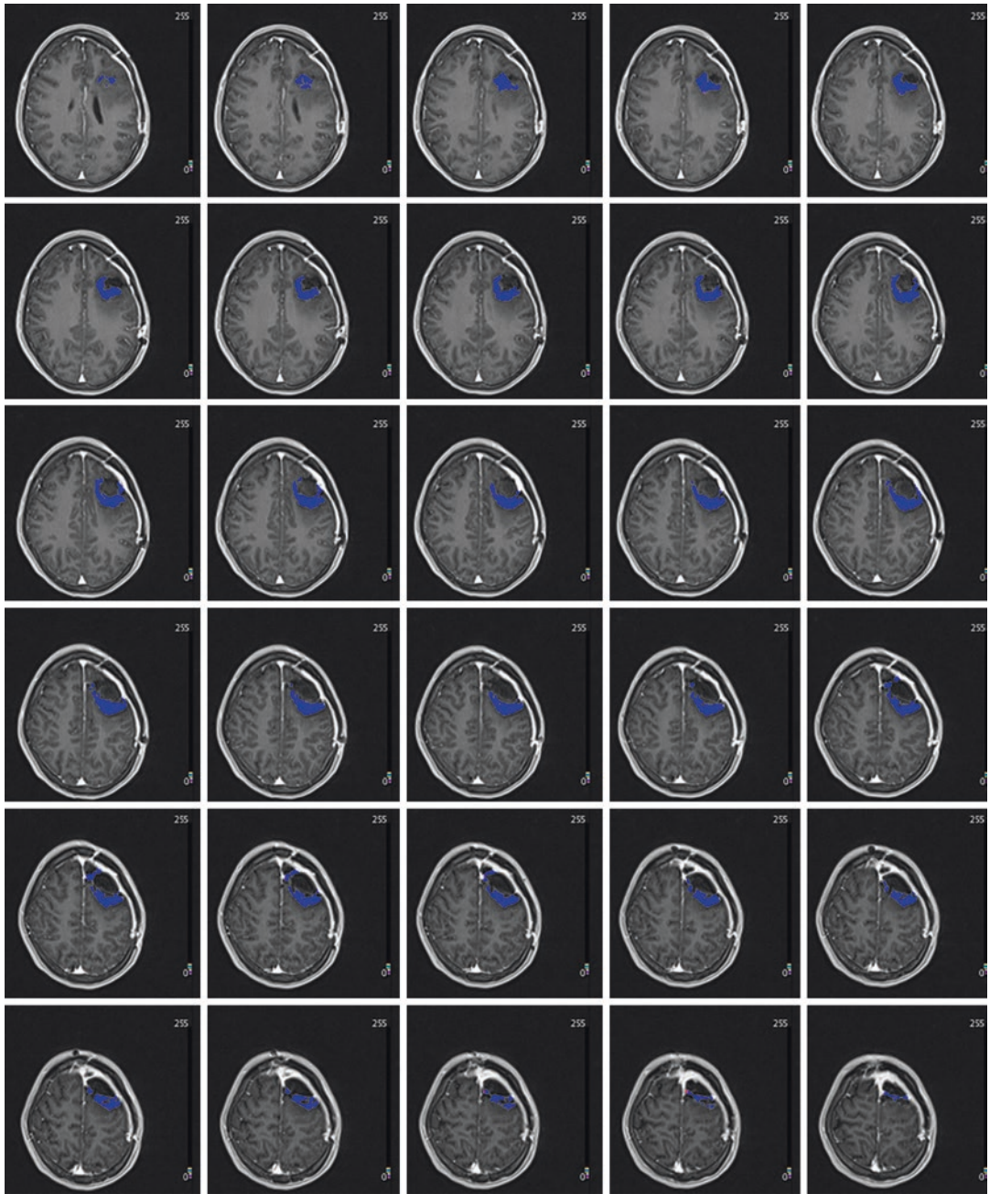

Fig. 15.16 Color encoded pixel by pixel segmentation of the enhancement region (blue representing treatment effect, purple: tissue in risk and red: relapse, correspondingly)

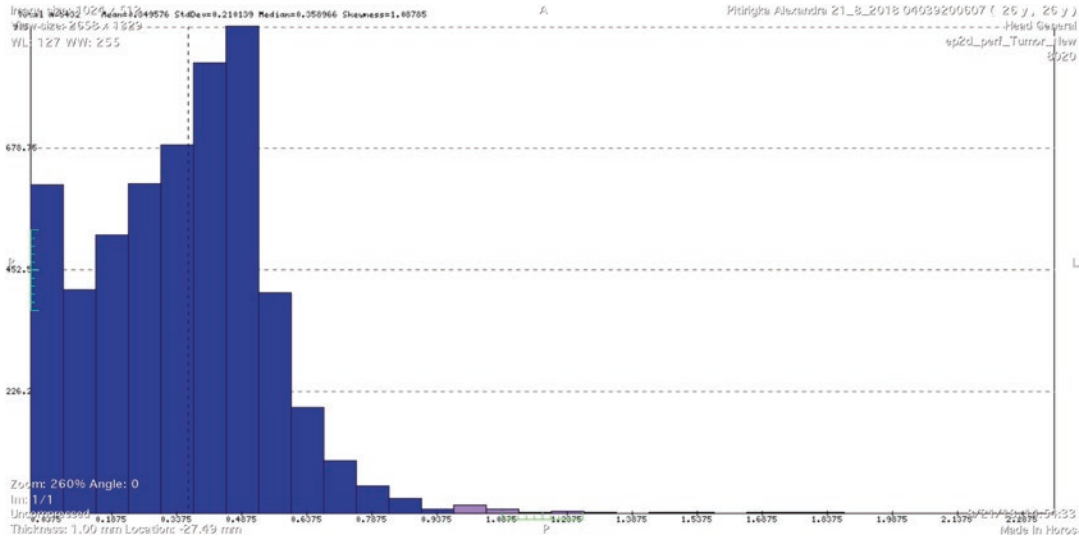

Fig. 15.17 Fractional tumor burden histogram

Fig. 15.18 Metrics of diffusion, permeability, and perfusion

ADC (RESEARCH) (registered)	**Extended Tofts Ktrans (linear) (RESEARCH) (registered)**	**rCBV (standardized) (leakage-corrected) (RESEARCH) (registered)**
(Tumor ROI)	(Tumor ROI)	(Tumor ROI)
Maximum = 3.12002	Maximum = 0.107118	Maximum = 2.33093
Median = 1.47427	Median = 0.00370638	Median= 0.360246
Mean = 1.67826	Mean = 0.00966315	Mean = 0.350478
Standard Deviation = 0.484946	Standard Deviation = 0.0135043	Standard Deviation = 0.21217
Volume = 9209.53	Volume = 9209.53	Volume = 9209.53

Preoperative Surgery Planning and Perioperative Imaging

16

Murat Şakir Ekşi, M. Memet Özek,
M. Necmettin Pamir, and Alp Dinçer

16.1 Pituitary Adenoma

A 68-year-old man was admitted to the clinic because of dizziness and new-onset hypertension. He was operated on via transsphenoidal way following radiological diagnosis of pituitary macroadenoma (Figs. 16.1–16.4). Pathology was consistent with pituitary macroadenoma with follicle stimulating hormone (FSH) and luteinizing hormone (LH) immunosuppressed type. The patient was well and took hormone-replacement therapy under supervision of endocrinologist in the postoperative period.

M. Ş. Ekşi (✉) · M. M. Özek · M. N. Pamir
Department of Neurosurgery, Acıbadem Mehmet Ali Aydınlar University School of Medicine, Istanbul, Turkey

A. Dinçer
Department of Radiology, Acıbadem Mehmet Ali Aydınlar University School of Medicine, Istanbul, Turkey

Y. Özsunar, U. Şenol (eds.), *Atlas of Clinical Cases on Brain Tumor Imaging*,
https://doi.org/10.1007/978-3-030-23273-3_16

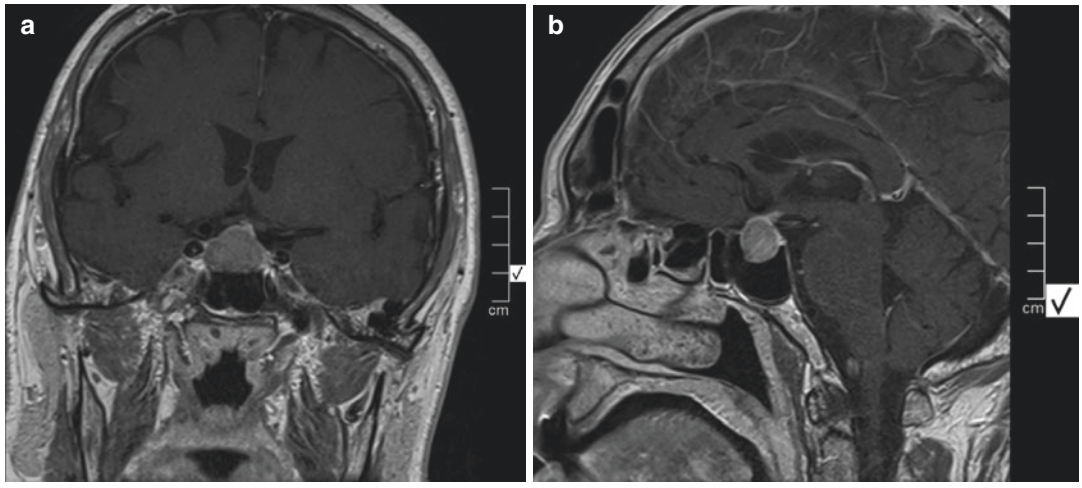

Fig. 16.1 Preoperative contrast-enhanced T1-weighted coronal (**a**) and sagittal (**b**) sellar magnetic resonance images (MRI) depicted sellar enlargement with a mass lesion enhancing diffusely and heterogenously**.** The mass lesion, compatible with pituitary macroadenoma, had diameters of 1.6 × 1.6 × 2.3 cm. The pituitary macroadenoma located in the anterior pituitary lobe had thrusted the optic chiasm upwards

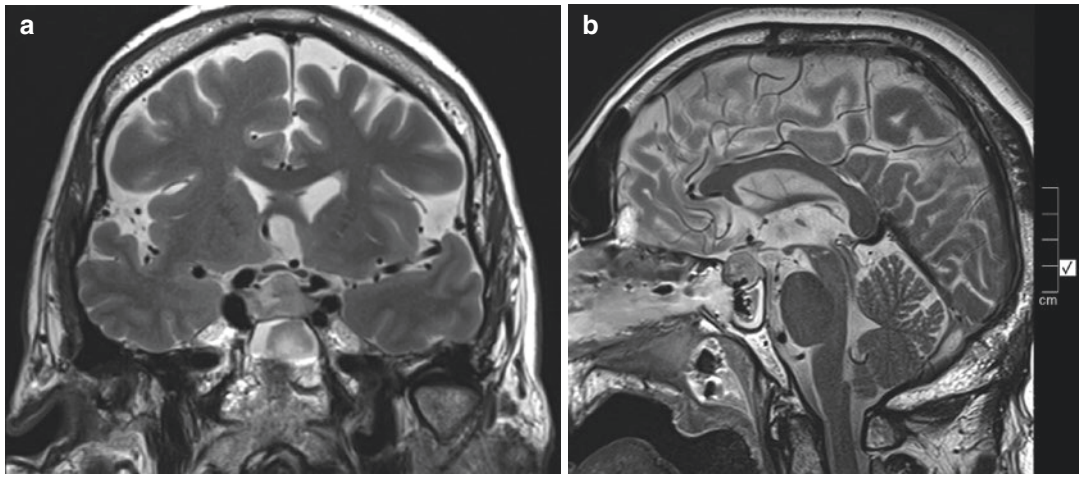

Fig. 16.2 Perioperative T2-weighted coronal (**a**) and sagittal (**b**) sellar MR views depicted operative changes beside residual pituitary adenoma, isointense to brain parenchyma. The patient was taken to the operating room for further resection of the adenoma

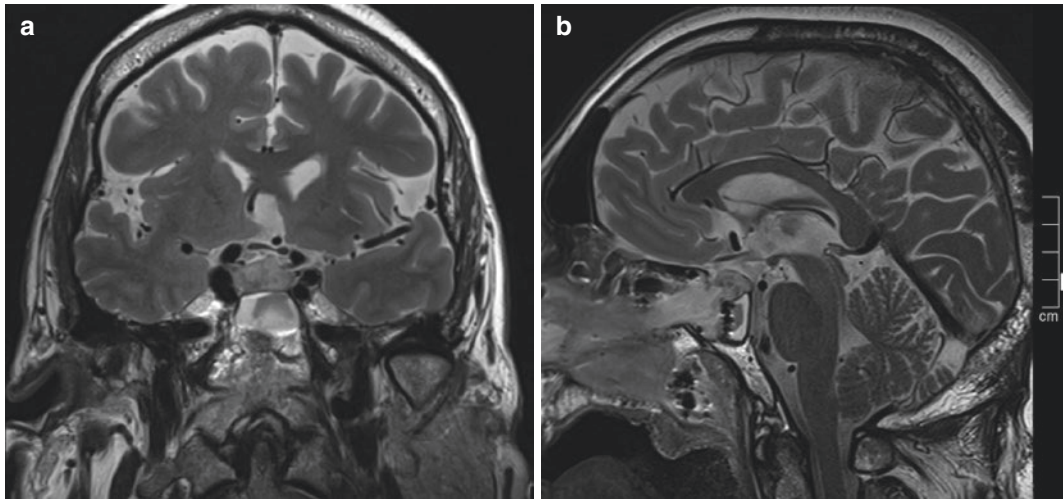

Fig. 16.3 Following further resection of the tumor, the patient was re-evaluated in the perioperative MR scanner. T2-weighted coronal (**a**) and sagittal (**b**) sellar MR images showed operative changes besides gross total resection of the pituitary adenoma. The patient was taken back to the operating room and the surgery was ended without any complication

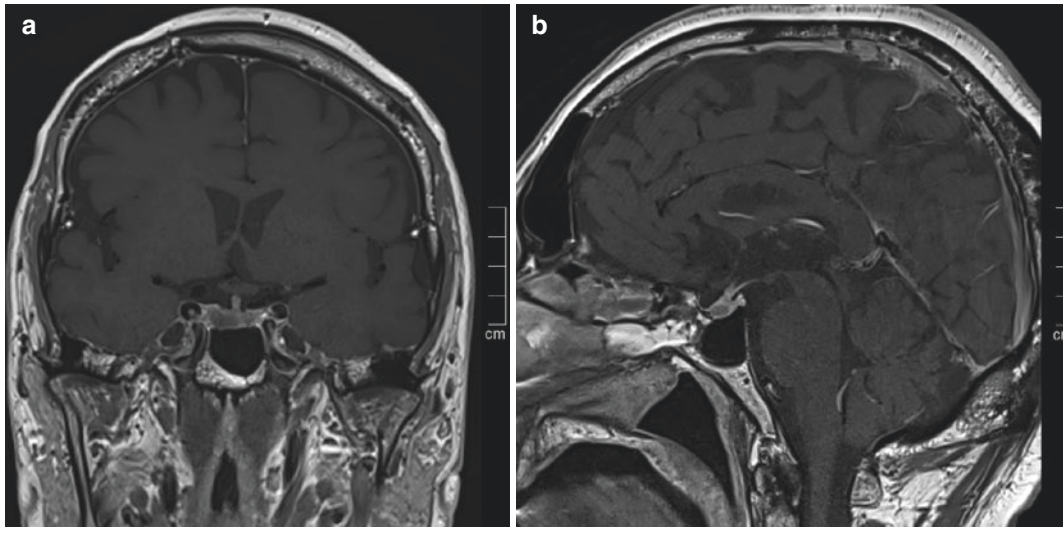

Fig. 16.4 Postoperative first year contrast-enhanced T1-weighted sellar MRI with coronal (**a**) and sagittal (**b**) views depicting the functional pituitary gland in situ

16.1.1 Epidemiology/Most Commonly Seen Types

Pituitary adenomas are the third most common intracranial neoplasms (14.1%) following meningiomas (35.5%) and gliomas (15.8%). Pituitary adenomas are categorized as microadenomas if their largest diameter is smaller than 10 mm; macroadenomas if their largest diameter is equal or greater than 10 mm. Pituitary macroadenomas occur at a rate of 1/600. Pituitary adenomas are also grouped based on their functional status. The most commonly diagnosed type of pituitary adenomas is prolactinoma (50% on average), followed by nonfunctioning pituitary adenoma (14–54%), somatotroph adenoma, corticotroph adenoma, and thyrotroph adenoma.

16.1.2 Pathology and Genetics

- The World Health Organization (WHO) Classification of Tumors of Endocrine Organs has been revised in 2017. In the new edition (fourth) of the classification, some changes have occurred.
- The term "atypical adenoma" has been eliminated from the new classification system.
- Pituitary blastoma, a very rare tumor seen in early childhood, has been introduced to the classification system for the first time.
- DICER1 mutations are seen in pituitary blastomas.
- A cell lineage-based classification system using immunohistochemistry for transcription factors and produced hormones has been introduced in the new system.
- Pituitary adenomas originate from the anterior pituitary lobe cells.
- There are three main pathways of cell differentiation in this lobe to produce hormones. These three pathways are directed by different transcription factors.
- Pituitary transcription factor 1 (PIT1) regulates somatotrophs (GH), lactotrophs (PRL), mammosomatotrophs (PRL and GH), and thyrotrophs (TSH).
- T-box pituitary transcription factor (TPIT) regulates corticotrophs (ACTH).
- Steroidogenic factor-1 (SF1) regulates gonadotrophs (FSH/LH).
- Treatment strategies are expected to be planned more effectively following the new classification system, yet more clinicopathological studies are necessary to make a conclusive statement in the future.

16.1.3 Clinical Management

Surgical intervention in symptomatic patients with pituitary macroadenomas via microsurgery, endoscopy, or combined technique leads to immediate tumor eradication and relief of signs and symptoms. Risk factors related with surgery are postoperative cerebrospinal fluid leak (3.9%), injury to normal pituitary gland and hence hypopituitarism (13%), diabetes insipidus (transient 18%, permanent 0.4%), transient isolated hyponatremia (21%), neurovascular injury (0–5.6%), and epistaxis (0.8–3.4%). Hormonal follow-up and replacement therapies, if necessary, should be commenced following the surgery.

16.1.4 Imaging Findings

Thin slices are obtained with smaller field of views (FOV) centered at the sella for inspection of pituitary gland. Dynamic contrast-enhanced sequences in coronal plane are acquired every 30 s for 3 min. Different contrast dynamics of adenomas, especially in case of microadenomas (<10 mm), are advantageous. Most adenomas enhance slowly (peak between 60–200 s). Normal pituitary gland enhances homogenously at 60–80 s. Maximum contrast difference between adenoma and normal pituitary gland appears at about 1 min and gradually decreases thereafter. Sometimes adenoma may enhance earlier than gland itself, due to a direct

arterial supply of the adenoma. Signal intensity on T2-weighted sequence could be variable due to cyst, necrosis, or hemorrhage present within the adenoma. Large adenomas result in displaced normal pituitary gland, and hence readily identifiable on MRI. Cavernous sinus infiltration could be differentiated on coronal pre- and postcontrast T1-weighted MR sequences. Perioperative T2-weighted coronal and sagittal images are useful in determining extent of resection in pituitary adenomas (Figs. 16.2 and 16.3). No complication is observed if the imaging procedure is done eloquently with caregiving both to the anesthesia and asepsis rules.

Key-Points

- Pituitary adenomas are the third most common intracranial neoplasms following meningiomas and gliomas
- A cell lineage-based categorization using immunohistochemistry has been introduced into the new WHO classification system of pituitary adenomas
- Dynamic contrast-enhanced coronal sellar MRI is successful in determining presence and location of pituitary adenoma within the pituitary gland itself at the preoperative era
- T2-weighted sellar MRI with coronal and sagittal views is useful in determining extent of resection of the pituitary adenoma during the surgery

Further Reading

1. Fomekong E, Duprez T, Docquier MA, Ntsambi G, Maiter D, Raftopoulos C. Intraoperative 3 T MRI for pituitary macroadenoma resection: Initial experience in 73 consecutive patients. Clin Neurol Neurosurg. 2014;126:143–149. doi: https://doi.org/10.1016/j.clineuro.2014.09.001
2. Ntali G, Wass JA. Epidemiology, clinical presentation and diagnosis of non-functioning pituitary adenomas. Pituitary. 2018;21:111–118. doi: https://doi.org/10.1007/s11102-018-0869-3
3. Aflorei ED, Korbonits M. Epidemiology and etiopathogenesis of pituitary adenomas. J Neurooncol. 2014;117:379–394. doi: https://doi.org/10.1007/s11060-013-1354-5
4. Inoshita N, Nishioka H. The 2017 WHO classification of pituitary adenoma: overview and comments. Brain Tumor Pathol. 2018;35:51–56. doi: https://doi.org/10.1007/s10014-018-0314-3
5. Mehta GU, Lonser RR. Management of hormone-secreting pituitary adenomas. Neuro Oncol. 2018;19:762–773. doi: https://doi.org/10.1093/neuonc/now130
6. Zamora C, Castillo M. Sellar and Parasellar Imaging. Neurosurgery. 2018;80:17–38. doi: https://doi.org/10.1093/neuros/nyw013

16.2 Pilocytic Astrocytoma Located in Pons

An 8-year-old boy was admitted with headache, vomiting, and gait ataxia. He was diagnosed of a left-sided brachium pontis lesion (Fig. 16.5). He was operated in October 2015 (Figs. 16.6 and 16.7). He had no deficit following the surgery. Pathological diagnosis was pilocytic astrocytoma (PA, grade I, WHO 2016). The lesion recurred 5 months later (Fig. 16.8). He was reoperated and the pathology was the same (Figs. 16.9–16.11). He was free of deficit following the second surgery. He received chemotherapy and fractionated radiotherapy following the second surgery. He was symptom free at his second year follow-up examination (Fig. 16.12).

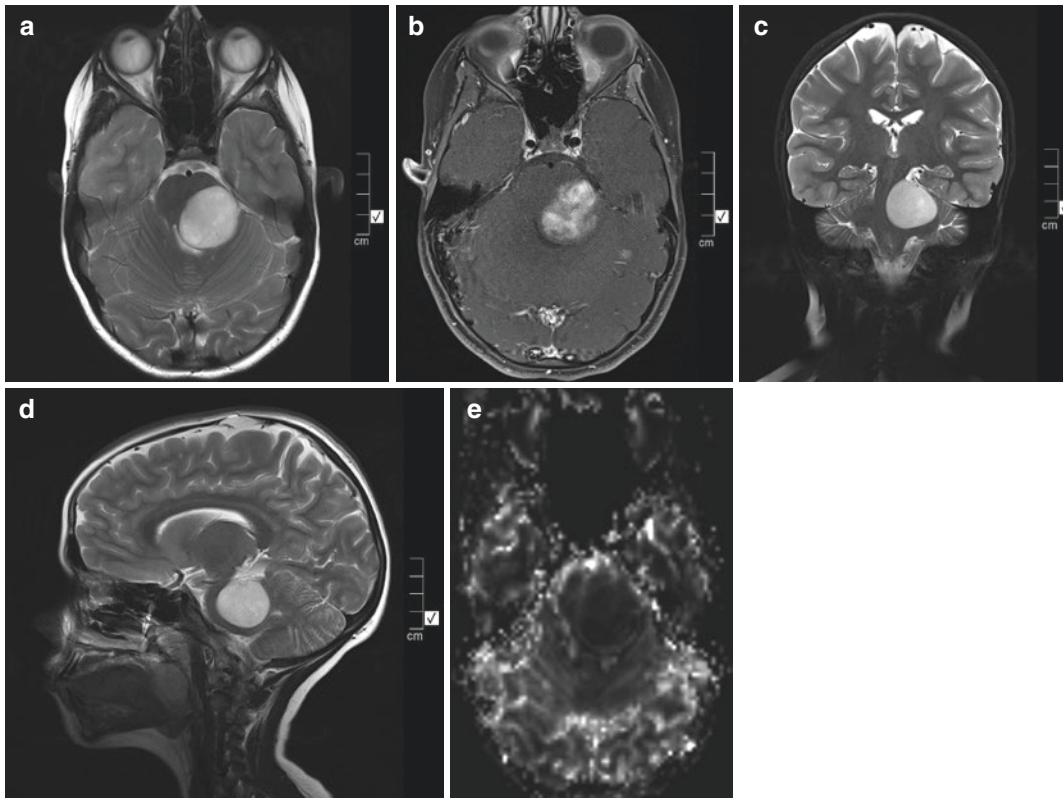

Fig. 16.5 A well-demarcated, expansile, intra-axial, nodular lesion was detected in the left side of the brachium pontis on T2-weighted brain MRI. Anteroposterior dimension of the lesion was 3 cm and it included multiple millimetric cysts. Edema was unclearly present at the border of the lesion. The fourth ventricle was compressed by the lesion (**a**, **c**, **d**). The lesion enhanced in patchy pattern (**b**). The lesion was hypoperfused on MR perfusion imaging (rCBV parametric map) (**e**). MR spectroscopy imaging was compatible with grade I glial lesion (**f**). No other concomitant lesion in supra- or infratentorial area was present. The relationship between the lesion and the left corticospinal tract was demonstrated on diffusion tensor imaging (**g**)

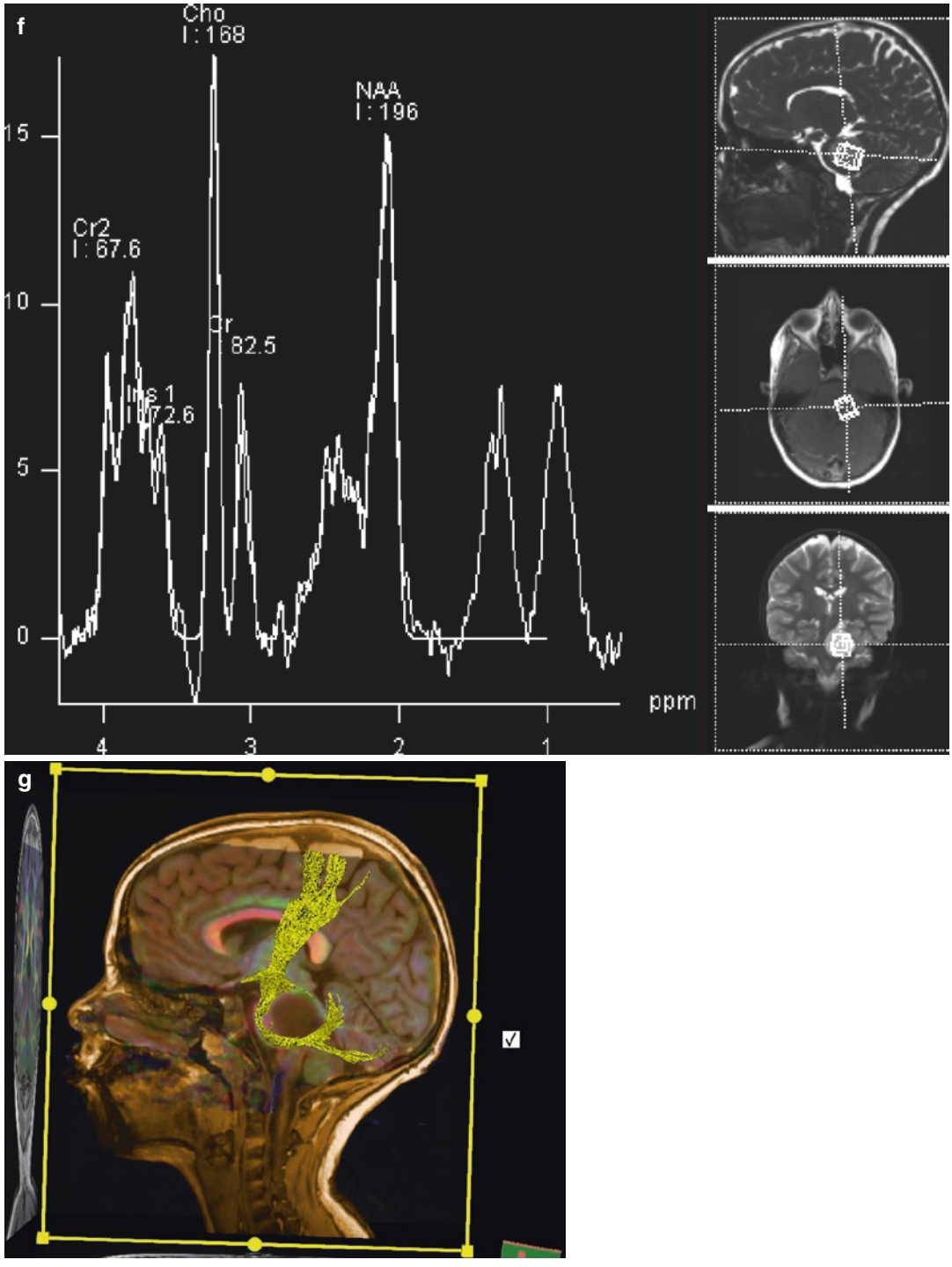

Fig. 16.5 (continued)

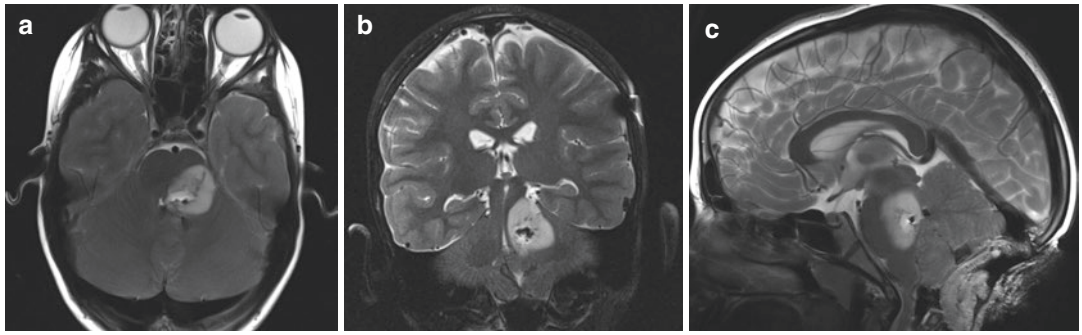

Fig. 16.6 The first perioperative imaging: axial, coronal, and sagittal T2-weighted brain MR images were obtained (**a**–**c**). There were operative changes besides the residual tumor, hyperintense to the parenchyma. The patient was taken back to the operating room for further resection of the tumor

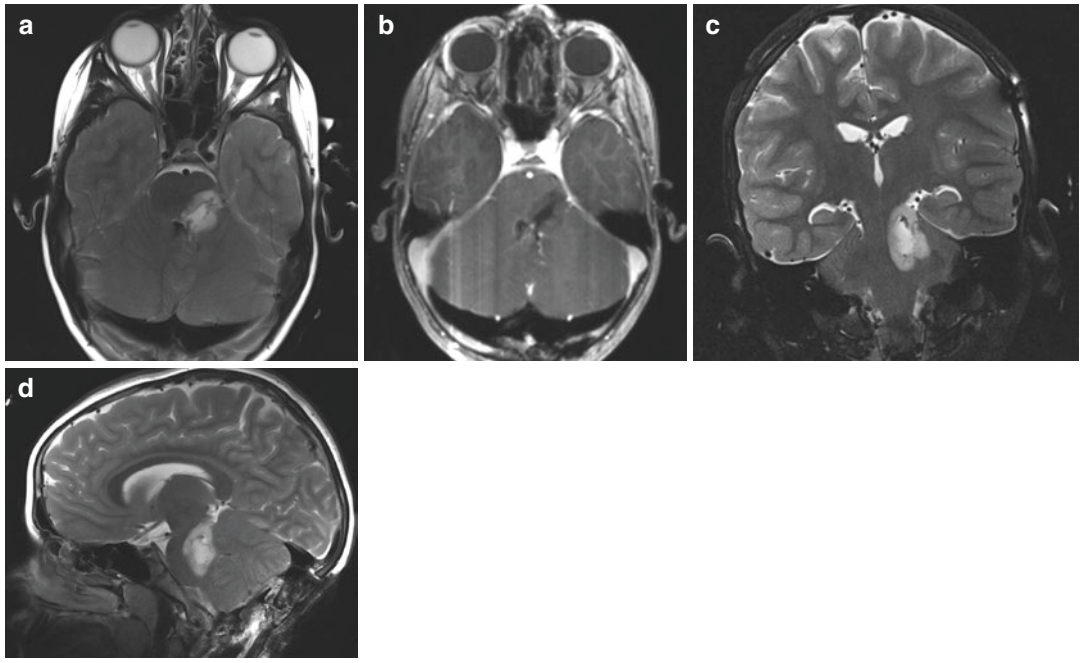

Fig. 16.7 Following further resection of the tumor, the patient was re-evaluated in the perioperative MR scanner. Axial T1- (**b**), axial, coronal and sagittal T2-weighted (**a**, **c**, **d**) brain MR images were obtained. The lesion was observed to have been further debulked. There was a rim-like hyperintensity enclosing previous lesion bed which enhanced in a limited fashion at the late term of I.V. contrast material administration. The patient was taken back to the operating room and the surgery was ended without any complication

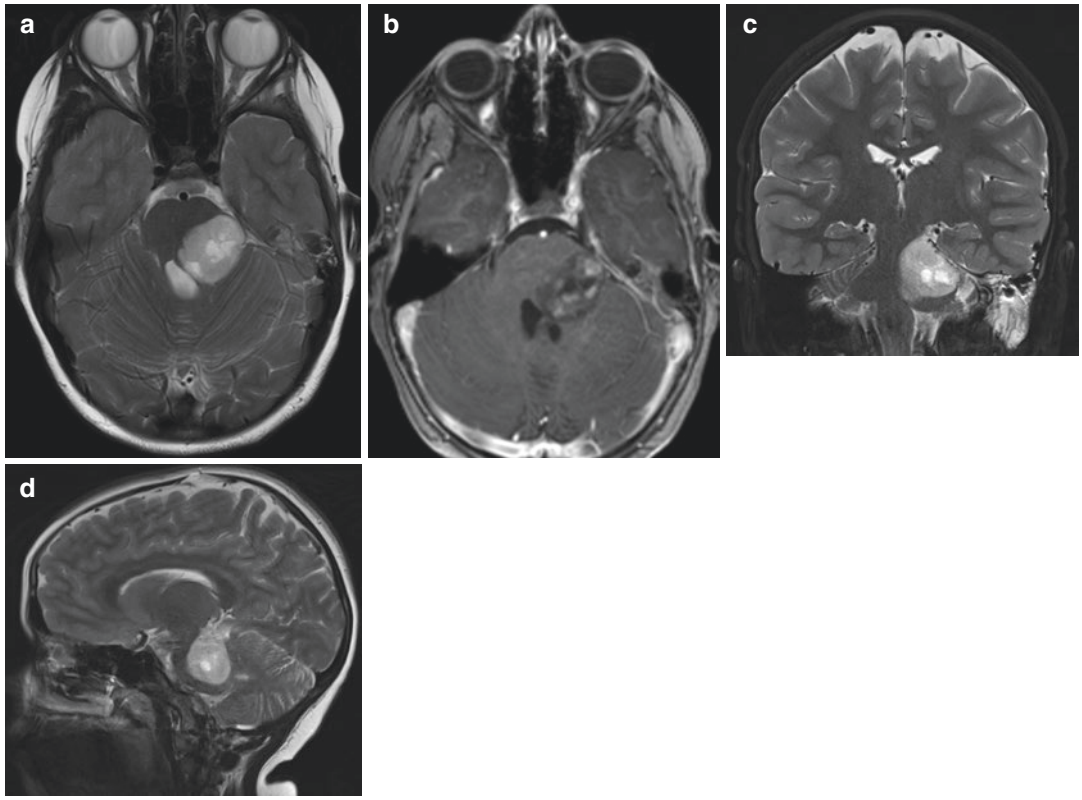

Fig. 16.8 The patient has been regularly followed up since the index surgery. The residual tumor progressed in dimensions and filled-up the previous tumor cavity in 5 months following the surgery. A solid, expansile, progressive lesion was observed inside the left brachium pontis. The lesion was hyperintense on T2-weighted brain MR scans (**a**, **c**, **d**) with cysts seeming more hyperintense compared to the lesion itself. The lesion had a mass effect resulting in effacement of basal cisterns and the fourth ventricle. The lesion was well demarcated from the normal tissue. There was heterogenous contrast enhancement on T1-weighted MR scans (**b**) and the enhancement became more obvious at the late phase of I.V. contrast material administration

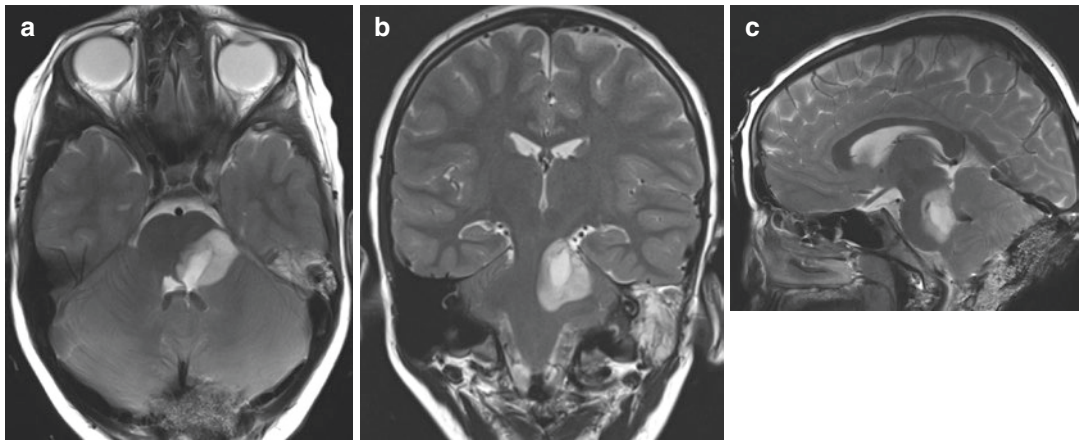

Fig. 16.9 The first perioperative imaging: T2-weighted axial, coronal, and sagittal brain MR images (**a**–**c**) were obtained. The residual tumor was seen surrounding the previous tumor bed. The patient was taken back to the operating room for further resection of the tumor

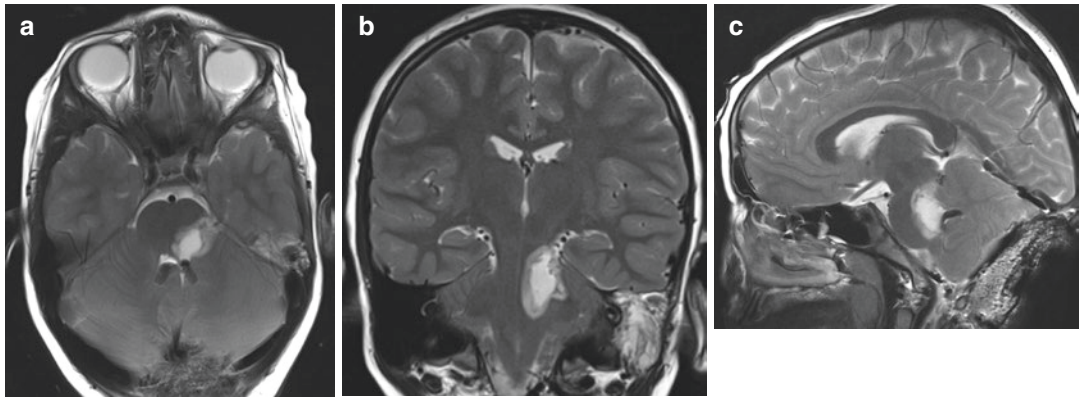

Fig. 16.10 Following further resection of the tumor, the patient was re-evaluated in the perioperative MR scanner. The lesion had been resected in gross total pattern (**a**–**c**). The patient was taken back to the operating room and the surgery was ended without any complication

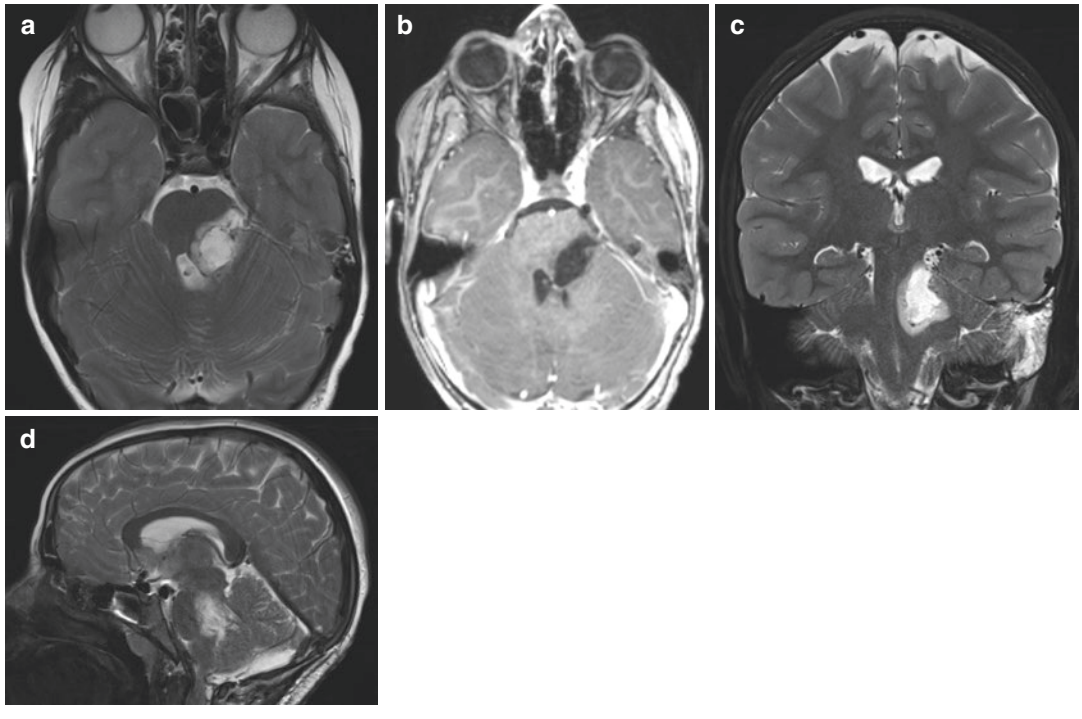

Fig. 16.11 T1-weighted (**b**) and T2-weighted (**a**, **c**, **d**) brain MR images were obtained at postoperative day 1. The lesion had been gross totally excised. There was a rim-like enhancement which was considered as a postoperative change rather than a tumor remnant which also had diffusion restriction on diffusion-weighted MR scans

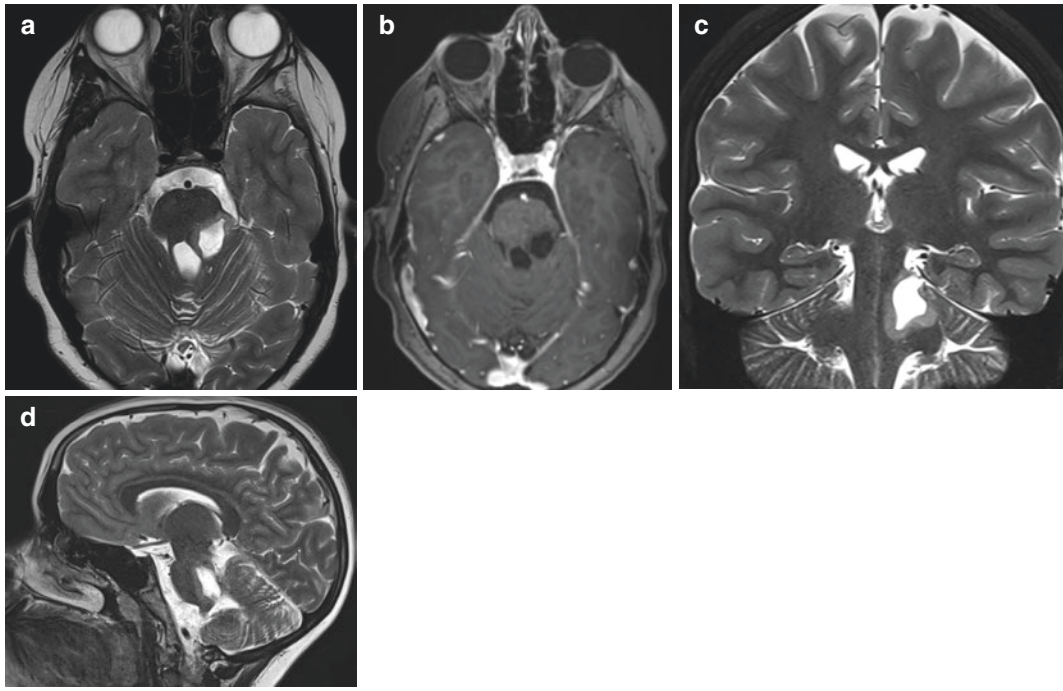

Fig. 16.12 Postoperative second year brain MR imaging: The resection cavity and the hyperintense zone around the cavity in the left brachium pontis was similar in extent following the second surgery and the adjuvant therapies (**a**–**d**). There was no pathological contrast enhancement (**b**). The lesion component extending to the left central tegmental tract was the same. The fourth ventricle was minimally dilated. The basal cisterns were open. There was neither intraparenchymal nor leptomeningeal new lesion

16.2.1 Epidemiology/Most Commonly Seen Types

Pilocytic astrocytoma is the most common pediatric brain tumor (20% of brain tumors in patients under the age of twenty years). The PA usually presents between 1 and 10 years (median: seven years). A few cases above age of thirty years have been reported, so far. There is no gender predilection of the PAs (M/F = 1). It is classified under glial tumors as grade I in the WHO classification of central nervous system tumors. The PA might arise from any site of the neuronal axis, yet it is mostly detected in the cerebellum, optic chiasm, and optic nerve. Survival rate of the PAs is 96% within a time frame of ten years besides a recurrence and progression rate of 20%.

16.2.2 Pathology and Genetics

- Pilocytic astrocytoma has a biphasic architecture of densely packed fibrillary tissue and loosely arranged microcystic areas.
- Pilocytic astrocytomas have eosinophilic granular bodies and Rosenthal fibers.
- The Ras/RAF/mitogen-activated protein kinase/extracellular signal-regulated kinase pathway has a key role in PA pathogenesis and regulates cell growth, proliferation, differentiation, and death in both malignant and nonmalignant cells.
- Tandem duplication at 7q34 and/or 3p25 leads to oncogenic process in the PA.
- Loss of NF1 could also result in PAs via activation of the Ras pathway.

16.2.3 Clinical Management

Pilocytic astrocytomas are well responsive to surgical resection when they present in brain areas amenable to total excision. Chemotherapy or radiotherapy is alternative first-line treatment modalities in case of inoperable, subtotal resected or progressive PAs. Pediatric patients under age of one year or with neurofibromatosis type 1 should receive only chemotherapy to avoid deleterious side effects of radiotherapy.

16.2.4 Imaging Findings

Pilocytic astrocytoma mostly presents as an expansive cystic mass with an enhancing mural nodule or as an infiltrative lesion elongating and widening the optic pathway. Sometimes it could be hard to define PAs due to their mimicking nature of malign tumors due to different growth and contrast enhancement patterns on MRI. Besides conventional MR imaging, MR spectroscopy and perfusion-weighted MR modalities could be useful in defining nature of the lesions. Diffusion tensor imaging could be lifesaving for tumors located in delicate brain/brainstem areas.

Key-Points

- Pilocytic astrocytoma is the most common pediatric brain tumor
- Ras/RAF/mitogen-activated protein kinase/extracellular signal-regulated kinase pathway has a key role in PA pathogenesis
- MR spectroscopy and perfusion-weighted MR modalities could be useful in defining nature of PAs located in unusual brain locations with unfamiliar imaging findings on conventional MRI
- Where applicable, PAs should be resected; if not possible, radio- and/or chemotherapy should be preferred
- Diffusion tensor imaging could be useful for safe resection of tumors located in delicate brain/brainstem areas

Further Reading

1. Sadighi Z, Slopis J. Pilocytic astrocytoma: a disease with evolving molecular heterogeneity. J Child Neurol. 2013;28: 625–632. doi: https://doi.org/10.1177/0883073813476141
2. Gaudino S, Martucci M, Russo R, Visconti E, Gangemi E, D'Argento F, Verdolotti T, Lauriola L, Colosimo C. MR imaging of brain pilocytic astrocytoma: beyond the stereotype of benign astrocytoma. Childs Nerv Syst. 2017;33: 35–54. doi: https://doi.org/10.1007/s00381-016-3262-4

16.3 Anaplastic Oligodendroglioma Located in the Left Frontal Lobe

A 52-year-old man was admitted with headache and generalized tonic-clonic seizure. An intra-axial mass lesion was detected in the left frontal lobe on brain MRI (Fig. 16.13). He was operated on and the pathological diagnosis was anaplastic oligodendroglioma (grade III, WHO 2016, IDH mutant type) (Fig. 16.14). He received adjuvant radiotherapy and chemotherapy (Fig. 16.15).

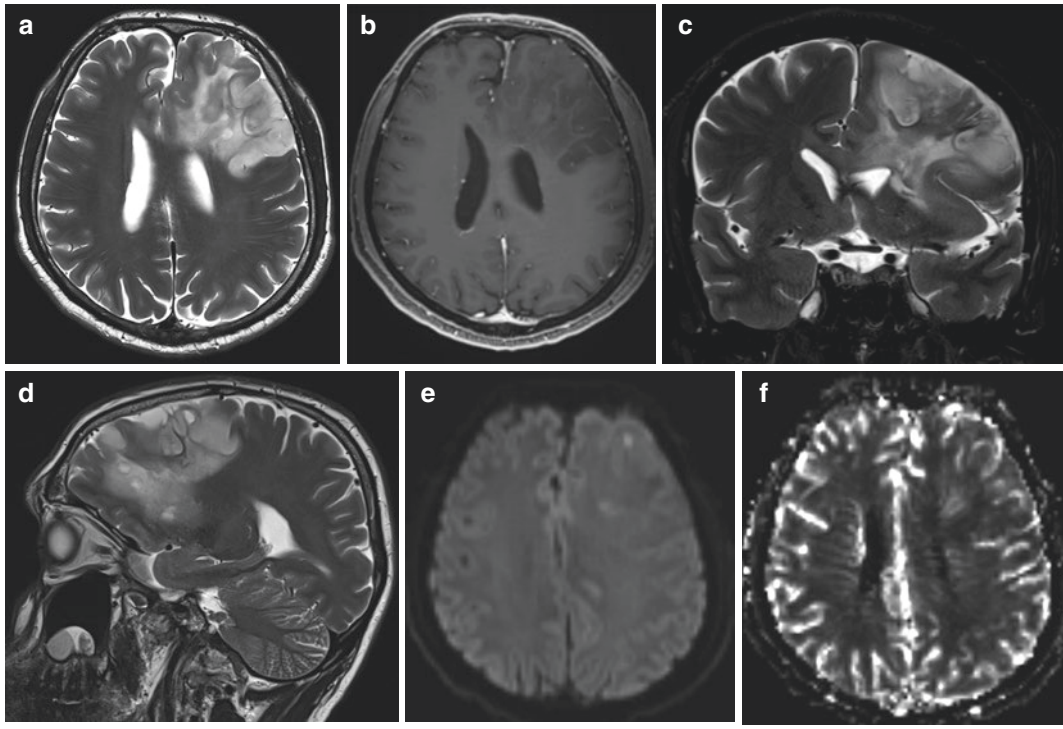

Fig. 16.13 On the preoperative brain MRI, there was an intra-axial mass lesion in the left frontal lobe extending to the anterior part of the left corpus callosum, the left forceps minor, with a limited extension to the contralateral hemisphere (**a**–**d**). The mass lesion was clutching both the gray and the white matter, while encompassing the frontal horn of the left lateral ventricle with a minimal midline brain shift (**c**). There were multiple cystic parts within the lesion and there was restriction on diffusion-weighted image (**e**). There was minimal contrast enhancement on T1-weighted sequences (**b**). Linear hyperperfusing areas were observed within the lesion on perfusion-weighted MRI (**f**). There was decrement in NAA and increment in choline on MR spectroscopy (**g**). The lesion was suspected to be a slowly progressive low-grade glioma, probably oligodendroglioma. On functional MRI (fMRI), the lesion was located just in front of the left pre-central sulcus. The Broca and Wernicke areas were present bilaterally. There was an intimate relationship of the left Broca area and the lesion itself (**h**). The lesion was present anterior to the corticospinal tracts on DTI. There was no tumor infiltration of the corticospinal tracts (**i**)

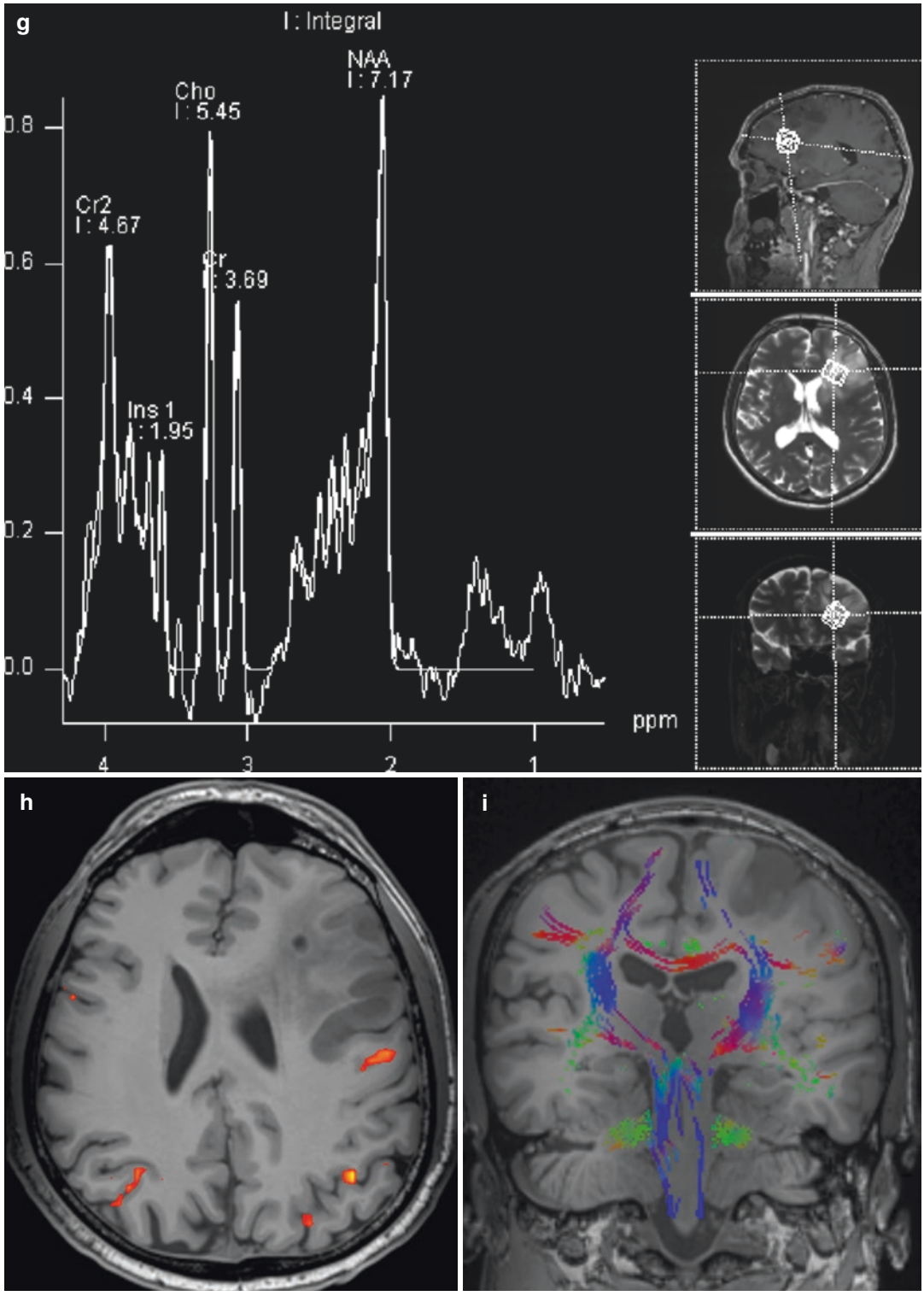

Fig. 16.13 (continued)

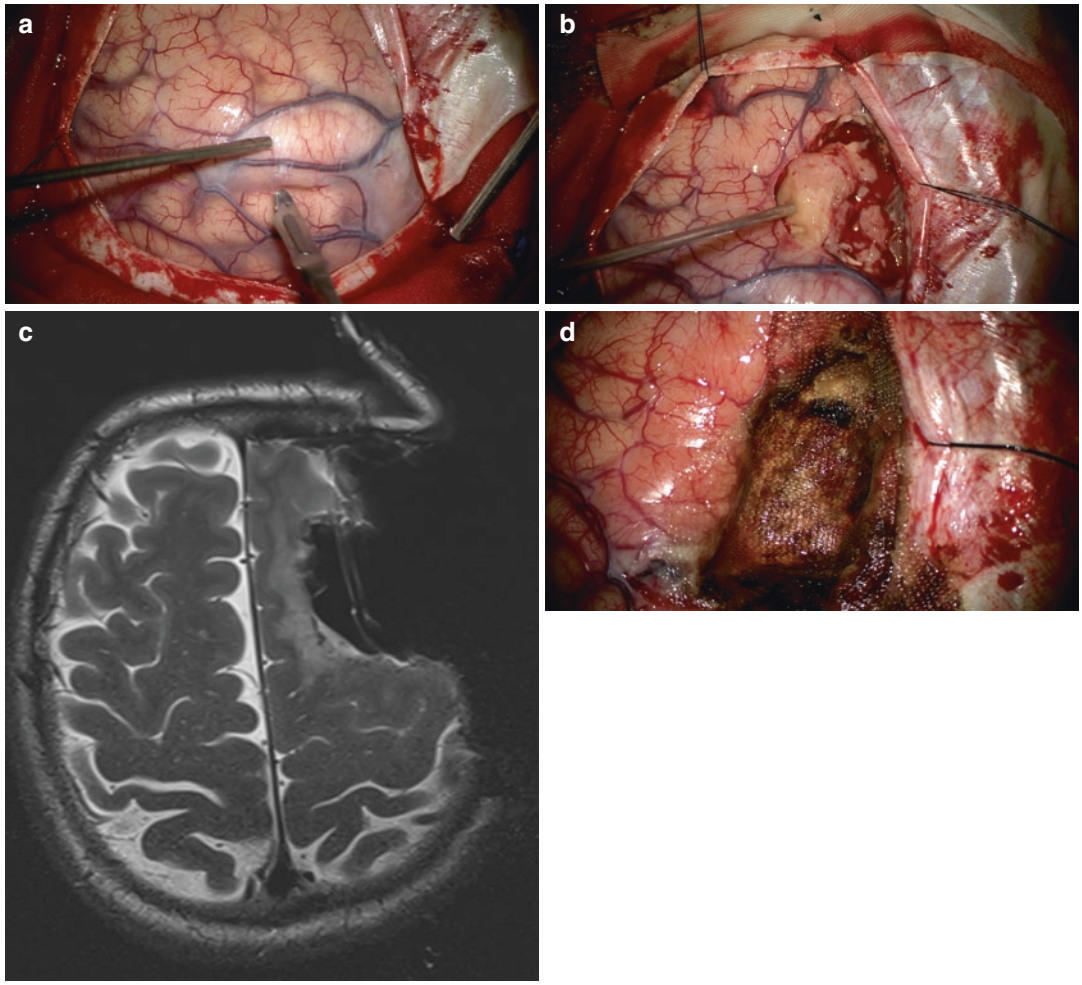

Fig. 16.14 The brain cortex was pale in color in the region of interest (**a**). The location and borders of the lesion were confirmed via perioperative ultrasonography. Tumor resection was done through the border of gliosis under stimulation of the brain cortex (**b**). Following tumor resection, the patient was taken into perioperative MR scanner. The resection cavity with the rim of tumor remnant close to the Broca area was observed on T2-weighted brain MRI (**c**). The patient was taken back to the operating room and the surgery was ended without any complication (**d**)

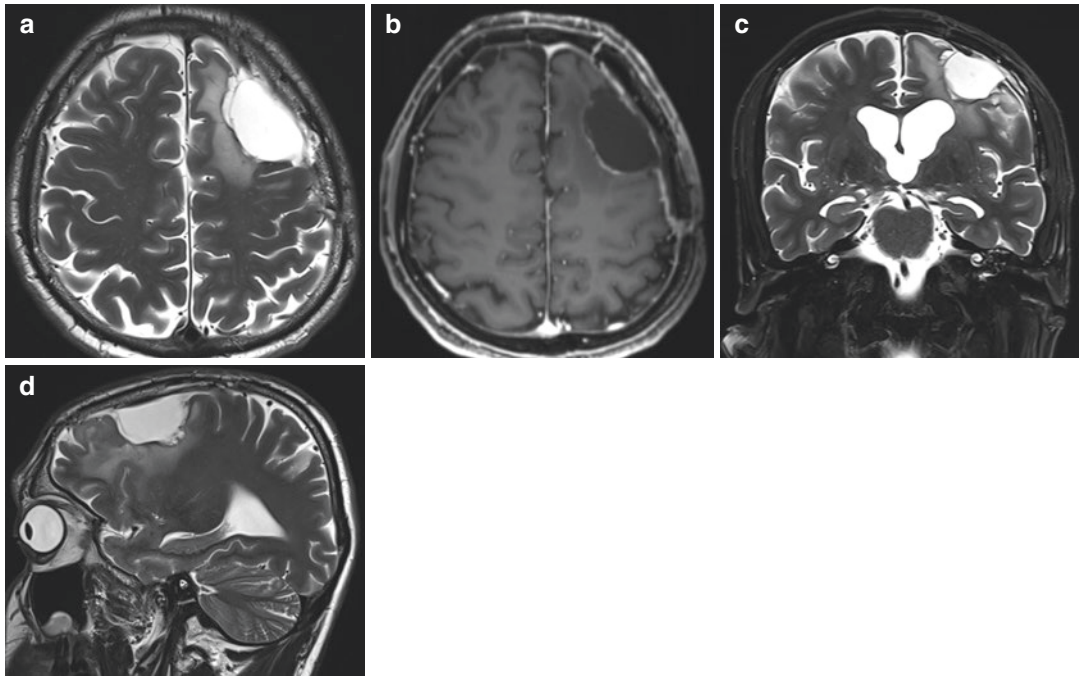

Fig. 16.15 The tumor remnant has regressed in diameters following the adjuvant therapies. No new lesion was observed at the final follow-up of 7 months since the surgery (**a-d**)

16.3.1 Epidemiology/Most Commonly Seen Types

Oligodendrogliomas compose 1.8% and 6.2% of primary brain tumors and of all central nervous system gliomas, respectively. According to the WHO classification, these tumors are categorized as grade II or grade III based on their histopathology.

16.3.2 Pathology and Genetics

- Anaplastic oligodendrogliomas (AO) infiltrate brain parenchyma diffusely with distinct borders.
- The WHO definition for AO is oligodendroglioma with focal or diffuse malignant properties and less favorable outcome.
- Low-grade oligodendrogliomas could progress to AOs as having high cell density, atypical nuclei, increased mitosis, microvascular proliferation, and necrosis.
- Anaplastic oligodendrogliomas could also emerge primarily without any low-grade precursor.
- There is no specific immunohistochemical marker for oligodendrogliomas whereas glial fibrillary acidic protein could be positive.
- Loss of 1p or co-deletion of 1p and 19q that harbor tumor suppressor genes is a molecular characteristic of oligodendrogliomas.
- Allelic loss of 1p/19q and mutations of IDH1 and TERT are detected in 60–90% of oligodendrogliomas.

16.3.3 Clinical Management

Surgery is the mainstay of the treatment of glial tumors to make final diagnosis, to relieve mass effect and to improve prognosis. Extent of resection of AOs is associated with survival rate. If tumor is unresectable, stereotactic biopsy could be applied to make the pathological diagnosis. Tumor grade (II or III) and 1p/19q status are the two most

important determinants of therapeutic decision-making process for oligodendrogliomas. Regardless of tumor grade, oligodedrogliomas with loss of heterozygosity of 1p/19q have better prognosis and are more responsive to chemo-radiation therapy than oligodendrogliomas with intact alleles. Nowadays, chemotherapy composed of procarbazine, lomustine, and vincristine (PCV) combined with radiotherapy is the standard of care in AOs. In the past; the brain tumor histopathology was enough to determine the treatment strategy, which has been replaced by the molecular structure of the tumor. The PCV therapy combined with radiation therapy is beneficial for AOs with IDH mutations, whereas patients with IDH wild type and MGMT promoter un-methylated AOs should be approached like having glioblastoma.

16.3.4 Imaging Findings

Tumor enhancement after I.V. gadolinium on MRI is a marker for malignancy of the glial tumors, yet it could sometimes be difficult to distinguish low-grade from high-grade oligodendrogliomas. In this respect, preoperative further work-up with perfusion MR and MR spectroscopy is key tool to make a delicate plan for treatment and to predict the prognosis. Perfusion MR with dynamic susceptibility contrast is used to calculate brain perfusion in several diseases such as gliomas. Maximum relative cerebral blood volume (rCBVmax) correlates with grade of brain tumors more than conventional MRI with contrast. A cutoff value of 1.75 has been selected for rCBVmax in the previous studies and higher rCBVmax is associated more with high-grade gliomas rather than low-grade. However, this correlation is more convenient for astrocytomas than oligodendrogliomas. So further workups are necessary. Perfusion MR, MR diffusion and MR spectroscopy combined with conventional MRI yield a sensitivity and specificity of 82% and 84%, respectively, in the preoperative era. These modalities never take the place of the histopathology for the final diagnosis; yet they supply enough arms to make proper preoperative management and therapeutic decision-making.

Key-Points

- Oligodendrogliomas compose 1.8% and 6.2% of primary brain tumors and of all central nervous system gliomas, respectively
- Loss of 1p or co-deletion of 1p and 19q that harbor tumor suppressor genes are molecular characteristics of oligodedrogliomas
- Surgery is the mainstay of the treatment for glial tumors to make final diagnosis, to relieve mass effect and to improve prognosis. Extent of resection of AOs is associated with survival rate
- Perfusion MR, MR diffusion, and MR spectroscopy combined with conventional MRI yield a sensitivity and specificity of 82% and 84%, respectively, to assist clinician to make proper preoperative management and treatment decision

Further Reading

1. Dolecek TA, Propp JM, Stroup NE, Kruchko C. CBTRUS statistical report: primary brain and central nervous system tumors diagnosed in the United States in 2005–2009 Neuro Oncol Suppl. 2012;5: v1–49. Doi: https://doi.org/10.1093/neuonc/nos218
2. Van Den Bent MJ, Bromberg JEC, Buckner J. Low-grade and anaplastic oligodendroglioma. Handb Clin Neurol. 2016;134: 361–380. doi:https://doi.org/10.1016/B978-0-12-802,997-8.00022-0
3. Jia Z, Geng D, Liu Y, Chen X, Zhang J. Low-grade and anaplastic oligodendrogliomas: differences in tumour microvascular permeability evaluated with dynamic contrast-enhanced magnetic resonance imaging. J Clin Neurosci. 2013;20: 1110–1113. doi: https://doi.org/10.1016/j.jocn.2012.09.019
4. Delgado AF, Delgado AF. Discrimination between glioma grades II and III using dynamic susceptibility perfusion MRI: a meta-analysis AJNR Am J Neuroradiol.

2017;38: 1348–1355. doi: https://doi.org/10.3174/ajnr.A5218

5. Fellah S, Caudal D, De Paula AM, Dory-Lautrec P, Figarella-Branger D, Chinot O, Metellus P, Cozzone PJ, Confort-Gouny S, Ghattas B, Callot V, Girard N. Multimodal MR imaging (diffusion, perfusion, and spectroscopy): Is it possible to distinguish oligodendroglial tumor grade and 1p/19q codeletion in the pretherapeutic diagnosis? AJNR Am J Neuroradiol. 2013;34: 1326–1333. doi: https://doi.org/10.3174/ajnr.A3352
6. Chawla S, Krejza J, Vossough A, Zhang Y, Kapoor GS, Wang S, O'Rourke DM, Melhem ER, Poptani H. Differentiation between oligodendroglioma genotypes using dynamic susceptibility contrast perfusion-weighted imaging and proton MR spectroscopy AJNR Am J Neuroradiol. 2013;34: 1542–1549. doi: https://doi.org/10.3174/ajnr.A3384

Acknowledgement *Conflict of Interest*: The authors declare that they have no conflict of interest related with the study.

Postoperative Imaging

17

Kamil Karaali

17.1 Decompressive Craniectomy, Fat Graft

A 42-year-old female presented with right hemiplegia and aphasia.

17.1.1 Images and Legends

K. Karaali (✉)
Department of Radiology, Akdeniz University Hospital, Antalya, Turkey

Y. Özsunar, U. Şenol (eds.), *Atlas of Clinical Cases on Brain Tumor Imaging*,
https://doi.org/10.1007/978-3-030-23273-3_17

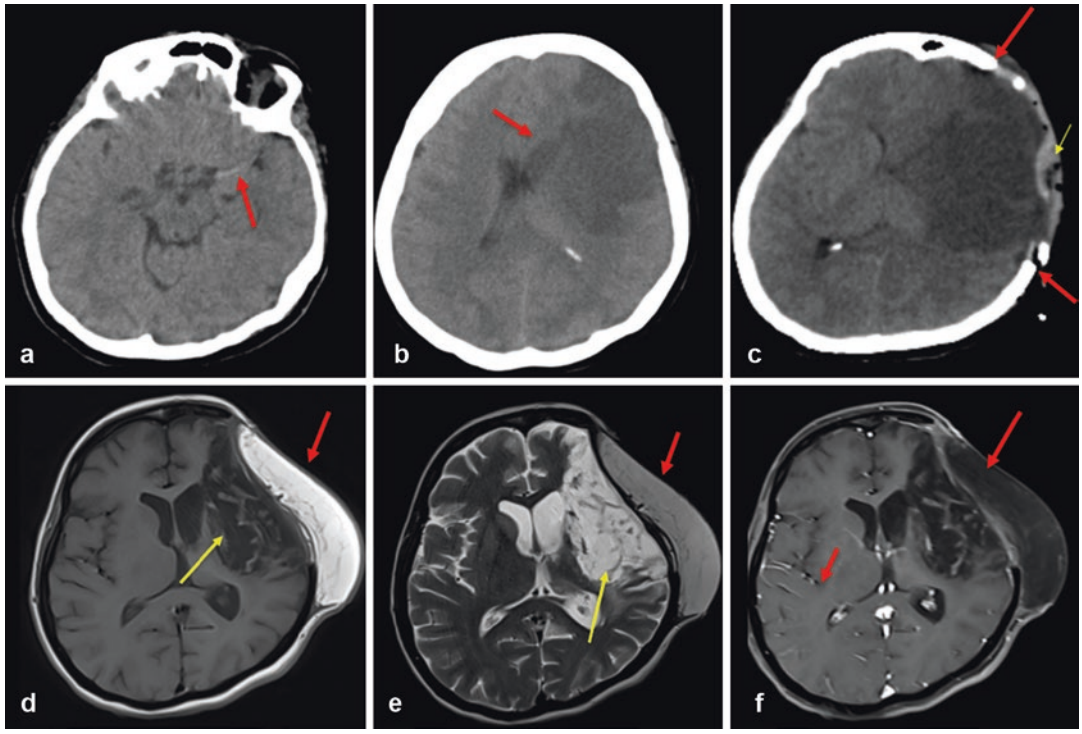

Fig. 17.1 A head CT after about 6 h from the start of the symptoms (**a**) show hyperdense left middle cerebral artery (MCA, arrow), which is an early indicator of a large MCA infarction. A day after (**b**), the infarction is prominent as hypodense areas, as well, left caudate head is hypodense and left lateral ventricle is compressed (arrow). A decompressive craniectomy is performed. Postoperative CT (**c**) shows bone defect (between red arrows) and air densities (yellow arrow). The defect was closed by resected calvarial bone 10 months after the first craniectomy, but osteomyelitis developed and it should be removed. Craniectomy defect was then closed with autologous fat tissue graft. An MRI was performed 11 months after the first CT. T1-weighted image (**d**) shows diffusely hyperintense fat graft (red arrow). Encephalomalacia is developed within the infarction area (yellow arrow). T2-weighted image (**e**) also shows diffusely hyperintense fat graft (red arrow). Encephalomalacia is close to fluid intensity (yellow arrow). T1-weighted fat suppressed image after contrast material injection (**f**) shows suppressed intensity of the graft. There is no pathologic enhancement

17.1.2 Clinical Management

- Decompressive craniectomy may be necessary in the management of strokes
- If the edema is remarkable, causing herniations or hydrocephalus due to fourth ventricle compression, decreasing the intracranial pressure is mandatory
- Large craniectomy defects are then closed by several type of materials. These include autologous bone, fat, fascia, and cranioplasty materials such as ceramics, alumina, bio-ceramics, polymers, and titanium. In this case, autologous fat was used

17.1.3 Imaging Findings and Differential Diagnosis

- Knowing the surgical technique and the type of the cranioplasty material is very useful for the evaluation
- Complications such as foreign material reaction and infection may occur after the surgery
- CT and MRI are frequently used to demonstrate collections, CSF leakage, and abscess formation
- An infection of the cranioplasty material needs resection, usually

Take-Home Messages

- Decompressive craniectomy may be necessary in the management of strokes
- Large craniectomy defects are closed by several type of materials
- There are various types of cranioplasty materials, such as autologous bone, fat, fascia, and cranioplasty materials such as ceramics, alumina, bio-ceramics, polymers, and titanium

Further Reading

- Khader BA, Towler MR. Materials and techniques used in cranioplasty fixation: a review. Mater Sci Eng C. 2016;66:315–22

17.2 Tumor Progress, Hematoma Within Resection Cavity

A 45-year-old male was being followed up for an intracranial mass. The mass was stable for the last four years. The patient developed severe headaches and MRI was performed.

17.2.1 Images and Legends

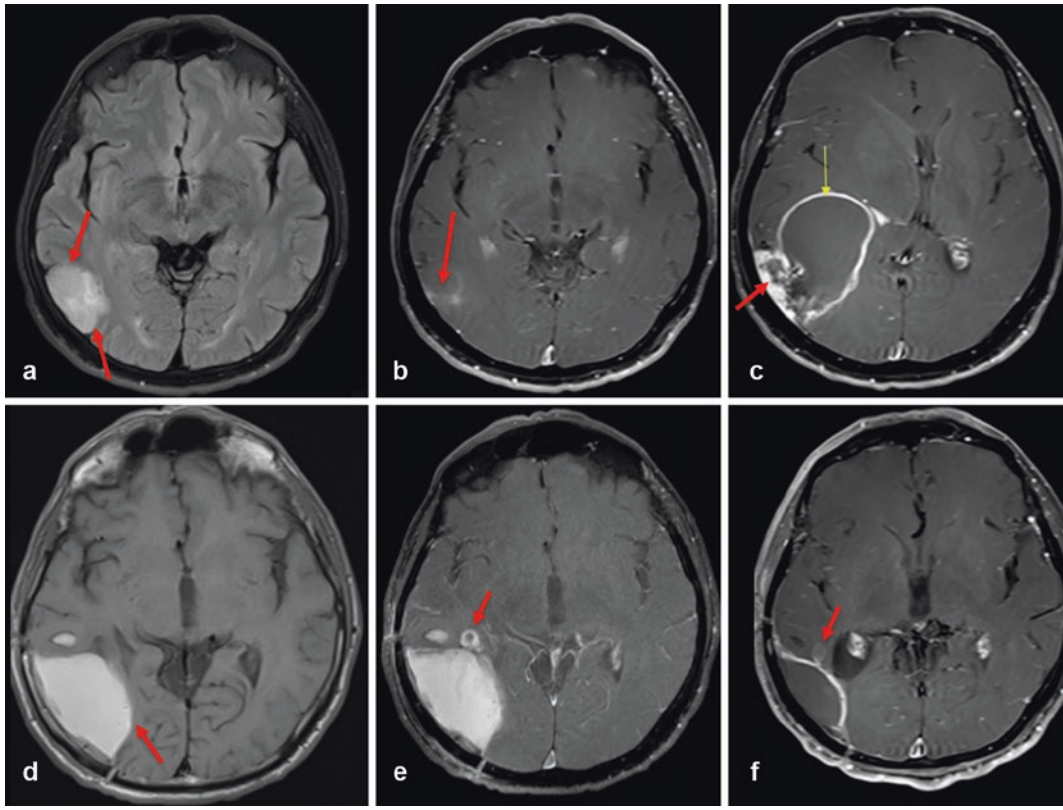

Fig. 17.2 FLAIR-weighted transverse (**a**) MR image shows a mass lesion on the right temporo-occipital junction. Tumor is peripherally located (arrow). On post-contrast T1-weighted MR image (**b**), there is mild linear enhancement centrally (arrow). The mass was stable on MRIs for the last four years. The patient was being followed up with yearly MRIs but he did not have the last scheduled MRI done. About 14 months after the last MRI, the patient developed severe headaches and an urgent MRI was performed. On this MRI, the mass was markedly enlarged, and has cystic, peripherally enhancing component (**c**, post-contrast T1-weighted image, yellow arrow), as well as peripheral solid component (**c**, red arrow). An urgent operation was done, early postoperative MRI was also performed. On T1-weighted image (**d**), there is homogeneous hyperintense area within the resection cavity, consistent with postoperative hematoma. On post-contrast T1-weighted image (**e**), there is a small nodular enhancement superior to the resection cavity, consistent with a small residual tumor. Five months after the operation, on post-contrast T1-weighted image (**f**); the size and the intensity of the hemorrhage is decreased, due to the resorption, as well, enhancement of the nodular residue is also decreased. Histopathologic diagnosis was anaplastic oligodendroglioma

17.2.2 Epidemiology/Most Commonly Seen Types

- Postoperative hematoma that causes neurological deficit is not very uncommon
- Its incidence is reported to be between 1 and 5%
- Usually, an immediate CT is obtained in almost every patient following the brain surgery
- A hematoma can be demonstrated as well as some other complications in this postoperative CT
- MRI is also recommended within 48 h after surgery, in order to show possible residual tumor and complications related to surgery

17.2.3 Pathology and Genetics

- Two most important complications of the brain surgery are hemorrhage and infarction
- Bleeding diathesis and some medications (e.g., anticoagulants) may increase the risk of postoperative hemorrhage
- Previous surgery also increases the risk of hemorrhage
- If the tumor is highly vascular, residue tumor tissue may also alter the hemostasis and cause hematoma within the resection cavity

17.2.4 Clinical Management

- Depending on the clinical status of the patient, hematomas could be reexplored and evacuated
- If the size is not too large and there is no related clinical deficit, follow-up may also be done
- The hemorrhage is usually resorbed and shrinked in several weeks, as in this case
- Another clinically important issue is possibility of rapid progress in a tumor, which was stable for years, as in this case. This was probably due to an "upgrade" in histopathology during follow-up period
- If a patient develops new neurologic symptoms during follow-up, an urgent MRI is necessary

17.2.5 Imaging Findings and Differential Diagnosis

- Hematomas are hyperdense on CT in acute and subacute phases
- The density decreases as the time proceeds, and within months, complete resorption is seen as hypodense areas on CT
- Depending on the MR imaging time, intensity of the hematoma varies on different sequences
- On hyperacute phase (less than 12 h) hemorrhage is isointense on T1-weighted images and isointense or hyperintense on T2-weighted images
- In the acute phase (12 h to 2 days) hemorrhage is isointense or hyperintense on T1-weighted images and hypointense on T2-weighted images
- In the subacute phase, on both sequences, hematoma is hyperintense, due to the methemoglobin formation
- Therefore, hematoma in the early postoperative MRIs is usually hyperintense on non-contrast T1-weighted images, as in this case
- As the hematoma resorption occurs, the intensity on T1- and T2-weighted images begin to decrease
- Hemosiderin formation begins at the periphery in late subacute phase, which is dark on T1- and T2-weighted images
- Sequences such as gradient echo T2 or SWI (susceptibility-weighted imaging) may also help in the detection of hemorrhage
- Hemorrhages may appear as restricted diffusion areas on DWI. In order not misinterpret as an infarction, all images should be evaluated, especially the non-contrast T1-weighted images

Take-Home Messages

- Postoperative hematomas are rare complications of brain surgery
- Hematoma appears differently on MRIs, depending on the imaging time. Usually, early postoperative MRIs is obtained within 48 h after surgery and hemorrhage is isointense or hyperintense on T1-weighted images in this period
- A previously stable tumor may show a rapid progress in size, during follow-up. This is probably due to an "upgrade" in histopathology

Further Reading

- Allkemper T, Tombach B, Schwindt W, et al. Acute and subacute intracerebral hemorrhages: comparison of MR imaging at 1.5 and 3.0 T—initial experience. Radiology. 2004;232:874–81
- Warnick RE, Petr MJ. Complications of surgery. In: Bernstein M, Berger MS, editors. Neuro-oncology. The essentials. New York: Thieme Medical Publishers; 2008

17.3 Early Postoperative Hypophysis

A 33-year-old male with the history of suprasellar mass lesion is operated. Early postoperative MR imaging is performed a day after the surgery.

17.3.1 Images and Legends

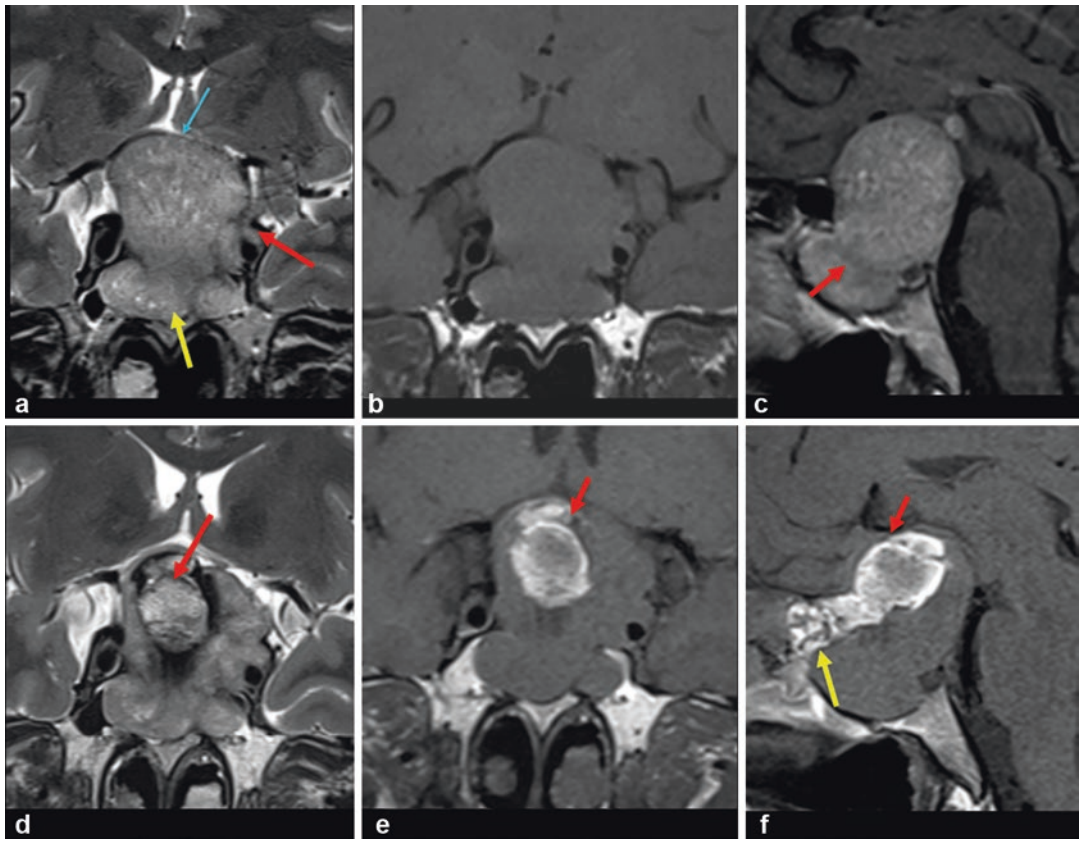

Fig. 17.3 T2-weighted coronal (**a**) MR image shows a large suprasellar mass lesion, a macroadenoma. The mass is homogeneously hyperintense. As well as the compression of optic chiasm (blue arrow), the mass is invading the sphenoid sinus (yellow arrow) and left cavernous sinus (red arrow). T1-weighted coronal (**b**) MR image shows that the mass is homogeneously isointense to brain parenchyma. On post-contrast sagittal T1-weighted image (**c**), the mas is enhancing intensely. The patient was operated by transsphenoidal approach. Postoperative images were obtained a day after. T2-weighted coronal (**d**) MR image shows hyperintense operation tract (arrow). Note hypointense hemorrhagic intensities (blood products) around the tract. Precontrast coronal T1-weighted image (**e**) shows hyperintense hemorrhagic intensities within operation cavity. On sagittal precontrast T1-weighted image (**f**), as well as the hyperintense hemorrhage (red arrow), surgical packaging material is also seen as heterogeneous hyperintensity (yellow arrow). Note, cavernous sinus component of the tumor is unchanged after the surgery. As well, there is residual tumor inferior to the hemorrhagic tract on sagittal postoperative image

17.3.2 Epidemiology/Most Commonly Seen Types

- Transsphenoidal surgery is the most common procedure for the treatment of pituitary macroadenomas
- In some selected cases, transcranial approach may still be preferred
- To evaluate the postoperative period, imaging characteristics of postoperative MR appearances should be known

17.3.3 Pathology and Genetics

- An early postoperative pituitary MRI after transsphenoidal surgery usually shows the surgical tract with hemorrhagic intensities
- Surgical packaging materials (fat, cartilage, gelfoam, etc.) are usually hyperintense
- Hemorrhage and surgical materials make the immediate postoperative images difficult to interpret
- The decrease in volume of the mass does not occur immediately after surgery. It may take 2–3 months to observe the full shrinkage
- The complexity of the early postoperative image also makes it difficult to identify the residue tumor
- It should also be remembered that, the portions of the tumor that extends into the cavernous sinus cannot be resected. Because of abundant hemorrhage risk, cavernous sinuses are avoided during the surgery

17.3.4 Clinical Management

- Early postoperative MRI of the pituitary is obtained in order to check possible complications of the surgery, as well as the residue tumors
- Some areas, as stated before, are avoided during the surgery and the portions of the tumor within those areas are left untouched
- Some residual tumors that are not within these areas and immediate second operation may be considered, before scarring and adhesions develop at the operation site
- MRIs show postoperative changes, as well as the possible residual tumor

17.3.5 Imaging Findings and Differential Diagnosis

- Preoperative and postoperative images should be compared thoroughly, to identify the changes related to surgery and possible residual tumors
- Hemorrhage within the surgical tract is usually hyperintense on both T1- and T2-weighted images
- There may be T2 hypointensities due to blood products, especially peripherally
- To control bleeding and prevent the CSF leaks, surgical packaging is frequently performed. Sellar floor and sphenoid sinus are usually filled with those materials
- Most of the surgical materials like autologous fat, cartilage, or gelfoam are hyperintense on T1-weighted images. To evaluate properly, information obtained from the surgeon will be very helpful
- Most surgical materials shrink with time
- Fat is usually absorbed completely after a year

Take-Home Messages

- Transsphenoidal surgery is the most common procedure for the treatment of pituitary macroadenomas
- To control bleeding and prevent the CSF leaks, surgical packaging is frequently performed. Most of these packaging materials (fat, cartilage, gelfoam, etc.) appear hyperintense on T1-weighted images. And most of them shrink with time
- Cavernous sinuses are avoided during transsphenoidal surgery. Tumor components within these areas will be seen as residual tumor postoperatively
- Early postoperative MRIs can show surgery-related changes as well as the residual tumors. Second immediate operation may be needed in huge macroadenomas with residual tumors

Further Reading

- Kremer P, Forsting M, Ranaei G, Wüster C, Hamer J, Sartor K, Kunze S. Magnetic resonance imaging after transsphenoidal surgery of clinically non-functional pituitary macroadenomas and its impact on detecting residual adenoma. Acta Neurochir (Wien). 2002;144:433–43
- Yoon PH, Kim DI, Jeon P, Lee SI, Lee SK, Kim SH. Pituitary adenomas: early postoperative MR imaging after transsphenoidal resection. AJNR Am J Neuroradiol. 2001;22:1097–104

17.4 Postoperative Abscess Development

A 16-year-old male with the history of intracranial mass lesion is operated. Early postoperative MR imaging is performed a day after the surgery. A month later, the patient developed high fever and headache. MRI was repeated.

17.4.1 Images and Legends

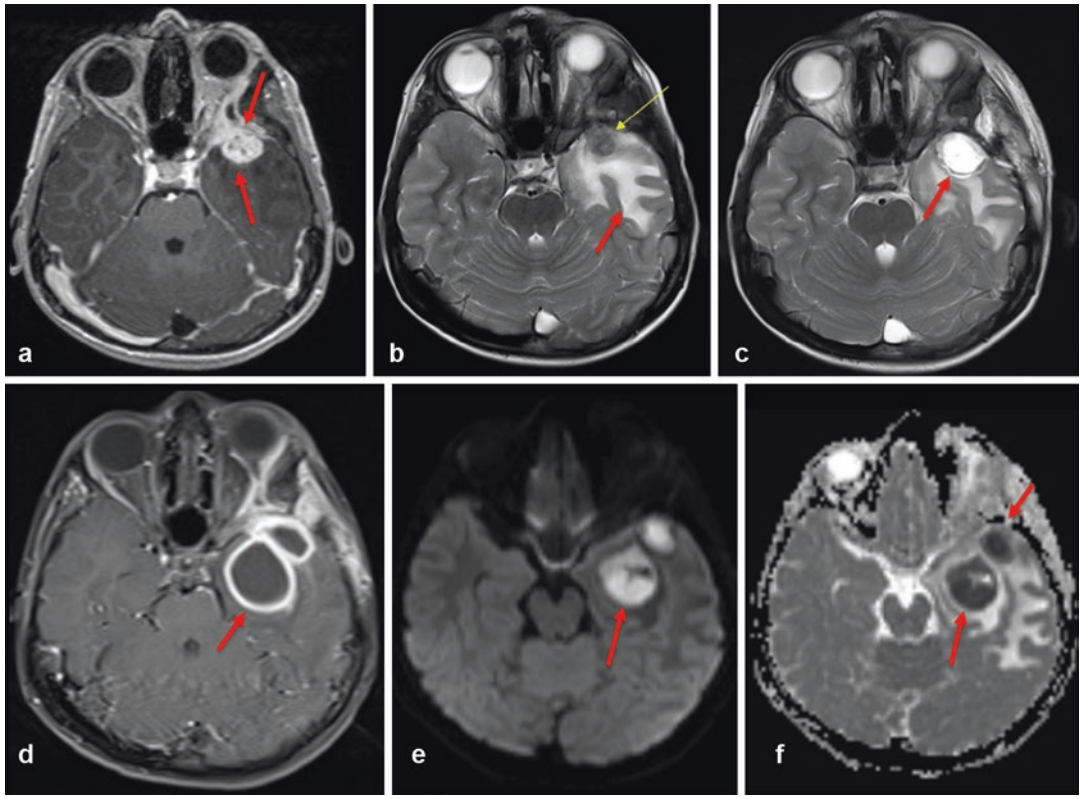

Fig. 17.4 T1-weighted post-contrast axial (**a**) MR image shows a mass lesion on the left anterior temporal fossa, behind the left sphenoid wing (arrow). T2-weighted axial image (**b**) shows surrounding vasogenic edema, the mass itself is hypointense (yellow arrow). Postoperative T2-weighted image (**c**) shows the resection cavity with fluid intensity. A month later, patient developed high fever and headache. MRI was repeated. T1-weighted post-contrast axial image (**d**) shows bilobulated lesion with marked peripheral enhancement. Inner contours of the enhancing margins are regular. On diffusion-weighted images (B1000 image, **e** and ADC map, **f**) there is marked diffusion restriction within the lesion (arrows)

17.4.2 Epidemiology/Most Commonly Seen Types

- Postoperative infection is a serious complication of brain surgery
- The incidence of postoperative infection is reported to be between 0.8 and 7%
- Most common symptoms are fever, headache, mental status change, seizures, and purulent drainage from the surgical wound
- Several types of postoperative infections may be seen: Subdural/epidural empyemas, meningitis, abscess, wound, or bone flap infections
- Early diagnosis of the type of the infection is necessary in order to plan the probable intervention, along with the antibiotherapy
- MRI is mandatory in the evaluation

17.4.3 Pathology and Genetics

- A typical abscess cavity shows peripheral enhancement with fluid intensity inside the lesion
- On DWI, abscess fluid usually show restricted diffusion. However, it is very important to remember that postoperative abscess may not show restricted diffusion
- The ratio of restricted diffusion is much higher in spontaneous abscesses than postoperative abscesses. Therefore, if the clinical findings suggest an infection, a peripherally enhancing fluid collection may be considered an abscess, even if restricted diffusion is not present
- Abscess margins usually show lower perfusion values than the tumors
- On SWI (susceptibility-weighted imaging), abscess margins have low intensity rims, which may also help for the differentiation

17.4.4 Clinical Management

- Along with the proper antibiotherapy, abscess cavities should be drained
- Antibiotherapy may be modified according to microbiologic evaluation of the abscess content. In this case, gram-positive cocci was present in the cavity fluid

17.4.5 Imaging Findings and Differential Diagnosis

Abscesses may look like peripherally enhancing or cystic tumors. Some clues to differentiate an abscess from tumor are:

- Abscesses have more regular enhancing margins, especially the inner contours, whereas tumors have usually irregular margins
- There is usually restricted diffusion within the abscess content. However, it is not a rule, especially in postoperative cases
- Abscess margins have lower perfusion values than tumors
- On SWI, abscess margins have low intensity rims

Take-Home Messages

- Urgent MRI is mandatory if a brain surgery patient develops fever, headache, personality changes, or seizures
- There are many types of postoperative infections and MRI gives valuable information for the differential diagnosis
- Typical postoperative brain abscess has regular, enhancing walls with fluid content. On DWI restricted diffusion may be present within the fluid portion

Further Reading

- Dashti SN, Baharvahdat H, Spetzler RF, et al. Operative intracranial infection following craniotomy. Neurosurg Focus. 2008;24(6):E10
- Lotan E, Hoffmann C, Fardman A, Ziv-Baran T, Komisar O, Harnof S. Postoperative versus spontaneous intracranial abscess: diagnostic value of the apparent diffusion coefficient for accurate assessment. Radiology. 2016;281:168–74
- Toh CH, Wei KC, Chang CN, et al. Differentiation of pyogenic brain abscesses from necrotic glioblastomas with use of susceptibility-weighted imaging AJNR Am J Neuroradiol. 33:1534–38

17.5 Postoperative Dural Enhancement

A 40-year-old male with the history of intracranial mass lesion (which is diagnosed as glioblastoma multiforme) is operated. Early postoperative MR imaging is performed a day after the surgery.

17.5.1 Images and Legends

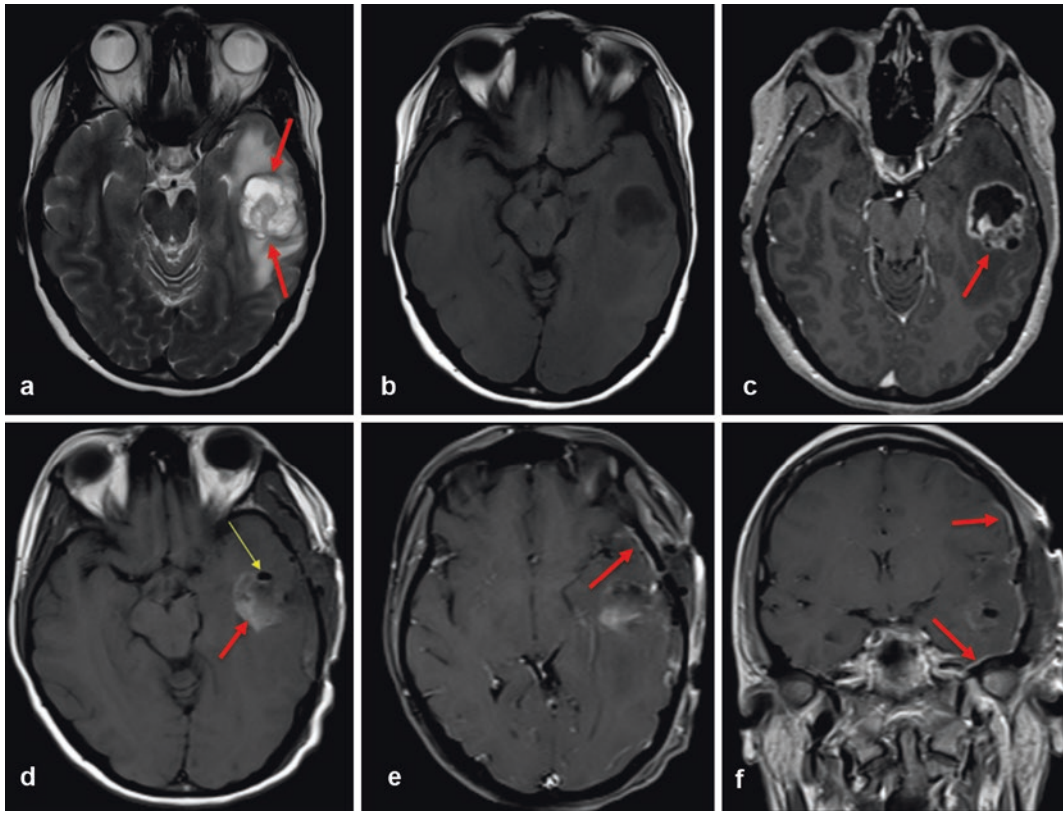

Fig. 17.5 MRI Images of T2-weighted (**a**), T1 (**b**), post-contrast T1 (**c**) images show a mass lesion on the left temporal lobe, which has cystic and solid portions with intense peripheral enhancement (arrows). There is no dural enhancement in preoperative images. After a day, early postoperative MRI shows resection cavity with hemorrhagic intensities (red arrow, **d**) and air (yellow arrow, **d**). On transverse (**e**) and coronal (**f**) post-contrast T1-weighted images, there is thin, asymmetric dural enhancement on the left side (arrows)

17.5.2 Epidemiology/Most Commonly Seen Types

- Two different types of extra-axial enhancement may be observed on postoperative MRIs: Thick (dural) and thin (leptomeningeal)
- Both types are observed very frequently after cranial surgery
- As well as surgery, stereotaxic biopsy, shunt catheter placement, and even lumbar punction may cause reactive dural enhancement

17.5.3 Pathology and Genetics

- Dural structures do not have blood-brain barrier and may show very thin and discontinuous enhancement in normal patients
- Surgery and hemorrhage may induce local inflammation on dura and vasodilatation and reactive changes develop afterwards. This causes thicker and more prominent appearance of dura on MR images

17.5.4 Clinical Management

- Dural thickness may be up to 3 mm in early postoperative period and may reach 6 mm within months, it is expected to decrease thereafter
- Thick dural enhancements persisting for year have been reported
- Dural enhancement alone does not require intervention

17.5.5 Imaging Findings and Differential Diagnosis

- Leptomeningeal enhancement is thin linear enhancement surrounding the gyral structures
- Dural enhancement is parallel to the inner table of calvarium and does not extend into the sulci
- Sometimes it can be difficult to differentiate residue or recurrent meningiomas from thick dural enhancements
- Cortical veins may also appear like dural enhancement in post-contrast T1-weighted images, especially if fat suppression is present. However, cortical veins are not seen on contiguous slices whereas dura is continuous

Take-Home Messages

- Early postoperative MRIs frequently show reactive dural enhancement
- Thickness of dural enhancement after the operation may reach 6 mm within months but decreases thereafter
- Dural enhancement rarely persists years after the surgery

Further Reading

- Burke JW, Podrasky AE, Bradlew WG. Meninges: Benign postoperative enhancement on MR images. Radiology. 1990;174:99–102
- Smirnotopoulos JG, Murphy FM, Rushing EJ, Rees JH, Schroeder JW. Patterns of contrast enhancement in the brain and meninges. Radiographics 2007;27:525–5
- Sato N, Bronen RA, Sze G, et al. Postoperative changes in the brain: MR imaging findings in patients without neoplasms. Radiology 1997;204:839–46

17.6 Postoperative Infarction

A 36-year-old male with the history of intracranial mass lesion is operated. Early postoperative MR imaging is performed a day after the surgery.

17.6.1 Images and Legends

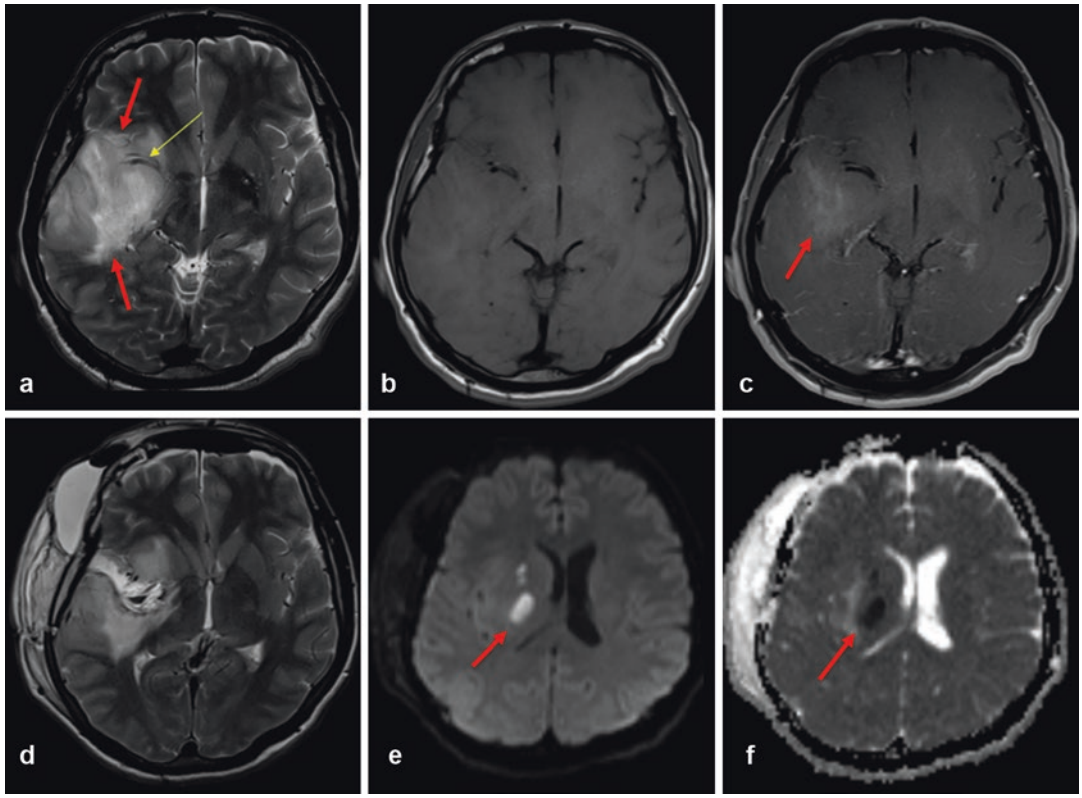

Fig. 17.6 T2-weighted (**a**), T1-weighted (**b**), post-contrast T1-weighted (**c**) MR images show a mass lesion on the right cerebral hemisphere around right Sylvian fissure (between red arrows) with a mild contrast enhancement (**c**, arrow). Right middle cerebral artery is passing through the mass (**a**, yellow arrow). After a day, early postoperative MRI shows the resection cavity. Edema and CSF leakage is also noted within the paracalvarial soft tissue (arrow, **d**). Just above the resection cavity, restricted diffusion is present on DWI (arrows on **e**: B1000 image, **f**: ADC map)

17.6.2 Epidemiology/Most Commonly Seen Types

- Majority of cerebrovascular incidents in brain tumor patients are related to treatment
- Infarctions are not infrequent postoperatively and they may be clinically silent, or may have subtle clinical findings. Therefore, they are usually identified on postoperative MRIs
- Diffusion-weighted sequences show restricted diffusion due to cytotoxic edema and they are the most valuable MRI sequence for showing cerebral infarctions in the early period
- Frequency of the postoperative infarctions is between 19 and 64%
- Infractions usually direct result of surgery. However, the patient's underlying stroke risk may also be increased by surgery

17.6.3 Pathology and Genetics

- Two most important complications of the brain surgery are hemorrhage and infarction
- Infarctions usually occur at the early postoperative period
- In cancer patients, it is known that thrombosis risk is increased. As well, arterial structures may also be compressed (as in the patient presented) or infiltrated by tumor, which also increase the likelihood of occlusion
- The infarctions usually occur around the resection cavity; however, remote infarctions have also been reported after cranial surgery

17.6.4 Clinical Management

- Cerebrovascular incidents after brain surgery increase the mortality and morbidity
- Early detection is important for the appropriate management
- Along with the medical treatment, decompression surgery may also be necessary if the infarction is large, and compression is remarkable
- External ventricular drainage is also performed if CSF flow obstruction is present due to the compression

17.6.5 Imaging Findings and Differential Diagnosis

- Restricted diffusion is the main finding of the acute brain parenchymal infarctions
- They appear bright on diffusion (e.g., B1000)-weighted images and dark on ADC (apparent diffusion coefficient) maps
- Findings begin to be detected 2–3 h after the incident. Other sequences such as T2 and FLAIR also show intensity changes but much later than the diffusion-weighted images
- Early postoperative MRIs should include diffusion-weighted sequences
- In early postoperative period, brain MRIs may be difficult to interpret, because hemorrhage may appear as areas of restricted diffusion; therefore, evaluating all the sequences along with the diffusion-weighted images is mandatory
- Hemorrhage is usually bright on T1-weighted images and dark on T2-weighted images in this period
- Sequences such as gradient echo T2 or SWI (susceptibility-weighted imaging) may also help in the detection of hemorrhage

Take-Home Messages

- Early postoperative (within 48 h after surgery) MRI should be obtained in all brain tumor patients who had surgical resection. Surgery-related enhancement is minimal in this period. Therefore, residual tumor detection is easier than later MRIs
- As well as showing the presence of a residual tumor, early postoperative MRIs are also valuable in showing complications such as hemorrhage, infarctions, and CSF leakage
- Diffusion-weighted images should always be included in the early postoperative MRI. Strokes may be undetected without these sequences
- Most infarctions after brain surgery is around the resection cavity; however, remote infarctions have also been reported

Further Reading

- Khan RB, Gutin PH, Rai SN, Zhang L, Krol G, DeAngelis LM. Use of diffusion weighted magnetic resonance imaging in predicting early postoperative outcome of new neurological deficits after brain tumor resection. Neurosurgery. 2006;59:60–6; discussion 60–6
- Kreisl TN, Toothaker T, Karimi S, et al. Ischemic stroke in patients with primary brain tumors. Neurology. 2008;70;2314–20
- Yoon SJ, Hong CK. Remote cerebellar infarction after supratentorial craniotomy and its management: two case reports. Brain Tumor Res Treat. 2015;3:141–6

17.7 Recurrent Tumor

A 56-year-old male with the history of intracranial mass lesion is operated. Preoperative and follow-up MRIs were obtained after the surgery.

17.7.1 Images and Legends

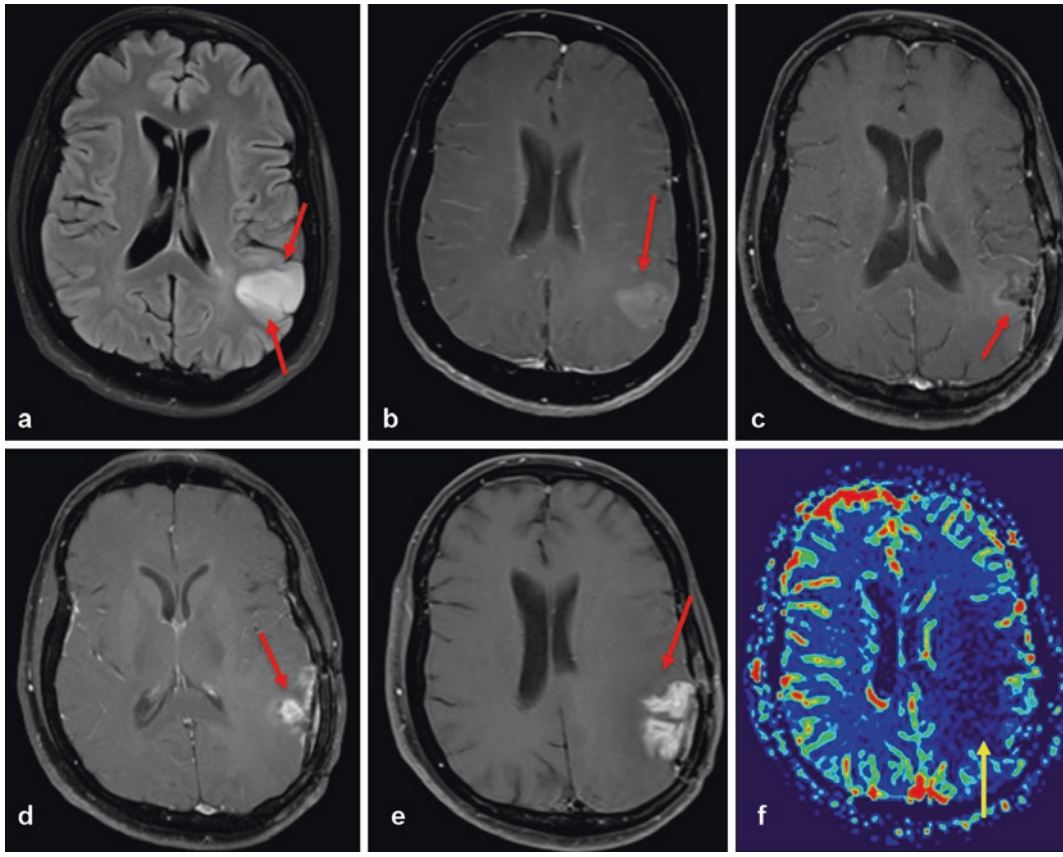

Fig. 17.7 FLAIR (**a**) MR image shows a mass lesion on the left parietotemporal junction. Tumor is peripherally located (arrow). On post-contrast T1-weighted MR image (**b**), there is mild enhancement (arrow). The patient was operated and the mass was completely resected. Pathologic diagnosis was anaplastic astrocytoma (WHO grade 3). Nine months after surgery, T1-weighted post-contrast MR image (**c**) shows no enhancement within or around the resection cavity. However, 15 months after the surgery, there is nodular enhancement within the resection site (arrow, **d**). And 18 months after the surgery, enhancement is much larger than previous MRI (arrow, **e**). Note: On perfusion MRI, there is no increased rCBV on the enhancing area (arrow, **f**). The patient was reoperated and pathologic examination confirmed recurrent tumor

17.7.2 Epidemiology/Most Commonly Seen Types

- Malignant gliomas (WHO grade 3 astrocytomas) and glioblastoma multiforme (WHO grade 4) have poor prognosis and this is mainly due to their extremely high recurrent rates
- Most recurrences occur within first year after the surgery
- MRI evaluation plays a very important role in the detection of recurrence

17.7.3 Imaging Findings and Differential Diagnosis

- Early postoperative MRIs is obtained usually within 48 h after surgery. This time interval is optimal for the early evaluation, because surgery-related enhancement is minimal
- Enhancing components of the possible residual tumor is evaluated much easier in early postoperative MRIs than later MRIs
- Opinion of the surgeon is also very important about the presence of residual tumor
- Even if the tumor is totally resected and no gross tumor left, recurrence still may occur, as in this case
- Reoperation of the recurrent tumor increases the median survival time
- Adjuvant chemo- and/or radiotherapy may also be added

Take-Home Messages

- Recurrence is the formation of tumoral mass after complete resection of the primary tumor
- Increased edema around the resection site and nodular enhancement are important signs of recurrence on MRIs
- On perfusion MR imaging, there is usually an increased rCBV in the recurrent tumors; however, there may still be a recurrence without increased perfusion, as in this case

Further Reading

- Barbagallo GMV, Jenkinson AD, Brodbelt AR. 'Recurrent' glioblastome multifoem, when should we reoperate. Br J Neurosurg. 2008;22:452–5
- Ekinci G, Akpınar İN, Baltacıoğlu F, et al. Early-postoperative magnetic resonance imaging in glial tumors: prediction of tumor regrowth and recurrence. Eur J Radiol. 2003;45:99–107

17.8 Postoperative Residue and Progress

A 47-year-old male with the history of intracranial mass lesion is operated. Preoperative and follow-up MRIs were as follows.

17.8.1 Images and Legends

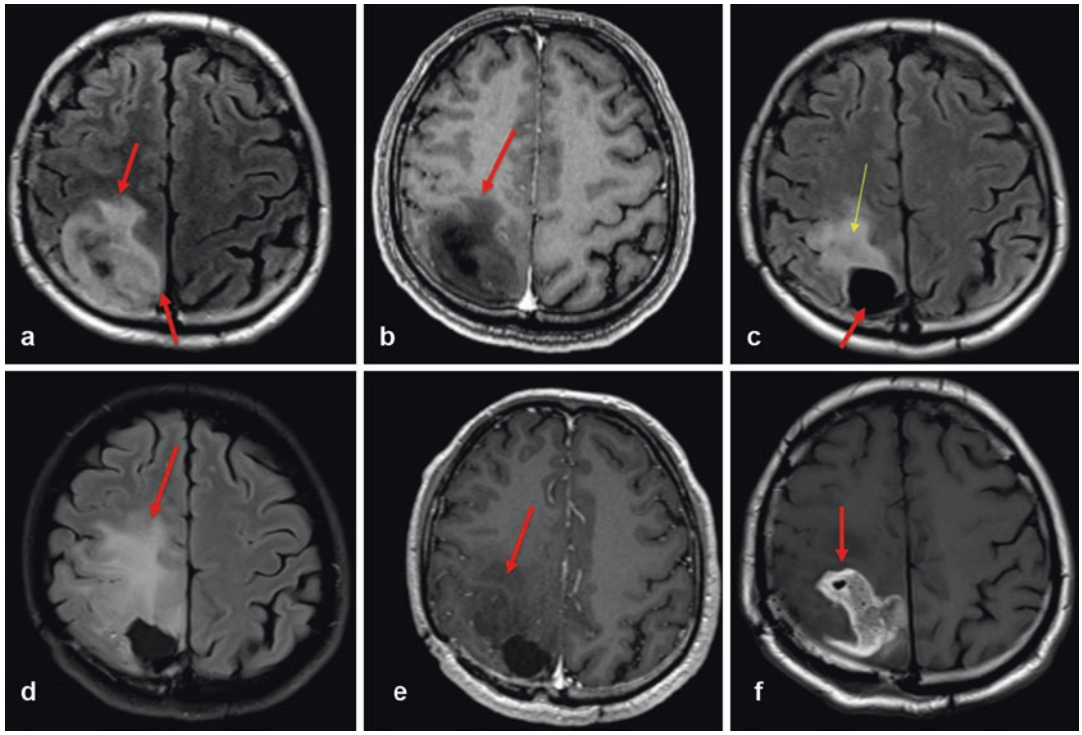

Fig. 17.8 Axial FLAIR (**a**) MR image shows a mass lesion on the right frontoparietal area (arrow). On the post-contrast T1-weighted image (**b**) there is no enhancement. MR examination on the fourth month after the surgery showed resection cavity (red arrow, **c**, axial FLAIR image) and residue tumor anterior to the resection site (yellow arrow, **c**). Patient was followed up with serial MRIs. The residue tumor increased on follow-up MRIs. Axial FLAIR image 18 months after the first surgery shows enlargement of the residue tumor volume (Arrow, **d**). There is still no contrast enhancement (post-contrast T1-weighted image, **e**). The patient was reoperated, postoperative T1-weighted axial image shows hyperintense hemorrhage within the resection cavity. Pathologic diagnosis was anaplastic astrocytoma (WHO grade 3) for both surgical excisions

17.8.2 Epidemiology/Most Commonly Seen Types

- Surgery is usually the main therapy in most brain tumors
- Depending on the pathologic evaluation, chemotherapy and radiotherapy may also be necessary
- The tumor cannot always be resected completely
- A patient's prognosis is better when all of the tumor can be surgically removed. There are four types of brain tumor surgery classifications:
  1. Gross total: The entire tumor was removed. Microscopic cells may still remain
  2. Subtotal: Large portions of the tumor were removed
  3. Partial: Only a part of the tumor was removed
  4. Biopsy only: Only a small portion, used for pathologic evaluation, was removed
- The amount of the residual tumor affects the prognosis, especially in high-grade glial tumors. As well, residual tumors may become larger in the follow-up period, which is considered as "progress."
- In the follow-up period, histopathologic grade of the residue tumor may also increase and this is considered as an "upgrade."
- If a previously non-enhancing tumor begins to show enhancement on follow-up, this is highly suggestive for tumor upgrade

17.8.3 Clinical Management

- Depending on the clinical findings, progress may need reoperation
- If imaging also suggests an upgrade, more aggressive treatments may be necessary. However, benefits of reoperation, especially in high-grade gliomas is still controversial

17.8.4 Imaging Findings and Differential Diagnosis

- In order to evaluate the possible residual tumor evaluation, first and foremost thing to know is the preoperative imaging characteristics of the tumor. Size, appearance on all sequences, enhancement, cystic and solid portions should be known and compared to the postoperative images

Take-Home Messages

- Early postoperative (within 48 h after surgery) MRI should be obtained in all brain tumor patients who had surgical resection
- Comparison of all sequences and slices of the preoperative and postoperative images is necessary to evaluate residue tumor and other findings related to surgery
- On follow-up MRIs, the size of the residue tumor may increase (progress) and may also show increase in tumor grade (upgrade)
- If a non-enhancing tumor begins to show enhancement on follow-up, this is highly suggestive for tumor upgrade

Further Reading

- Barbagallo GM, Jenkinson MD, Brodbelt AR. 'Recurrent' glioblastoma multiforme, when should we reoperate? Br J Neurosurg. 2008;22:452–5
- Cha S. Update on brain tumor imaging: from anatomy to physiology. AJNR Am J Neuroradiol. 2006;27:475–87

Follow-Up and Treatment Changes

18

Osman Kızılkılıç and Burak Koçak

18.1 Radiation and Chemotherapy-Related Injuries

18.1.1 Patient 1

61-year-old female with history of lung carcinoma, central nervous system metastasis, and whole brain radiotherapy.

18.1.2 Patient 2

18-year-old female with a history of surgery and radiotherapy for suprasellar germinoma. During follow-up, the patient also suffers from a sudden onset of headache.

18.1.3 Images and Legends

O. Kızılkılıç (✉)
Cerrahpasa Medical Faculty, Department
Of Radiology, Istanbul University-Cerrahpasa,
Istanbul, Turkey
e-mail: osmank@istanbul.edu.tr

B. Koçak
Istanbul Training and Research Hospital,
Istanbul, Turkey

Y. Özsunar, U. Şenol (eds.), *Atlas of Clinical Cases on Brain Tumor Imaging*,
https://doi.org/10.1007/978-3-030-23273-3_18

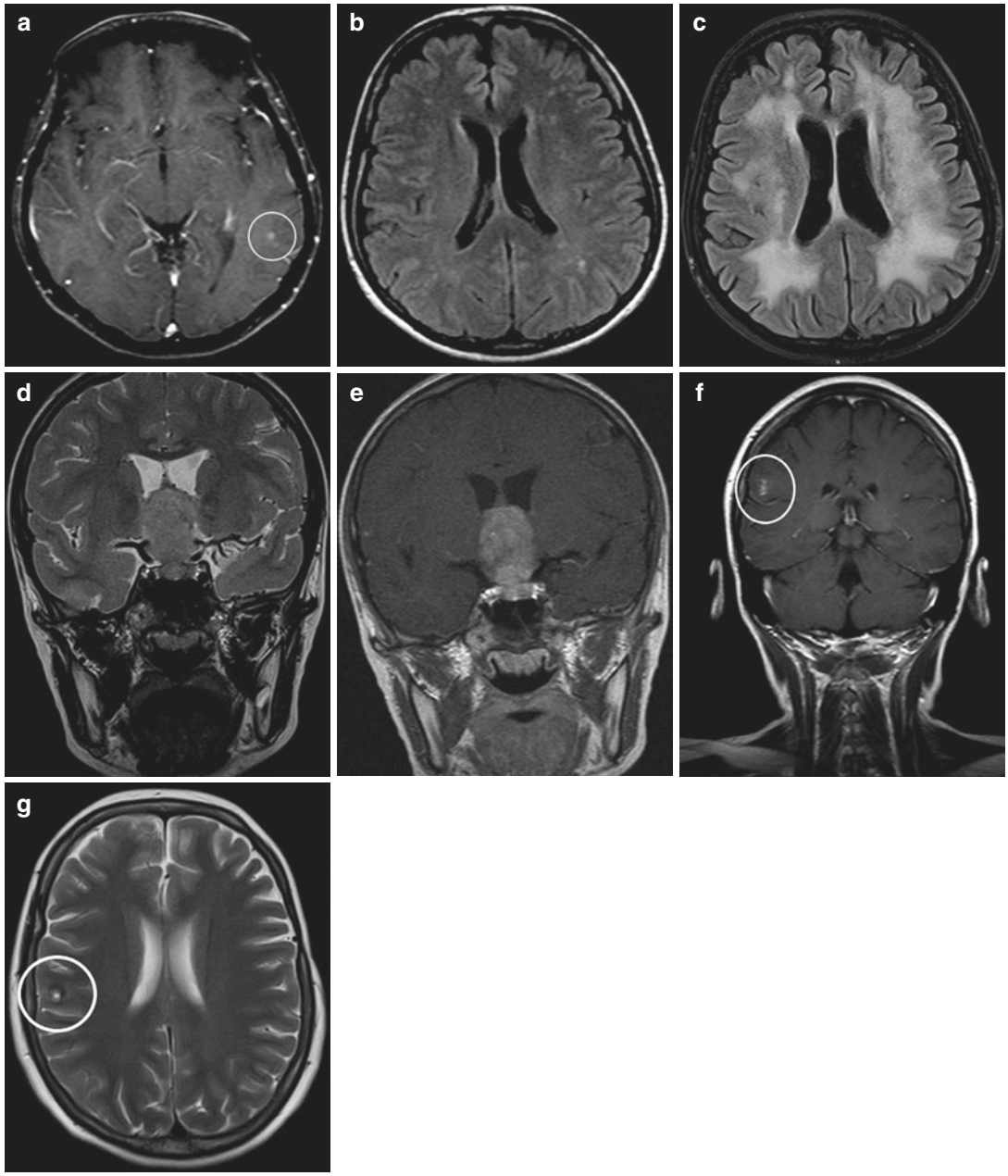

Fig. 18.1 Patient 1: Axial post-contrast T1-weighted image (**a**) shows a left-sided metastatic focus (circle) in the temporo-parietal subcortical region. Axial FLAIR (**b**) image shows nonspecific foci in bilateral cerebral white matter. Following radiation therapy, axial FLAIR image (**c**) shows extensive white matter signal intensity increase in both cerebral hemispheres, corresponding to radiation-related leukoencephalopathy. Patient 2: Coronal T2-weighted (**d**) and post-contrast T1-weighted (**e**) images show a suprasellar germinoma. Following surgery and radiation therapy, a new enhancing lesion with T2-weighted hypointense rim is seen on coronal T1-weighted (**f**) and axial T2-weighted (**g**) images, which corresponds to the radiation-related cavernous malformation (circles)

18.1.4 Epidemiology

- After fractionated partial or whole brain irradiation and/or chemotherapy
- Often observed acute (days to weeks), early delayed (1–6 months), and late delayed (6 months to years) phase

18.1.5 Pathology

- Acute: edema
- Early delayed: transient demyelination
- Late: vascular abnormalities, demyelination, gliosis, and white matter necrosis

18.1.6 Clinical Management

- Acute and subacute injuries are reversible
- Delayed injury is irreversible
- Prognosis is worse in young patients

18.1.7 Imaging Findings

- Radiation injury (**Please see the next case**)
  - From mild edema to necrosis
- Leukoencephalopathy (**Patient 1; Figure a–c**)
  - T2/FLAIR high signal in white matter, but U-fibers spared
  - Usually focal after radiation therapy
  - Diffuse or in large territories after chemotherapy
- Necrotizing leukoencephalopathy
  - After radiation and/or chemotherapy
  - White matter necrosis
- Capillary telangiectasia.
  - Usually occur 3–9 months after irradiation
  - With intervening neural parenchyma
- Cavernous malformation (**Patient 2; Figure d–g**)
  - Especially patients underwent radiation therapy in childhood
  - No intervening neural parenchyma
  - Take a longer time to develop after radiation compared to capillary telangiectasia
- PRES
  - Associated with chemotherapy and immunosuppressive agents
  - White matter edema in posterior circulation areas
- Mineralizing microangiopathy
  - Following radiation (generally) and/or chemotherapy
  - Calcification in basal ganglia, subcortical white matter
  - Atrophic changes

Take-Home Messages

- Radiation and chemotherapy for brain tumors can cause several pathologies
- Acute and subacute injuries are reversible
- Imaging findings depends on the pathology (edema, vascular damage, and demyelination) and severity of the injury

Further Reading

1. Sundgren PC, Cao Y. Brain irradiation: effects on normal brain parenchyma and radiation injury. Neuroimaging Clin N Am. 2009;19(4):657-68. doi: https://doi.org/10.1016/j.nic.2009.08.014
2. Lincoln CM, Fata P, Sotardi S, Pohlen M, Uribe T, Bello JA. Imaging spectrum of immunomodulating, chemotherapeutic and radiation therapy-related intracranial effects. Br J Radiol. 2018;91(1082):20170553. doi: https://doi.org/10.1259/bjr.20170553

18.2 Radiation Necrosis

18.2.1 Images and Legends

54-year-old female with a history of surgery due to glioblastoma and radiation therapy.

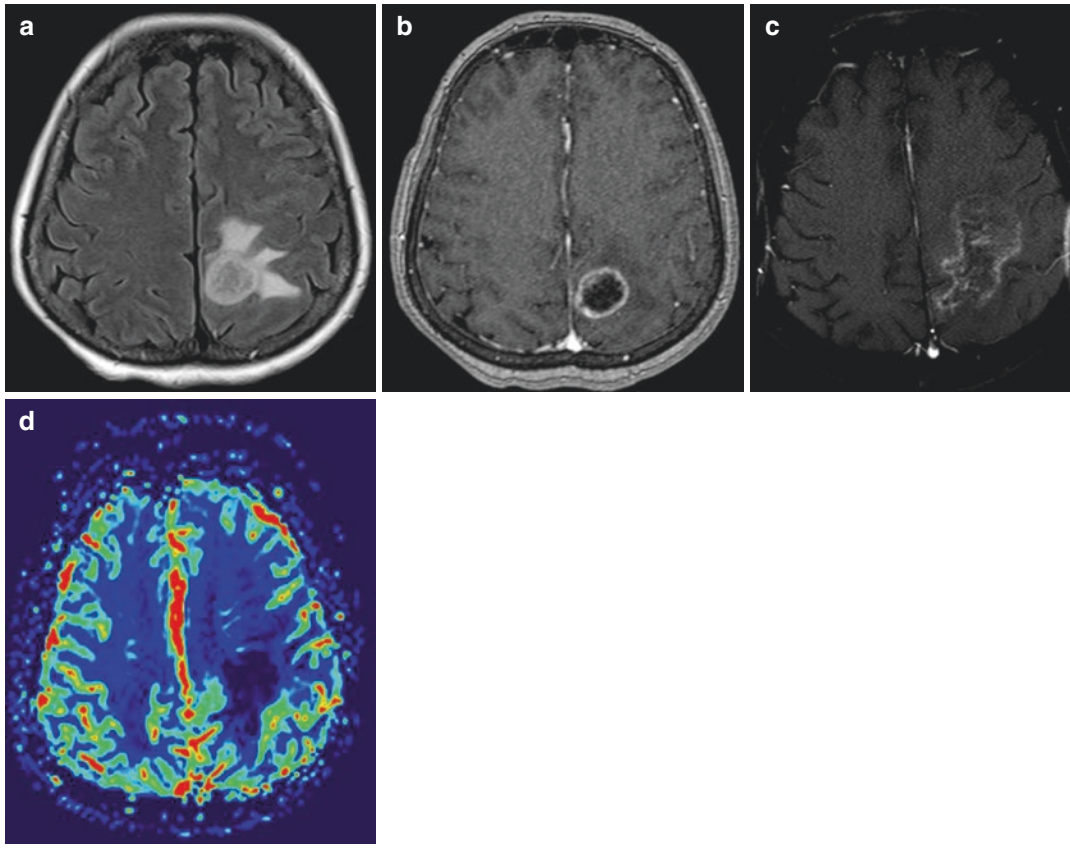

Fig. 18.2 Axial FLAIR (**a**) and post-contrast T1-weighted (**b**) images show left parietal enhancing mass with perilesional edema. Two years after surgery, axial post-contrast T1-weighted image (**c**) shows a mass-like enhancing lesion. Axial rCBV map of perfusion-weighted imaging (**d**) shows low rCBV

18.2.2 Epidemiology

- Following intracranial or regional radiation
- Appears months to several years after radiation therapy

18.2.3 Pathology

- Vascular injury
- Oligodendrocytes and white matter damage
- Fibrinolytic enzyme system activation
- Immune mechanisms

18.2.4 Clinical Management

- Can cause serious neurologic injury secondary to cerebral edema and mass effect
- Initial management includes corticosteroids
- Surgery may be the only therapy that halts the process or leads to improvement of symptoms
- Patients developing progressive lesions may require surgical intervention to remove the cause of an advancing front of destructive inflammation
- Many nonoperative treatment approaches have been used in an attempt to treat radionecrosis, including anticoagulants, pentoxifylline, deferoxamine, pentobarbital, hyperbaric oxygen, and, more recently, bevacizumab, a monoclonal antibody targeted against VEGF

18.2.5 Imaging Findings

- High signal of white matter on T2/FLAIR
  - Early period: edema and mass effect
  - Late period: volume loss
- Enhancement on CE-MRI
  - In white or gray matter
  - "Soap-bubble" or "Swiss-cheese" enhancement
  - Occasionally ring enhancement
  - Single or multiple enhancing components
  - Might be nodular or curvilinear
- Hypometabolism on MR-S
  - Low choline, creatine, and NAA
- Low rCBV
- Usually hypometabolic in FDG-PET

Take-Home Messages

- Appears months to several years after radiation therapy
- Conventional imaging can be misleading
- "Soap-bubble" or "Swiss-cheese" enhancement
- Hypometabolism on MR-S and FDG-PET
- Low rCBV

Further Reading

1. Sundgren PC, Cao Y. Brain irradiation: effects on normal brain parenchyma and radiation injury. Neuroimaging Clin N Am. 2009;19(4):657–68. doi: https://doi.org/10.1016/j.nic.2009.08.014
2. Lincoln CM, Fata P, Sotardi S, Pohlen M, Uribe T, Bello JA. Imaging spectrum of immunomodulating, chemotherapeutic and radiation therapy-related intracranial effects. Br J Radiol. 2018;91(1082):20170553. doi: https://doi.org/10.1259/bjr.20170553
3. Eisele SC, Dietrich J. Cerebral radiation necrosis: diagnostic challenge and clinical management. Rev. Neurol. 2015;61(5):225–32

18.3 Pseudo-Progression

65-year-old patient with glioblastoma diagnosis and a history of radiation therapy and temozolomide treatment.

18.3.1 Images and Legends

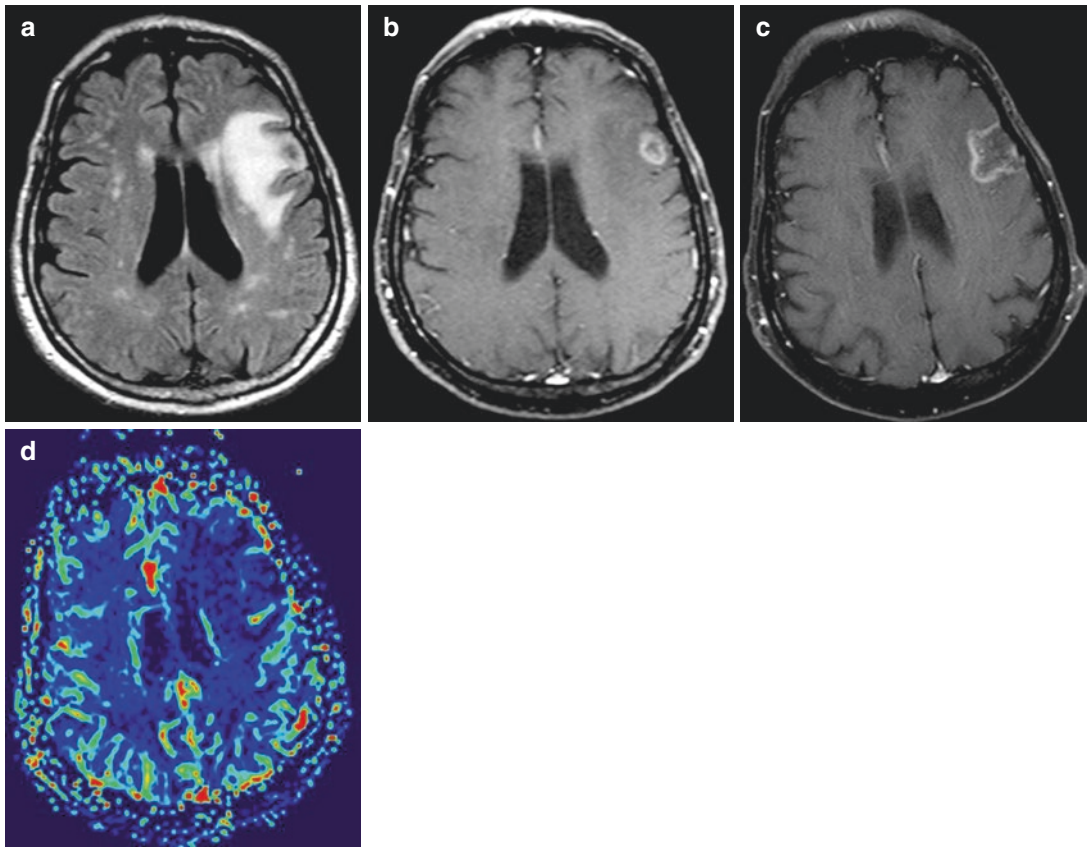

Fig. 18.3 Axial FLAIR (**a**) and post-contrast T1-weighted (**b**) images show a left frontal enhancing mass with perilesional edema. 7 months later, axial T1-weighted image (**c**) shows increased size of the enhancing lesion with a low rCBV on perfusion-weighted imaging (**d**)

18.3.2 Epidemiology

- Typically seen after concurrent radiation therapy (RT) and chemotherapy with temozolomide
- Occurs in almost 30–50% of the patients with malignant gliomas under chemoradiotherapy (RT and temozolomide)
- RT alone (15% of the patients) is less likely to result in pseudo-progression

18.3.3 Pathology

- Related to endothelial damage and tissue hypoxia following chemoradiotherapy
- Nearly 60% of the cases develop in the first 3 months after treatment
- Possible to occur from first few weeks to 6 months

18.3.4 Clinical Management

- A marker of robust response to treatment
- Self-limiting process
- Resolve without additional treatment
- Associated with longer survival

18.3.5 Imaging Findings

- New contrast enhancement and increased size of the lesion
- With or without increased T2W and FLAIR signal
- Higher ADC ($\geq$1300 × 10-6 mm^2/s) compared with tumor
- Lower rCBV in comparison with tumor
- Lower mean K_{trans} than progressive tumor
- Low choline, choline/NAA $\leq$ 1.4, increased lactate and lipid in MR spectroscopy
- MRS trace may be flat, indicating hypometabolism

Take-Home Messages

- Not all new enhancement means progressive tumor
- Knowing timing of chemoradiotherapy is key to diagnosis
- Advanced sequences (DWI, MR perfusion, and MR spectroscopy) are helpful
- Look for higher ADC, lower rCBV, and lower K_{trans}

Further Reading

1. Nowosielski M, Wen PY. Imaging criteria in neuro-oncology. Semin Neurol. 2018;38(1):24–31. doi: https://doi.org/10.1055/s-0038-1,627,468
2. Ellingson BM, Chung C, Pope WB, Boxerman JL, Kaufmann TJ. Pseudoprogression, radionecrosis, inflammation or true tumor progression? Challenges associated with glioblastoma response assessment in an evolving therapeutic landscape. J Neurooncol. 2017;134(3):495–504. doi: https://doi.org/10.1007/s11060-017-2375-2
3. Aquino D, Gioppo A, Finocchiaro G, Bruzzone MG, Cuccarini VJ. MRI in glioma immunotherapy: evidence, pitfalls, and perspectives. Immunol Res. 2017;2017:5813951. doi: https://doi.org/10.1155/2017/5813951

18.4 Pseudo-Response

50-year-old male with a history of residual glioblastoma following surgery and tumor progression after temozolomide, with a recent history of bevacizumab treatment.

18.4.1 Images and Legends

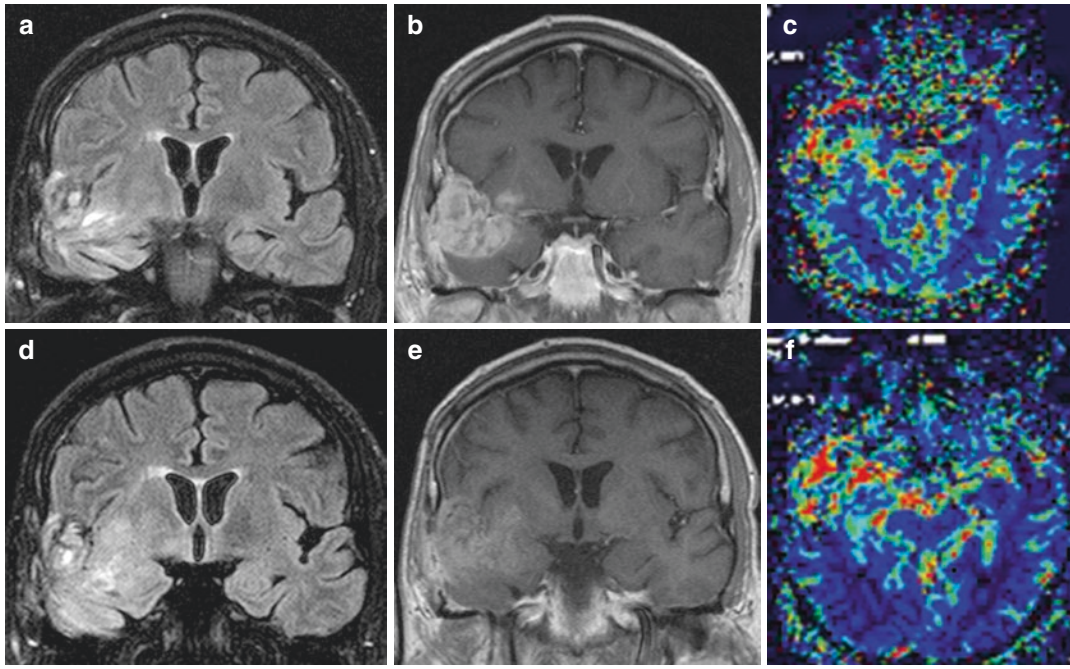

Fig. 18.4 Coronal FLAIR (**a**) and post-contrast T1-weighted (**b**) images show a right temporal mass. During follow-up, FLAIR (**d**) abnormalities persist. However, on post-contrast images (**e**), a decrease in enhancement is apparent. On the other hand, previous (**c**) and last (**f**) rCBV maps of the perfusion-weighted images show increased rCBV on the last image (**f**) in the location of the tumor. Courtesy of Cem Calli, MD

18.4.2 Epidemiology

- Use of antiangiogenic agents in glioblastomas
- Anti-VEGF (Bevacizumab; Avastin) is the main antiangiogenic agent
- VEGF receptor tyrosine kinase inhibitor (Cediranib) is another antiangiogenic agent, being currently tested in trials

18.4.3 Pathology

- Antiangiogenic agents restore blood–brain barrier
- Reduced or normalized vascularity by antiangiogenic agents

18.4.4 Clinical Management

- Antiangiogenic agents improve 6-month progression-free survival, not overall survival
- Local response to tumor growth is controlled
- Diffuse infiltration and distant metastasis are common

18.4.5 Imaging Findings

- Decreased contrast enhancement
- Persistent FLAIR hyperintensity and high ADC
- Decreased enhancement during follow-up may be true response or pseudo-response
- Early change in rCBV after therapy distinguishes PR from true response

Take-Home Messages

- Antiangiogenic agents are responsible for pseudo-response
- Decreased contrast enhancement under antiangiogenic agents
- Decreased enhancement during follow-up may be true response or pseudo-response
- ADC is an important biomarker for pseudo-response

Further Reading

1. L.C. Hygino da Cruz, I. Rodriguez, R.C. Domingues, E.L. Gasparetto and A.G. Sorensen Pseudoprogression and pseudoresponse: imaging challenges in the assessment of posttreatment glioma. Am J Neuroradiology 2011;32(11):1978–1985
2. Fatterpekar GM, Galheigo D, Narayana A, Johnson G, Knopp E. Treatment-related change versus tumor recurrence in high-grade gliomas: a diagnostic conundrum--use of dynamic susceptibility contrast-enhanced (DSC) perfusion MRI. AJR Am J Roentgenol. 2012;198(1):19–26. doi: https://doi.org/10.2214/AJR.11.7417

18.5 Tumor Progression/ Recurrence

52-year-old female with glioblastoma and progressive neurologic symptoms following repeated surgeries.

18.5.1 Images and Legends

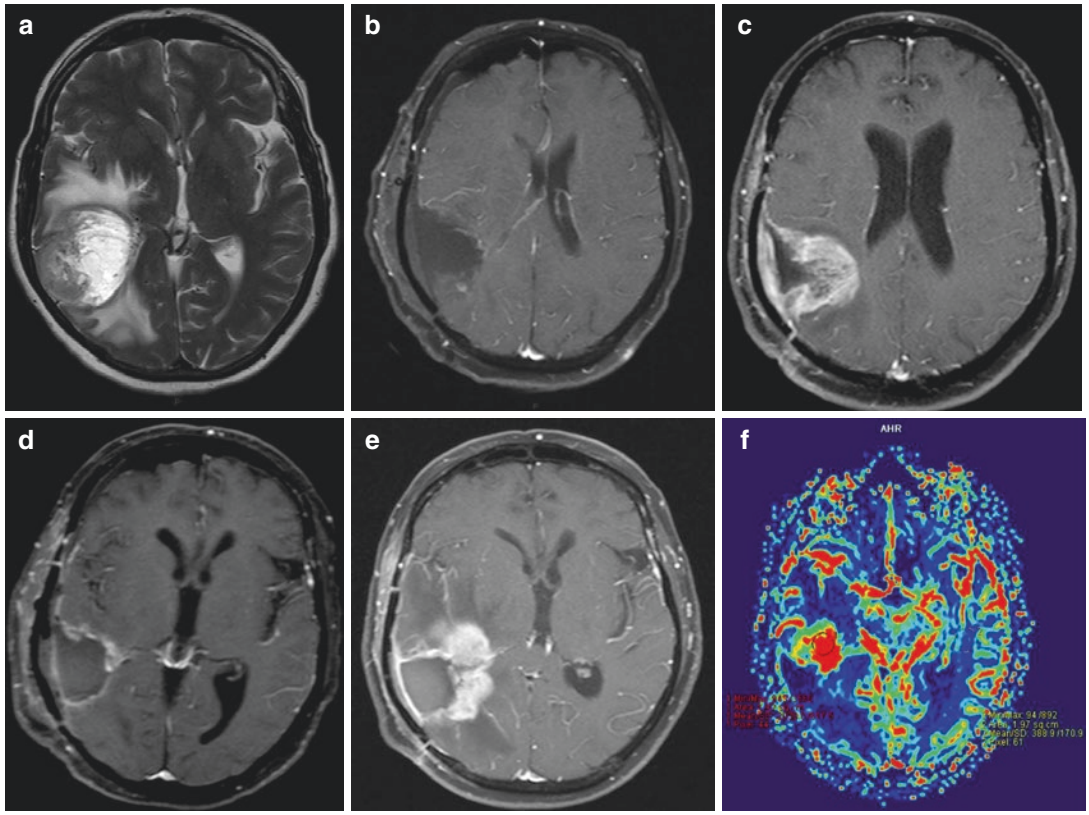

Fig. 18.5 Axial post-contrast T1-weighted image (**a**) shows right parieto-temporal enhancing mass. Following first operation, postoperative cavity with no enhancing focus is seen on the post-contrast T1-weighted image (**b**). One month later, axial post-contrast T1-weighted image (**c**) shows development of new enhancing components. Following second operation, the border of the operation cavity slightly enhances (**d**). Sixteen days later, control post-contrast T1-weighted image (**e**) shows progression of tumor with new enhancing components. Axial rCBV map from perfusion-weighted imaging (**f**) shows increased rCBV in the enhancing areas

18.5.2 Epidemiology

- Almost only 10% of patients with glioblastoma may live five years or longer
- Vast majority occurs in the surgical cavity and the high-dose radiation field

18.5.3 Pathology

- The O6-methylguanine-DNA methyltransferase (MGMT) DNA repair gene is the most important molecular prognostic factor, as well as predictive marker of response to temozolomide
- In pathological specimens, glioma cells go far beyond the abnormality shown in these imaging techniques

18.5.4 Clinical Management

- Upon recurrence, patients have a very poor prognosis, with an approximate median PFS and OS of 1.8 and 6.2 months
- Prognostic factors include multifocal and large lesions, tumor location, baseline KPS, steroid use, and age. Until now, there has been no treatment algorithm that can guide therapeutic decisions. Systemic therapy is the preferred treatment upon recurrence
- Surgery remains largely controversial in this setting. Still, there is preliminary evidence that re-operation may have some survival benefit in well-selected patients
- Clinical deterioration
- Clinical status is not attributable to other non-tumor causes and not due to steroid decrease
- The extent of surgical resection is associated with an improved outcome

18.5.5 Imaging Findings

- RANO criteria for progression
  - 25% or more increase in enhancing lesions despite stable or increasing steroid dose
  - Increase (significant) in non-enhancing FLAIR/T2W lesions, not attributable to other non-tumor causes
  - New lesions

Take-Home Messages

- Vast majority occurs in the surgical cavity and the high-dose radiation field
- Remember RANO criteria for tumor progression
  - 25% or more increase in enhancing lesions
  - Significant increase in non-enhancing FLAIR/T2W lesions
  - New lesions

Further Reading

1. Benjamin M. Ellingson, Patrick Y. Wen, Timothy F. Cloughesy. Modified criteria for radiographic response assessment in glioblastoma clinical trials. Neurotherapeutics. 2017; 14(2): 307–320
2. Telles BA1, D'Amore F, Lerner A, Law M, Shiroishi MS. Imaging of the posttherapeutic brain. Top Magn Reson Imaging. 2015;24(3):147–154